GRAVITATIONAL WAVE DATA ANALYSIS WORKSHOP

A VOLUME of TRANSPARENCIES

M.I.T., Cambridge, Massachusetts

December 6-8, 1996

LIGO G960253-00-M

GEO 600
Progress Report

H. Ward

MIT, December 1996

GEO 600 – rationale

- 600m baseline, low cost, high performance system
- planned sensitivity close to that of first stage LIGO or VIRGO above a few hundred Hertz
- construction on a timescale equivalent to that of the longer detectors
- can participate in coincidence experiments with LIGO and VIRGO
- can undertake meaningful stand-alone pulsar searches
- will allow development of advanced interferometric techniques

GEO 600 collaboration

- Garching (30m prototype)
  - power recycling
  - signal recycling
  - auto-alignment
- Glasgow (10m prototype)
  - seismic isolation
  - monolithic pendulum suspensions
  - computer control
- Hannover (600m detector)
  - buildings
  - vacuum system
  - laser system
- Cardiff / Potsdam
  - data acquisition
  - data analysis

Interferometer outline

- The main detector is a recycled Michelson interferometer with :
  - 600m arm length
  - power recycling with a factor of 1500
  - signal recycling tunable in bandwidth and centre frequency
  - external modulation for signal recovery

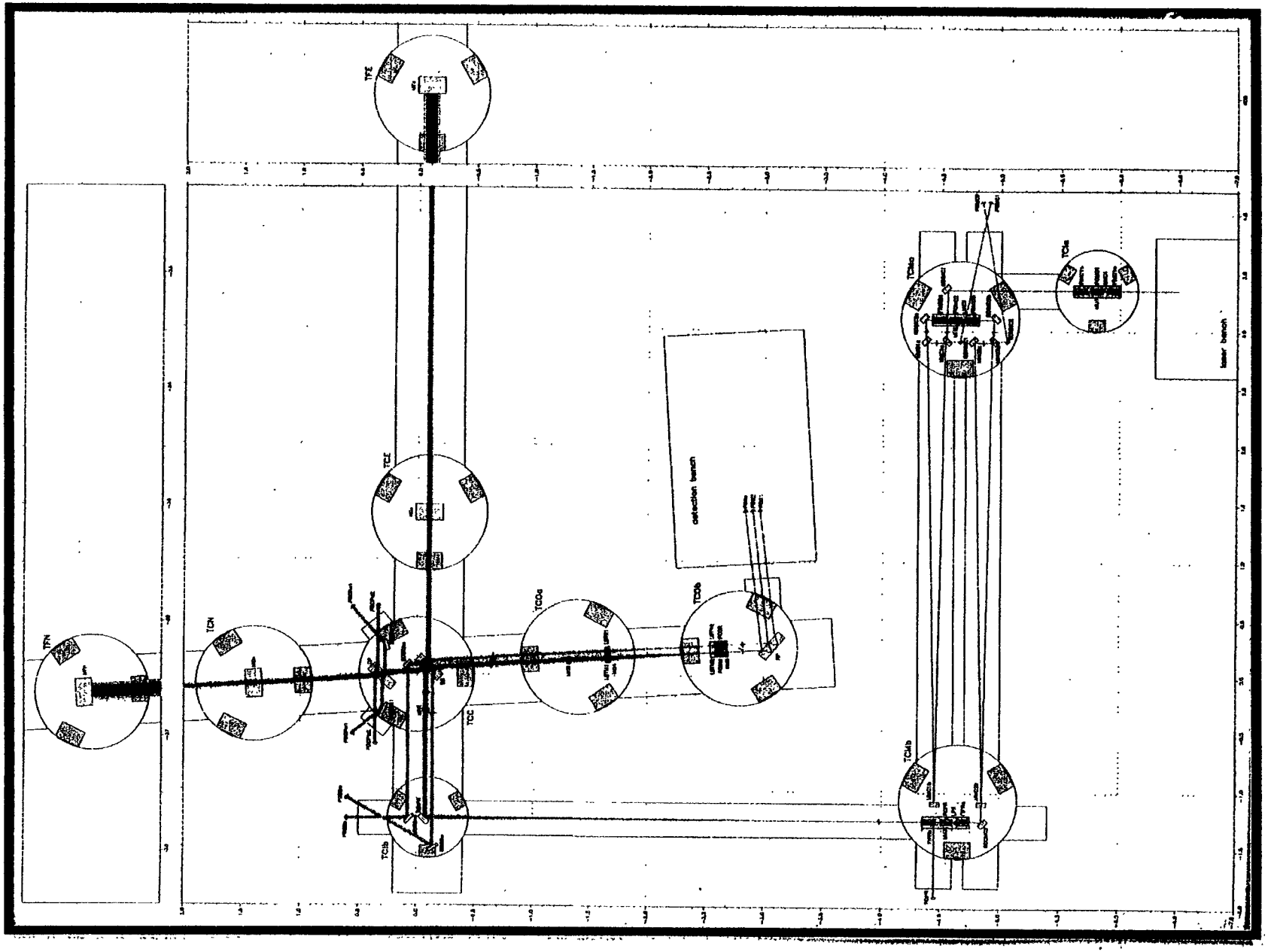

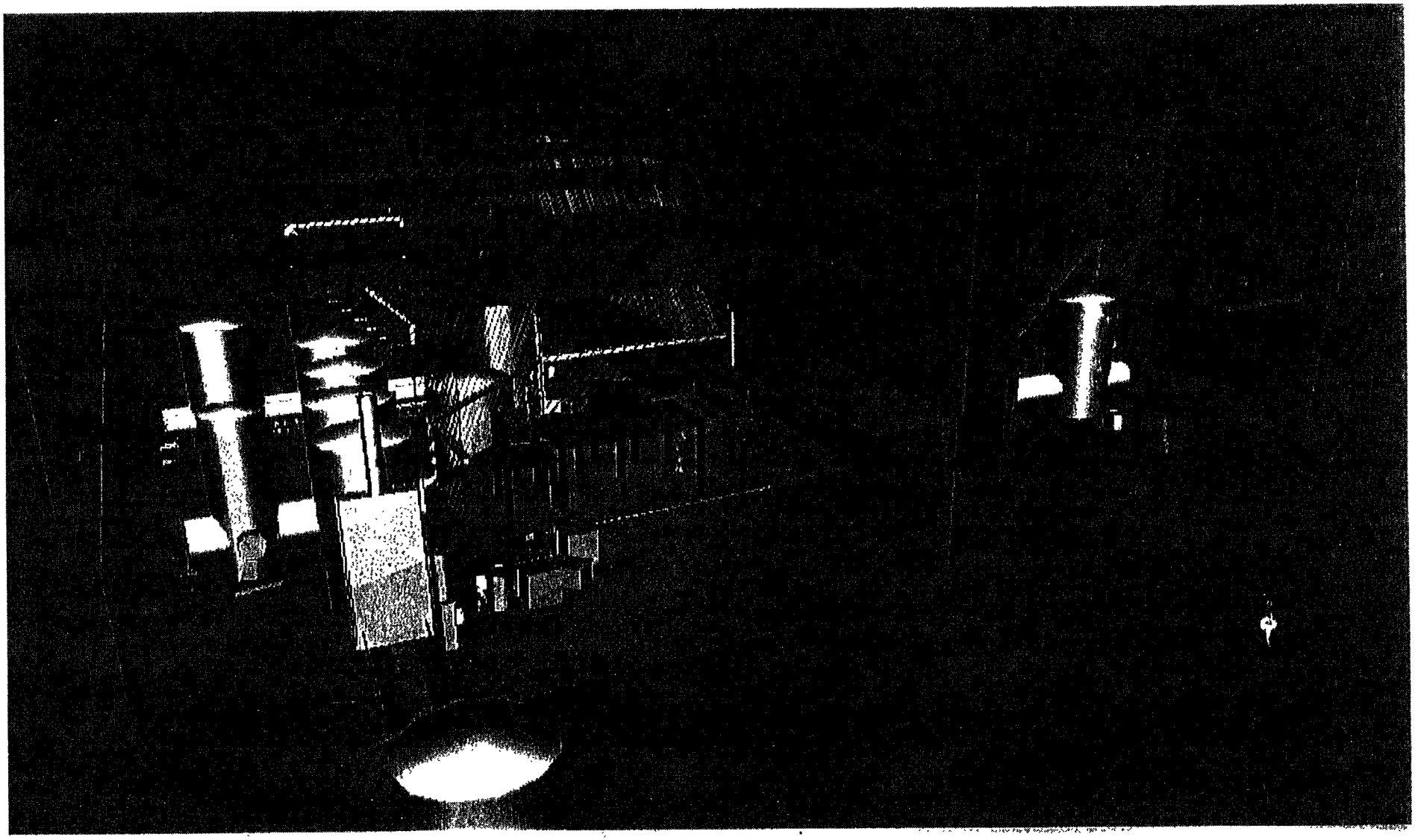

GEO 600 specifications – 1

- Arms
  - 2 x 600m, bearing NNW and ENE, near Ruthe, close to Hannover
- Laser system
  - Nd:YAG, diode-pumped, 1064nm, master/slave system with injection lock
  - frequency and intensity stabilised
  - twin mode-cleaner cavities
- Optics
  - 25cm diameter, 15cm thick OH^--free fused silica, absorption < 1ppm/cm
- Mirrors
  - ionsputtered, absorption loss < 1ppm/cm

GEO 600 specifications – 2

- Seismic isolation / suspension
  - 2-layer stacks plus 2 vertical springs
  - double pendulums with reaction masses where required
  - lower stage monolithic fused silica
- Vacuum
  - 60cm diameter pipes
  - 5×10^{-8} mbar for Hydrogen, 5×10^{-9} mbar for other gases
  - hydrocarbon-free

GEO600 End-mirror Suspension

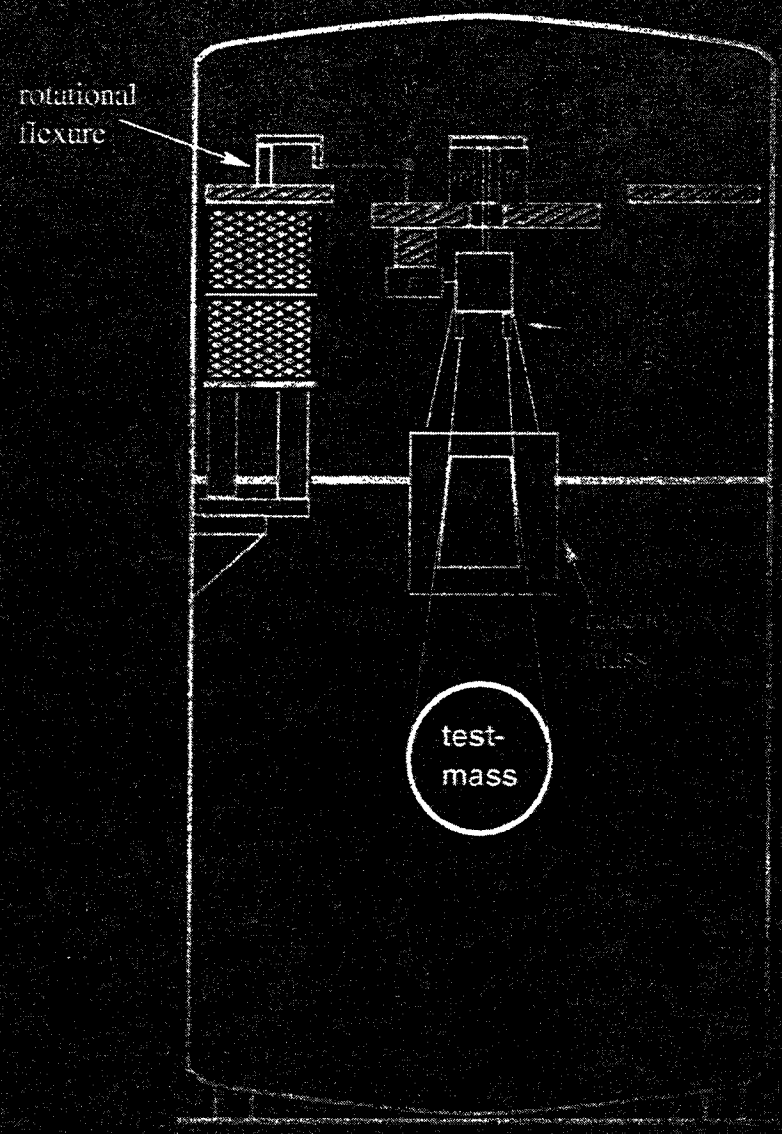

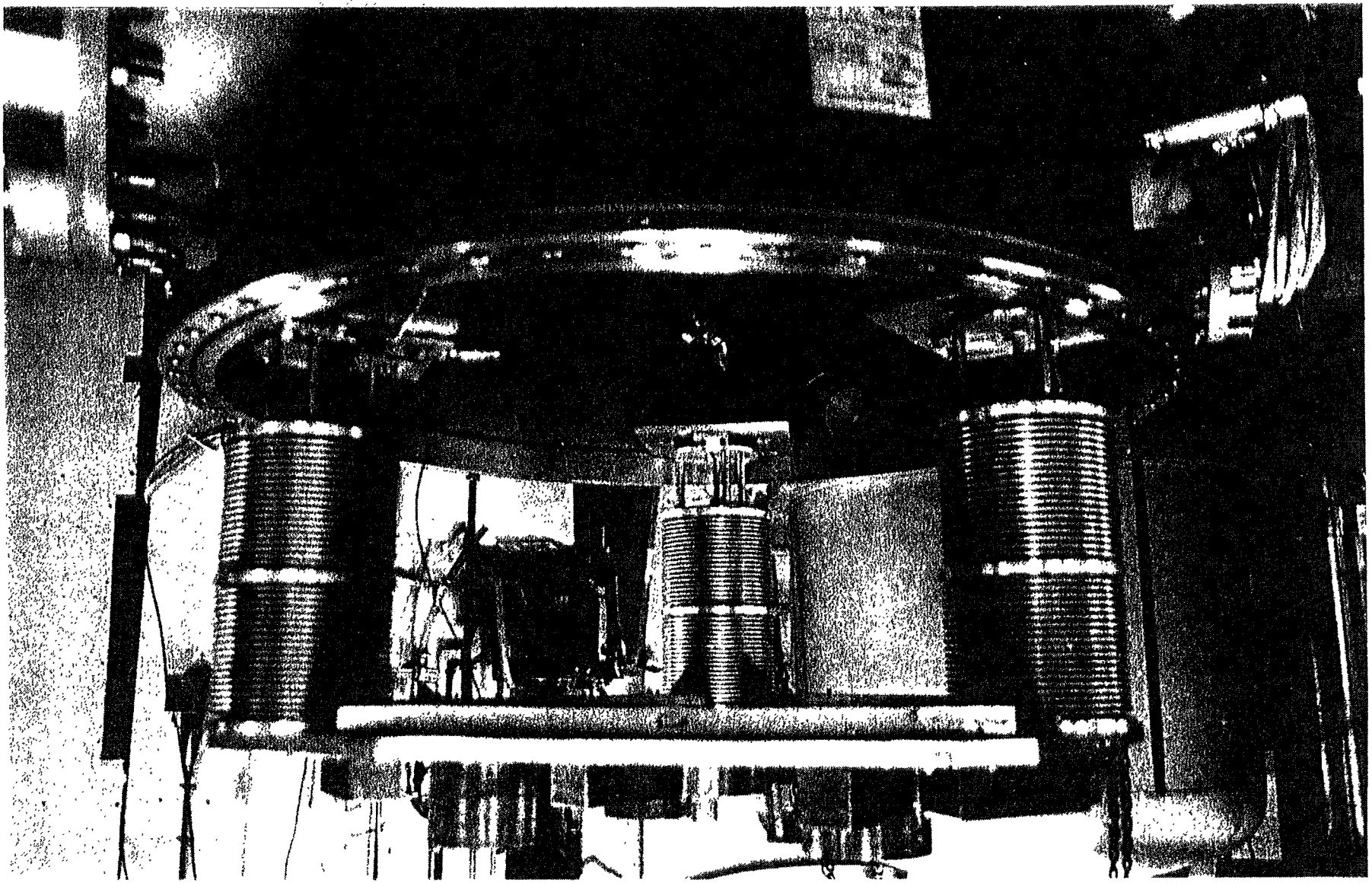

GEO 600 specifications – 3

- Power recycling
  - up to 10kW of circulating power
- Signal recycling
  - up to 1000-fold signal power enhancement
  - tunability from 50Hz to 1500Hz, with bandwidth from 5Hz to 500Hz
- Sensitivity
  - depending on chosen bandwidth

    $h \sim 2 \times 10^{-22} / Hz^{-1/2}$ to

    $h \sim 3 \times 10^{-23} / Hz^{-1/2}$

THE SENSITIVITY OF GEO600

- Seismic Noise
- Overall Sensitivity

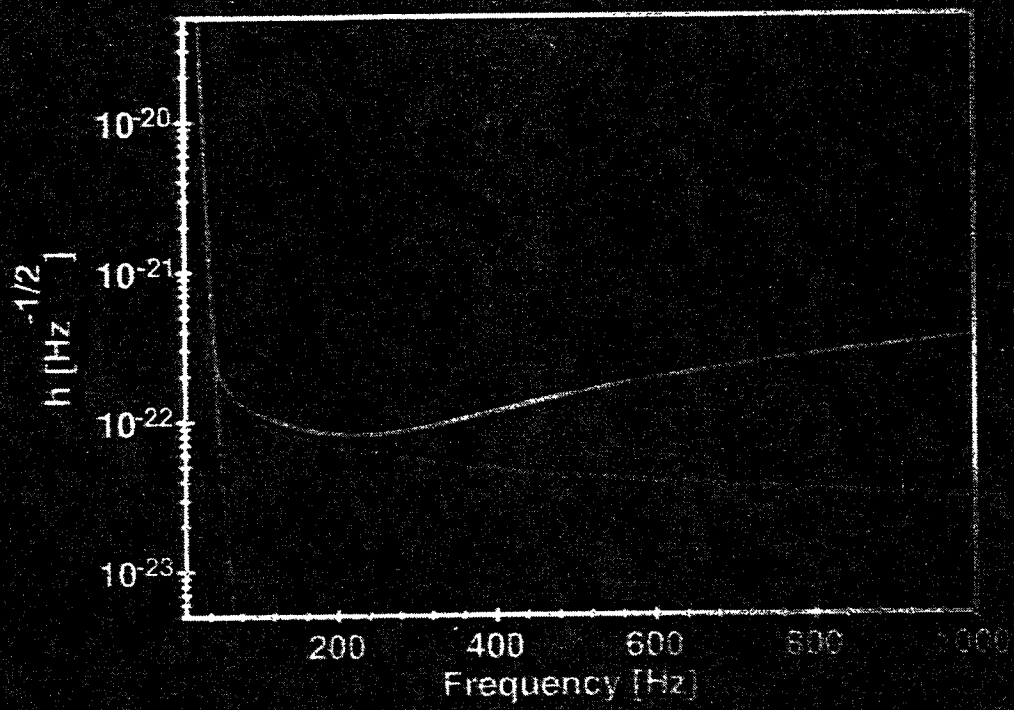

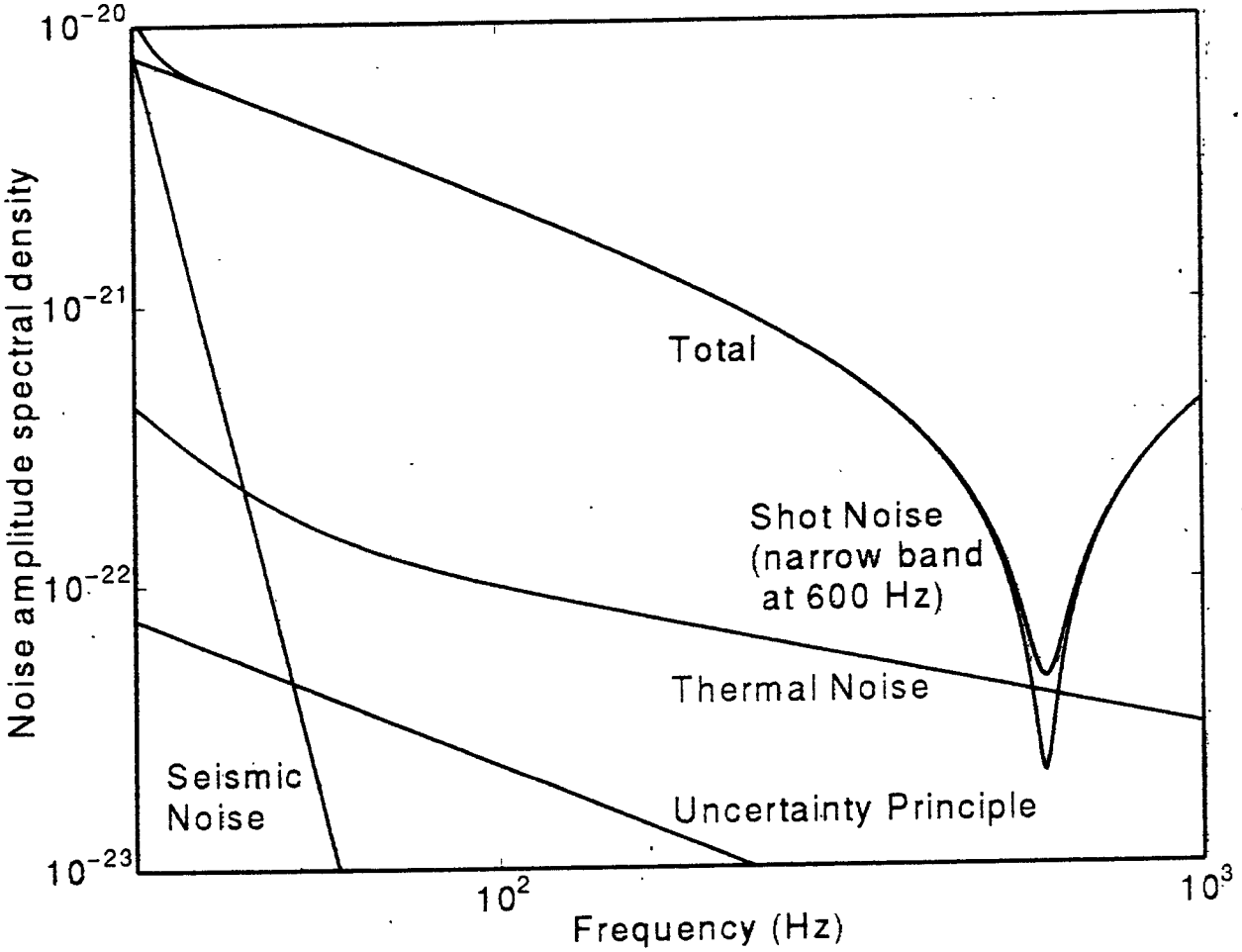

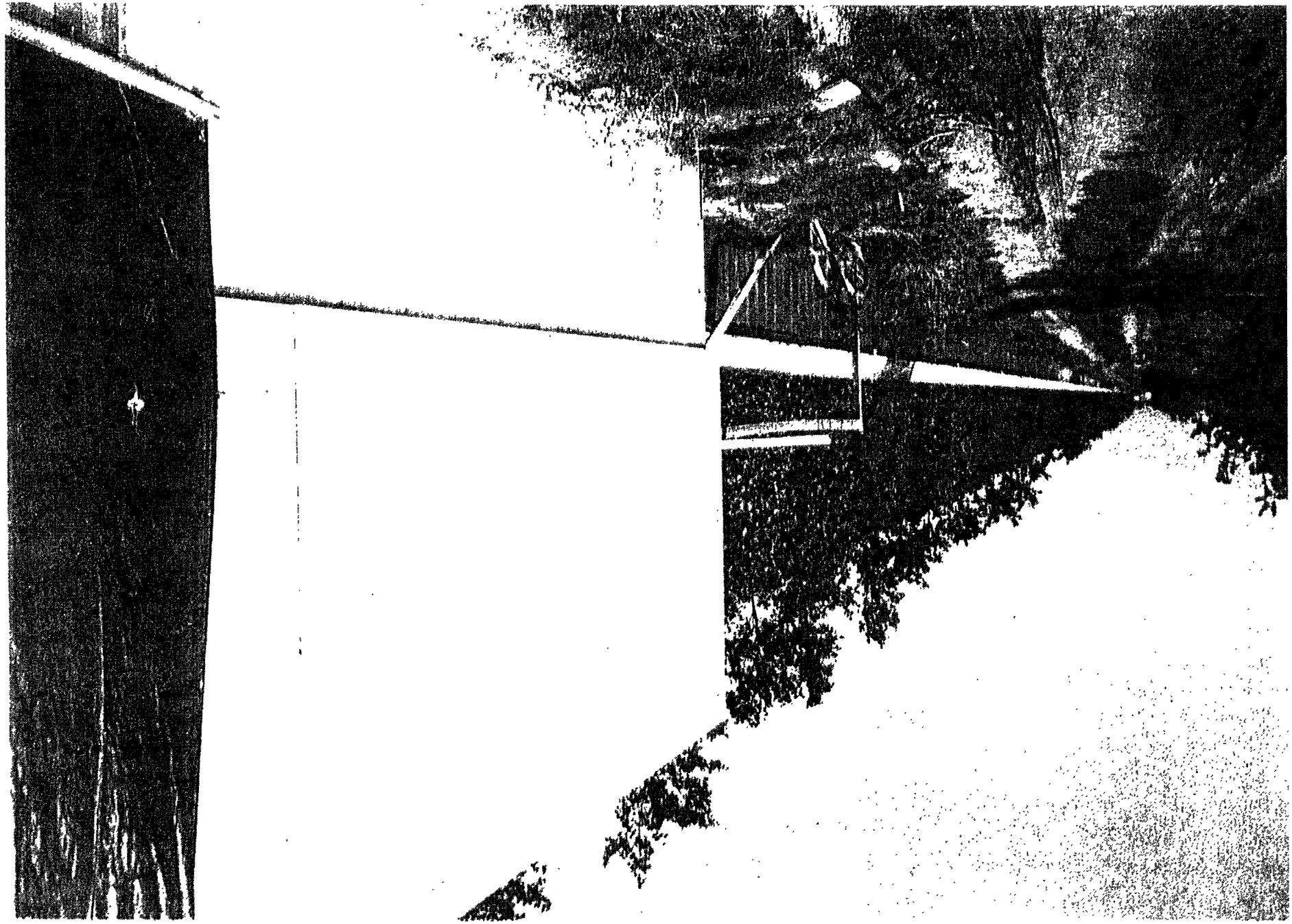

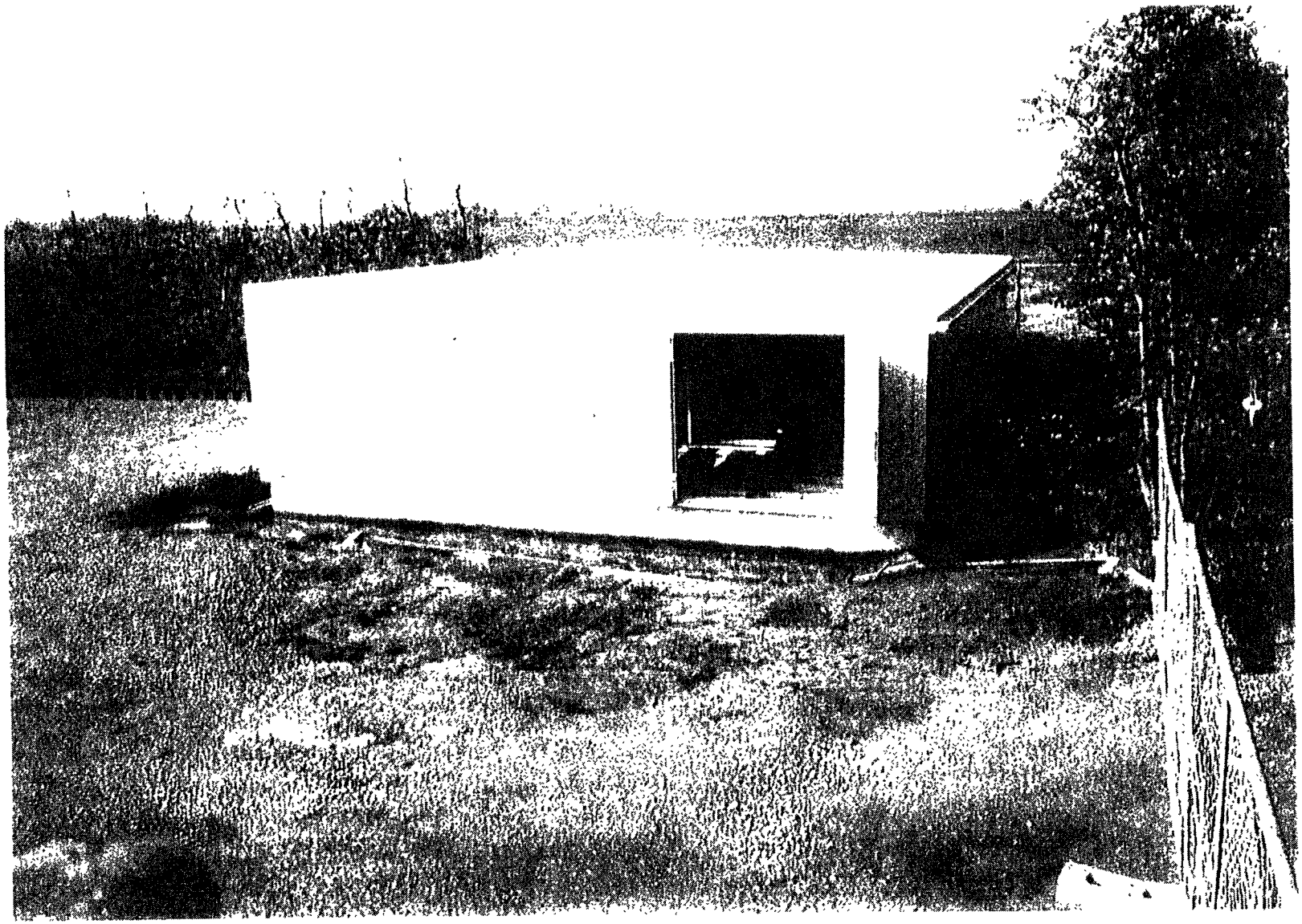

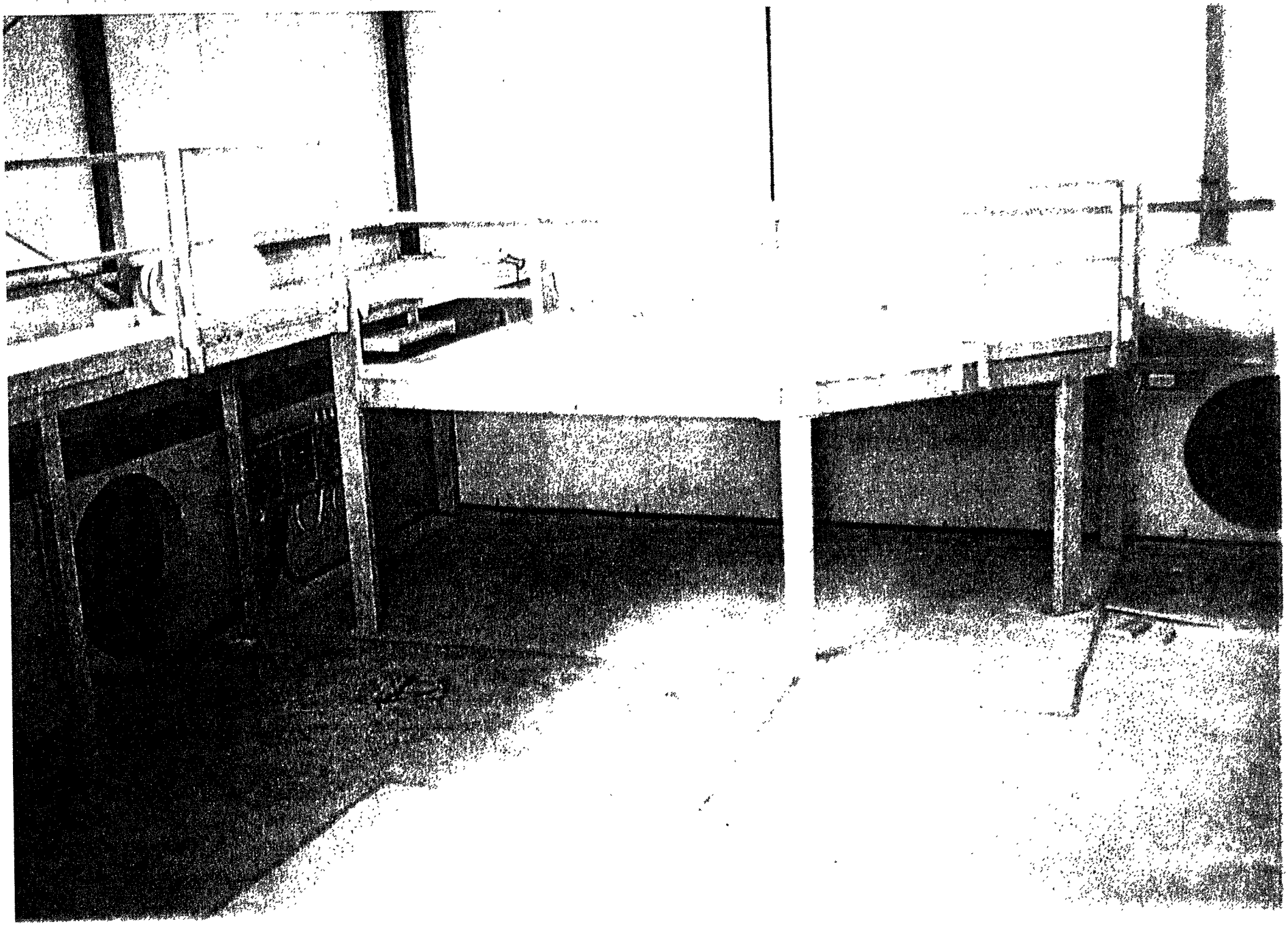

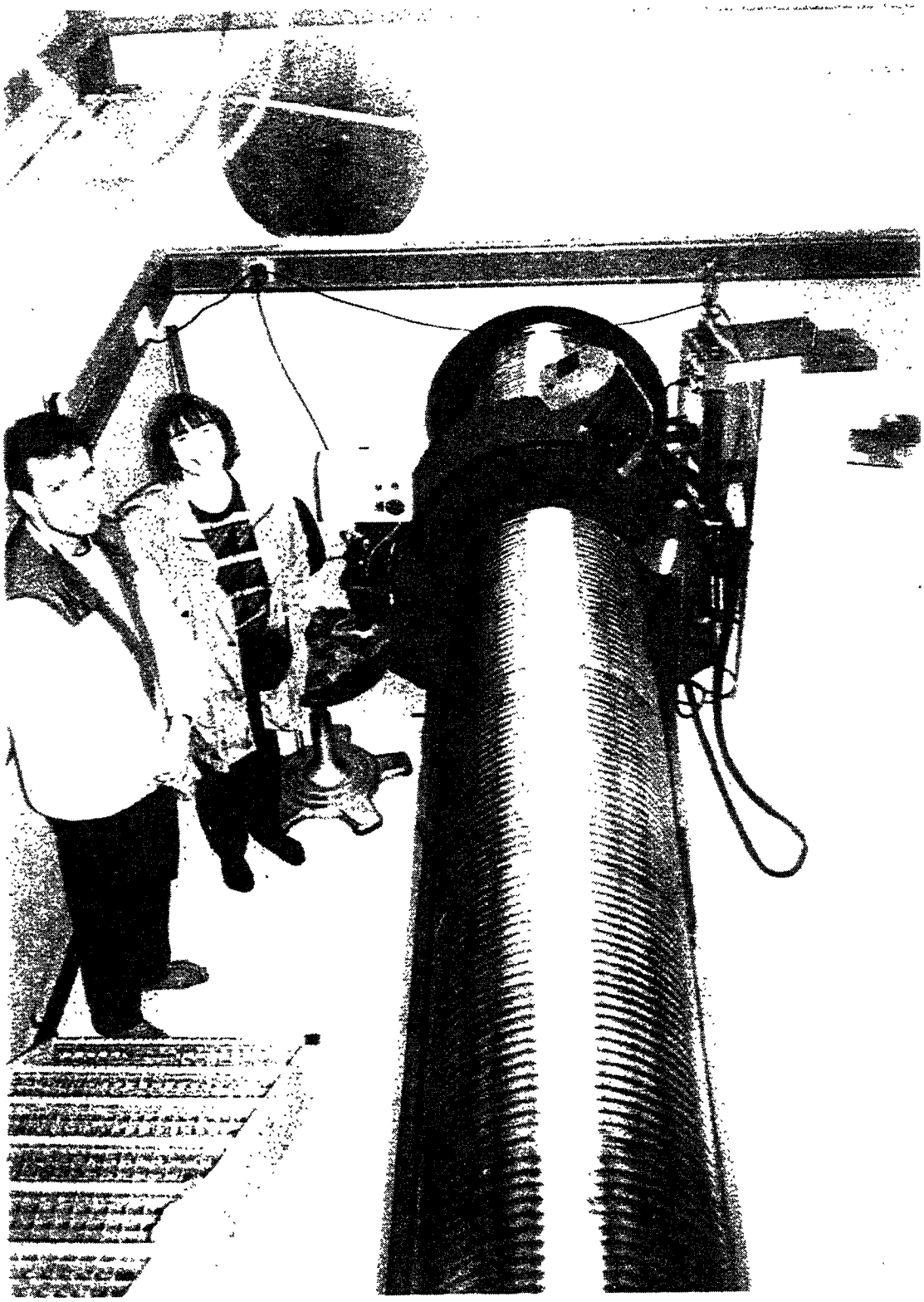

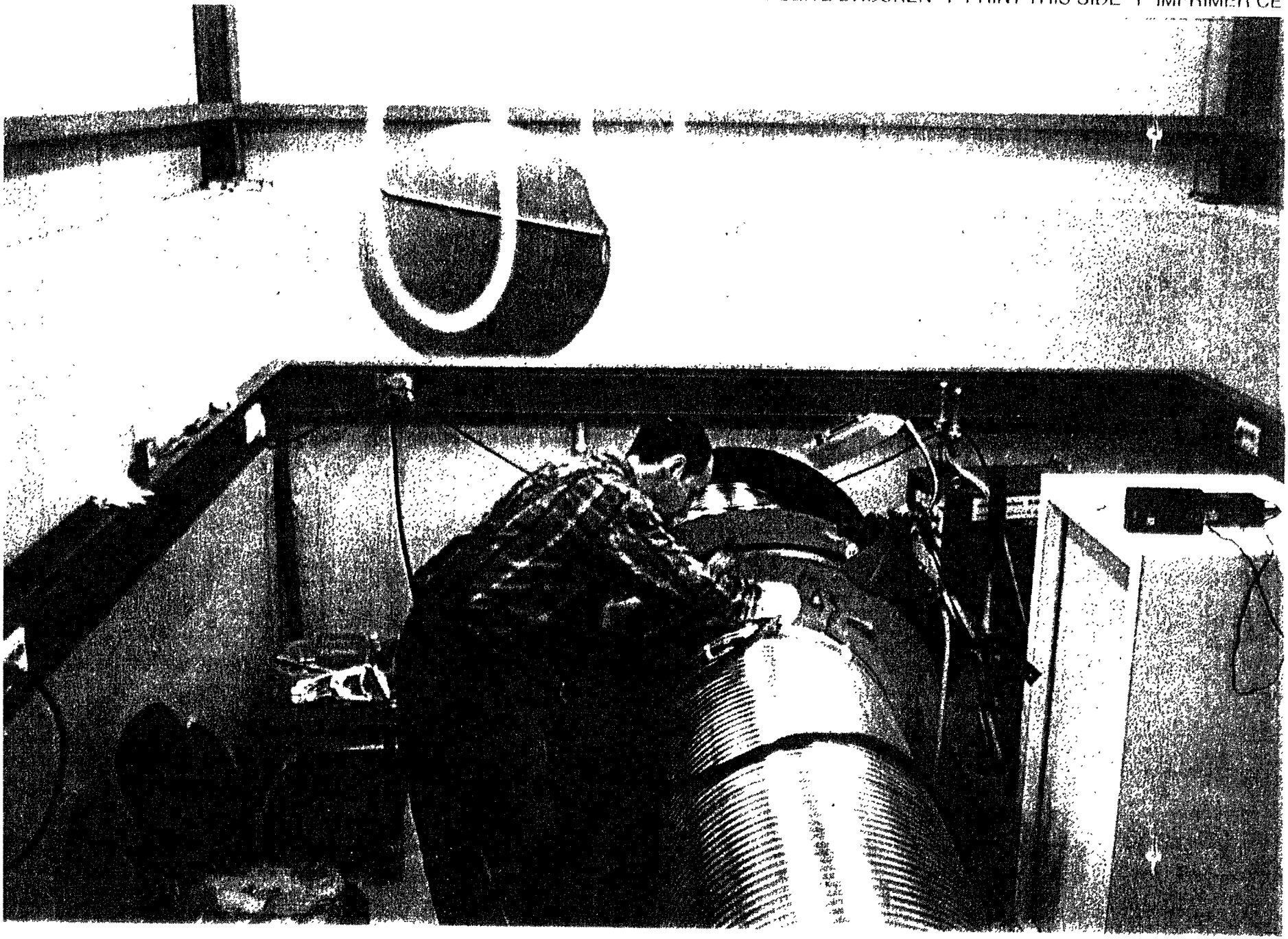

Timetable

- 1966
  - vacuum system
- 1997
  - mode-cleaners, laser bench
- 1998
  - investigations with a 1200m long cavity formed from single arm
- 1999
  - 600m Michelson interferometer
- 2000
  - final optics

DATA TAKING

Construction Update

LIGO

Barry Barish

GWDAW Workshop

MIT

Dec 5-7, 1996

LIGO-G960105-00-M

h_{rms} Noise Envelopes for Initial LIGO and Advanced Subsystems/Detectors

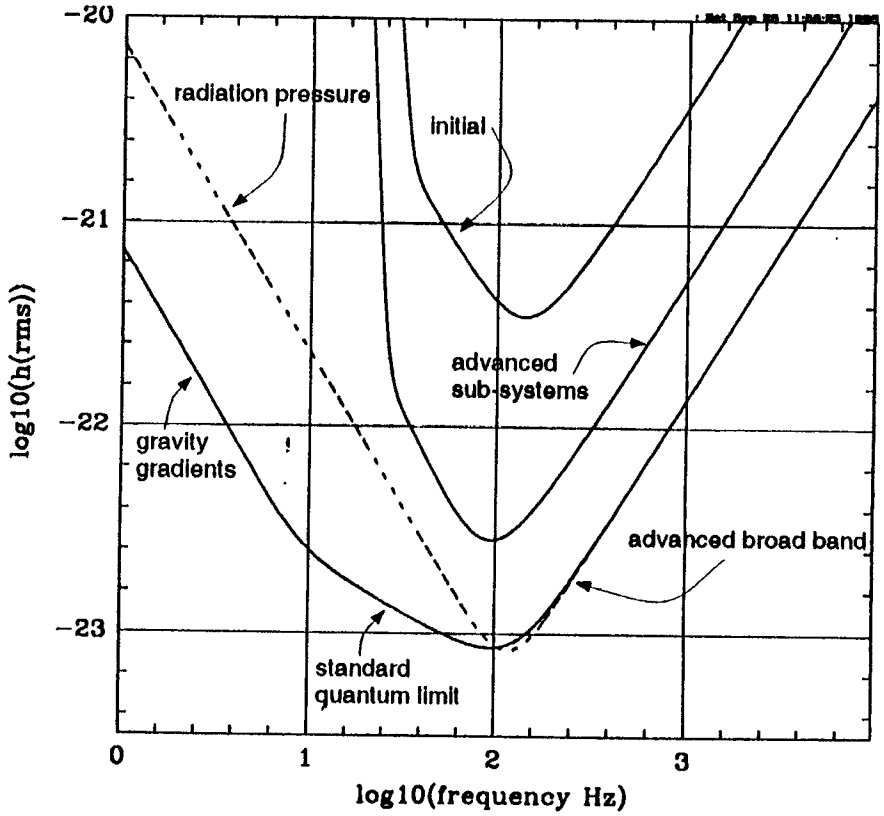

LIGO Plans

- Main Activity

1996	Construction Underway
	-mostly civil
1997	Facility Construction
	-vacuum system
1998	Interferometer Construction
	-complete facilities
1999	Construction Complete
	-interferometers in vacuum
2000	Commission Detectors
	-first light; testing
2001	Engineering Tests
	-sensitivity; engineering run
2002	Initial LIGO Detector Run
	- $h \sim 10^{-21}$

Civil Construction

- WA site
  - completed finish grade and slip form of slab
  - completed service road and distributed electric power along arms
  - Completed precast approx 1500 BT enclosure segments
  - demo'd installation technique
  - completed final design and initiated construction of WA bldgs
  - awarded BT enclosure installation contract

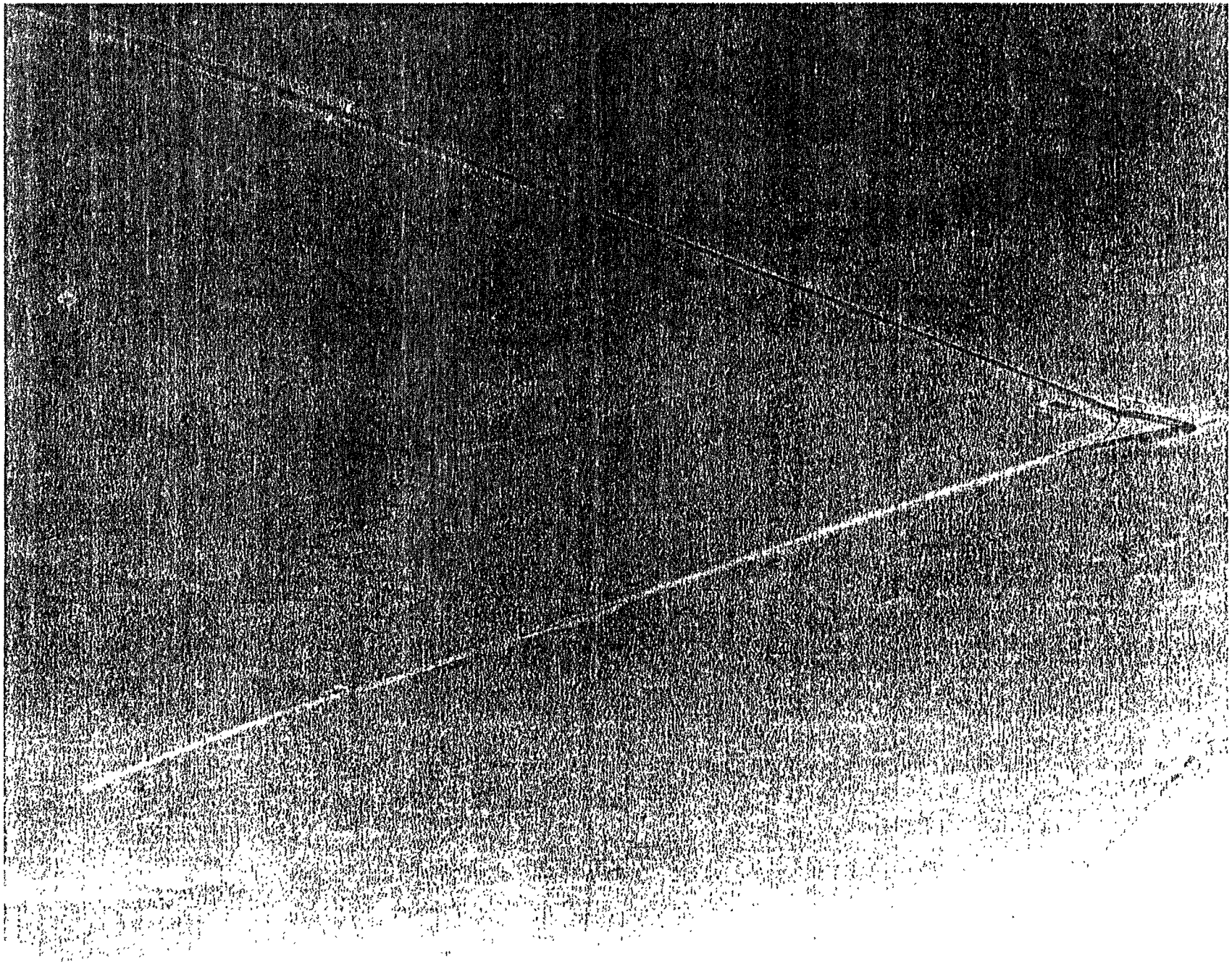

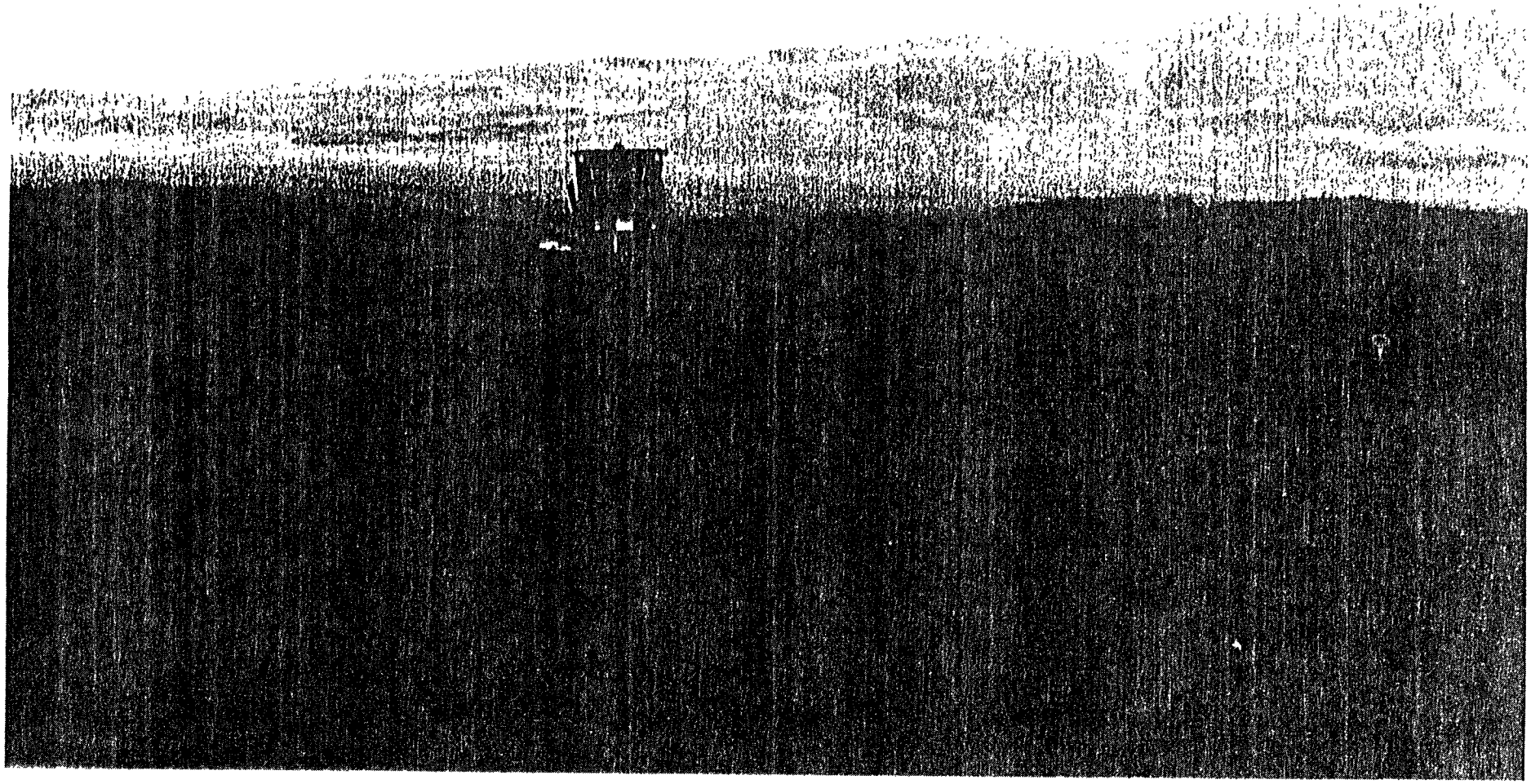

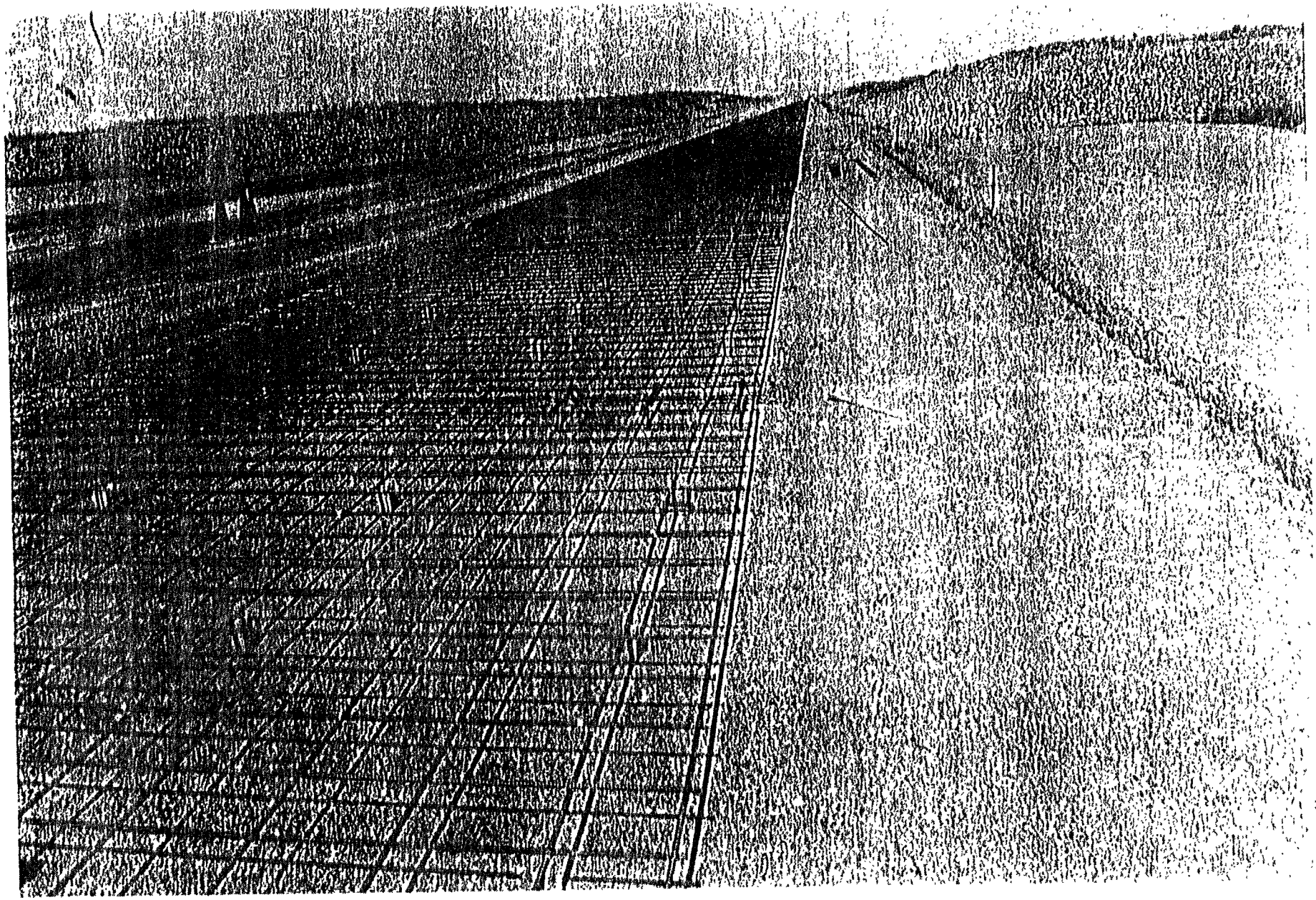

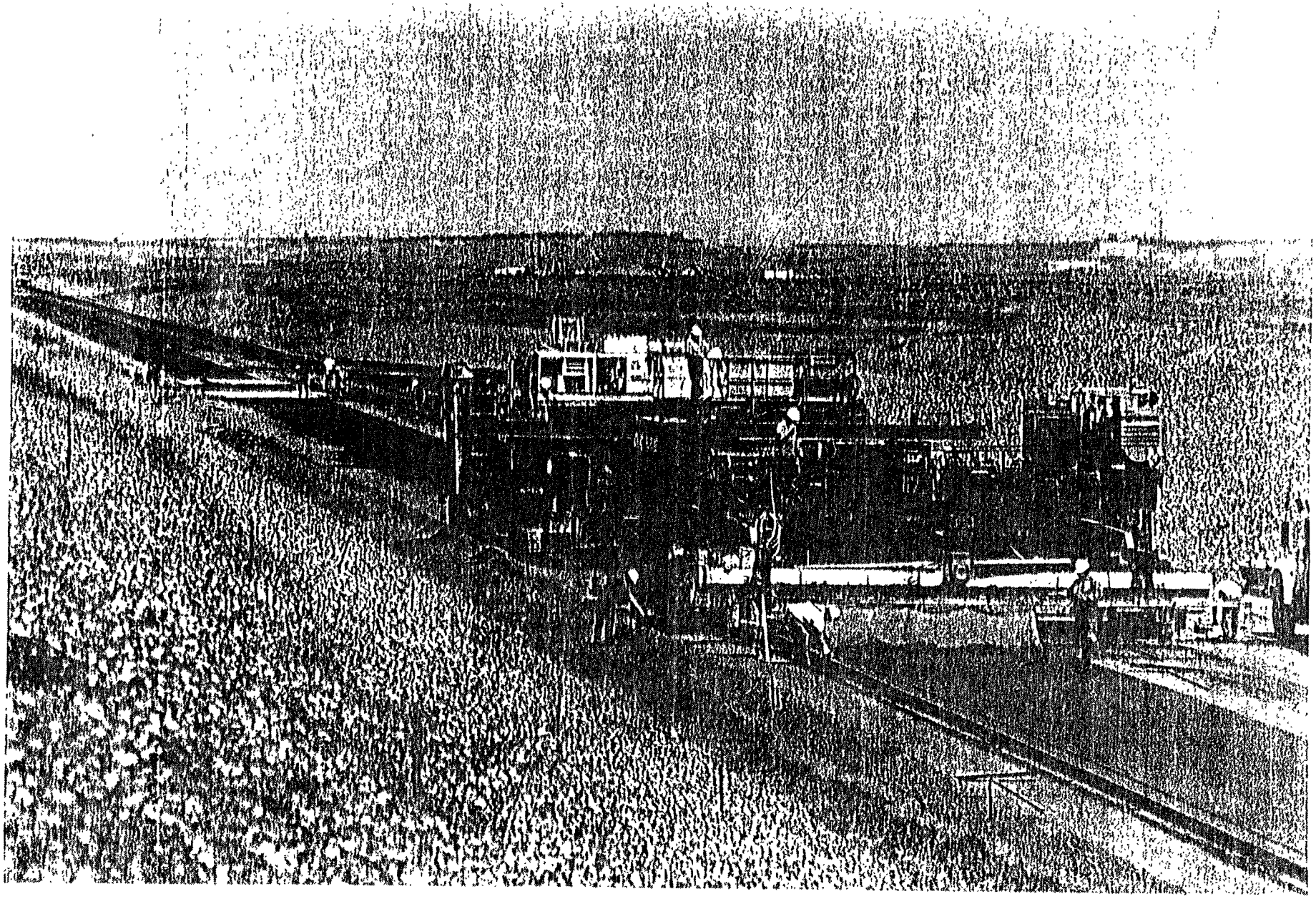

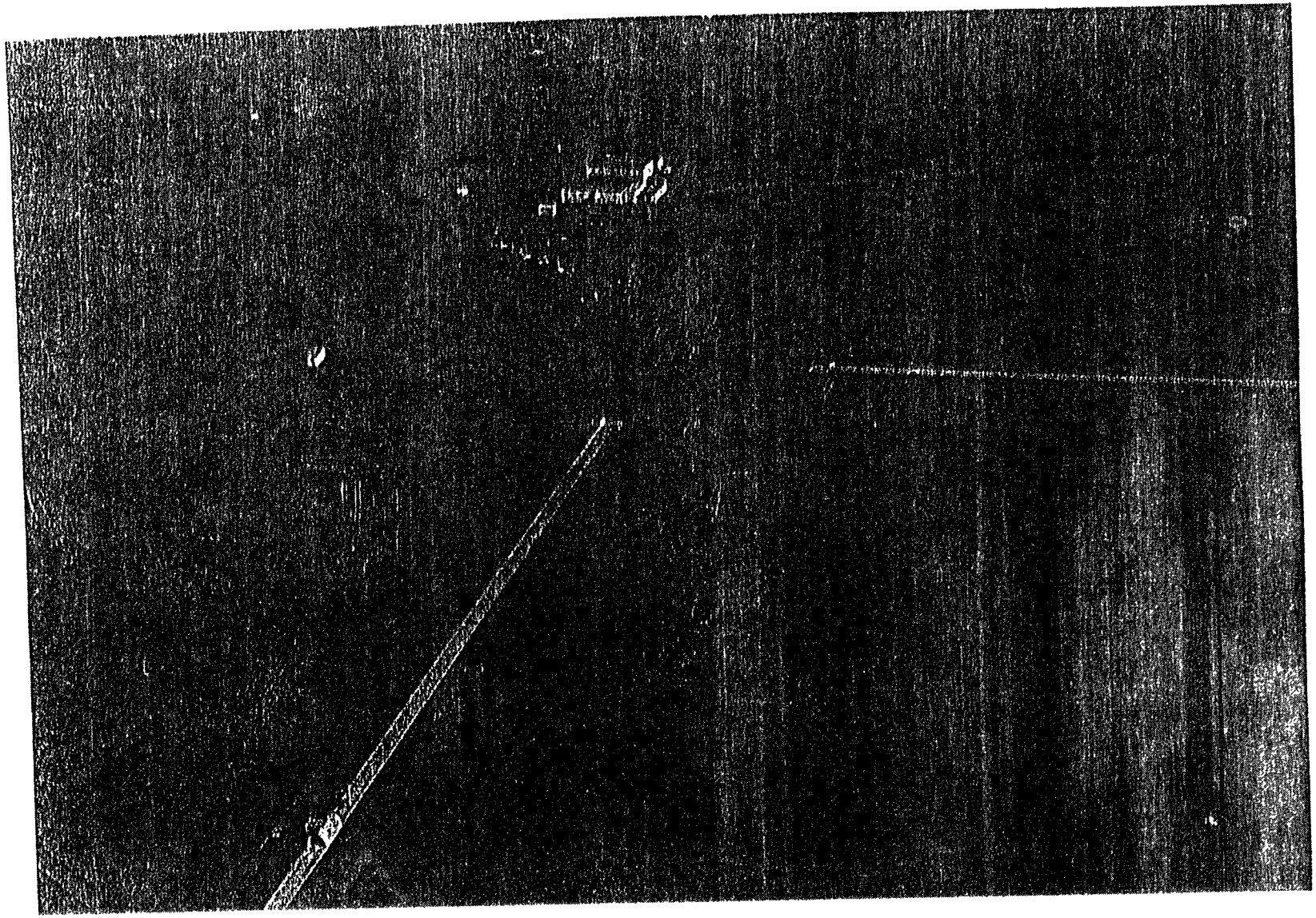

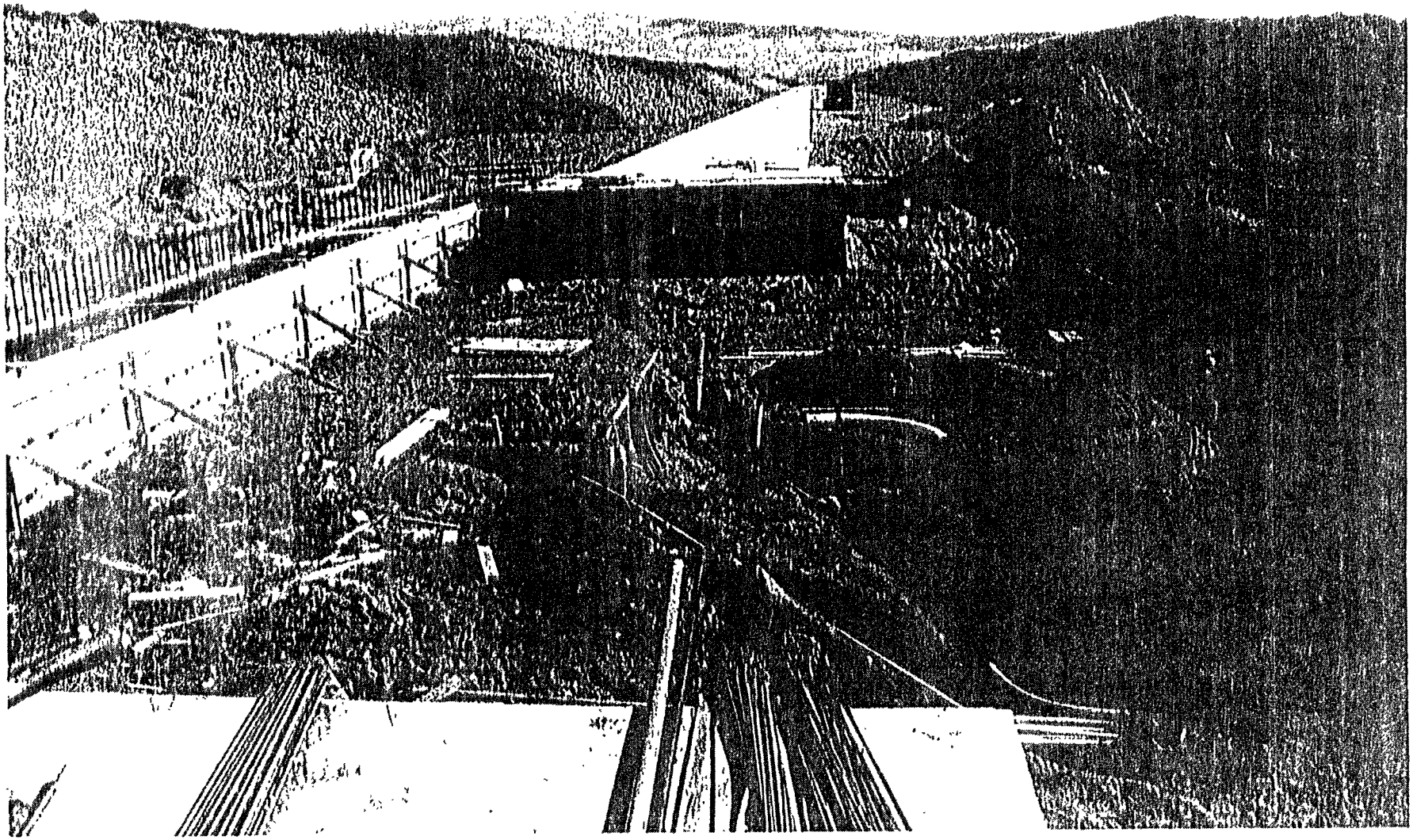

LA Civil Construction Status

Otto Matherny, Fred Asiri

- Bids opened for slabs, enclosures, roads, buildings
  - apparent low bidders within budget.
- Rough grading:
  - It rains a lot in LA
  - approximately 150 days lost to weather delay
  - arms at full height since July
    - » should allow sufficient time for settlement for Feb 97 slab installation
    - » monitoring of settlement plates to look at creep rate.

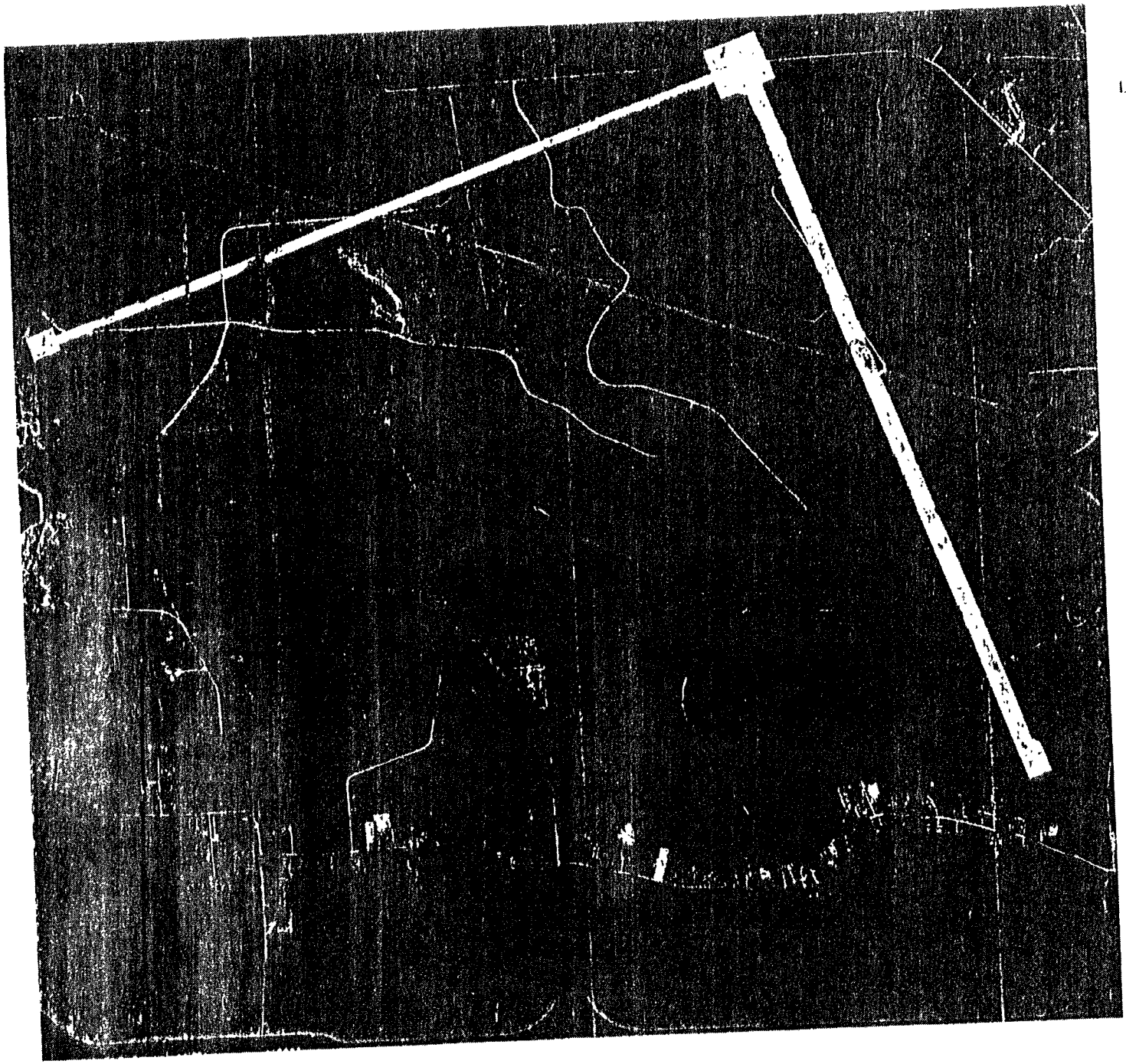

LIGO

LIVINGSTON PARISH

LOUISIANA

AERIAL PHOTO BY:

GULF COAST AERIAL MAPPING

FLOWN: AUGUST 25, 1996

ALTITUDE: 12,000 FEET

Beam Tube

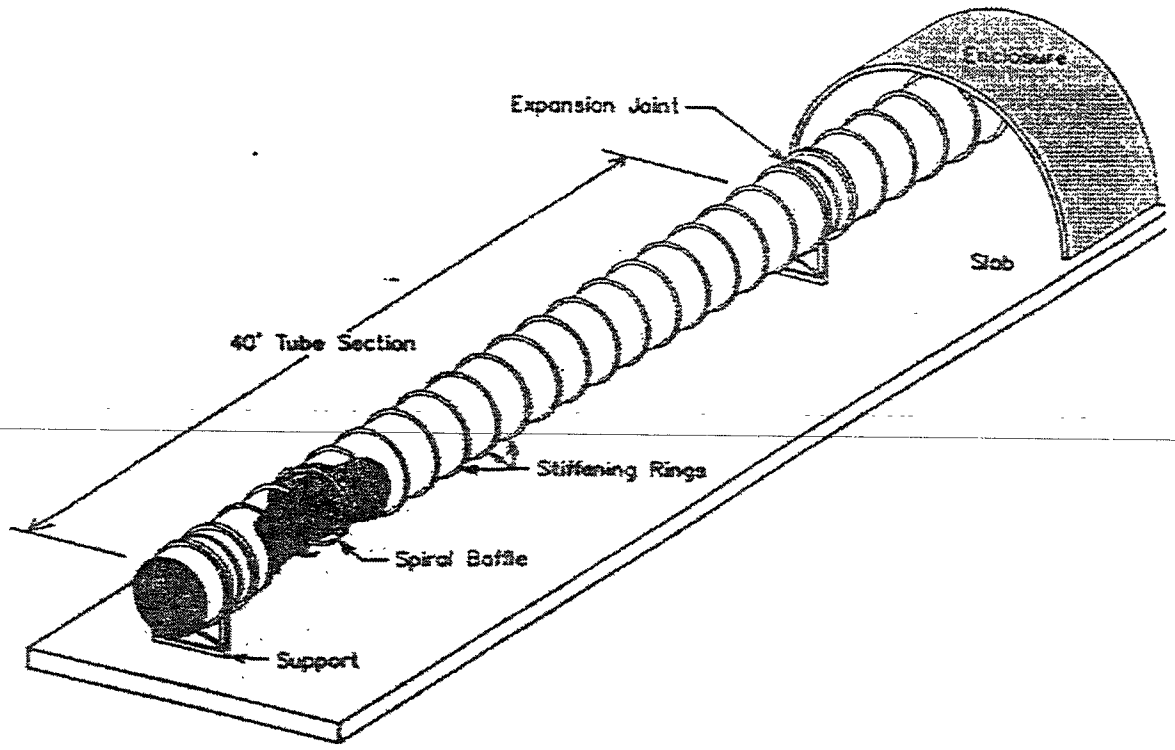
Enclosure
Expansion Joint
Slab
40' Tube Section
Stiffening Rings
Spiral Baffle
Support

BIG PASCO

WAREHOUSE #5, BAYS #1 & #2

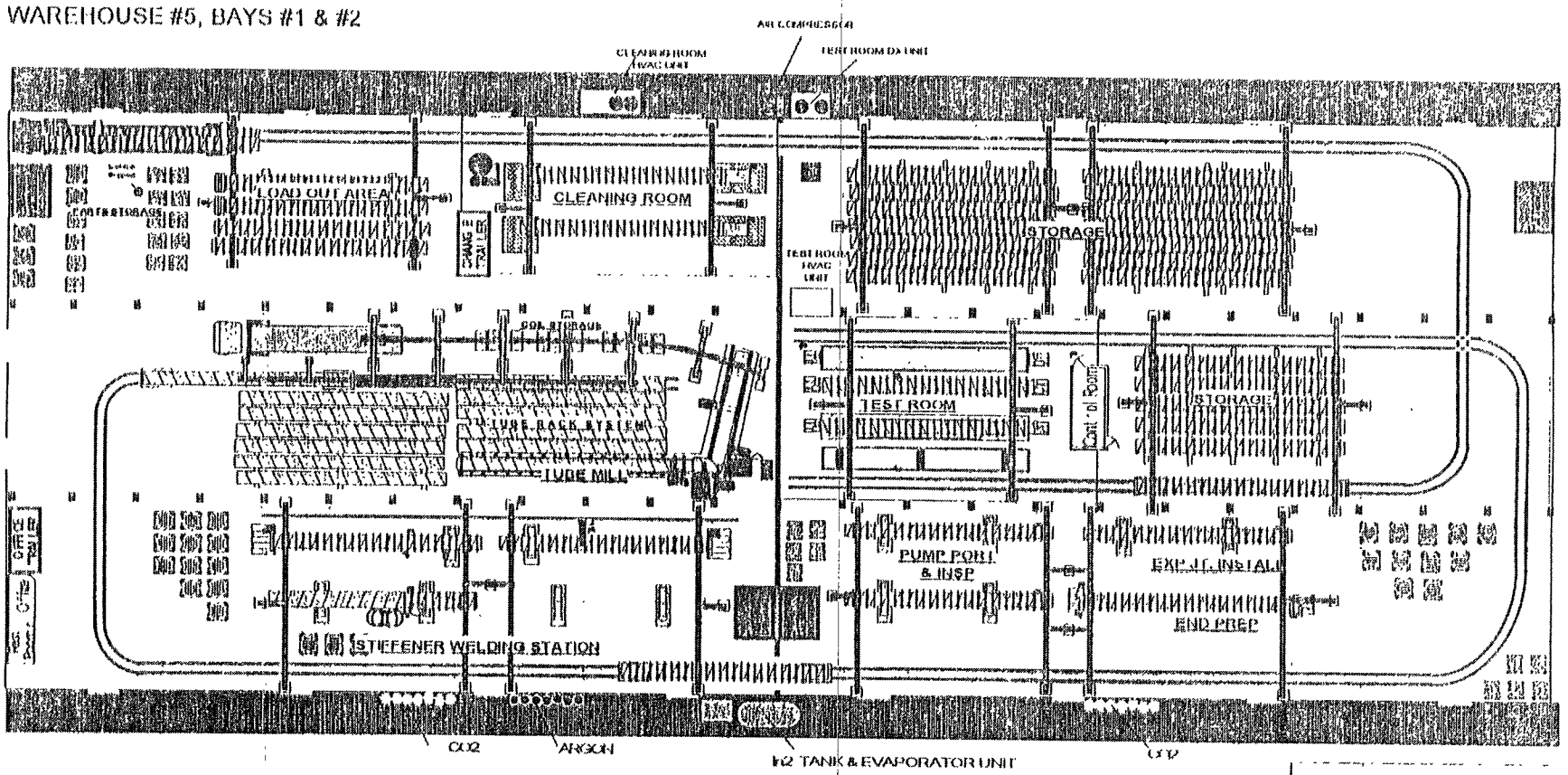

LIGO

HANFORD LOCATION

FABRICATION FACILITY

BIG PASCO WHSE #5, BAYS 1 & 2

PC181520

BIGPASO1.CVS

NEW

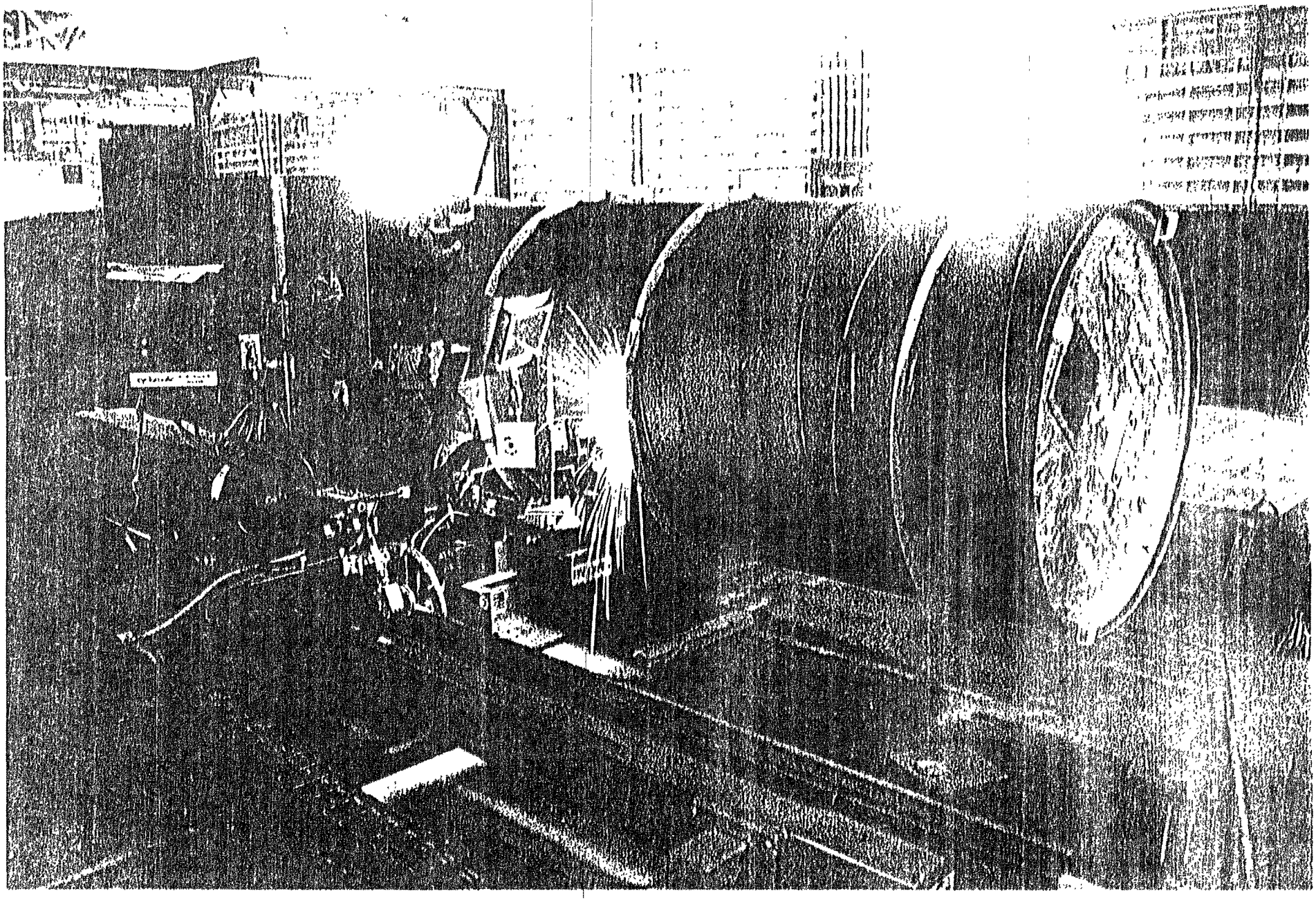

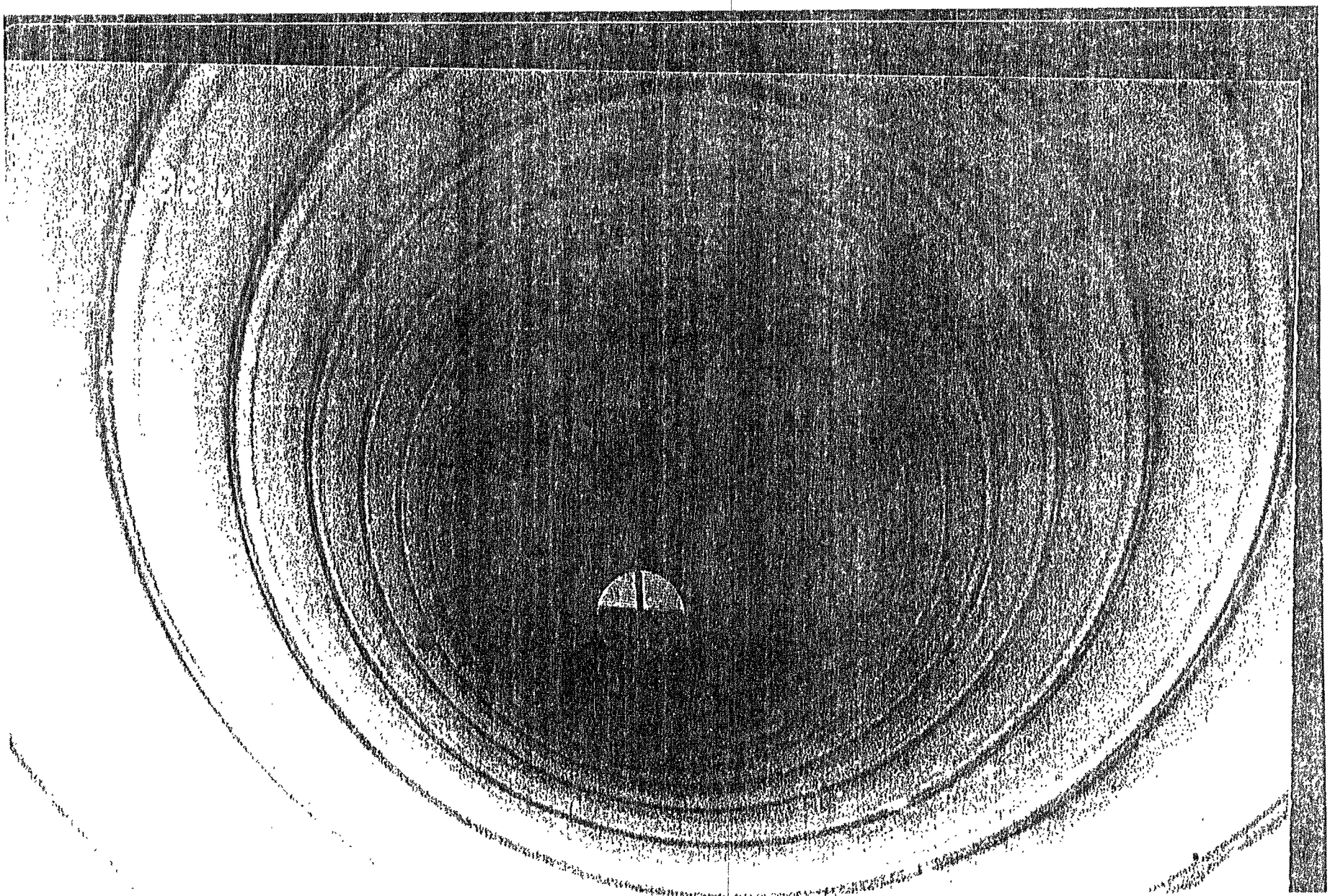

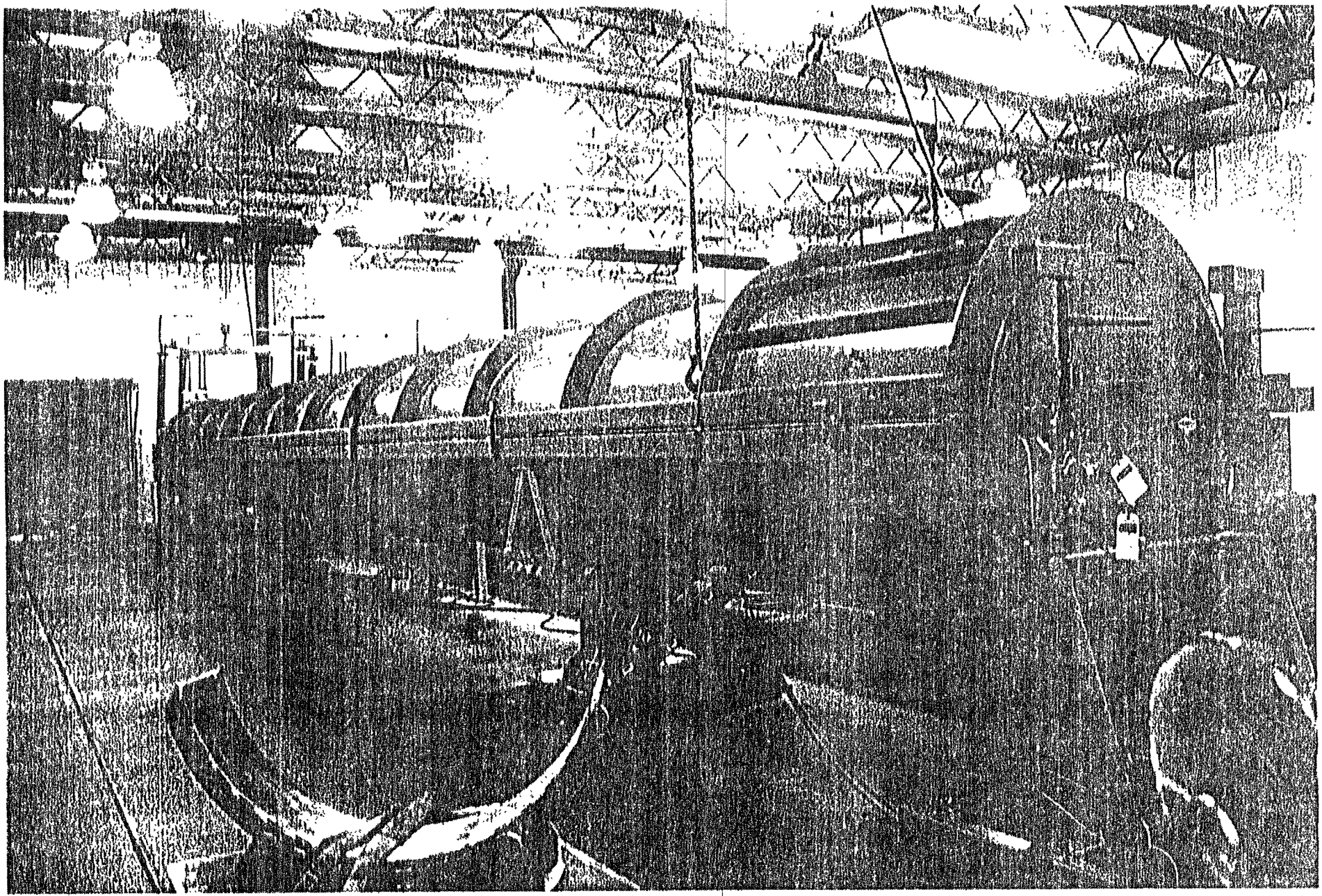

LIGO Facilities

Beam Tube Enclosure

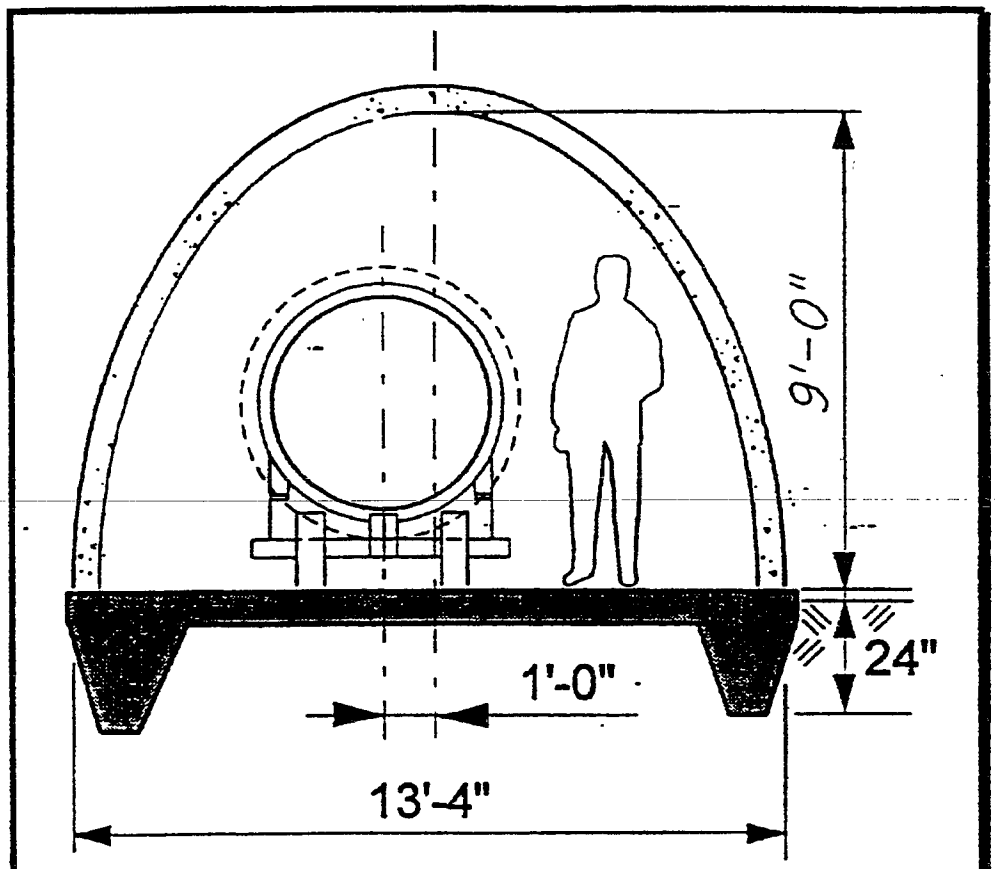

Figure 2.1-1 — Cross Section of Design Baseline at Hanford

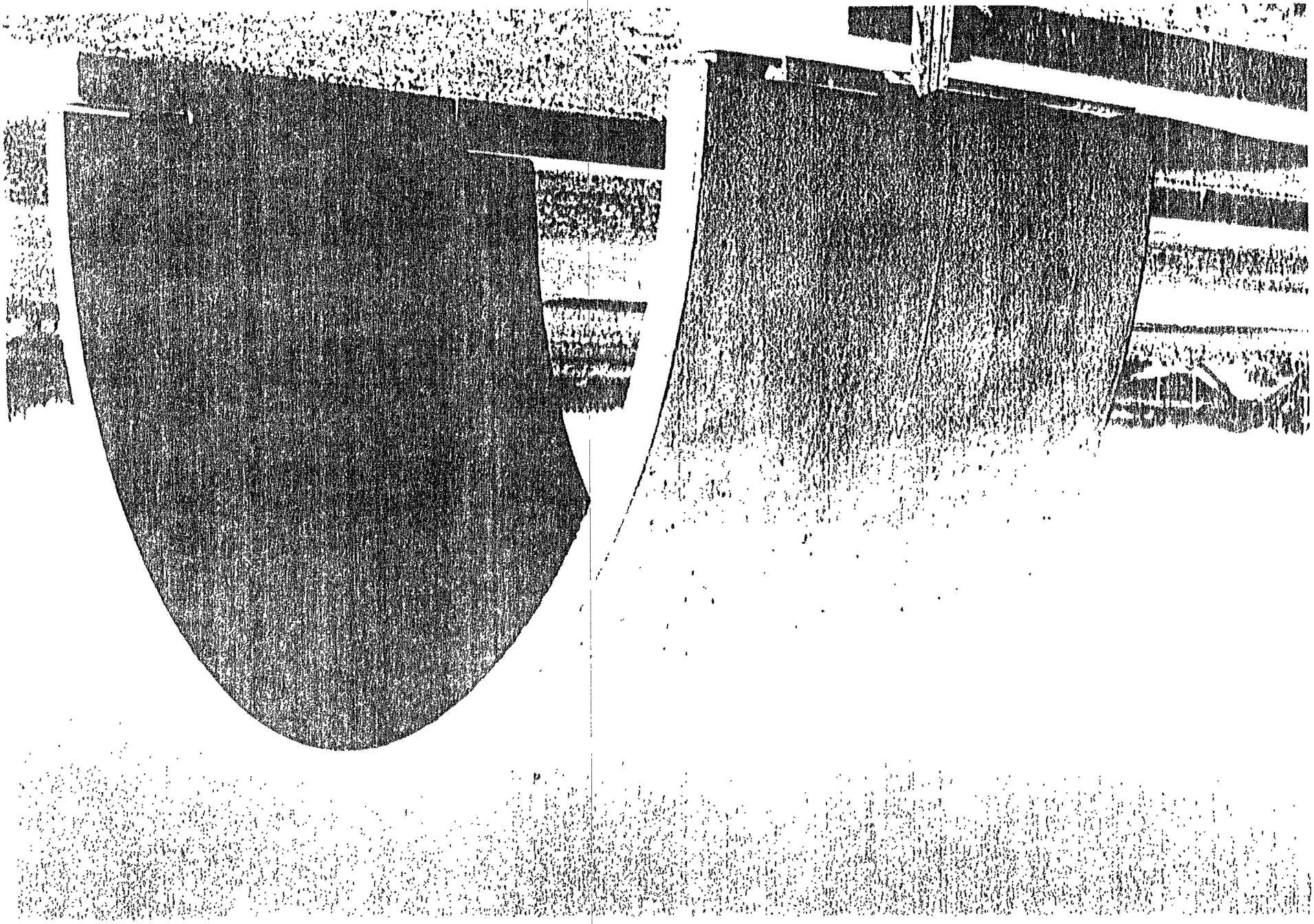

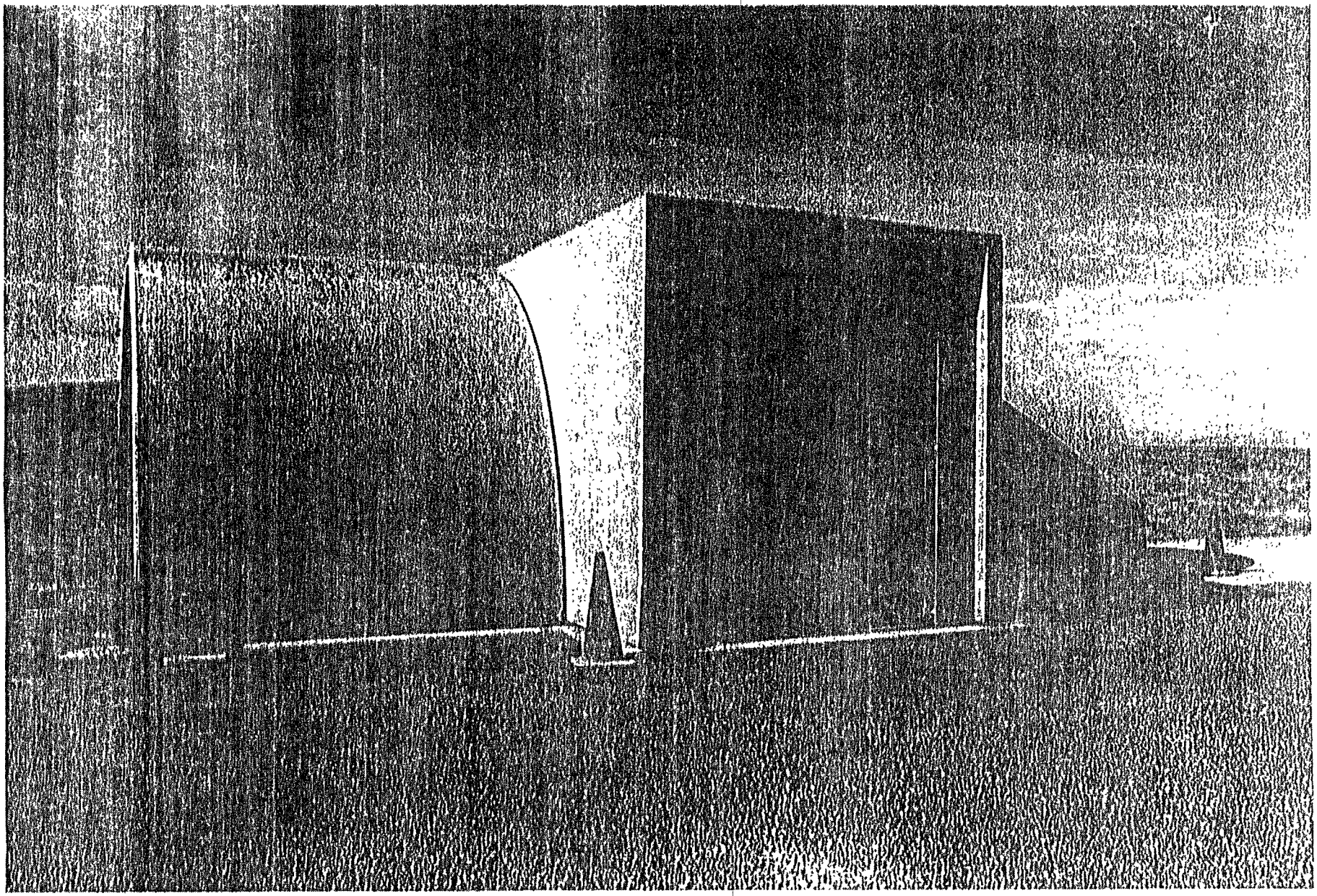

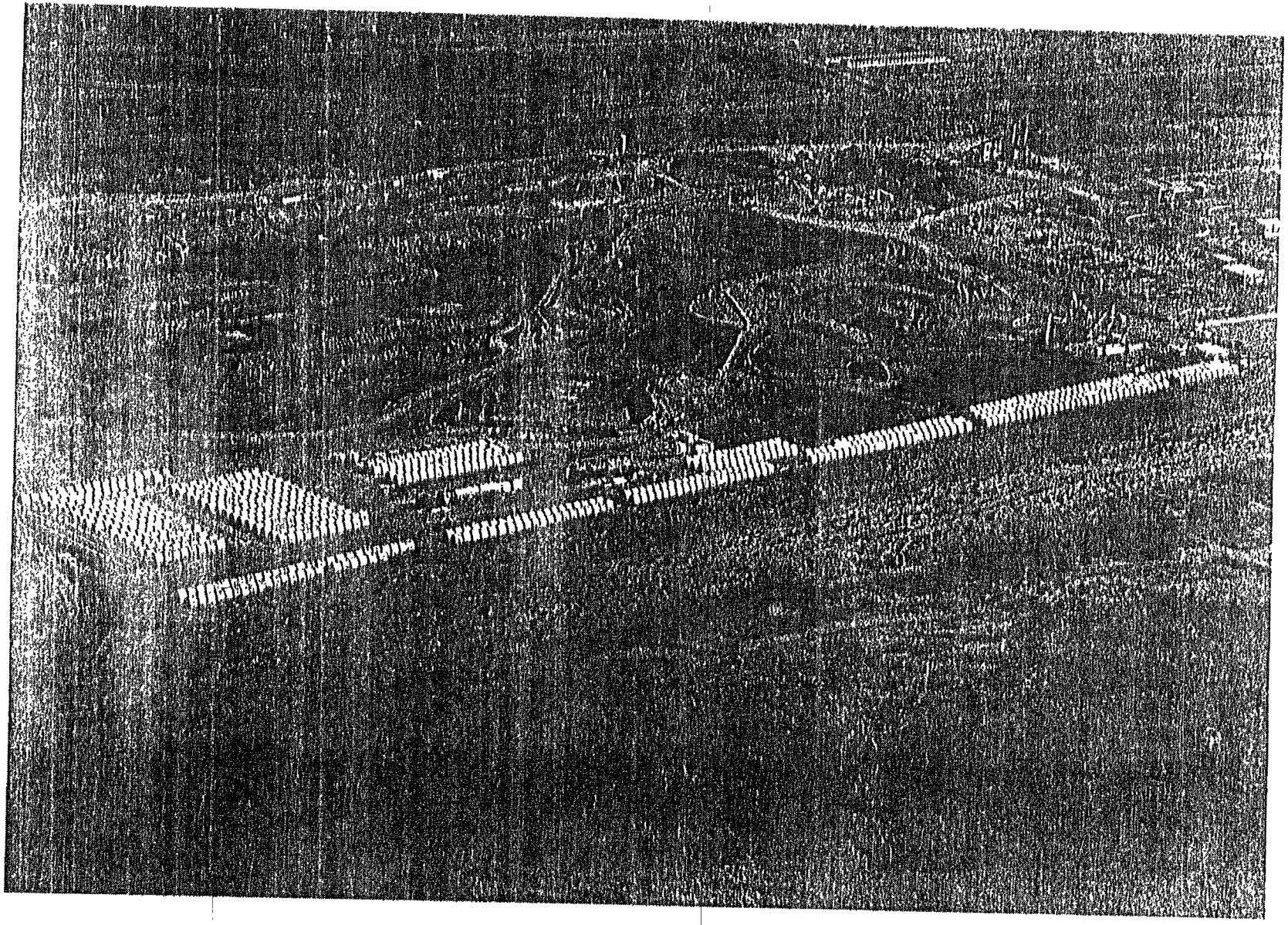

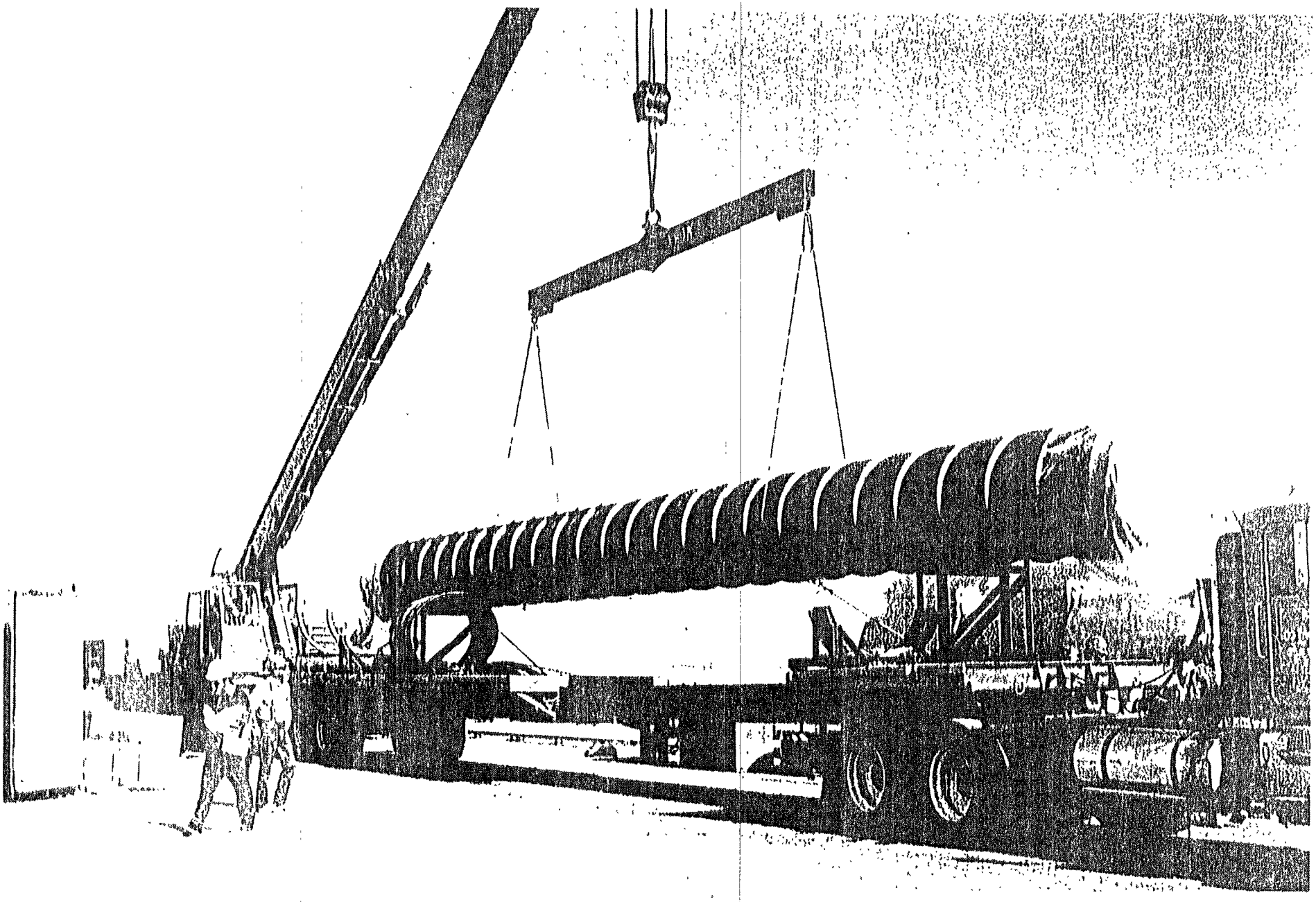

INSTALLATION WORK AREA - INSTALLING TUBES

ATTACHEMENT "D"

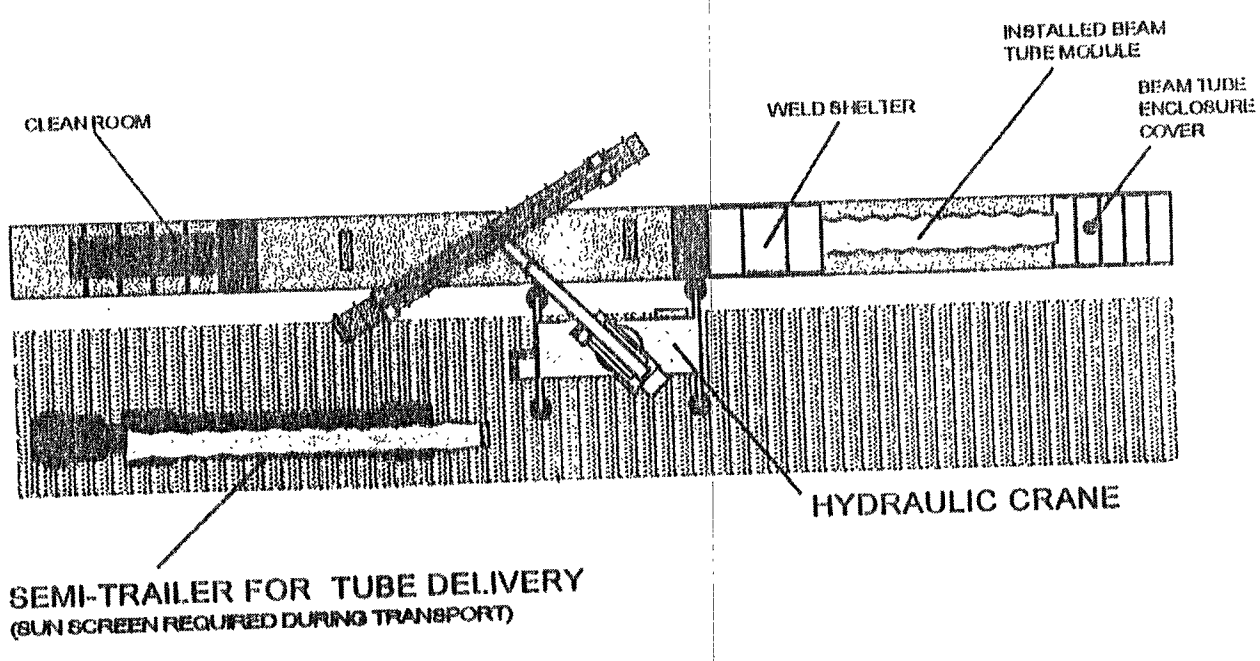

PLAN VIEW AT TYPICAL TUBE LOCATION

INSTALLATION PLAN

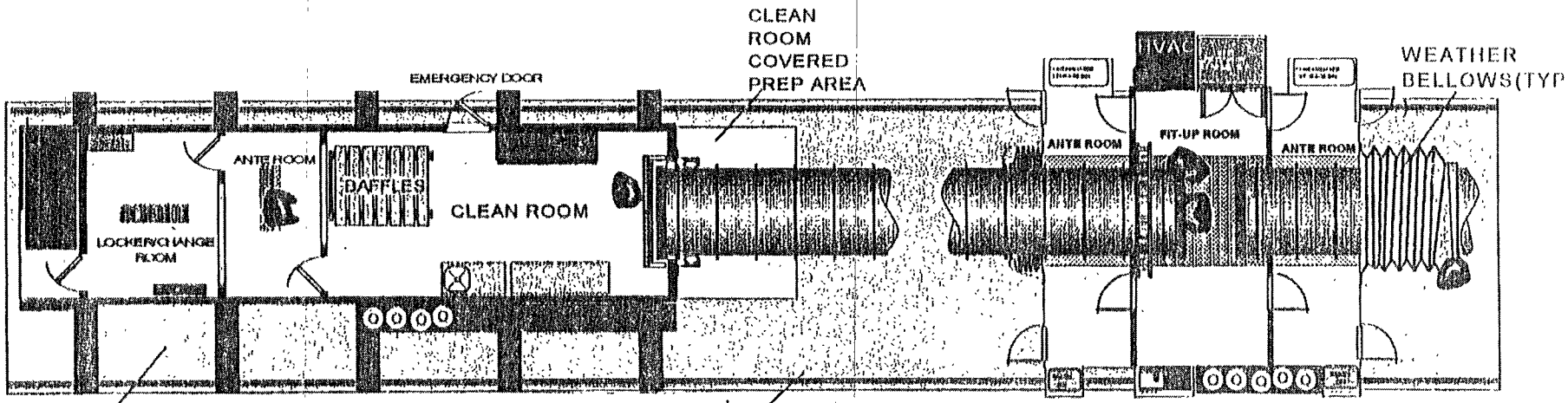

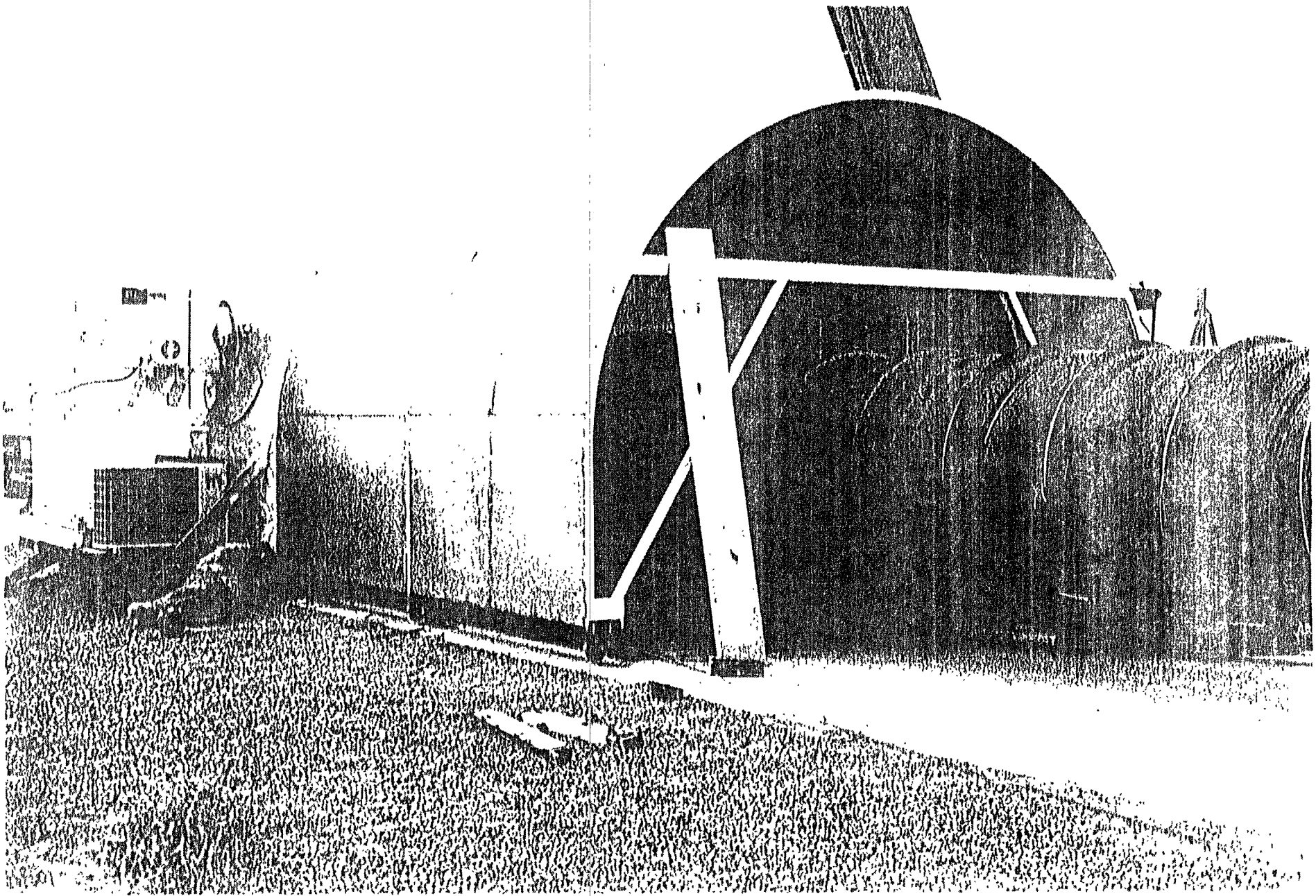

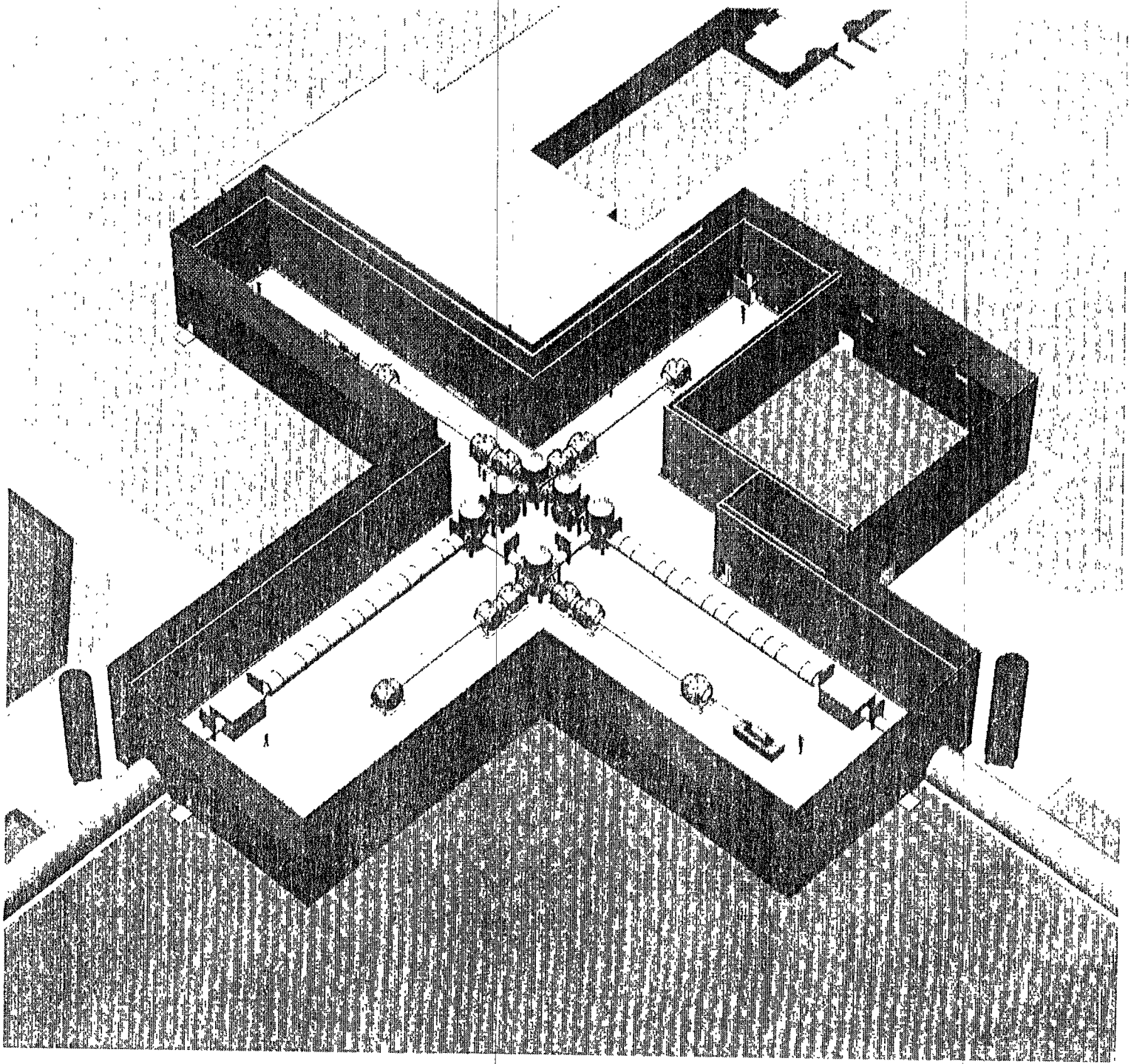

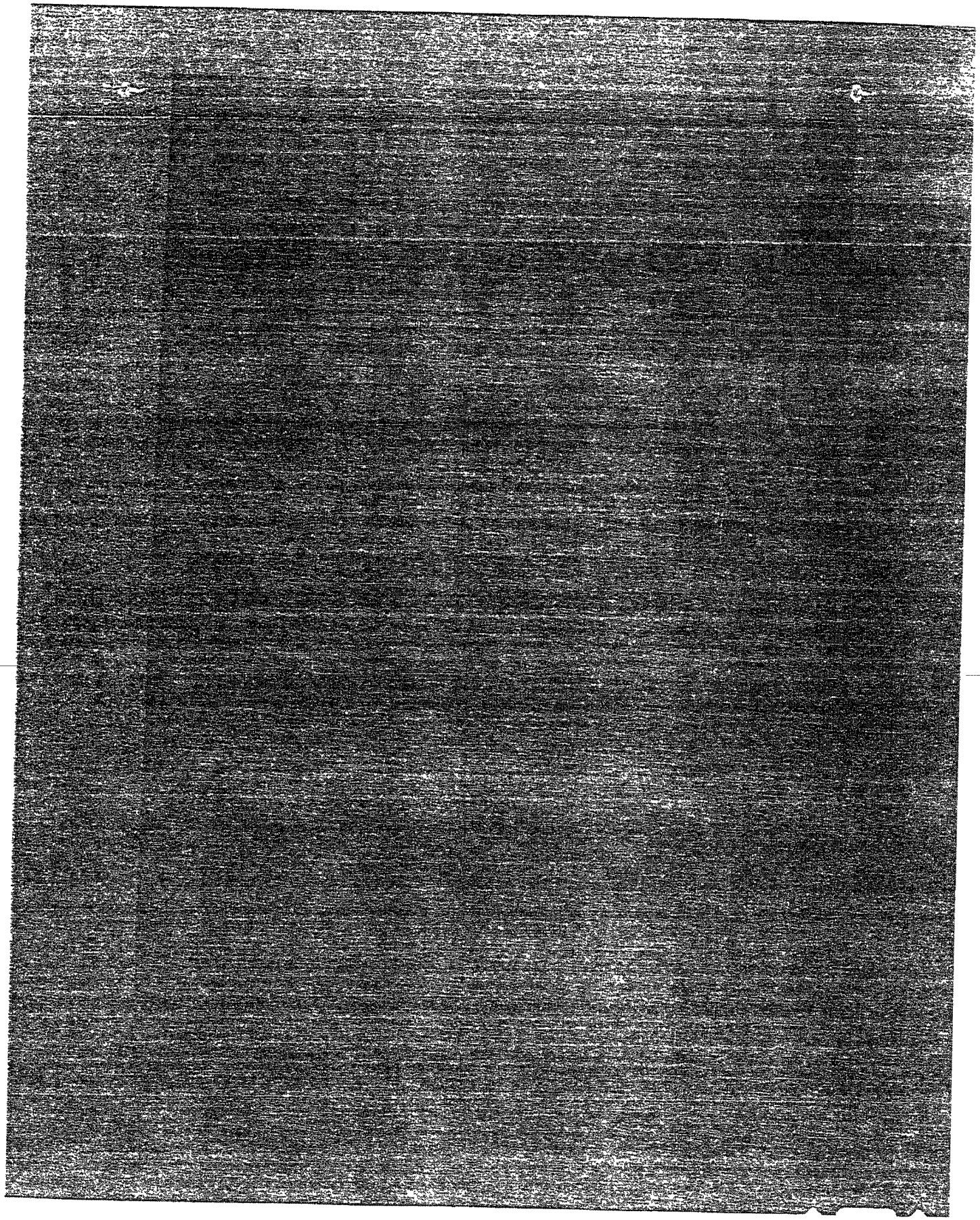

Advanced Subsystems R&D

- Double Pendulum Suspension
- Reduced Thermal Noise
- Reduced Internal Test Mass Thermal Noise: Sapphire
- Higher Laser Power and Core Optics for Higher Power
- Increased Mass (Sapphire)

What We Propose

- A program of research to define advanced subsystems intended to be enhancements to the initial LIGO interferometers
- A program of research to define new advanced detectors
- A five year program in each thrust
  - ›› Some areas of research will enable implementation proposals
  - ›› Some research areas will not be completed and will become part of a following R&D proposal
- A program based upon the benchmark gravitational wave sources, but intended to be flexible if the course of physics research dictates a different evolution of LIGO capabilities

LIGO Funding by NSF Task and by Year

Fiscal Year	*Construction*	*R&D*	*Operations*	*Proposed Upgrade R&D*	*Total*
Thru 1994	**35.9**	**11.2**			**47.1**
1995	**85.0**	**4.0**			**89.0**
1996	**70.0**	**2.4**			**72.4**
1997	**55.0**	**1.6**	**0.3**		**58.6**
1998	**27.1**		**7.3**	**2.7**	**37.1**
1999			**20.9**	**2.7**	**23.6**
2000			**21.1**	**2.7**	**23.8**
2001		**10 months >**	**19.1**	**2.6**	**21.7**
All funds shown in 'then'-year $M					

LIGO

Future Expansion

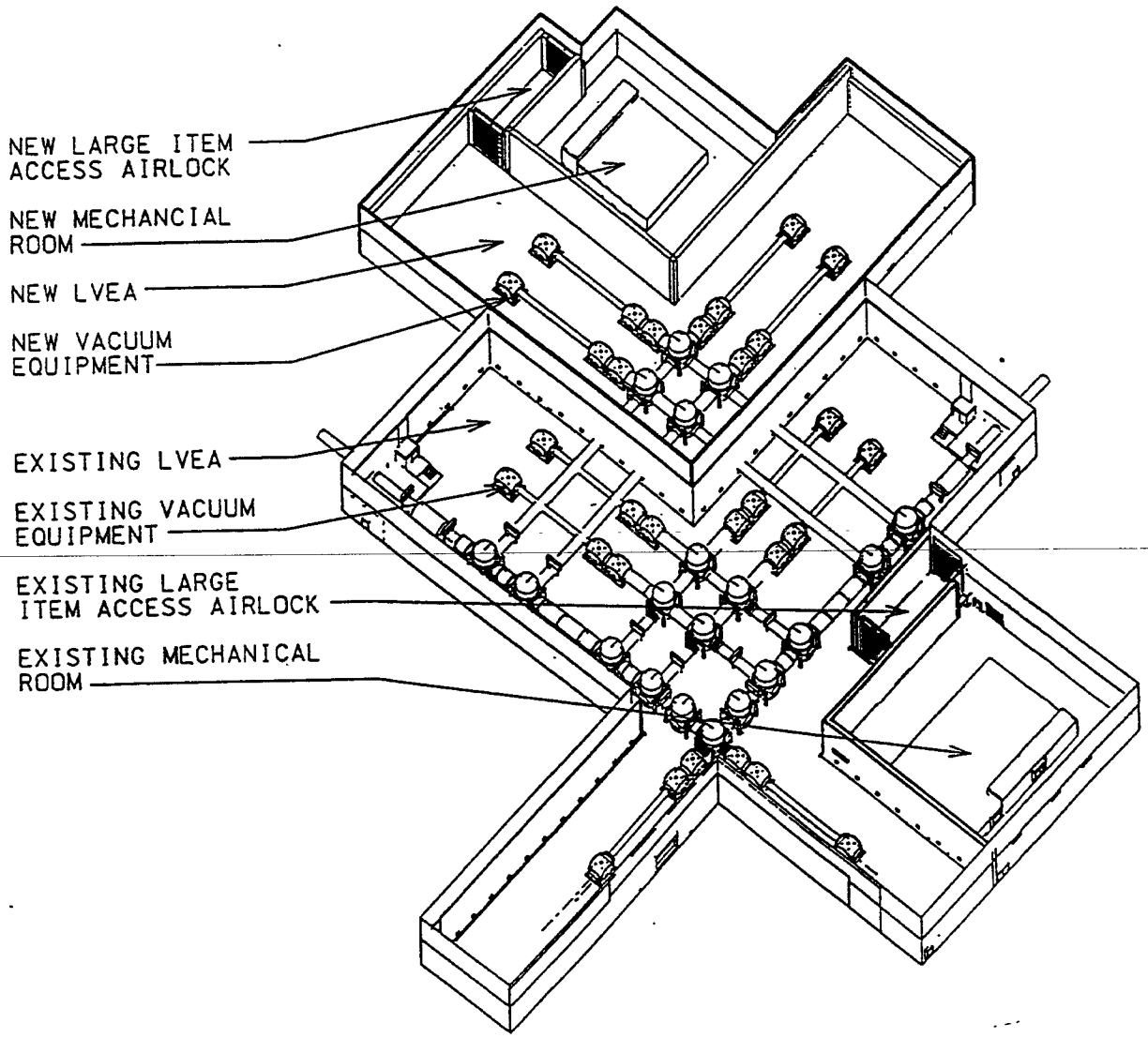

LIGO

LIGO-G960108-00-M

LIGO Site-to-site Communications

- Hanford-Livingston link permits real-time cross-correlations among instruments
- Caltech-MIT link provides high speed link to data archives; data tapes to be archived at university.
- Site-University links provides site scientific staff access to archived data
- University gateways provide broader access to database
- Data tapes transported to University repository

Data Analysis for Initial LIGO

On-line Processing Computing Resources & Distribution

- Redundant systems at LA & WA Observatories
- Support for 1x, 2x, 3x operations independently
  - Diagnostics -- especially during commissioning
  - 2x/3x operations between sites feasible with reduced datastreams
    - Transient/burst signals ($\Delta T < 1s$) -- GW + superveto/QA
    - Inspiral & coalescence waveforms ($10s < \Delta T < 1000s$) -- events
- System configuration (target: $\mathbf{M_{NS}>0.3\ M_{SUN}}$)
  - Volatile data storage for 3 hours of data + 3 hours of analysis (FIFO) for 2 IFOs (WA) @ 100% data stream: 125GB+125GB
  - Template storage for:300 GB
  - ~ 2-50 GFLOP CPU system -- intrinsically parallel computational requirements:
    - Parallel processor(s) -- *monolithic/efficient/more expensive*
    - Workstation cluster -- *versatile/less efficient/less expensive*
    - Specialized (DSP) system -- *less versatile/efficient/least expensive/upgrade difficult*

Data Analysis for Initial LIGO
On-line Processing Computing Resources & Distribution

- System configuration (cont.)
  - ›› Site-to-site communication link to provide 2x and 3x real-time cross-correlation
    - Selected (pre-processed) data subsets (GW + super-veto; event lists)
    - Two way: WA->LA & LA->WA
      - Can support independent algorithms
    - T1: 0.2 MB/s is barely sufficient for GW WA->LA
    - T3 (6 MB/s) or ATM (20 MB/s) will be available by time needed

Data Analysis for Initial LIGO

On-line Processing Computing Resources & Distribution

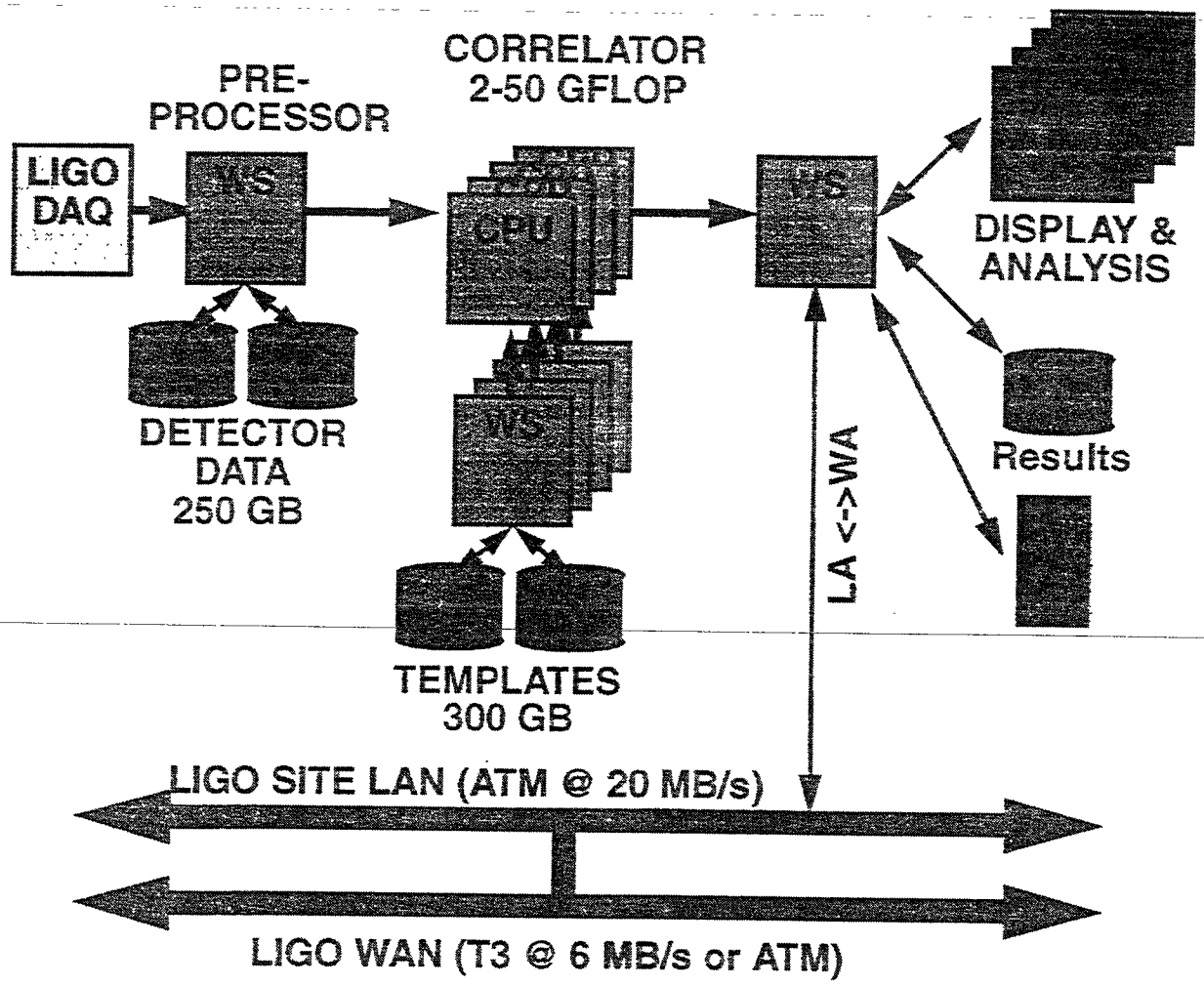

Data Analysis for Initial LIGO

Off-line Processing Computing Resources & Distribution

- Single system at a LIGO Laboratory University*
- Supports analyses either not feasible or not required on-line.
  - Stochastic background
  - Pulsar searches (directed/partial sky)
  - Inspiral with combined IFOs (vector data for max. SNR)
  - Research on algorithm development & signal processing
  - Refined analyses
  - Novel searches
- Provides/manipulates data archive.
- Data access via WAN to other LIGO sites and users.
- Utilizes and is designed around existing University resources for maintenance, availability, communications & support.

Data Analysis for Initial LIGO
Off-line Processing Computing Resources & Distribution

- System configuration (target: max. capability for multiple users)
  - Large data archive
    (~ 500 TB/yr => 10k tapes/yr @ 50 GB/tape => $0.5M/yr @ $50/tape)
  - Robotic tape access -- size TBD
  - Disc cache system capable of storing 450GB of data
    - 8 hours of 100% data ~ 450 GB
    - ~ 5 weeks of GW data (suitably filtered to not require ancillary channels)
  - Processors for computationally intense analyses (100+ GFLOPS)
    - Support multiple, independent analyses (4 - 6)
    - Parallel processor(s) -- *monolithic/efficient/more expensive*
    - Workstation cluster -- *versatile/less efficient/less expensive*
    - Distinctions will fade with time
  - High bandwidth communication to other LIGO sites & collaborating institutions
    - T3 (6 MB/s) or ATM (20 MB/s)

Data Analysis for Initial LIGO

Off-line Processing Computing Resources & Distribution

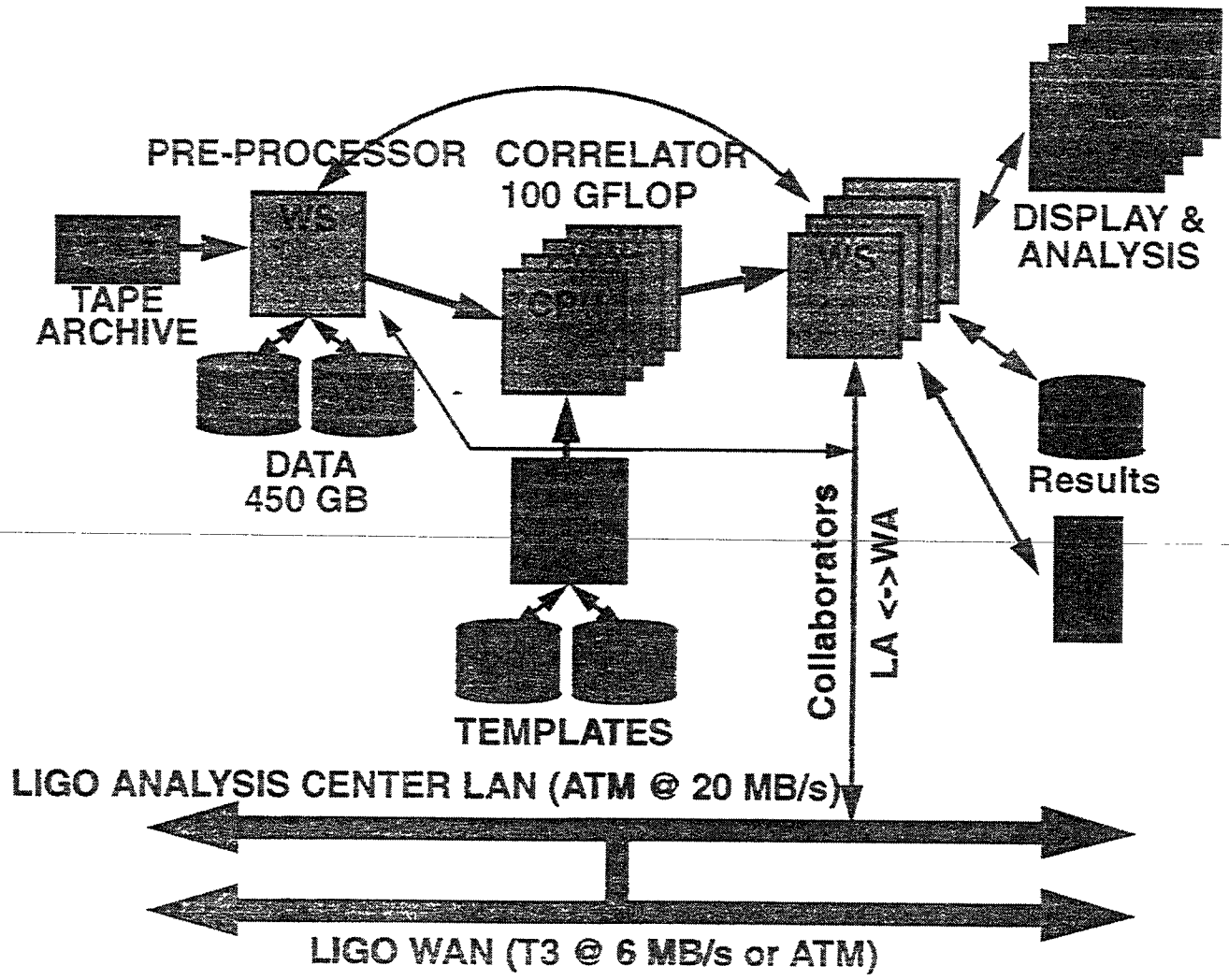

LIGO Data Stream and Data Frame Design

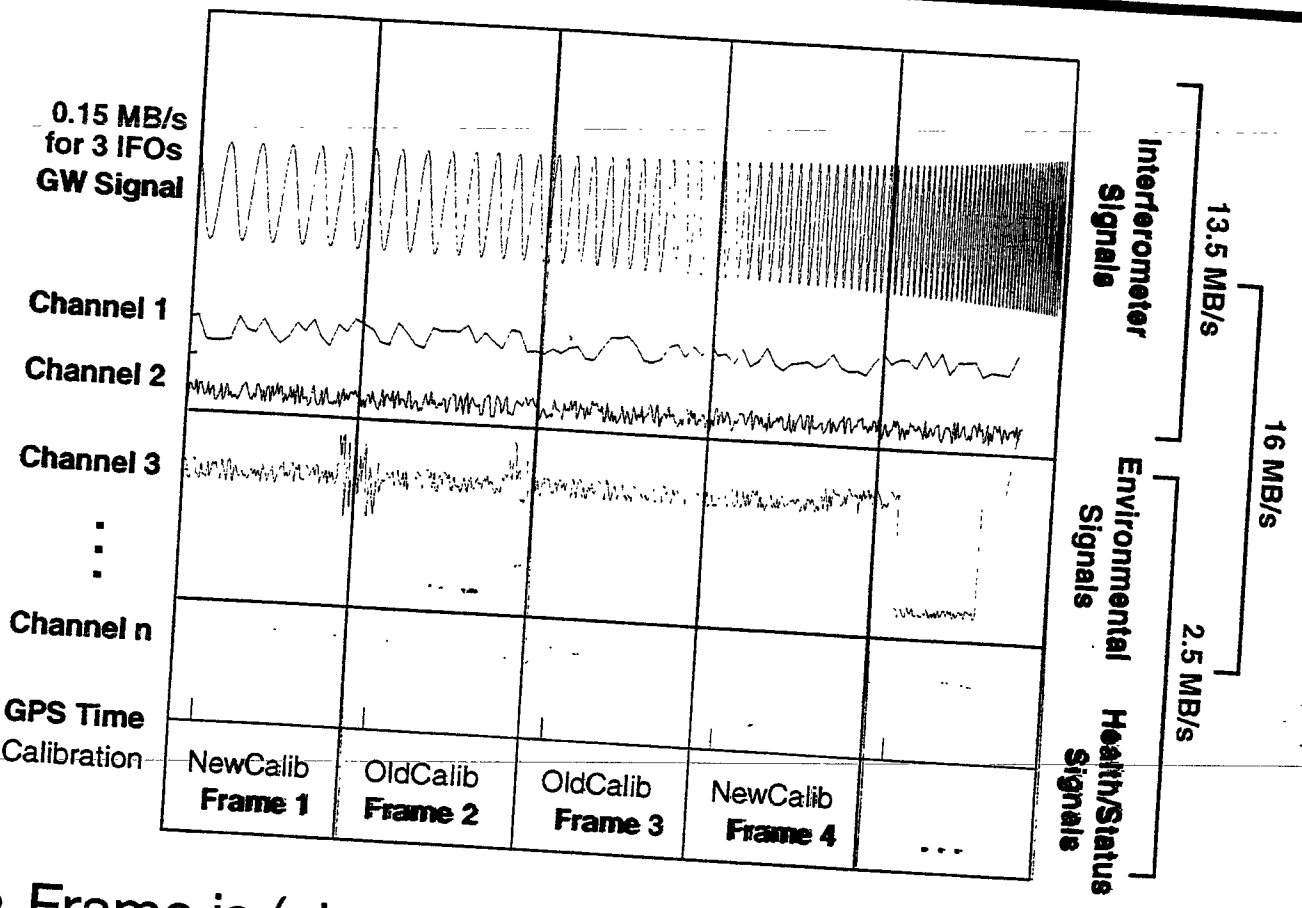

- Frame is (structured) self-contained snapshot of data for a period of time
  - GW channel & ancillary IFO channels
  - Environmental monitoring (veto) channels
  - Facilities/Vacuum health & status

LIGO Physics Analysis

Physics Schedule

- First Physics Run (~2002)
  - » LIGO Collaboration -- (being formed)
- Enhancements
  - » Advanced R&D to reach h ~ 10^{-22}
  - » implemented from 2002 over 5-10 years
- Physics runs interleaved
- Advanced Detectors

Collaboration includes Data Analysis

- develop analysis tools, etc
- access to data thru collaboration only

Open access to the data

- someday??

Project Director

Yoshihide KOZAI

National Astronomical Observatory (NAO)

20m FP

Institute for Cosmic Ray Research (ICRR)

resonat. X-pendulum

National Laboratory for High Energy Physics (KEK)

Institute of Space and Astronautical Science (ISAS)

100 ~ DL.

University of Tokyo suspension system.

3m FP

University of Electro-Communications

Laser

Kyoto University Theory

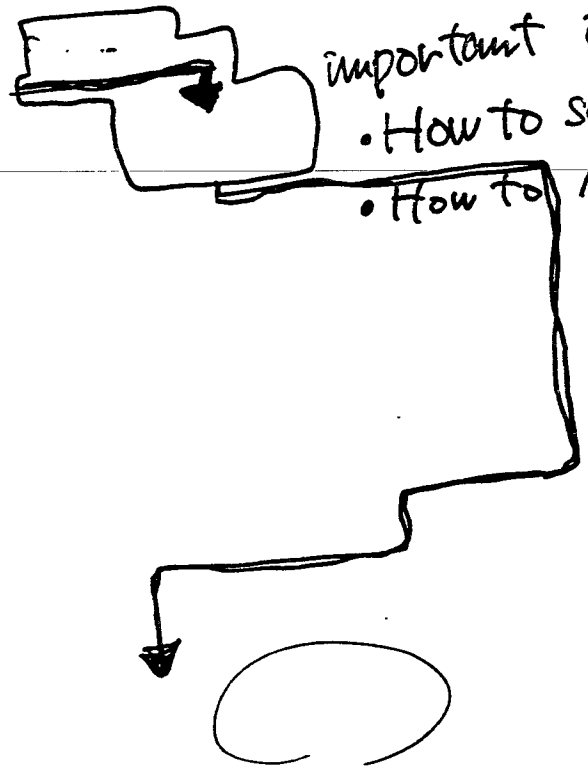
important issue
• How to select GW event.
• How to reduce noise

Data Flow of TAMA 300

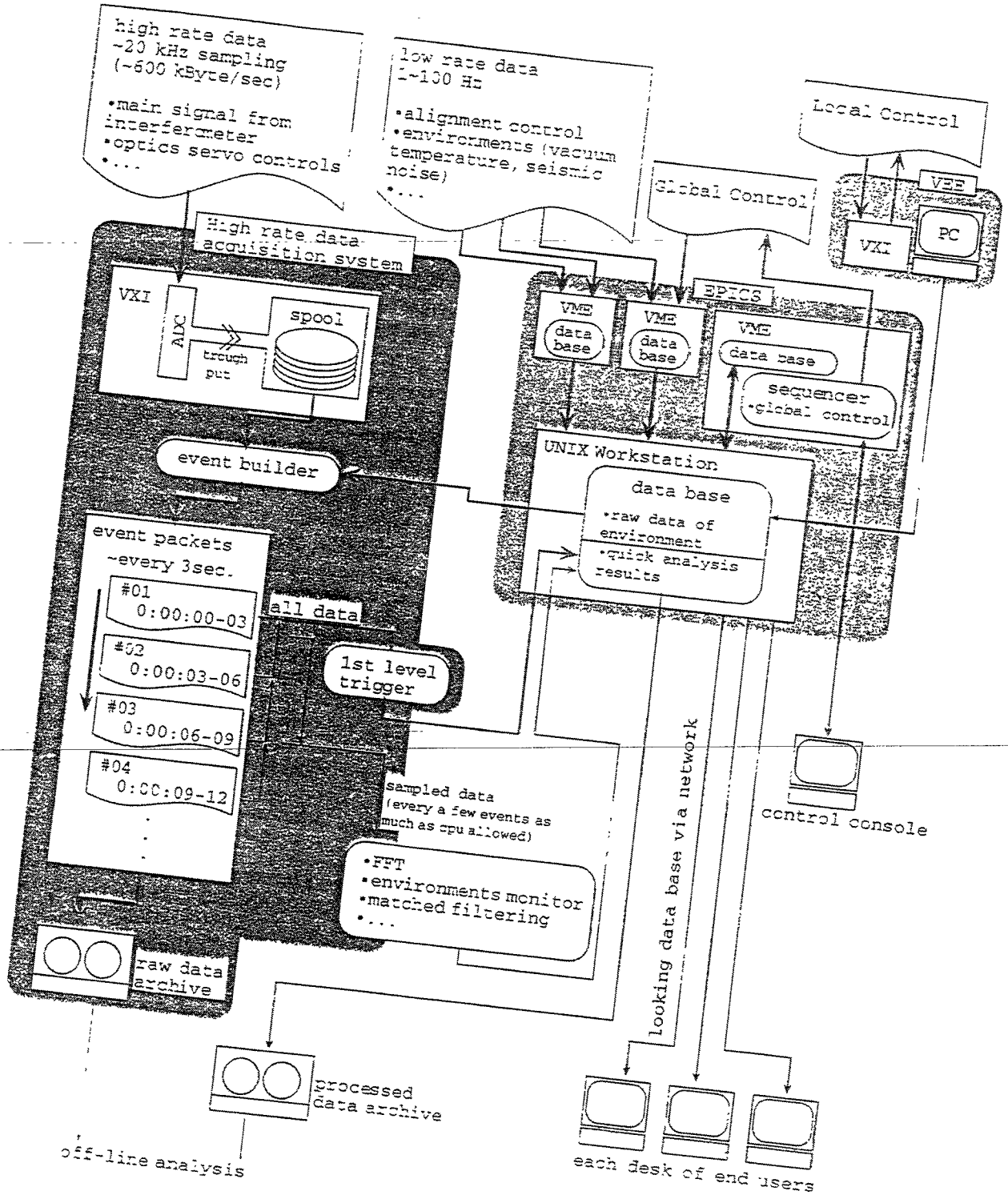

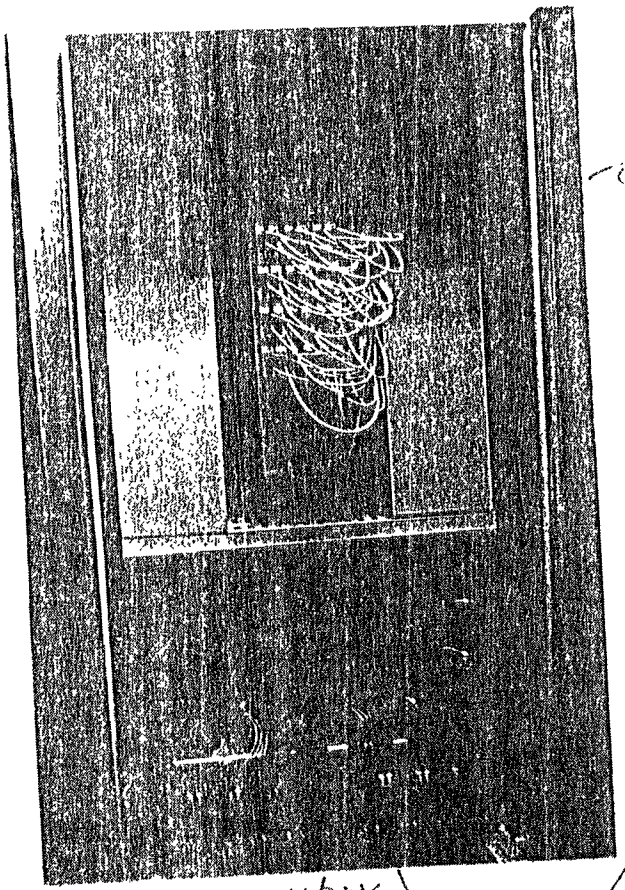

fiber junction box

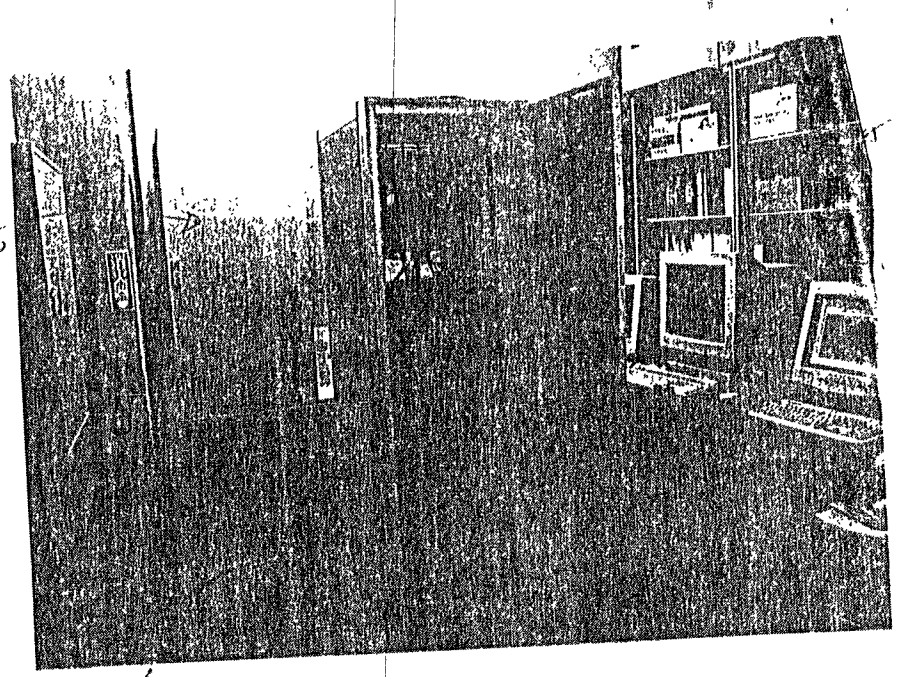

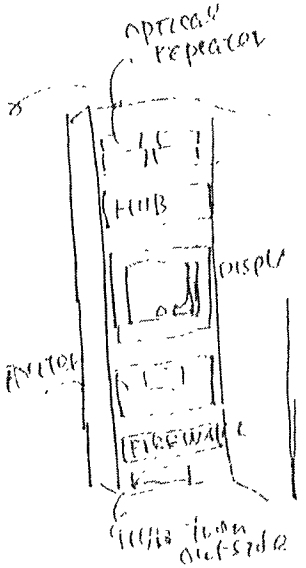

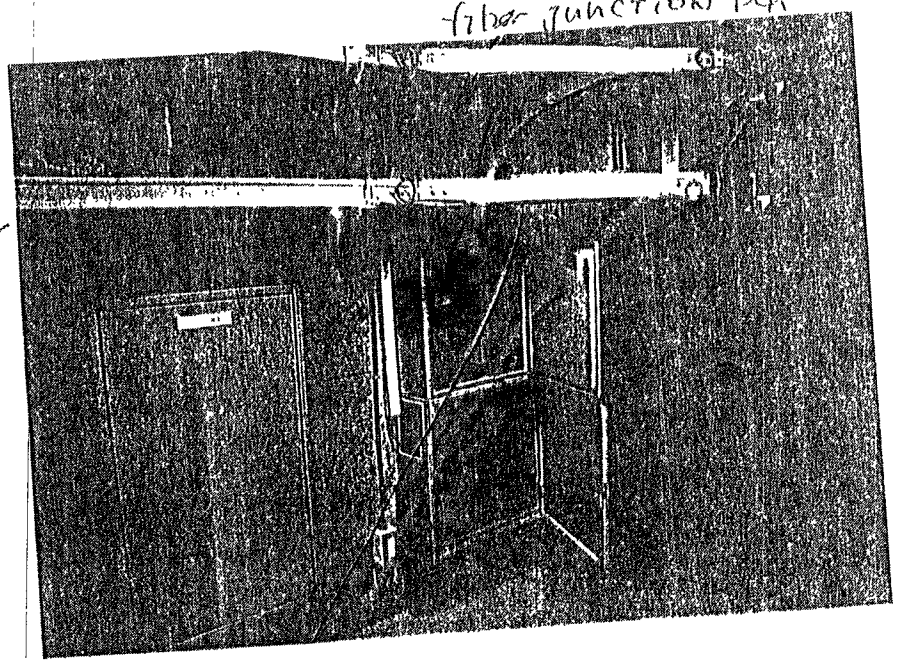

fiber junction box

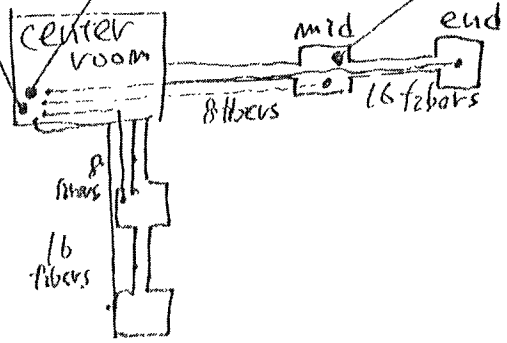

Signals from the interferometer system

High sampling-rate signals

- main interferometer signal, Fabry=Perot cavity error signal, etc.
- most important signals for GW detection
- 20 kHz or more high rate sampling
- 600 kByte/sec (dominate the amount of total data)

Low sampling-rate signals

- environments as vacuum status, temperature
- optical elements, suspension system with slow feedback
- distributed along the interferometer arm
- many channels

Data Flow of TAMA 300

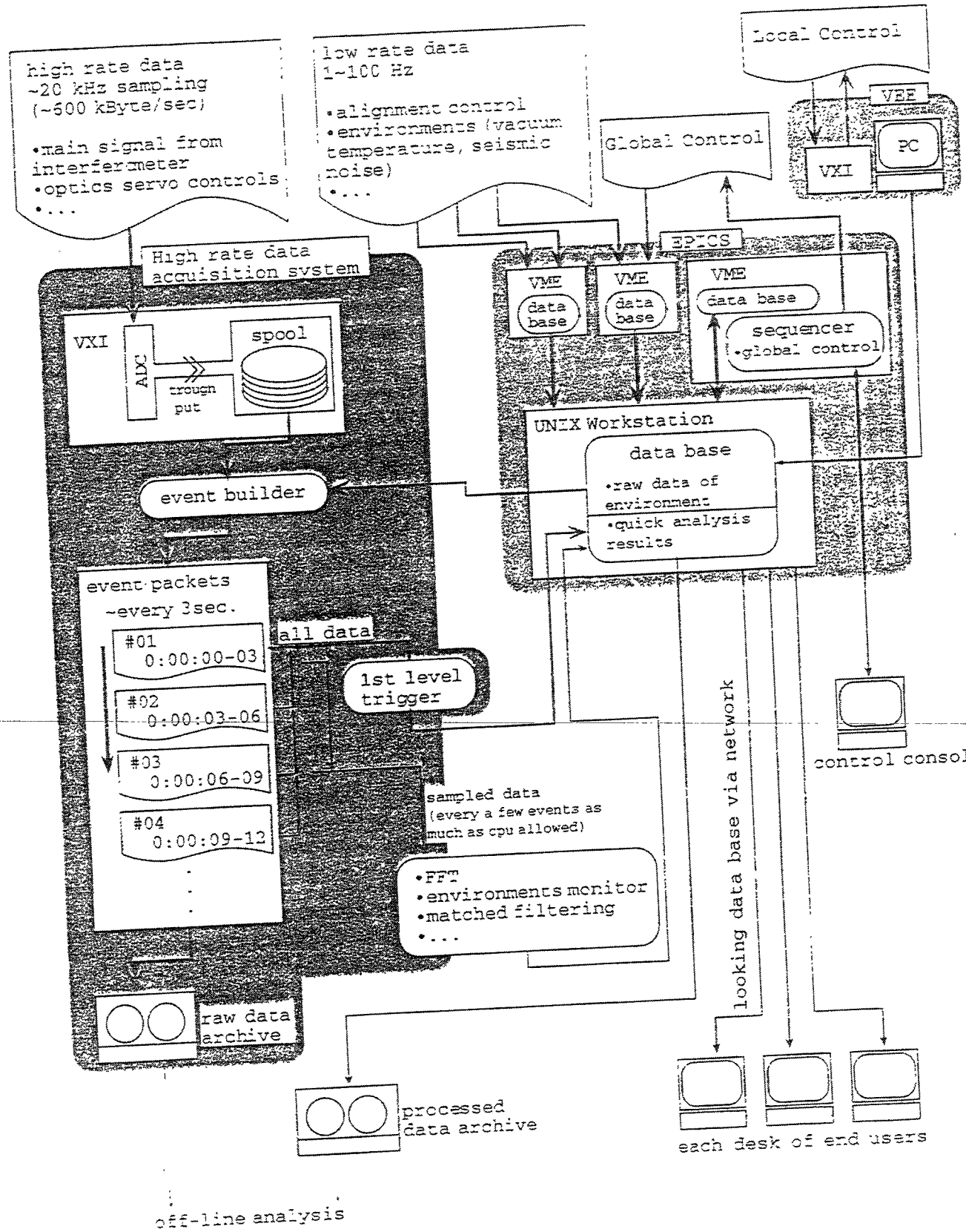

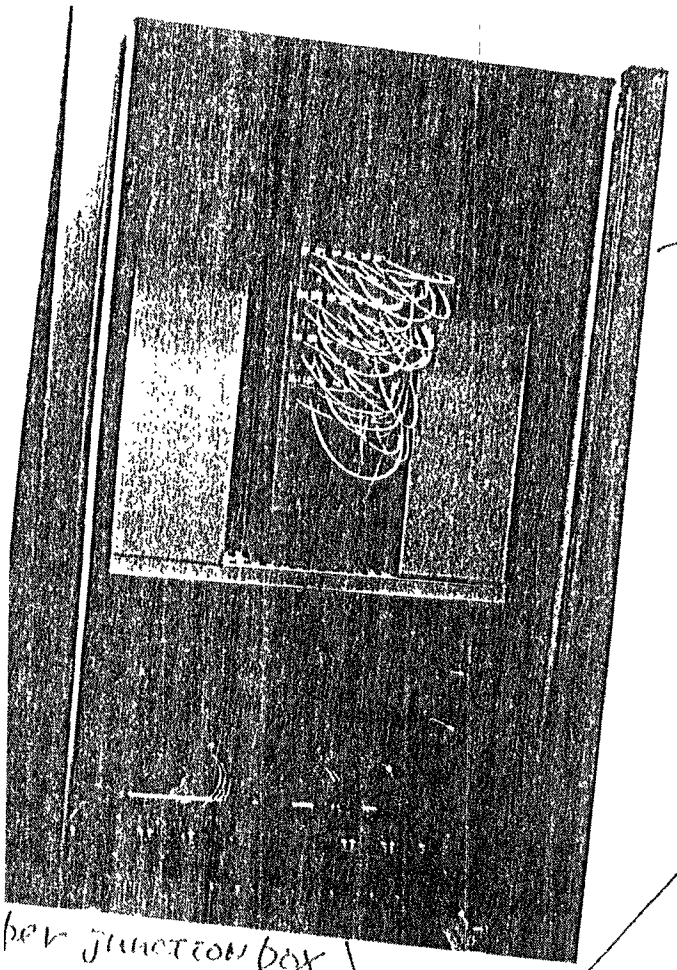

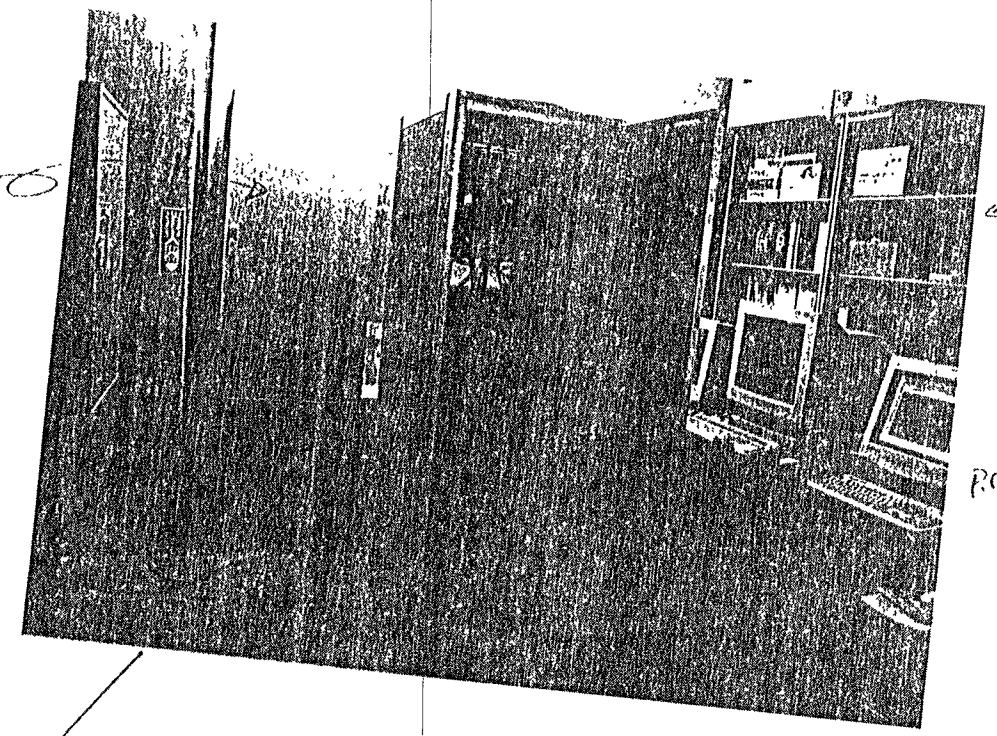

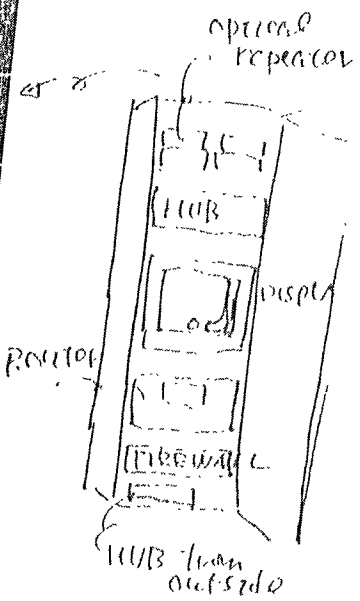

fiber junction box

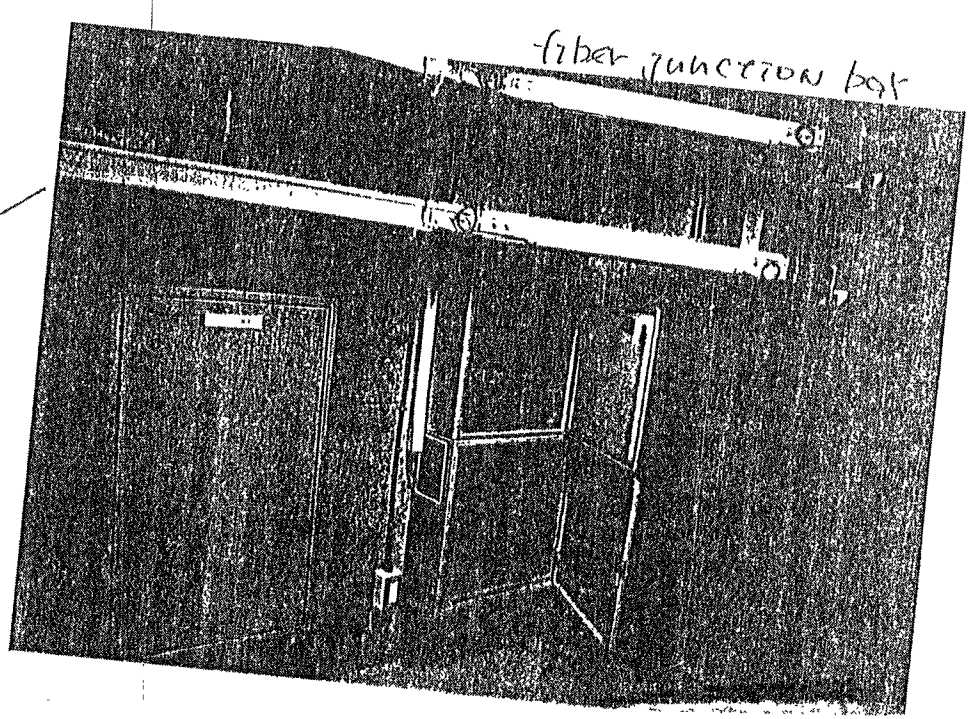

fiber junction box

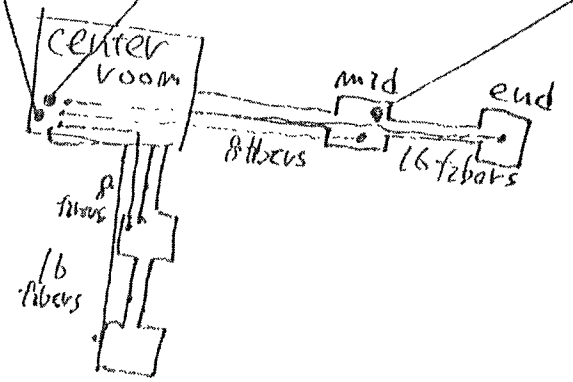

I/O signals of TAMA online sytem

signal name	ch#	kind	bit depth	sampling rate [Hz]	Note
High rate input signals					VXI + DSP engine
Fabry=Perot Michelson					
L- error signal (main interference signal)	1	ADC	16	20k	
L- feedback	1	ADC	16	20k	
L+ error	1	ADC	16	20k	
L+ feedback	1	ADC	16	20k	
beam splitter error	1	ADC	16	20k	
beam splitter feedback					
Mode cleaner, Recycling					
mode cleaner error	1	ADC	16	20k	
mode cleaner feedback	1	ADC	16	20k	
recycling mirror error	1	ADC	16	20k	
recycling mirror feedback	1	ADC	16	20k	
Laser					
laser power	1	ADC	16	20k	
laser frequency stabilization error	1	ADC	16	20k	
Instant physical calculations					
strain :*h*	1	ADC	16	20k	
(reserved)	2	ADC	16	20k	
	amount of data			**600 kByte/sec**	

Low rate Input signals					VXI+PC, VME
alignment monitor	8	ADC	12	~50	
Fabry=Perot cavity	1	ADC	12	~100	
photo detector DC current (main signal)	16	ADC	12	0.1	
X-pendulum tilt monitor					
vacumme related					
ion pump status	20	ADC	12	~1	
turbo pump status	8	ADC	12	~1	
temperature	12	ADC	12	~1	
	amount of data			**~800 Byte/sec**	

Output signals					
alignment feedback	8	DAC	12	~50	
roughly alignment control (thermal drift correction)	2	GPIB	-	~1	pico motor control
initial position of optiocal elements suspension	28	GPIB	-	manual	pico motor control
X-pendulum tilt feedback	24	DAC	12	0.1	
	amount of data			**~600 Byte/sec**	

total amount of data ~600 kByte/sec

~2 GByte/hour

On-line feedback loops

Feedback during operation

- local control
  - example: X-pendulum
  - feedback between local devices
  - operate independently on others
- global control
  - example: correction of drift due to thermal expansion
  - feedback between remote devices (center room <-> end room)
  - operation via Network system

Digital control for initial setup

- example: Initial alignment of optical elements

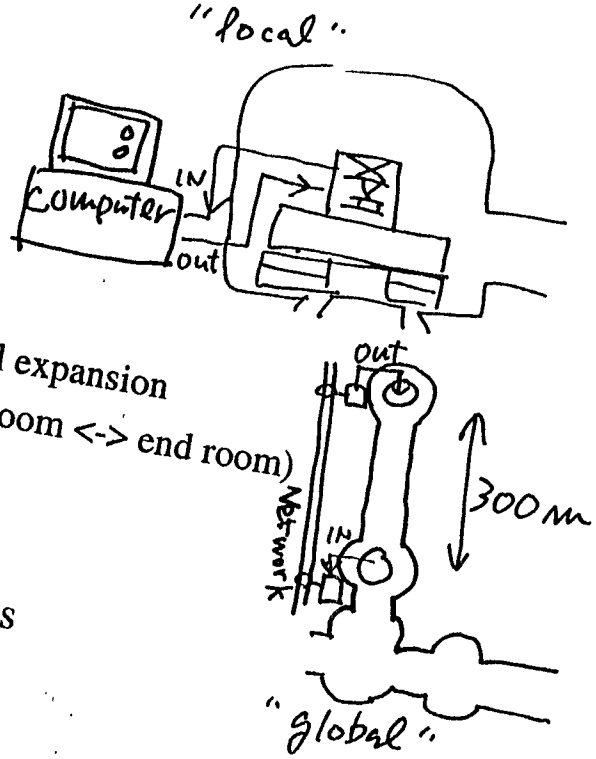

Prototype 2.

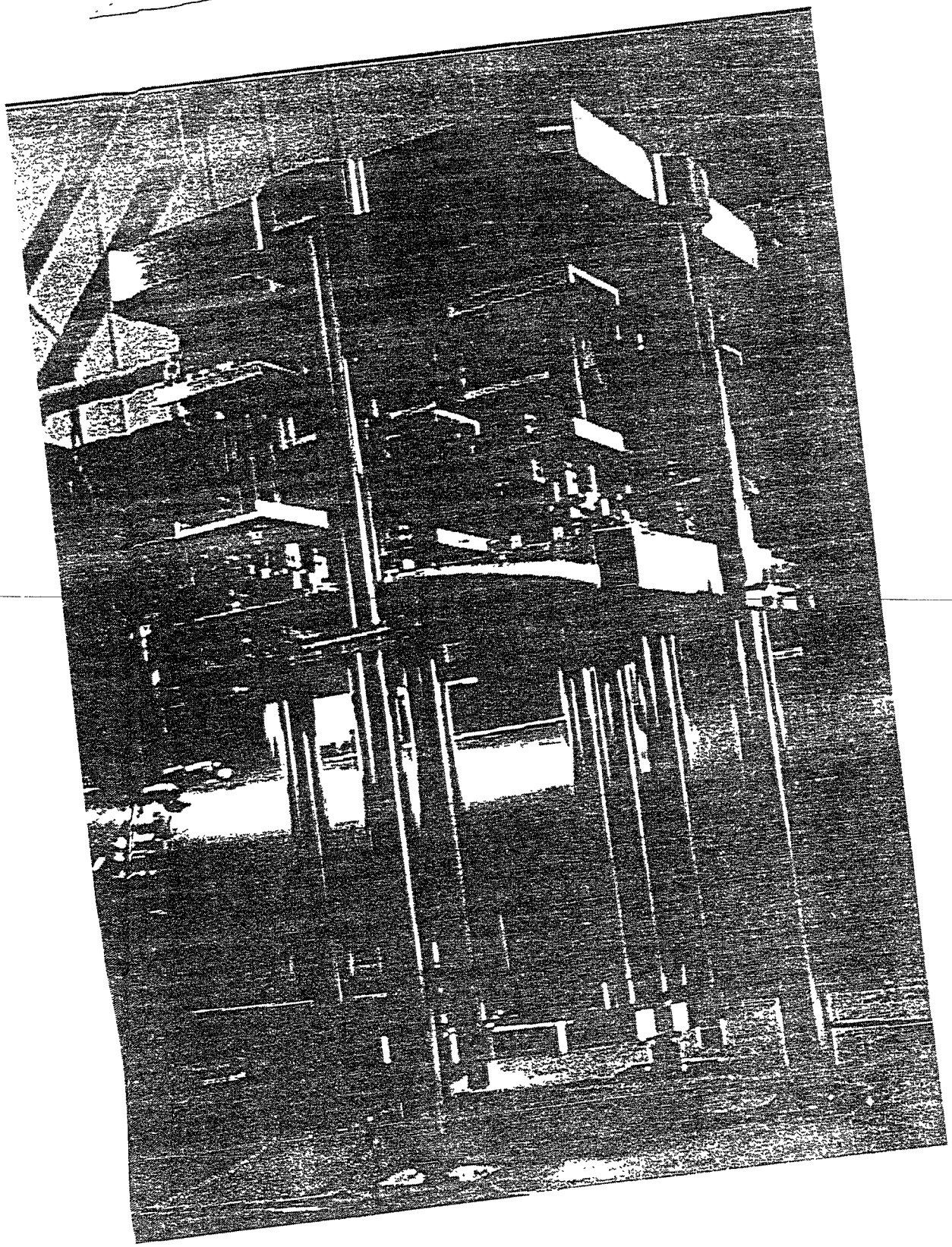

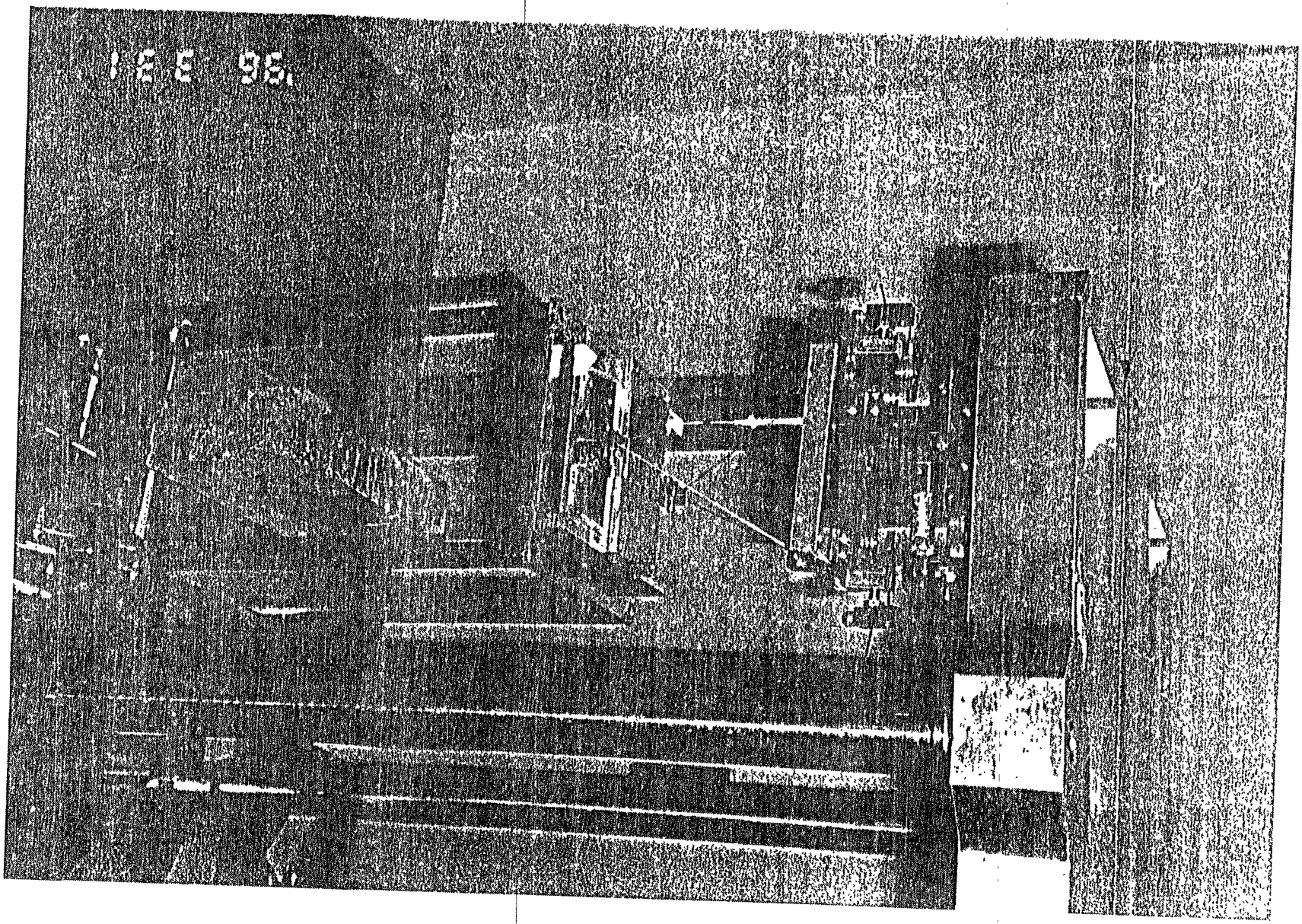
IEE 98.

Naive 2D X-Pendulum

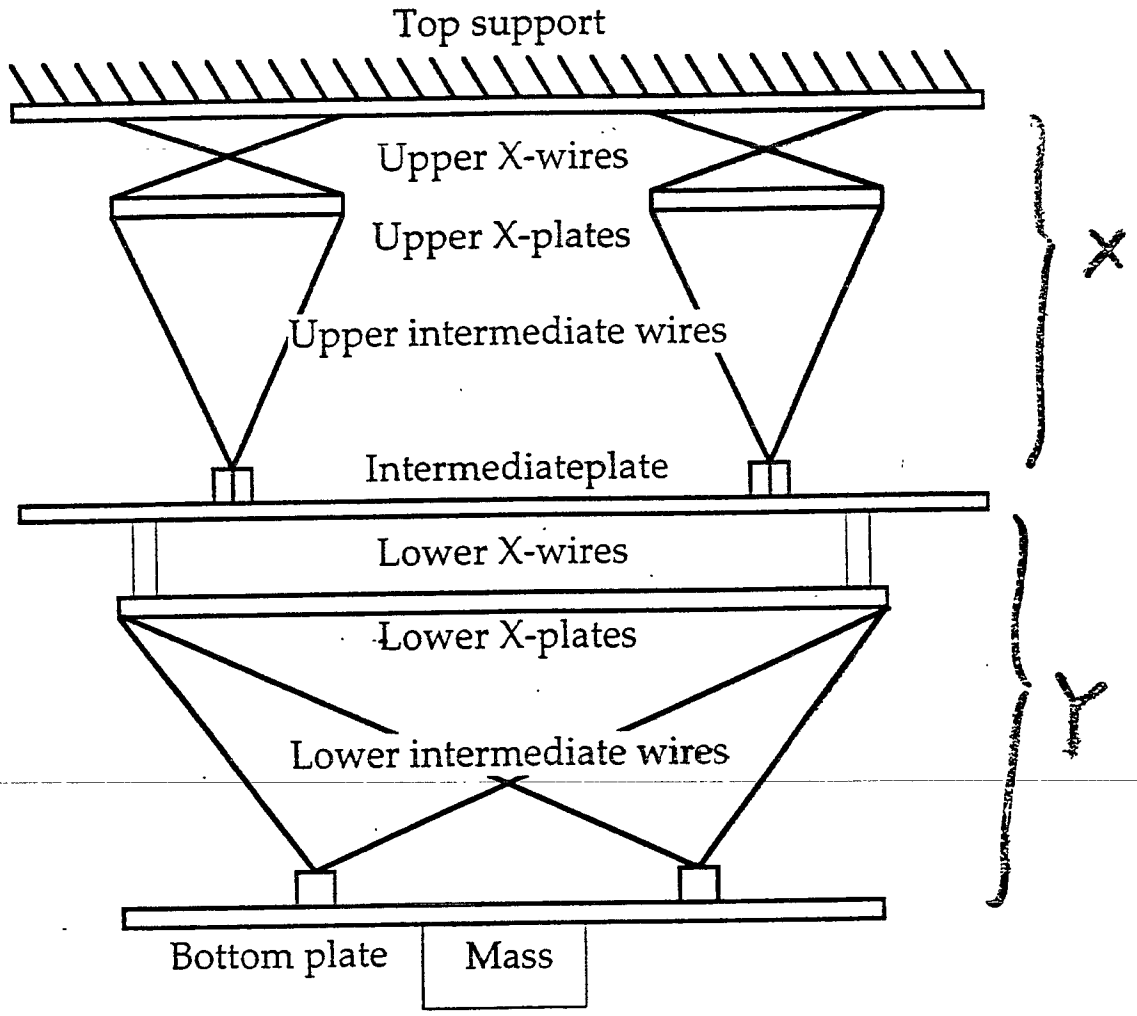

Disadvantages

- Inconveniently tall
- Many low frequency elastic modes

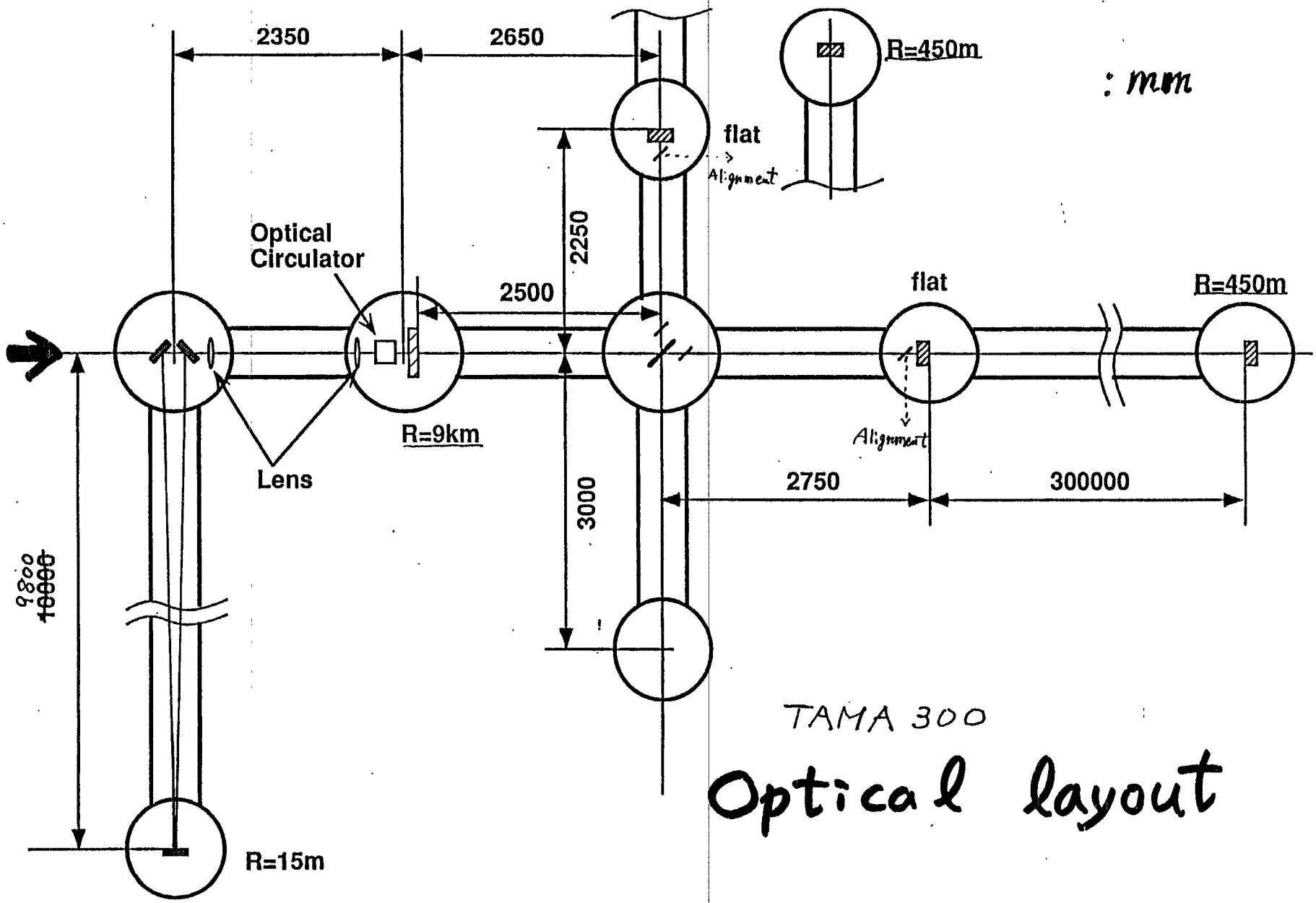

TAMA 300

Optical layout

Vacuum design

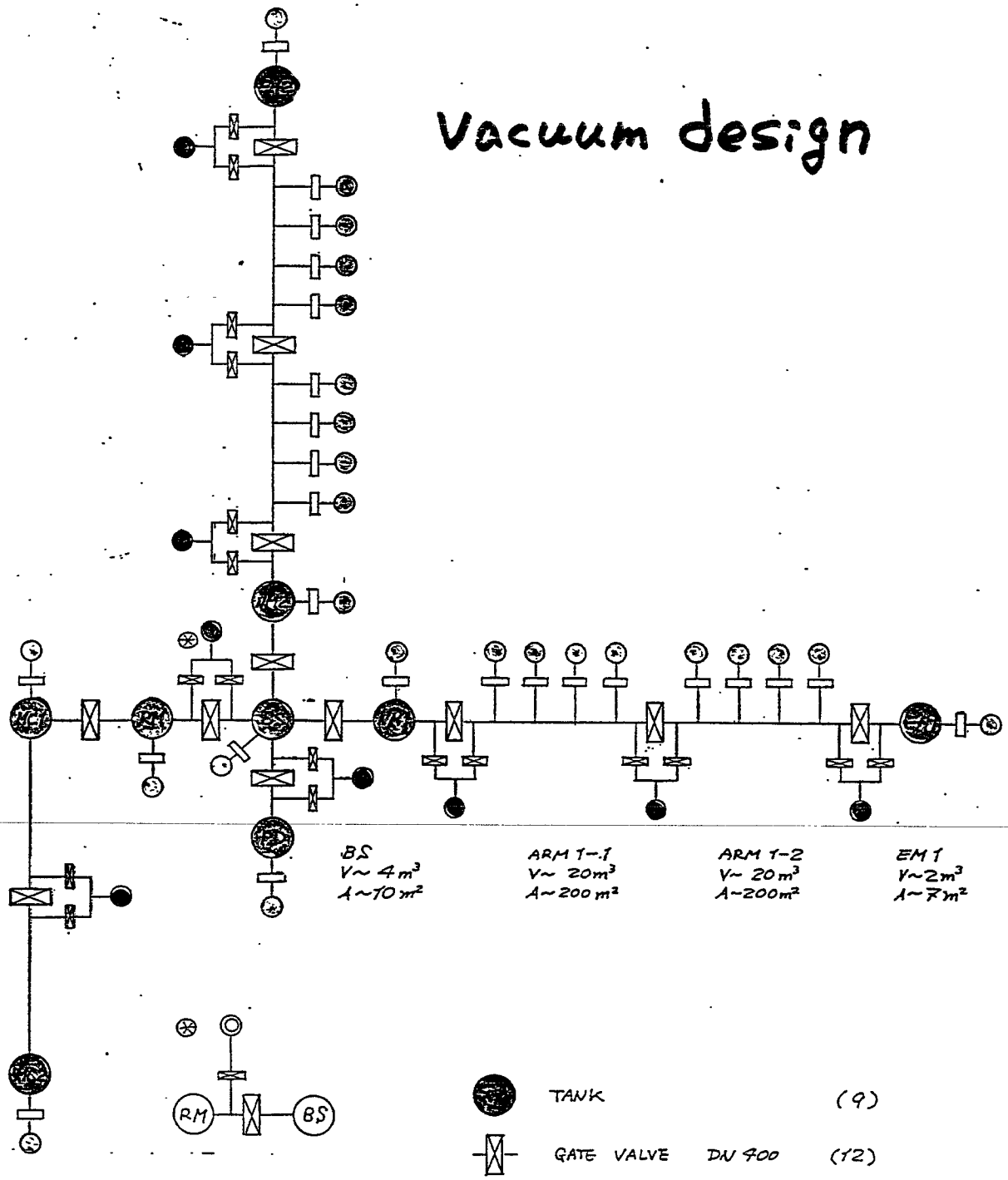

TANK (9)

GATE VALVE DN 400 (12)

PUMP UNIT (9)

- GATE VALVES DN 200 <18>
- TMP 1000 ℓ/s <9>
- RP 2000 ℓ/min <9>

PUMP UNIT. (9+76); TANK+ARM

- GATE VALVE DN 150
- SPUTTER ION PUMP 400ℓ/s

VACUUM SYSTEM

Oct. 27 '94 Y. Saito

平面図

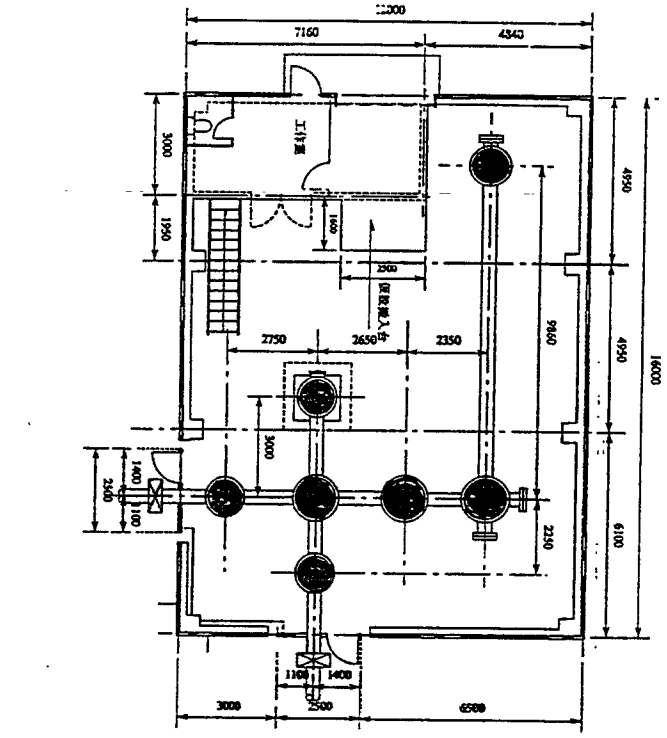
11300
7160
4340
3000
1950
1400
2500
保安職員入口
工作室
4950
4950
4950
16000
2750
2650
2350
5940
3000
1400
2400
100
2250
6100
1100
1400
3000
2500
6500

側面図

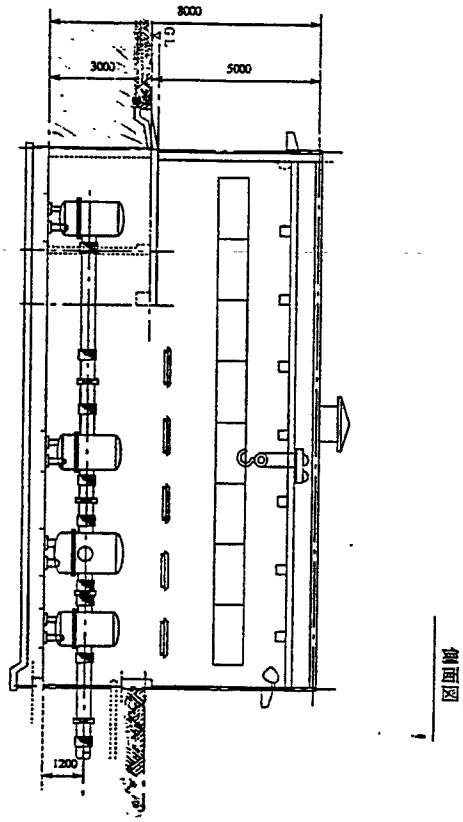
8000
3000
5000
GL
1200

N

正面図

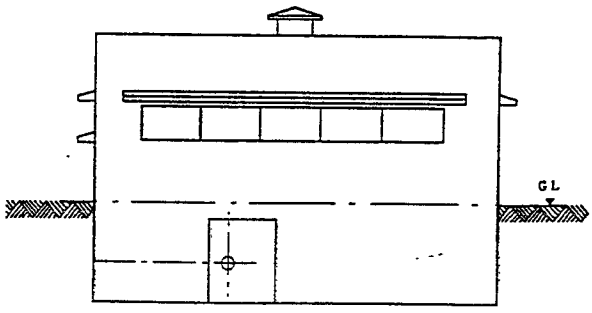
GL

配管路及び端部真空槽

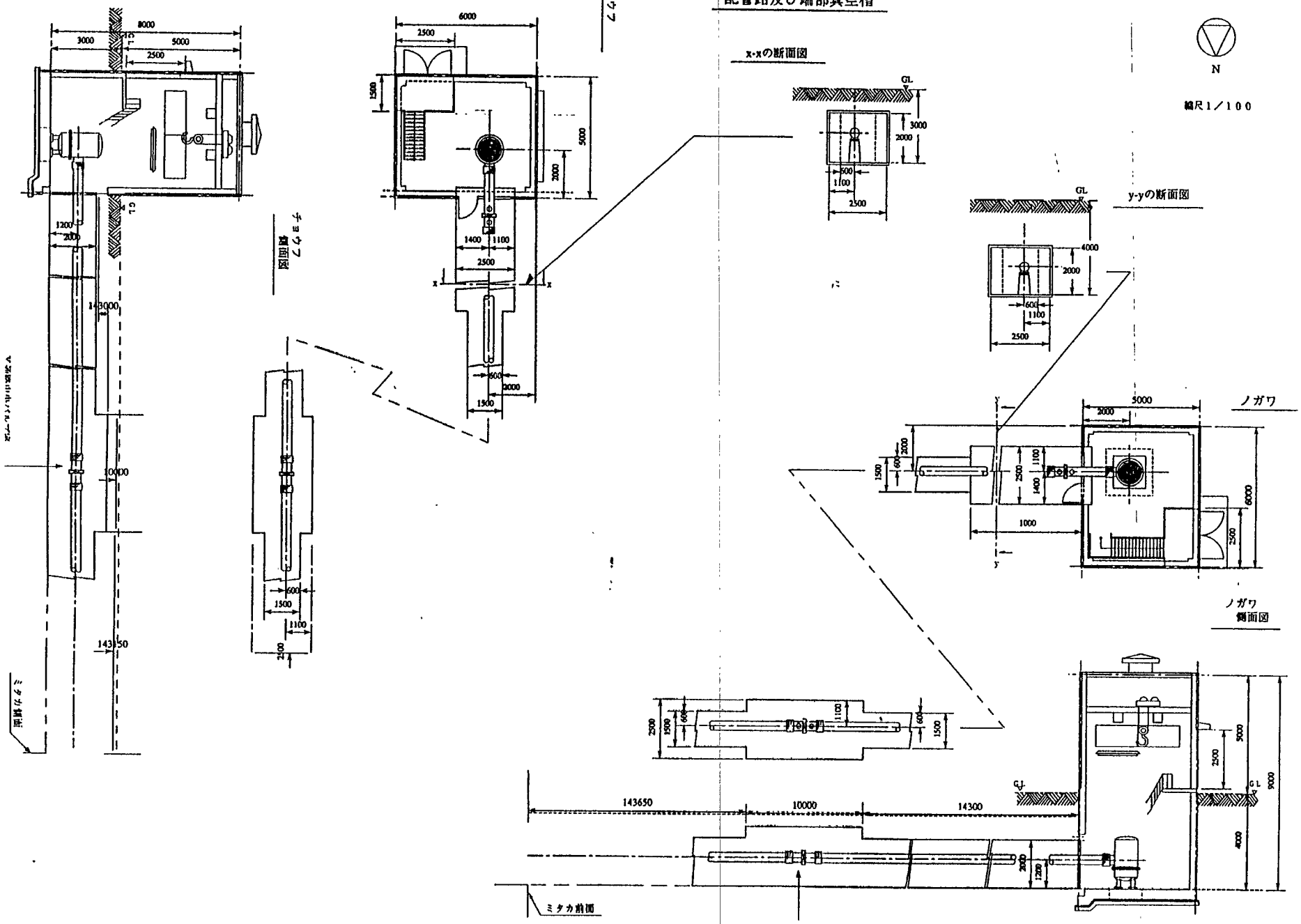
N
縮尺1／100
x-xの断面図
y-yの断面図
チョウフ
ノガワ
ノガワ
側面図
ミタカ前面
GL
8000
3000
5000
2500
6000
1200
200
143000
10000
143650
14300
1400
1100
600
1500
2000
1000
250
4000
5000
9000
1220

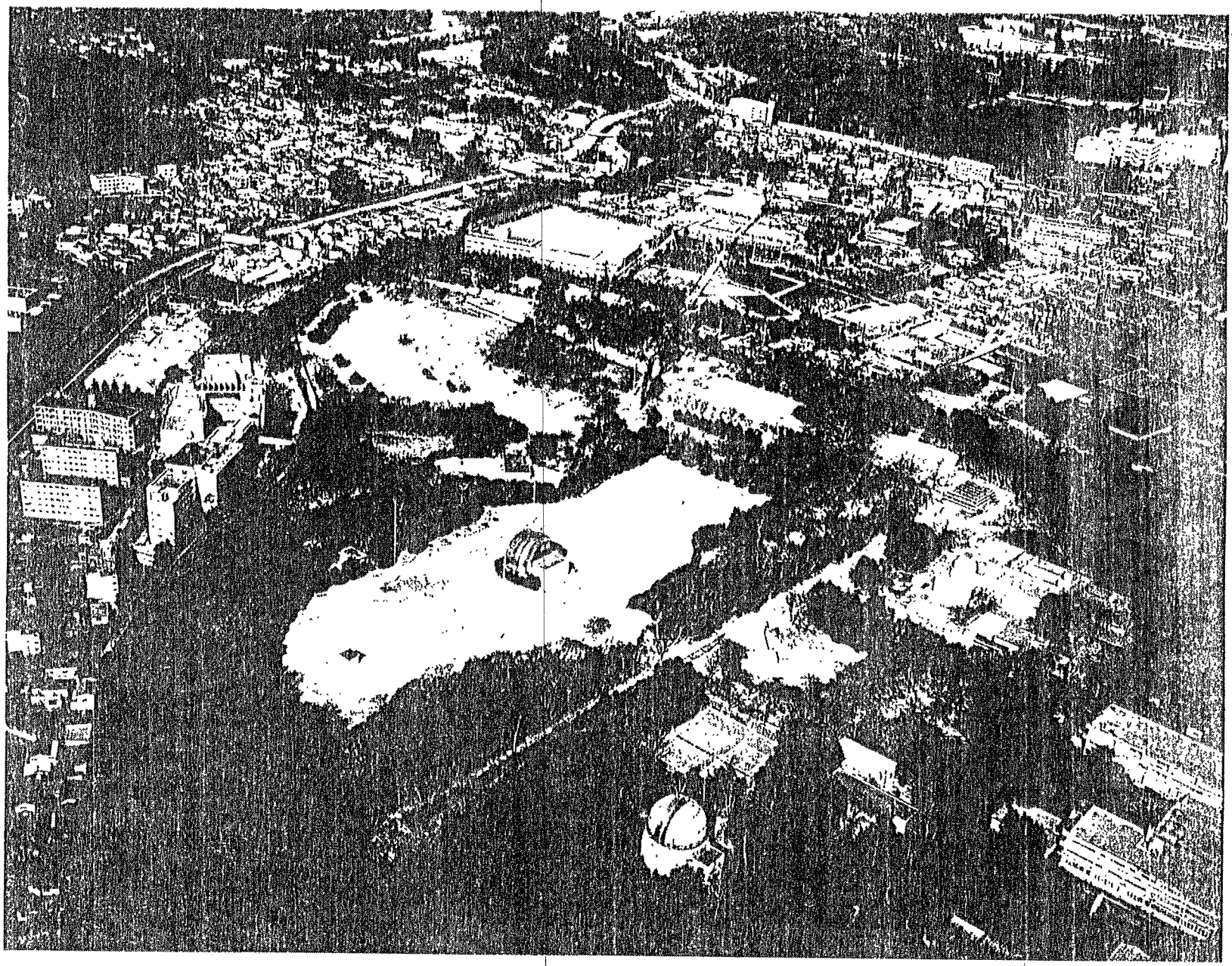

Nov. 1995

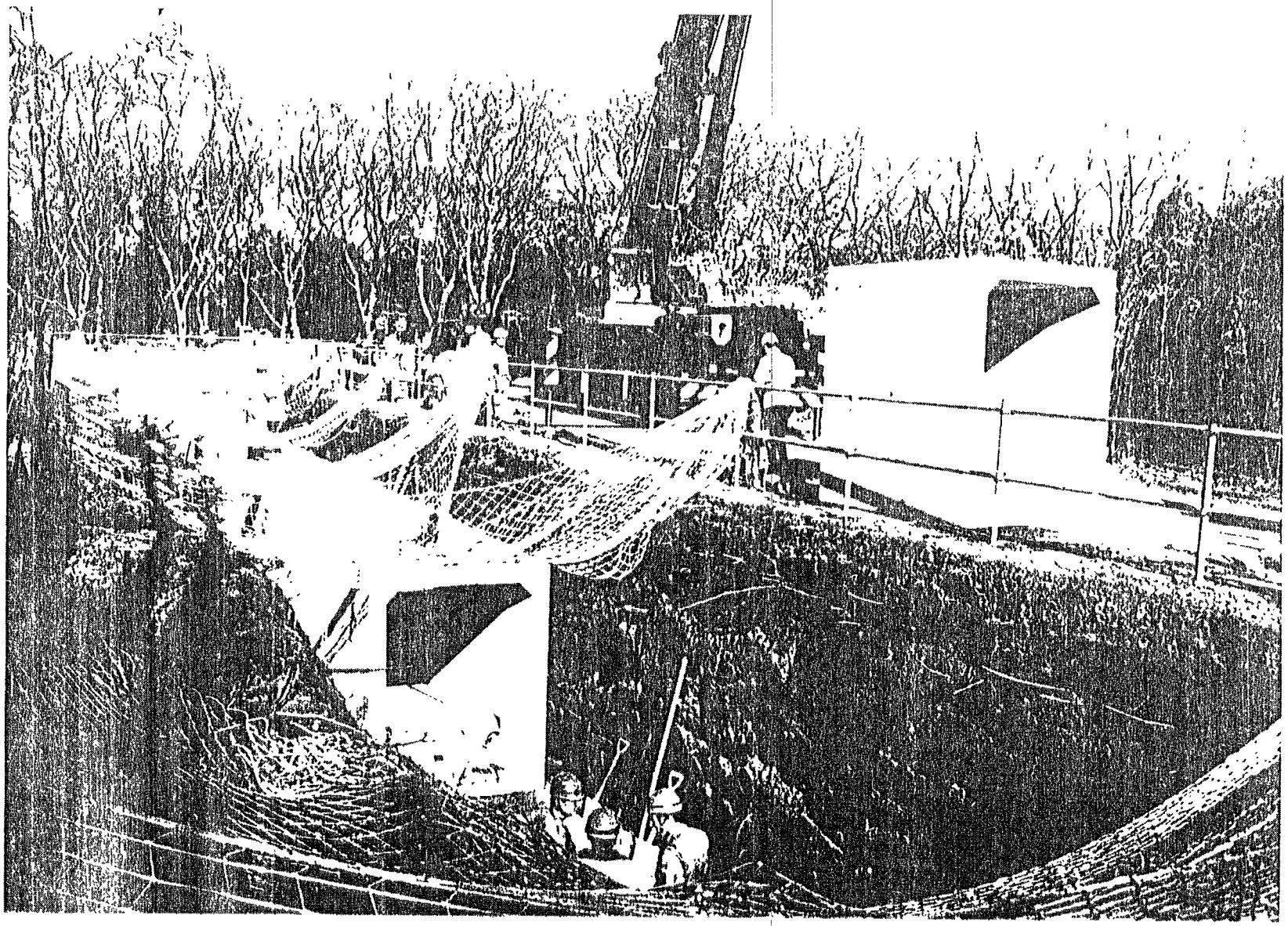

February. 1996

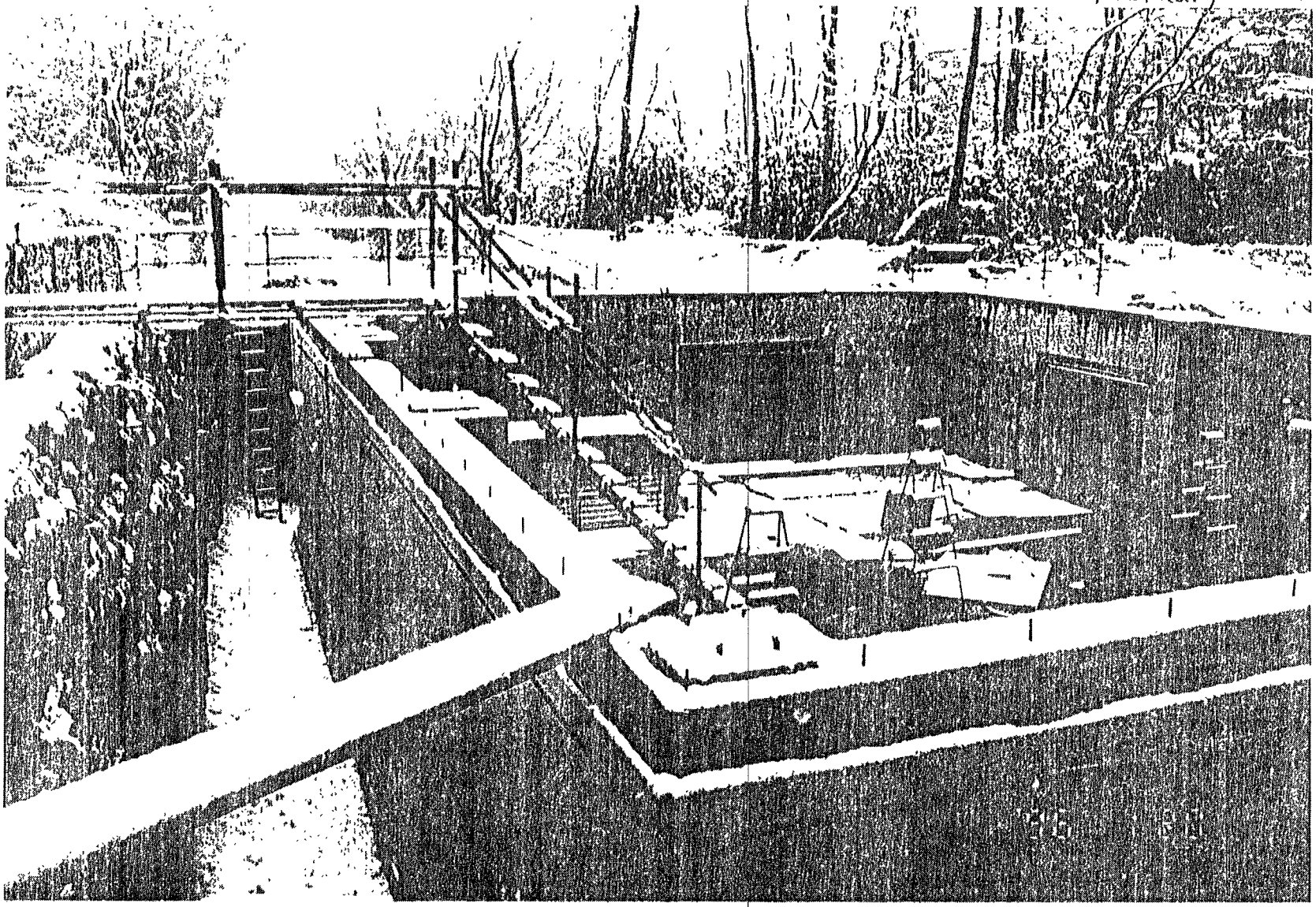

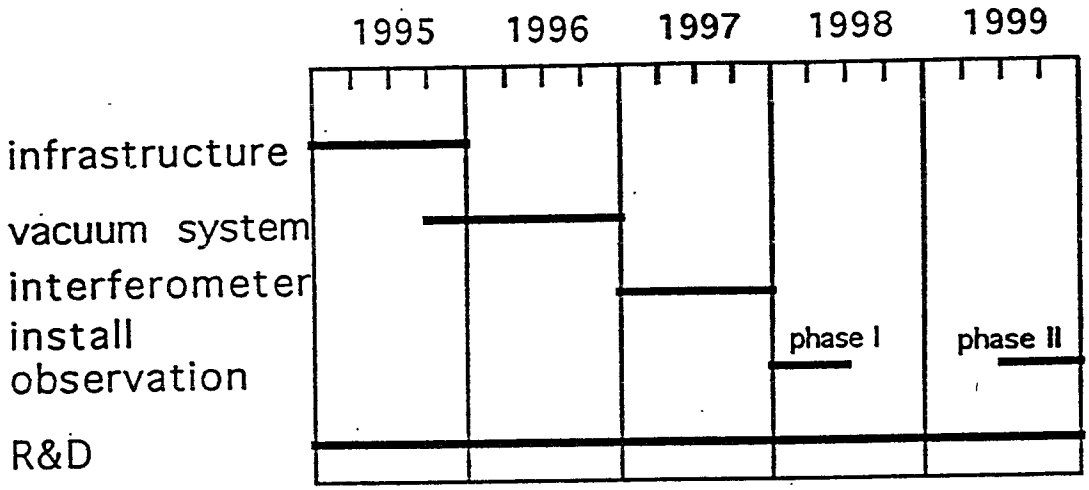

Time schedule of the construction of the detector

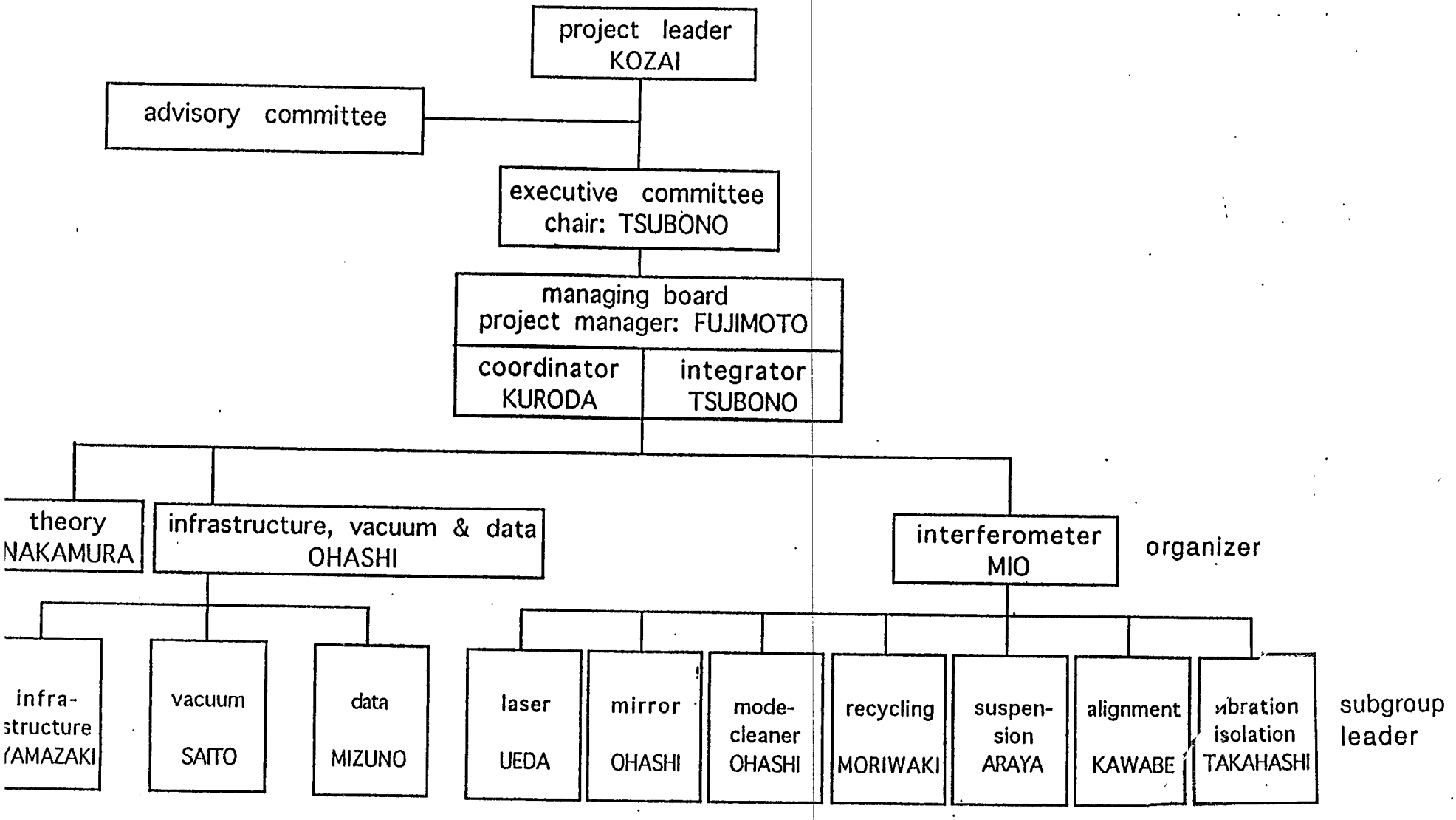

TAMA300 organization

Ideas for on-line trigger of gravitational wave

N.Kanda, ICRR/Univ.Tokyo

1. Requirement for ON-LINE trigger method

- Fast processing
- Clear signature of real signal

  -> On-line trigger is not selection of event. It is veto for fake signal.
- High efficiency

2. for CHIRP wave from binary coalescence of binary stars

2.1. Resampling

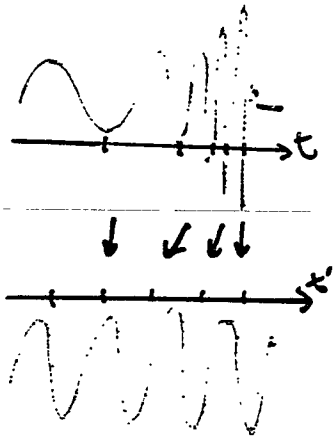

.Distort time axis according to chirp of frequency, then chirp wave reformed as sinusoidal.

.-> Get line spectra when resampling rate is matched

Ref: Smith S., Phys.ReV.D.36.2901(1987)

R.Flaminio etal. LAPP-EXP-93.13

.Resampling parameters are:

- mass parameter $k=\frac{m_1 m_2}{(m_1+m_2)^{(1/3)}}$
- arrival time t_0
- final frequency ν_0
- Power spectra density is not sensitive for a final phase of the chirp wave.

.The resampling rate is given as:

$$Rn=\frac{\nu(t)}{\nu_0}=(1-1.53\times10^{-6}\nu_0^{8/3}kt)^{3/8}\ [1/Hz]$$

$$\text{resampling rate}=\frac{\text{ADC continuous sampling rate}}{Rn}$$

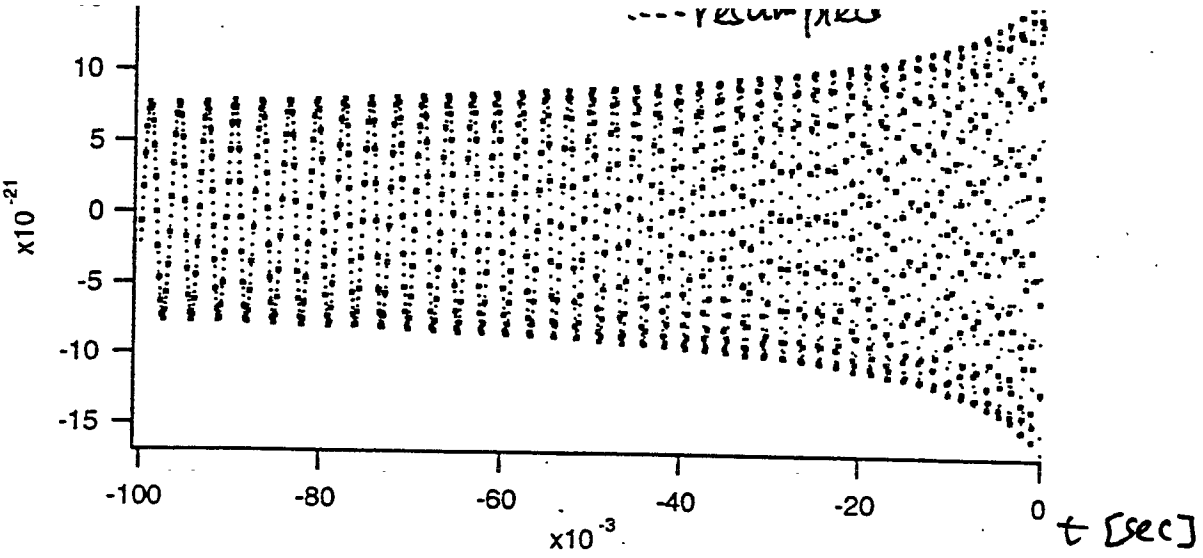
10
5
0
-5
-10
-15
x10^-21
-100
-80
-60
-40
-20
0
x10^-3
t [sec]

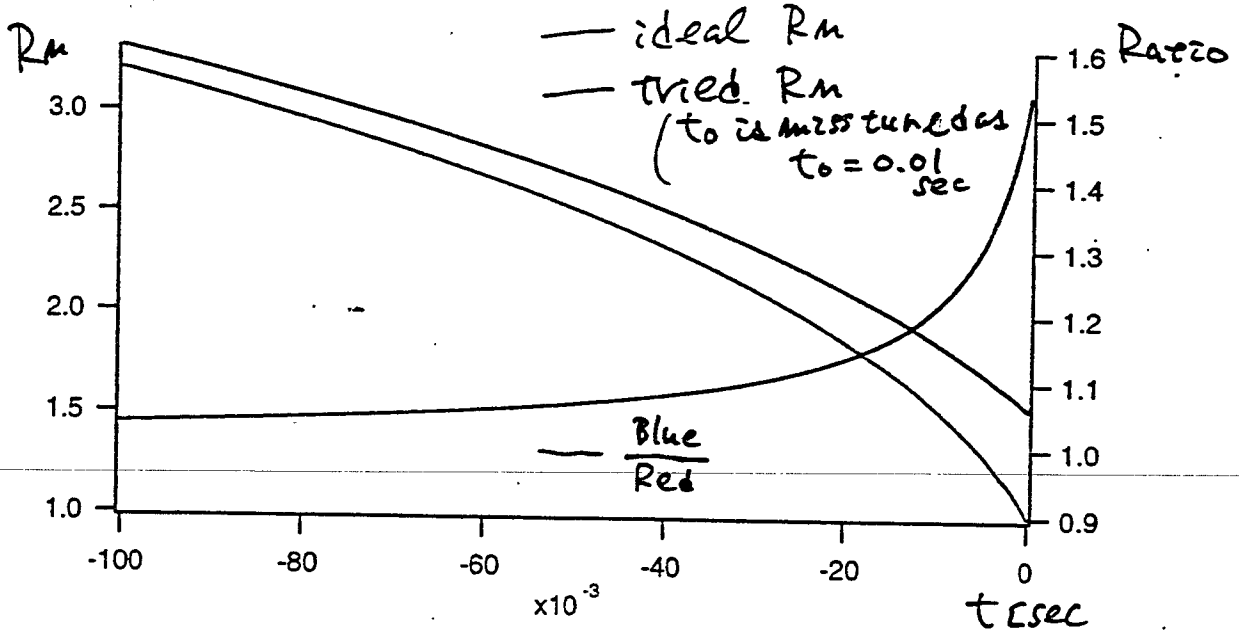
Rn
ideal Rn
tried Rn
(to is mistuned as
to = 0.01 sec
Blue / Red
Ratio
3.0
2.5
2.0
1.5
1.0
1.6
1.5
1.4
1.3
1.2
1.1
1.0
0.9
-100
-80
-60
-40
-20
0
x10^-3
t [sec]

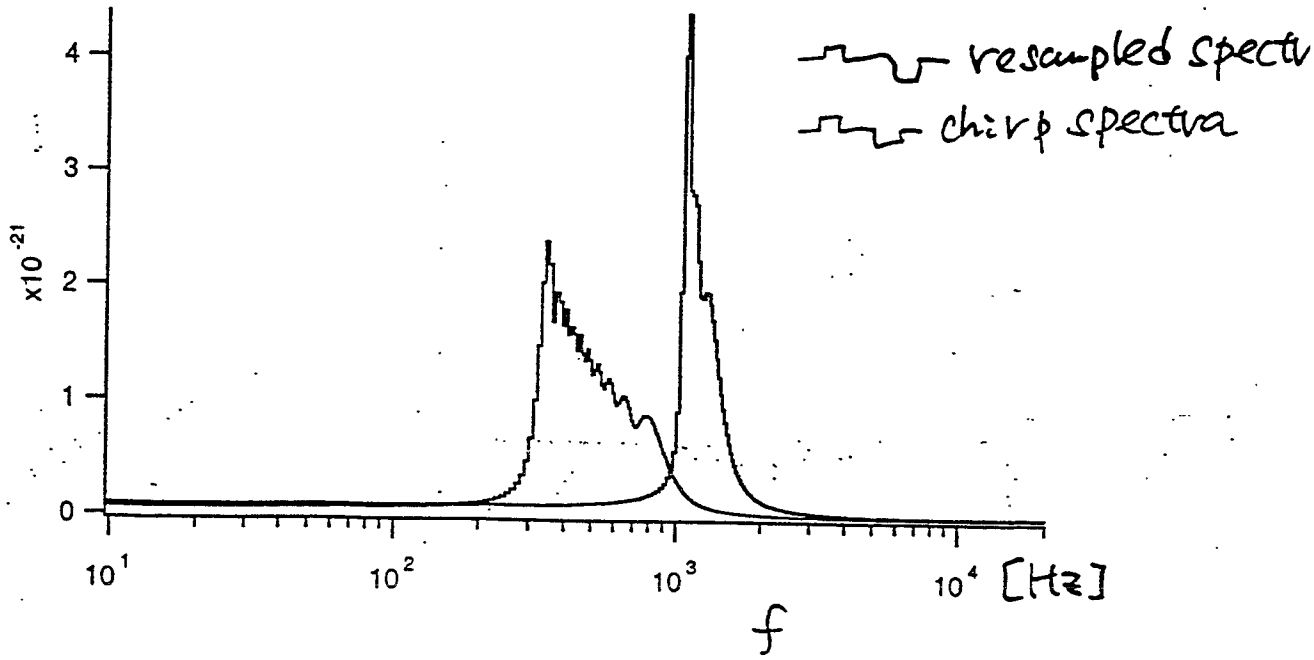
resampled spectra
chirp spectra
4
3
2
1
0
x10^-21
10^1
10^2
10^3
10^4 [Hz]
f

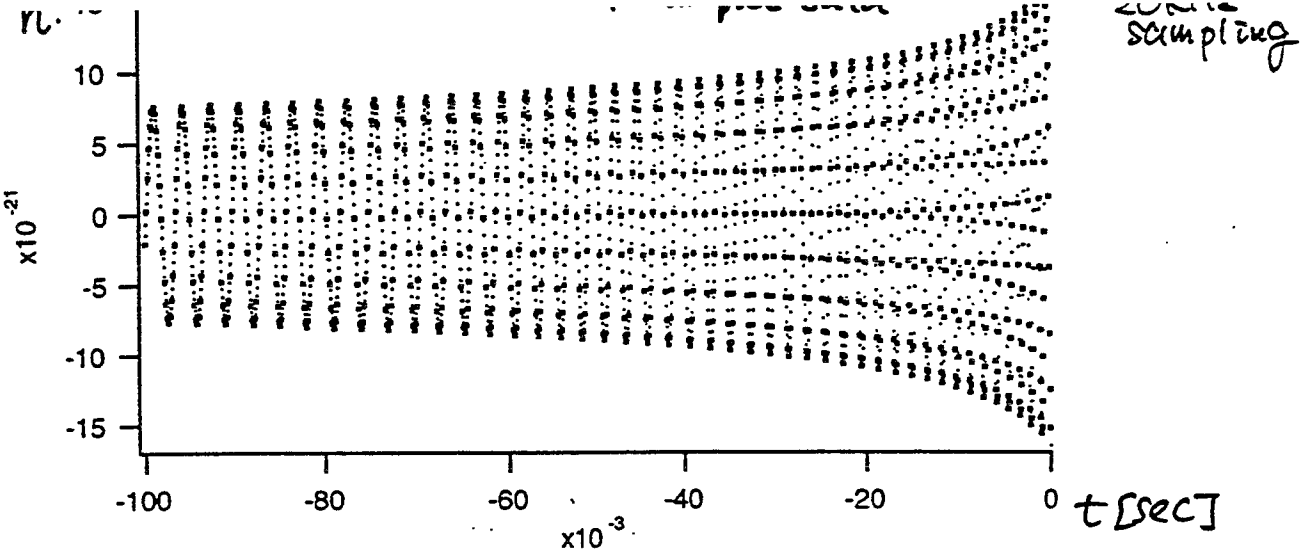
10
5
0
-5
-10
-15
x10^-21
-100
-80
-60
-40
-20
0
x10^-3
t [sec]

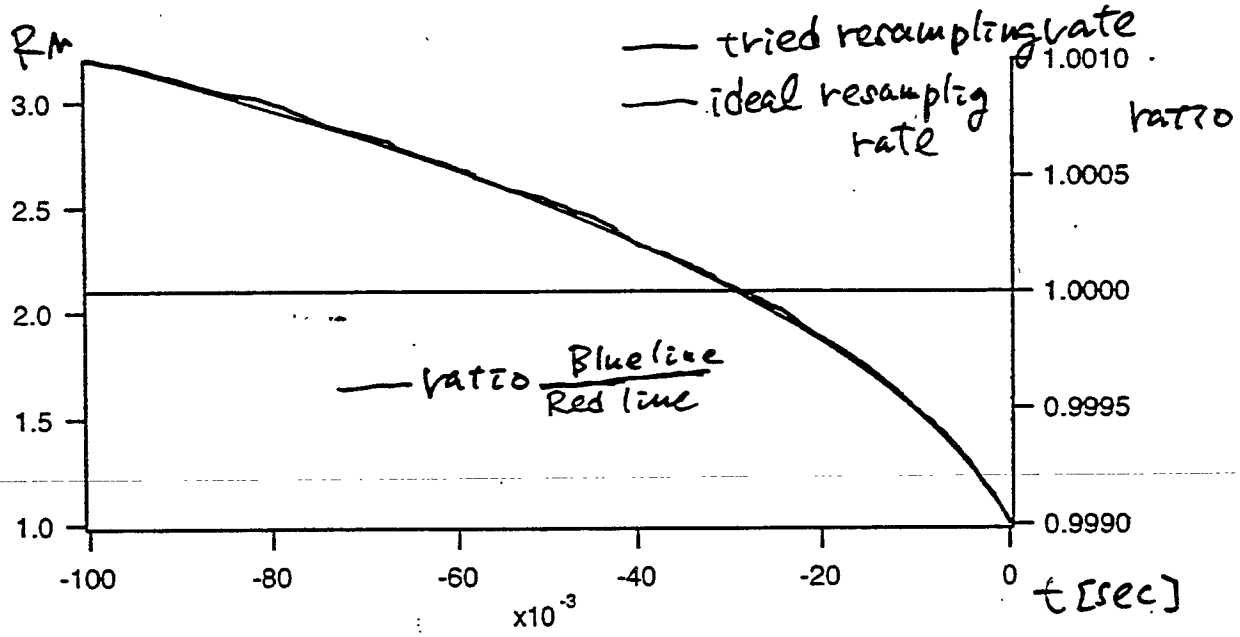
RM
tried resampling rate
ideal resampling rate
ratio Blue line / Red line
3.0
2.5
2.0
1.5
1.0
1.0010
1.0005
1.0000
0.9995
0.9990
ratio
-100
-80
-60
-40
-20
0
x10^-3
t [sec]

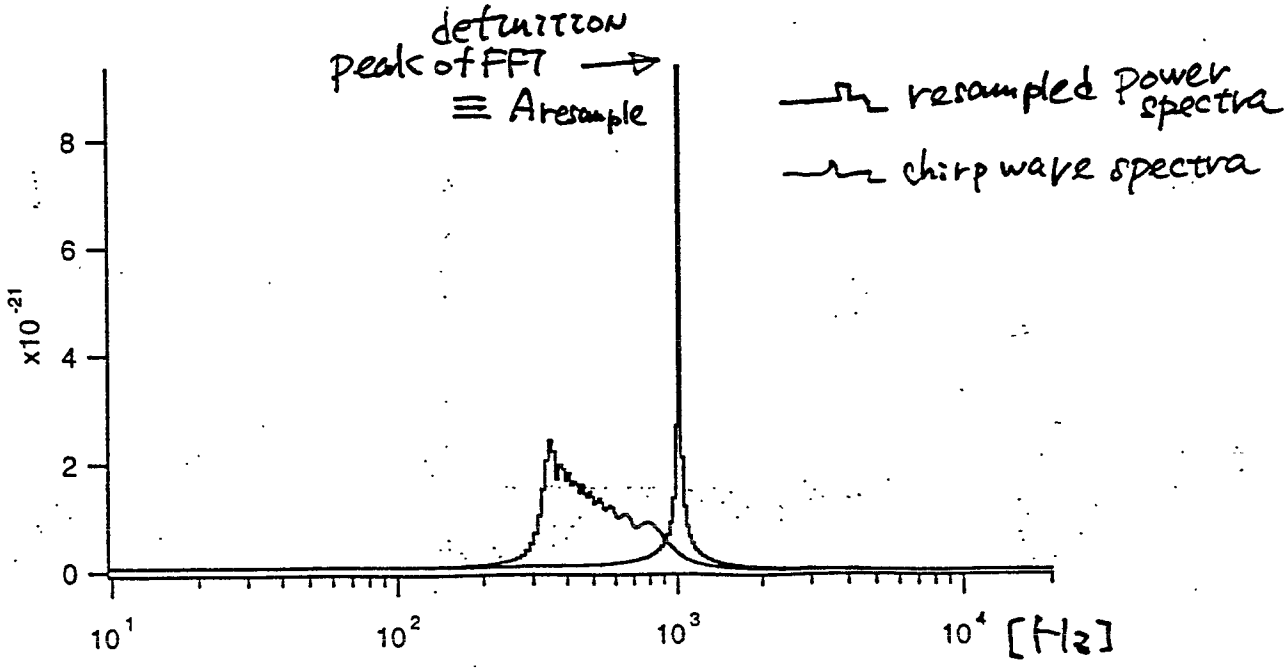
detuning
peak of FFT
≡ Δresample
resampled Power spectra
chirp wave spectra
8
6
4
2
0
x10^-21
10^1
10^2
10^3
10^4 [Hz]

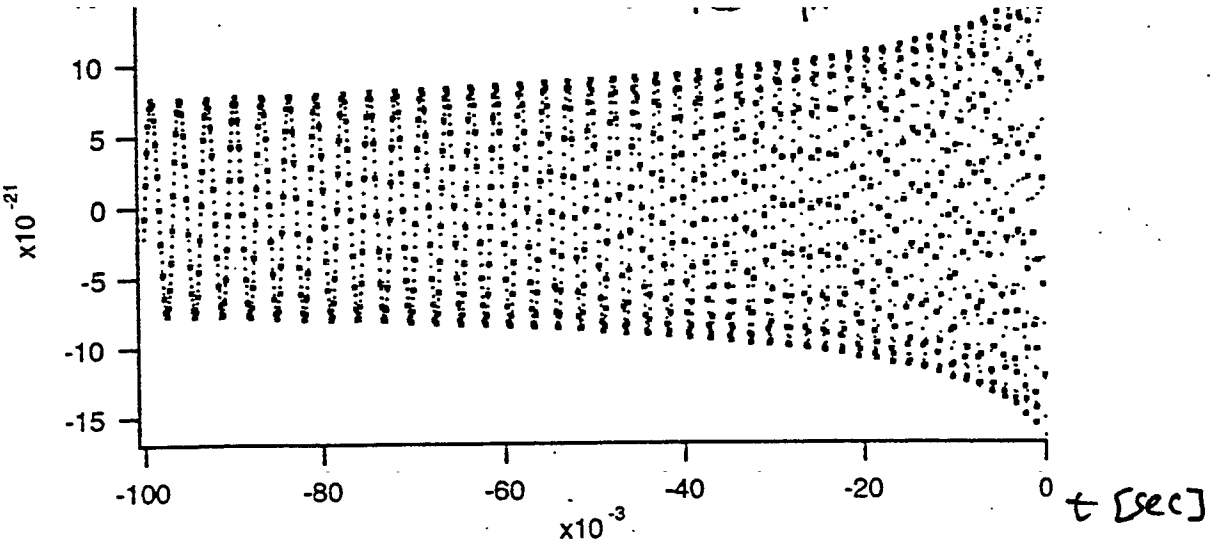
10
5
0
-5
-10
-15
x10^-21
-100
-80
-60
-40
-20
0
x10^-3
t [sec]

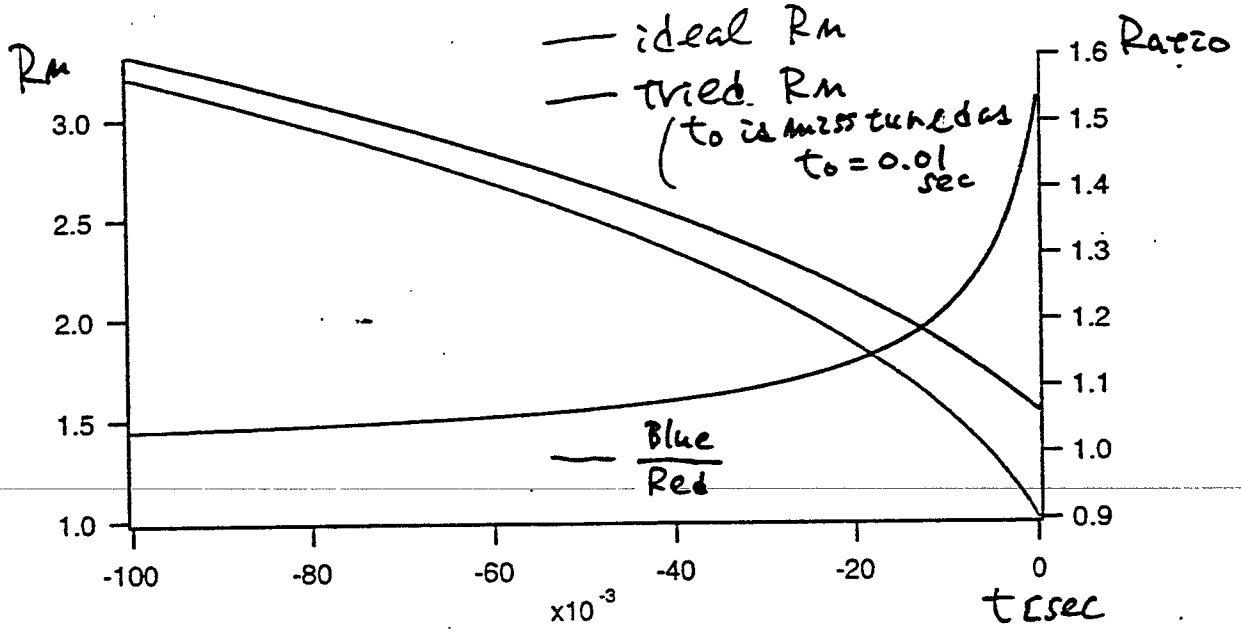
Rn
ideal Rn
tried Rn
(to is miss tuned as
to = 0.01 sec
Ratio
Blue / Red
3.0
2.5
2.0
1.5
1.0
1.6
1.5
1.4
1.3
1.2
1.1
1.0
0.9
-100
-80
-60
-40
-20
0
x10^-3
t [sec]

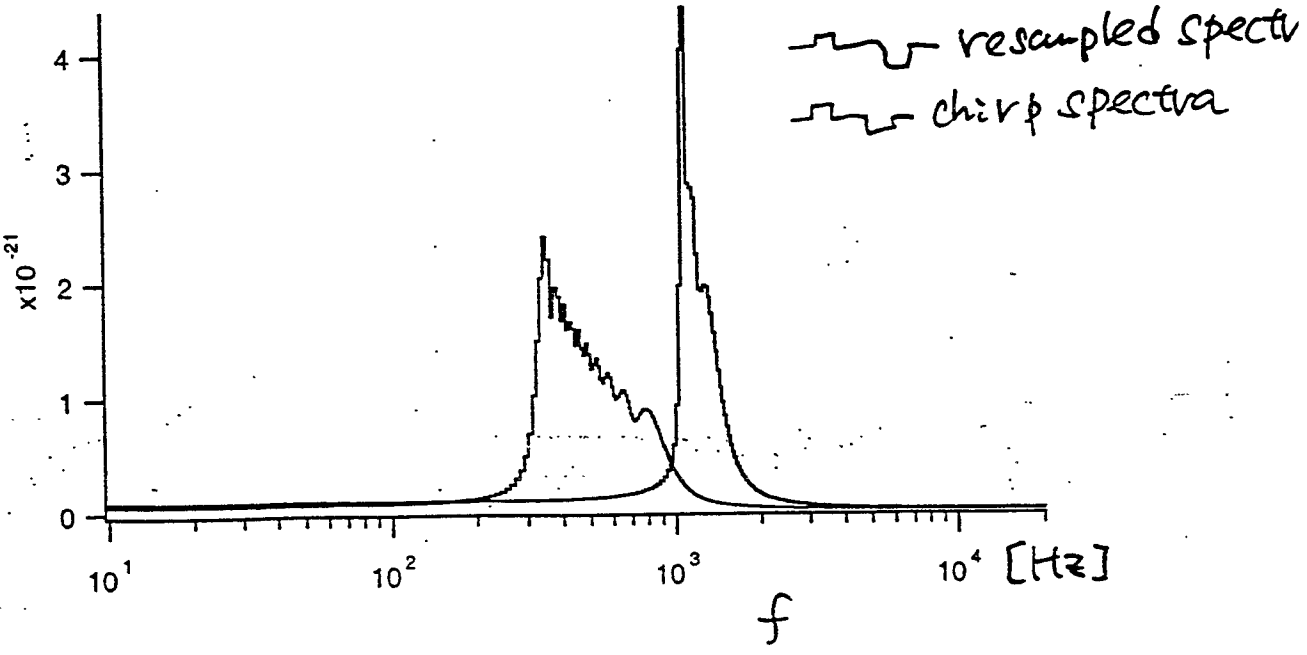
resampled spectra
chirp spectra
4
3
2
1
0
x10^-21
10^1
10^2
10^3
10^4 [Hz]
f

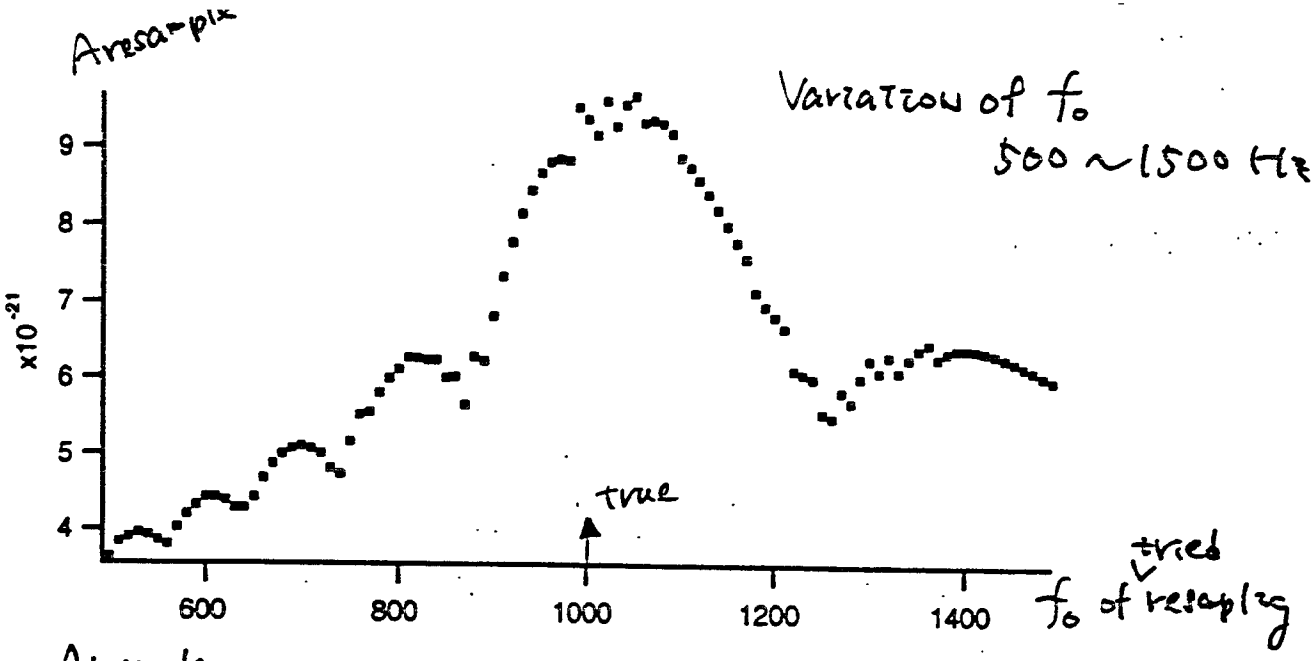
Aresample
Variation of f_0
500 ~ 1500 Hz
x10^-21
true
tried
f_0 of resampling

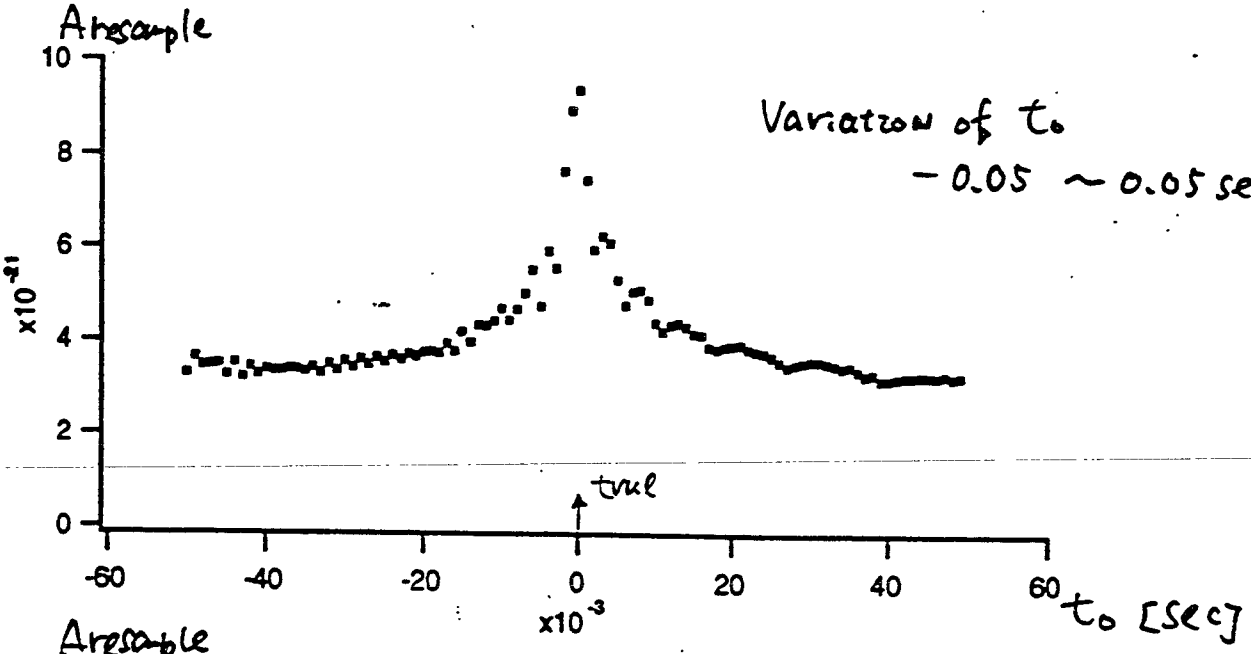
Aresample
Variation of t_0
-0.05 ~ 0.05 sec
x10^-21
true
x10^-3
t_0 [sec]

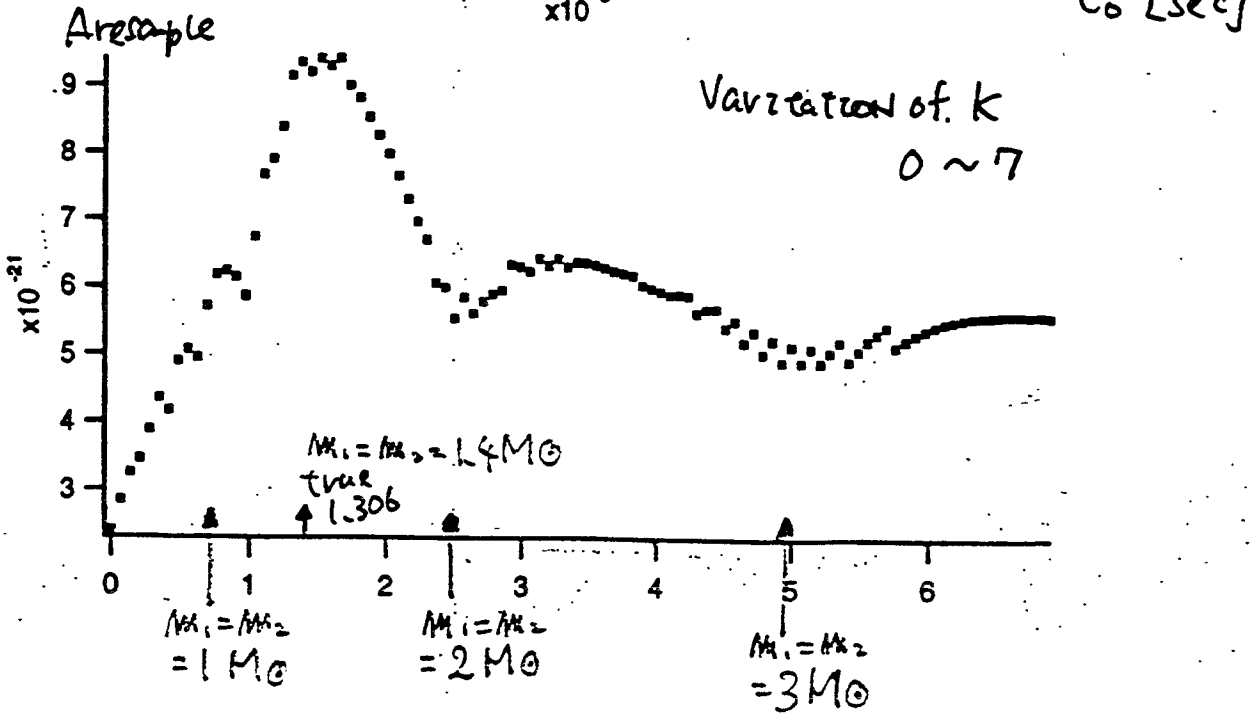
Aresample
Variation of k
0 ~ 7
x10^-21
$M_1 = M_2 = 1.4 M_\odot$
true
1.306
$M_1 = M_2$
$= 1 M_\odot$
$M_1 = M_2$
$= 2 M_\odot$
$M_1 = M_2$
$= 3 M_\odot$

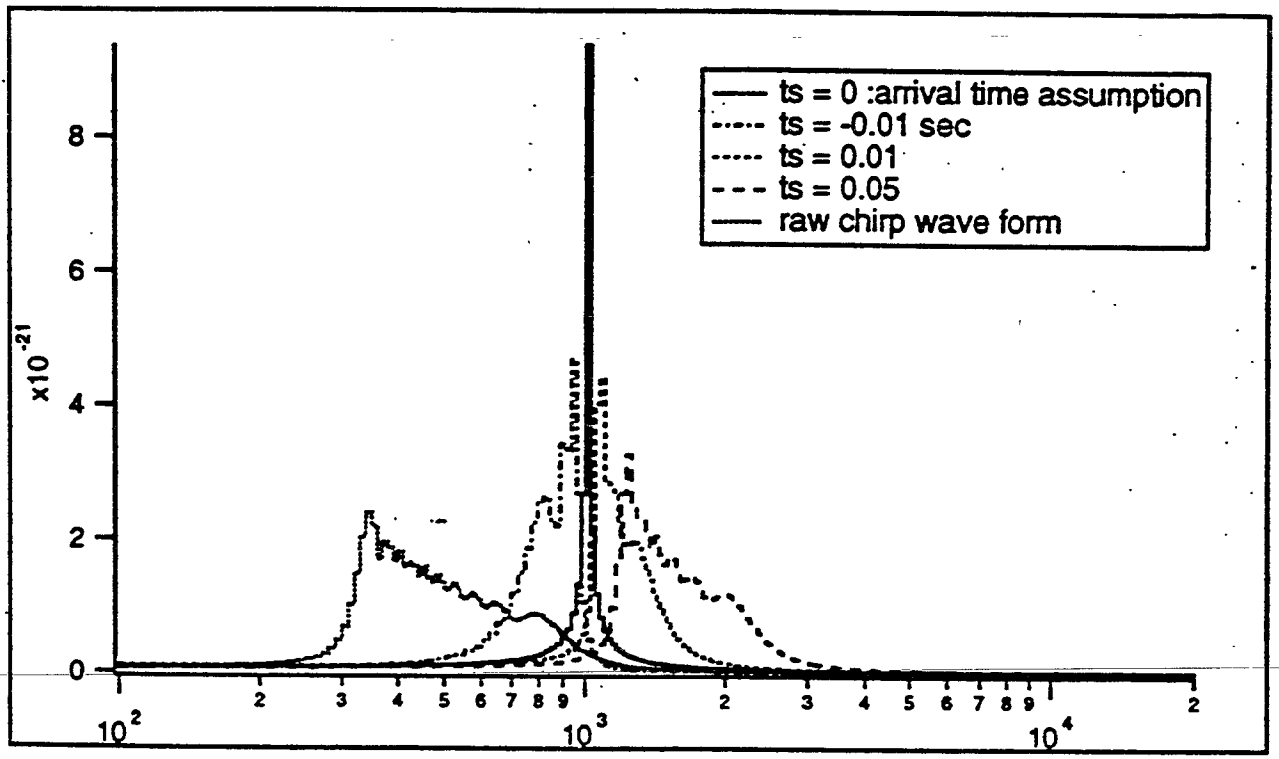
ts = 0 :arrival time assumption
ts = -0.01 sec
ts = 0.01
ts = 0.05
raw chirp wave form
x10^-21
8
6
4
2
0
10^2
10^3
10^4

.My guess are:

- reduce parameters (Only k is tuning parameter.)
- pipeline process for time domain signal

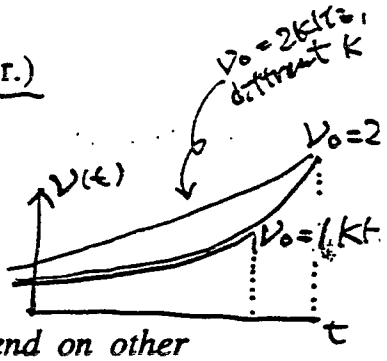

Why?

reason(1) $\frac{\dot{\nu}}{\nu} = 0.1248\ k\ \nu^{8/3}$

->$\dot{\nu}$ is decide with k and ν itself ! It is not depend on other parameters of chirp form.

reason(2)

In case of different ν_0 , however, if k is matched, resampling rate will match after t=0. (->SHOW analysis sample!)

Therefore, process time domain signal as pipeline with resampling variations according to k. No need to prepare for other parameters !

Benefit

- The signature is quite simple.
- The resampling is simple. Only variation of k is required.
- FFT can be done fast procedure.
- The process is lighter than Matched filtering.

(note)

$$h_+ = 0.5 \times (1+\cos^2\beta)\, h(t) \cos\phi(t)$$

$$h_\times = \cos\beta\, h(t) \sin\phi(t)$$

where

$$h(t) = 1.19 \times 10^{-22} \frac{k}{d} \nu(t)^{2/3}$$

$$\phi(t) = \phi_0 - \frac{8}{5} 2\pi\nu_0\tau\,(1-t/\tau)^{5/8}$$

$$\nu(t) = \nu_0(1-t/\tau)^{-3/8}$$

Ref: S.Bourzeix et al., Phys.Lett.A.151, 371(1990)

f_0. different template used....

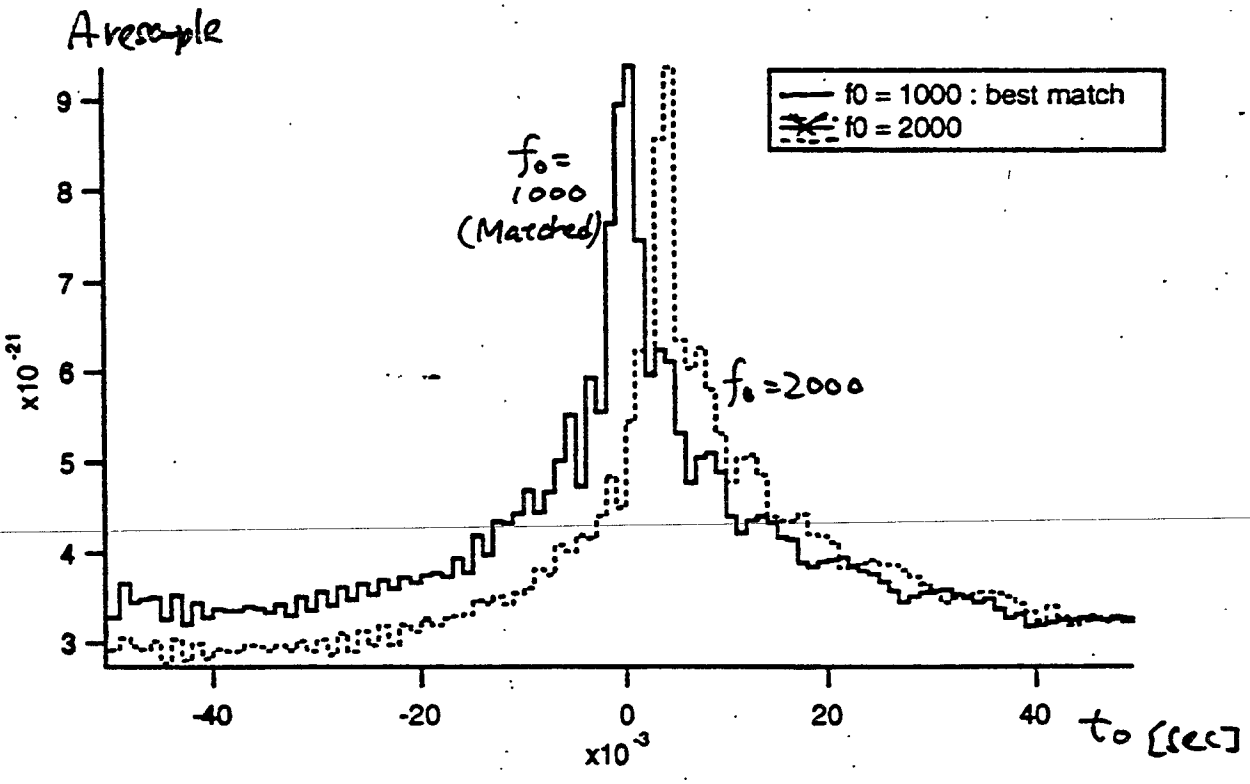

If K= Matched, we can get enough amplitude Aresample with different f_0.

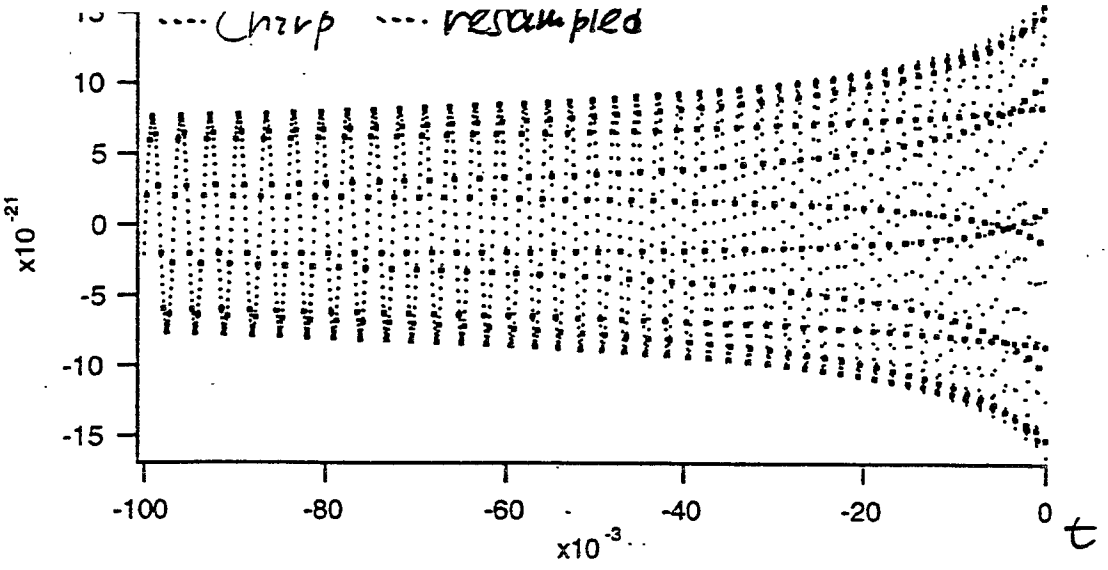
chirp
resampled
10
5
0
-5
-10
-15
x10^-21
-100
-80
-60
-40
-20
0
x10^-3
t

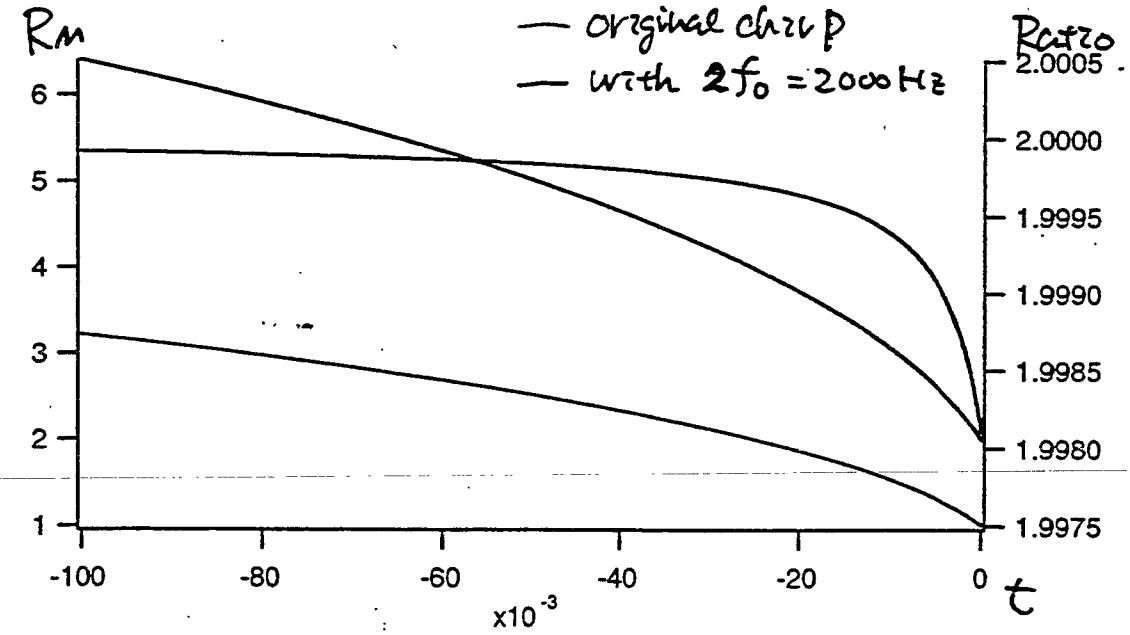
Rm
original chirp
with 2f0 = 2000Hz
Ratio
2.0005
2.0000
1.9995
1.9990
1.9985
1.9980
1.9975
6
5
4
3
2
1
-100
-80
-60
-40
-20
0
x10^-3
t

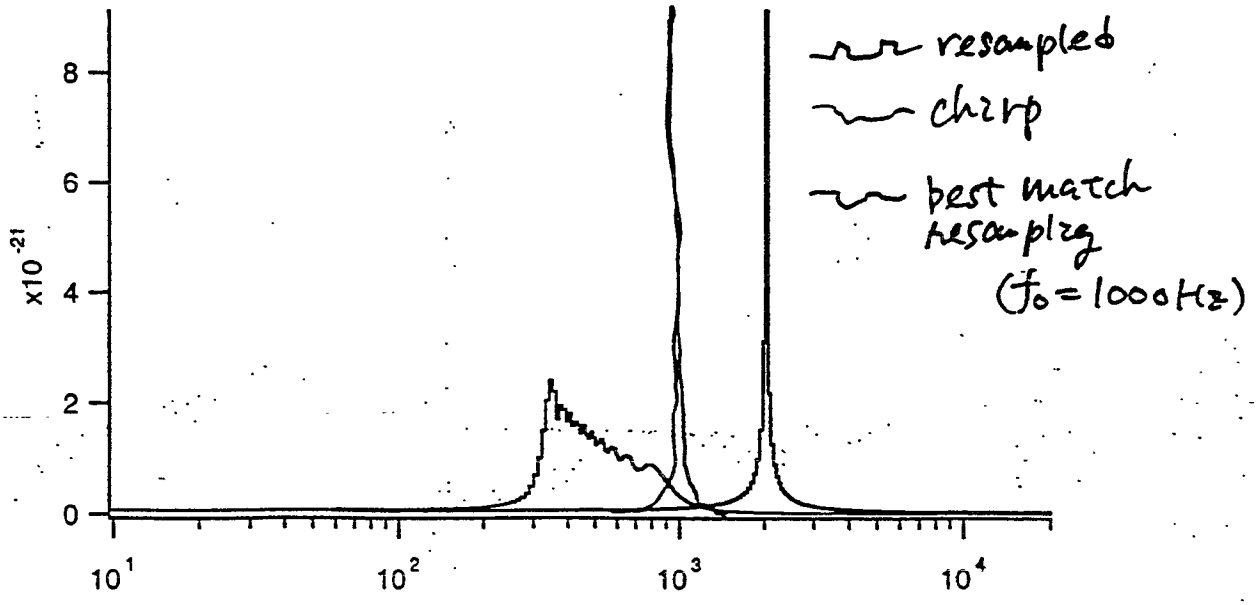
resampled
chirp
best match resampling
(f0 = 1000Hz)
8
6
4
2
0
x10^-21
10^1
10^2
10^3
10^4

2.2.Matched filtering

- (no need to explain...)
- Need large numbers of templates with parameters
- heavy calculations
- Require high performance of computing...
- (require much money also...)
- Need appropriate noise spectrum of interferometer

difficulty to keep optimal condition during long experiment period (= robustness require stable operation of interferometer)

3.for BURST from supernova explosions

3.1.Wide band strain mean

- Use h(ω) spectra in short time
- $\frac{h(\omega)}{\omega}$ > Threshold
- Take ω as wide range

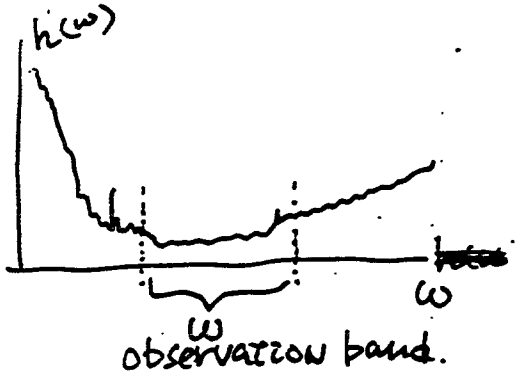

3.2.Narrow band strain

- Use h(ω) spectra in short time
- Choose several narrow frequency regions escape from noise spikes

1. • sum of ($h(\omega_i)$) > Threshold
2. • one of $h(\omega_i)$ >Threshold
3. • $h(\omega_i)$ >$Threshold_1$ and $h(\omega_2)$ >$Threshold_2$ and $h(\omega_3)$ >$Threshold_3$ and ....

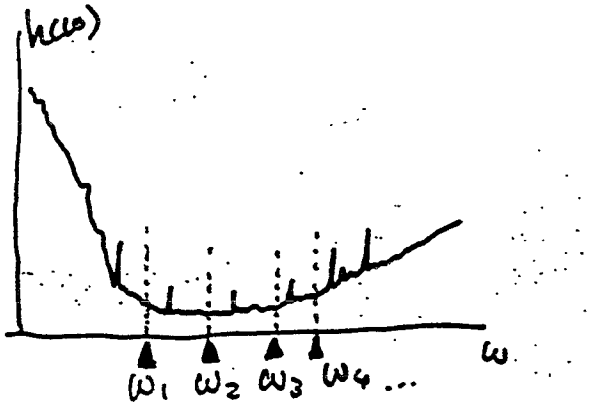

3.3.Phase sensitive process in narrow band

.Requirement !

- At ω_0, thermal noise of pendulum or of test mass internal is dominant in noise spectral density.

  -> remove electrical noise at ω_0

- If thermal noise is dominant, the noise has a coherence due to high Q of pendulum or of mass.

  <- as a resonant mass detector

.How to do?

- Extract time-domain signal on w_0 with narrow band pass
- Process signal into complex form with reference signal. (as lock-in amplifier)

  -> $Z(t) = X(t) + i\,Y(t)$ $\propto h(\omega_0)$

- Calculate "phase/amplitude jump" in complex

  $\Delta Z(t) = |Z(t+\Delta t) - Z(t)|$ $\propto Z \times \frac{\Delta t}{2}$

- Chose optimal Δt
- $\Delta Z(t)$ > Threshold

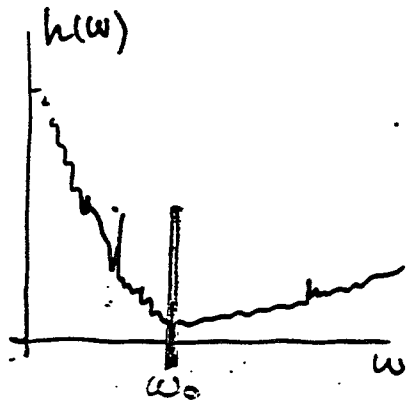

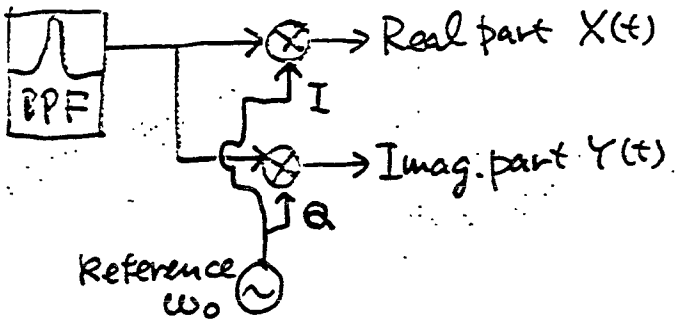

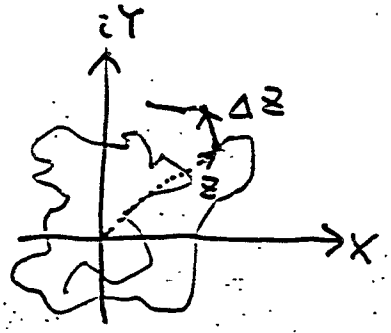

(多摩300)

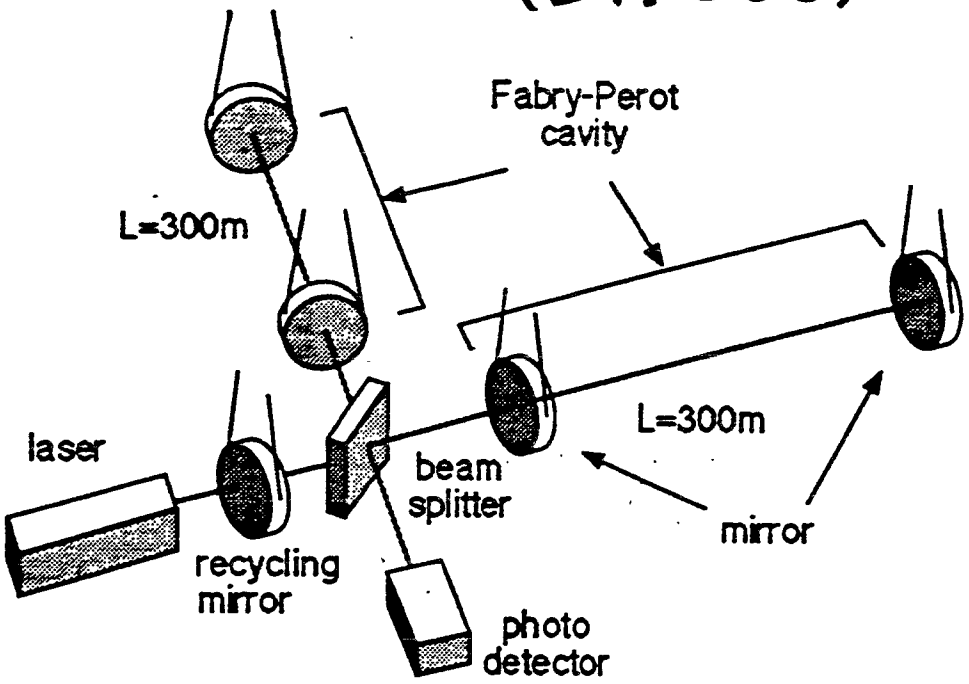

図 1: 日本のTAMA300プロジェクト. 300m基線長レーザー干渉計の概念デザインを示す.

finish to construction

国	プロジェクト名	設置場所	タイプ、基線長	完成予定
アメリカ	LIGO	Hanford(Washington) Livingston(Louisiana)	FP 4km(2基)	2000
イタリア/フランス	VIRGO	Pisa(Italy)	FP 3km	1999
ドイツ/イギリス	GEO	Hannover(Germany)	DR 600m	1998
日本	TAMA	三鷹 MITAKA	FP 300m	1998

表 1: 世界で現在進行中の大型レーザー干渉計計画(FP:Fabry Perot, DR:Dual Recycling)

目標感度	$h_{\min} = 3 \times 10^{-21}$@300Hz (帯域幅300Hz)
干渉計タイプ	Fabry-Perot-Michelson
基線長	300m
ファブリー・ペロー共振器フィネス	520
光源 laser	注入同期方式Nd:YAGレーザー、出力 10W、波長 1064nm power λ
パワーリサイクリング Recycling	利得10倍 (干渉計入力実効パワー 30W) gain10
真空容器内真空度	10^{-6} Pa
真空パイプ直径	40cm

表 2: TAMA300 レーザー干渉計の基本仕様

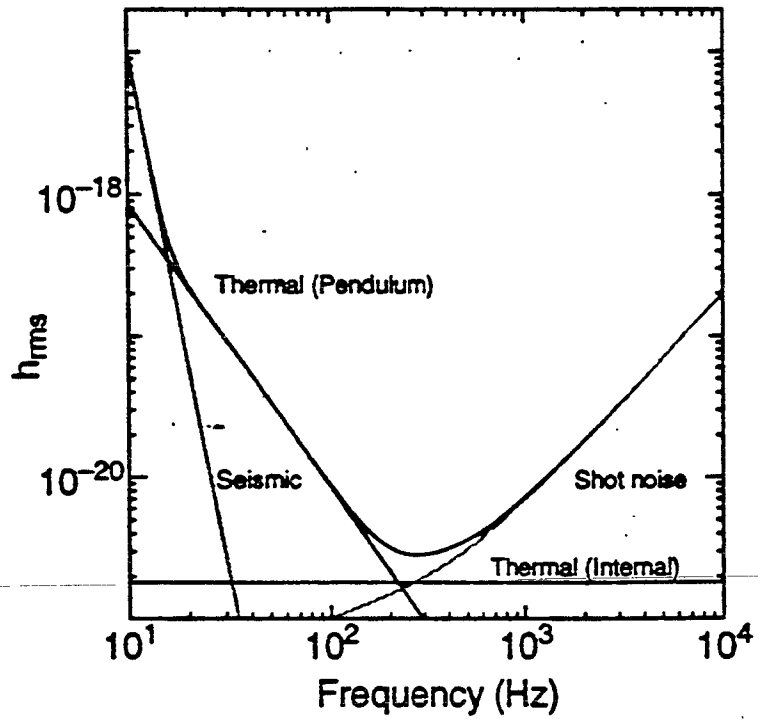

図 2: TAMA300で予想される感度曲線.

2 Design

次に干渉計の各部分のデザインについて説明する.

2.1 光学デザイン

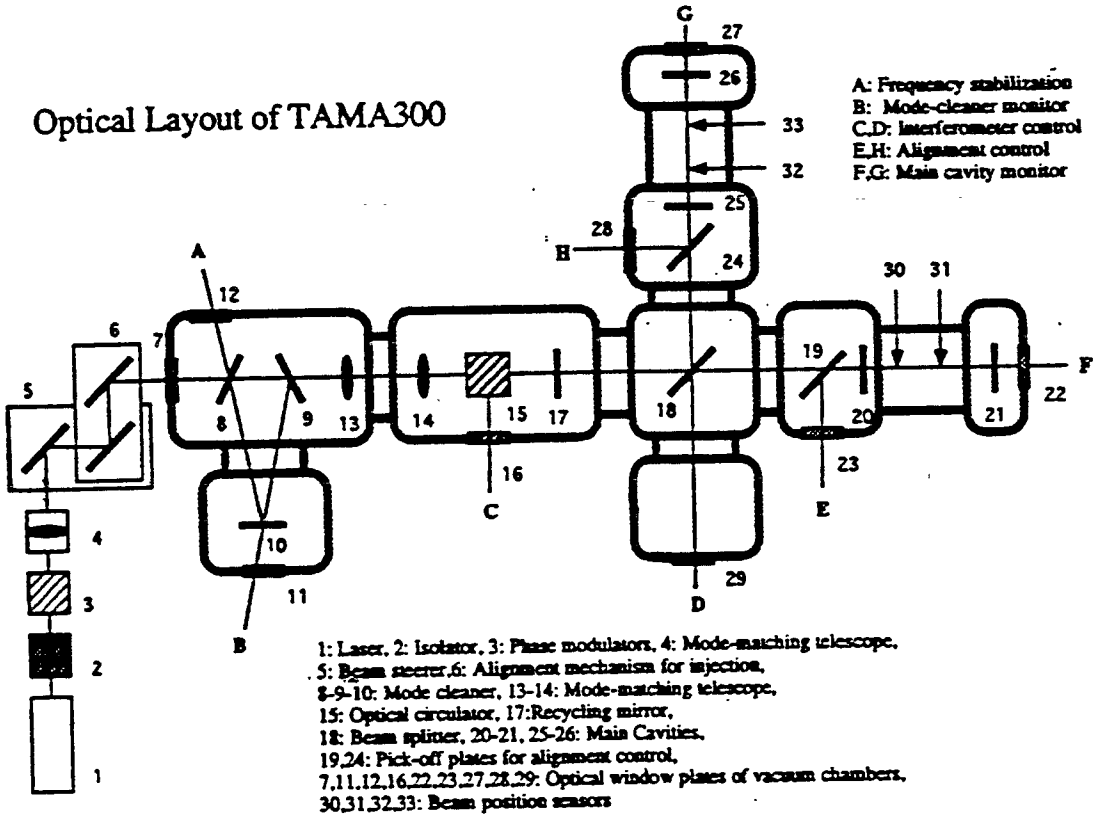

図 3: TAMA300の基本光学デザイン.

光学デザインは次の制御系デザインとともに干渉計の根幹をなすものである. 図3には干渉計全体の基本的な光学系デザインが描かれている. あらかじめ周波数安定化が施されたレーザー出力はEOM(Electoro-Optical Modulator)により15.25MHzの変調がかけられる. その後入射光のパラメータを調整するためのレンズ類を通過した後、モードクリーナーとよばれるリング型の光共振器に入射される. モードクリーナーを出た光はもう一度モードマッチングのためのレンズをとおり、リサイクリングミラーから干渉計本体に入射する. ビームスプリッターによって2つに分けられた光はそれぞれ300m長さのファブリー・ペロー共振器に入射されるが、ビームスプリッターとそれぞれのファブリー・ペロー共振器の手前のミラーの間の距離は両方向で50cmの差がある. これはpre-modulationというテクニックであり、2つの腕からの反射光が干渉するさい、先ほど述べた15.25MHzの変調が残るようにするためのものである. この変調を利用することにより信号の復調が可能となる. それぞれのファブリー・ペロー共振器の手前には反射光を一部抜き取るピックオフとよばれるプレートがある. これは光ビームとミラーの間のアライメントの情報を取り出すために使われる.

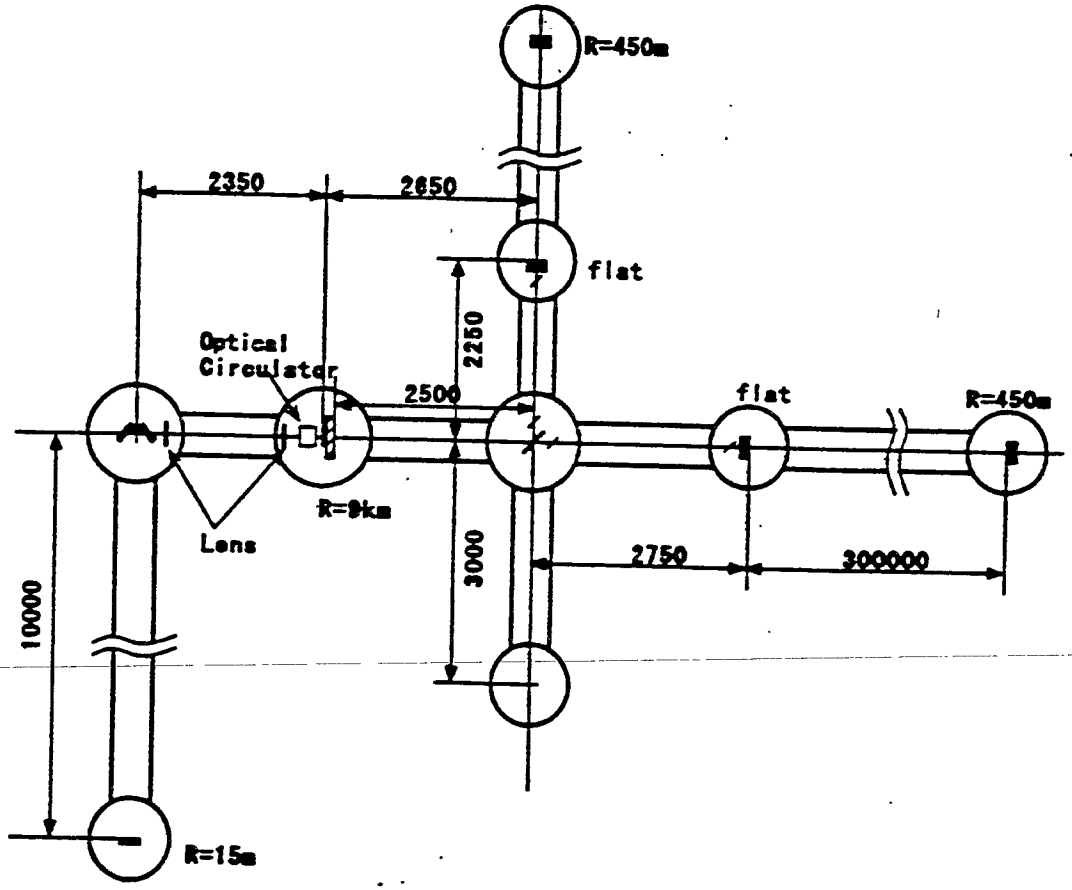

図 4: TAMA300の光学デザイン.

2.2 制御デザイン

干渉計の制御は大きく分けて3つの部分に分かれる．ひとつはフリンジ制御とよばれる干渉縞の制御であり、ミラーの光軸方向の位置を調整する．ふたつめはビームアライメントであり、この場合は光ビーム軸方向に対してミラーの姿勢を制御する．3つ目はパワーリサイクリングのための制御である．

2.2.1 フリンジコントロール

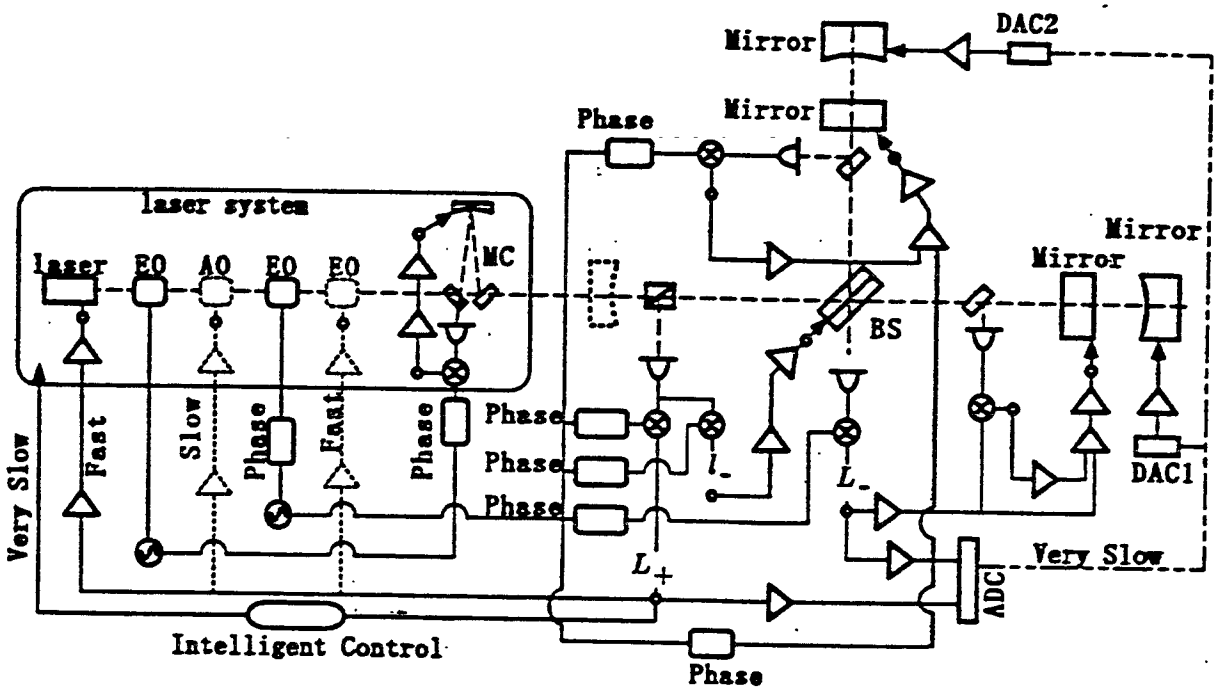

図 6: TAMA300の基本制御デザイン．

まずフリンジ制御について説明する．各ミラーの光軸方向の位置制御の問題である．300m基線長は長時間の間には温度変化や潮汐効果などにより距離が変化する．この大きさは最大2mm程度と見積もられるが、2枚のミラーの位置を制御することによりこれを補正する必要がある．これはゆっくりした距離の変化であるが、干渉縞を常にダーク（暗縞）に保つには速い変化も抑え込む必要がある．この速い制御については、ミラーの後に貼り付けた磁石とコイルをアクチュエーターとして用いる．フリンジ制御を考えるとき、2つのファブリー・ペロー共振器の同相変化(L_+)と差動変化(L_-)およびファブリー・ペロー共振器の手前のミラーが作るマイケルソン干渉計の同相変化(l_+)と差動変化(l_-)の4つの独立自由度に対する制御と考えた方がわかりやすい．これをブロックダイアグラムの形で表したのが図6である．重力波信号が含まれているのはL_-の信号の中であり、ミラーに対する制御信号から取り出すことができる．

2.2.2 アライメントコントロール

ビームアライメントに関してはwave front sensing法という方法を用いる．これはファブリー・ペロー共振器からの反射波をピックオフで一部取り出し、その反射光の光路上の適当な位置に4分割の光検出器を置き、変調周波数(15.25MHz)と同じ周波数で復調することにより、2枚のミラーの傾き（あおり(pitch)と横回転(yaw)）に関する情報を独立に抜き出す方法である．この信号を適当に処理してミラーの懸架部分の

	diameter (mm)	thickness (mm)	curvature (m)	reflectivity (%)	trans.	injection angle	wedge	pol.	N
300mFP front	100	60	flat	98.80		0	1′		2
300mFP end	100	60	450±25	≥ 99.99	≥ 60ppm	0	1°		2
300mFP BS	150	40	flat	50±0.1		45°		S	1
10m ring MC near	100	30	flat	99.82 ± 0.05		45°		S	2
10m ring MC far	100	60	15 ± 1	≥ 99.99	≥ 60ppm	0			1
recycling mirror	100	60	9,000	96.67		0			1

Mirror Specs.

表 3: TAMA300 ミラー仕様

3.7.5 コーティング

ミラーで最も重要なのがコーティングである．FP 共振器の性能はコーティングで決まると言っても過言ではない．まず、2つのFPのフィネス（反射率）を揃えるためには、非常に良く制御された成膜が必要である．特にエンドミラーに関してはなるべく高い反射率が要求されるので、これは損失の問題に直結している．例えば損失が10ppmあると、可能な最高反射率は99.99950ppm以下という仕様になる．ニアミラーの場合は反射率は低いのだが、レーザーパワーを有効に使うために、やはり低損失であることが要求される．共振器中では等価的に光パワーはフィネス倍になるので、50ppmといっても、そこで発生する熱はかなり大きい．この熱によりミラー基材が変形してレンズのようになるので、熱膨張率が小さく、熱伝導率が大きい素材を選ぶことが大事である．この点に関しては合成石英はあまり良い素材とは言えないので、損失は低ければ低いほど良いことになる．このようなコーティングはIom Beam Sputter法で唯一可能であり、直径1cm程度の小さなサンプルでは1ppmのオーダーの吸収損失が報告されている．TAMAミラーのコーティングはそのような技術を持つ日本航空電子に発注される．

以上の検討により、表3のような仕様が決められた．

3.8 テストマス懸架

ミラーなどのテストマスを懸架する部分のデザインは制御性、防振特性、熱雑音などを考慮して決められる．基本的なデザインはミラーを2重振り子で懸架し、光軸方向の並進以外は振り子の支点で制御するというものである．2重振り子の上側のマスのまわりには強力な永久磁石が配置されていてeddy currentの効果により振り子の振動に制動がかかる．これにより通常行われるローカルコントロールといわれる制御系が不要になり、大幅にデザインが簡素化され信頼性が向上する．防振特性も単振り子に比べて向上するはずであるが、縦方向の振動が横方向に結合する効果が比較的大きいためこれを軽減する対策が必要となる．振り子の支点にはXYZ方向および2つの回転方向を制御するためのアクチュエーターが取り付けられている．粗調にはピコモーターという電動マイクロメータを用い、微調のためにはPZT（圧電素子）を併用する．熱雑音の効果としては振り子運動にともなうものと、ミラーの弾性体としての固有振動にともなう熱振動がある．振り子運動は周期1秒程度であるが、その熱雑音のスペクトルの裾である300Hz周辺の成分が雑音に寄与する．同様にミラーの内部モードは共振周波数が30kHz以上であるが、スペクトルの低周波数部分が効いてくる．振り子のQ値としては10^5以上、内部モードのQ値は10^7以上が要求される．

Vibration Isolation System for the 300m Interferometer

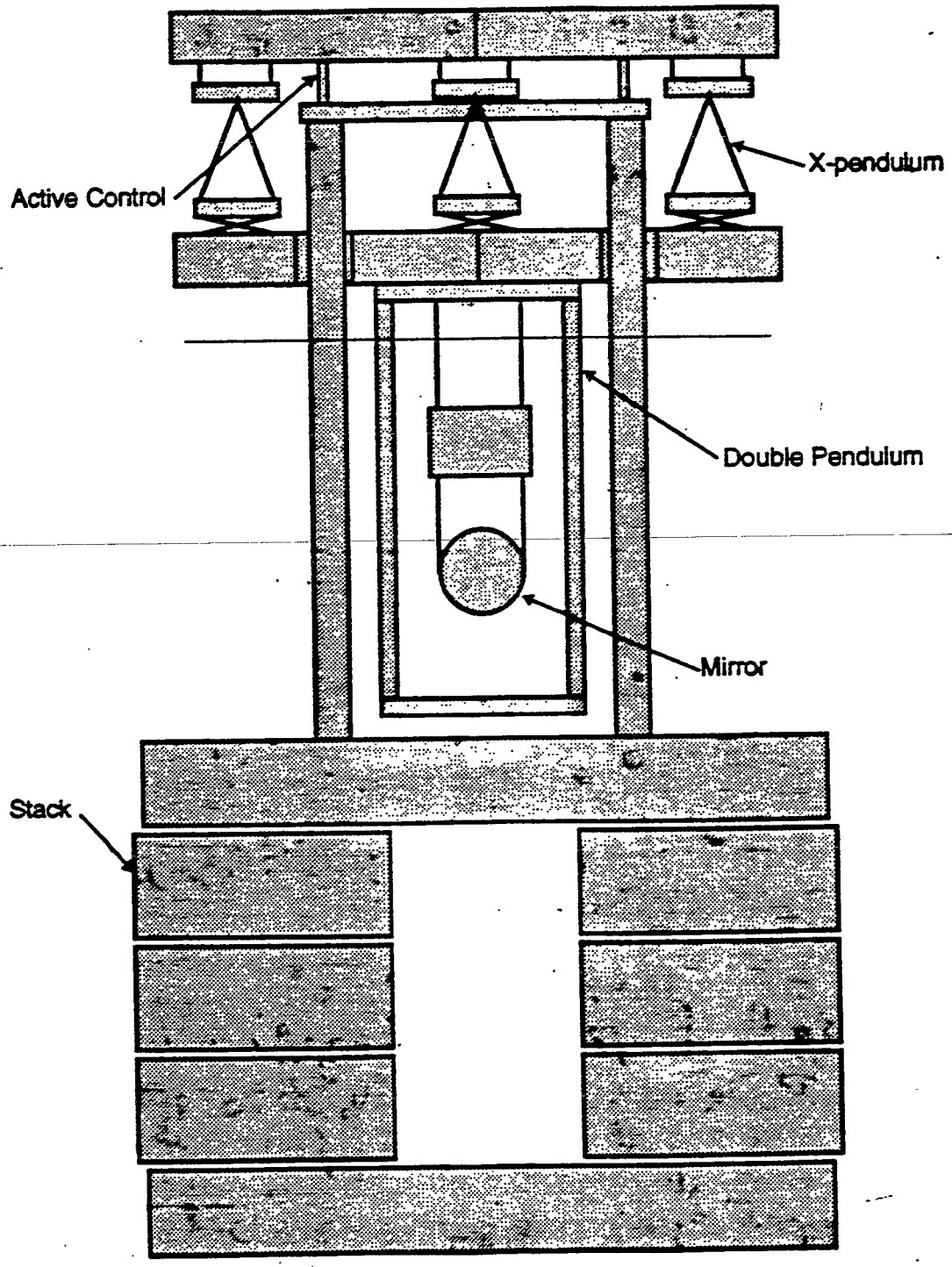

図 18: ミラー懸架を含む防振系全体.

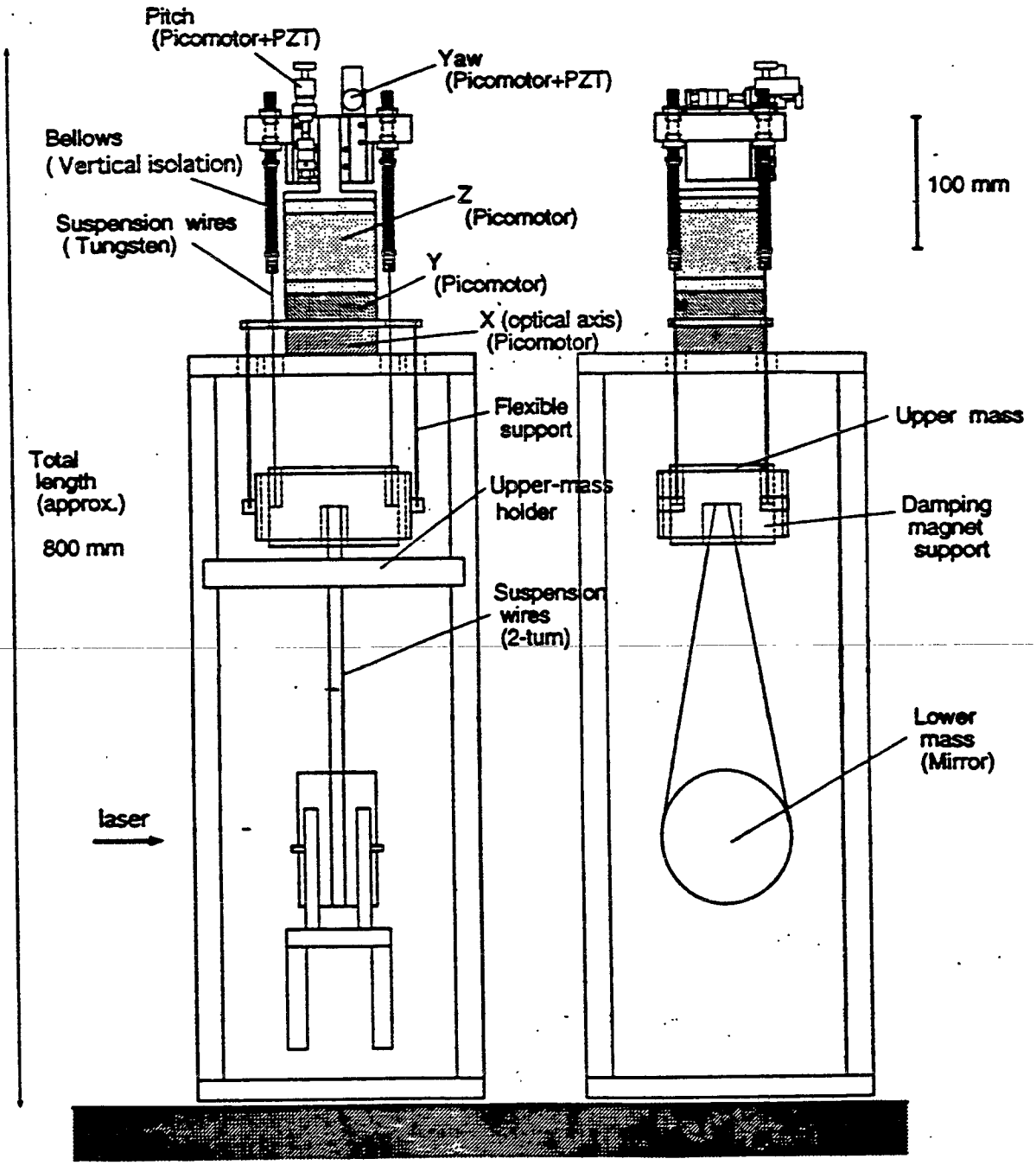

Preliminary Suspension Design for TAMA300

図 13: ミラー懸架システム.

図 14: スタック配置系.

Data Flow of TAMA 300

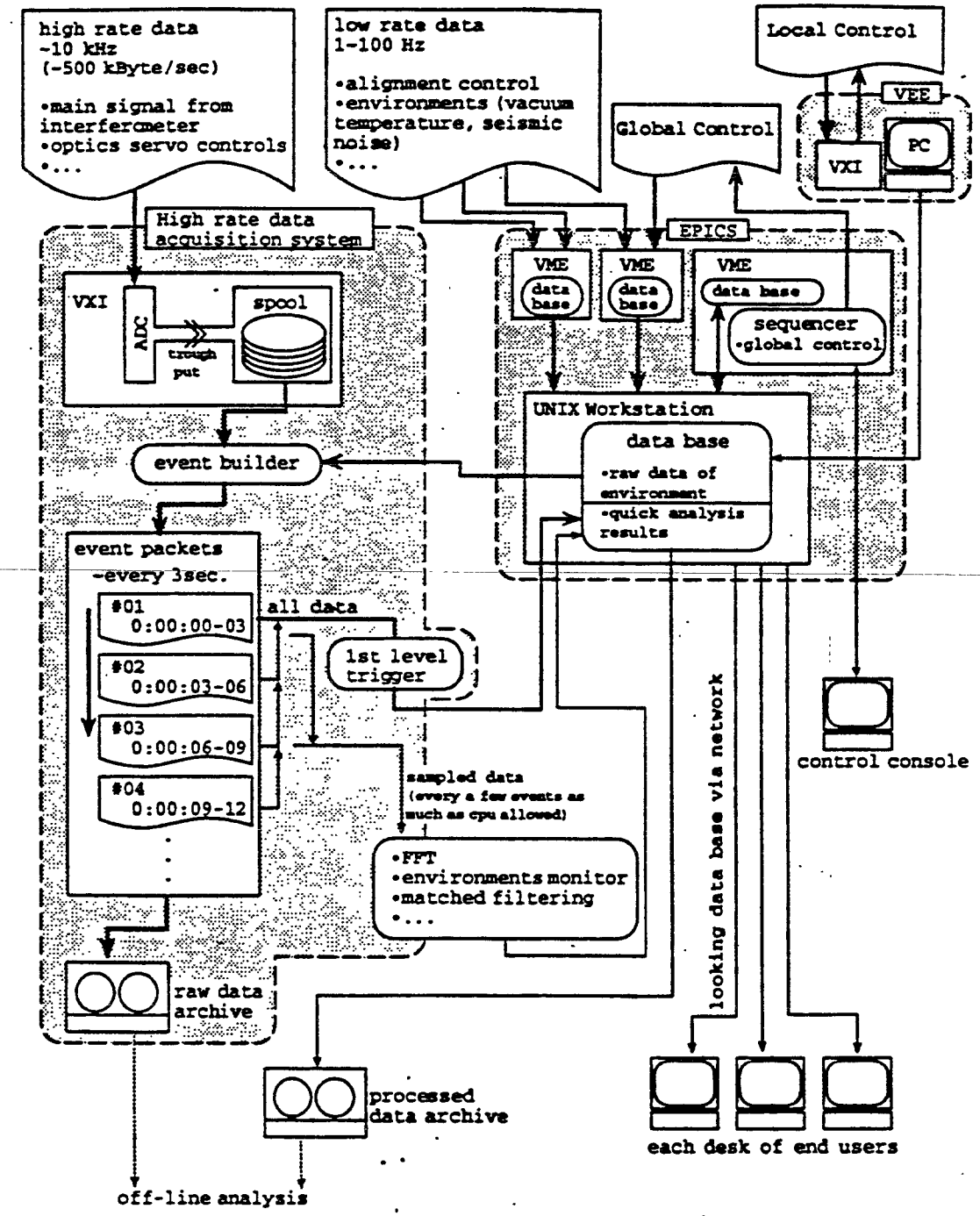

図 20: TAMA300のデータ流れを示す図.

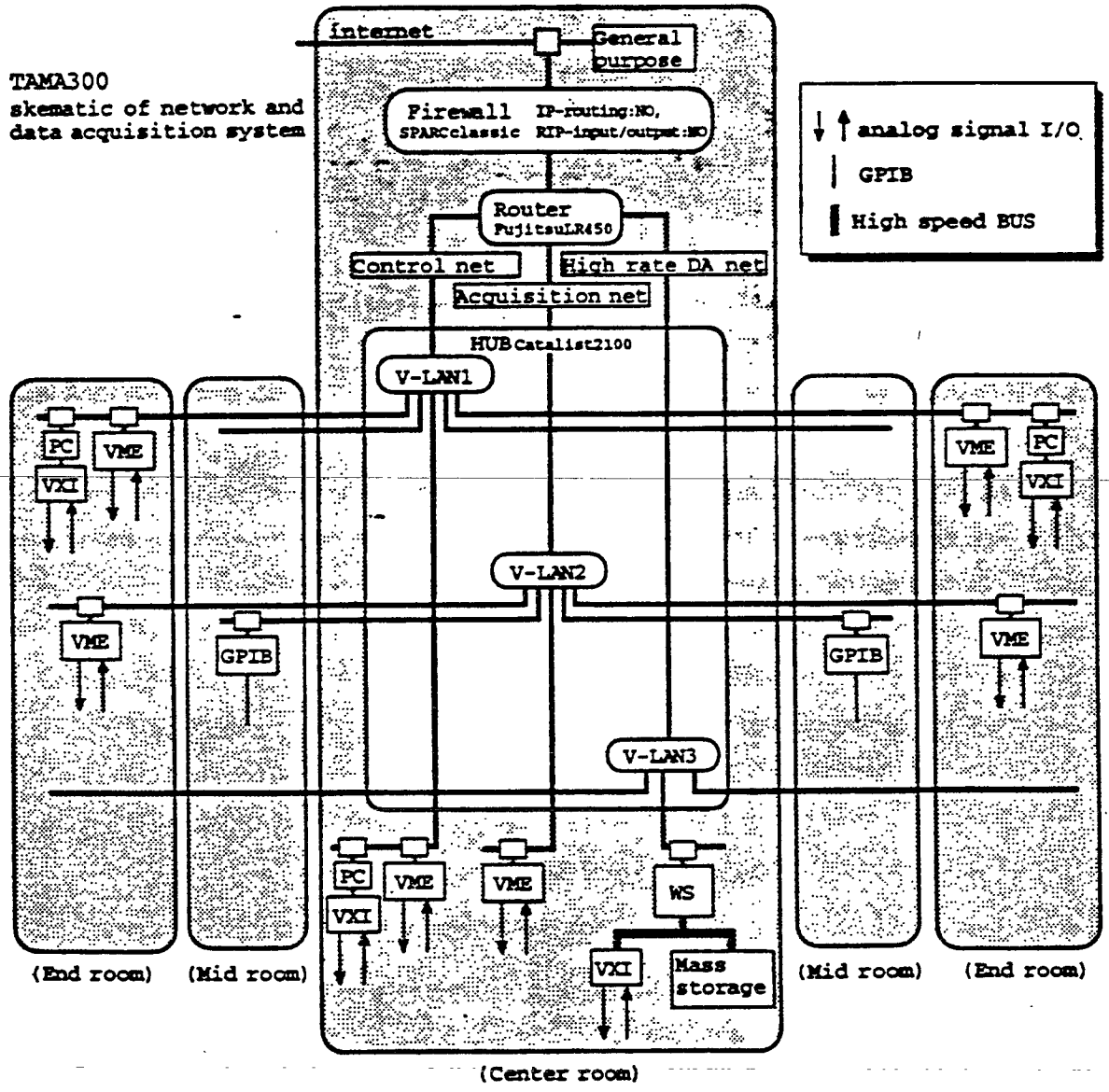

図 19: TAMA300 ネットワークシステム概念図.

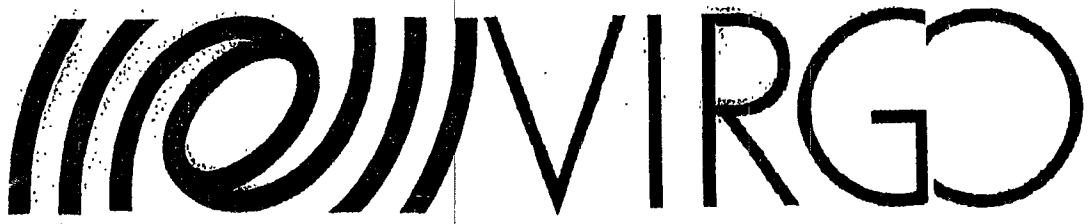

STATUS OF THE VIRGO PROJECT

Fulvio Ricci
University of Rome La Sapienza and INFN Roma 1

GRAVITATIONAL WAVE DATA ANALYSIS WORKSHOP
M.I.T. DEC. 1996

VIRGO

Fabry-Perot	L= 3 km
Band width	$\Delta\nu$= 4 Hz - 6 kHz
Cavity finesse	F= 50
Power Recycling	R= 50
Nd-YAG Laser	W= 20 w
Vacuum Pipe	Φ =1.2 m
Tube vacuum pressure	p= 10^{-8} mbar
N. of baffles	220

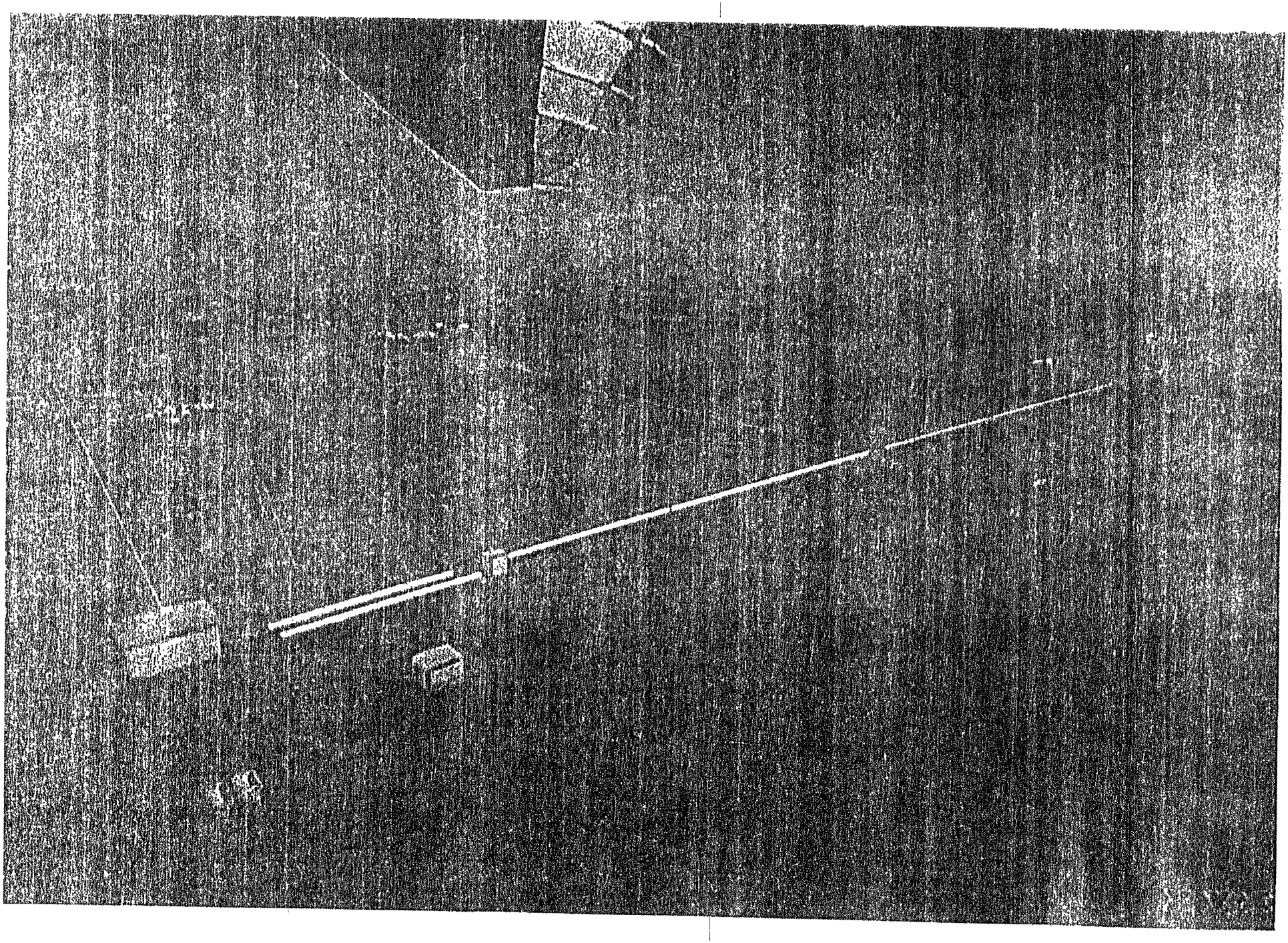

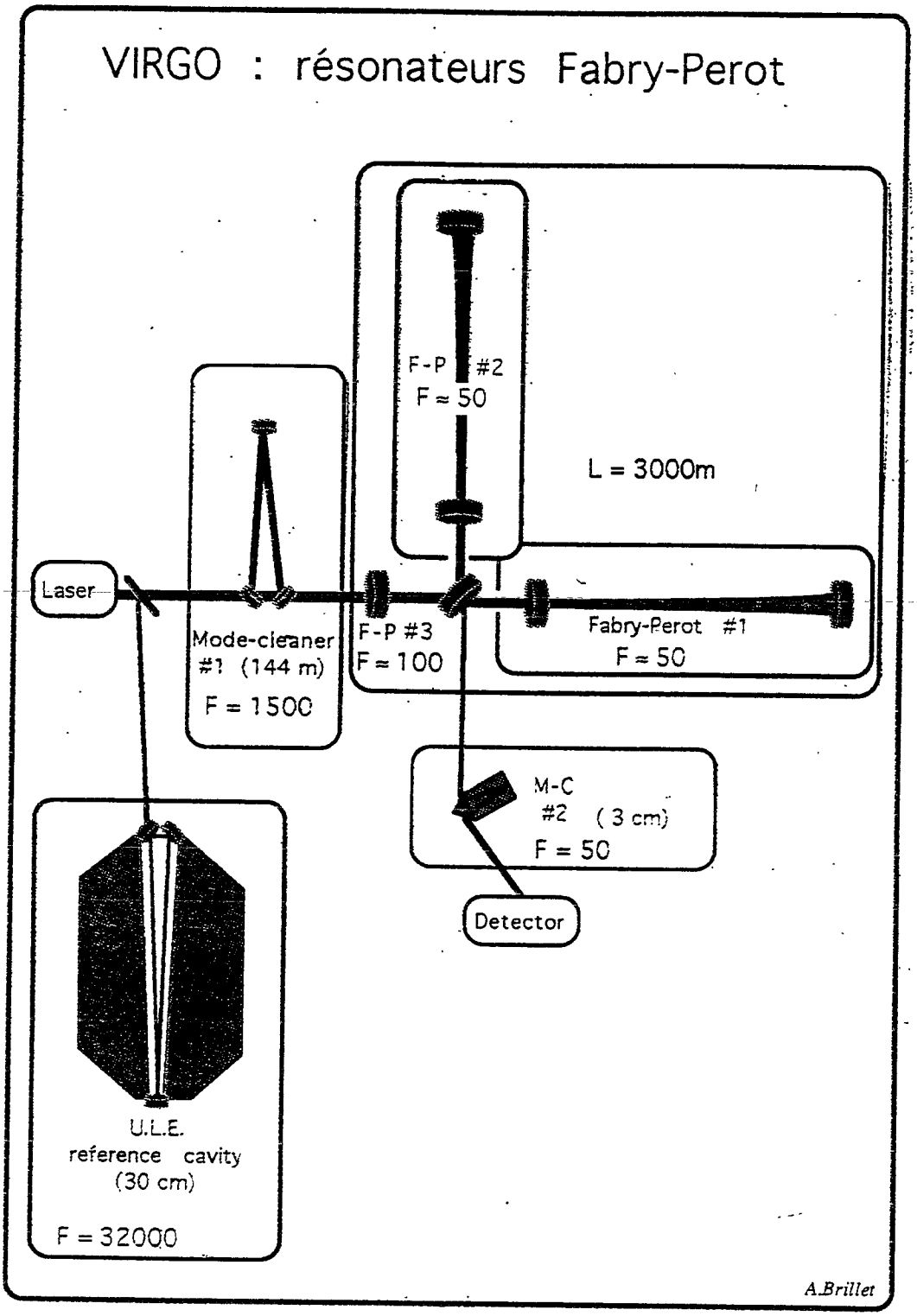
VIRGO : résonateurs Fabry-Perot
F-P #2
F ≈ 50
L = 3000m
Laser
Mode-cleaner
#1 (144 m)
F = 1500
F-P #3
F ≈ 100
Fabry-Perot #1
F ≈ 50
M-C
#2 (3 cm)
F = 50
Detector
U.L.E.
reference cavity
(30 cm)
F = 32000
A.Brillet

The 98' Interferometer

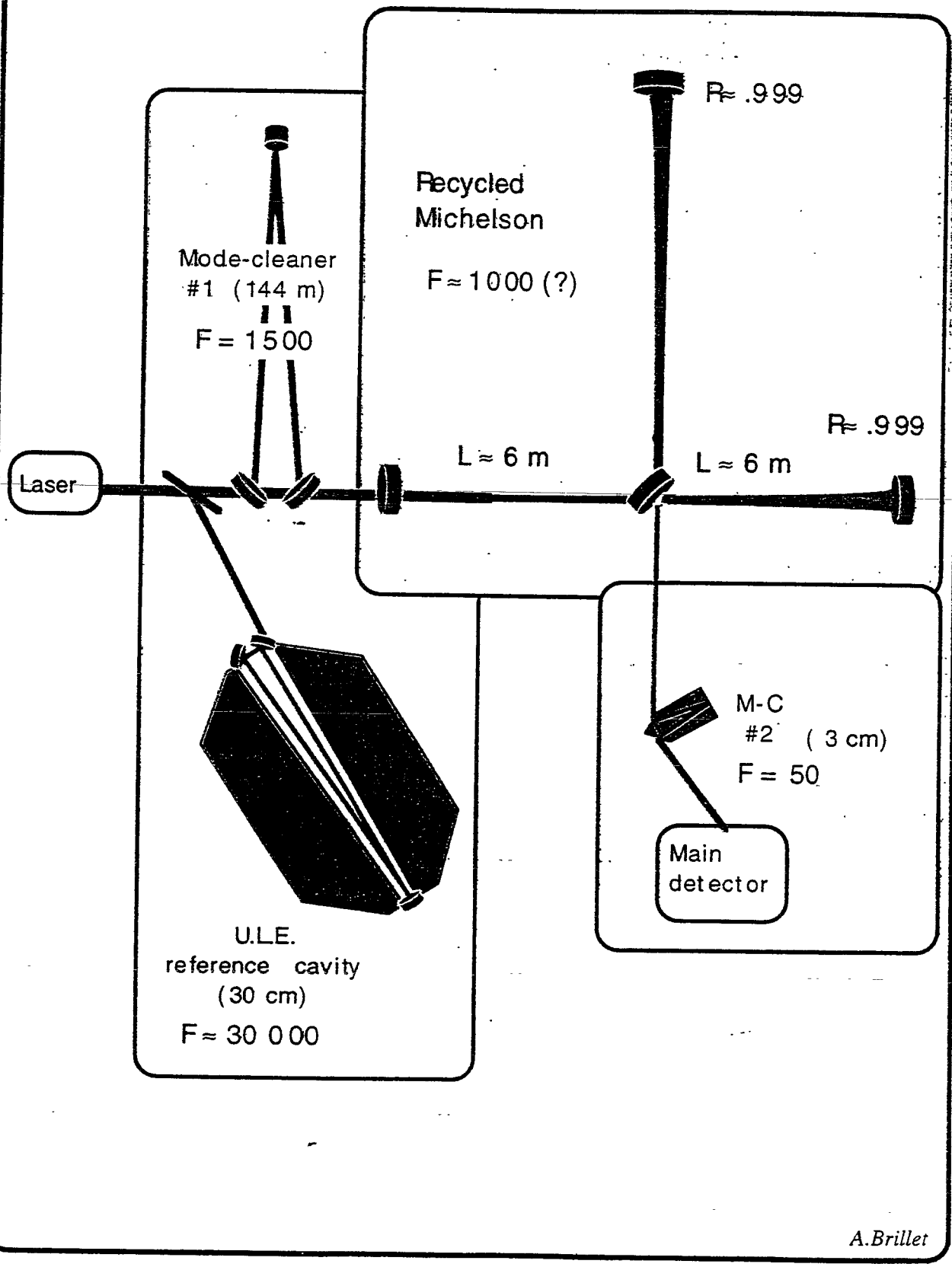

A.Brillet

- Construction started , April 1996
- Site available, August 1996
- Central buildings available, June 1997
- Test interferometer, End 1998
- End of construction Mid 2001
-
- Remarks planning is constrained by budget issues

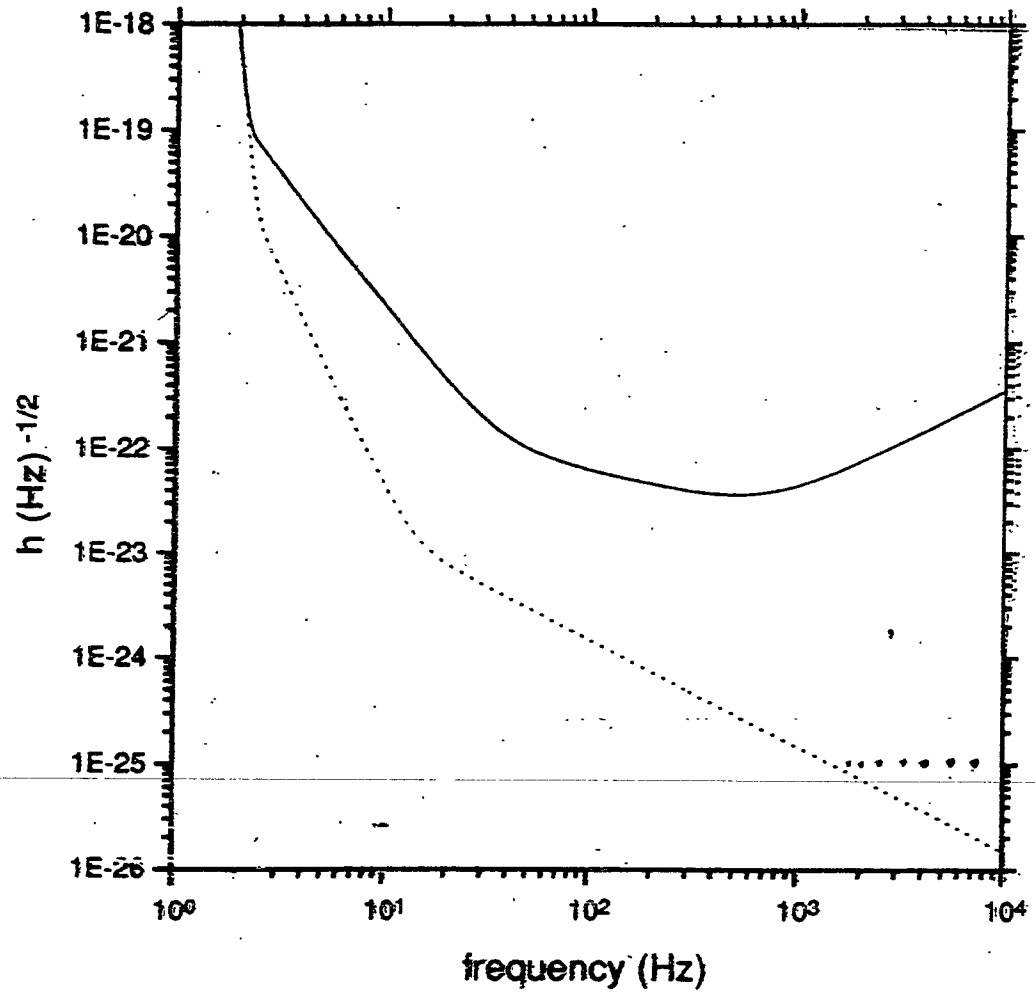

VIRGO → FEW EVENTS / YEAR (BINARIES)

ULTIMATE SENSITIVITY → 50 000 EVENTS / YEAR

Signal detection and ITF locking

Many PD ; 16 bit ADC sampled at 100 KHz for high dynamical range (10+7) ADC resampled at 20 KHz, the FB loop bandwidth. These signals are sent to the suspension control CPU by means of DOL.

Signal	# of chanels	rate	bits
Longitudinal photo. signals(5 signalsx3)	15	20KHz	16
longitudinal feedback (5 mirrors+laser)	6	20KHz	16
Alignment signal (2x4 quadrant diodes)	16	1KHz	16
Alignment data (5mirrors x 2corrections)	10	1KHz	16
Laser power&frequency	2	20KHz	16
Mode cleaner locking (signal + correction)	2	20KHz	16
Mode cleaner alignment	8	1KHz	16
Seismic noise (6 per tower)	6x9	100Hz	16
Acoustic noise (one per building)	4	20KHz	8
elec. mag. noise (one per building)	4	20KHz	8
Line voltage (one per building)	4	20KHz	8

DATA STORAGE

Raw Data	Triggered Data
~ 2 Mbyte/s	~ 10 Kbyte/s

1) Raw data (6.10+4 Gbyte/year)possible storage on DAT (4 Gbyte):
   -300 Kbyte/s, 15000 cassettes/year
   -cost/cassette 12 ECU,
   -Total cost/year 180 KECU
   -Total volume/year 1 m3

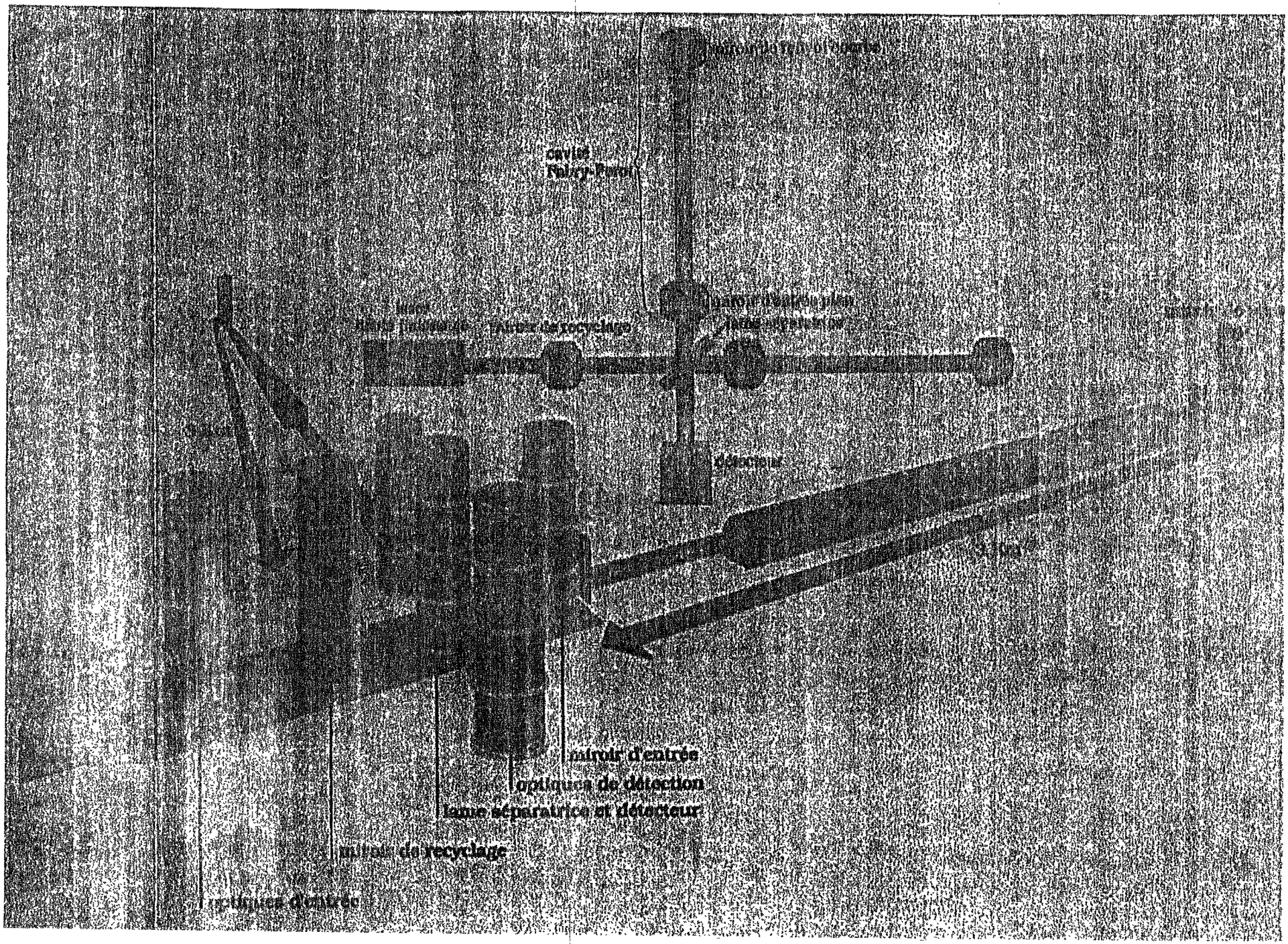
cavité
Fabry-Perot
miroir d'entrée
optiques de détection
lame séparatrice et détecteur
miroir de recyclage
optiques d'entrée

Electronics

- Architecture is defined
- Standardization effort

Control

- Totally digital
  (except for the fast laser control)

Data Management

- Data format
- Acquisition and storage prototype

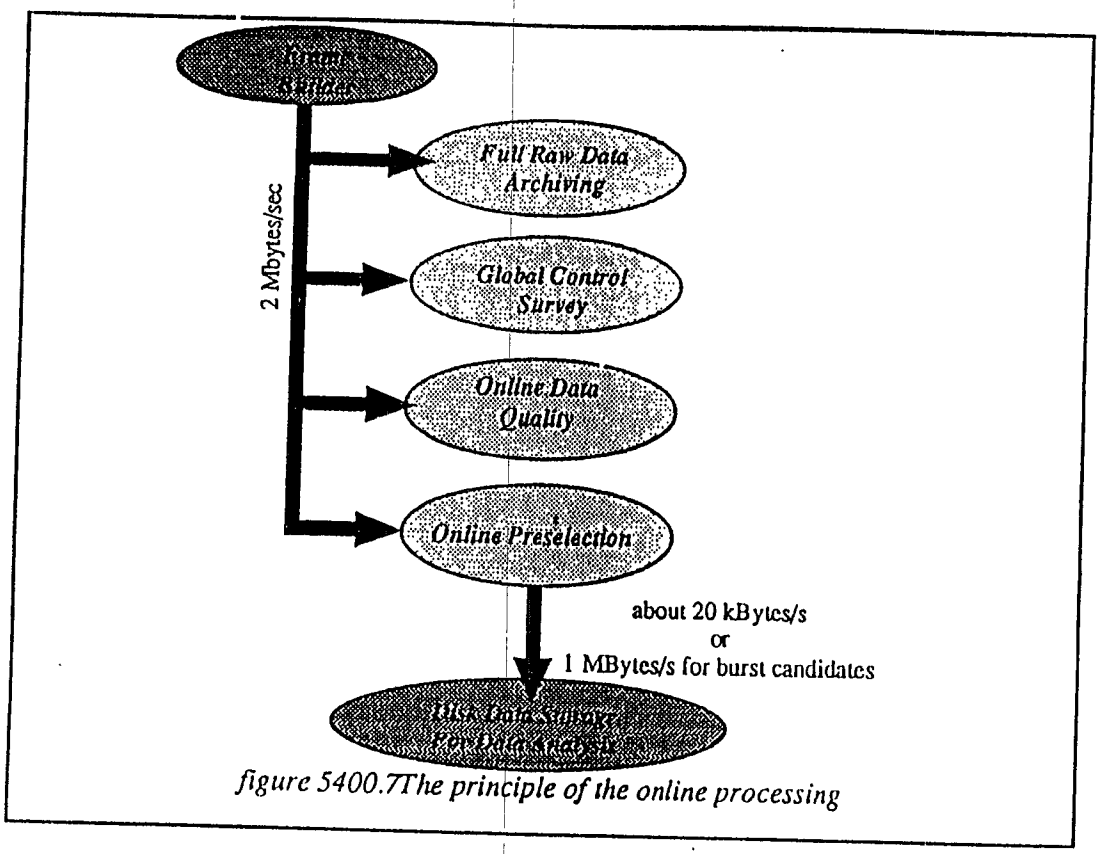

figure 5400.7The principle of the online processing

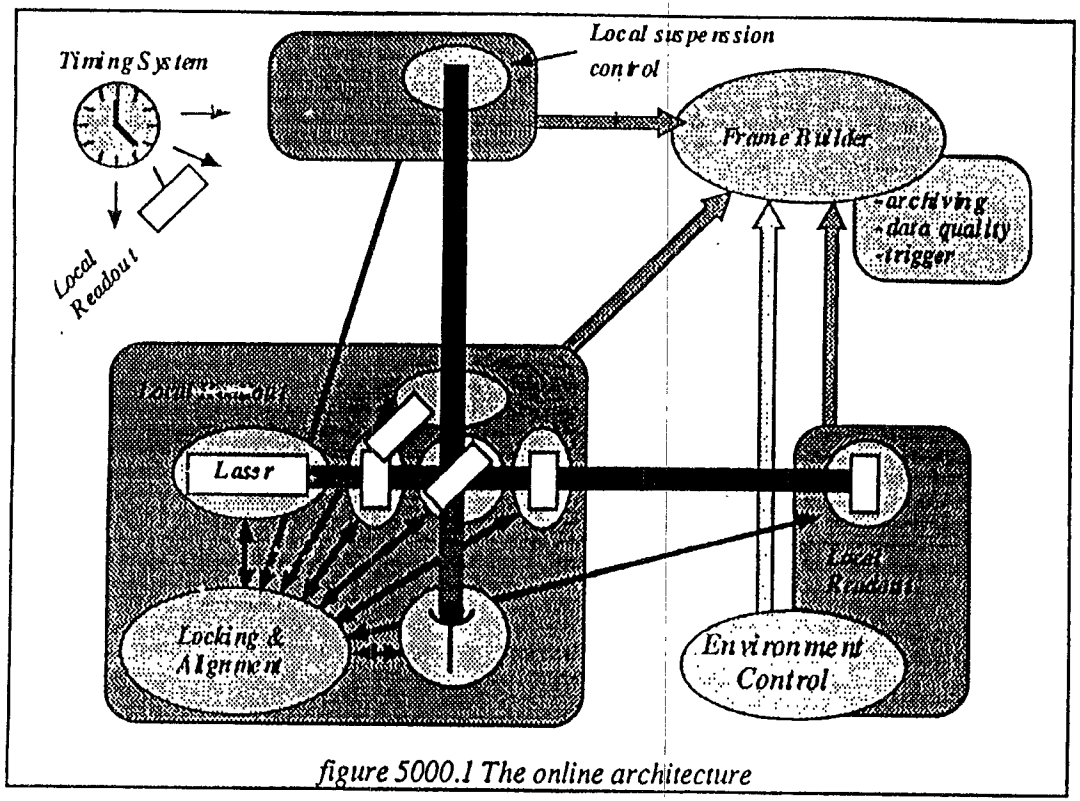

figure 5000.1 The online architecture

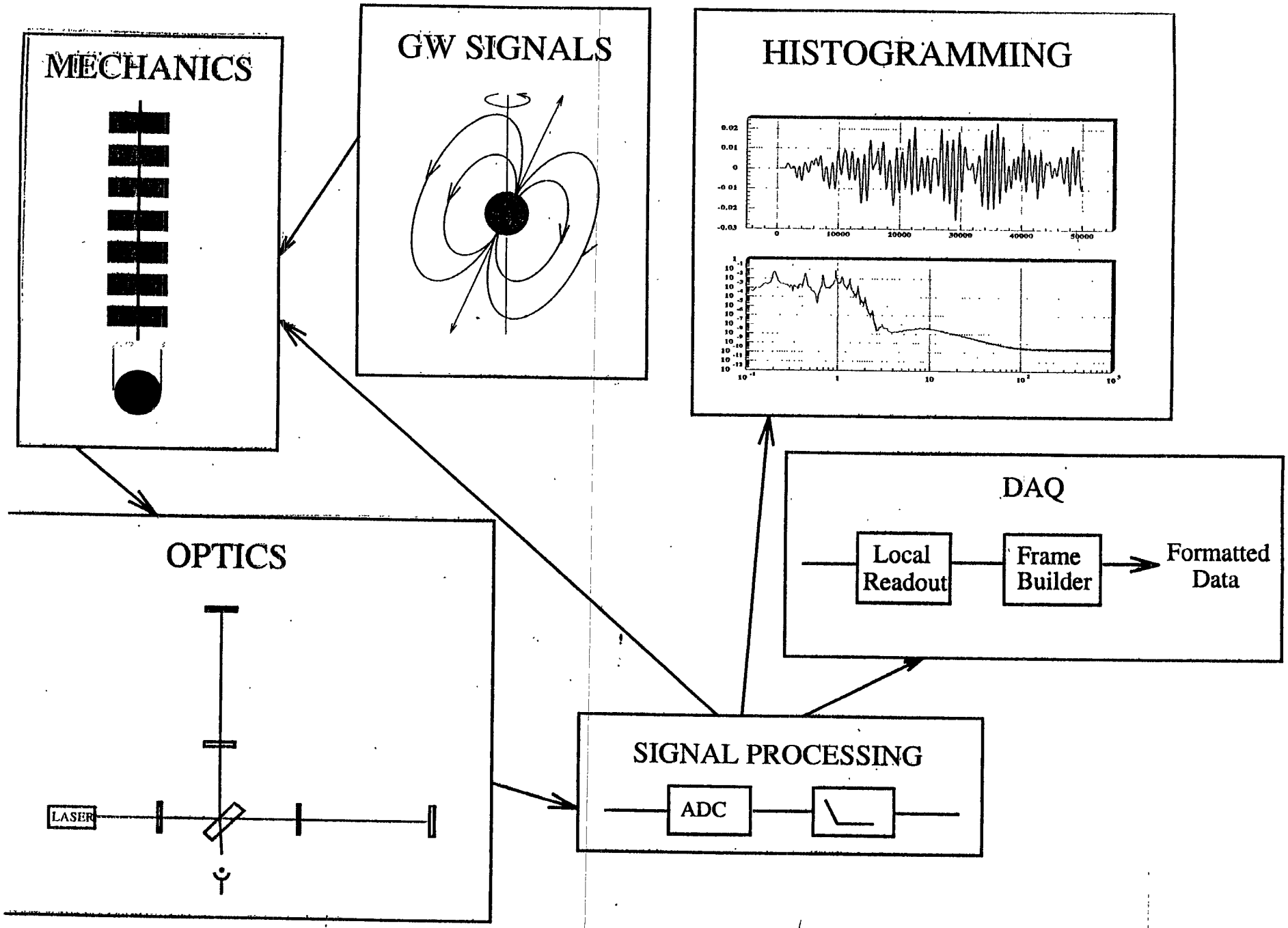
MECHANICS
GW SIGNALS
HISTOGRAMMING
OPTICS
LASER
DAQ
Local Readout
Frame Builder
Formatted Data
SIGNAL PROCESSING
ADC

Conclusion

1. Birefringence : between 0 and 1 mrad
2. Optical Thickness : better than $\lambda/50$ p.v. on 64 cm^2
3. Wedge : 960+/−70 µrad
4. Bubbles : objective, to detect point defects down to 0.1 µm diameter

②Optical Thickness

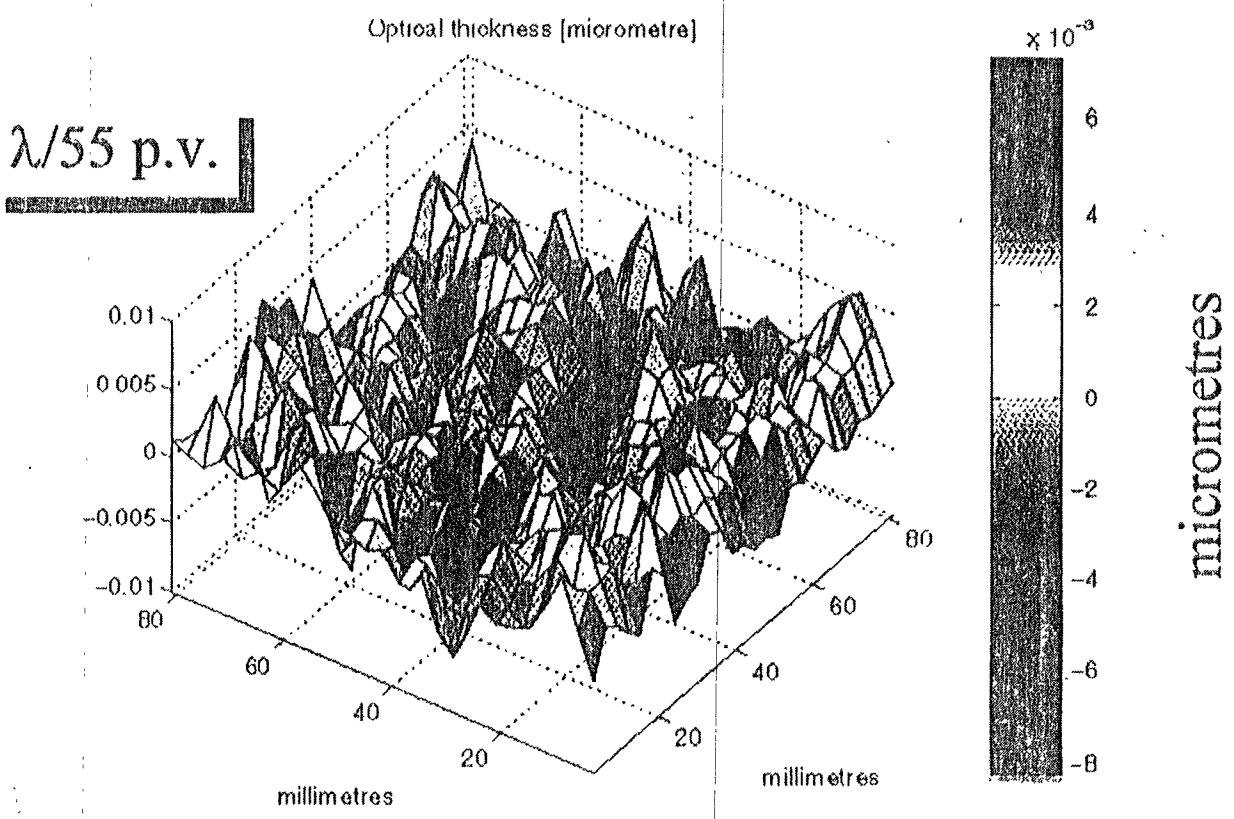

8 cm X 8 cm

ESPCI *Optique*

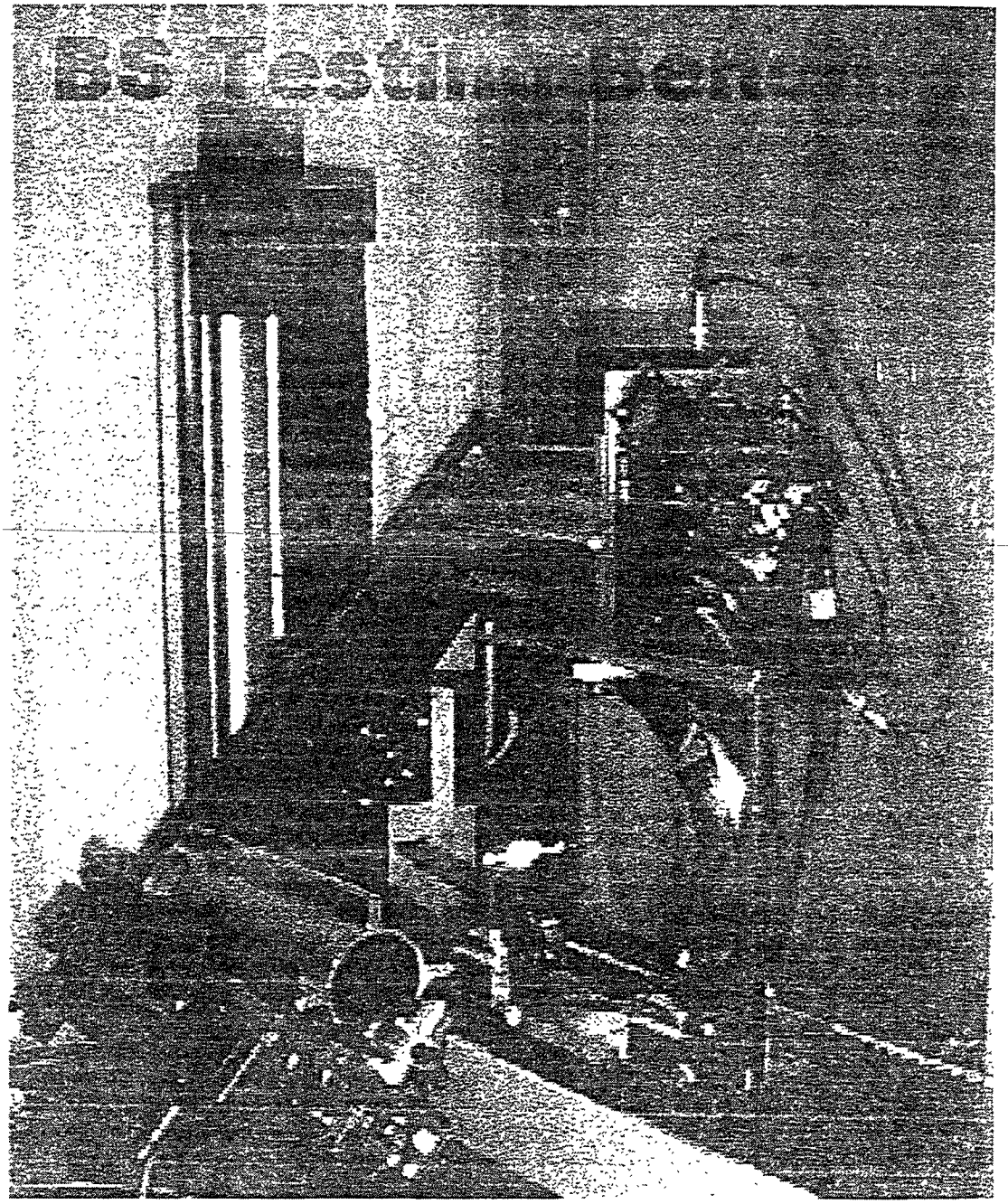

Mode Cleaner

Coatings from LMA-IN2P3-VIRGO

IPN Lyon

SMA

2" Mirror

Wavefront after automatized corrective coating

(Deformation before correction : 40 nm P.V.)

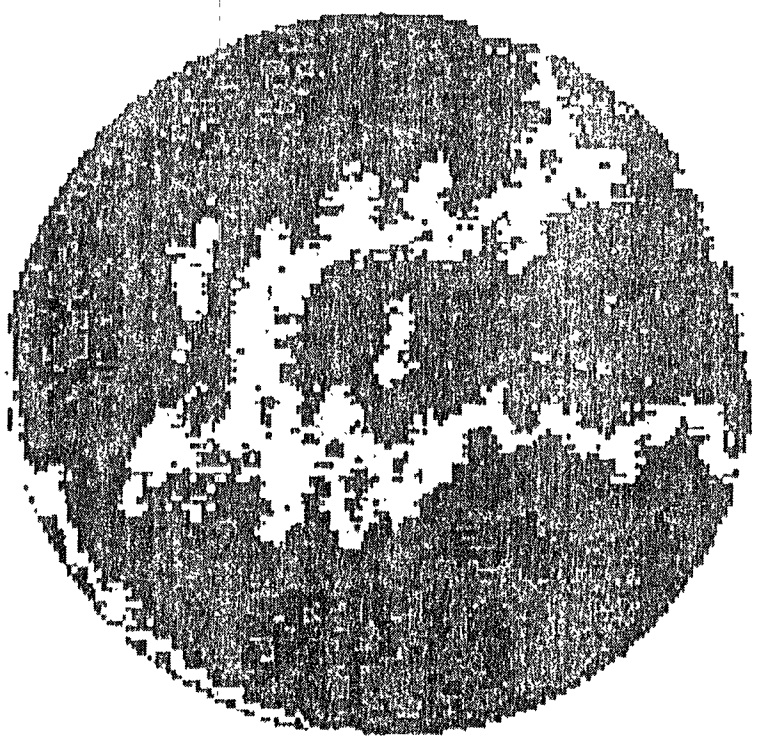

12 nm

0

The Cycle of correction

mirror to correct

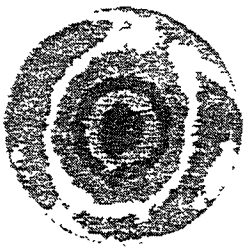

Mesure of the mirror with the interferometer zygo

file

Program "Caract"

Determination and simulation of the correction

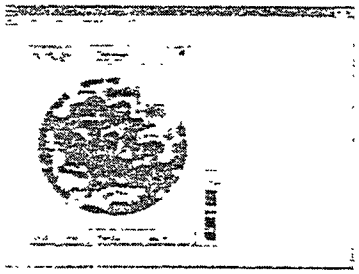

file

Program "Robot"

Pilots the robot for executing the correction

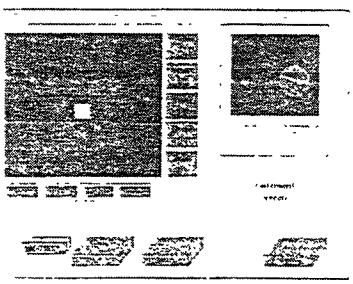

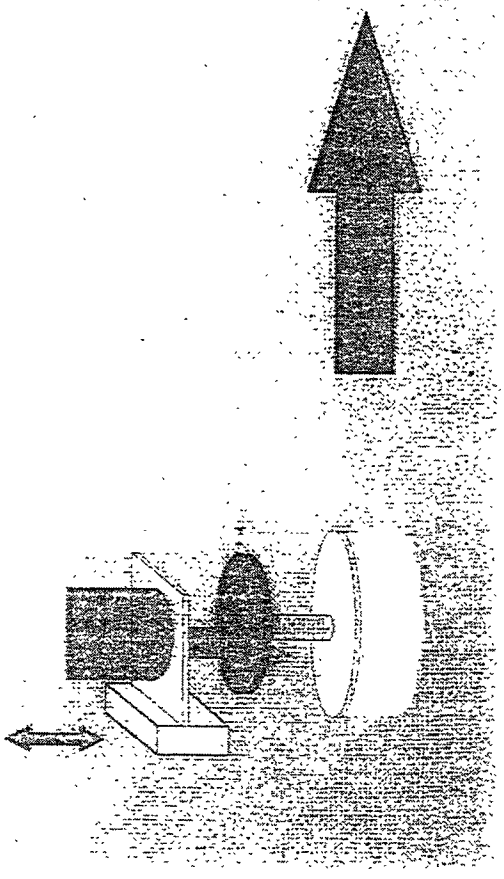

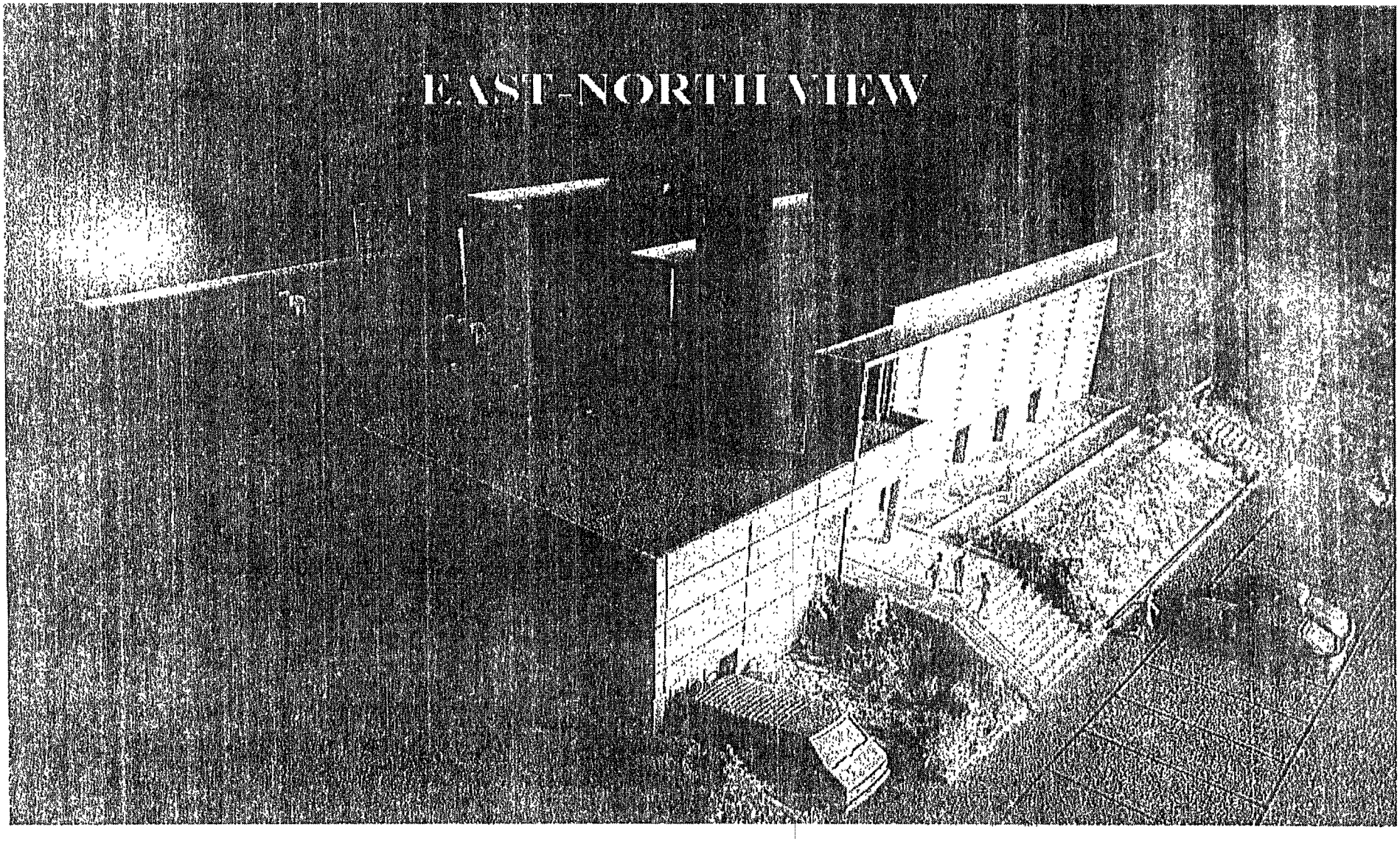

DURABLE 8552

MIRRORS

	Diam.(mm)	Thick.(mm)
Input cavity FP	350	100
Output cavity FP	350	100
Beam splitter	350	100
Recycling	350	100
Substrate absorption		< 2 ppm/cm

COATINGS

Results obtained by the group of Lyon on mirrors with 50 mm in diameter:

Absorption	$\lesssim$ 1 ppm
Scattering	< 1 ppm

The centre of the bandwidth is defined within 10 nm

These values are well within the specification of VIRGO

At LYON the VIRGO collaboration started the construction of a facility to produce mirrors with a coating of 300 mm in mirrors of 350 mm in diameter

Laser 10 W diode pumped 1.064 µm Nd:YAG-Laser

Injection locking

master laser (stable) transfers stability to
slave laser (high power)

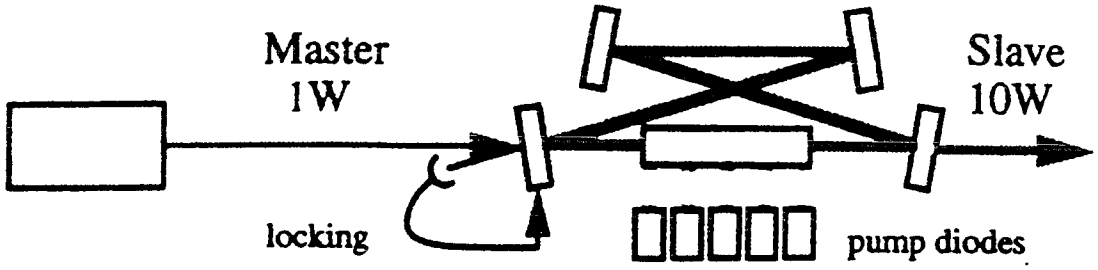

Frequency stabilisation

Prestabilisation to reference cavity
Main stabilisation to interferometer

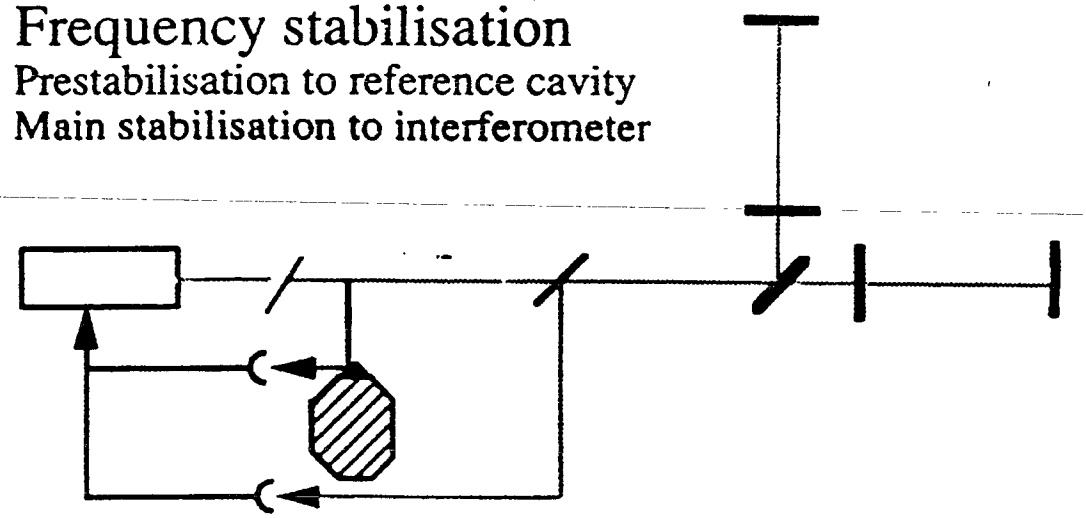

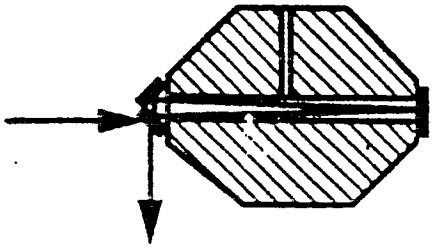

Material: ULE
expansion $5 \cdot 10^{-9}$/°C
Q ≈ 100 000
Resonance > 9 kHz

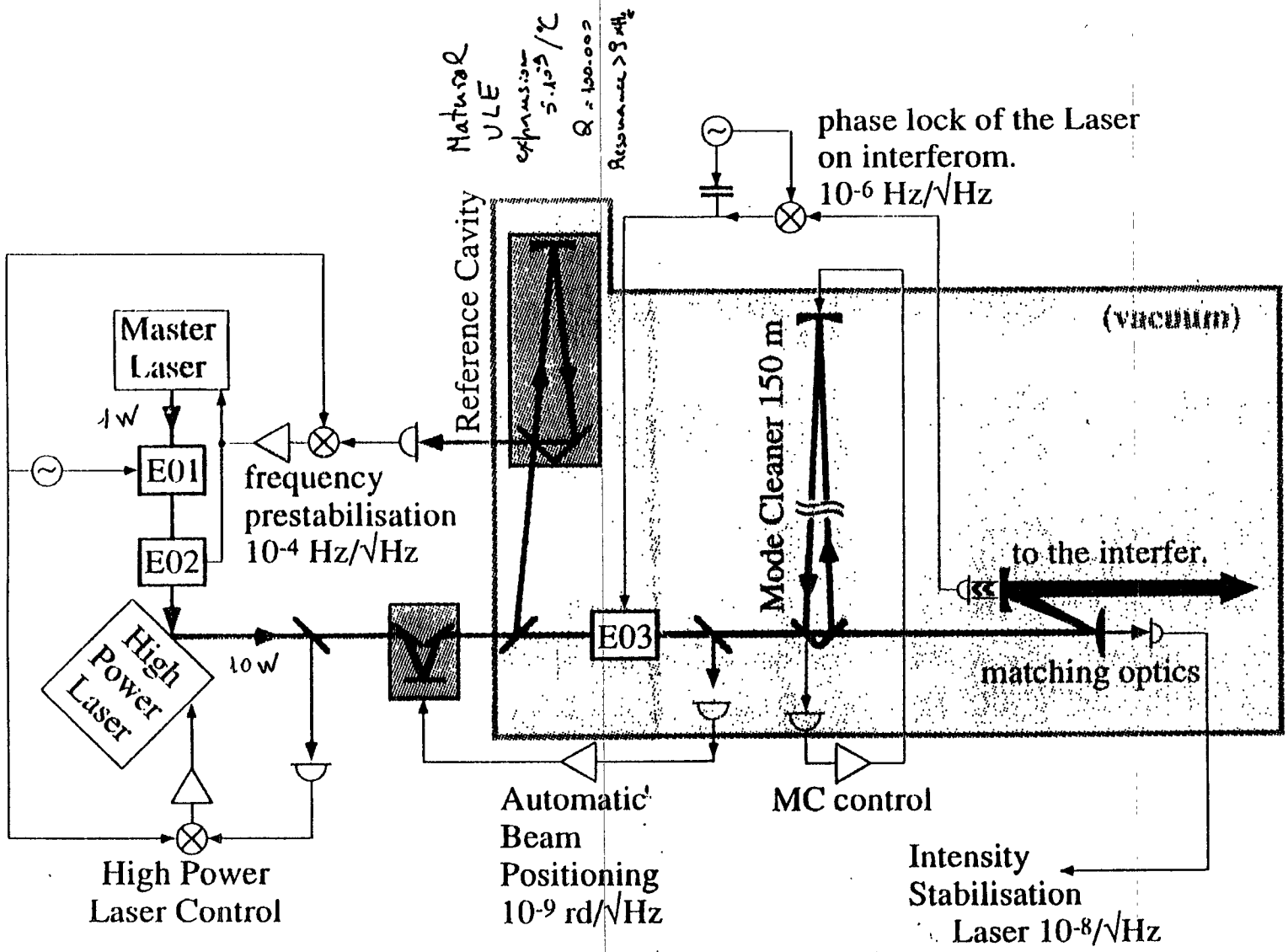

Stabilised High Power LASER and Input Optics.

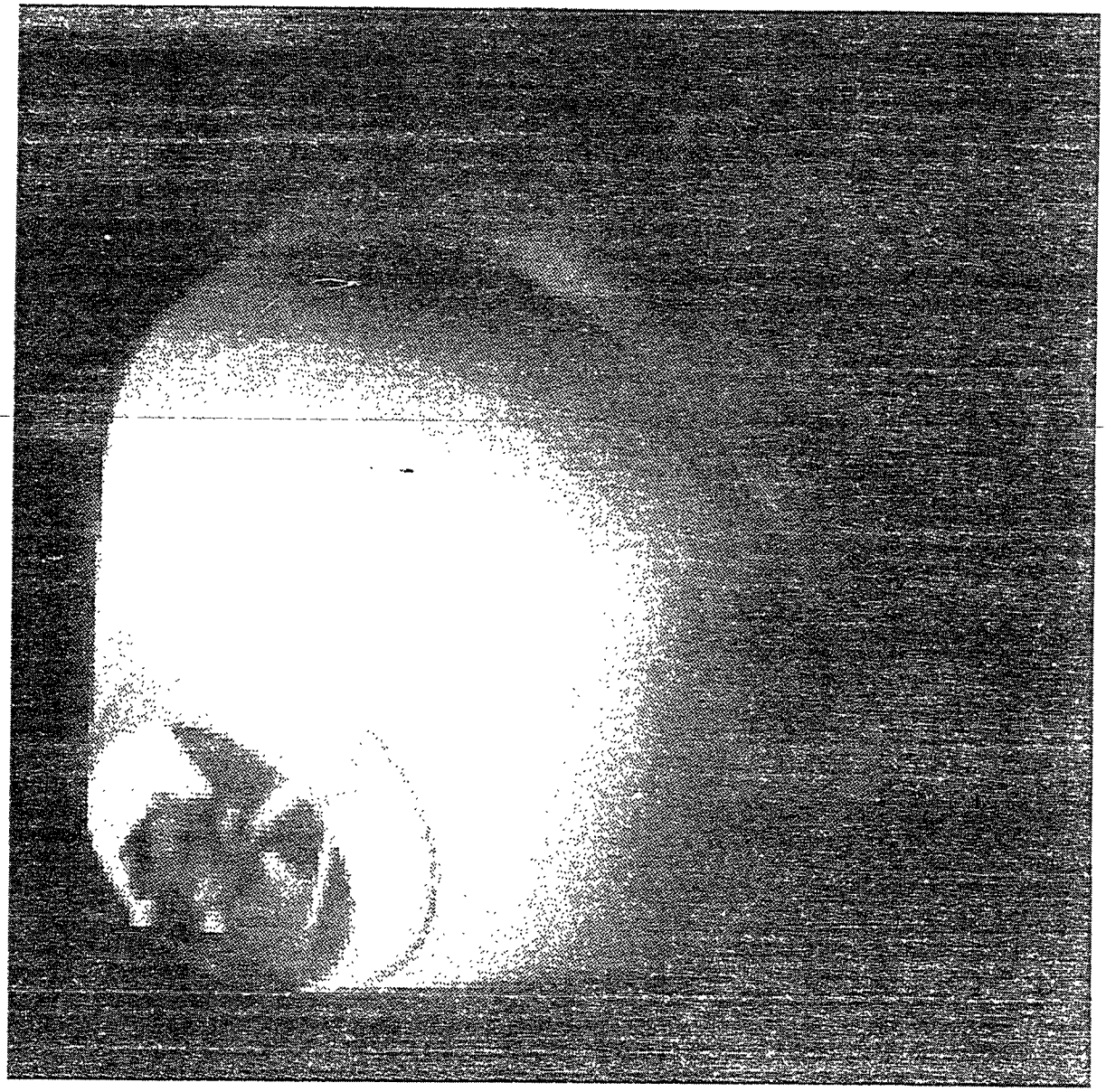

SDMS
SDMS

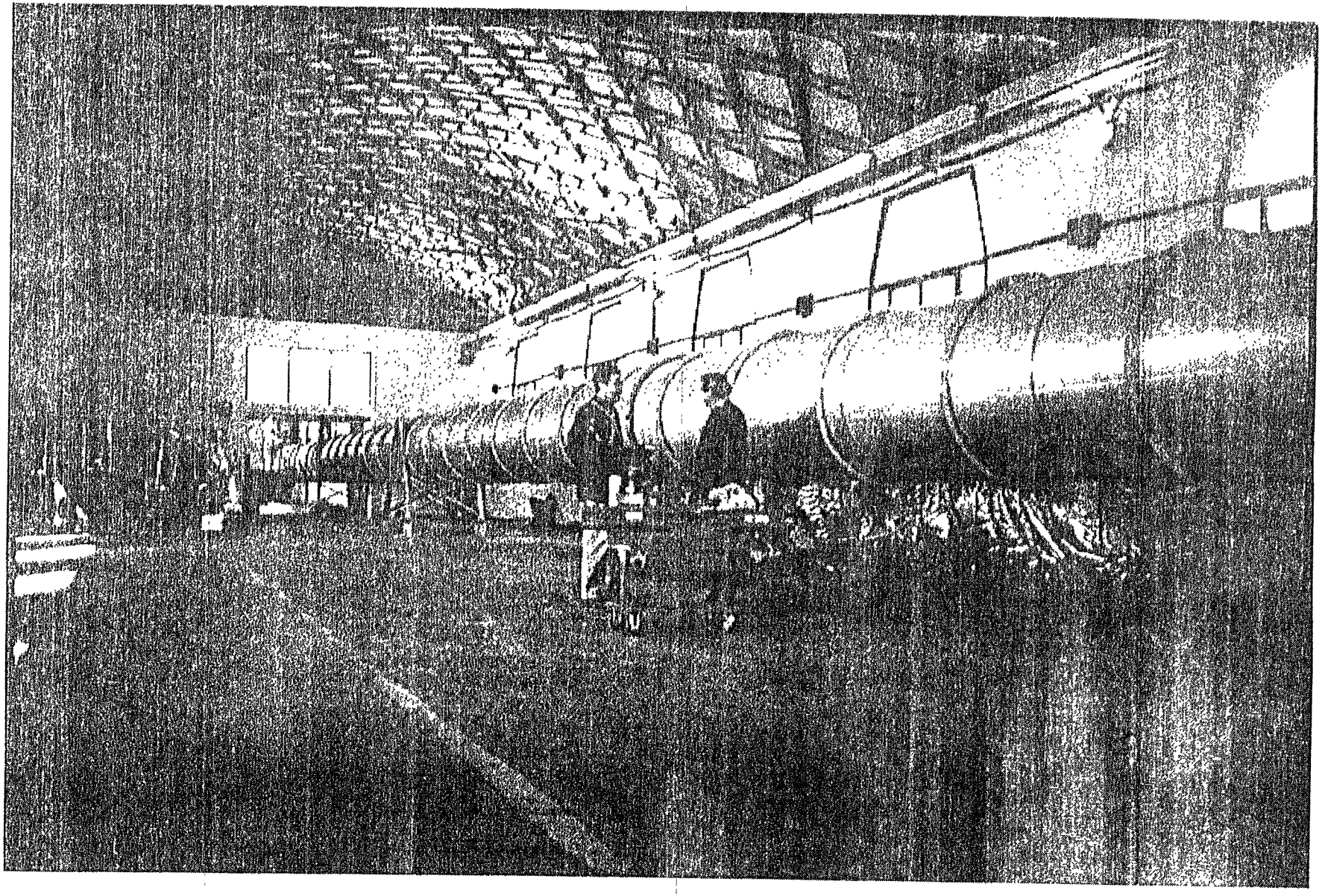

The VIRGO vacuum system

The vacuum tube:

SPECIFICATIONS:
diameter: 1200 mm
length: 2*3000 m
material Stanley steel 304
The tube will be entirely welded on the site.
Outgassing rate : 3 10^{-12} [torr lt/(cm^2 s)]

RESULTS OBTAINED ON A PROTOTYPE
diameter: 1200 mm
length: 60 m
thickness 5 mm
tube firing in air at 450 C
baking at 150 C
Outgassing rate : 5 10^{-15} [torr lt/(cm^2 s)]

The pumping system

SPECIFICATIONS

Final pressure in the tube and in the lower part of the towers	1 10^{-8} mbar
Final pressure in the upper part of the towers	1 10^{-6} mbar

REFERENCE SOLUTION:

Vacuum pumping system for the tube:
1 pumping station each 300 m of 1000 l/s
Oil free system which includes
rotary pump, turbomolecular pump with magnetic bearings and Ti sublimation pump

Vacuum pumping system for the towers:
For the *lower* part of the towers
1 pumping station of 1000 l/s
Oil free system which includes
Turbomolecular pumping group with magnetic bearings

For the *upper* part of the towers
1 pumping station of 2000 l/s
Turbomolecular pumping group with magnetic bearings

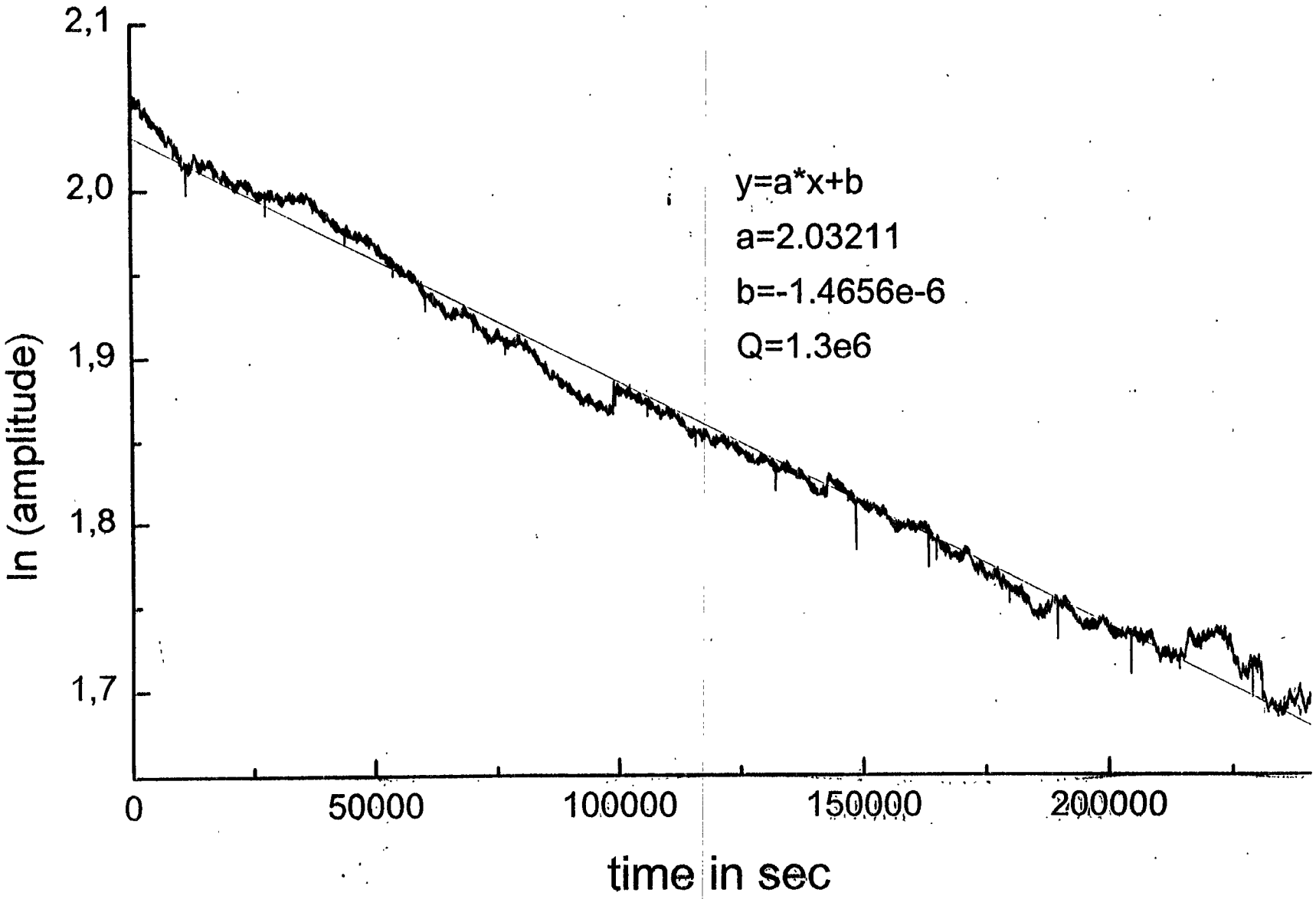
2,1
2,0
1,9
1,8
1,7
ln (amplitude)
y=a*x+b
a=2.03211
b=-1.4656e-6
Q=1.3e6
0
50000
100000
150000
200000
time in sec

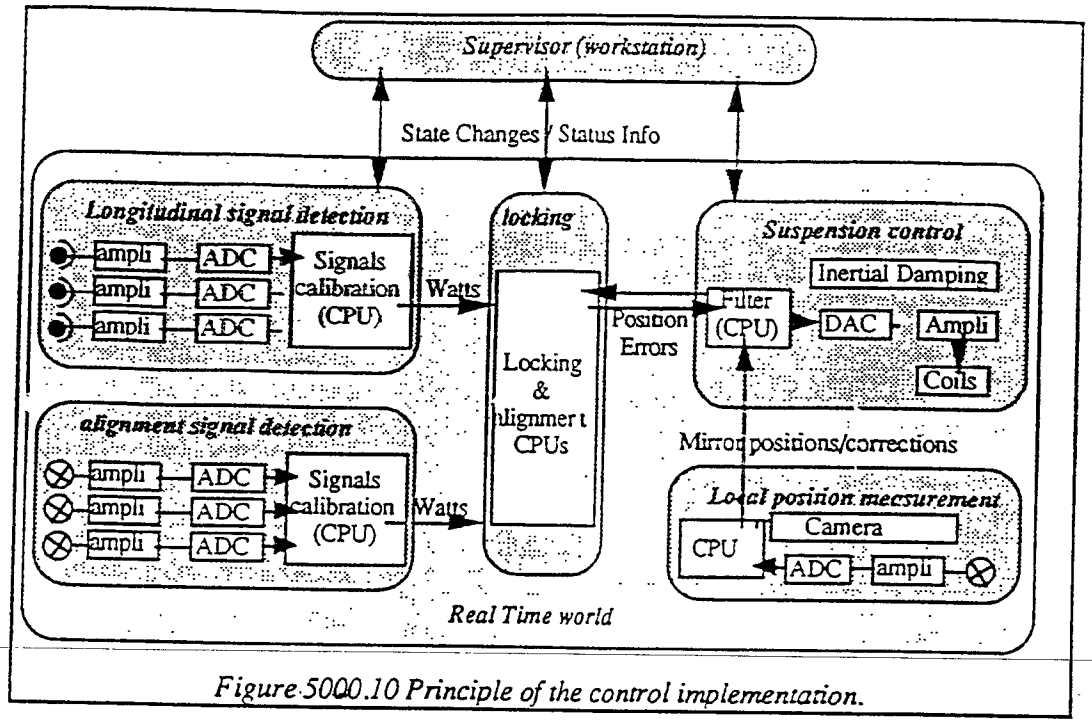

Figure 5000.10 Principle of the control implementation.

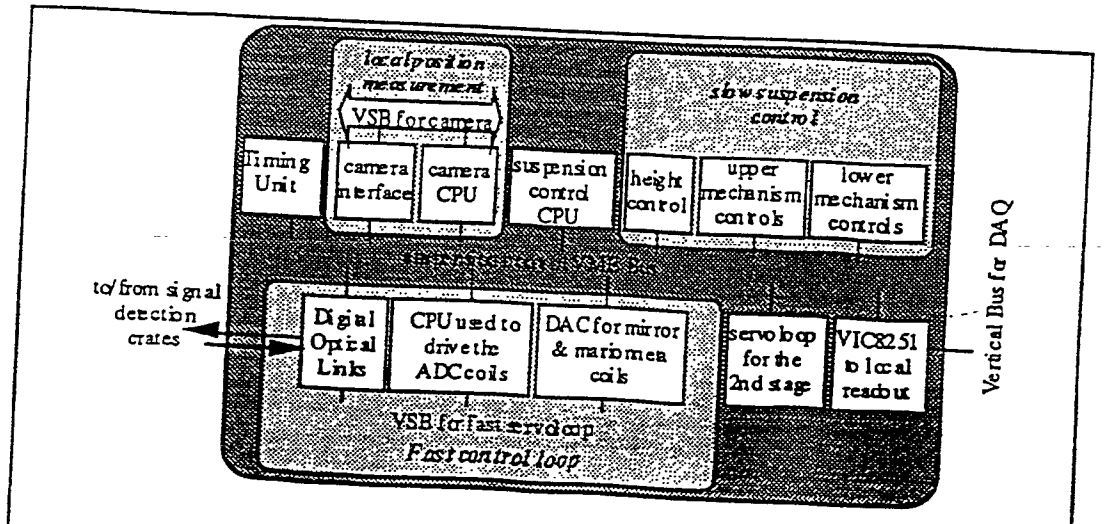

Figure 5000.11 VME crate for a suspension control (crates for the analogic electronic are not shown)

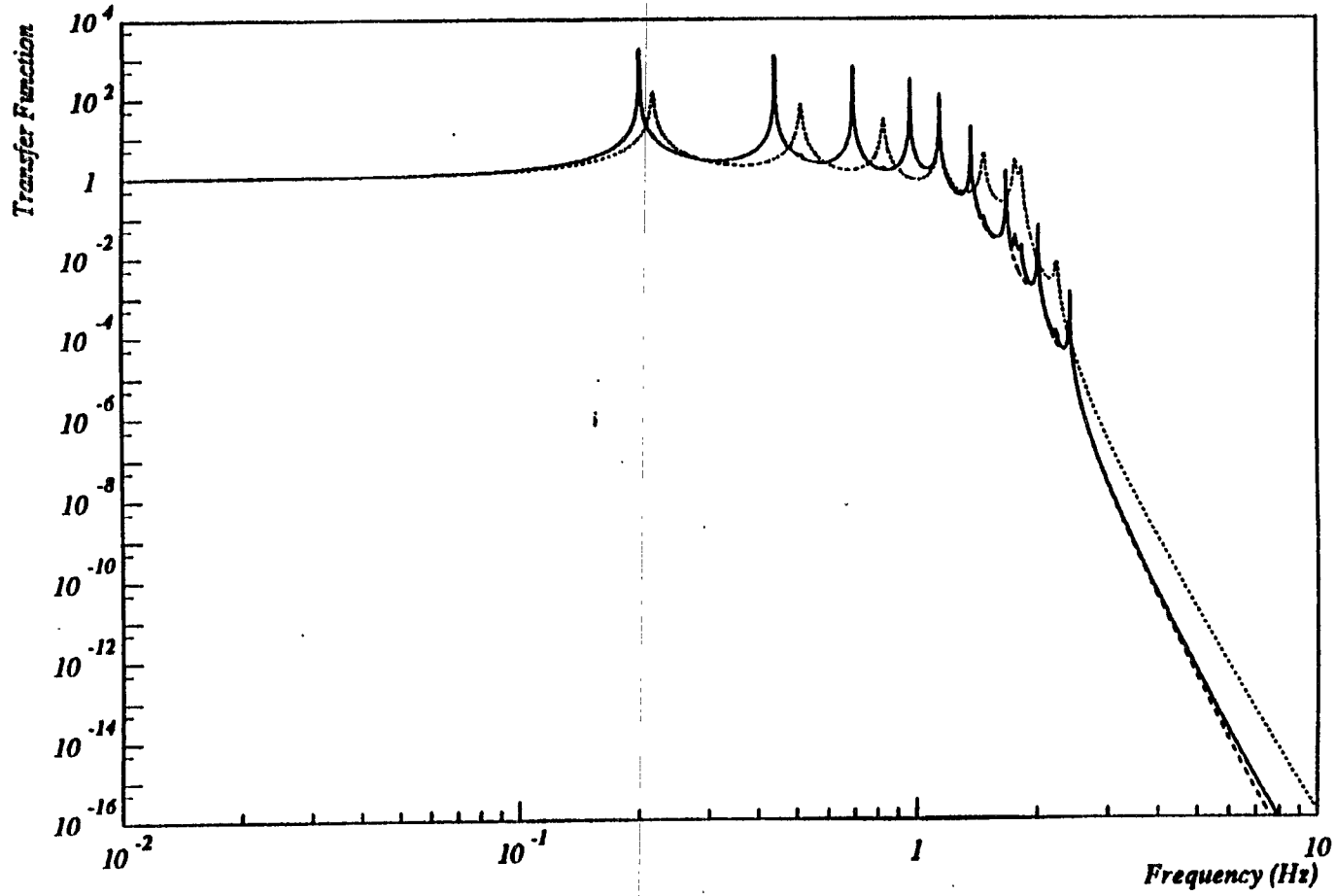

Figure 1: Superattenuator transfer functions from the suspension point to the mirror. The dashed and dotted lines refer to the horizontal and the vertical direction respectively. The continuous line refers to the combined effect of the horizontal and vertical TF (vertical to horizontal coupling of 10^{-2}).

ONE STAGE

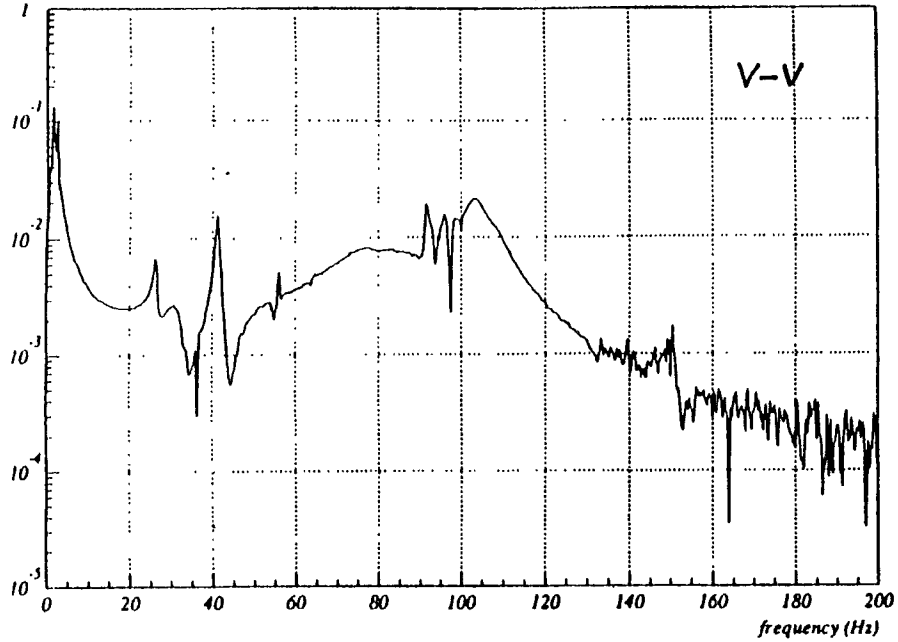

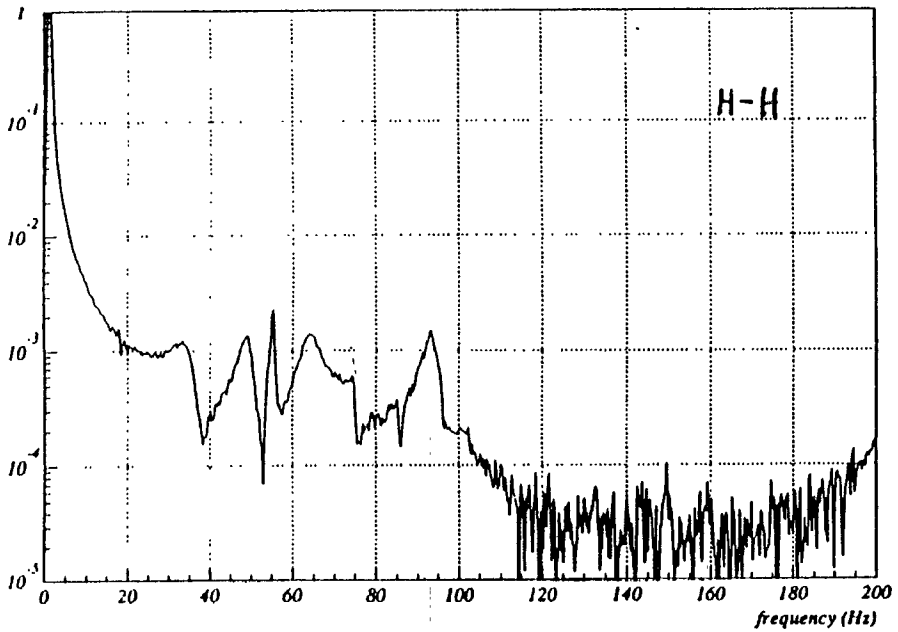

TWO STAGES

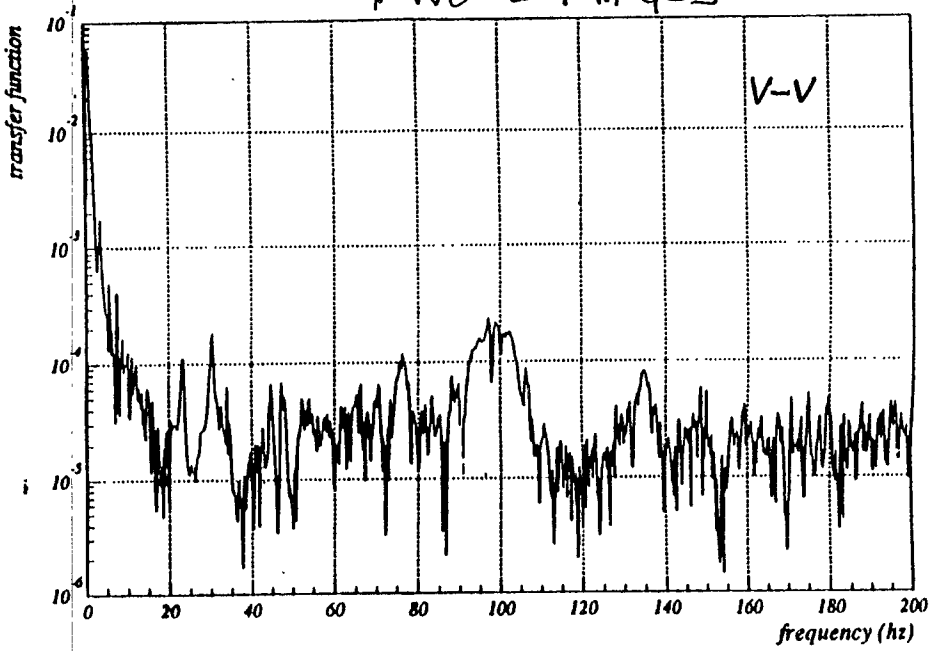

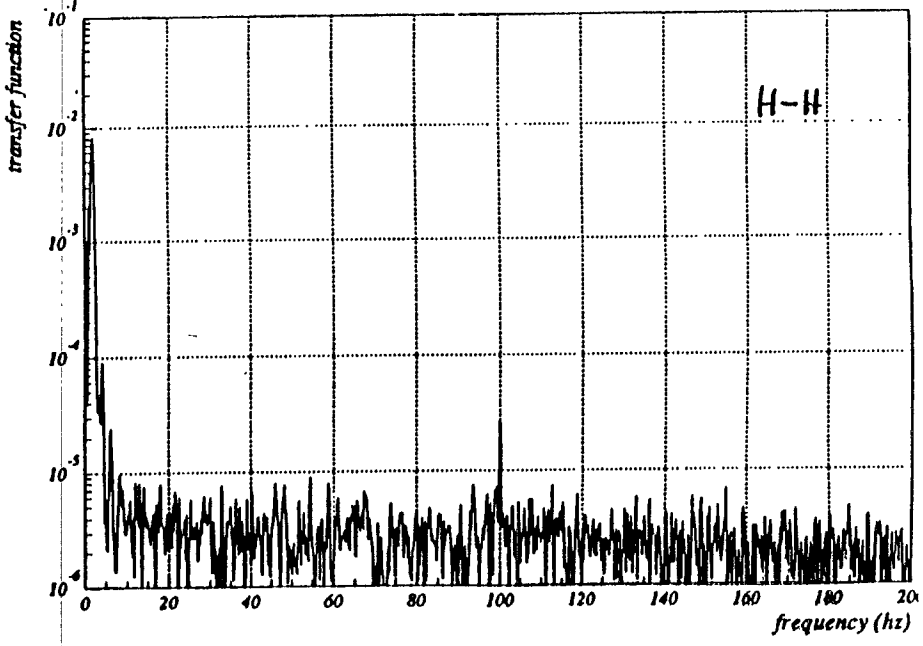

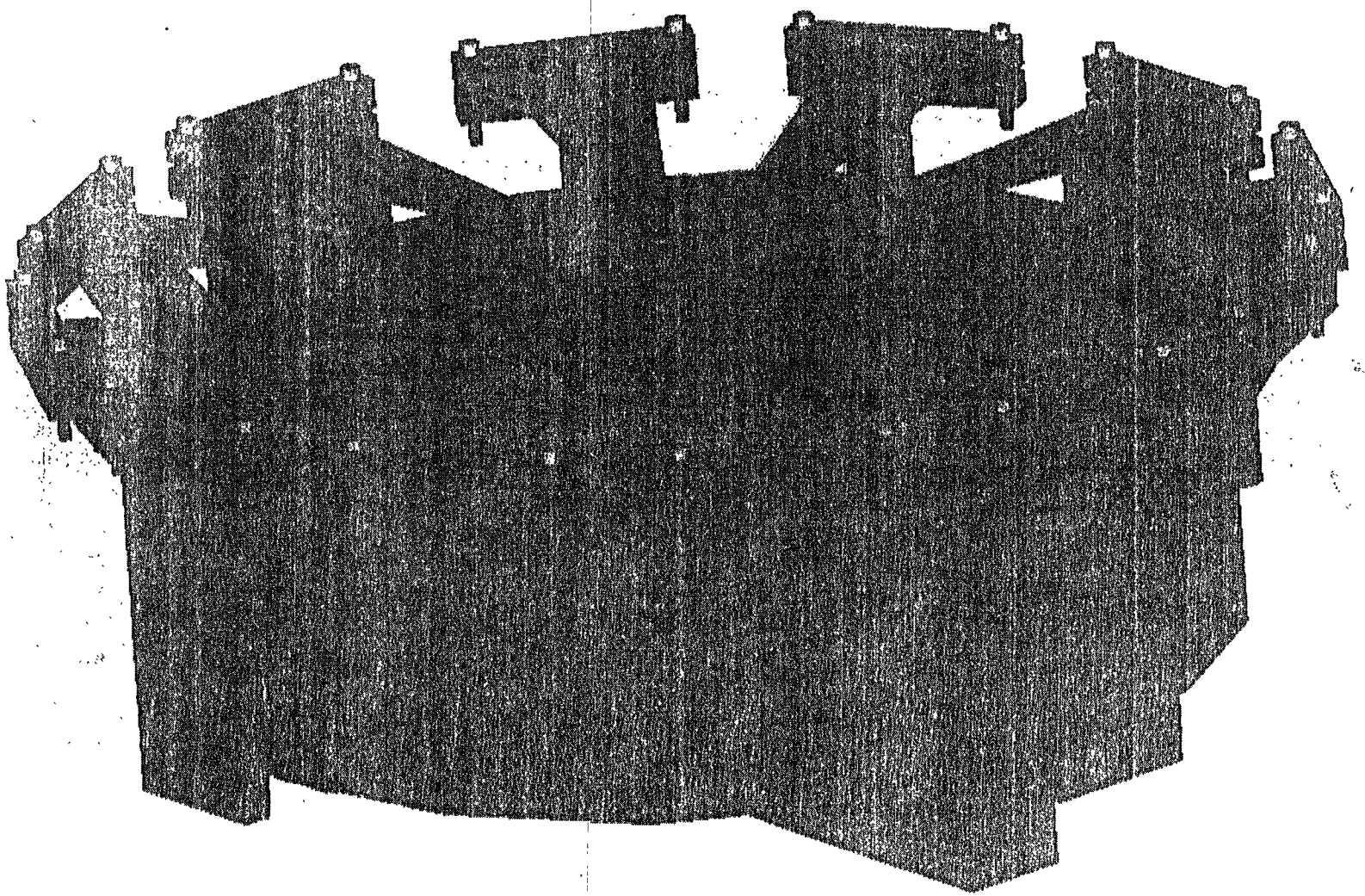

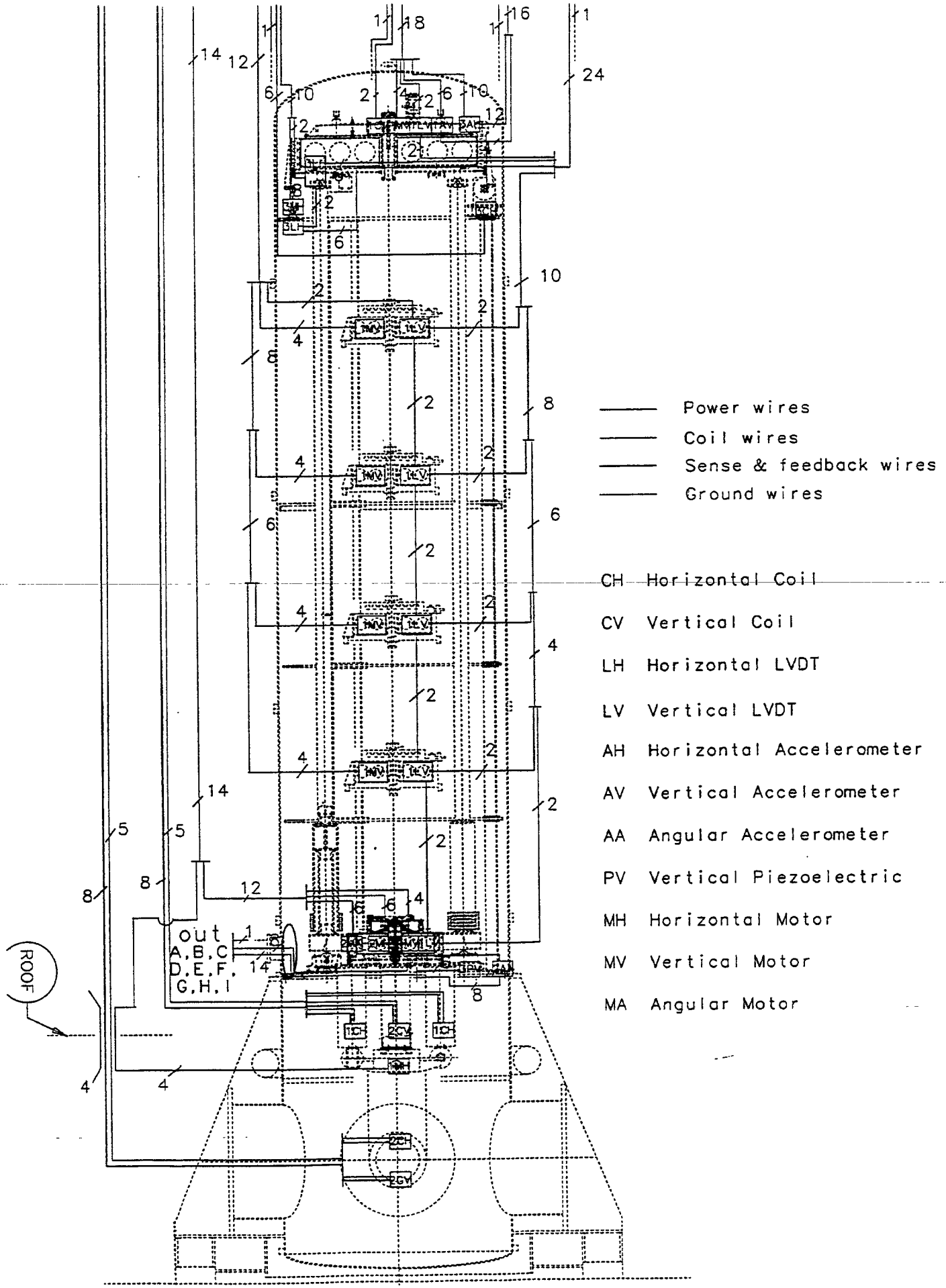
Power wires
Coil wires
Sense & feedback wires
Ground wires
CH Horizontal Coil
CV Vertical Coil
LH Horizontal LVDT
LV Vertical LVDT
AH Horizontal Accelerometer
AV Vertical Accelerometer
AA Angular Accelerometer
PV Vertical Piezoelectric
MH Horizontal Motor
MV Vertical Motor
MA Angular Motor
ROOF
out
A,B,C
D,E,F,
G,H,I

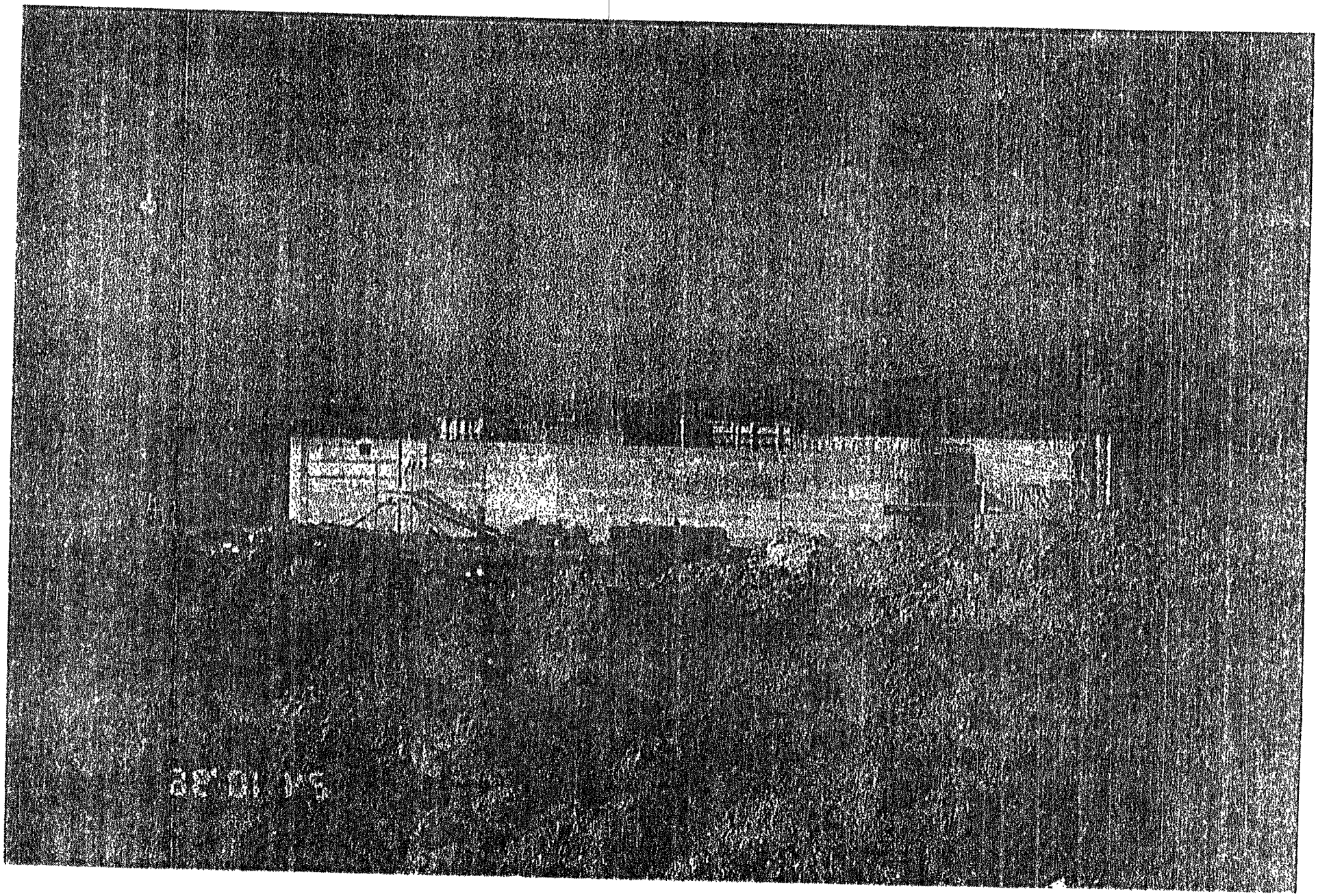

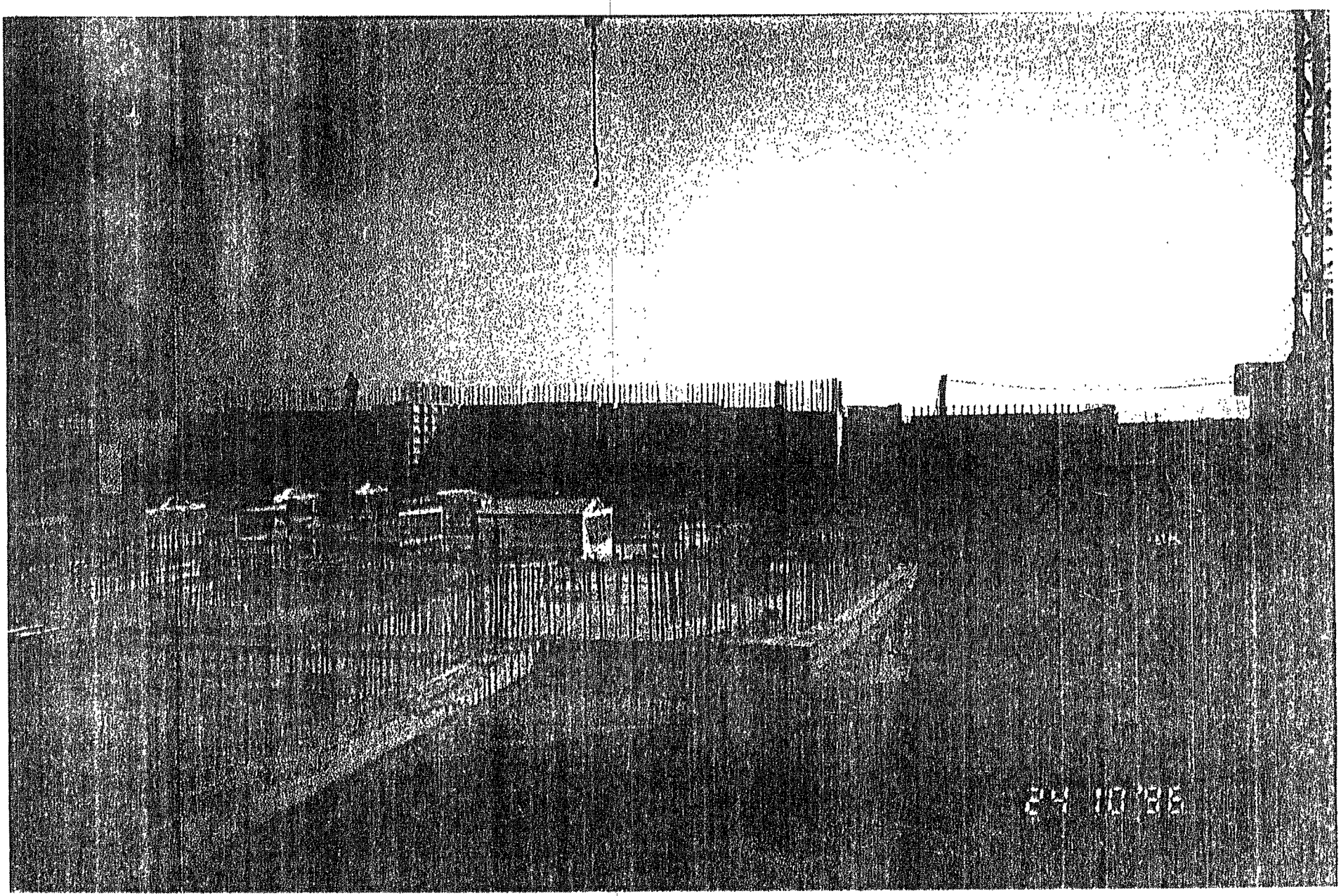
24 10 86


32°01 E

Stato dei lavori a Cascina, 10 settembre 1996

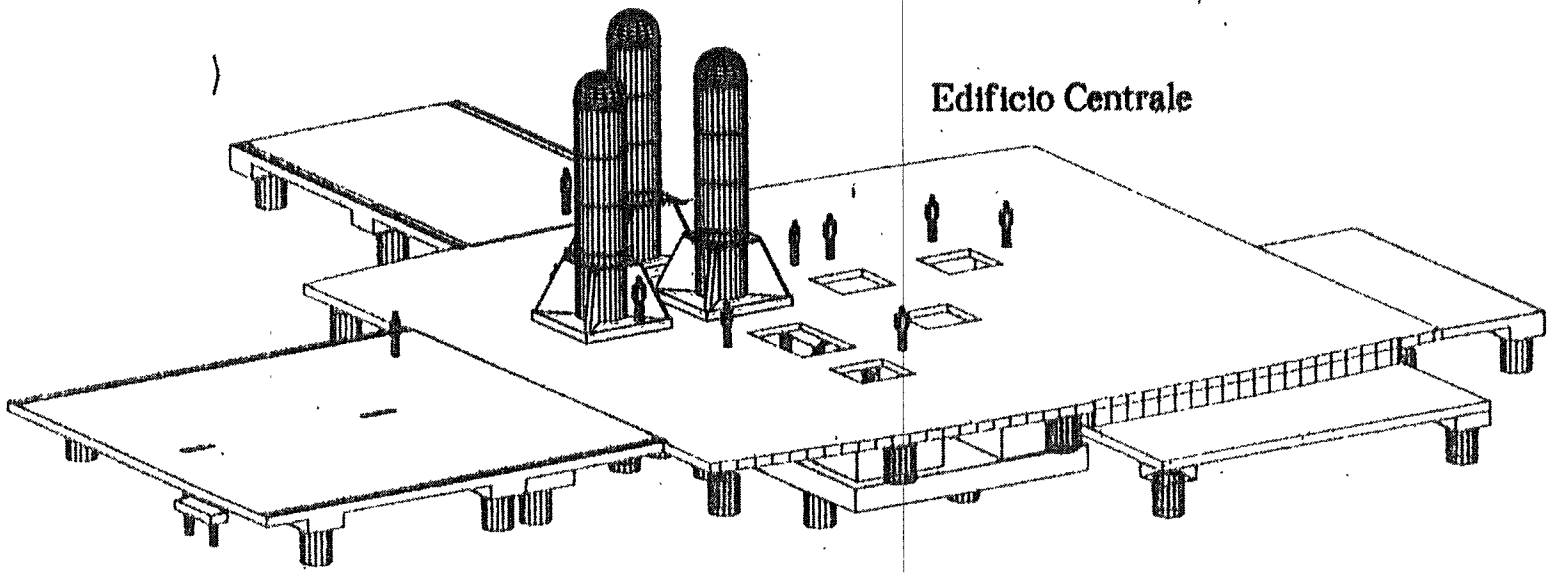

Edificio Centrale

Edificio Tecnologico

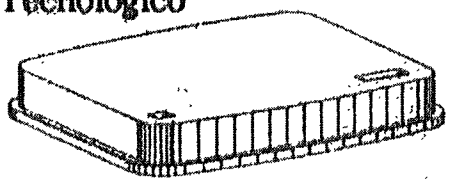

Edificio Controllo

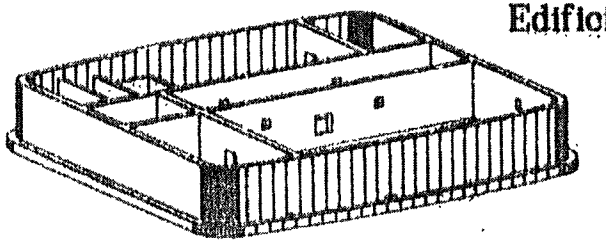

P.I. G. De Carolis

MARINA Soc. di Piso
Cascina, 20/08/96 - De Carolis

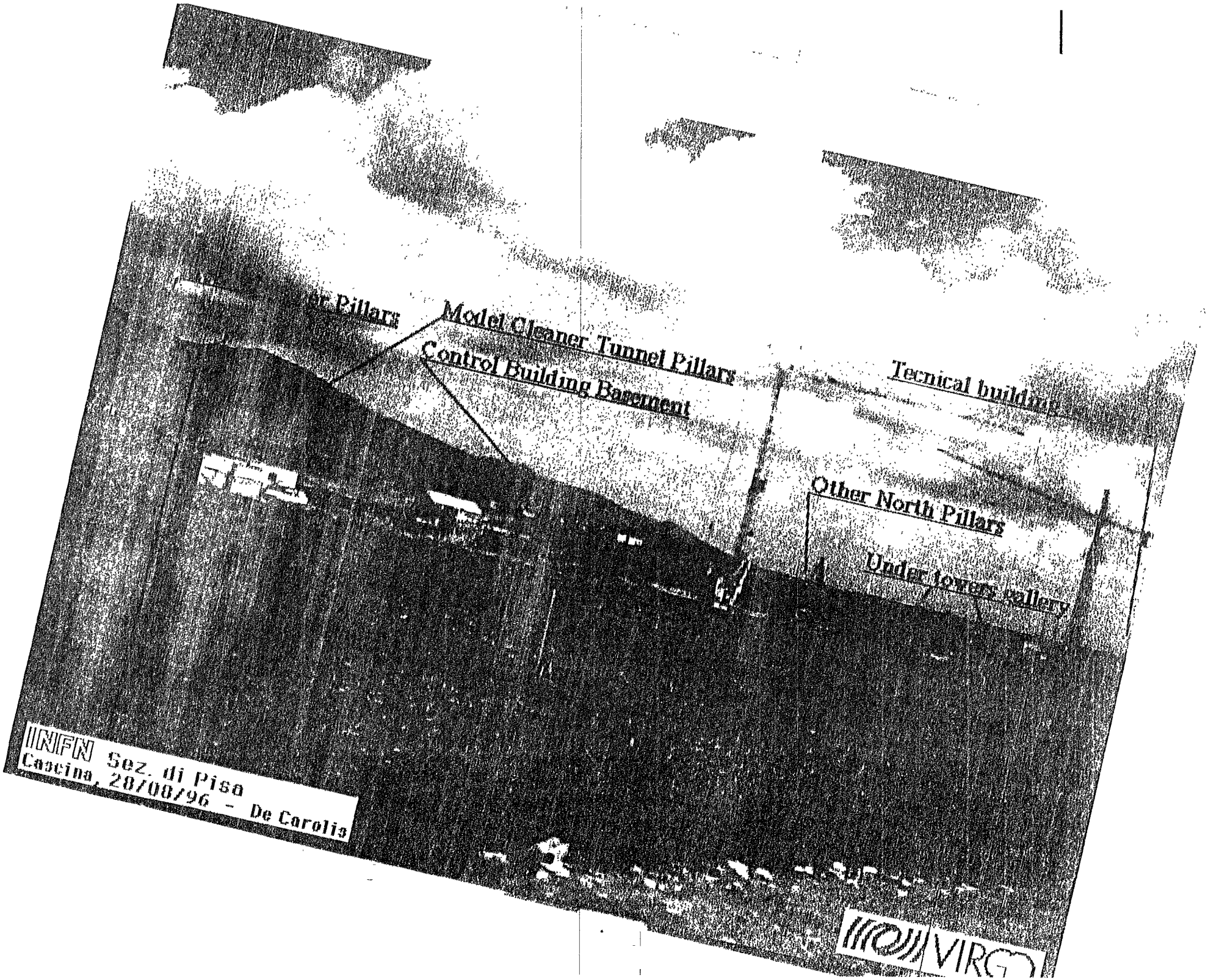
Model Cleaner Tunnel Pillars
Control Building Basement
Tecnical building
Other North Pillars
Under towers pillars
INFN Sez. di Pisa
Cascina, 28/08/96 - De Carolis
VIRGO

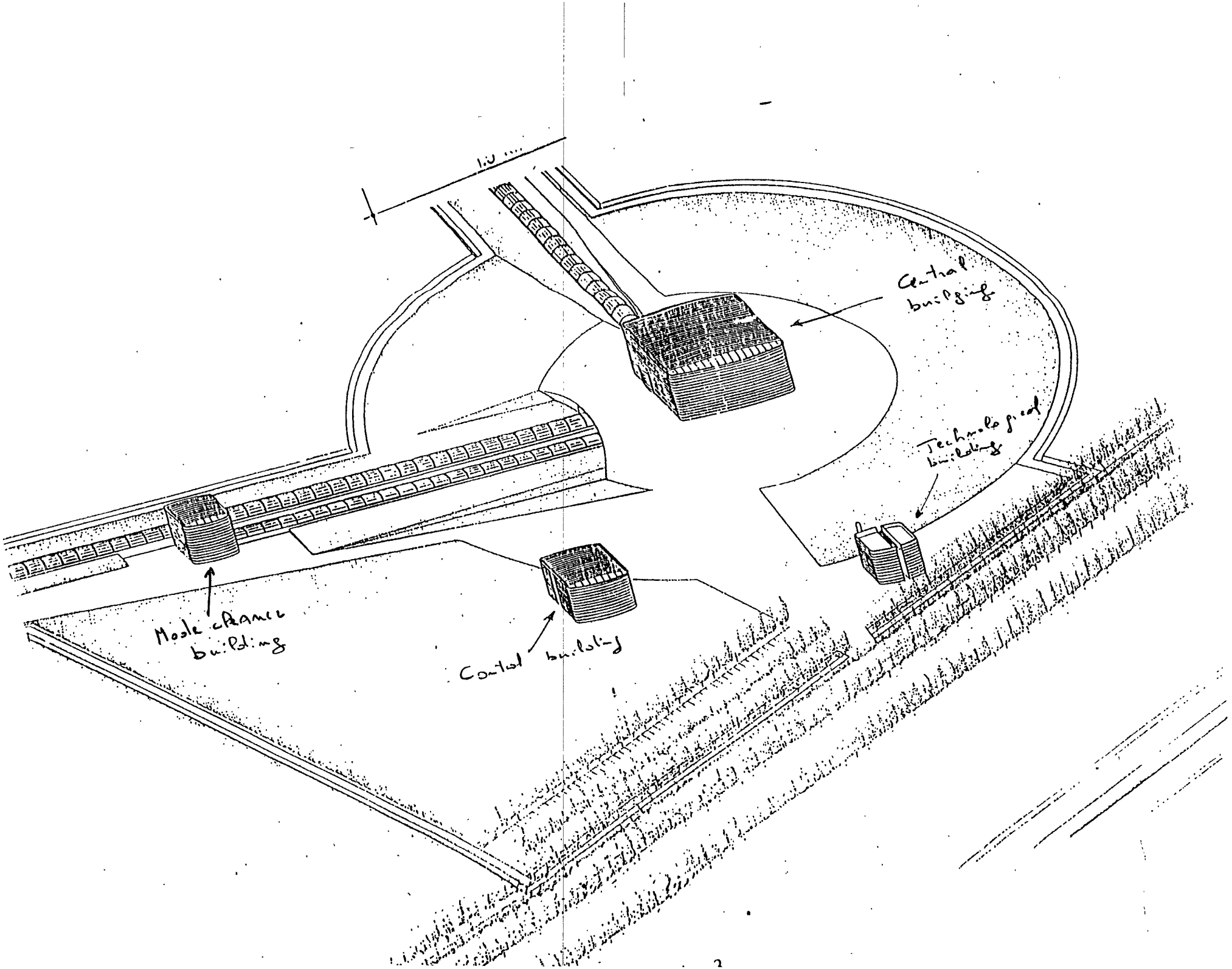
Central building
Technological building
Mode change building
Control building

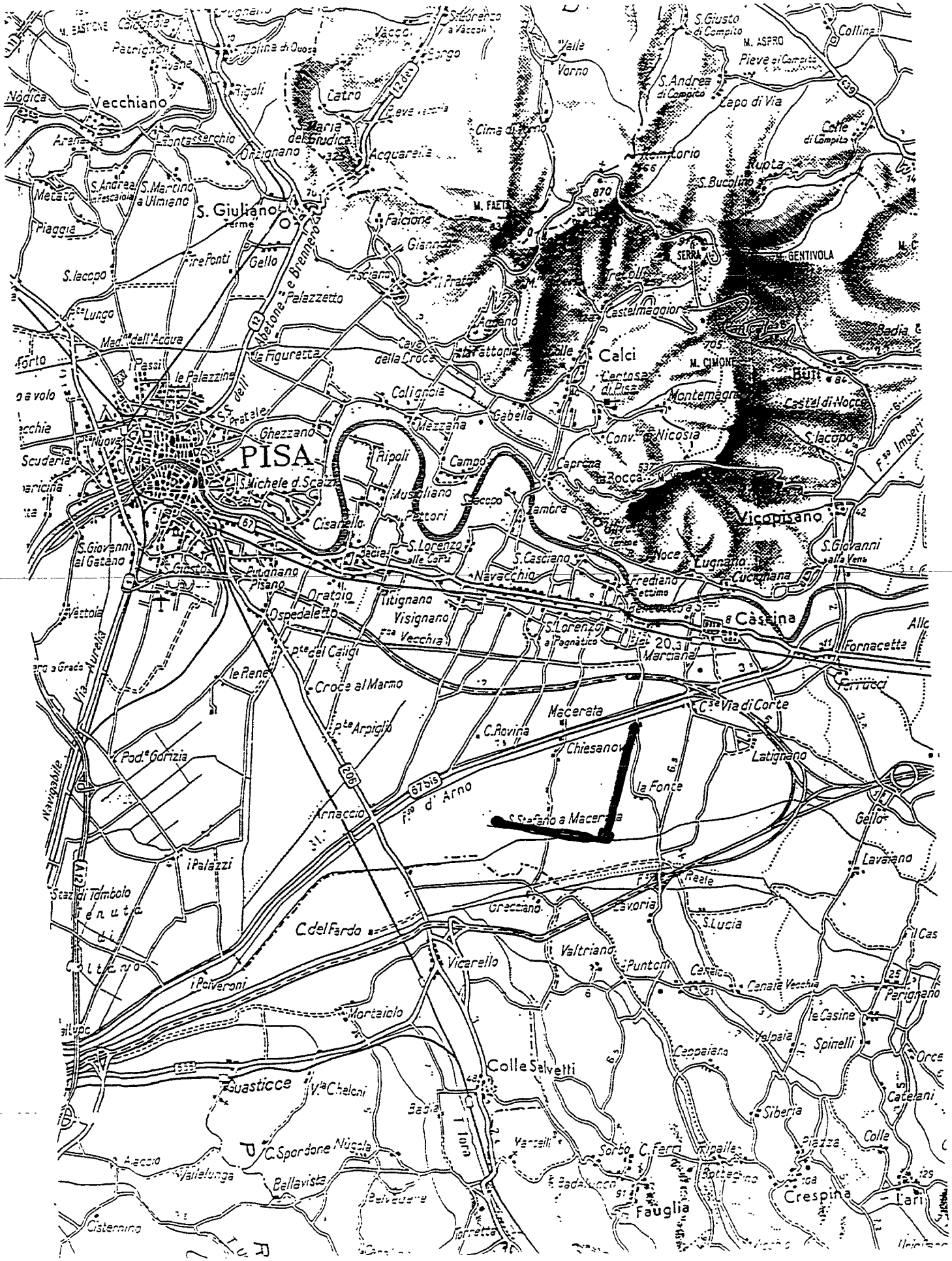

M. BASTONE
Patrignone
Molina di Quosa
Vecchiano
Nodica
Rigoli
Catro
Maria del Giudice
Acquarella
Pieve
Cima di Vorno
Vorno
Valle
Vacco
S. Lorenzo a Vaccoli
S. Giusto di Compito
M. ASPRO
Pieve di Compito
S. Andrea di Compito
Capo di Via
Colle di Compito
Collina
Rupta
S. Bucolino
Romitorio
Arena
Orzignano
Metato
S. Andrea in Pescaiola
S. Martino a Ulmiano
S. Giuliano Terme
Piaggia
Falcione
M. FAETA
SERRA
M. GENTIVOLA
S. Iacopo
Tre Ponti
Gello
Asciano
Palazzetto
Il Prato
Agnano
Tre Colli
Castelmaggiore
Badia
Madonna dell'Acqua
Brennero
Abetone e Brennero
Forto
La Figuretta
Cava della Croce
La Fattoria
Calci
Certosa di Pisa
M. CIMONE
Buti
Montemagno
Castel di Nocco
I Passi
Le Palazzine
Gavolo
Pratale
Colignola
Gabella
Mezzana
Ghezzano
Conv. di Nicosia
S. Iacopo
Nuova
Scudaria
PISA
Ripoli
Campo
Caprona
La Rocca
S. Michele d. Scalzi
Musigliano
Zambra
Cisanello
Pettori
Uliveto Terme
Vicopisano
S. Giovanni al Gatano
Bacia
S. Lorenzo alle Corti
S. Casciano
Noce
Lugnano
Cucignana
S. Giovanni alla Vena
S. Giusto
Putignano Pisano
Navacchio
S. Frediano a Settimo
Vettola
Oratoio
Titignano
Visignano
Ospedaletto
Zambra
S. Lorenzo a Pagnatico
Cascina
Fornacette
Marciana
Via Aurelia
Pte del Caligi
Le Rene
Croce al Marmo
Macerata
Ferrucci
Case Via di Corte
C. Rovina
Chiesanova
Latignano
Pte Arpiglio
Pod.e Gorizia
206
67 bis
F.so d'Arno
La Fonce
Navigabile
Arnaccio
S. Stefano a Macerata
Gello
A12
I Palazzi
Lavaiano
Staz.di Tombolo
Tenuta di Coltano
Reale
Grecciano
Lavoria
C. del Fardo
S. Lucia
Valtriano
Vicarello
Puntoni
Cenaia
Cenaia Vecchia
Perignano
I Polveroni
Le Casine
Mortaiolo
Ceppaiano
Volpaia
Spinelli
Colle Salvetti
Guasticce
V.la Chelcni
Badia
T. Tora
Siberia
Catelani
C. Spordone
Nugola
Vallelunga
Bellavista
Belvedere
Sorbo
C. Ferri
Ripaile
Bottegino
Colle
Piazza
Crespina
Badalucco
Fauglia
Lari
Cisternino
Torretta

2. Level 1

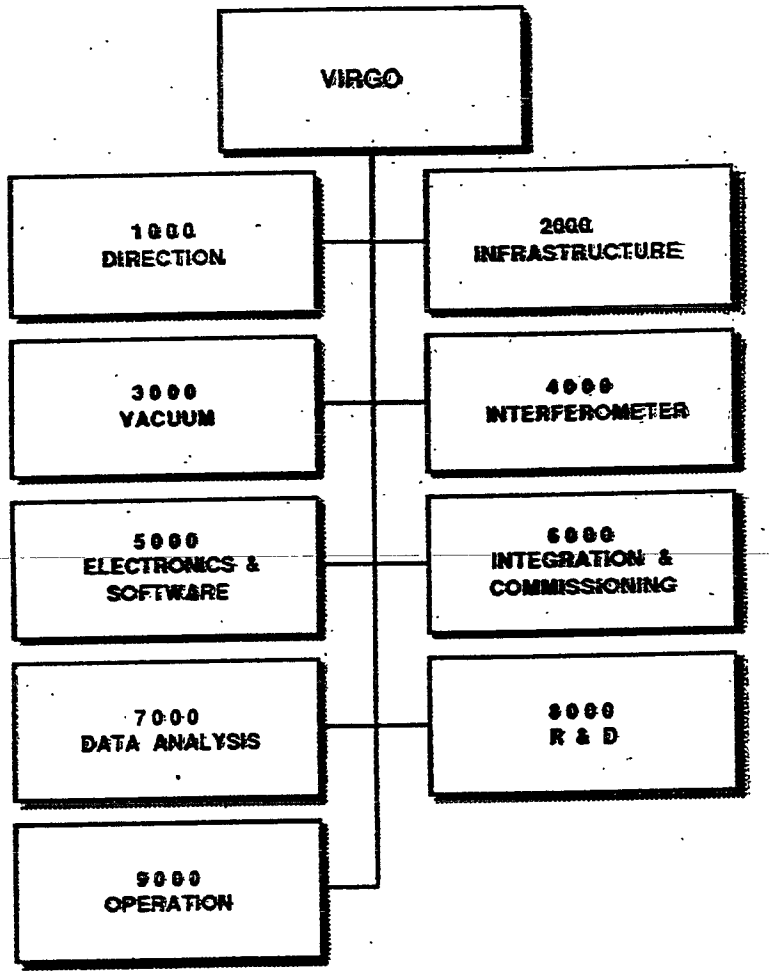
VIRGO
1000
DIRECTION
2000
INFRASTRUCTURE
3000
VACUUM
4000
INTERFEROMETER
5000
ELECTRONICS &
SOFTWARE
6000
INTEGRATION &
COMMISSIONING
7000
DATA ANALYSIS
8000
R & D
9000
OPERATION

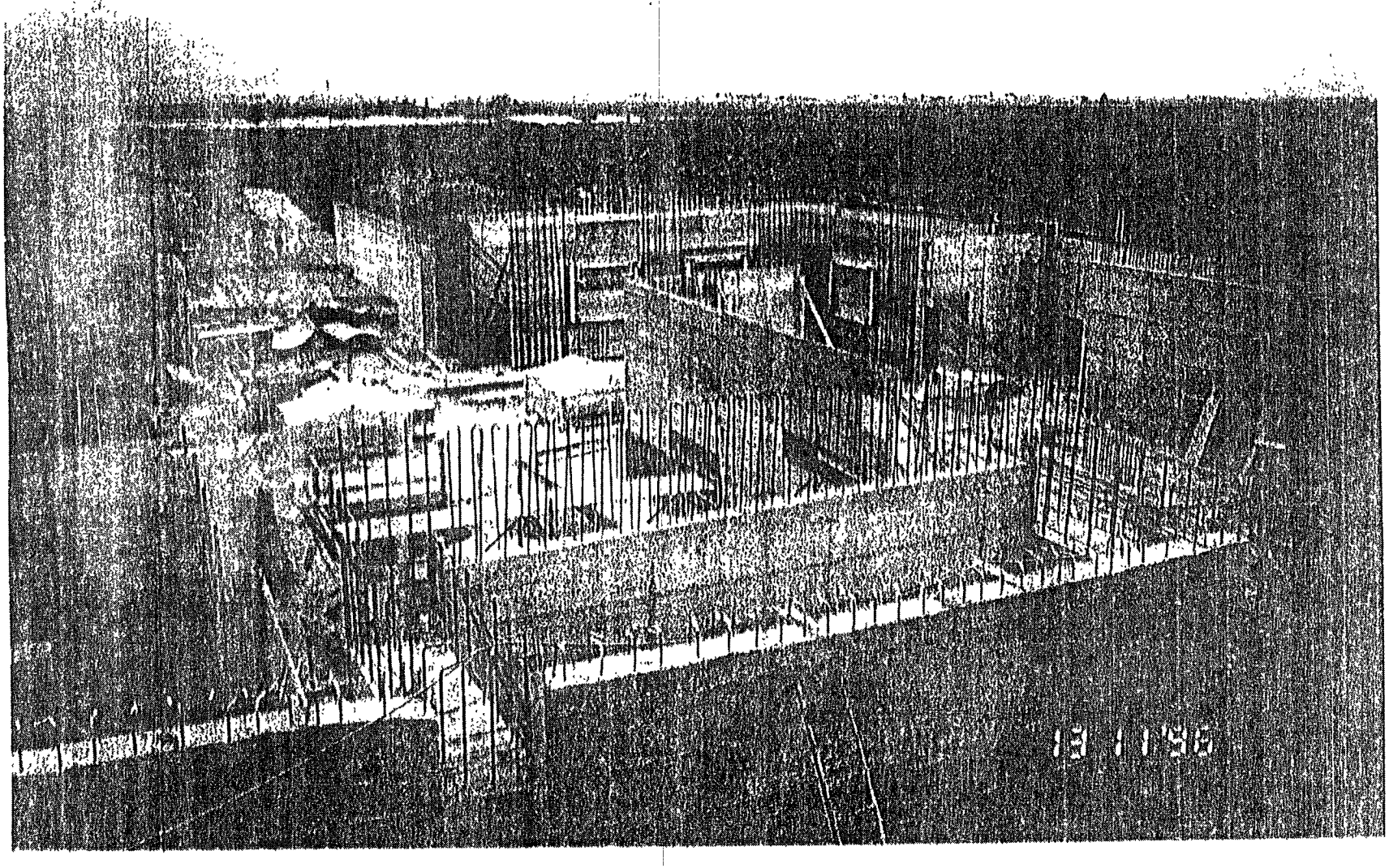

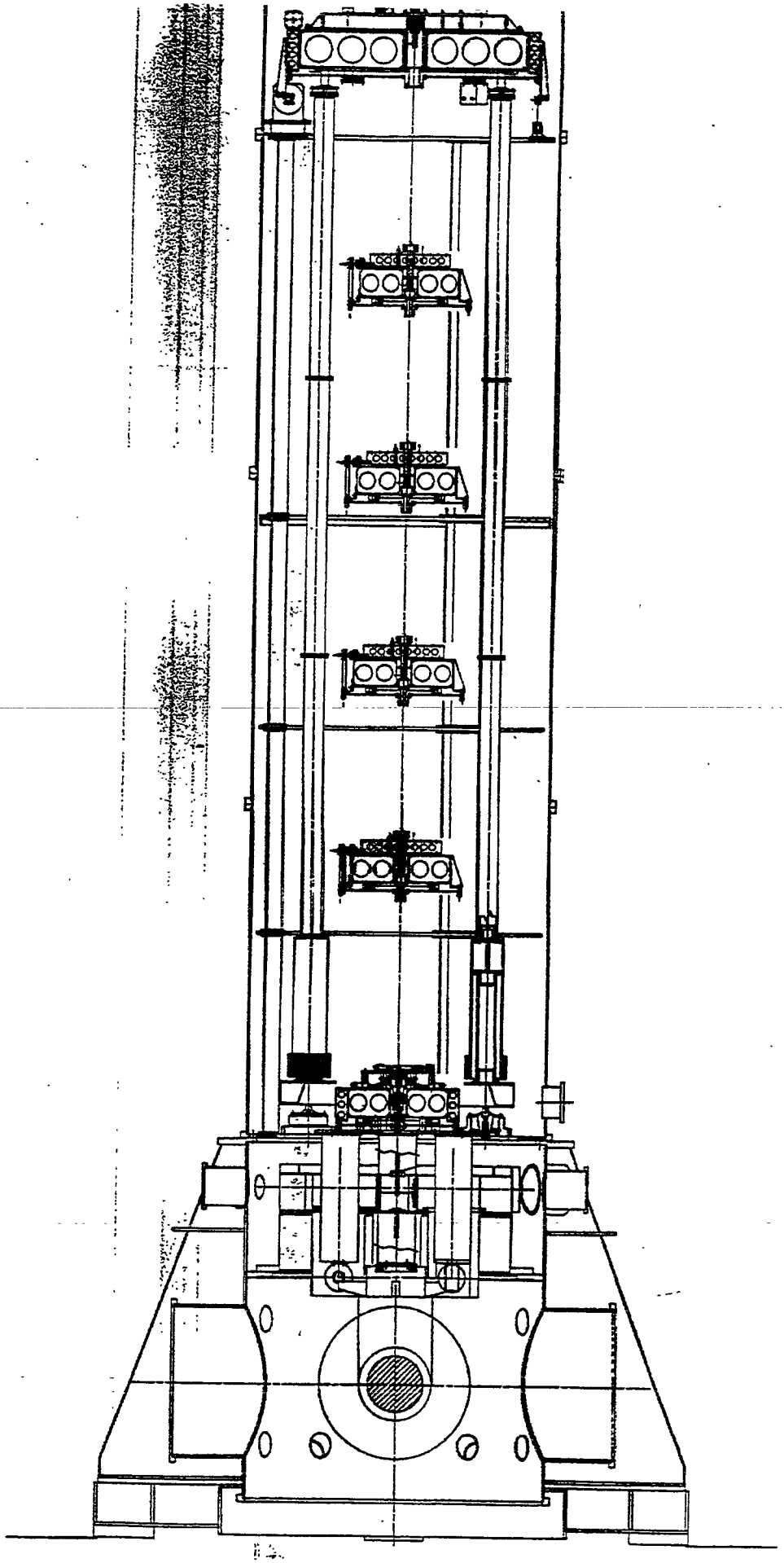

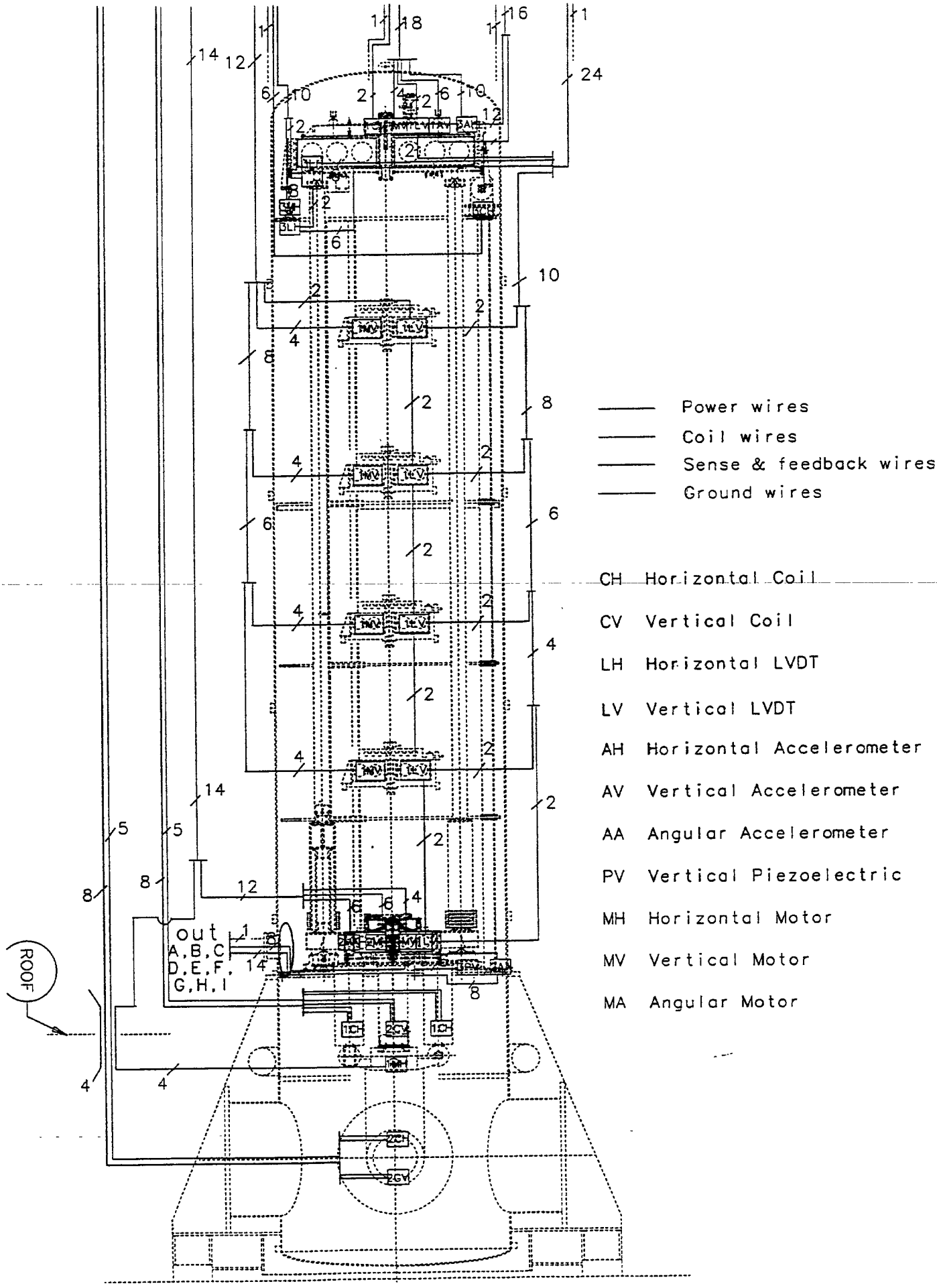
Power wires
Coil wires
Sense & feedback wires
Ground wires
CH Horizontal Coil
CV Vertical Coil
LH Horizontal LVDT
LV Vertical LVDT
AH Horizontal Accelerometer
AV Vertical Accelerometer
AA Angular Accelerometer
PV Vertical Piezoelectric
MH Horizontal Motor
MV Vertical Motor
MA Angular Motor
ROOF
out
A,B,C
D,E,F,
G,H,I

CENTRAL ZONE
NORTH INPUT TOWER
WEST INPUT TOWER
DETECTION TOWER
INJECTION TOWER
BEAM SPLITTER TOWER
RECYCLING TOWER
NORTH TERMINAL TOWER
TERMINAL COMPENSATOR
WEST TERMINAL TOWER
MODE CLEANER TOWER
3000m
4km
LAYOUT OF VIRGO

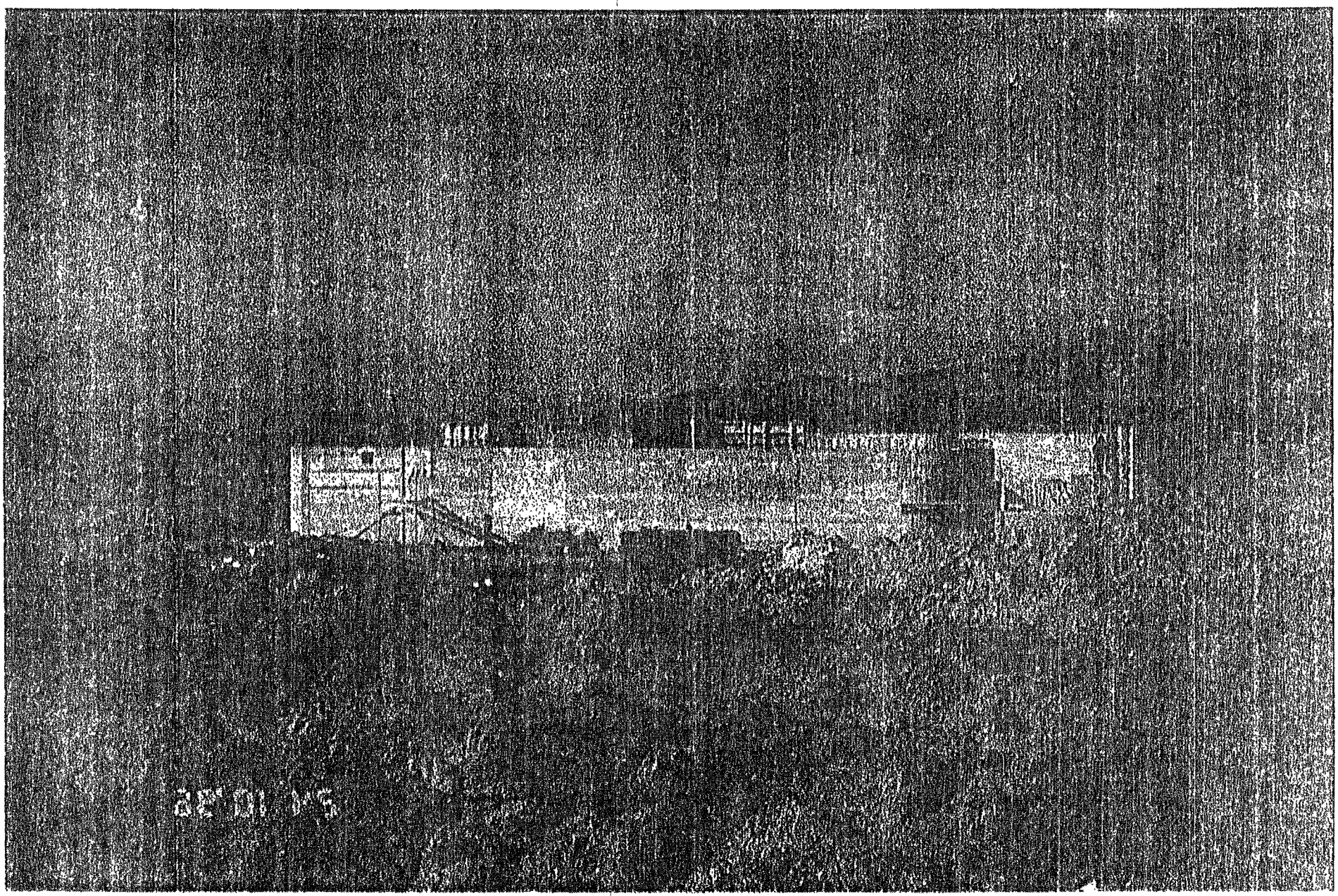

VIRGO

Organisation

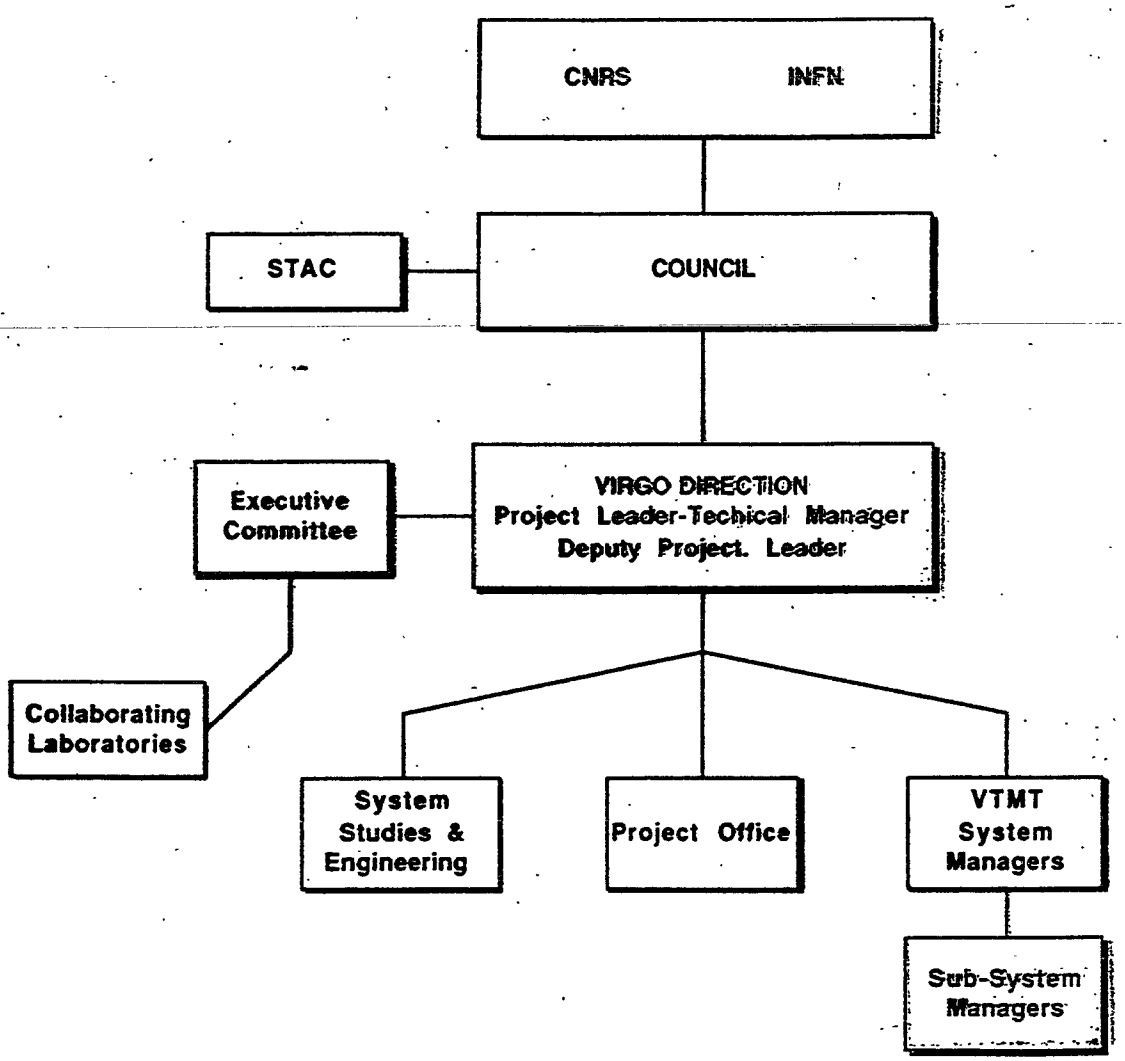

History

1982-1989 Feasibility studies in Orsay and Pisa

1989 --> May : Virgo proposal

1990 Validation by CNRS and INFN committees

1992 --> March : Final conceptual Design

Costs and planning estimates validated by INFN-CNRS joint committee

--> June : project approved by CNRS
--> October : project approved by INFN

1994 --> July : CNRS-INFN agreement

Site acquisition by INFN, in Cascina
Prototype tower in Annecy (vacuum and cleanliness tests)

VIRGO COLLABORATION

ITALY

INFN Frascati

Physicists	*Technicians*	*Administrant*
D. Babusci	E. Cima	S. Giromini
S. Bellucci	M. Iannarelli	
S. Candusso	D. Orecchini	
G. Giordano	E. Turri	
G. Matone		

INFN Firenze

(to be confirmed)

Physicists

E. Bougleax
M. Mazzoni
P. Pelfer
R. Stanga

INFN Napoli

Physicist

F. Barone	M. Flagiello
E. Calloni	M. Longo
L. Di Fiore	M. Lops
F. Garufi	S. Marano
A. Grado	
L. Milano	
S. Solimeno	

INFN Perugia

Physicists

G. Cagnoli
M. Punturo
L. Gammaitoni
J. Kovalik
F. Marchesoni

INFN Pisa

Physicists		*Engineers*	*Technicians*	*Administrant*
M. Beccaria	A. Giassi	A. Basti	L. Berretta	P. Benfatti
M. Bernardini	P. La Penna	D. Enard	E. Carboni	L. Lilli
S. Braccini	G. Losurdo	A. Gaddi	R. Cosci	P. Villani
C. Bradaschia	S. Mancini	A. Gennai	G. De Carolis	
G. Cella	F. Palla	H.B. Pan	A. Di Sacco	
A. Ciampa	D. Passuello	A. Pasqualetti	M. Iacoponi	
E. Cuoco	R. Poggiani	P. Popolizio	F. Paoletti	
G. Curci	A. Viceré	F. Raffaelli	E. Pucciarelli	
R. De Salvo	Z. Zhou		A. Ragonesi	
R. Del Fabbro			R. Ruberti	
A. Di Virgilio				
I. Ferrante				
F. Fidecaro				
A. Giazotto				

INFN Roma

Physicists	*Engineers*	*Technicians*	*Administrant*
V. Ferrari	F. Bronzini	L. Andreanelli	L. Russo
E. Majorana		M.Perciballi	
P. Puppo		E. Serrani	
P. Rapagnani		G. Caparadossi	
F. Ricci		A. Mattei	
		F. Pellegrino	

VIRGO COLLABORATION

FRANCE

LAPP Annecy

Physicists		*Engineers*	*Technicians*	*Administrant*
B. Caron	B. Mours	M. Axeline	D. Boget	C. Lemarec
A. Dominjon	V. Sannibale	F. Bellachia	B. Bourdas	
C. Drezen	M. Yvert	C. Girard	P.-Y. David	
R. Flaminio		J.-C. Lacotte	L. Derome	
X. Grave		J. Lecoq	G. Gaillard	
F. Marion		B. Lieunard	L. Giacobone	
L. Massonnet		S. Lieunard	R. Hermel	
C. Mehmel		P. Mugnier	J.-C. Lemarec	
R. Morand			R. Sottile	

IPN Lyon

Physicists	*Engineers*
J.M. Mackowski	L. Dognin
L. Pinard	P. Ganau
	C. Michel
	M. Napolitano

ESPCI Paris

Physicists

C. Boccara
P. Gleyzes
J.P. Roger
V. Loriette

LAL Orsay

Physicists	*Engineers*	*Technicians*	
M. Barsuglia	C. Arnault	R. Combeau	G. Lissillour
V. Brisson	J.L. Beney	P. Corona	R. Marie
F. Cavalier	R. Bilhaut	J.P. Coulon	J.C. Marrucho
M. Davier	R. Chiche	S. Cuzon	P. Rivoirard
P. Hello	M. Dialinas	M. Dehamme	M. Taurigna
P. Heusse	A. Ducorps	C. Eder	
F. Lediberder	A. Hrisoho	C. Garnier	
P. Marin	A. Reboux	M. Gaspard	
	P. Roudier	E. Jules	

Laser Optics Orsay

Physicists		*Engineers*	*Technicians*	*Administrant*
B. Bhawal	C. Nary Man	Y. Acker	P. Bindzi	E. Ruillere
A. Brillet	M. Pham-Tu	R. Barillet	J.-C. Lucenay	
F. Bondu	M. Taubman	J. Cachenaut	T. Redon	
H. Heitmann	E. Tournier	F. Cleva		
J.-M. Innocent	J.Y. Vinet	V. Reita		
L. Latrach				

VIRGO

A laser interferometer for the detection of Gravitational waves

Location: Cascina (Pisa) - Italy

Centre National de Recherche Scientifique (CNRS)
France
Laboratoire d'optique - LAL Orsay
IN2P3 - LAL, Orsay
IN2P3- LAPP, Annecy
EPSCI, Paris
IPN, Lyon

Istituto Nazionale di Fisica Nucleare (INFN)
Italia
INFN, Laboratori Nazionali di Frascati
INFN, Sezione di Firenze
INFN, Sezione di Napoli
INFN, Sezione di Perugia
INFN, Sezione di Pisa
INFN, Sezione di Roma 1

The Data Stream

- Properties of the interferometric detector data
  - ›› Large dynamic range > 160 db
    - servo control and filtering
    - need for "whitening"
  - ›› Large frequency range $\frac{F_{max}}{F_{min}} > 1000$
- Characteristics of the noise
  - strongly colored
  - components with different correlation times τ_{cor}
  - steady state component - the typical noise curves presented
  - slowly varying part : time of day, temperature.....
  - time domain: rare, large amplitude (non-Gaussian) component
  - freq. domain: few, large amplitude (non Rayleigh) components

The Data Stream

- The data recorded
  - Gravitational wave strain at antisymmetric port
    - 16 bit words sampled at 16.4 kHz
    - absolute timing accuracy 10 μsec, resolution 1μ sec
    - calibration accuracy better than 10%
    - continuous record > 40 hours
    - annually integrated "availability" single interferometer > 90 %
    - averaged double coincidence availability > 85 %
    - averaged triple coincidence availability > 75 %
  - Ancillary instrument information
    - laser frequency, amplitude, beam jitter.....
    - suspension motions, orientation, transverse translations .....
    - common and differential mode longitudinal and angular control
    - .....
    -

The Data Stream

- Environmental and facility information
  - 3 axis seismic motion
  - 2 axis tilt
  - 3 axis acceleration of chambers
  - 3 axis magnetic fields
  - radio frequency interference
  - power line fluctuations
  - residual gas fluctuations
  - .....

The Data Stream

- Goals:
  - Development of reduced data sets
    - calibrated in standard units h(t) or h(f)
    - instrument signatures removed
    - correlations with environmental parameters removed or vetoed
    - size of set to permit meaningful real time analysis

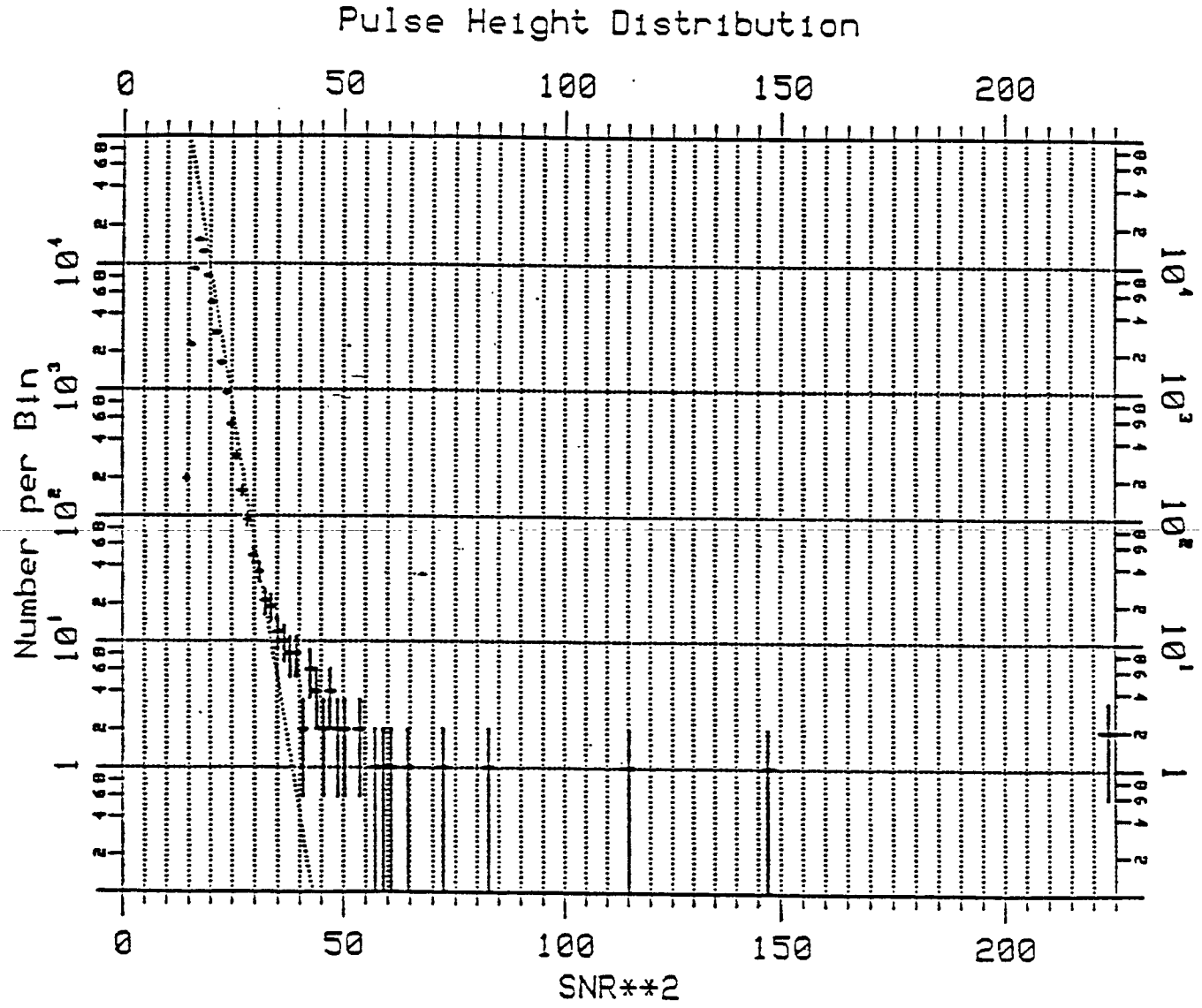

Figure 7.20 PHD from All Templates Excluding the "102" Events

O.OEWE'

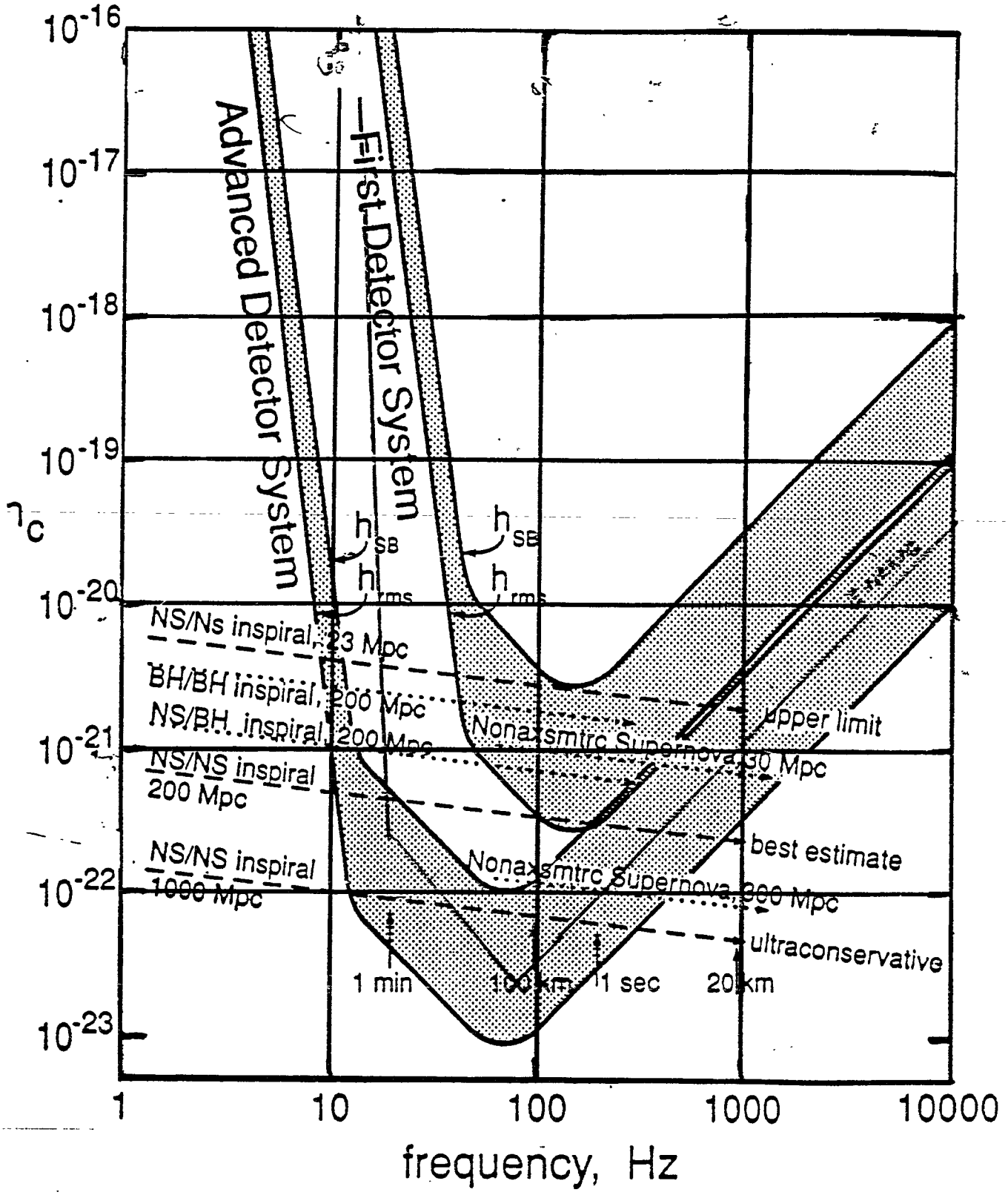
Advanced Detector System
First Detector System
h_{SB}
h_{rms}
h_{SB}
h_{rms}
NS/Ns inspiral, 23 Mpc
BH/BH inspiral, 200 Mpc
NS/BH inspiral, 200 Mpc
NS/NS inspiral 200 Mpc
NS/NS inspiral 1000 Mpc
Nonaxsmtrc Supernova, 30 Mpc
Nonaxsmtrc Supernova, 200 Mpc
upper limit
best estimate
ultraconservative
1 min
100 km
1 sec
20 km
h_c
10^{-16}
10^{-17}
10^{-18}
10^{-19}
10^{-20}
10^{-21}
10^{-22}
10^{-23}
1
10
100
1000
10000
frequency, Hz

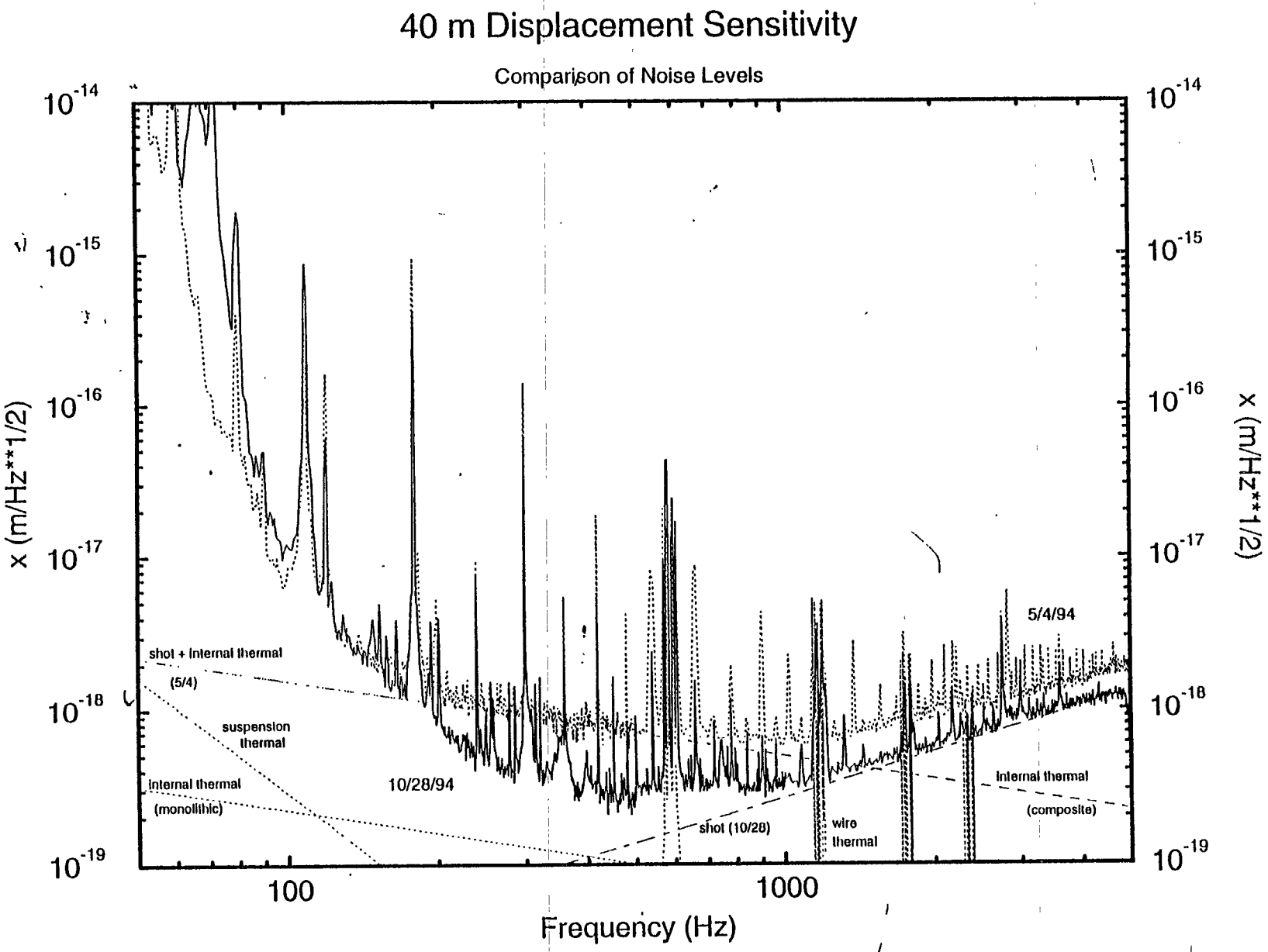
40 m Displacement Sensitivity
Comparison of Noise Levels
x (m/Hz**1/2)
Frequency (Hz)
100
1000
10^-14
10^-15
10^-16
10^-17
10^-18
10^-19
shot + internal thermal
(5/4)
suspension
thermal
internal thermal
(monolithic)
10/28/94
5/4/94
shot (10/28)
wire
thermal
internal thermal
(composite)

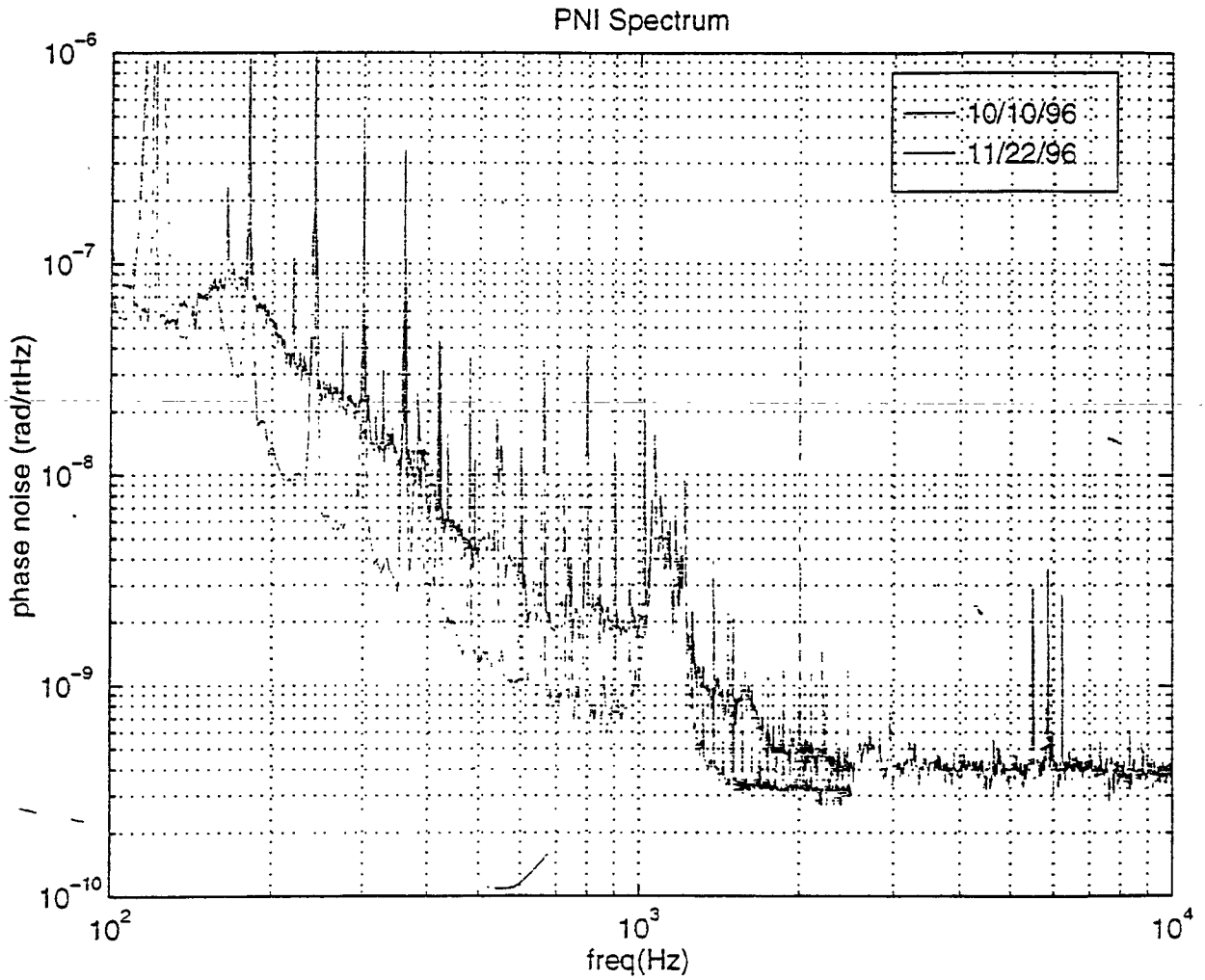
PNI Spectrum
10/10/96
11/22/96
phase noise (rad/rtHz)
10^{-6}
10^{-7}
10^{-8}
10^{-9}
10^{-10}
10^{2}
10^{3}
10^{4}
freq(Hz)

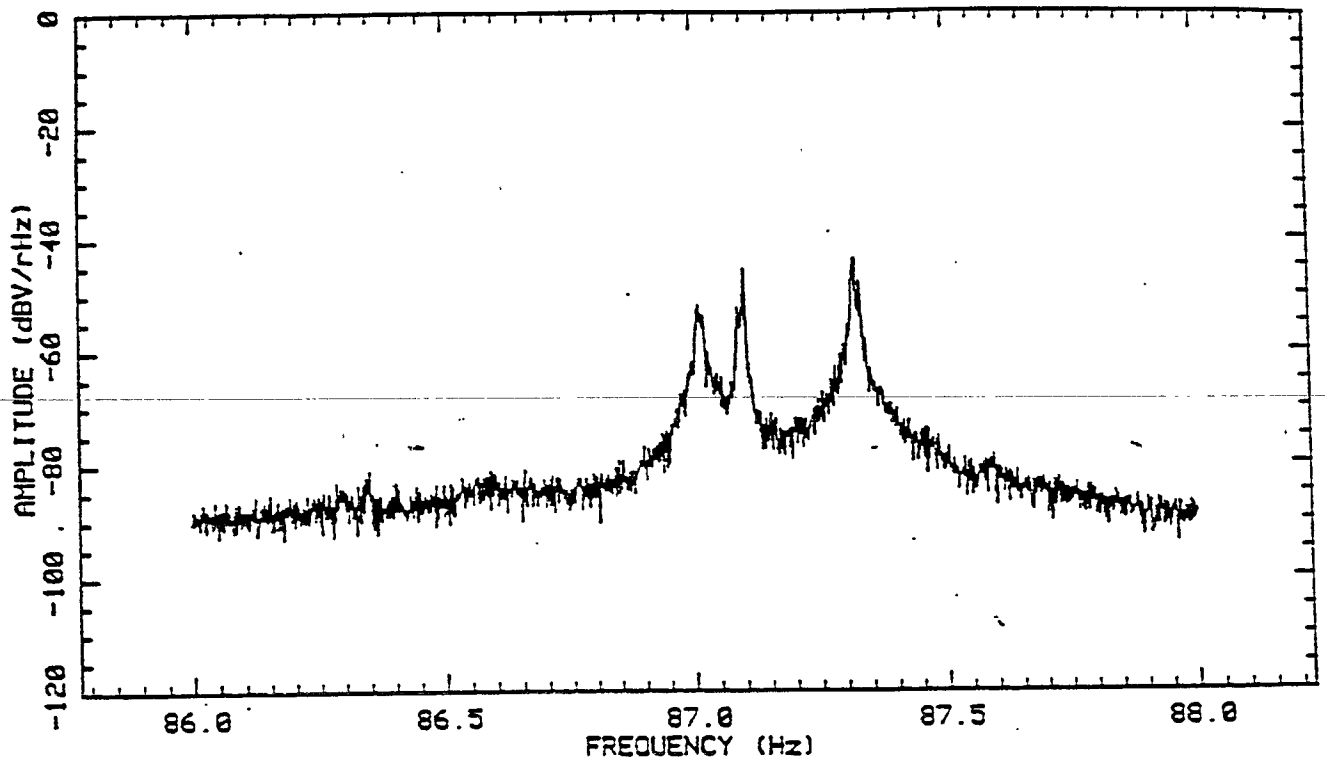

Figure 5.19
Suspension wire "string" mode resonances.

J. LIVAS

Quantization noise

- Dynamic range

	$h(f)$ $1/(\sqrt{\text{Hz}})$	f Hz	t_{int} sec	h_{rms}
tides		$1-2\times10^{-5}$		1×10^{-7}
microseismic and seismic	5×10^{-11}	0.1 - 10		
pendulum		1	10 servo damped	1×10^{-15}
wire vertical 1×10^{-3} cross couple		16	1×10^{3}	6×10^{-20}
wire horizontal		450	1×10^{4}	1×10^{-20}
mirror mode		16 k	1×10^{2}	7×10^{-20}
minimum initial det noise	1×10^{-23}	150	1×10^{7}	3×10^{-27}

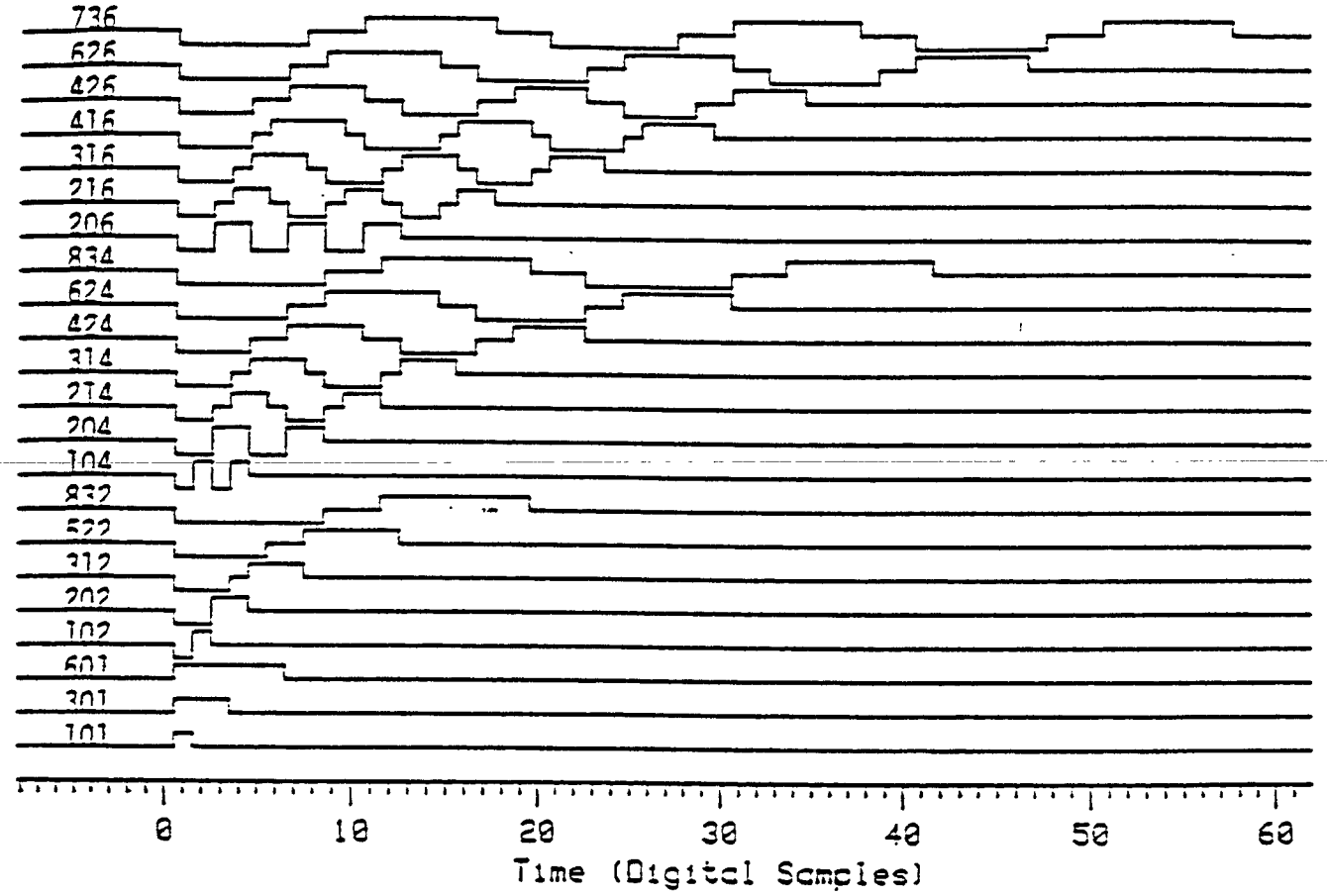

Figure 6.5 The Set of Templates and their N_1, N_0, NHC Codes

D. DEVROY

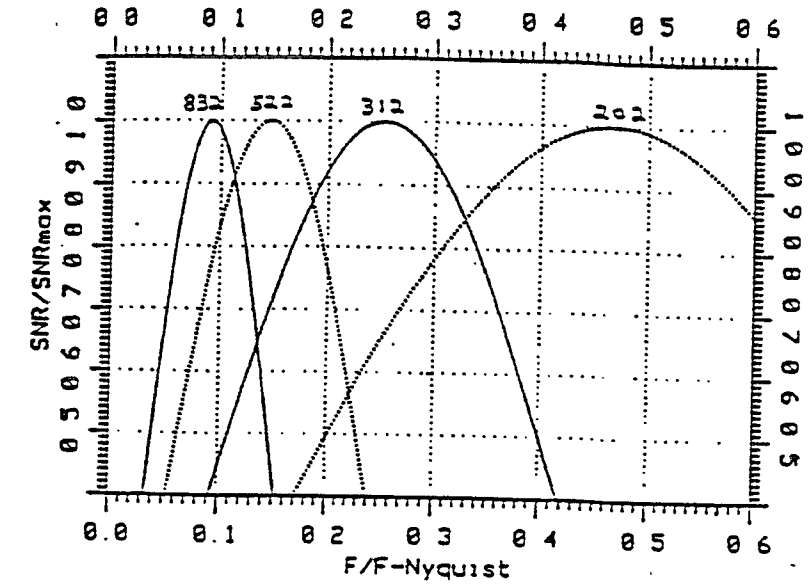

NHC = 2

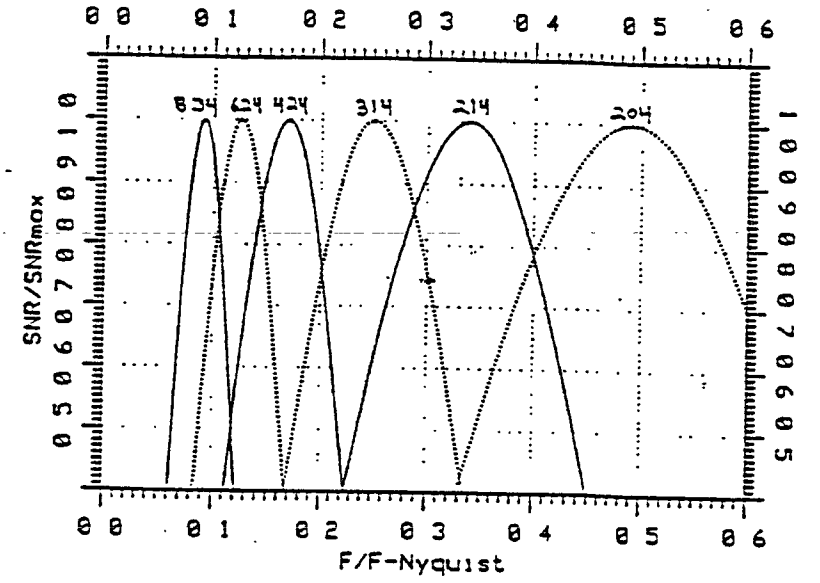

NHC = 4

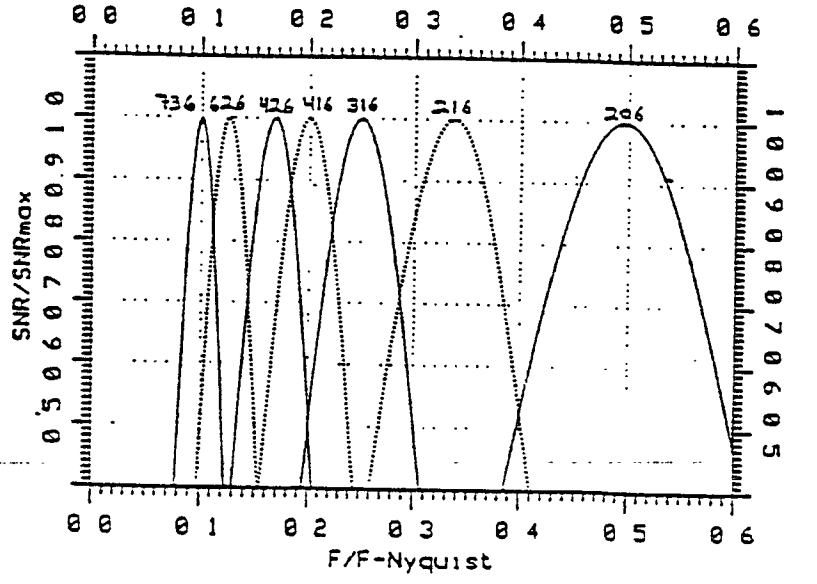

NHC = 6

D. DREW

Figure 6.6 SNR Response of the Digital Templates

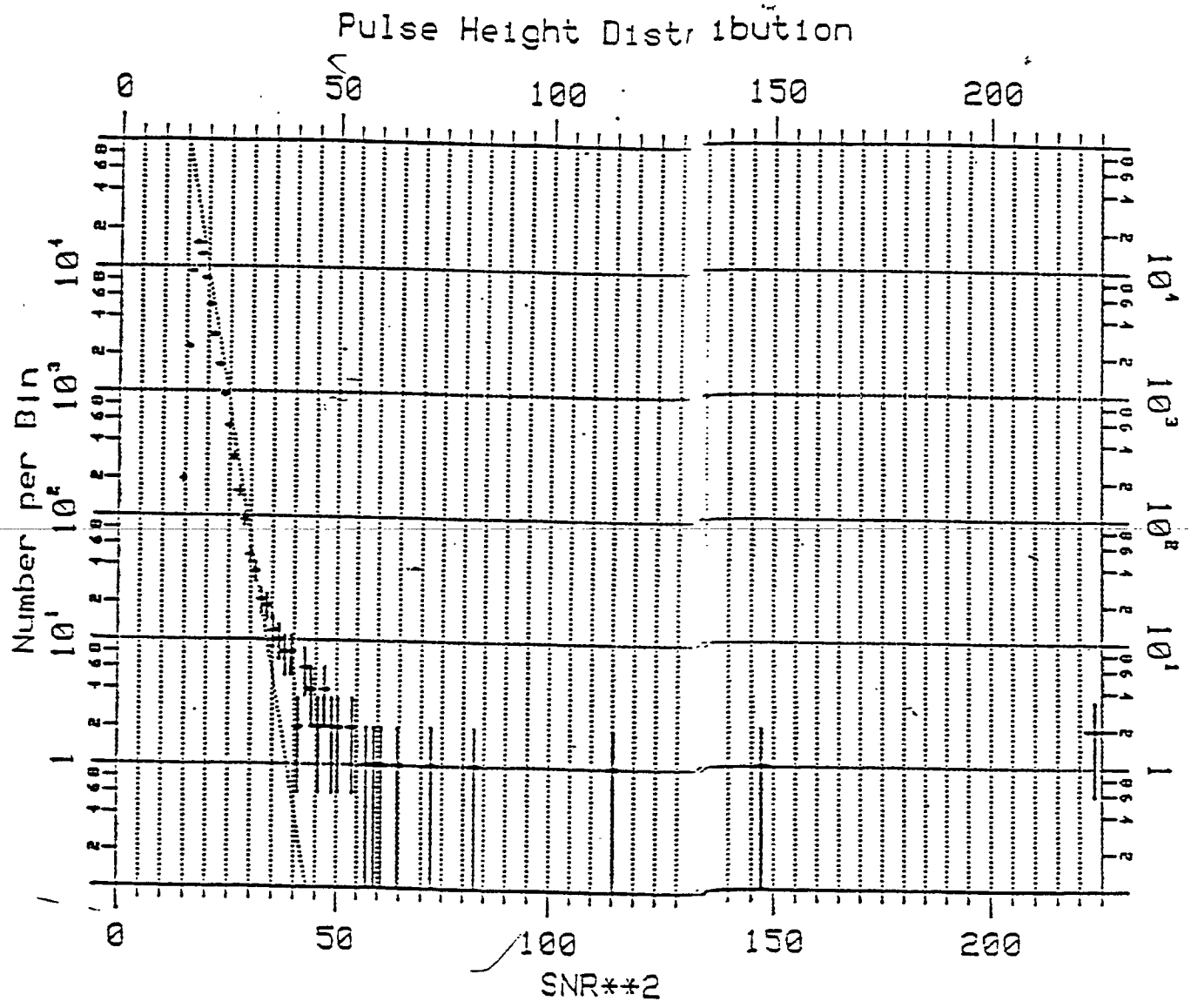

Figure 7.20 PHD from All Templates Excluding the "102" Events

O. OREWY

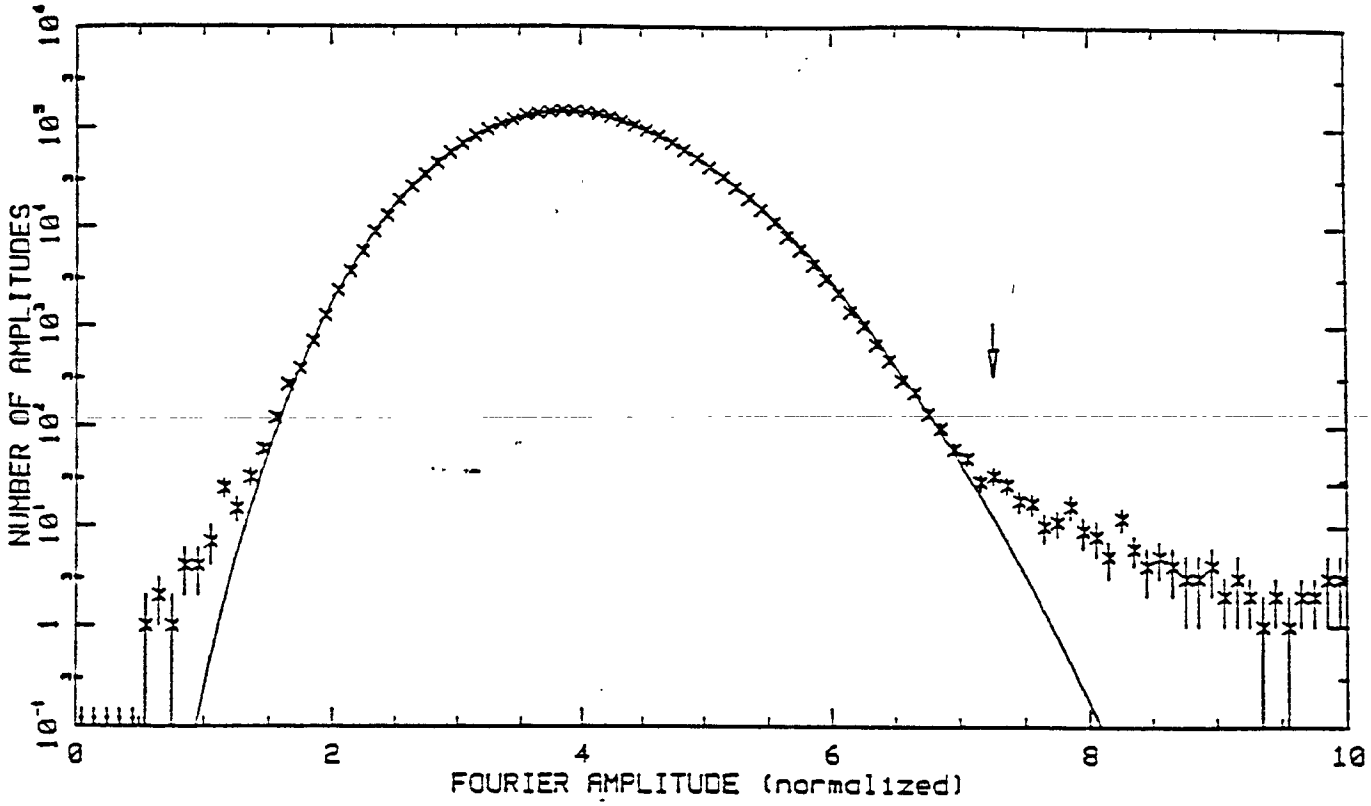

Figure 5.14

8-tape rms averaged power spectrum amplitude distribution.

Table 1: Estimated IFO Data Channels and Rates

System	*Number of Channels/Sample Rate*				
	2 Hz	*256 Hz*	*2048 Hz*	*16384 Hz*	*Total*
Sensitive Component Suspension	120	90	30	60	300
Prestabilized Laser	20	10	5	8	43
Mode Cleaner	30	20	10	20	80
Injection Optics	20	15	5	10	50
Interferometer Readout	20	15	0	30	65
Auto Alignment	20	15	0	0	35
Total Acquisition Channels/IFO	230	165	50	128	573
Total Data Rates (KBytes/sec)/IFO	0.9	84.5	204.8	4194.3	4484.5

Table 2: Estimated LIGO PEM/Control & Monitoring Data Channels and Rates

System	*Number of Channels / Sample Rate*				
	2 Hz	*256 Hz*	*2048 Hz*	*16384 Hz*	*Total*
Auxillary	0	200	10	30	240
Housekeeping	300	50	20	0	370
Total Channel Counts	300	250	30	30	610
Data Rates (KBytes/sec)	1.2	128	122.9	983.0	1235.1

Table 3: Estimated Site Data Channels and Rates

System	*Number of Channels*				
	2 Hz	*256 Hz*	*2048 Hz*	*16384 Hz*	*Total*
Hanford	760	580	130	286	1756
Livingston	530	415	80	158	1183
Total Channel Counts	1290	995	210	444	2939
Data Rates (KBytes/sec)	5	509.4	860.2	14549.0	15923.6

Gravitational-Wave Data Analysis Workshop

Kent Blackburn
Albert Lazzarini
LIGO Integration Group

MIT
6 - 8 December 1996

LIGO-G960240-00-E

/home/lazz/Presentations/Talks/GWDataAnalysisMITMtg.fm5

LIGO Data Stream and Data Frame Design

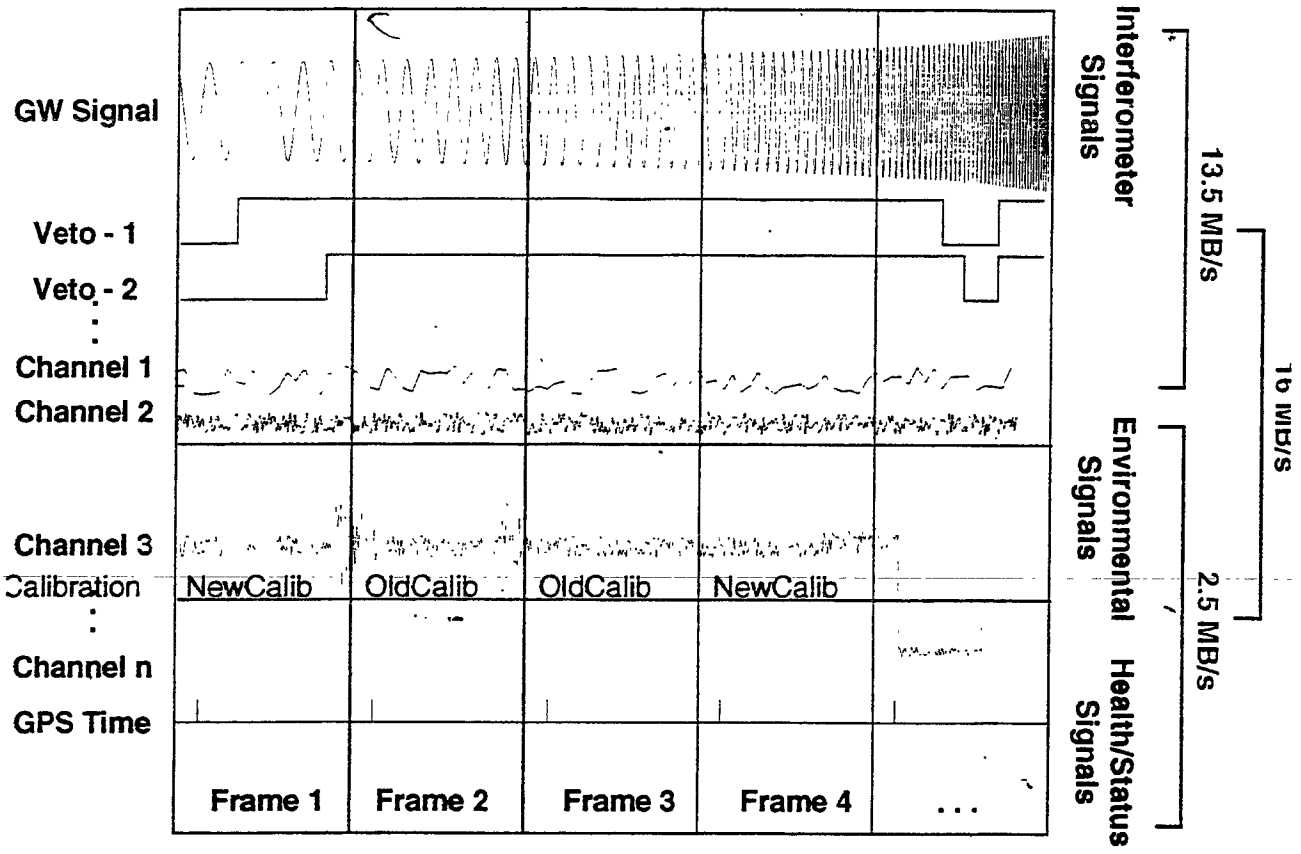

- Frame is (structured) self-contained snapshot of data for a period of time
  - GW channel & ancillary IFO channels
  - Environmental monitoring (veto) channels
  - Facilities/Vacuum health & status
  - Hierarchical organization of data reflects IFO subsystems for more efficient veto utilization

LIGO-VIRGO DATA FORMAT

Status

- Initial meeting with VIRGO in April hosted by LIGO
  - VIRGO format presented, compared with LIGO needs
  - Attractive (to LIGO) because of maturity & availability of existing I/O libraries
  - Tuned for time-series data stream (vs. events or images)
- Alternatives explored by LIGO
  - Public domain standards - CDF/HDF
  - Used for image frame data distribution (NASA)
  - Greater overhead per frame than VIRGO
  - Well suited for eventual data distribution
- Continued interaction with VIRGO
  - Format evolving under collaborative effort
  - Software availability: commited to public domain access of libraries

LIGO-VIRGO DATA FORMAT

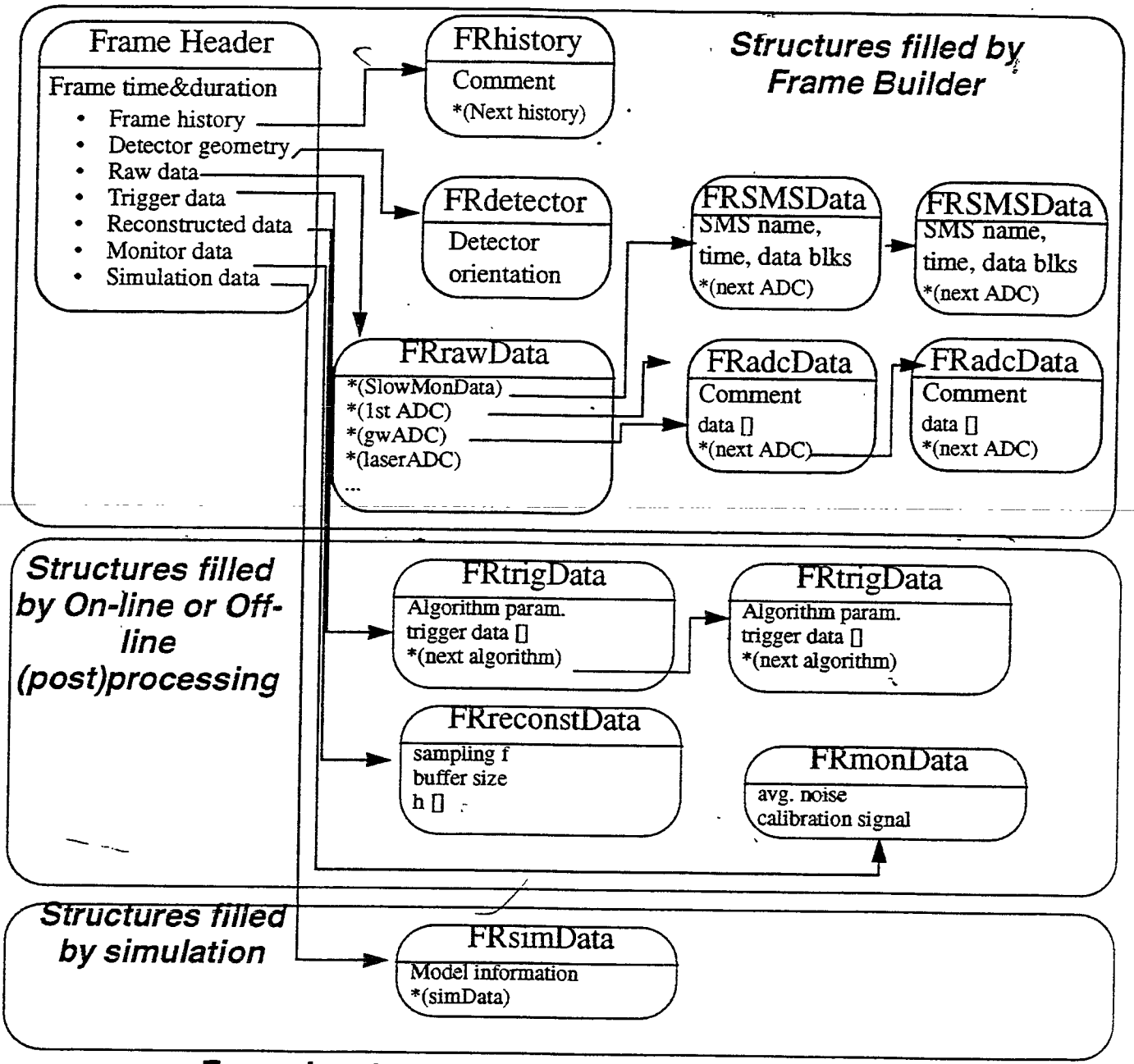

- **Frame has tree structure:**
- **Individual blocks are C structures**
- **Extensible to arbitrary length with design evolution**
- **Utilized for both on-line & off-line analyses**

LIGO-G960240-00-E

LIGO-VIRGO DATA FORMATS

- PROPOSED FORMAT (Adopted from VIRGO)
  - FRAMES (unit of information containing all information needed to understand the interferometer behavior over a finite time interval)
  - C STRUCTURES (frames are organized as a set of C structures)
  - FRAME HEADER (holds pointers to additional structures that contain all information)
  - LINK LISTS (used to collect generic data types, PEM, ADC, etc.)
  - HEADER HOOKS (pointing to frame elements used by on-line processing or by off-line reprocessing)
  - 2^N DATA POINTS (allowing faster FFT analysis on individual frames)
  - DICTIONARY (acts as a catalog of C structures and pointer offsets)

LIGO Data Analysis Flow -- Baseline

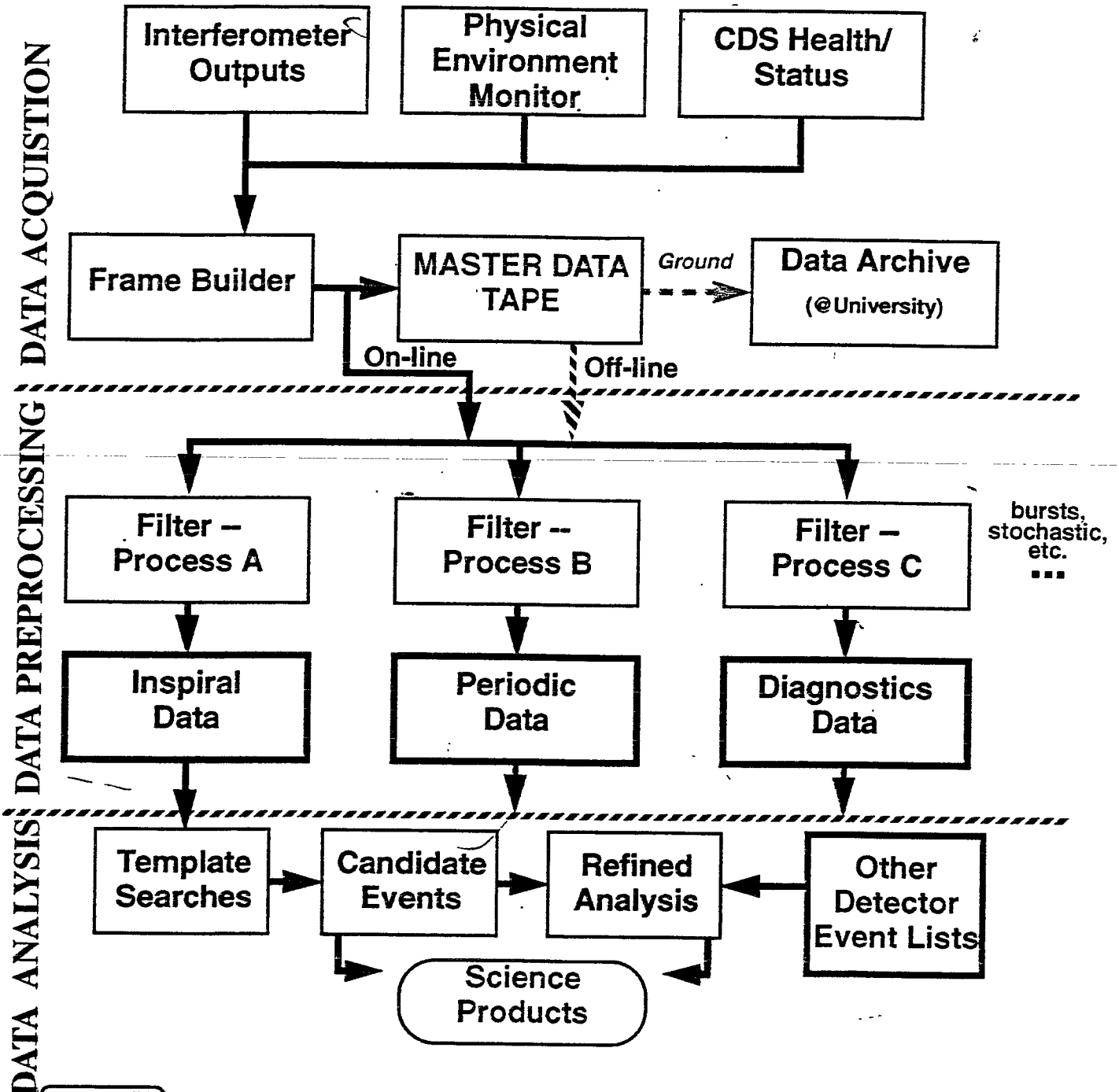

LIGO

LIGO-G960240-00-E

/home/lazz/Presentations/Talks/GWDataAnalysisMTMtg.fm5

Data Analysis for Initial LIGO

Processing Computing Resources & Distribution

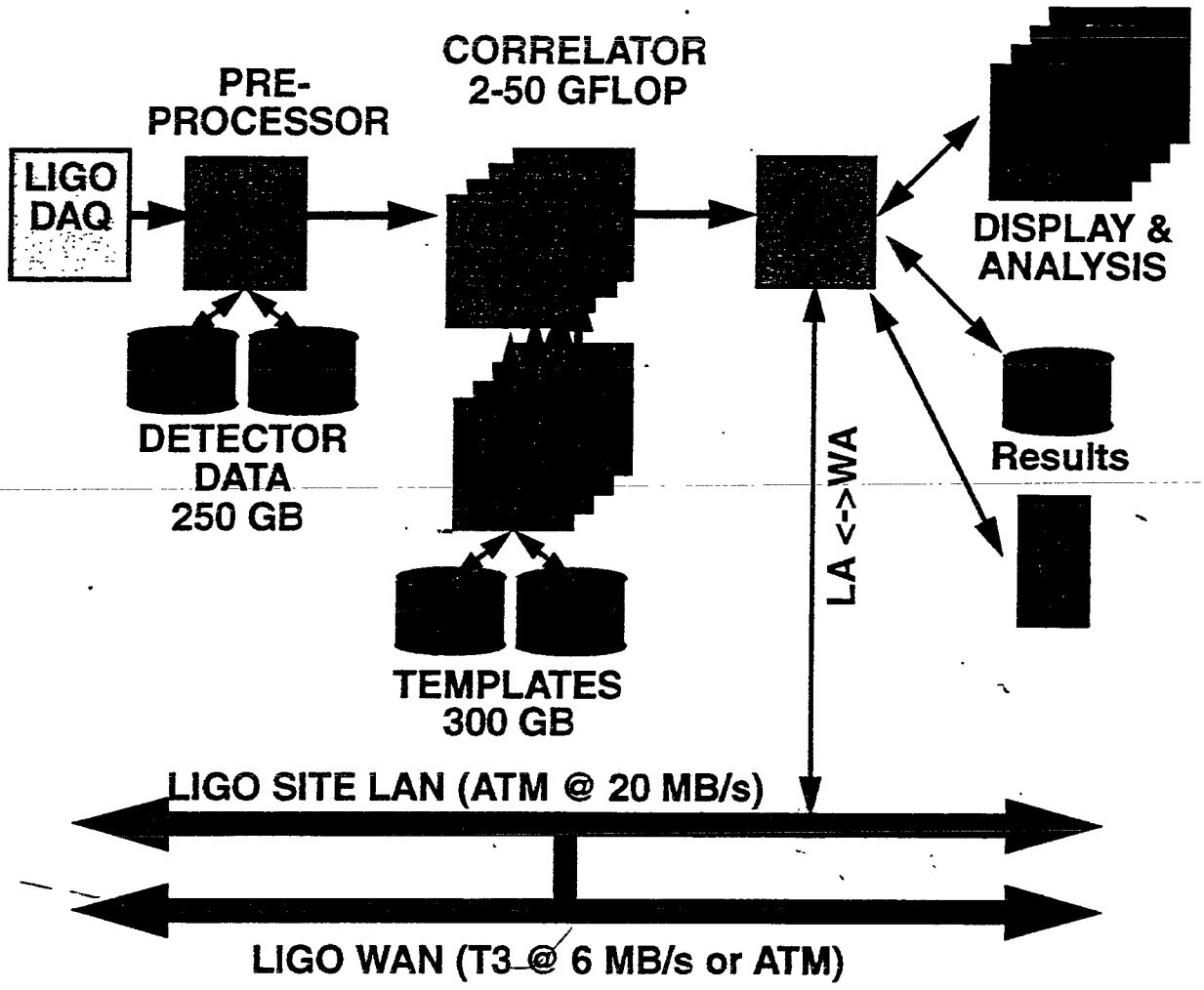

/home/lazz/Presentations/Talks/GWDataAnalysisMITMtg.fm5

Ongoing Activities
Prototyping

- Detector construction phase is developing a prototype DAQ system for the 40m facility
  - Utilize 40m to acquire datasets of substantial length (1/2 day) on a regular basis
  - Experimental use of ancillary channels for data qualification
- LIGO co-authored joint proposal for IBM Sponsored University Research (SUR) Grant funding - $800k of processor hardware will be awarded
  - LIGO will participate in hardware configuration definition; to be shared with other campus groups
  - Hardware to be installed at Center for Advanced Computing Research (CACR)
  - CACR already has similar NSF-funded hardware for astrophysics data analysis
- Use ongoing work to provide realistic scaling of parallel analysis algorithms for large data sets
- Establish data link from 40m to CACR

Planned Activities
Timeline for Development

Milestone or Event	Date	Communications	Hardware	Software
Begin Coincidence Operations	7/00	Common		
On-Line System Available	1/00	Common		
	3/99-12/99	Implementation	Procurement & Integration	Verification
	11/98	Agreements	Specifications	Development
System FDR	11/98	Definition	Design & Prototyping	Specifications
System PDR	11/97			Design & Prototyping
System DRR	5/97			

LIGO Standards

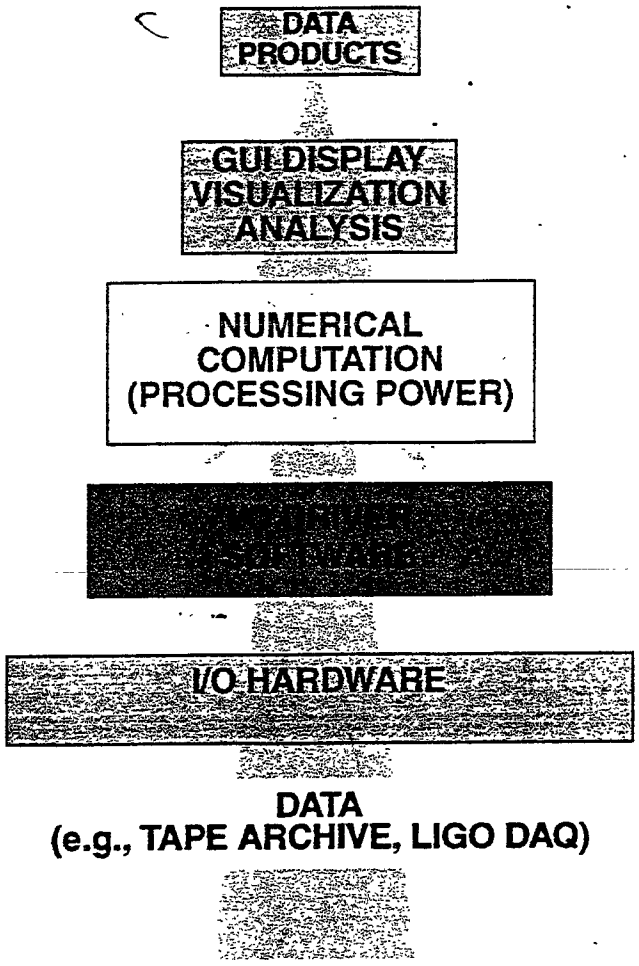

- Software libraries are modular,addressing various analysis functions: analysis/visualization; computation; I/O; etc.
- Limit the sources of potential platform-dependent occurrences of software routines to low-level (standardized) drivers

NON-GAUSSIAN NOISE

"Backgrounds" for detection

'EXTERNAL' ≠ VETOABLE
NON VETOABLE

'INTERNAL' !

"POTENTIALLY" CRIPPLING
BECAUSE FALSE ALARM IS SO COSTLY

ALLEGRO HISTORY

DESCRIPTION
(CAUSES)

LESSONS

MORE DETECTORS REQUIRED

PROBLEM IS UNQUANTIFIED UNTIL
SERIOUS SEARCHES ARE DONE.
HISTOGRAMS BEAT SPECTRA.

ALLEGRO

A Louisiana Low-temperature Experiment
and Gravitational Radiation Observatory

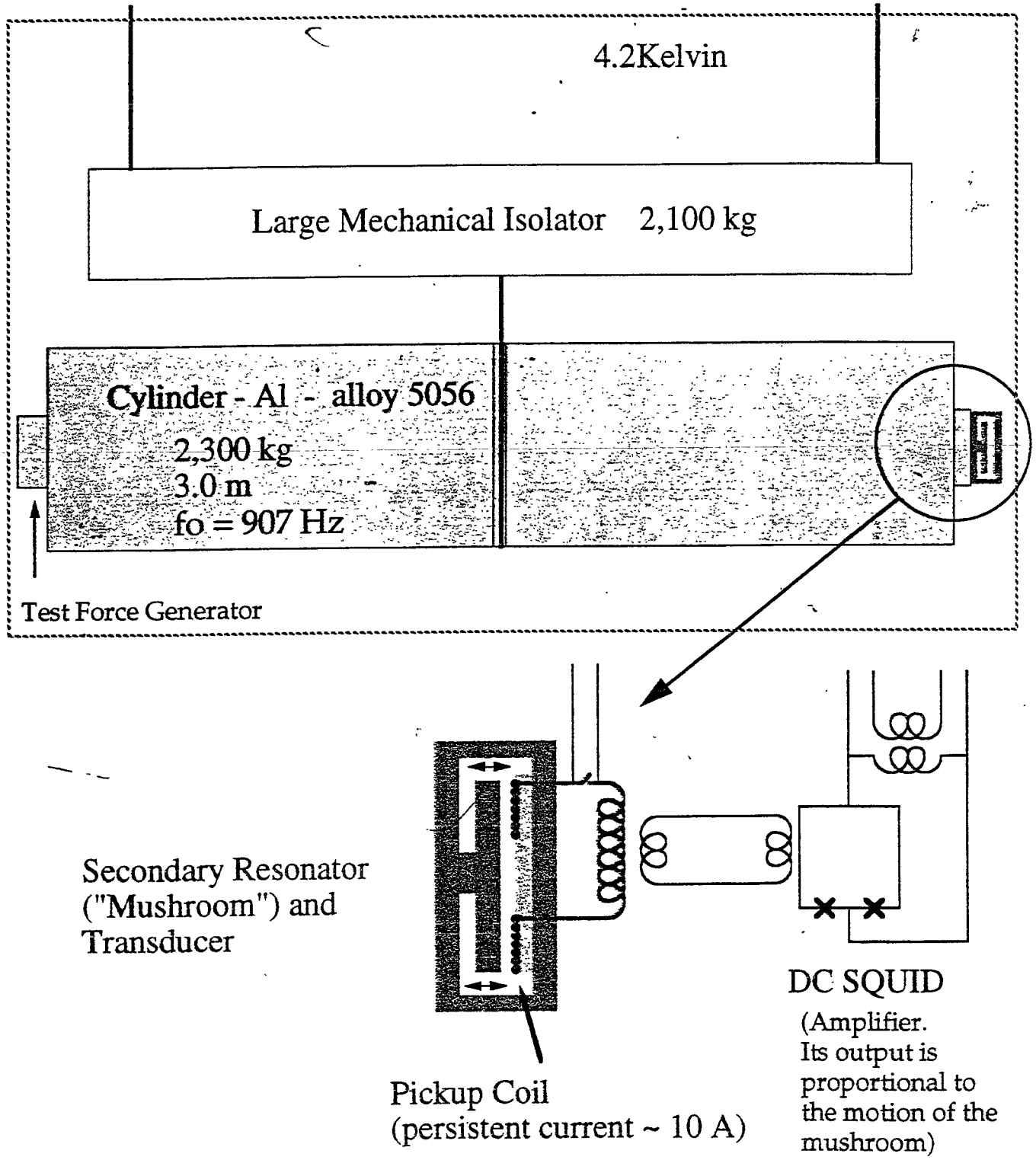

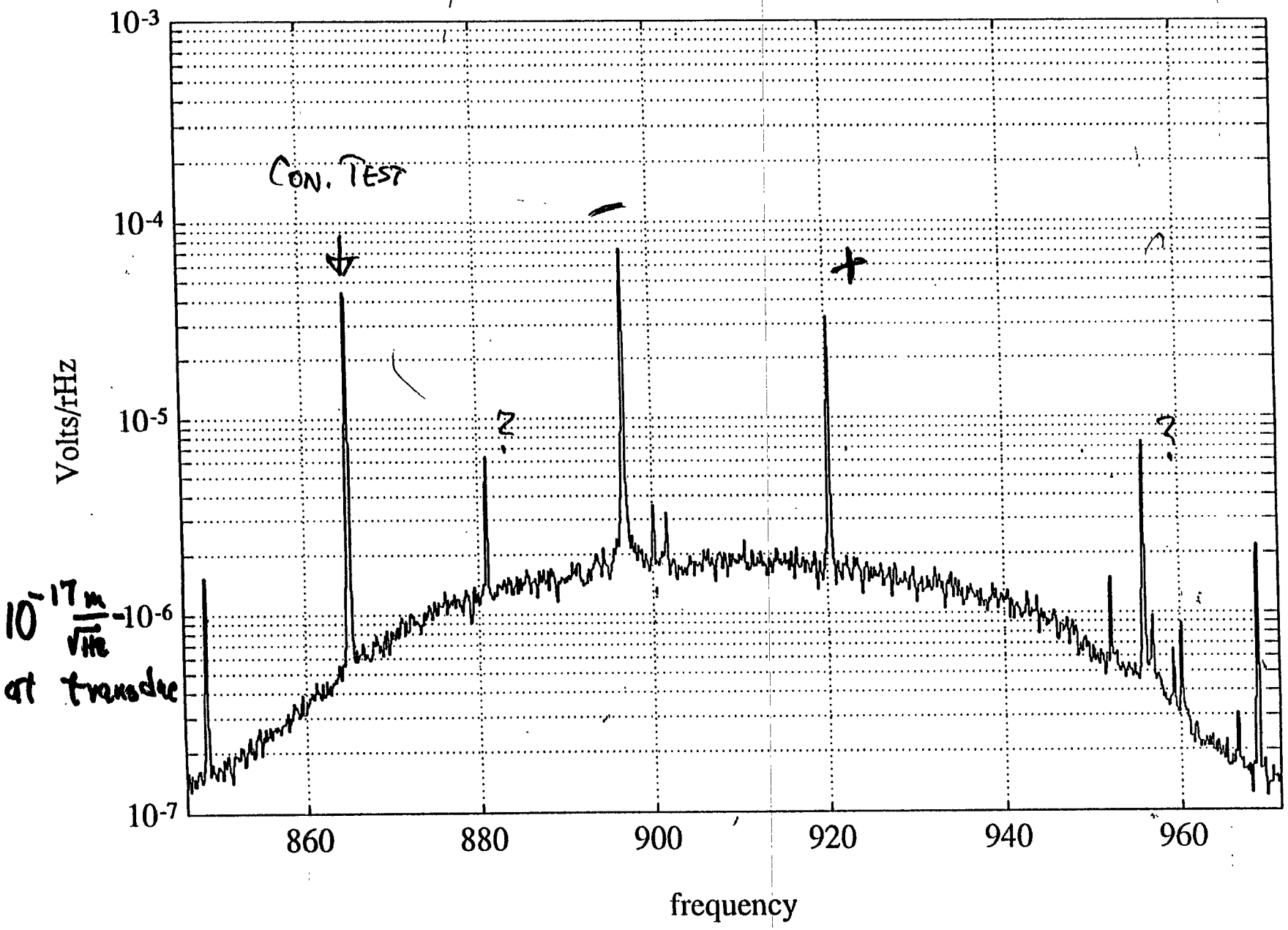
NOISE_SPEC8: file: day162 , recnum= 1001:1008
ut = 5:33:40
CON. TEST
Volts/rHz
frequency
10-3
10-4
10-5
10-6
10-7
860
880
900
920
940
960
10-17 m/√Hz at transducer

NOISE BUDGET - ALLEGRO '93

—— RESONATOR THERMO-MECHANICAL FORCE ("BROWNIAN")

..... ANTENNA " "

-.-.-.- AMPLIFIER (SQUID) NOISE

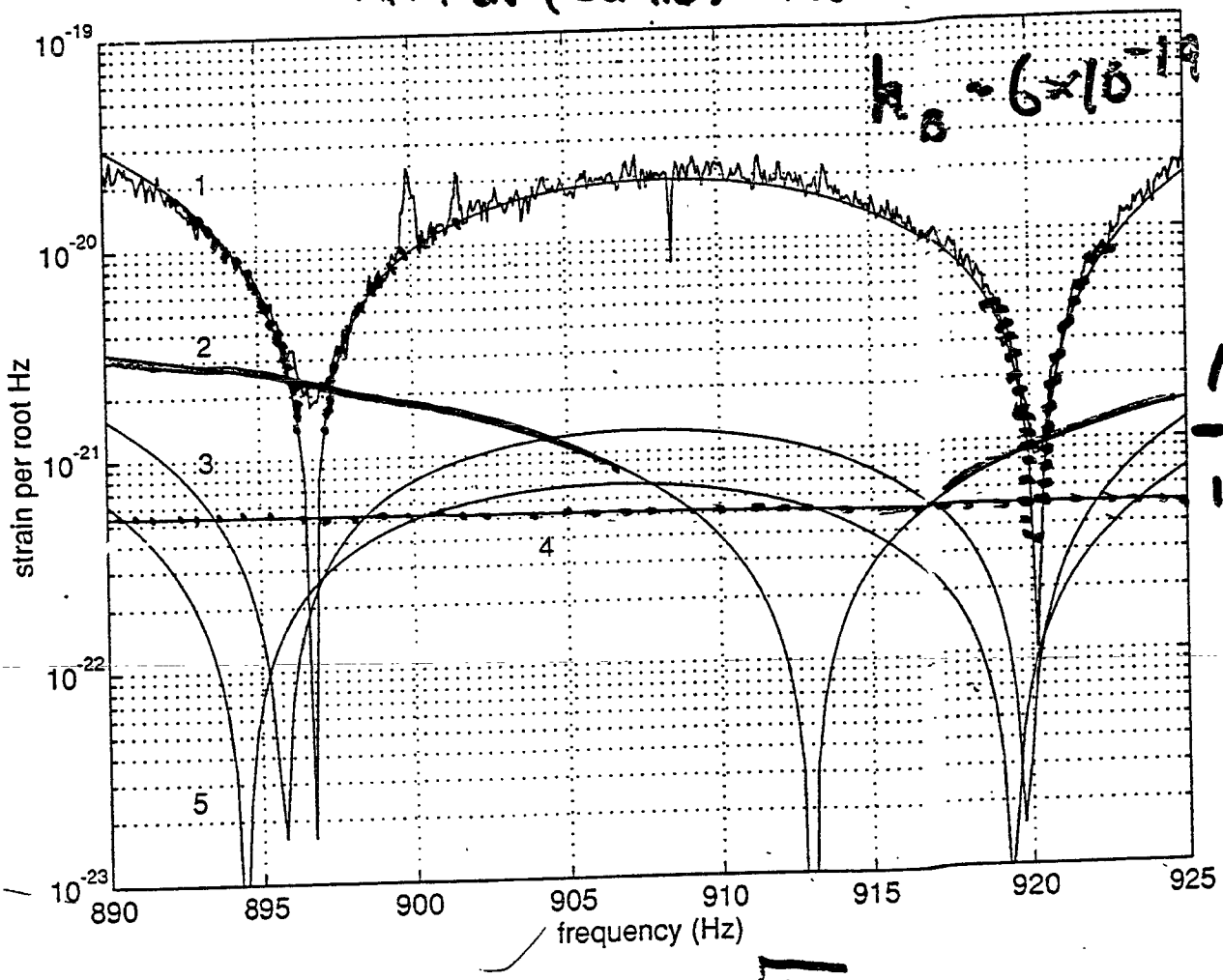

THERMO-MECHANICAL NOISE $\propto \sqrt{\frac{T}{mQ}}$

AMP NOISE $\propto$ $\frac{\text{ADDITIVE NOISE}}{\text{COUPLING STRENGTH}}$

What can be done with cryogenic techniques

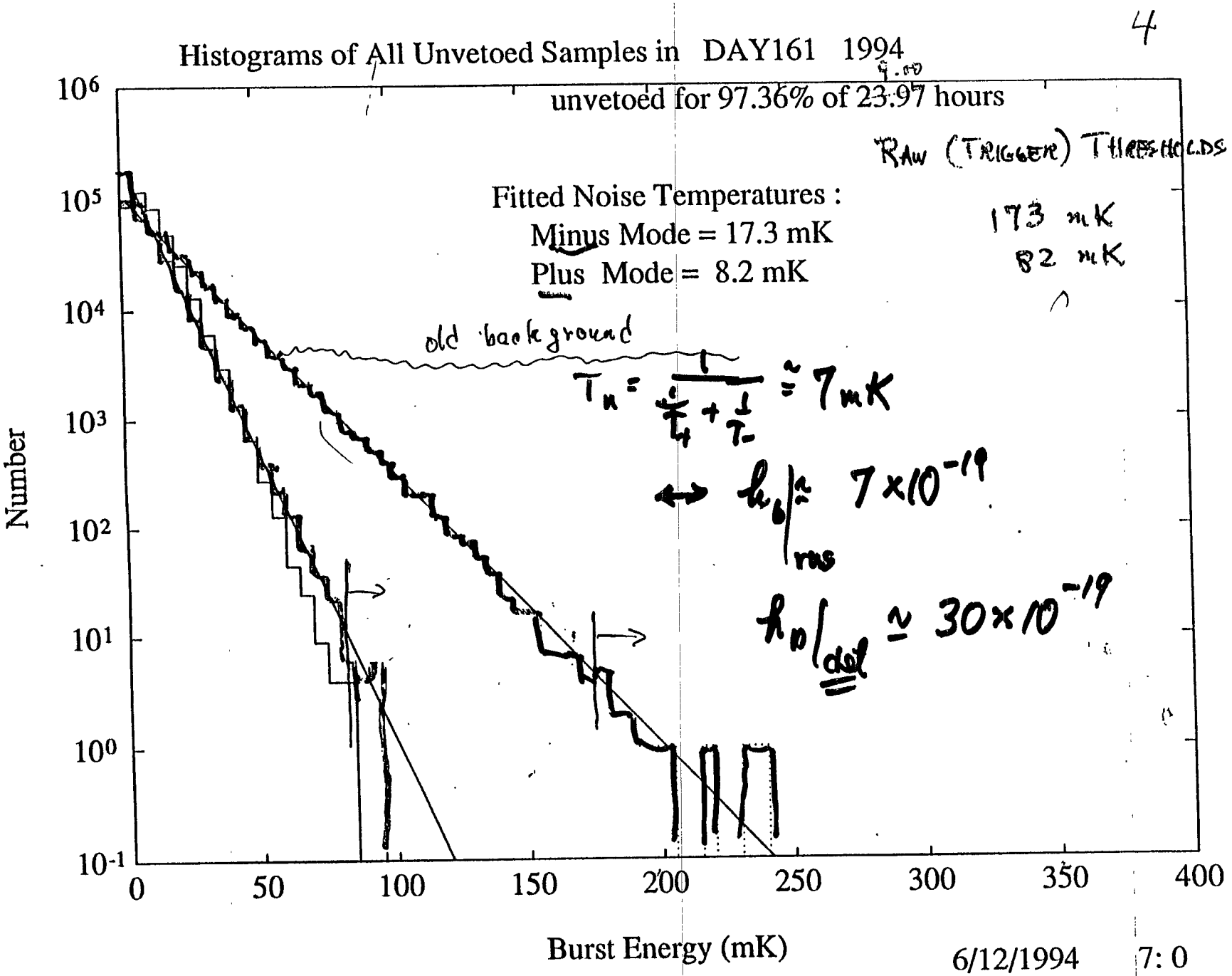
Histograms of All Unvetoed Samples in DAY161 1994
unvetoed for 97.36% of 23.97 hours
Fitted Noise Temperatures :
Minus Mode = 17.3 mK
Plus Mode = 8.2 mK
RAW (TRIGGER) THRESHOLDS
173 mK
82 mK
old background
$T_n = \frac{1}{\frac{1}{T_+} + \frac{1}{T_-}} \simeq 7\,mK$
$\leftrightarrow h_0|_{rms} \simeq 7 \times 10^{-19}$
$h_0|_{det} \simeq 30 \times 10^{-19}$
Number
Burst Energy (mK)
6/12/1994 7: 0

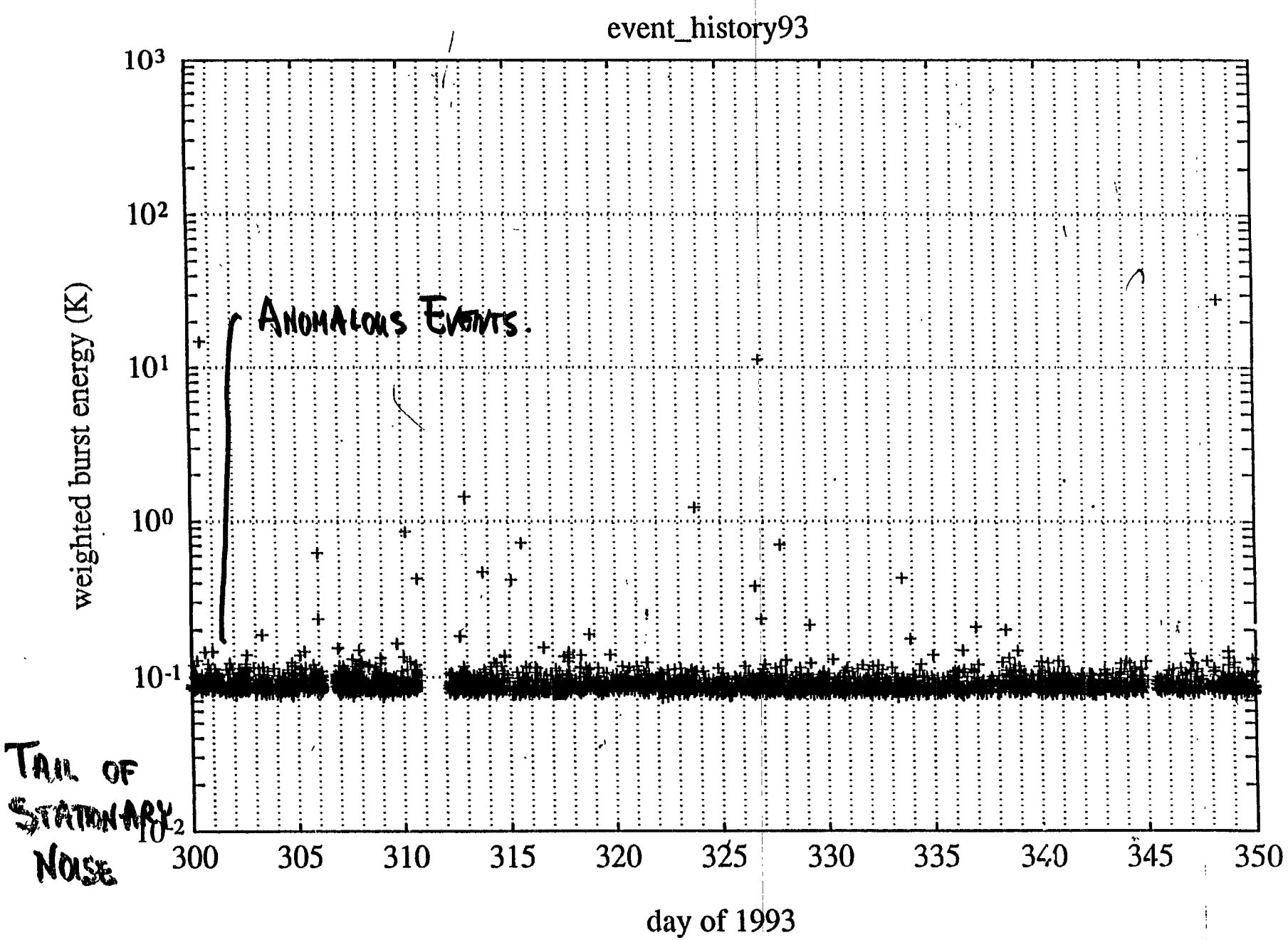
event_history93
weighted burst energy (K)
10^3
10^2
10^1
10^0
10^{-1}
10^{-2}
ANOMALOUS EVENTS.
TAIL OF STATIONARY NOISE
300
305
310
315
320
325
330
335
340
345
350
day of 1993

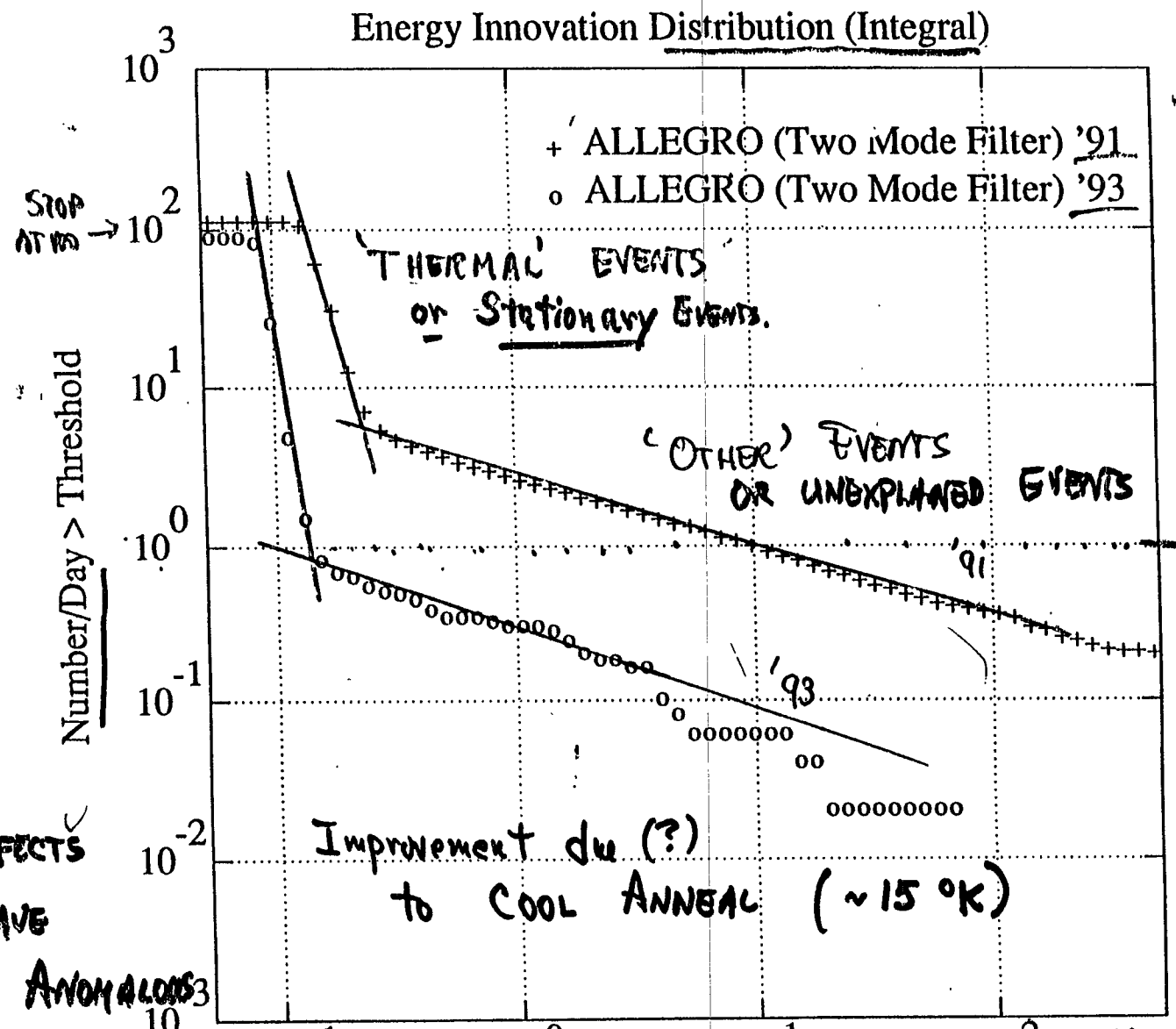

STOP AT 100 →

1 event/day × 1 day/10^5 sec ⇒ 10^{-5} probability of anomalous event.

MANY EFFECTS MIGHT HAVE PRODUCED ANOMALOUS EVENTS. BUT DID NOT.

USE COINCIDENCE WITH SECOND DETECTOR TO CONFIRM OR DENY.

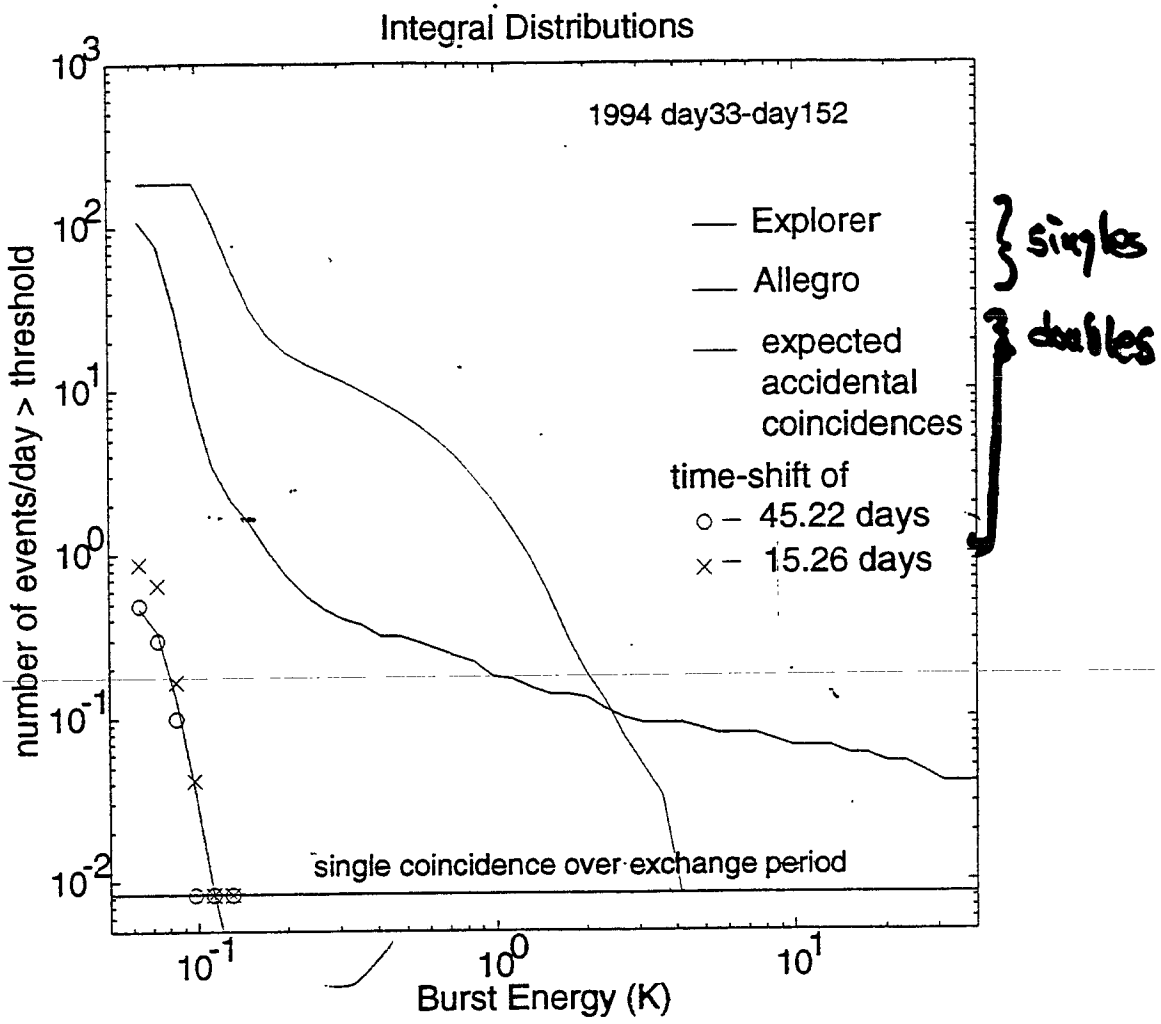
Integral Distributions
1994 day33-day152
Explorer
Allegro
expected accidental coincidences
time-shift of
○ – 45.22 days
× – 15.26 days
singles
doubles
single coincidence over exchange period
number of events/day > threshold
Burst Energy (K)
10^3
10^2
10^1
10^0
10^{-1}
10^{-2}
10^{-1}
10^0
10^1

GRAVITATIONAL WAVE DATA ANALYSIS WORKSHOP, BOSTON, DEC 9.

BINARY INSPIRAL SIGNAL MODELING I

Thibault Damour
IHES

WORK WITH B.R. IYER AND B.S. SATHYAPRAKASH

GRAVITATIONAL WAVEFORM FROM INSPIRALLING BINARY

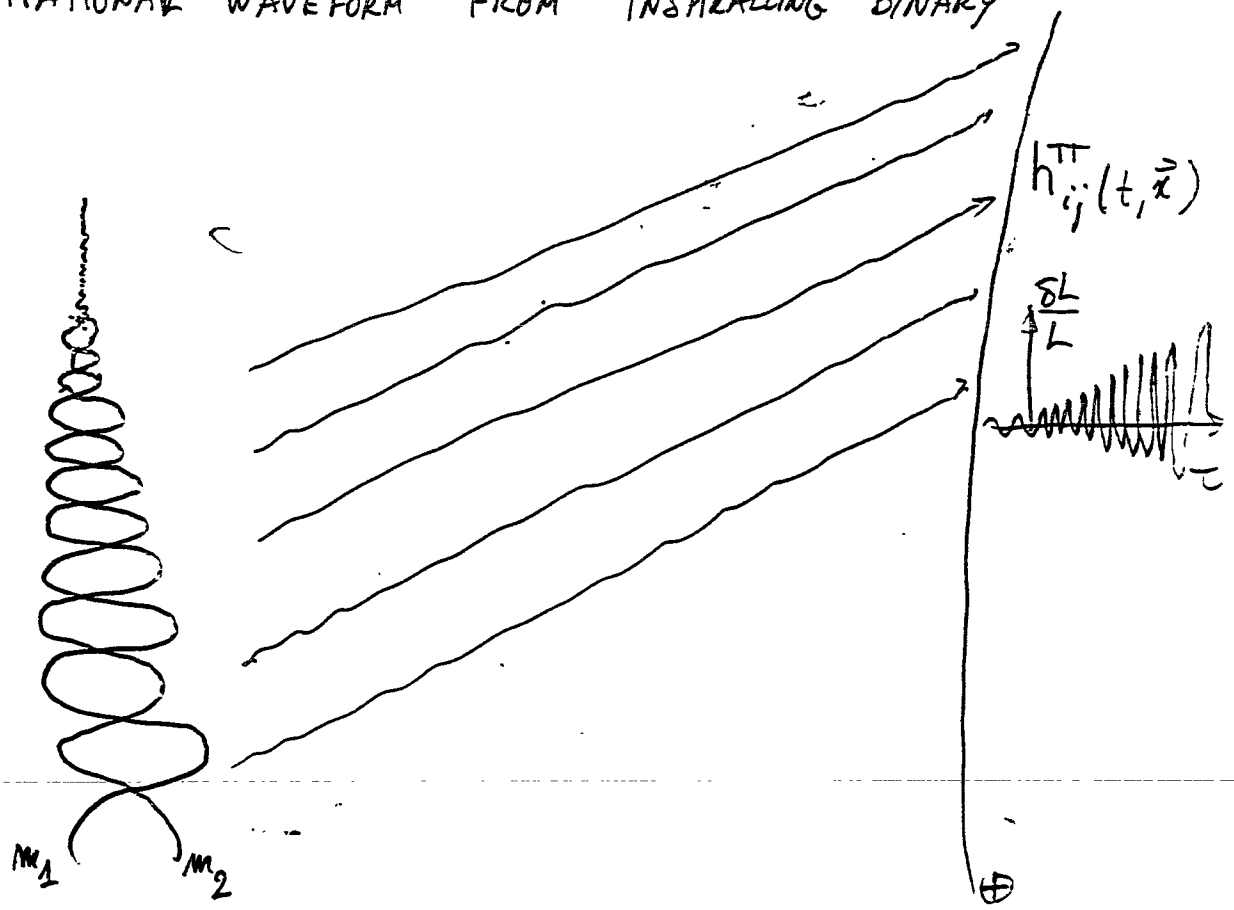

ROUGHLY SEPARABLE IN TWO (COUPLED) PROBLEMS:

- GENERATION PROBLEM : h^{TT}_{ij} = FUNCTIONAL [STRUCTURE and MOTION OF SOURCE]
- PROBLEM OF MOTION : EQS OF MOTION OF THE SOURCE, INCLUDING RADIATION REACTION

TEST MASS CASE ($m_2 \ll m_1$) [CIRCULAR] — Poisson (93), Cutler et al (93), Tagoshi Nakamura (94), Sasaki (94), Tagoshi Sasaki (94), ...

COMPARABLE MASSES — GENERATION: Blanchet, T.D., Iyer, Will, Wiseman 95; Blanchet, T.D., Iyer 95, Blanchet 96, Will Wiseman 96

EQS MOTION: T.D., Deruelle '81, T.D. '82, '83

HERE: CIRCULAR, NO SPINS (EXPECTED FOR 2 NS)

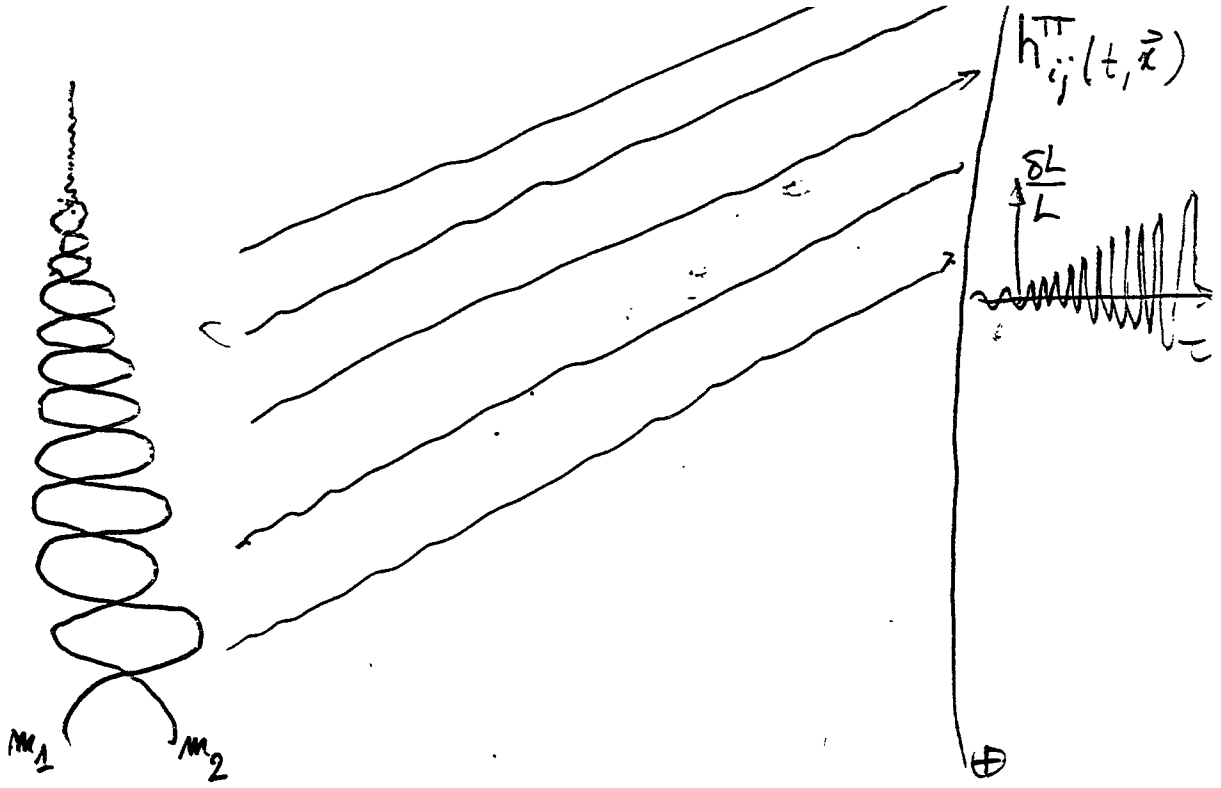

ROUGHLY SEPARABLE IN TWO (COUPLED) PROBLEMS:

- GENERATION PROBLEM : h^{TT}_{ij} = FUNCTIONAL [STRUCTURE and MOTION OF SOURCE]
- PROBLEM OF MOTION : EQS OF MOTION OF THE SOURCE, INCLUDING RADIATION REACTION

TEST MASS CASE ($m_2 \ll m_1$) [CIRCULAR] : Poisson (93), Cutler et al (93), Tagoshi Nakamura (94), Sasaki (94), Tagoshi Sasaki (94), ...

COMPARABLE MASSES / GENERATION: Blanchet, T.D., Iyer, Will, Wiseman 95
Blanchet, T.D., Iyer 95, Blanchet 96, Will Wiseman 96
\ EQS MOTION: T.D., Deruelle '81, T.D. '82, '83

HERE: CIRCULAR, NO SPINS (EXPECTED FOR 2 NY)

QUESTION: ARE THE PRESENT $\left(\frac{v}{c}\right)^5$ RESULTS SUFFICIENTLY ACCURATE OR NOT ?
[IF NOT, NEED NOT ONLY TO IMPROVE GENERATION, BUT ALSO (DELICATE) 3PN EQS OF MOTION

PREVIOUS ATTACKS : PESSIMISTIC RESULTS

CUTLER + ... + THORNE 93 v^5 NOT ENOUGH FOR ACCURATE DETECTION

ROUGH CRITERION: CUTLER, FINN, POISSON, SUSSMAN 93 ~ BEYOND v^6 NEEDED ($> v^6$, OR $\geq v^6$?)

PHASE COUNTING

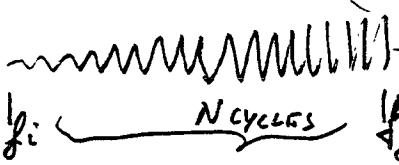

TAGOSHI, NAKAMURA 94 1.4×1.4 : v^7 NEEDED

TAGOSHI, SASAKI 94 1.4×10, 10×10 : $\geq v^8$ OR $\geq v^9$ NEEDED

HERE PRECISE CRITERION:

REDUCTION IN SNR

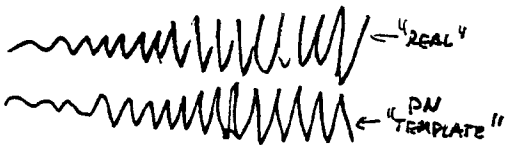

POISSON 95 1.4×1.4 ; v^5 / v^6 GIVE $\frac{SNR|_{actual}}{SNR|_{max}} \simeq 0.5$

$R \equiv \frac{SNR}{SNR} \sim \begin{cases} 0.76 \\ 0.95 \leftarrow \text{WITH EXACT MOTION} \end{cases}$

10×1.4 v^6 $R \sim \begin{cases} 0.61 \\ 0.68 \leftarrow \text{EXACT MOTION} \end{cases}$

+ CRUCIAL IMPORTANCE OF LOCATION OF LAST STABLE ORBIT (LSO)

PRESENT ATTACK (TD, IYER, SATHYAPRAKASH)

- REDUCTION IN SNR AFTER OPTIMIZING IT OVER TEMPLATE PARAMETERS
- INTRODUCTION OF NEW "IMPROVED" ENERGY FUNCTION
- SYSTEMATIC USE OF (OPTIMIZED) PADÉ APPROXIMANTS, INSTEAD OF TAYLOR ONES

GUIDED BY "STRUCTURAL STABILITY" $\eta = 0 \rightarrow \eta \neq 0$

BASIC IDEA: TRY TO INJECT A PRIORI ALL THE AVAILABLE THEORETICAL KNOWLEDGE TO FIND OPTIMIZED REPRESENTATIONS

THE "PHASING FORMULA"

- ACCURACY ON TENSORIAL AMPLITUDE $h_{ij}^{TT} = \left(\frac{v}{c}\right)^5$: ENOUGH
- PROBLEM : <u>EVOLUTION OF PHASE</u>

RESTRICTED WAVEFORM : $h(t) = a^{GW}(t) \cos \phi^{GW}(t)$

ESSENTIALLY $\phi^{GW}(t) = 2\,\Phi(t)$ ← ORBITAL PHASE

ANALOGY
- BINARY PSR "TIMING FORMULA": $\Phi_n^{PSR} = F[t_n ; P_i]$ ← STROBOSCOPIC SPINNING PHASE; ← PARAMETERS
- BINARY SYSTEM "PHASING FORMULA": $\phi^{GW} = 2\Phi = F[t ; P_i]$

HEURISTICALLY [APPROXIMATELY], $\Phi(t)$ DETERMINED BY TWO (INVARIANT) FUNCTIONS
- ENERGY FUNCTION $\tilde{E}(v)$
- FLUX FUNCTION $F(v)$

INSTANTANEOUS <u>ORBITAL ANGULAR FREQUENCY</u> $\Omega = \dot{\Phi}$

$G = c = 1$

$$v \equiv (m\Omega)^{\frac{1}{3}} \equiv x^{\frac{1}{2}}$$

$$E_{tot} \equiv m\,(1 + \tilde{E})$$

F = GRAVITATIONAL LUMINOSITY

$m \equiv m_1 + m_2$

NB : ALL INVARIANTLY DEFINED (COORD-INDEPENDENT) IN C. OF MASS FRAME

PARAMETRIC REPRESENTATION OF PHASING FORMULA

$$\Phi(t) \begin{cases} t(v) \\ \Phi(v) \end{cases}$$

$$\eta \equiv \frac{m_1 m_2}{(m_1+m_2)^2} \qquad 0 \le \eta \le \frac{1}{4}$$

$$\tau \equiv \eta^{\frac{3}{5}} m \qquad \text{(CHIRP TIME)}$$

$$\frac{t(v)}{\tau} = \frac{t_c}{\tau} + \eta^{-\frac{3}{5}} \int_v^{v_{lso}} dv \; \frac{\tilde{E}'(v)}{F(v)}$$

$$\Phi(v) = \Phi_c + \int_v^{v_{lso}} dv \; v^3 \; \frac{\tilde{E}'(v)}{F(v)}$$

PROBLEM: ? BEST REPRESENTATION OF $\tilde{E}'(v)$, $F(v)$ GIVEN FINITE POST-NEWTONIAN EXPANSIONS ?

A NEW, IMPROVED ENERGY FUNCTION

TEST MASS LIMIT

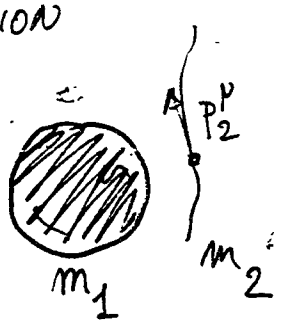

CONSERVED ENERGY ← $E_{TOT} = m_1 + \mathcal{E}_2 = m_1 - k_\mu p_2^\mu$ ← KILLING VECTOR

AT INFINITY $E_{TOT} = m_1 - \dfrac{p_{1\mu} p_2^\mu}{m_1} = m_1 - \dfrac{(p_1 \cdot p_2)}{m_1}$

↑ VERY DISSYMETRIC EXPRESSION

- INTRODUCE USUAL KINEMATIC VARIABLE: $s = -(p_1+p_2)^2 = E_{tot}^2 = m_1^2 + m_2^2 - 2 p_1 \cdot p_2$

OR EQUIVALENTLY

$$\frac{s - m_1^2 - m_2^2}{2 m_1 m_2} = -\frac{(p_1 \cdot p_2)}{m_1 m_2} + O\left(\frac{m_2}{m_1}\right) = \frac{\mathcal{E}_2}{m_2} + O(\eta)$$

USED IN RELATIVISTIC QUANTUM MECHANICS cf. ITZYKSON, ZUBER

- USE INFORMATION THAT IN SCHWARZSCHILD $\dfrac{\mathcal{E}_2}{m_2} = \dfrac{1-2x}{\sqrt{1-3x}}$ WITH $\boxed{x \equiv v^2}$

↑ BRANCH CUT IN COMPLEX x-PLANE

DEFINE

$$\boxed{e(x) \equiv \left(\frac{s - m_1^2 - m_2^2}{2 m_1 m_2}\right)^2 - 1}$$

WHERE $s \equiv E_{TOT}^2$

PROPERTIES:

- SYMMETRIC EXPRESSION IN m_1, m_2 ; FUNCTION OF s-VARIABLE
- WHEN $\eta \to 0$ $\quad e(x)\big|_{\eta=0} = -x\,\dfrac{1-4x}{1-3x}$ = RATIONAL FCN OF x WITH POLE AT $x = \frac{1}{3}$

EXPECTATION : WHEN $\eta \neq 0$, $e(x)$ PLAUSIBLY A MEROMORPHIC FUNCTION OF $x \in \mathbb{C}$

⇒ WELL SUITED TO PADÉ APPROXIMANT

TEST MASS LIMIT

CONSERVED ENERGY ↓ — KILLING VECTOR ↓

$$E_{TOT} = m_1 + \mathcal{E}_2 = m_1 - k_\mu P_2^\mu$$

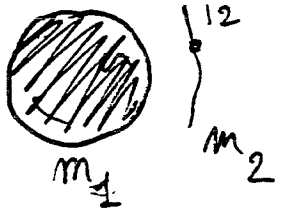

AT INFINITY $\quad E_{TOT} = m_1 - \dfrac{P_{1\mu} P_2^\mu}{m_1} = m_1 - \dfrac{(P_1 \cdot P_2)}{m_1}$

↑ VERY DISSYMETRIC EXPRESSION

- INTRODUCE USUAL KINEMATIC VARIABLE: $s = -(P_1+P_2)^2 = E_{TOT}^2 = m_1^2 + m_2^2 - 2(P_1 \cdot P_2)$

OR EQUIVALENTLY

$$\frac{s - m_1^2 - m_2^2}{2 m_1 m_2} = -\frac{(P_1 \cdot P_2)}{m_1 m_2} + O\left(\frac{m_2}{m_1}\right) = \frac{\mathcal{E}_2}{m_2} + O(\eta)$$

USED IN RELATIVISTIC QUANTUM MECHANICS see ITZYKSON, ZUBER

- USE INFORMATION THAT IN SCHWARZSCHILD $\quad \dfrac{\mathcal{E}_2}{m_2} = \dfrac{1-2x}{\sqrt{1-3x}}$ WITH $\boxed{x \equiv v^2}$

↳ BRANCH CUT IN COMPLEX x-PLANE

DEFINE

$$\boxed{e(x) \equiv \left(\frac{s - m_1^2 - m_2^2}{2 m_1 m_2}\right)^2 - 1}$$

WHERE $s \equiv E_{TOT}^2$

PROPERTIES:

- SYMMETRIC EXPRESSION in m_1, m_2 ; FUNCTION OF s-VARIABLE
- WHEN $\eta \to 0$ $\quad e(x)\big|_{\eta=0} = -x\,\dfrac{1-4x}{1-3x}$ = RATIONAL FCN OF x, WITH POLE AT $x = \frac{1}{3}$

EXPECTATION : WHEN $\eta \neq 0$, $e(x)$ PLAUSIBLY A MEROMORPHIC FUNCTION OF $x \in \mathbb{C}$

⇒ WELL SUITED TO PADÉ APPROXIMANT

BASIC IDEA: "STRUCTURAL STABILITY" UNDER $\eta = 0 \Rightarrow \eta \neq 0$

STRATEGY FOR ENERGY FUNCTION

- COMPUTE PN EXPANSION OF $\mathcal{E}(x)$
- PADÉ IT AS

$$\mathcal{E}_{P_n}(x) = -x \cdot \cfrac{c_0}{1 + \cfrac{c_1 x}{1 + \cfrac{c_2 x}{1 + c_3 x}}} \quad \cdots$$

P_n: LABEL PRECISION IN v^n — CONTINUOUS FRACTION FORM OF P^N_{N+1}

E.G. $P_4 \equiv 2PN \equiv v^4$

- COMPUTE FROM $\mathcal{E}_{P_n}(x) \longrightarrow$

$$\tilde{E}_{P_n}(x) \equiv \sqrt{1 + 2\eta\left[\sqrt{1 + \mathcal{E}_{P_n}(x)} - 1\right]} - 1$$

ENTERING THE PHASING FORMULA

FROM $\tilde{E}_{P_n}(x)$ —

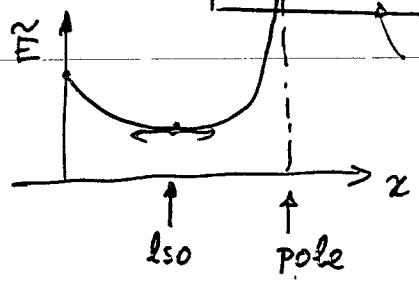

COMPUTE LOCATION OF LAST STABLE ORBIT: $\tilde{E}'(v_{lso}) = 0$

APPLICATION

$\eta = 0 \Rightarrow$ 2PN $\Rightarrow$ EXACT $\tilde{E}_{\eta=0}$

$\eta \neq 0$: DD EQS OF MOTION + SCHWARZS $\Rightarrow$

η-CORRECTIONS ARE FRACTIONALLY $< \eta < \frac{1}{4}$

$$\mathcal{E}(x) = -x\left[1 - \left(1 + \frac{\eta}{3}\right)x - \left(3 - \frac{35}{12}\eta\right)x^2\right.$$

[BETTER BEHAVIOUR THAN "HYBRID"]

$$\left. - \left(9 + O(\eta)\right)x^3 - \cdots - \left(3^{n-1} + O(\eta)\right)x^n - \cdots\right]$$

TO TEST SENSITIVITY TO UNKNOWN HIGHER-ORDER η-CORRECTIONS, AND QUALITY OF CONVERGENCE DEFINE A FIDUCIAL "EXACT" $\mathcal{E}$

$$\mathcal{E}_X(x) \equiv -x\left[1 - \left(1 + \frac{\eta}{3}\right)x - \left(3 - \frac{35}{12}\eta\right)x^2 - \frac{9\left(1 + k_3\eta\right)x^3}{1 - 2\left(1 + k_4\eta\right)x}\right]$$

- COMPUTE PN EXPANSION OF $\mathcal{E}(x)$

- PADE' IT AS

$$\mathcal{E}_{P_n}(x) = -x \cfrac{c_0}{1 + \cfrac{c_1 x}{1 + \cfrac{c_2 x}{-1 + c_3 x}}} \quad \cdots$$

CONTINUOUS FRACTION FORM OF P^N_{N+1}

$\mathcal{E}_{P_n}(x)$ ↑ LABEL PRECISION IN v^n

E.G. $P4 \equiv 2PN \equiv v^4$

- COMPUTE FROM $\mathcal{E}_{P_n}(x) \longrightarrow$ $\boxed{\tilde{E}_{P_n}(x) \equiv \sqrt{1 + 2\eta\left[\sqrt{1+\mathcal{E}_{P_n}(x)} - 1\right]} - 1}$

ENTERING THE PHASING FORMULA

FROM $\tilde{E}_{P_n}(x)$

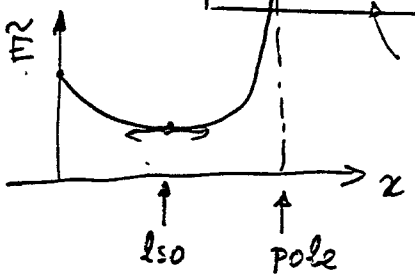

COMPUTE LOCATION OF LAST STABLE ORBIT: $\tilde{E}'(v_{lso}) = 0$

APPLICATION

$\eta = 0 \Rightarrow$ 2PN $\Rightarrow$ EXACT $\tilde{E}_{\eta=0}$

$\eta \neq 0$: DD EQS OF MOTION + SCHWARZS $\Rightarrow$ $\mathcal{E}(x) = -x\left[1 - \left(1 + \frac{\eta}{3}\right)x - \left(3 - \frac{35}{12}\eta\right)x^2 - (9 + O(\eta))x^3 - \cdots - (3^{n-1} + O(\eta))x^n - \cdots\right]$

η-CORRECTIONS ARE FRACTIONALLY $0 < \eta < \frac{1}{4}$

[BETTER BEHAVIOUR THAN "HYBRID"]

TO TEST SENSITIVITY TO UNKNOWN HIGHER-ORDER η-CORRECTIONS, AND QUALITY OF CONVERGENCE DEFINE A FIDUCIAL "EXACT" $\mathcal{E}$

$$\mathcal{E}_X(x) \equiv -x\left[1 - \left(1 + \frac{\eta}{3}\right)x - \left(3 - \frac{35}{12}\eta\right)x^2 - \frac{9(1 + k_3\eta)x^3}{1 - 3(1 + k_0\eta)x}\right]$$

$k_0 \sim O(1) \sim k_3$

TWO PARAMETERS TO VARY SHAPE, AND LOCATION LSO

PADE APPROXIMATION

Let $G_{\mathrm{T}_3}(x)$ be a Taylor series in x to order x^3 :

$$G_{\mathrm{T}_3} = \sum_{n=0}^{3} a_n x^n.$$

The *continued fraction* form of Padé approximant to $G_{\mathrm{T}_3}(x)$ is:

$$G_{\mathrm{P}_3}(x) = \cfrac{c_0}{1 + \cfrac{c_1 x}{1 + \cfrac{c_2 x}{1 + c_3 x}}}$$

c_n are obtained by demanding that to order x^3, $G_{\mathrm{P}_3} = G_{\mathrm{T}_3}$

$$c_0 = a_0$$

$$c_1 = -\frac{a_1}{a_0}$$

$$c_2 = -\frac{a_2}{a_1} + \frac{a_1}{a_0}$$

$$c_3 = \frac{a_0(a_1 a_3 - a_2^2)}{a_1(a_1^2 - a_2 a_0)}$$

STRATEGY FOR FLUX FUNCTION $F(v)$ [PRELIMINARY]

CONCENTRATE ON PN-CONVERGENCE PROBLEMS (KEEP $\eta = 0$)

TEST MASS CALCULATIONS : POISSON 93 ——— TAGOSHI-SASAKI 94

$$\begin{cases} F(v) = \dfrac{32}{5}\eta^2 v^{10}\left[\sum_{k=0}^{8} A_k v^k + B_6 v^6 \ln v + B_8 v^8 \ln v + O(v^9 \ln v)\right] \\ + F(v) \quad \text{"EXACT" NUMERICAL (POISSON 95)} \end{cases}$$

- FACTORIZE LOGARITHMS AFTER INTRODUCING A WORKING POINT v_0
- WORK WITH THE INVERSE FLUX FUNCTION

$$\frac{1}{F(v)} \equiv \frac{5}{32\eta^2 v^{10}} Q(v) \leftarrow \text{ENTERS DIRECTLY PARAMETRIC PHASING FORMULA}$$

$$Q(v) = \left[1 - \ln\frac{v}{v_0}\left(B_6 v^6 + (B_8 - A_2 B_6) v^8\right)\right] \times \left[1 + C_2 v^2 - C_3 v^3 q(v)\right]$$

NUMERICALLY VERY SMALL

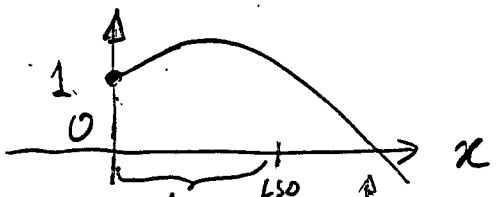

ONLY DOMAIN OF IMPORTANCE KNOWN TO HAVE SIMPLE ZERO AT $x = 3$

- PADÉ $\quad q(v) \underset{P_n}{=} \dfrac{1}{1 + \dfrac{C_1 v}{1 + \dfrac{C_2 v}{1 + C_3 v}}}$ ——

SUGGESTS PADÉ

OVERALL STRATEGY:

COMPARE TAYLOR/PADÉ APPROXIMANTS (QUALITY CONVERGENCE) IN / PHASING FORMULA INGREDIENT ($\hat{E}$, F, v_{LSO})
VERSUS "EXACT" \ SNR

BINARY SIGNAL MODELLING

T. Damour, B.R. Iyer and B.S. Sathyaprakash

GWDAW 6-9 December 1996, MIT, Boston

AMBIGUITY FUNCTION

Let $h(t;\lambda_k)$ be a signal with λ_k its parameters and $g(t;\mu_k)$ a template with μ_k its parameters. (Shapes of h and g and their parameters, including their number, are assuemed to be in general different.) Their scalar product (also statistic of Wiener filtering)

$$(h,g)(\lambda_k,\mu_k) = 4\int_0^\infty \tilde{h}(f;\lambda_k)\tilde{g}^*(f;\mu_k)e^{-2\pi i f t_0}\frac{df}{S_n(f)}$$

- t_0 is the lag parameter (shift of filter relative to signal)
- $\tilde{h}$ denotes the Fourier transform
- $S_n(f)$ is detector noise power spectral density.

Ambiguity Function: Absolute value of the scalar product of normalized (i.e.(h,h)=1) wave forms maximized over the lag parameter t_0 :

$$\mathcal{A}(\lambda_k,\mu_k) = \max_{t_0}|\langle h,g\rangle|$$

$\mathcal{A}(\lambda_k,\mu_k)$ SNR obtained using a template that is not necessarily matched on to the signal. When template wave forms are not identical to signal shapes

$$\max_{\mu_k}\mathcal{A} \leq 1, \quad \mu_k \neq \lambda_k.$$

SIGNAL FAITHFULNESS AND RELIABILITY

- Choose *intrinsic* parameters of the signal and the template to the same.

If $1 - \mathcal{A}(\lambda_k, \lambda_k) \leq 3\%$ we have a *faithful signal model.*

- Keeping the signal parameters maximize the ambiguity function over all *intrinsic* template parameters.

If $1 - \max_{\mu_k} \mathcal{A} \leq 3\%$ we have a *reliable signal model.*

As a general rule

- Every faithful signal model is also a reliable signal model.
- A faithful signal model produces large SNR and low bias.
- A reliable signal model produces large SNR but may not produce low bias.

BREAKDOWN OF STATIONARY PHASE APPROXIMATION

$$\text{Overlap} = \frac{(H_1, H_2)}{\sqrt{(H_1, H_1)(H_2, H_2)}}$$

$$(H_1, H_2) = 4 \int_0^\infty \tilde{H}_1(f) \tilde{H}_2^*(f) \frac{df}{S_n(f)}$$

Table 1: Overlap integrals of a test mass wave form whose Fourier transform is computed using stationary phase approximation with the same wave-form but whose Fourier transform is computed numerical FFT. N=Newtonian, Tn=Taylor to order v^n, X=Exact.

Flux—Energy	Overlap
N—N	0.987
T4—N	0.986
T5—N	0.982
T6—N	0.980
T7—N	0.980
T8—N	0.977
X—N	0.981
N—T4	0.970
N—T6	0.955
N—T8	0.958
N—X	0.932
X—X	0.922

DISCRETE AND STATIONARY PHASE FOURIER TRANSFORMS

EXACT WAVE FORM—TEST MASS CASE

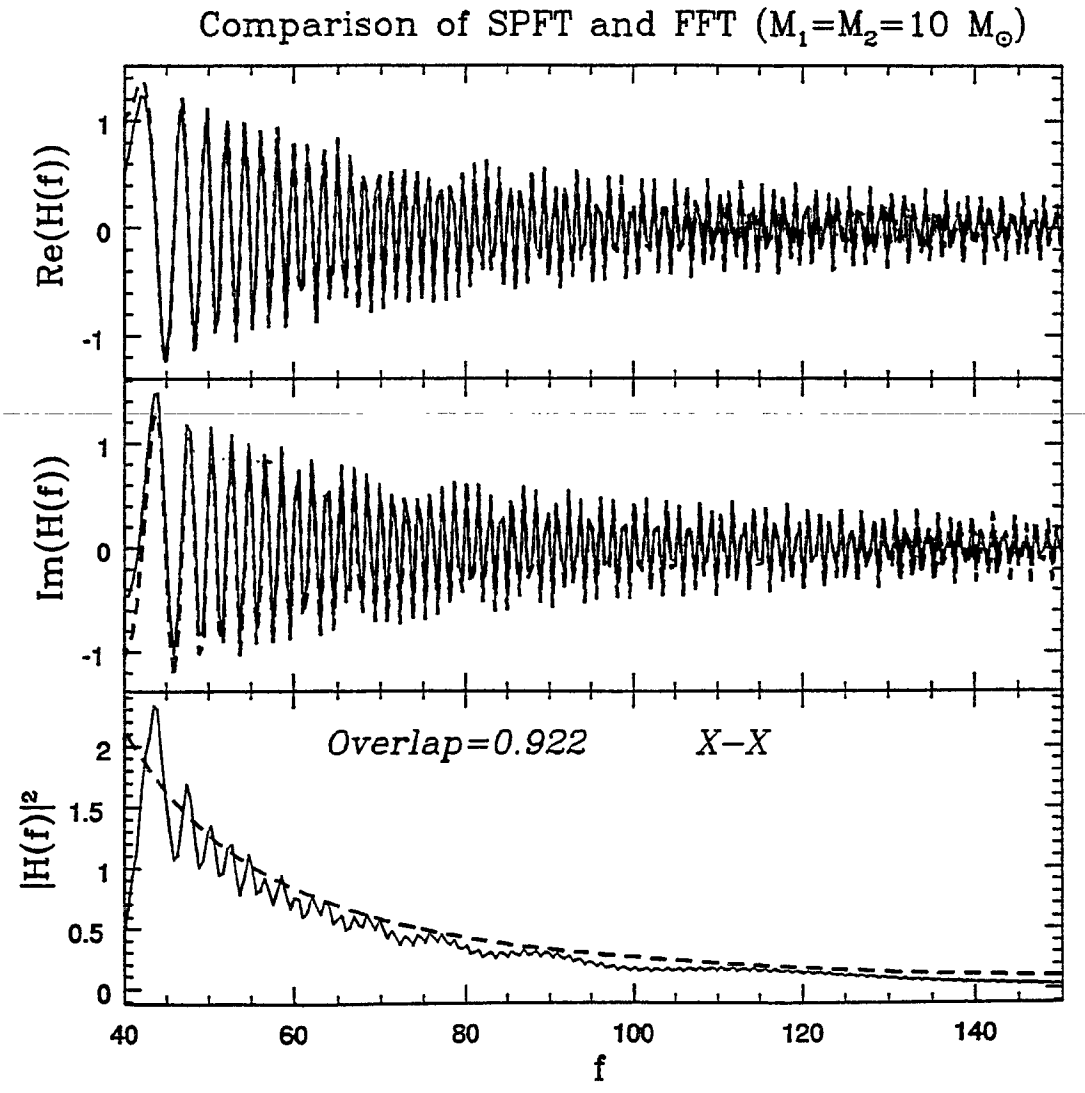

DISCRETE AND STATIONARY PHASE FOURIER TRANSFORMS

NEWTONIAN WAVE FORM—TEST MASS CASE

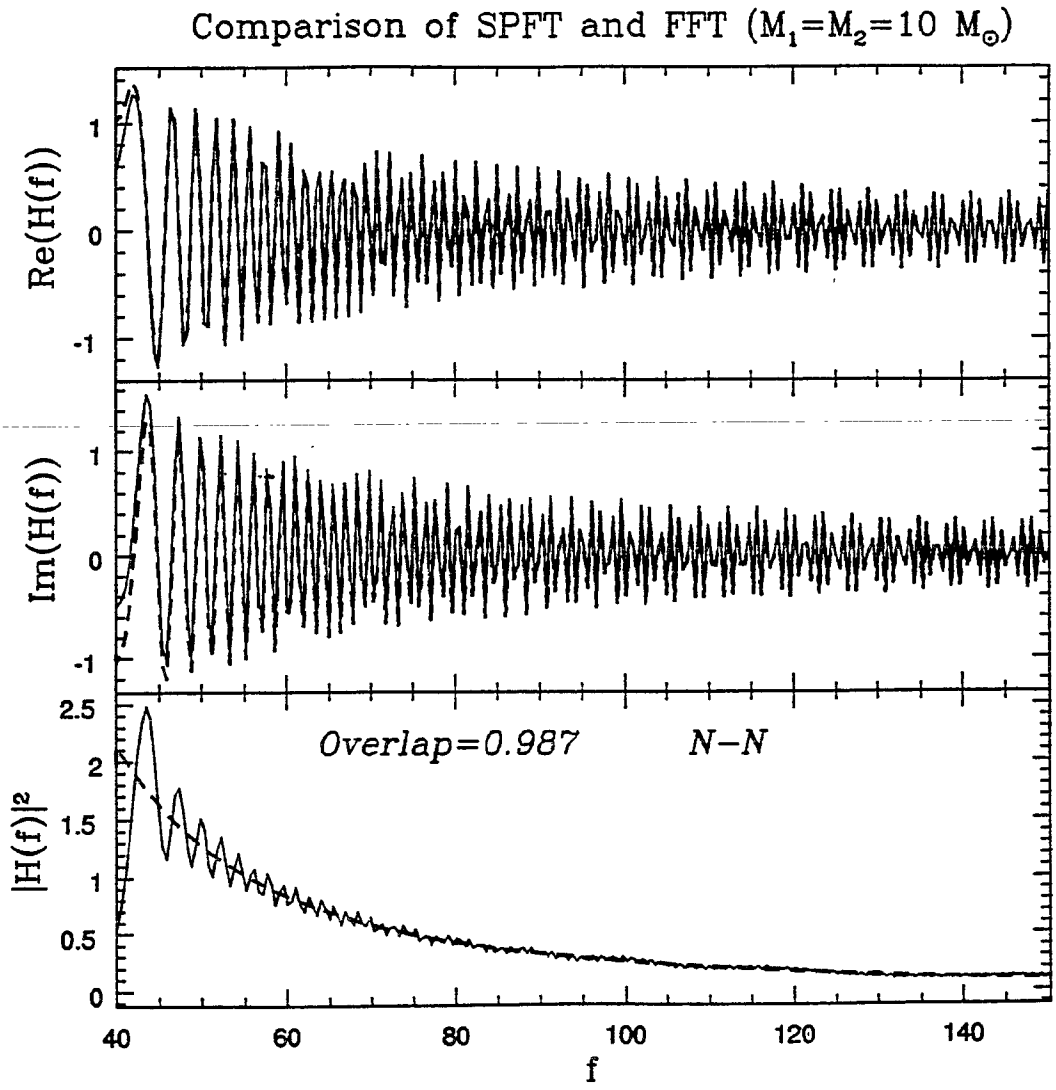

PHASING FORMULA

Energy balance $dE_{\rm tot}/dt = -F$, gives phasing of the orbit

velocity-time relationship

$$\frac{t_c - t}{\tau} = T_\eta(v)$$

$$T_\eta(v) = \eta^{-3/5} \int_v^{v_{\rm lso}} dv \left[-\frac{\tilde{E}'(v)}{F(v)} \right]$$

velocity-time relationship

$$\Phi_c - \Phi(t) = \Phi_\eta(v)$$

$$\Phi_\eta(v) = \int_v^{v_{\rm lso}} dv v^3 \left[-\frac{\tilde{E}'(v)}{F(v)} \right]$$

- $v_{\rm lso}$ is a fiducial velocity (e.g. velocity at *last stable circular orbit*; $1/\sqrt{6}$ for a test mass orbiting a black hole.)
- τ is the *chirp time* and t_c, Φ_c are arbitrary constants (time and phase at $v_{\rm lso}$.
- Given a t solve for v iteratively using $T_\eta(v)$.
- Use this v in $\Phi_\eta(v)$ to)compute the phasing of the wave.

PADE APPROXIMANTS TO FLUX AND ENERGY FUNCTIONS

$$Q(v) = \frac{32\eta^2 v^{10}}{5F(v)}, \quad R(v) = \frac{-\tilde{E}'(v)}{\eta v}$$

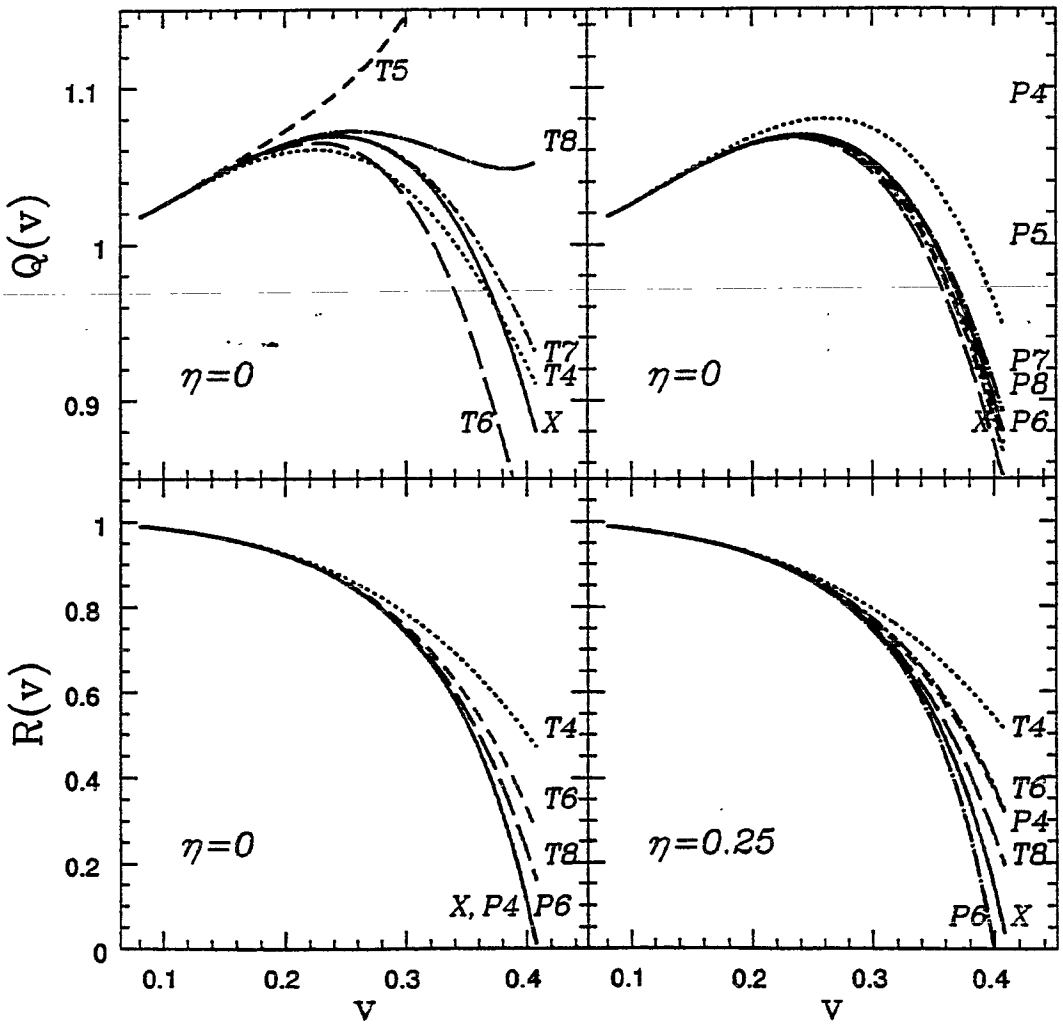

LOCATION OF LAST STABLE ORBIT

TEST MASS CASE

Table 2: In the test mass case Padé approximant to the energy function is exact at order v^4 and higher.

$6x_{\rm lso} = 6v^2_{\rm lso}$		
Order	Taylor	CFA
4	1.4415	1
6	1.1705	1
8	1.0783	–

FINITE MASS CASE

Table 3: Values of $6x_{\rm lso}$ for $\eta = 0.25$ for various orders of Taylor and Continued Fraction Approximants. The Exact values corresponding to $\kappa_0 = -1$, 0, 1 are 1.0695, 1.0126 and 0.9518, respectively. Note that the Padé approximants capture the LSO better than Taylor approximants in all cases.

$6x_{\rm lso} = 6v^2_{\rm lso}$			
Order	κ_0	Taylor	CFA
4	–	1.5348	1.1916
6	–	1.2040	0.9575
8	-1	1.1206	1.0341
8	0	1.0997	0.9995
8	1	1.0811	0.9511

OVERLAP INTEGRALS OF APPROXIMATE WAVE FORMS WITH EXACT WAVE FORM

TEST MASS CASE

Table 4: N=Newtonian; T_n Taylor approximation of order n and P_n Pade approximation of order n.

$M_1 = M_2 = 10M_\odot$		
FLUX	ENERGY	Overlap
N	N	0.446
T4	X	0.997
T5	X	0.747
T6	X	0.983
T7	X	1.000
T8	X	0.977
P4	X	0.966
P5	X	0.995
P6	X	0.993
P7	X	0.996
P8	X	1.000

OVERLAP INTEGRALS OF APPROXIMATE WAVE FORMS WITH EXACT WAVE FORM

TEST MASS CASE

Table 5: N=Newtonian; T_n Taylor approximation of order n and P_n Pade approximation of order n.

$M_1 = M_2 = 10M_\odot$		
FLUX	ENERGY	Overlap
X	N	0.442
X	T4	0.773
X	T6	0.934
X	T8	0.984
X	P4	1.000
X	P6	1.000
T4	T4	0.820
T5	T4	0.555
T6	T6	0.982
T7	T6	0.934
T8	T8	0.955

Threshold Levels for Stochastic Background Searches

(i) data analysis strategy

(ii) threshold criterion

(iii) implications for observation times

Data Analysis Strategy

(i) correlate the outputs of two detectors

(ii) assume noise statistically independent

$$x := d_1 d_2 = (h_1 + n_1)(h_2 + n_2)$$

$$\mu := \langle x \rangle = \langle h_1 h_2 \rangle$$

$$\sigma^2 := \langle x^2 \rangle - \langle x \rangle^2 \approx \langle n_1^2 \rangle \langle n_2^2 \rangle$$

(iii) make repeated correlation measurements

$$x_1, x_2, \cdots, x_n \qquad (n \geq 10^6)$$

Threshold Criterion

$$z := \frac{\bar{x} - \mu}{s/\sqrt{n}}$$

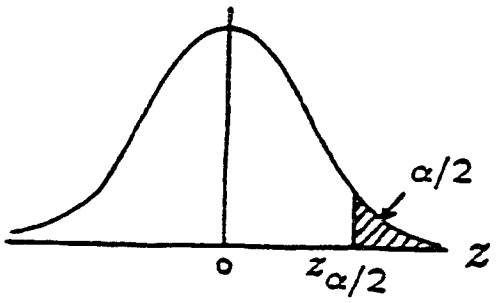

$(1-\alpha) \cdot 100\%$ confidence

$$\bar{x} - z_{\alpha/2}\,\frac{s}{\sqrt{n}} < \mu < \bar{x} + z_{\alpha/2}\,\frac{s}{\sqrt{n}}$$

$\beta \cdot 100\%$ relative error

$$\text{Maximum Error} = z_{\alpha/2}\,\frac{s}{\sqrt{n}} < \beta\ \bar{x}$$

$$\text{S/N Ratio} = \sqrt{n}\,\frac{\bar{x}}{s} > \frac{z_{\alpha/2}}{\beta}$$

Observation Times

$$\sqrt{n}\,\frac{\bar{x}}{s} > \frac{z_{\alpha/2}}{\beta}$$

(i) Signal Detection: $(\beta = 1)$

$$0 < \mu$$

Initial LIGO, $\Omega_0 = 3 \times 10^{-6}$,
90% confidence $\Rightarrow$ 2 months

(ii) Parameter Estimation: $(0 < \beta \leq 1)$

$$(1-\beta)\ \bar{x} < \mu < (1+\beta)\ \bar{x}$$

Initial LIGO, $\Omega_0 = 3 \times 10^{-6}$,
90% confidence, 10% relative error
$\Rightarrow$ 300 months

G.W. STOCHASTIC BACKGROUND

$\tilde{h}$ spectral amplitude

Physics Letters B, 385 (1996)

Upper limit

using the data of the EXPLORER detector

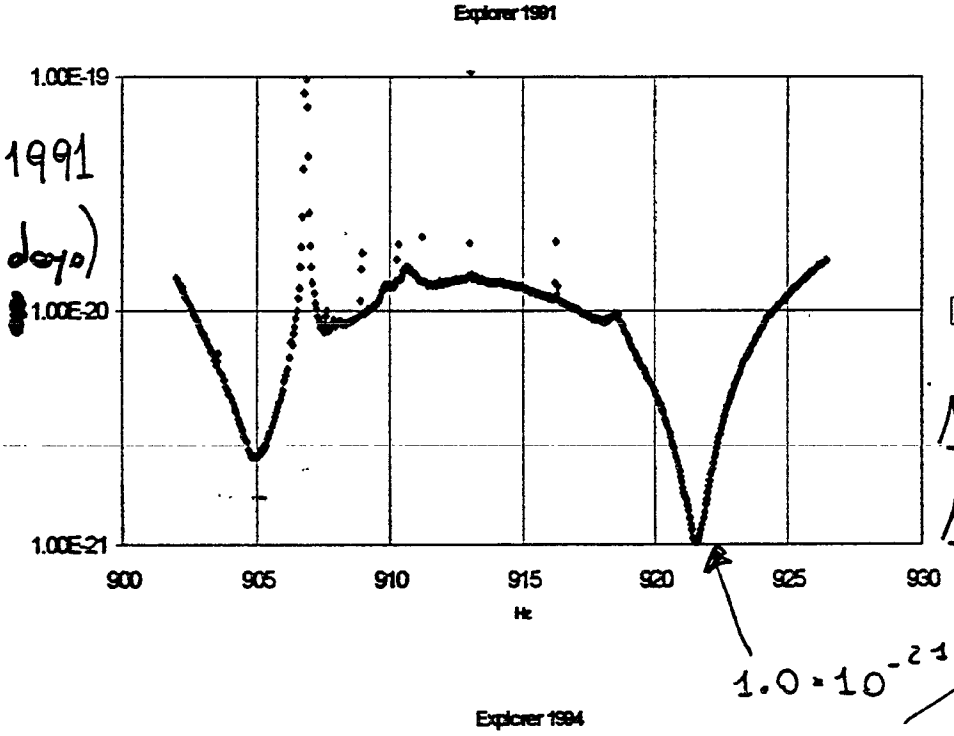

$\tilde{h}$

Explorer 1991

(t_m = 31 days)

$Q \sim 10^6$

T ~ 2.9 K

$\Delta\nu_- \sim 1.5$ Hz

$\Delta\nu_+ \sim 0.9$ Hz

$1.0 \cdot 10^{-21} / \sqrt{Hz}$

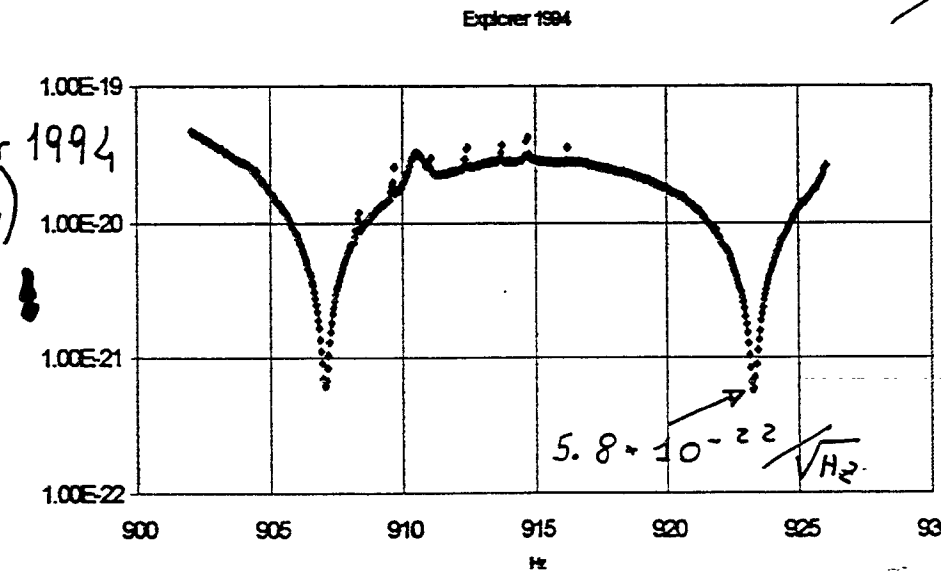

$\tilde{h}$

Explorer 1994

(t_m = 36 h)

$Q \sim 5 \cdot 10^6$

T ~ 2.9 K

$\Delta\nu_- \sim 0.2$ Hz

$\Delta\nu_+ \sim 0.2$ Hz

$5.8 \cdot 10^{-22} / \sqrt{Hz}$

Here the time t_m is not important: increasing t_m only reduces the variance of the estimation (the thickness of

Target for the year 1999

Nautilus at 100 mk, with an improved transducer

SIMULATION

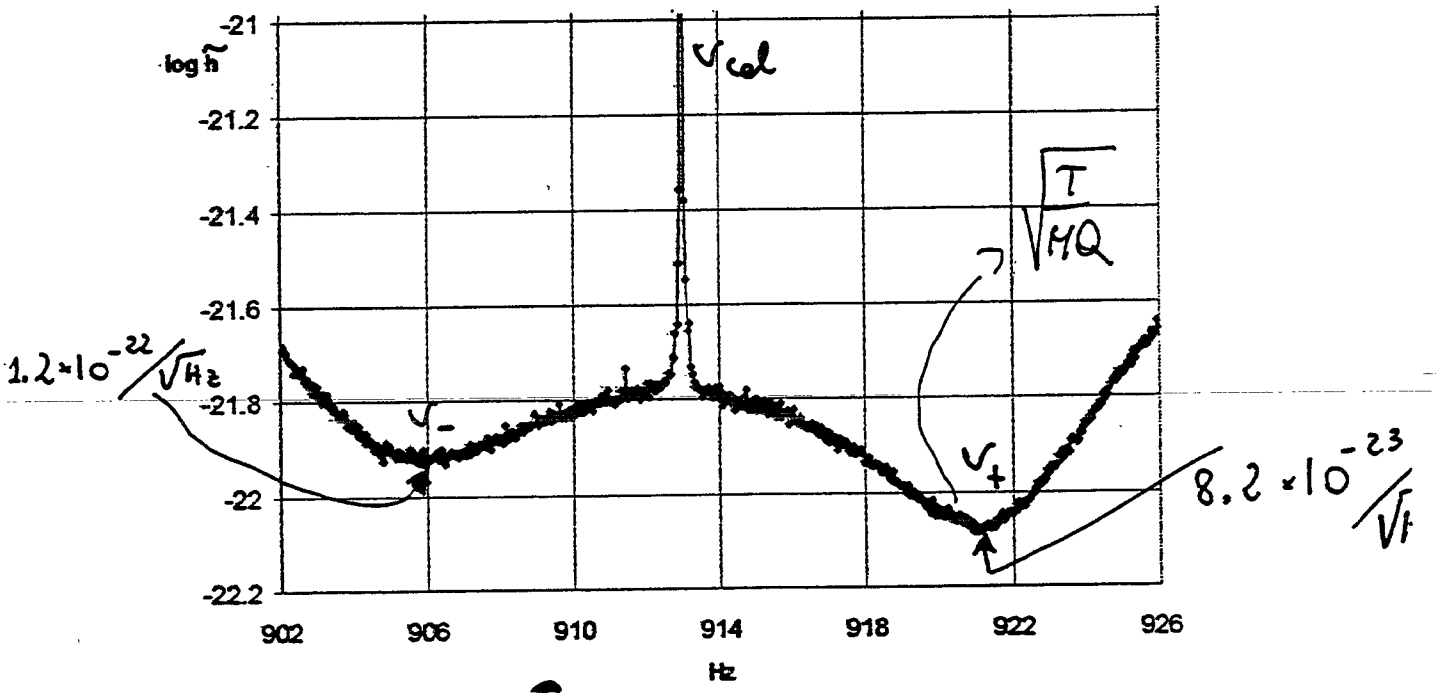

Q=8.5 10^6

Bandwidth=5 Hz

$\tilde{h}_1 = 8 \times 10^{-23}\ 1/\sqrt{(Hz)}$

Nautilus - Auriga

$f_1 = 920\,Hz$, $\Delta f = 5\,Hz$, $S_{h_1} = 7 \cdot 10^{-45}\,/Hz$

$S_{h_2} = 7 \cdot 10^{-45}\,/Hz$

if near and aligned: $\Omega_{G.W.} = 5.2 \cdot 10^{-4}$

present location: $\Omega_{G.W.} \cong \Omega_{G.W.} * 10$

(VITALE et al.)

Nautilus - GEO600

$f_1 = 920\,Hz$, $\Delta f = 5\,Hz$, $S_{h_1} = 7 \cdot 10^{-45}\,/Hz$

$$S_{h_2}^{INT} = 3 \cdot 10^{-45} \left(\frac{f_1}{200}\right)^2$$

if near and aligned: $\Omega_{G.W.} = 1.3 \cdot 10^{-3}$

present location: $\Omega_{G.W.} \cong \Omega_{G.W.} * 20$

(SCHUTZ, COMPTON et al.)

Nautilus - VIRGO

$f_1 = 920\,Hz$, $\Delta f = 5\,Hz$, $S_{h_1} = 7 \cdot 10^{-45}\,/Hz$

$$S_{h_2}^{INT} = 1 \cdot 10^{-46} \left(\frac{f_1}{200}\right)^2$$

if near and aligned: $\Omega_{G.W.} = 2.3 \cdot 10^{-4}$

present location: $\Omega_{G.W.} \cong \Omega_{G.W.} * 10$

(-> Auriga-VIRGO at present location is a factor ~ 2 better)

(VITALE et al.)

STOCHASTIC BACKGROUND

- the sensitivity is not strongly affected by the detector bandwidth, $(\Delta f)^{-1/4}$

- it depends strongly on $S_h(f \pm \Delta f)$ and on the detectors separation and orientation

$\Rightarrow$ the feasibility of a BAR - INTERFEROMETER or a BAR - BAR experiment is high if compared to an INTERFEROMETER - INTERFEROMETER experiment

- the search could be done at $f \sim 1$ kHz with a BAR "near" and "aligned" to the INTERFEROMETER
- the best sensitivity can be reached if the interferometer is narrow banded down to the bar bandwidth.

"Near detectors means at a distance $R < \lambda/2\pi$

$R \sim 50$ Km $\Rightarrow$ 1 KHz ; $R \sim 250$ Km $\Rightarrow$ 200 Hz

"Aligned" detectors means that they are sensitive to the same polarization components of the wave

$$\Omega_{G.W.} = \Omega_{G.W.}^{\text{near and aligned}} / |\gamma(f)|$$

present location and orientation

$\gamma(f)$ is the overlap reduction function, defined by E. Flanagan

It depends on

- frequency of the wave
- location of the detectors
- orientation of the detectors

Example of $\gamma(f)$ for the two LIGO detectors (3000 Km apart)

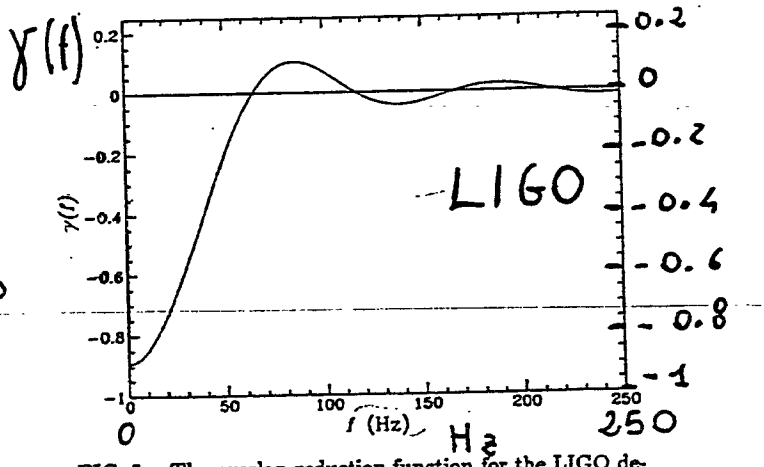

FIG. 5. The overlap reduction function for the LIGO detectors using their currently planned orientations. Flanagan

COMPARISON OF ALGORITHMS FOR THE DETECTION OF BURST SOURCES IN RESONANT MASS DETECTORS

S. Frasca and M.A. Papa
(INFN and Univ. of Roma 1 and 2)

- WHEN THE NOISE IS STATIONARY THE OPTIMAL SOLUTION TO SEARCHING FOR A BURST SIGNAL EXISTS: THE MATCHED FILTER

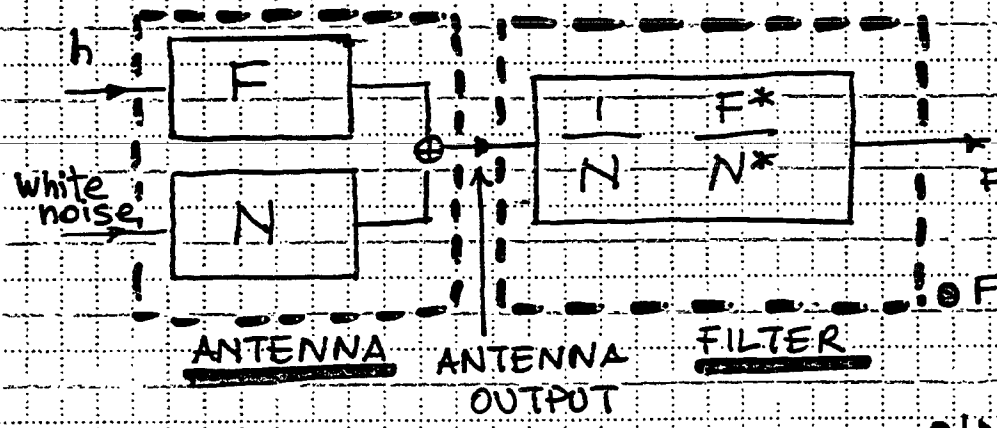

- F: ANTENNA TRANSFER FUNCTION
- $|N|^2$: POWER SPECTRUM OF NOISE

- WHAT IF THE SYSTEM IS NOT STATIONARY?
  - AT DIFFERENT TIMES THE SYSTEM IS NON STATIONARY IN DIFFERENT WAYS (not just a trivial and known time dependence of noise statistics)
  - THIS AFFECTS WHAT THE BEST (most efficient) ESTIMATE OF $|N|^2$ IS

- SPOT SOME (GENERAL) TYPES OF NON STATIONARY BEHAVIOURS THAT THE SYSTEM MAY EXHIBIT AND

  - DEFINE PARAMETERS TO DISTINGUISH AMONG THEM DURING OPERATION (for control purpouses)

  - DEFINE, IN CORRESPONDENCE, DIFFERENT WAYS TO ESTIMATE THE POWER SPECTRUM $|N|^2$ WELL IN ALL THE CIRCUMSTANCES

This has been implemented on the new high frequency - 5000 Hz - data acquisition and on-line analysis system of the antennas of the Rome Group, DAGA2_HF

DATA ANALYSIS ARAVITATIONAL ANTENNAS HIGH FREQUENCY

I for stationary noise the optimal filter to detect a pulse signal is the matched filter.

To implement a matched filter you need to know

- F
- the power...

Our filters are adaptive in the sense that the ps is estimated not by any model of the noise but by using the data.

J one of the issues I'm addressing is that when the system is non stationary the estimate of the power sp. becomes a more delicate pb because it affects the perform. of filter

- BRIEFLY, THE DIFFERENT WAYS OF ESTIMATING THE POWER SPECTRUM IN ORDER TO BEST CURE THE EFFECTS OF DIFFERENT TYPES OF NON STATIONARY BEHAVIOUR ARE:

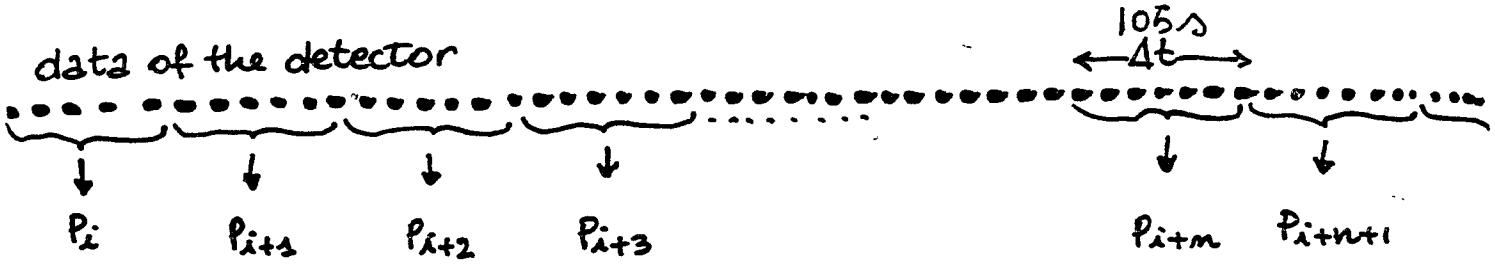

P_i is the "periodgram" at time i

- $S = \sum_i^{2\,\text{hours}} P_i$ ... OLD MATCHED FILTER SPECTRUM
- $S_i = P_i (1-w) + w S_{i-1}$ $\quad w = e^{-\Delta t/\tau}$ WHOLE SPECTRUM
- $S_i = \begin{cases} S_{i-1} & \text{if } P_i \text{ is too noisy} \\ P_i (1-w) + w S_{i-1} & \text{otherwise} \end{cases}$ CLEAN SPECTRUM
- $S_i = P_i \left[1 - w(S_{i-1})\right] + w(S_{i-1})\, S_{i-1}$ VARYING MEMORY SPECTRUM

where $w = w(S_{i-1})$ because $\tau = \tau(S_{i-1})$:

$$\chi := \frac{S}{\bar{S}}$$

$\bar{S}$ ← EXPECTED VALUE OF S IN GOOD OPERATING CONDITIONS

$$\tau(\chi) = \frac{\tau_0}{1 + \chi^\alpha \beta}$$

Integral histogram of 1 minute
average data from different
filters on the Nautilus antenna.

I've drawn a 50% line & correspondingly
I've defined an effective temperature,
~~with the~~ meaning that for 50%
of the Total time the one minute
averages of the data had values
below this effective temperature.

NAUTILUS DATA
27/10/96 → 3/11/96

number

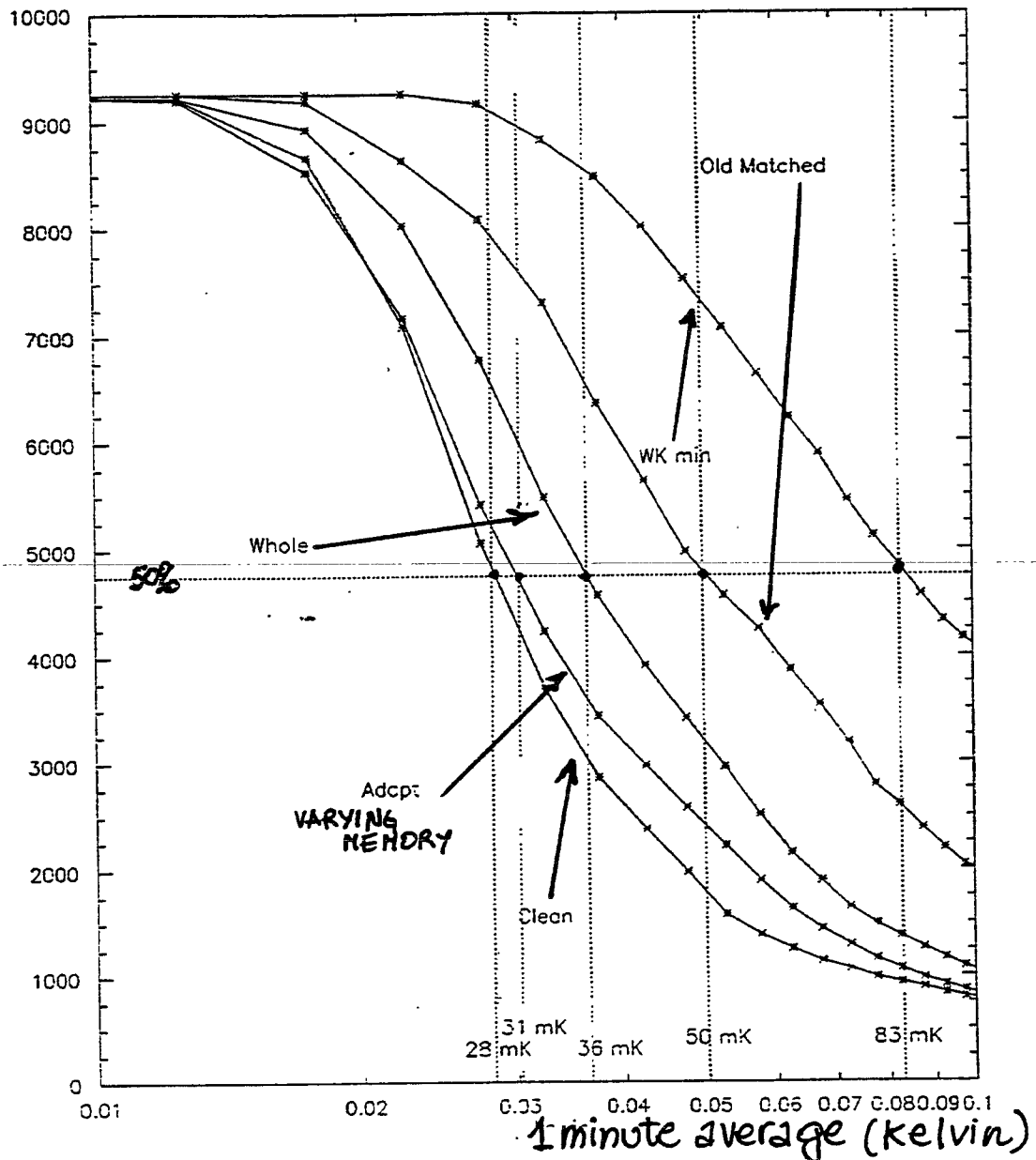

Integral histogram of one minute average data, expressed in Kelvin, from the different filters. The 50% line refers to half the total data and indicates, on the temperature axis, the effective temperature T_{eff} of the filters.

0.01

0.1

difference between # of 1 minute average above T

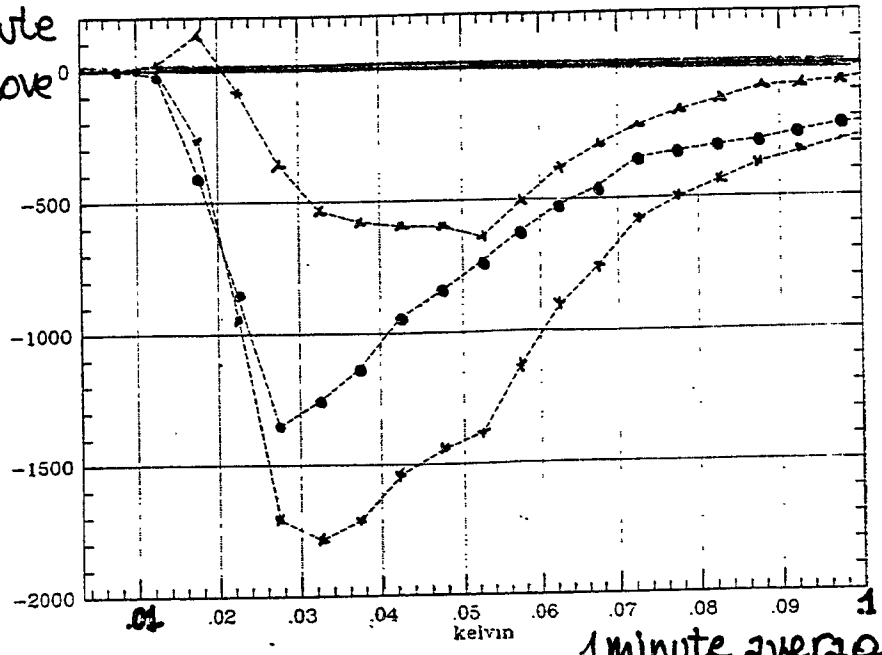

1 minute average (Kelvin)

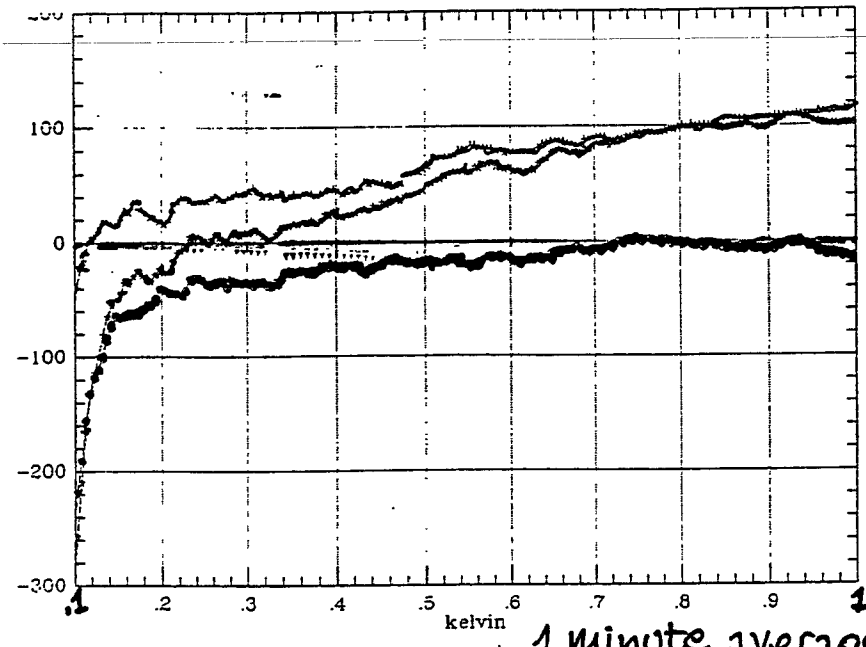

1 minute average (Kelvin)

1 CLEAN - VAR MEM

* CLEAN - WHOLE

● VAR MEM - WHOLE

SO:

- DIFFERENT PERFORMANCE OF DIFFERENT ALGORITHMS IN DIFFERENT NOISE CONDITIONS WHICH MAKE IT DIFFICULT TO TELL **A PRIORI** THE BEST STRATEGY.

  IN FACT, IF THE SAME STUDY WERE REPEATED OVER ANOTHER DATA SET, ONE WOULD GET CONSISTENT RESULTS AND MORPHOLOGICALLY THE SAME BEHAVIOUR, BUT NOT MORE THAN THIS.

- WE HAVE TO ABBANDON THE IDEA THAT WE CAN IMPLEMENT **ONE** FILTERING ALGORITHM WHICH IS OPTIMAL AT ALL TIMES

suggestion: HAVE A SET OF ALGORITHMS PROCESSING THE DATA IN PARALLEL. **A POSTERIORI** CHOOSE THE BEST ON THE BASIS OF THE SNR RESPONSE TO SIMULATED EVENTS SUMMED TO THE DATA AT PREDETERMINED TIMES BEFORE THE DATA ARE FED INTO THE FILTERING ALGORITHMS.

has had the best behaviour because
On the whole, the variance filter
it has detected ~~nearly all the false~~
~~events~~ the highest % of the false events.

The % of coincidences between the different
algorithm says that these are actually
seeing the same events, and this is
due to the fact that

- SNR is high
- the filter is the same, the
algorithm is different

~~By looking at the SNRs from the~~
~~different algorithms~~

Here are the SNR for the

SNR d'ingresso
~ 1
~ 2
~ 10

SNRs OF DIFFERENT FILTERS FOR OUR SIMULATED EVENTS

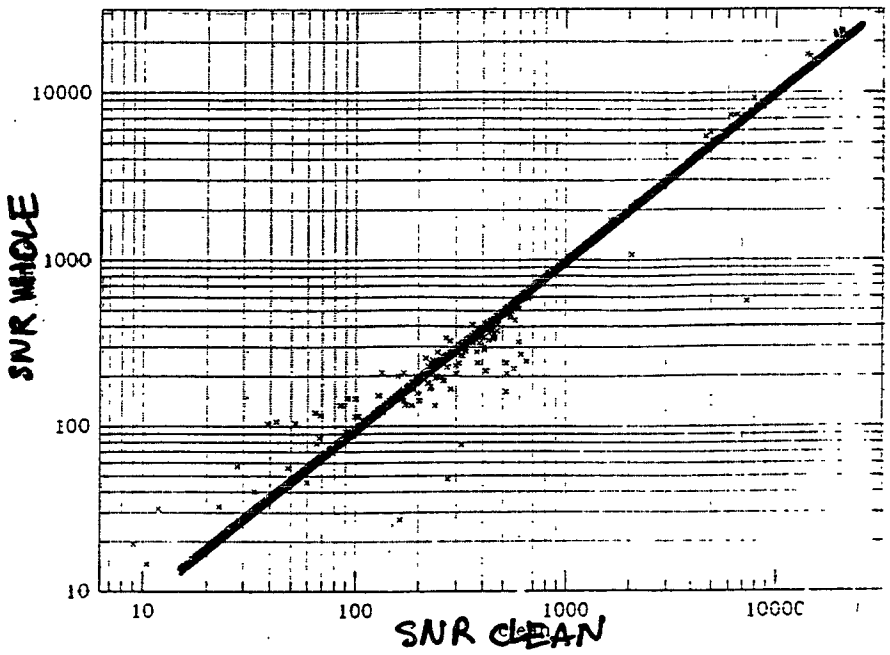

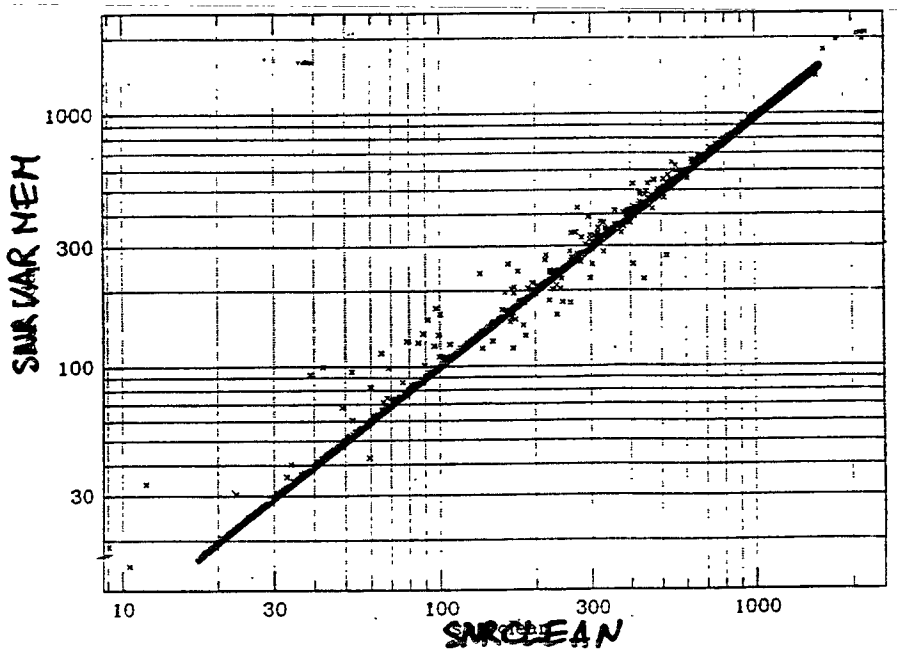

% OF DETECTED FALSE EVENTS WITH RESPECT TO TOTAL

WHOLE	66.2%
CLEAN	86.8%
VAR MEM	90.3%

% OF COINCIDENCES AMONG THE DIFFERENT FILTERS

WH - CL	94.8%
WH - VAR M	96.5%
CL - VAR M	97.3%

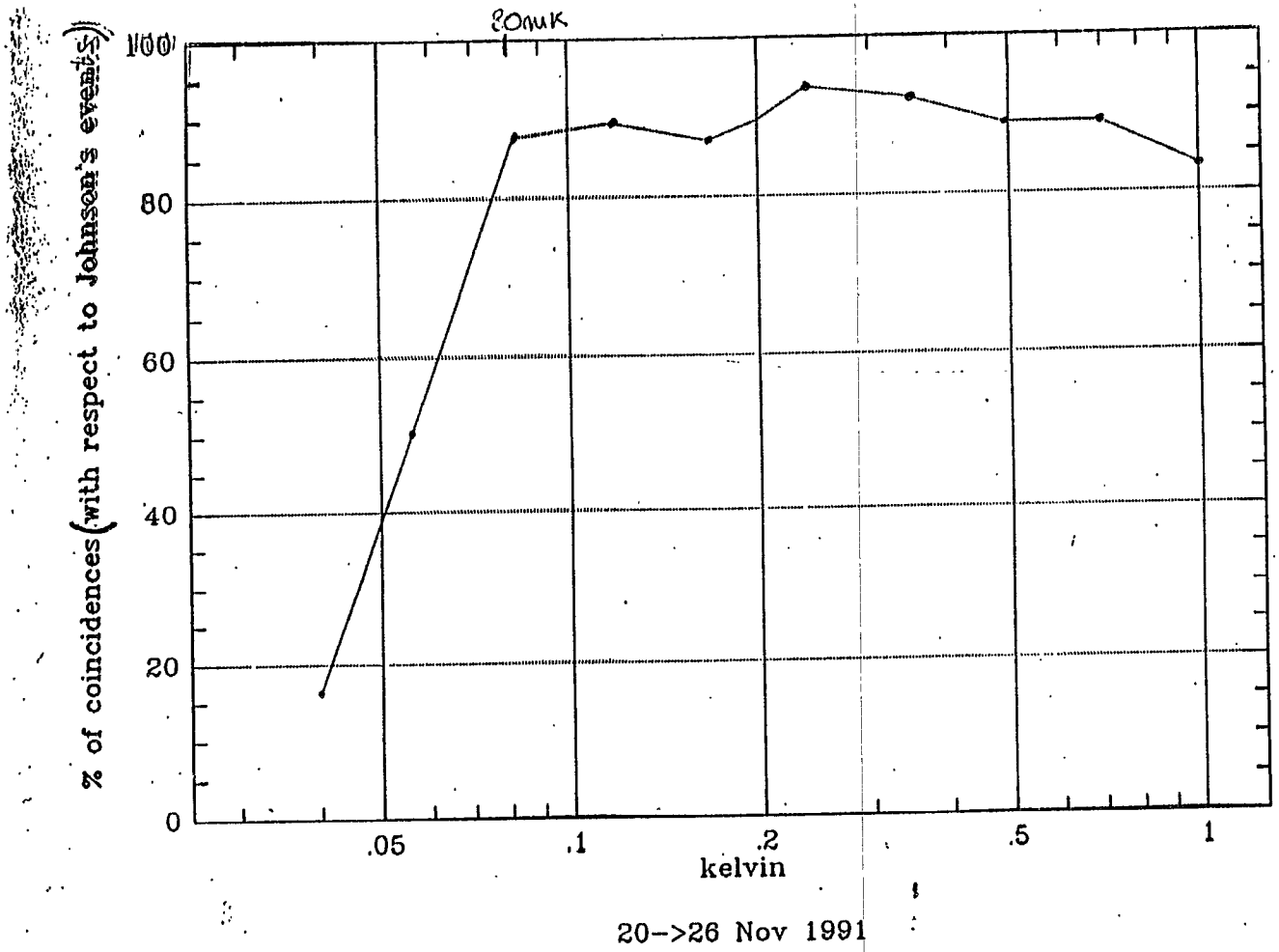

- EVENTS FROM THE RAW DATA OF THE ALLEGRO DETECTOR FILTERED WITH A **WHOLE** TYPE SPECTRUM ALGORITHM.

- THE SENSITIVITY OF THE INSTRUMENT IS NOT THE SAME AT ALL TIMES.

  - get rid of disturbed data — need to define what disturbed data are
  - treat all the data on equal footing, try to get best SNR in all conditions, store all relevant information on the status of the system.

- IT IS NOT POSSIBLE TO PREDEFINE THE OPTIMUM ALGORITHM — is this a problem? no

the solution to this by

- TESTING FILTERING PERFORMANCE IN THE REAL CASE, ON-LINE

also allows to tackle other issues

- LEARNING ABOUT THE NON-STATIONARITIES IN THE SYSTEM
- TEST EFFECTS OF NON PERFECT SIGNAL-TEMPLATE MATCHING
- KNOWING EXACTLY WHAT ONE'S LOOSING BY SETTING THRESHOLDS IN COINCIDENCE EXPERIMENTS

THESE ARE

Flanagan and Hughes

Gravitational-wave measurements of merging binary black holes

We break the waveform into 3 evolutionary phases:

1. **Inspiral**: bodies are well-separated, orbital evolution driven by radiation reaction.

   $h(t)$: Post-Newtonian, "IBBH" techniques

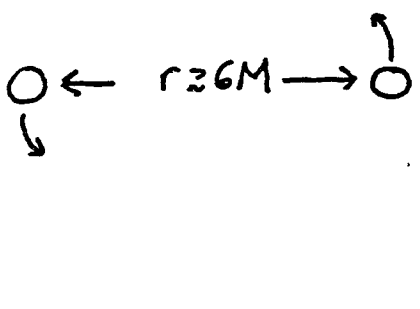

$$f \leq f_M \lesssim 200\,\mathrm{Hz}\left(\frac{20M_\odot}{M}\right)$$

2. **Merger**: the orbit becomes dynamically unstable, and the binary merges into a single body.

   $h(t)$: numerical relativity.

WAVEFORM NOT KNOWN!

$$f_M \leq f \leq f_R$$

3. **Ringdown**: tail end of merger. Gravitational waves of the $\ell = |m| = 2$ quasi-normal mode.

$h(t)$: damped sinusoid, from perturbation theory.

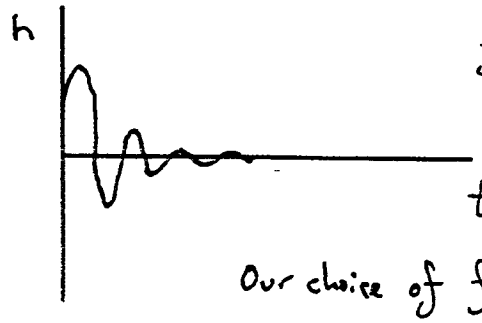

$$f \sim f_R \sim 1300\,\mathrm{Hz}\left(\frac{20M_\odot}{M}\right)$$

Our choice of f_R corresponds to a final spin of $\frac{a}{M} = .98$

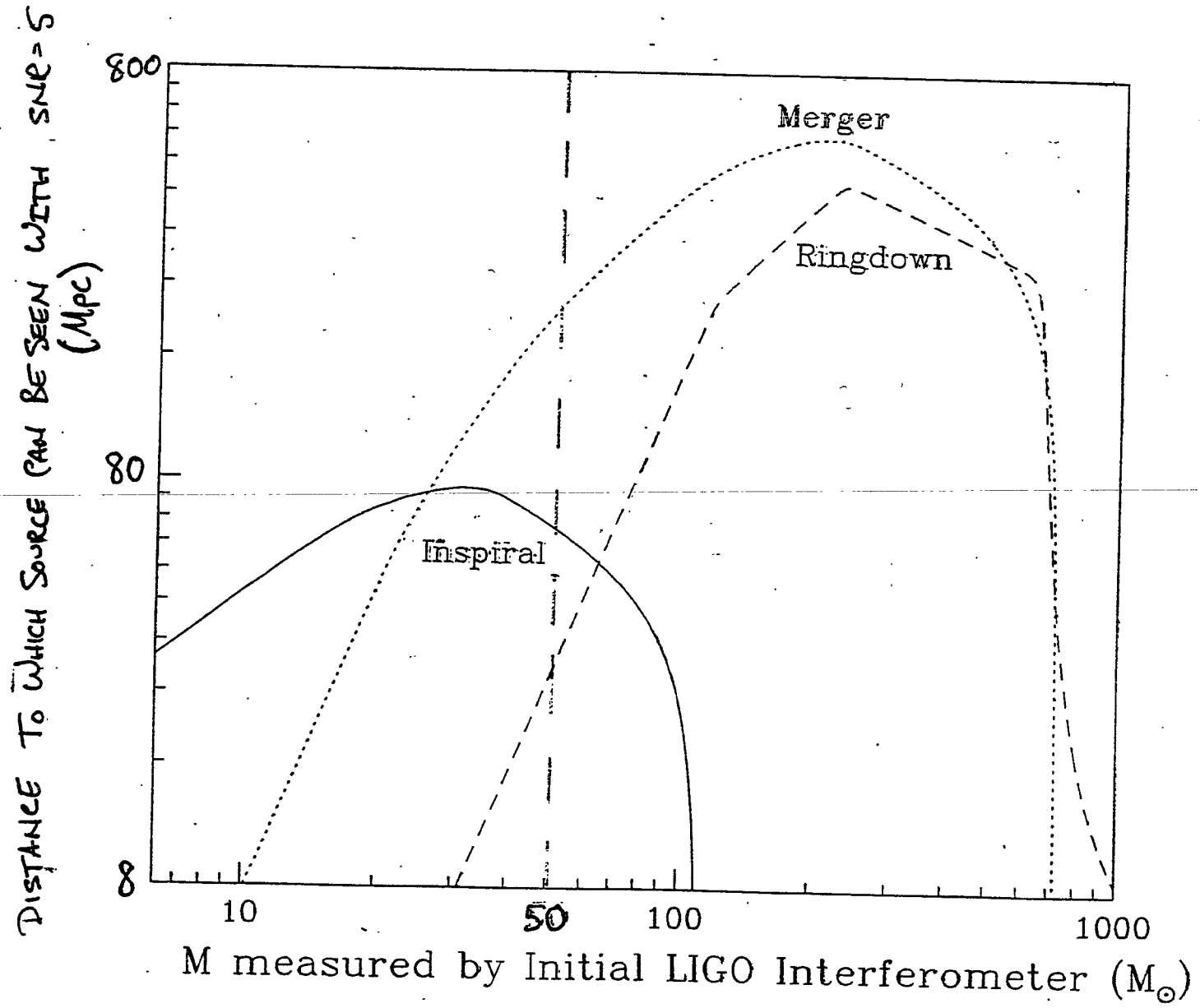
DISTANCE TO WHICH SOURCE CAN BE SEEN WITH SNR=5 (Mpc)
800
80
8
Merger
Ringdown
Inspiral
10
50
100
1000
M measured by Initial LIGO Interferometer ($M_\odot$)

Which signals are visible in which mass regime:

$(1+z)M \lesssim 40\,M_\odot$: Inspiral and merger are strongest. May be able to search for inspiral, then look for merger afterwards. DIFFICULTY: Especially for the larger mass systems, the inspiral signal comes only from the last few orbits. These will be best described with "IBBH" templates - which don't yet exist.

$(1+z)M \gtrsim 100\,M_\odot$: Ringdown and merger are strongest. Should be possible to search for ringdown (requires $\lesssim 10^4$ templates - low computational cost), then merger.

For intermediate masses, all three phases might be visible. Could "trigger" with inspiral + ringdown - this would tell duration + bandwidth of merger. Then, go in and look closely for merger using information learned from inspiral and ringdown.

NOTE: For $(1+z)M \gtrsim 20\,M_\odot$, the merger is potentially the strongest of the signal phases. If templates exist, gravitational-wave observatories should search for the merger directly.

Event Rates

Highly uncertain. However, the larger intrinsic system masses mean that events will be detectable out to greater distances – hence, a greater volume of the universe is seen.

Since $h \sim M$, $\frac{N_{BBH}}{N_{NSNS}} \approx \frac{R_{BBH}}{R_{NSNS}} \left(\frac{M_{BBH}}{M_{NSNS}}\right)^3$

R_{BBH}: system birth rate; N_{BBH}: detected rate

Need to know the highly uncertain birth rate of binary black hole systems! (Irregardless, the highest event rates come at the largest masses, where waveforms are most poorly known.)

One result (Lipunov et al, 1996 preprint) finds the rate depends most strongly on the kick one of the progenitors imparts to the other at supernova; they find (roughly) $\frac{R_{BBH}}{R_{NSNS}} \sim .1 - .01$. If a typical BBH total system mass is $20-30\ M_\odot$, we could have

$$\frac{N_{BBH}}{N_{NSNS}} \sim 4 \text{ to } 100$$

But there are a LOT of uncertainties in these estimates:

- details of mass transfer, mass loss
- separation of final black holes (if too large, won't inspiral in a Hubble time)
- distribution of progenitor binaries

NOTE – these processes only build $M \lesssim 50\ M_\odot$ binaries! Larger binaries will have to be "built" from repeated mergers.

What if templates for the merger do not exist?

Data analysis will proceed using other filtering techniques. Consider a "worst-case": simple band-pass filters that "chop out" data not in the relevant frequency range. The SNR is reduced compared to the optimal filter value:

$$\left(\frac{S}{N}\right)_{\substack{\text{BAND}\\ \text{PASS}}} \approx \frac{1}{\sqrt{N_{bins}}} \left(\frac{S}{N}\right)_{\text{OPTIMAL}}$$

Here, $N_{bins} \equiv 2 T \Delta f$

- Δf → Signal bandwidth
- T → Signal duration

is the number of Fourier coefficients required to describe a signal with duration T and bandwidth Δf.

We put $\Delta f = 1100\ \text{Hz}\left(\frac{20 M_\odot}{M}\right)$, and estimate that T may range

from $T \approx 2.5\ \text{ms}\left(\frac{M}{20 M_\odot}\right)$ [2 Schwarzschild black holes, merger dominated by QNR]

to $T \approx 10\ \text{ms}\left(\frac{M}{20 M_\odot}\right)$ [2 Kerr black holes]

Using these guesstimates, $2 \lesssim \sqrt{N_{bins}} \lesssim 5$

> The merger SNR is likely reduced by a factor less than or of order 5 when templates are not used for data analysis.

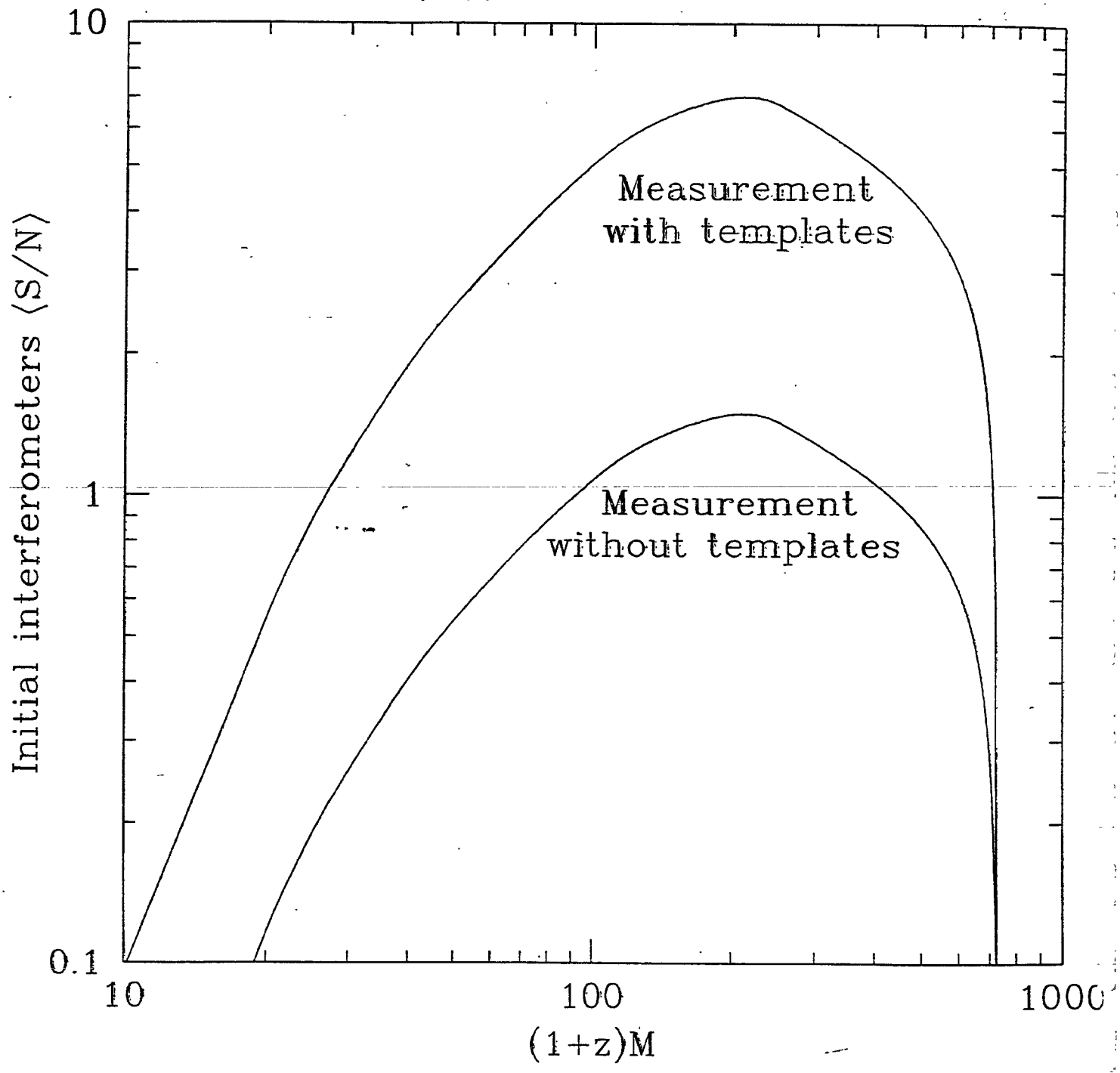
10
1
0.1
Initial interferometers ⟨S/N⟩
Measurement
with templates
Measurement
without templates
10
100
1000
(1+z)M

Example tilings: 64 pts, Sine + Impulse

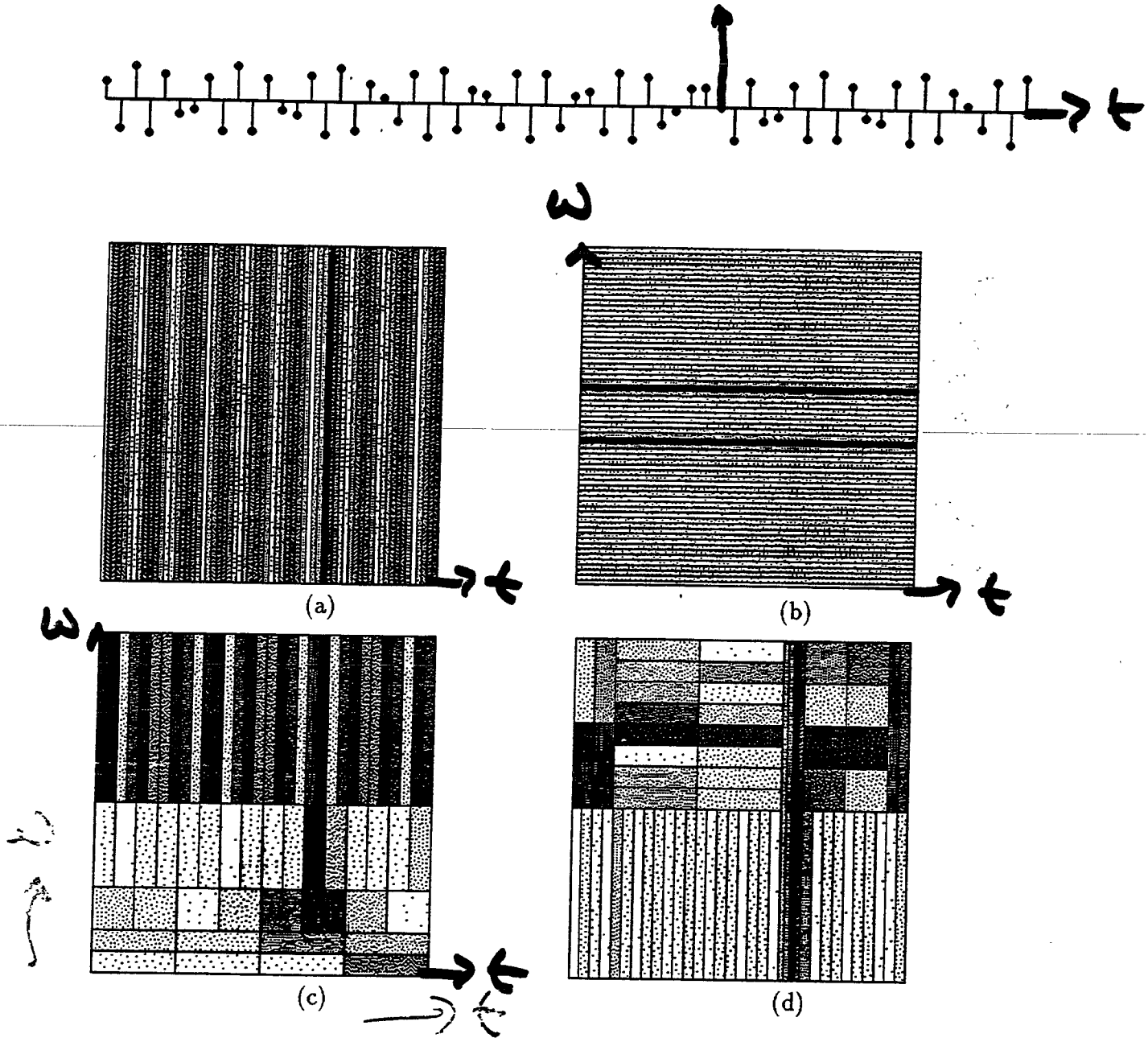

(a) Identity basis. (b) Discrete Fourier Transform. (c) Discrete wavelet transform. (d) Arbitrary tiling. [From Herley, thesis 1993]

SPIE PROCEEDINGS: WAVELET APPLICATIONS IN SIGNAL AND IMAGE PROCESSING IV. VOLUME 2825.

Comparison of algorithms for the fast computation of the continuous wavelet transform

Michael J. Vrhel, Chulhee Lee, and Michael Unser

Biomedical Engineering and Instrumentation Program, Bldg. 13, Room 3N17,
National Center for Research Resources, National Institutes of Health,
Bethesda, MD 20892, USA

ABSTRACT

We introduce a general framework for computing the continuous wavelet transform (CWT). Included in this framework is an FFT implementation as well as fast algorithms which achieve $O(1)$ complexity per wavelet coefficient. The general approach that we present allows a straight forward comparison among a large variety of implementations. In our framework, computation of the CWT is viewed as convolving the input signal with wavelet templates that are the oblique projection of the ideal wavelets into one subspace orthogonal to a second subspace. We present this idea and discuss and compare particular implementations.

Keywords: wavelet, continuous wavelet transform, fast algorithms, oblique projection.

1. INTRODUCTION

The continuous wavelet transform (CWT) is an often used tool in the analysis of non-stationary and fractal signals (e.g. EEG)[8, 16]. The typically long length of these signals and the large number of scales computed in their analysis provides a motivation for considering fast algorithms to compute the CWT. In this paper, we present a general framework for computing the CWT. This framework encompasses fast algorithms with complexity $O(1)$ per wavelet coefficient as well as an FFT implementation. Here we define the real CWT of the signal $s(t)$ as the inner product

$$W_s(\alpha,\tau) = \frac{1}{\sqrt{\alpha}}\left(s(t) * \psi\left(\frac{\tau - t}{\alpha}\right)\right)\Big|_{t=\tau} = \frac{1}{\sqrt{\alpha}}\int_{-\infty}^{+\infty} s(t)\,\psi\left(\frac{\tau - t}{\alpha}\right)dt \qquad (1)$$

$\alpha = 2^j \quad t = K2^{-j}$

where α and τ are respectively the continuously varying scaling and shifting parameters, and the real function $\psi(t)$ is the mother wavelet* .

In practice, the variables α and τ are sampled over the plane of values. Fast algorithms exist for computing the wavelet transform at the dyadic scales $\alpha = 2^i$ when the wavelet is associated with a multi-resolution [1, 3, 7, 11]. In this paper, we are interested in a finer sampling of the scale axis.

Previous methods for calculating the CWT include an approach which obtained the coefficients at the integer sample values $\alpha = i$, $\tau = k$, with $O(N)$ number of operations per scale [16]. Another approach which computes the CWT along arbitrary scales, again with $O(N)$ complexity per scale, is discussed in [13]. This last method is restricted to Gabor-like wavelets (i.e., modulated Gaussians). A method which achieved $O(N)$ operations per scale, with no restrictions on the shape of the wavelet, and with arbitrarily fine exponential sampling along the scale axis was introduced in [17]. This last method approximated wavelets at several scales by their orthogonal projection onto a space defined by a compact scaling

* : To simplify the notation throughout the paper, we use a definition of the wavelet transform that is a time-reversed version of the conventional one.

FILTER BANK $F\,H = I$

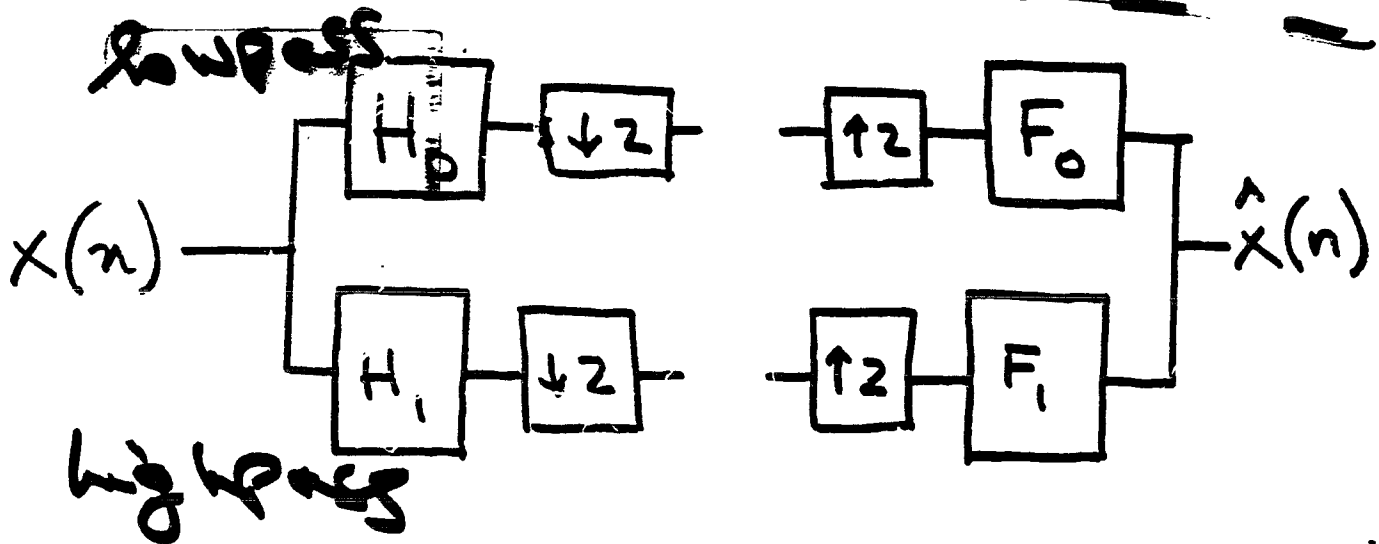

* ORTHOGONAL FILTER BANK

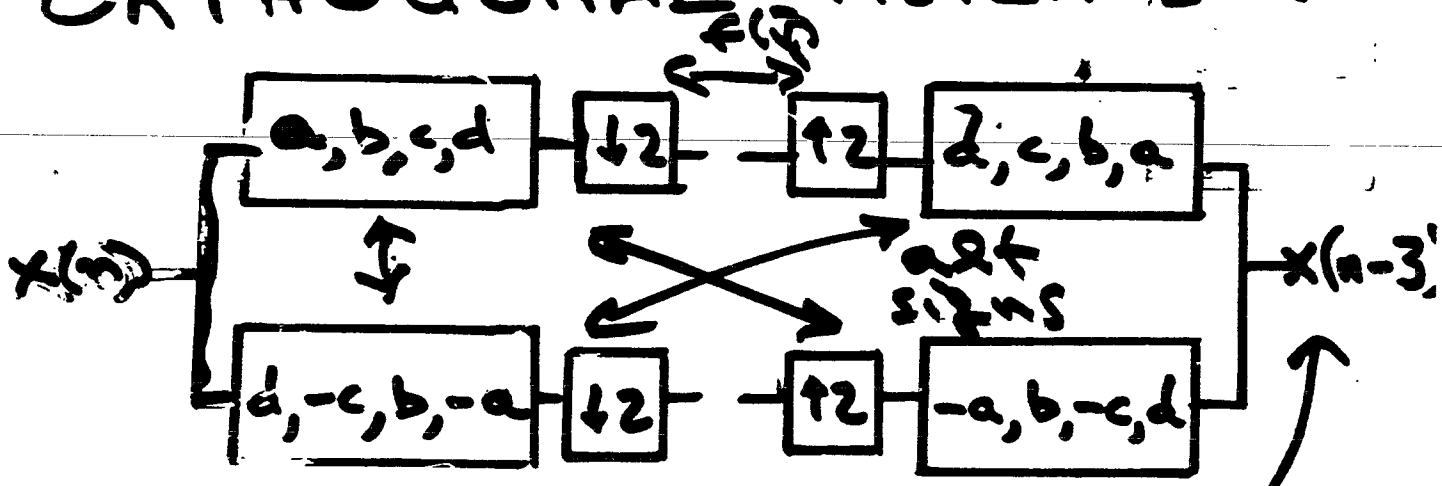

perfect reconstruction

$(a,b,c,d) * (d,c,b,a) =$ "halfband"

$(-1,0,9,16,9,0,-1)/16$

Daubechies coefficients

important zeros

3 DOMAINS: time, ω, z

FILTER IN TIME DOMAIN:

TOEPLITZ MATRIX (Convolution)

$$y_0 = H_0 x = \begin{bmatrix} \cdot & \cdot & & & \\ h(2) & h(1) & h(0) & & \\ \underline{h(3)} & \underline{h(2)} & \underline{h(1)} & \underline{h(0)} & \\ & h(3) & h(2) & h(1) & h(0) \\ & & h(3) & h(2) & h(1) \\ & & & \cdot & \cdot \\ & & & & \cdot \end{bmatrix} \begin{bmatrix} \cdot \\ x(-1) \\ x(0) \\ x(1) \\ x(2) \\ \cdot \end{bmatrix}$$

$$y(n) = \sum h(k)\, x(n-k)$$

$$y_0 = (\downarrow 2)\, y_0(n) = y_0(2n)$$

$$(\downarrow 2)\, H_0 = \begin{bmatrix} h(1) & h(0) & & & \\ h(3) & h(2) & h(1) & h(0) & \\ & & h(3) & h(2) & h(1) & h(0) \\ & & & & h(3) & h(2) & \cdot \\ & & & & & & \cdot \end{bmatrix}$$

"Double-shift"

ITERATE THE LOWPASS FILTER

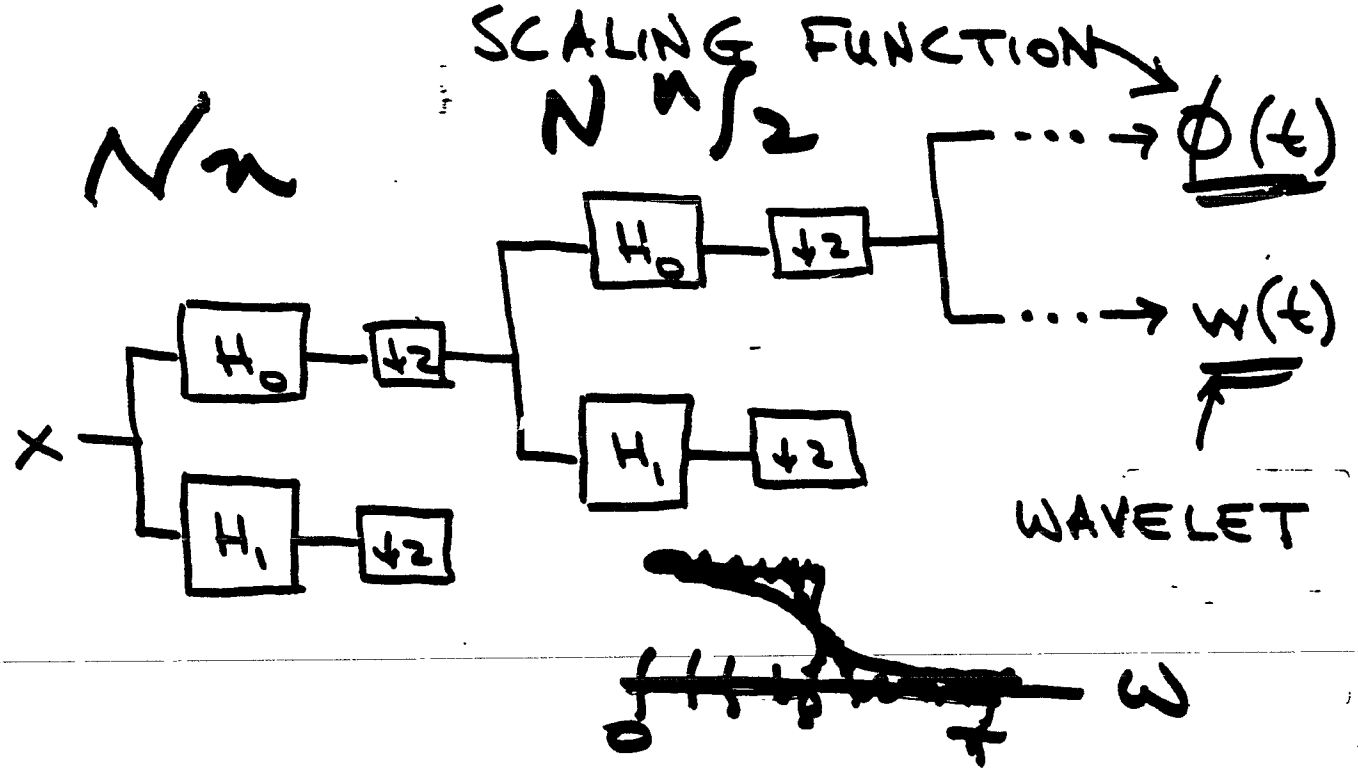

Normalize to $H(0) = \sum h(k) = 1$

(divide by $\sqrt{2}$) (H is H_0: lowpass)

ITERATION = CASCADE ALGORITHM

$$\phi^{(i+1)}(t) = \sum 2\, h(k)\, \phi^{(i)}(2t-k)$$

constant area

analog of $2n$

$$\int \phi^{(i+1)}(t)\,dt = \int \phi^{(i)}(t)\,dt$$

$\phi^{(0)}(t) =$ box

IF the iteration converges then

$$\phi(t) = \sum_{0}^{N} 2\, h_0(k)\, \phi(2t-k)$$

DILATION EQN (REFINEMENT EQN)

Then the wavelet comes from one highpass step

$$w(t) = \sum 2\, h_1(k)\, \phi(2t-k)$$

Similarly $\tilde{\phi}(t)$ and $\tilde{w}(t)$ from $f_0(k)$ and $f_1(k)$

BIORTHOGONAL $\int \phi(t)\, \tilde{\phi}(t+k)\, dt = \delta_{0k}$

$$\int \phi(t)\, \tilde{w}(2^j t+k)\, dt = 0 = \int \tilde{\phi}(t)\, w(2^j t+k)\, dt$$

$$\int w(2^j t+k)\, \tilde{w}(2^J t+K)\, dt = \delta_{jJ}\, \delta_{kK}$$

Wavelets and Filter Banks

Gilbert Strang
Massachusetts Institute of Technology

Truong Nguyen
University of Wisconsin

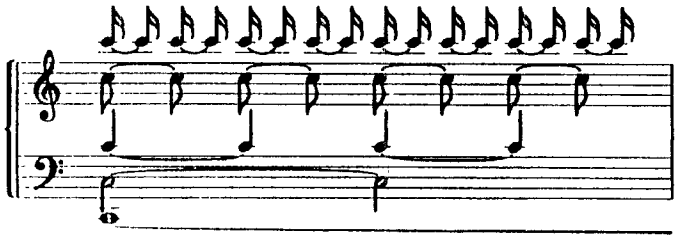

Wellesley-Cambridge Press
Box 812060
Wellesley MA 02181

email address: gs@math.mit.edu

Contents

Date: Fri, 16 Feb 1996 17:55:58 -0500
From: Geoff Davis <gdavis@cs.dartmouth.edu>

Strang and Nguyen's text, _Wavelets and Filter Banks_, is by far the best introduction to wavelets that I have seen.

One of the nicest things about the text is that it achieves a balance between the language of engineers and the language of mathematicians, and it presents material in a manner that is accessible to people with a wide range of backgrounds. My current graduate seminar on wavelets is attended by graduate students, some advanced undergraduates, and several professors. The members of the class come from the math department, the computer science department, the engineering school, and the business school. All seem to have found the book useful.

I have been extremely pleased with the book overall and give it an enthusiastic endorsement!

GW data → Gaussian Noise Component
GW data → Excess Noise Component (Non-Gaussian)

* Even with a clean spectrum → register excess events

* Caused by transients in narrow band spikes or broad band noise

Laser Interferometers => spectra have many spikes (known & unknown)
=> transients can mimic bursts

Bars => learning lessons on how to get max information out of data with non-stationary noise.

VARIOUS APPROACHES TO BURST DETECTION

1/ ZOP: Search for transients in amplitude & phase poor amplitude & time resolution.

2/ Non-adaptive Weiner: Better time resolution and SNR.

3/ Adaptive Weiner: Better SNR as adapts parameters as noise changes.

However Intrinsically suppresses non-thermal events if these are part of the noise model

Do we really want to do this?

Typical Spectrum

$P_{sig} = -21$ dBm

10dB + 40dB LNA BPF in readout system

Input CH1 Rng: 223.87 mVrms DC, Float CH2 Rng: 891.25 mVrms DC, Float

Date: 03-30-93 Time: 05:39:00 PM

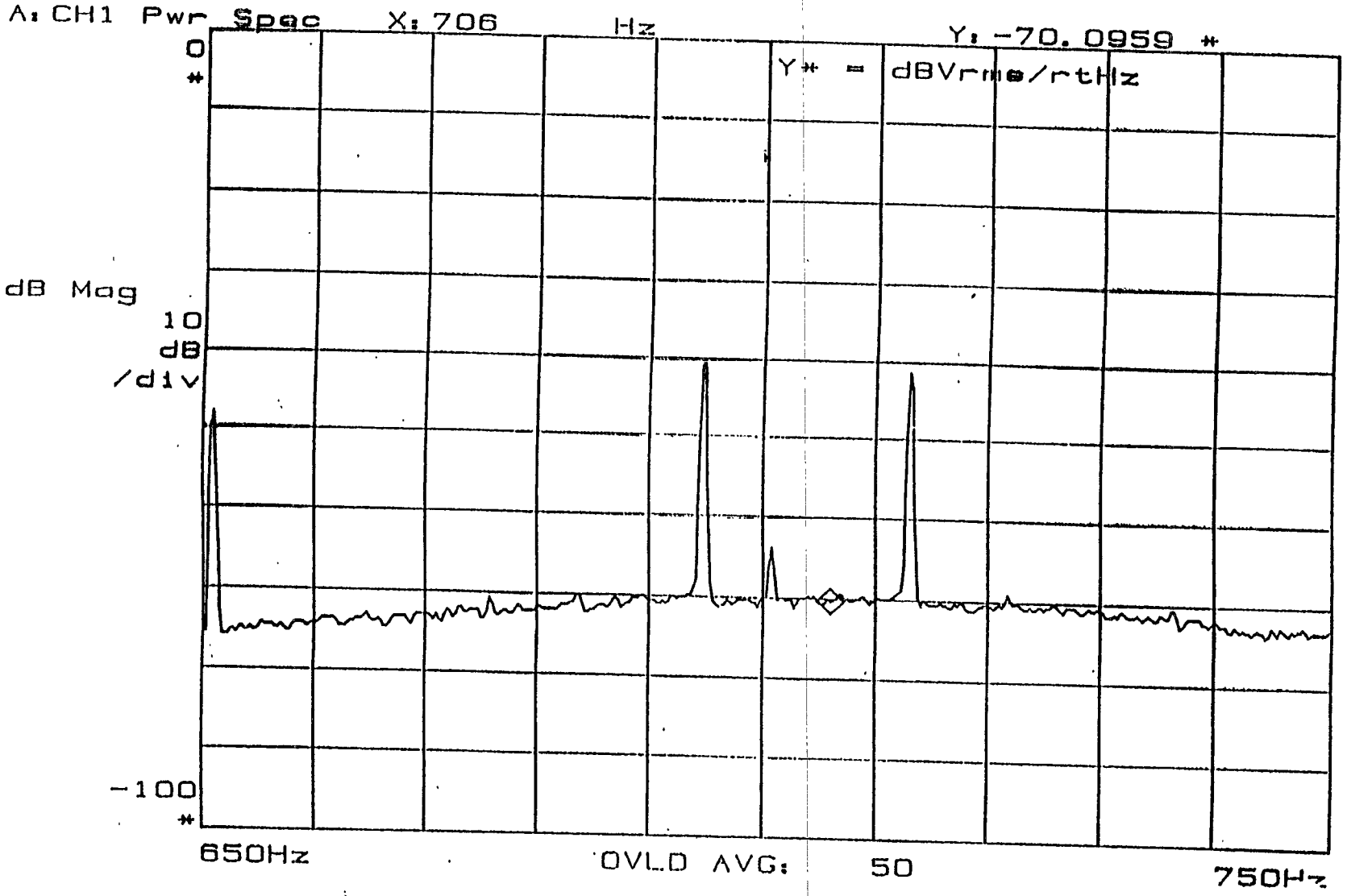

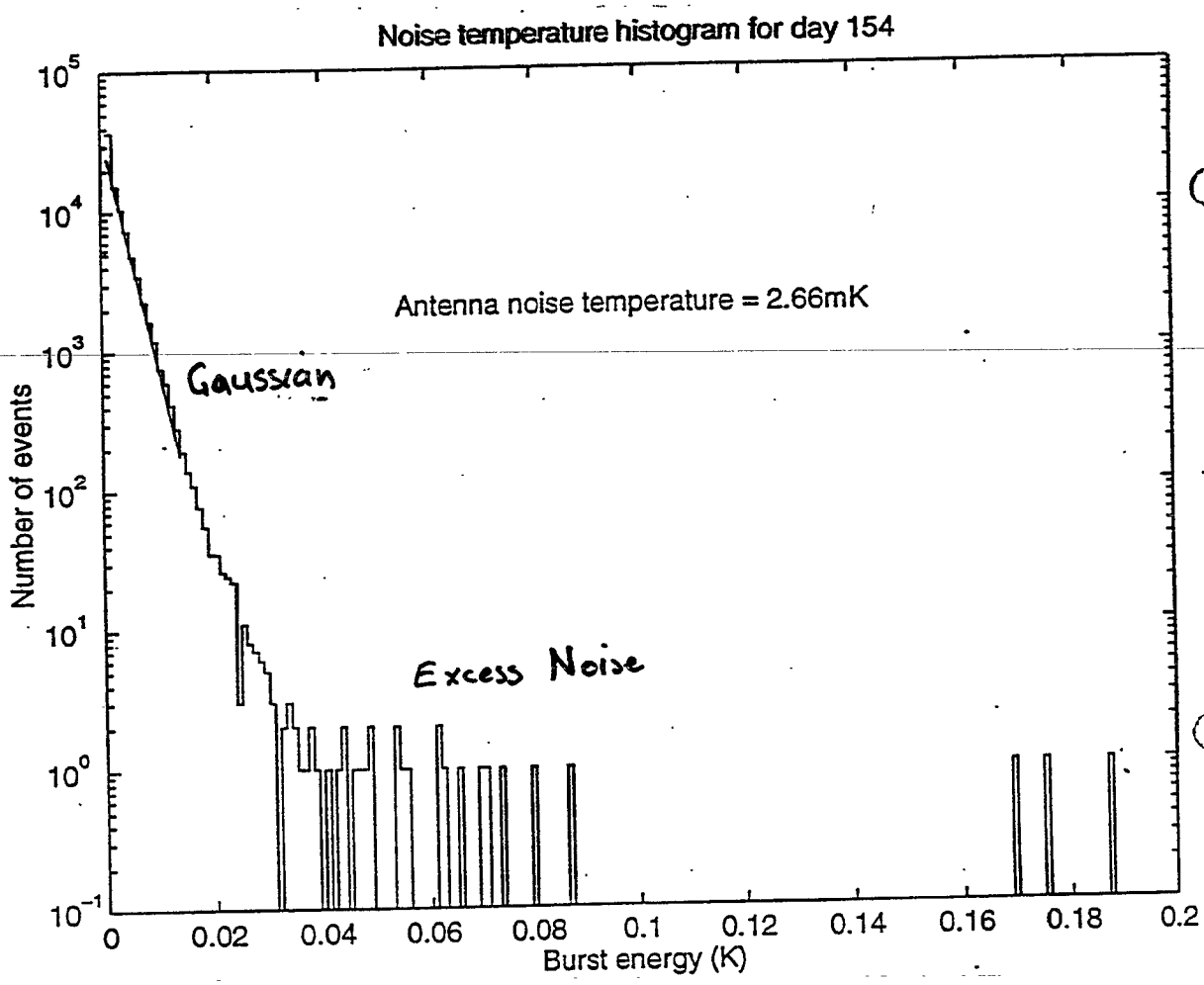
Noise temperature histogram for day 154
Antenna noise temperature = 2.66mK
Gaussian
Excess Noise
Number of events
Burst energy (K)
10^5
10^4
10^3
10^2
10^1
10^0
10^{-1}
0
0.02
0.04
0.06
0.08
0.1
0.12
0.14
0.16
0.18
0.2

Amplitude Modulated Calibration Pulses

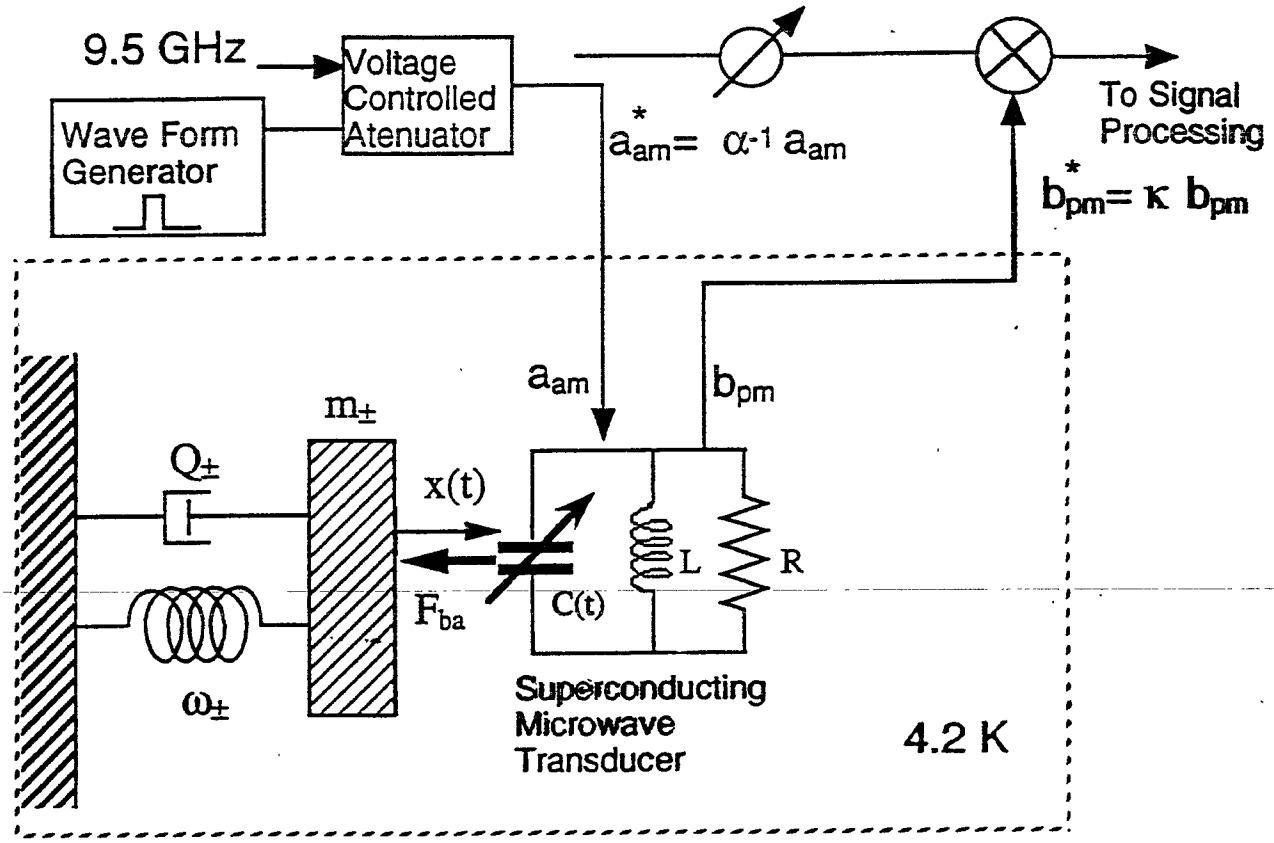

* Amplitude modulated carrier causes a back-action force which excites the antenna

* Excited antenna causes a phase modulation which is demodulated by a phase sensitive detector

* Transducer is represented by scattering parameter matrix

$$\begin{bmatrix} b_{pm} \\ F \end{bmatrix} = \begin{bmatrix} S_{pu} & S_{pa} \\ Z_{in} & S_{fa} \end{bmatrix} \begin{bmatrix} \dot{x} \\ a_{am} \end{bmatrix}$$

* If configured properly $S_{pa} = 0$
(no am->pm conversions on reflection)

The energy deposited into the antenna can be calculated from;

$$E_c = \frac{\pi N_c \, a_{am} \, bpm(\Delta t)}{\Omega_o \, (\beta + 1)}$$

$$= \frac{\gamma \, \pi \, (N_c \, a_{am})^2}{2\omega} \qquad \gamma = \frac{b_{pm}(\Delta t)}{N_c \, a_{am}} \frac{\omega}{\Omega_o} \frac{(\beta+1)}{2}$$

Measure

$$a^*_{am} \, b^*_{pm}(\Delta t) = \alpha^{-1} \, \kappa \, a_{am} \, b_{pm}(\Delta t)$$

* Some uncertainty due to attenuation and gain from outside the dewar to the transducer

---

*Self calibration technique is more accurate, however this technique may be used to check the self calibration technique.

*Moreover, this method provides an easy way to apply pulses to calculate relative timing and energy performance of the data aquisition system.

Test Pulses

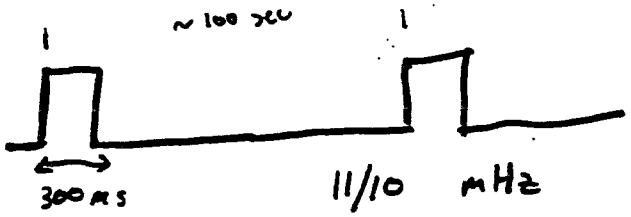

* Test relative performance
of ZOP
Weiner
Adaptive Weiner

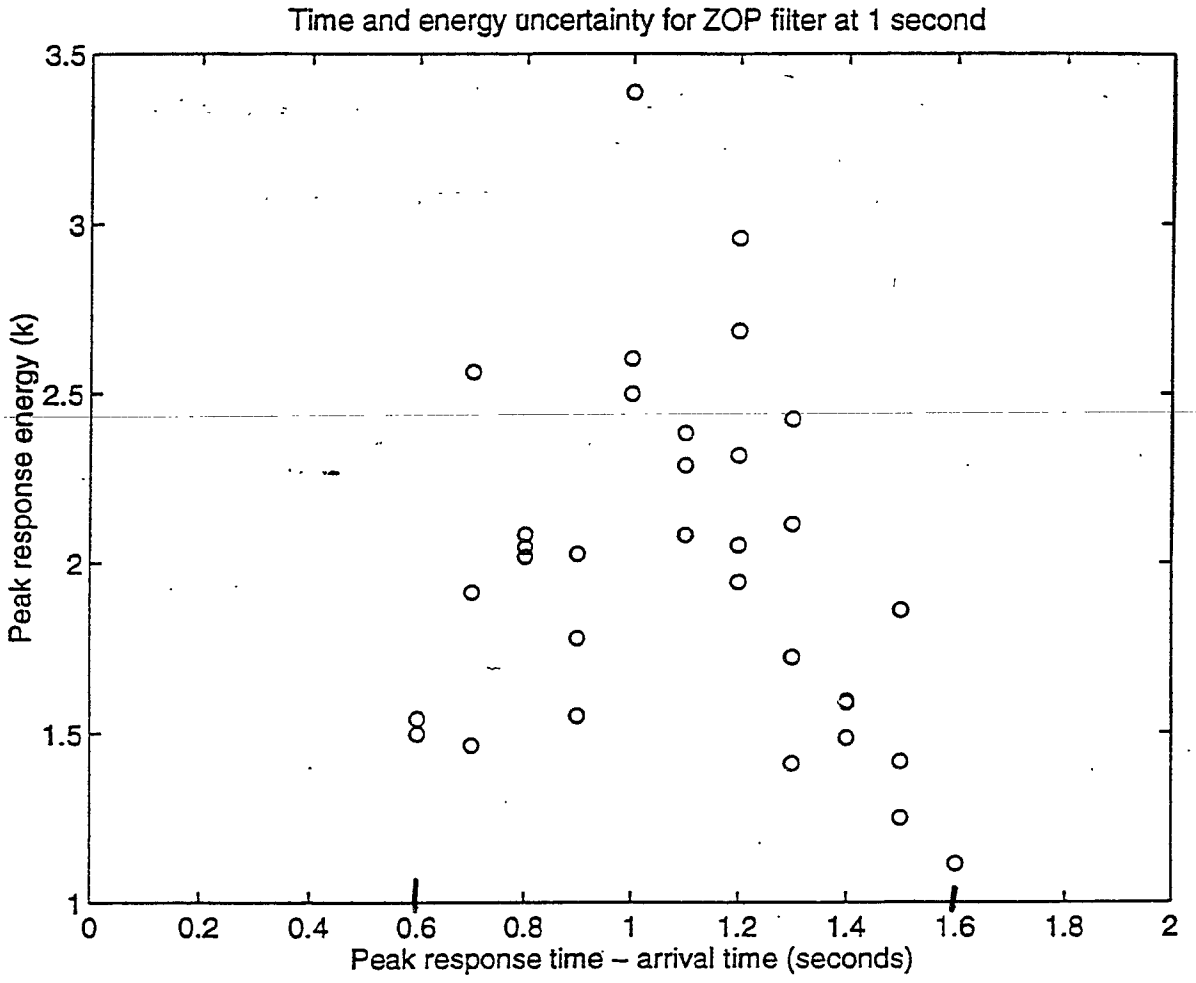

$\Delta t \Rightarrow 0.6$ to 1.6

Simulation $\Delta t \Rightarrow 0.2$ to 1.2

Suggests 0.4 sec error

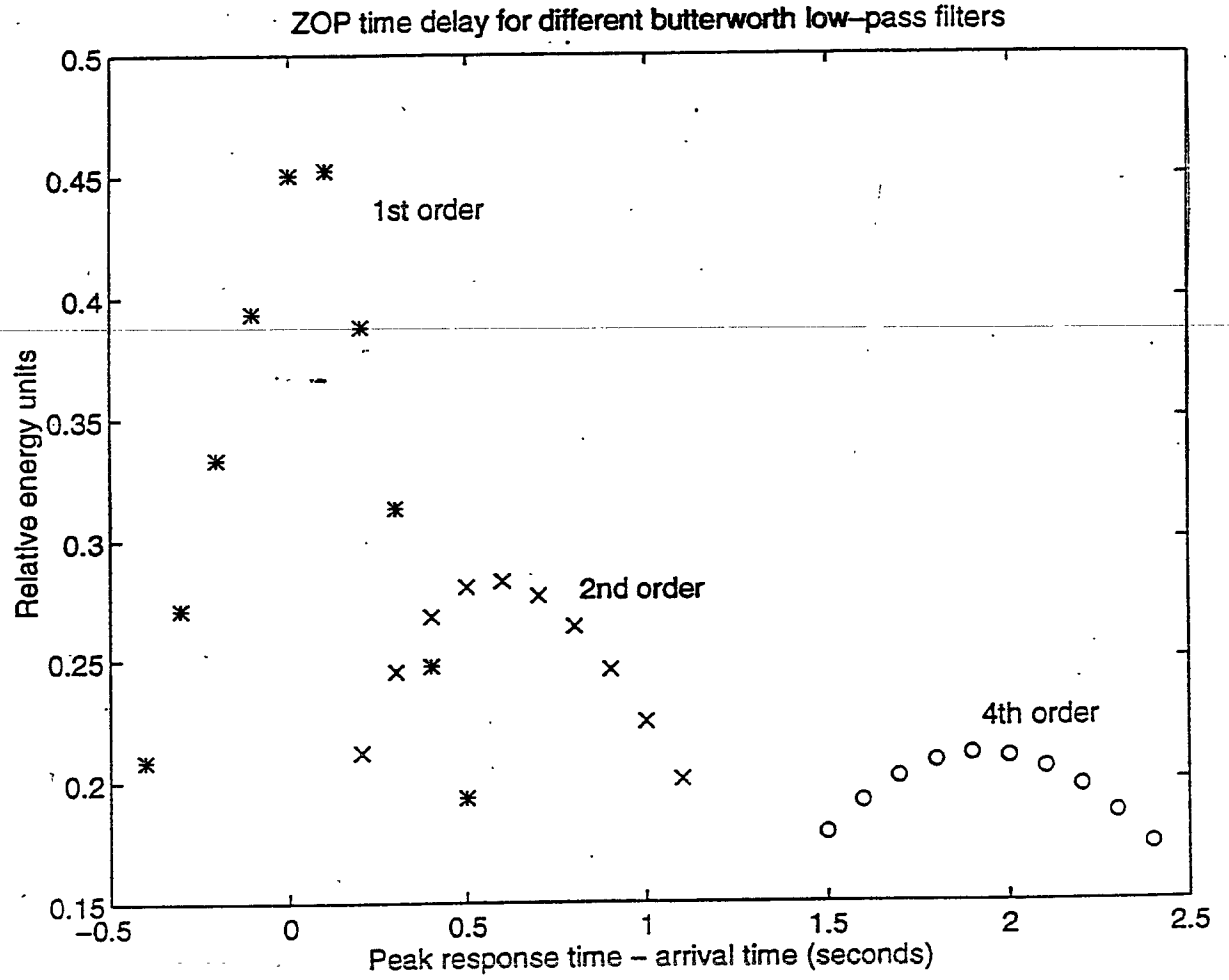

From Simulations

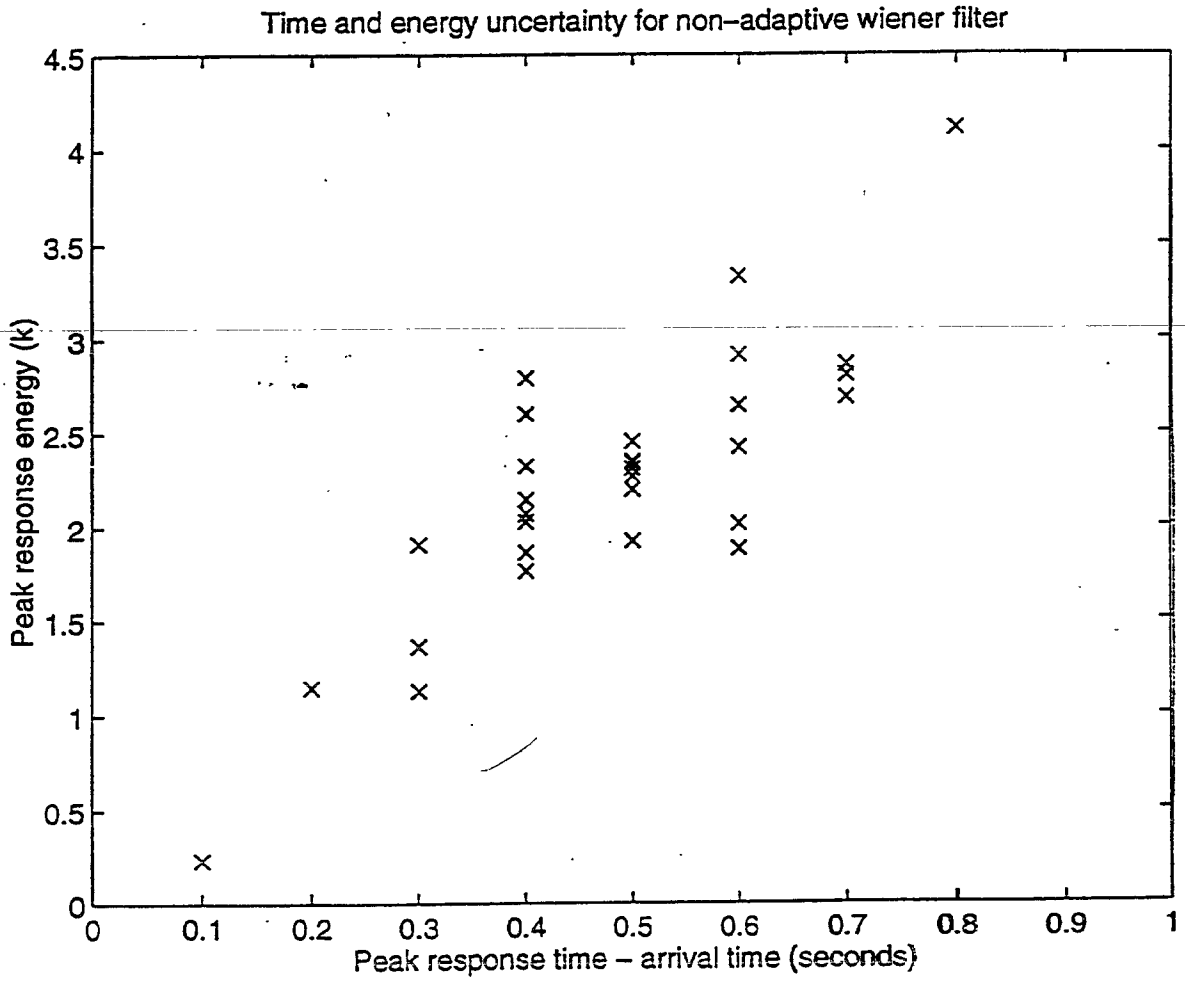

$\Delta t \Rightarrow 0.1$ to 0.8

energy diff : 0.1 2.

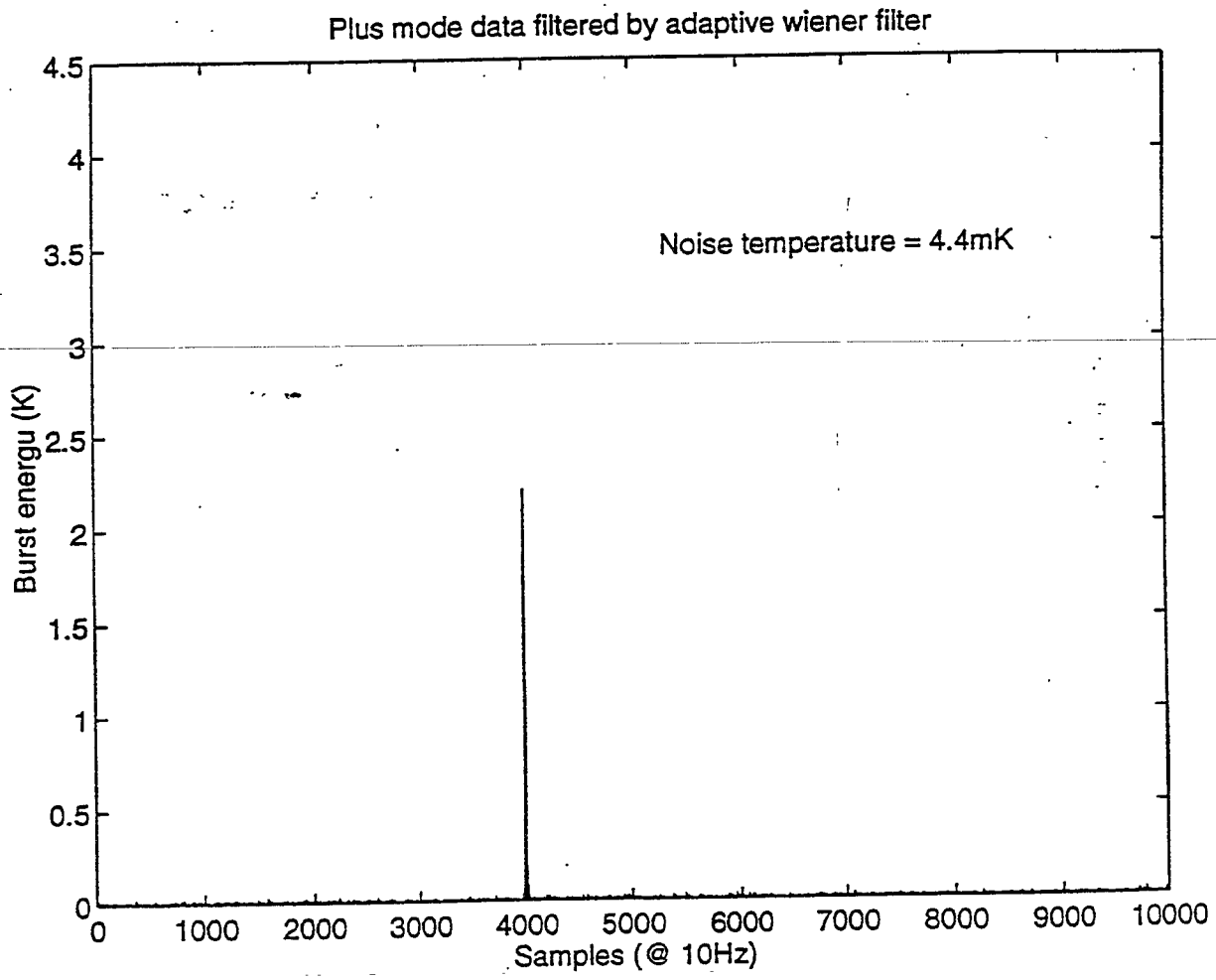
Plus mode data filtered by adaptive wiener filter
Noise temperature = 4.4mK
Burst energu (K)
Samples (@ 10Hz)
0
0.5
1
1.5
2
2.5
3
3.5
4
4.5
0
1000
2000
3000
4000
5000
6000
7000
8000
9000
10000

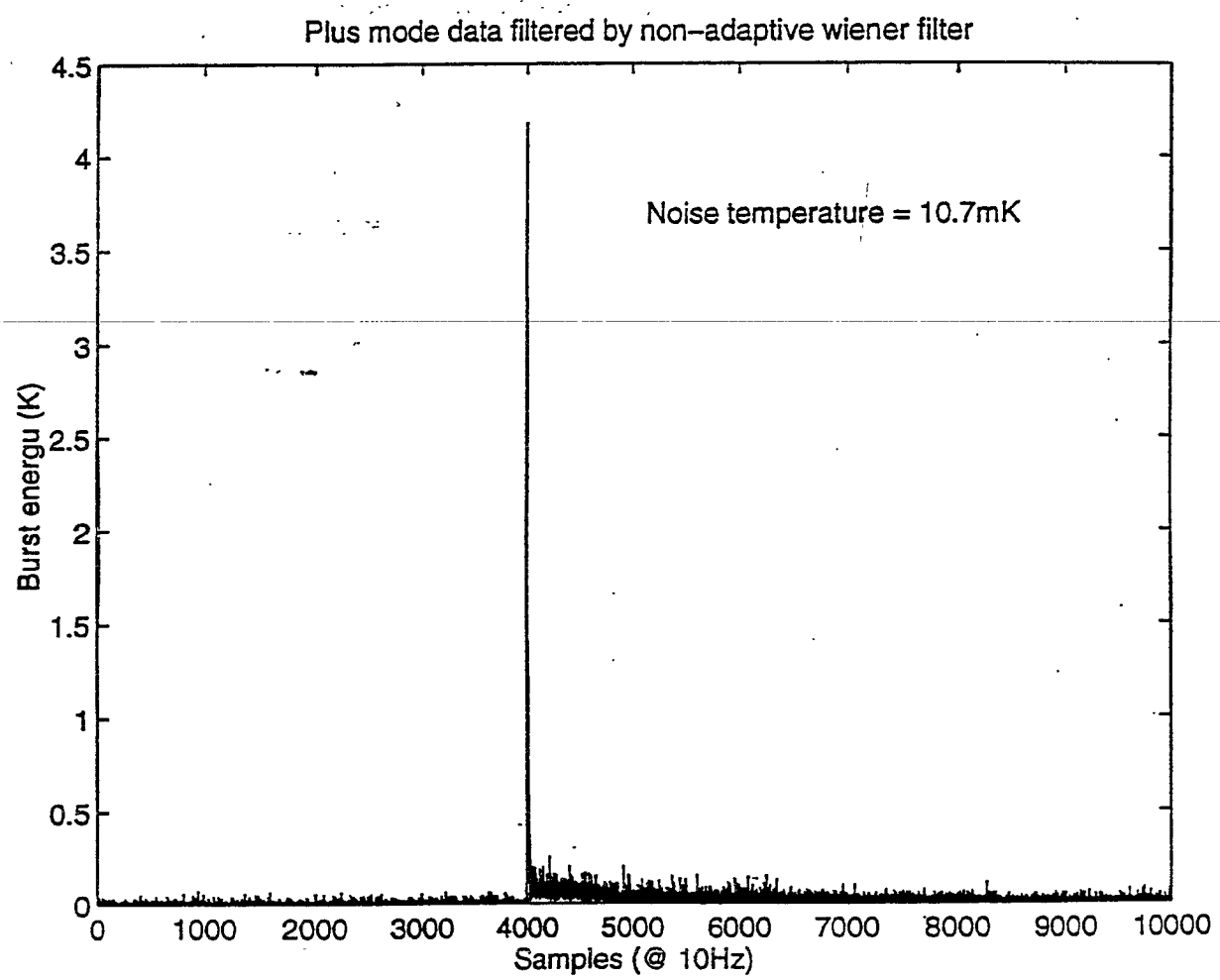
Plus mode data filtered by non–adaptive wiener filter
Noise temperature = 10.7mK
Burst energy (K)
Samples (@ 10Hz)
0
0.5
1
1.5
2
2.5
3
3.5
4
4.5
0
1000
2000
3000
4000
5000
6000
7000
8000
9000
10000

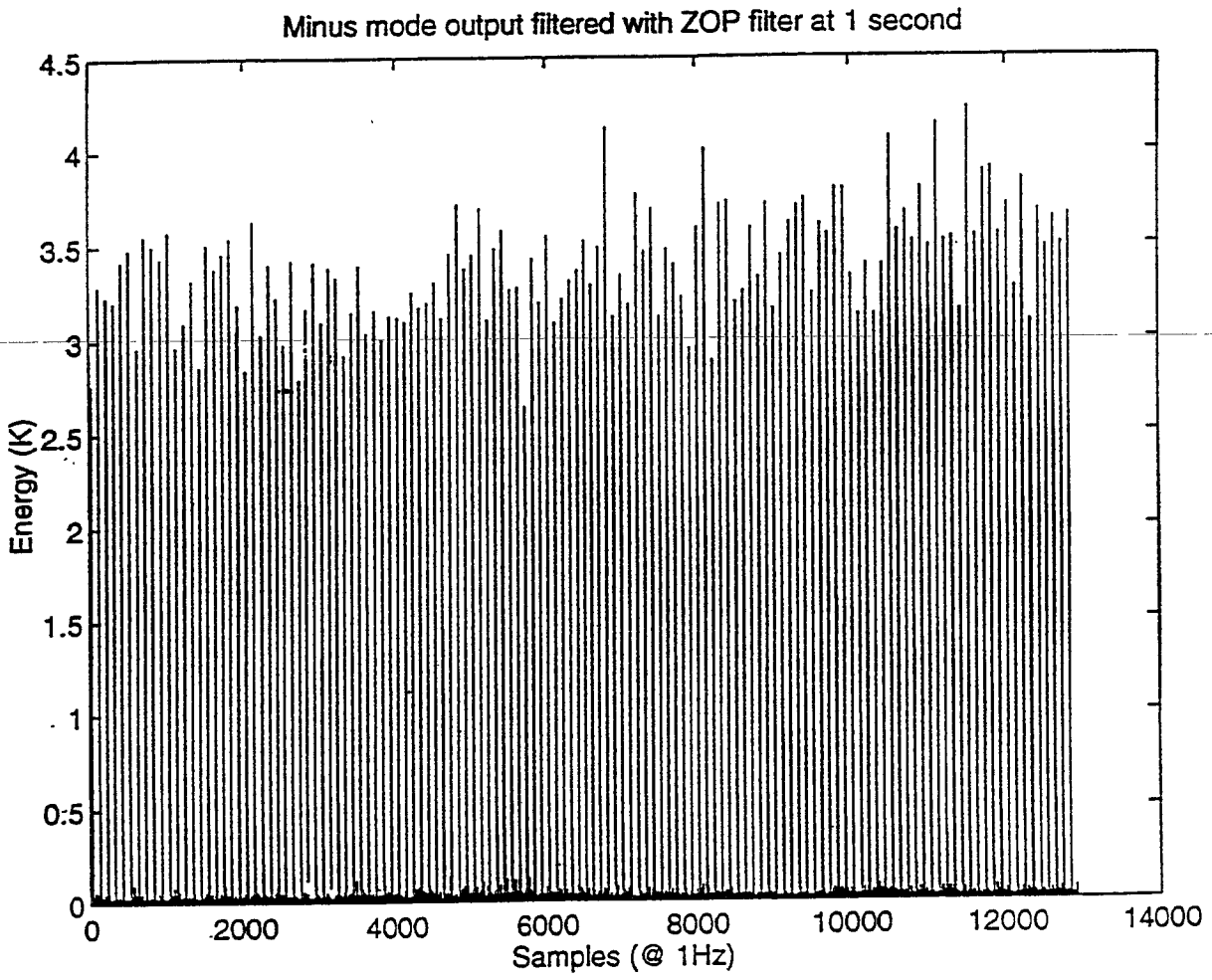
Minus mode output filtered with ZOP filter at 1 second
Energy (K)
Samples (@ 1Hz)
0
0.5
1
1.5
2
2.5
3
3.5
4
4.5
2000
4000
6000
8000
10000
12000
14000

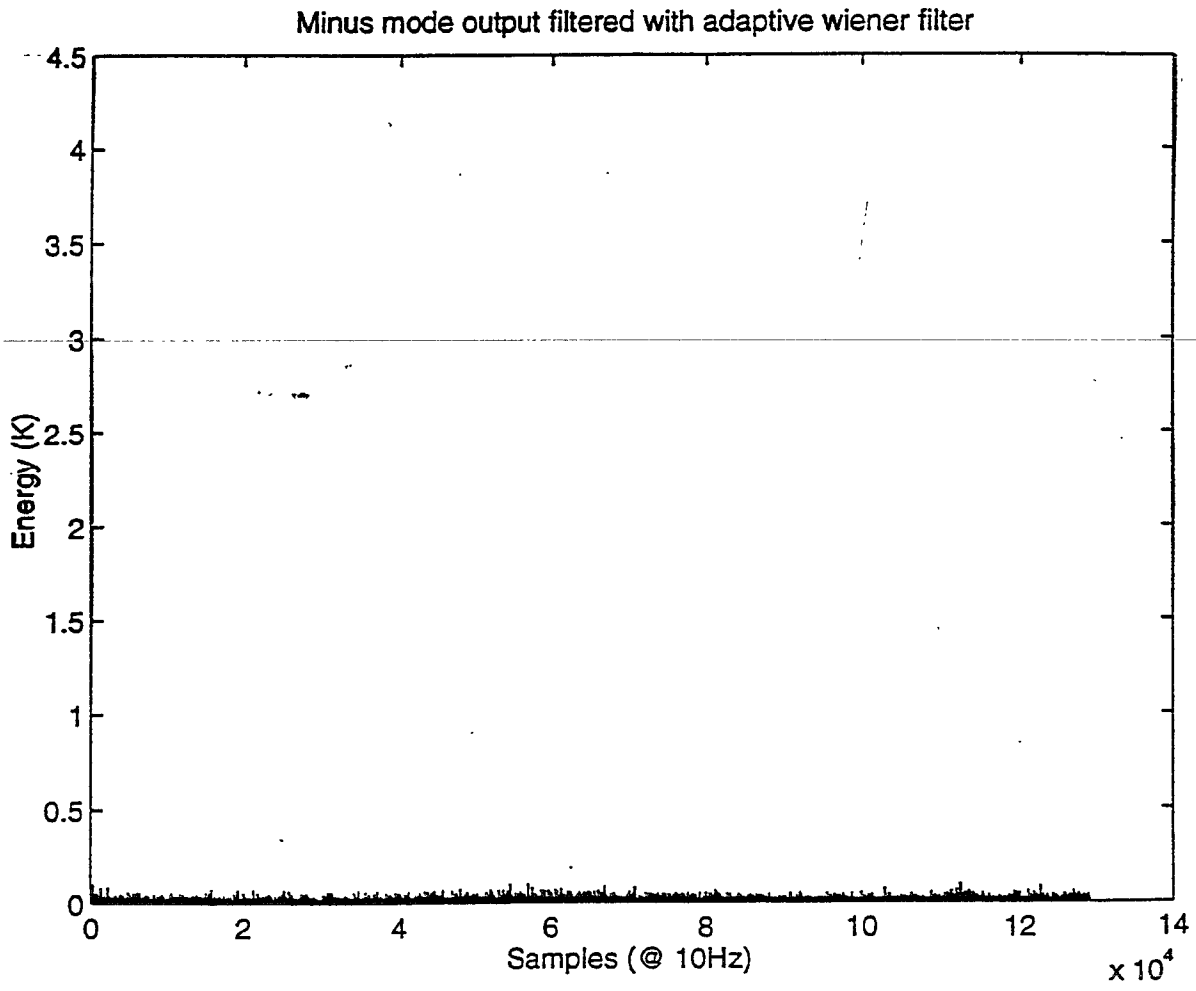
Minus mode output filtered with adaptive wiener filter
Energy (K)
4.5
4
3.5
3
2.5
2
1.5
1
0.5
0
0
2
4
6
8
10
12
14
Samples (@ 10Hz)
x 10^4

Summary

* Energy & Timing Considerations are non-trivial

* Important to be able to apply pulses or ~~signals~~ expected signals to test the performance of a real detector.

* There is doubt of the performance of interferometers amongst Non-Gaussian noise.
  → should ~~make~~ a priority to insert calabrators.
  → Use a function generator to apply a chirp and test templates amongst Non-Gaussian noise.
  → check accuracy of signal and timing ~~am~~ with varying SNR.

* When doing coincident analysis it simplifies the procedure if we use the same filter & sampling time.

- The CW problem for resonant acoustic detectors -

P. Astone S. Frasca

- The Rome group of resonant detectors -

Pulsars, sensitivities at ~ 1 kHz:

$t_m = 1$ year, known source, $h = \sqrt{\frac{25}{t_m}}$

Explorer: $\sim 2 \cdot 10^{-25}$ in ~ 2 Hz around the resonances

$\sim 2 \cdot 10^{-24}$ in ~ 16 Hz between the resonances

Nautilus: $\sim 1 \cdot 10^{-26}$

Auriga

GEO 600: $\sim 5 \times 10^{-26}$

GEO 600 narrow: $\sim 5 \cdot 10^{-27}$

VIRGO: $\sim 1 \cdot 10^{-26}$

LIGO advanced: $\sim 2 \times 10^{-26}$ / $\sim 3 \cdot 10^{-27}$

} Schutz

$\Rightarrow$ joint searches (also) between bdrs and interferometers

SPECTRAL DATA BASE

Due to the Doppler effect
the maximum sweeping in frequency is:

during one year	$\sim$ 0.62 Hz
during one day	$\sim$ 0.011 Hz

An individual spectrum is taken over a time period of 0.6617 hours and covers the frequency range

900 -927.5 Hz

During this time we have

$\Delta\nu_{Doppler}$=0.28 mHz

smaller than the frequency step in the spectrum

$\Delta\nu$ = 0.42 mHz

In conclusion, we have 13239 spectra in one year

HEADER:
it is used for vetoing the experimental data

- **Date**
- **Brownian noise, minus mode**
- **Brownian noise, plus mode**
- **frequencies, minus and plus**
- **decay times, minus and plus**
- **wide band noise**
- **calibration**
- **other information**

In one year we have 13239 spectra

Explorer 1991
Search for Monochromatic Waves

One spectrum, $\Delta t_0 = 0.66$ hours

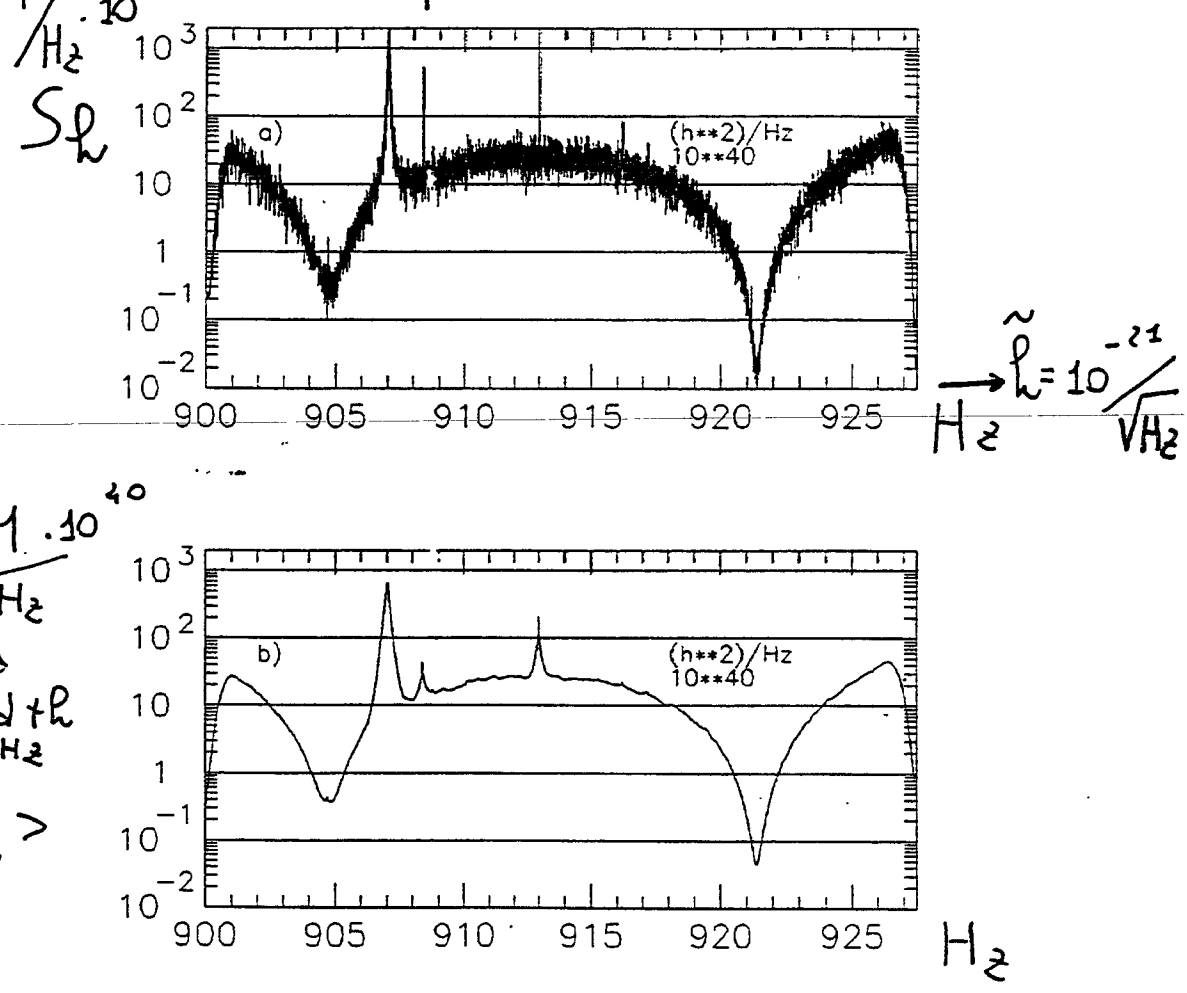

Figure 1: *a) One spectrum in the data base (1 august 1991). b) Its smoothing filter*

for $t_m = 0.66$ hours $h_0 = \sqrt{\frac{2 S_h}{t_m}} = 3 \times 10^{-23}$ experimental

over one year $h_0 = 3 \times 10^{-23} \times \left(\frac{365 \cdot 24}{0.66}\right)^{1/4} =$

$= 2.8 \cdot 10^{-22}$

Procedure – candidate lines REGISTRATION

in each spectrum of the Data base
$i = 1, 13239$
$j = 1, 65536$

the procedure

reads $(\nu_{ji}, \tilde{h}^2_{ji})$ in the j channel of the i-spectrum

registers $(time_i, \nu_{ji}, \tilde{h}^2_{ji} - \langle \tilde{h}^2_i \rangle)$

if $\tilde{h}^2_{ji} \geq K \tilde{h}^2_{MIN\,i}$

(actually $K = 8$)

where $\tilde{h}^2_{MIN_i}$ is a MINIMUM value of the spectrum, evaluated again each time a new datum is registered. (register the LOCAL MAXIMA)

One file/year contains all these information that can be easily read by the analysis program

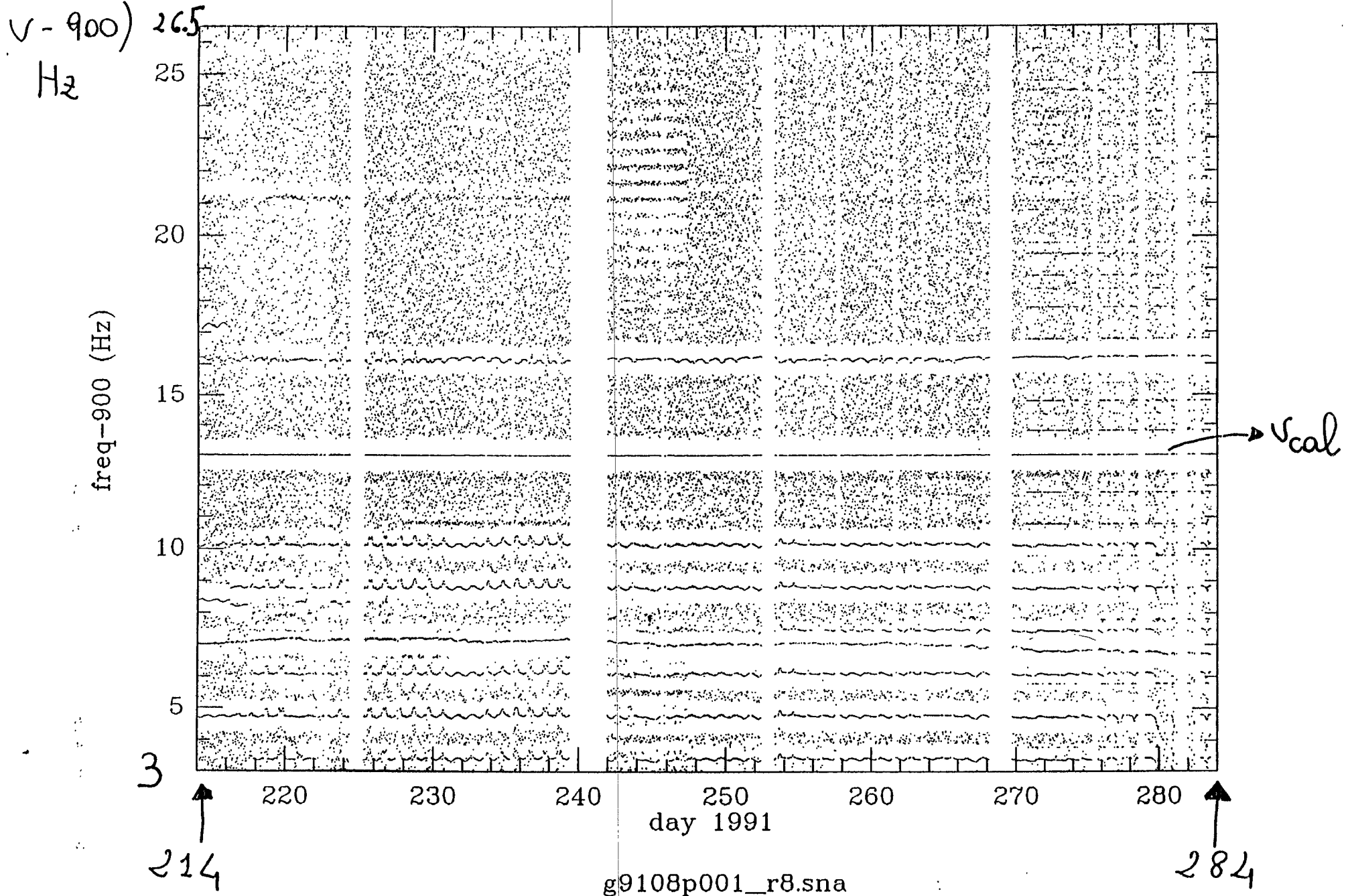
(ν - 900) 26.5
Hz
25
20
15
10
5
freq-900 (Hz)
ν_{cal}
3
220
230
240
250
260
270
280
day 1991
214
284
g9108p001_r8.sna
DAY, 1991

Spectral line at 916.3 Hz

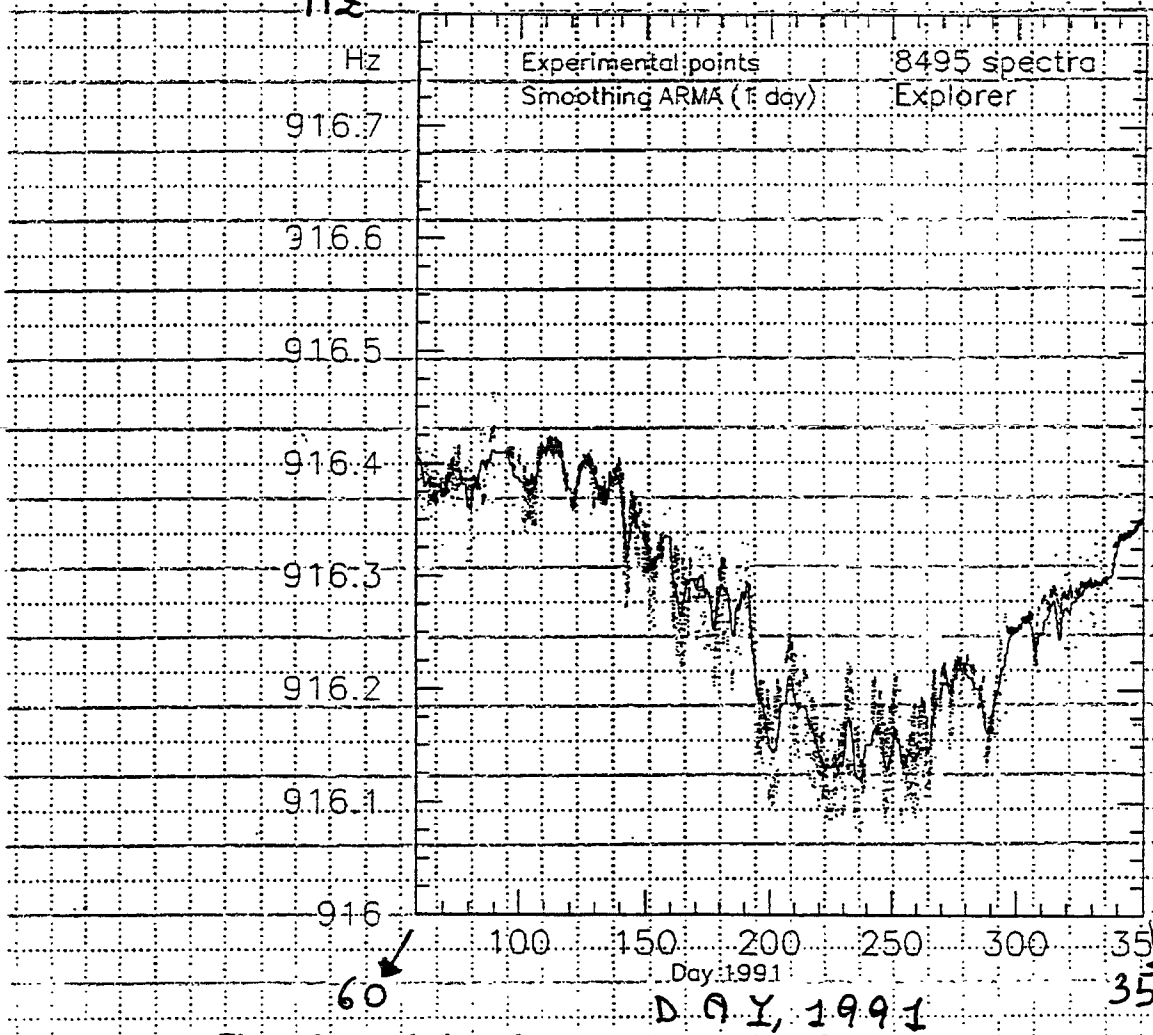

Figure 2: march-december 1991, 8495 spectra. Spectral line at 916 Hz and its smoothing, with an AR (Filt+Tlif)filter with $\tau = 1$ day.

8495 spectra

We analyze the frequency and amplitude patterns of each candidate spectral line in order to identify, or to exclude, a certain locus of points as possible g. w. emitters.

Using ~ 20000 point sources

$\Delta \nu < 0.4$ mHz

(less than the frequency step in each spectrum)

$\Delta h^2 \lesssim 10\%$

We fit the frequency and the amplitude with the expected modulations from various sources.

The first step might consist in fitting the frequencies and chosing the direction which gives the best fit.

The energies are averaged as a function of the SIDEREAL TIME and we test if the fit for them, using the SAME direction, is satisfactory

The sensitivity:

in each spectrum the (noise) standard deviation is $\sigma_i \sim (3 \times 10^{-23})^2$ experimental

$(h_0 = 3 \times 10^{-23})$

in each spectrum we registere as a possible candidate of a spectral line

$\tilde{h}^2_{j\tilde{i}}$ than can be $<< \sigma_i$

This number is not significant for a single spectrum

But when we average the information of all the N spectra ($N = 13239$ if $t_m = 1$ year)

$$\sigma_i \longrightarrow \sigma_i / \sqrt{N}$$

$$h_0 = \frac{3 \times 10^{-23}}{N^{1/4}} = 2.8 \times 10^{-24}$$

Disadvantage

It has a reduced sensitivity, compared to the "long" FFT

$$h_0^{"long"} = \sqrt{\frac{2 S_h}{t_m}}$$

$$h_0 = \sqrt{\frac{2 S_h}{\sqrt{t_m \Delta t}}}$$

$$\Rightarrow \frac{h_0}{h_0^{"long"}} = \left(\frac{t_m}{\Delta t}\right)^{1/4}$$

if t_m = one year
$\Delta t = 0.66\,h$

$$\Rightarrow \frac{h_0}{h_0^{"long"}} \sim 10$$

A Montecarlo, using the experimental data + simulated continuous signals, is in progress to confirm experimentally

Advantages, DETECTOR

Even if the detector works properly, it is really difficult (impossible?) to have, say, 1 year of data at the SAME level of sensitivity, with the SAME level of STATIONARY noise, WITHOUT disturbances

hence it is important to have a DATA BASE of SPECTRA in which each spectrum is completely characterized

Advantages, SOURCE

- it is very simple and doesn't require the use of lots of templates

- it measures the frequency and amplitude patterns of the spectral lines. Hence:

- soure frequency indetermination is not so crucial, as it is in a "long" FFT

- soure frequency variation with time can be directly measured

- in case the frequency (amplitude) pattern matches with the expected from one direction in the sky, it is simple to test if the amplitude (frequency) pattern matches with the same direction

Advantages, EXPERIMENTER

- study spectral lines periodicity (if there are)
- correlations between the lines
- time dependance of the lines
- the same procedure can be used to investigate spectral peaks that can be due to noise

---

In case of interesting results from one direction in the sky it is still possible to apply the "long" FFT method, removing in the data the modulation due to the Doppler from the candidate source, and using all the information obtained with the present analysis (e.g. frequency decreasing, if observed)

Spectral line at 916.3 Hz

- frequency versus time -

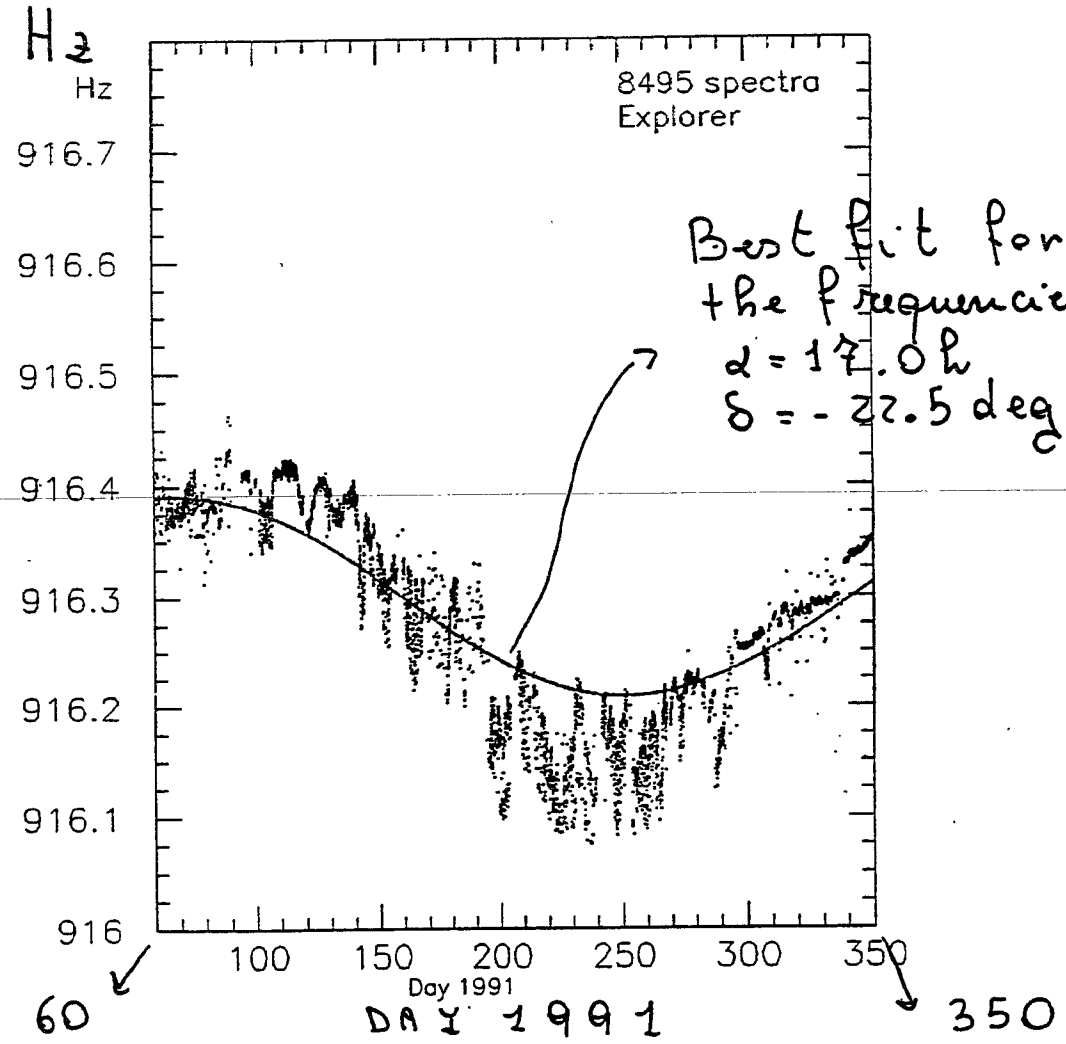

Figure 1: march-deccmber 1991; 8495 spectra. Experimental data, cleaned using ARMA filt+ tlif 1 day, and expected if the source were at α=17.03 hours, δ=-22.5 degrees, that is the best fit for the frequencies.

Results of the ~ 20000 frequencies fits

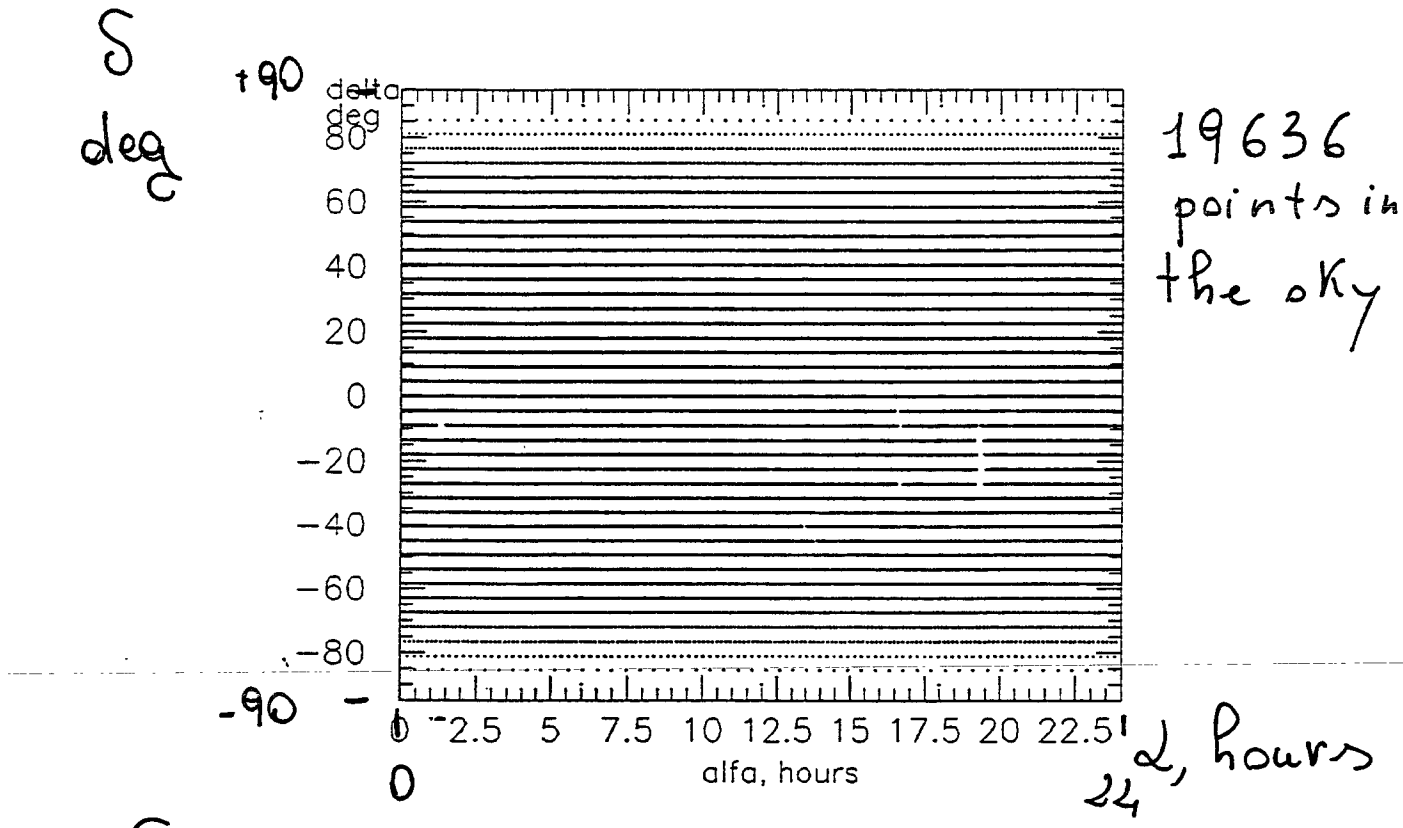

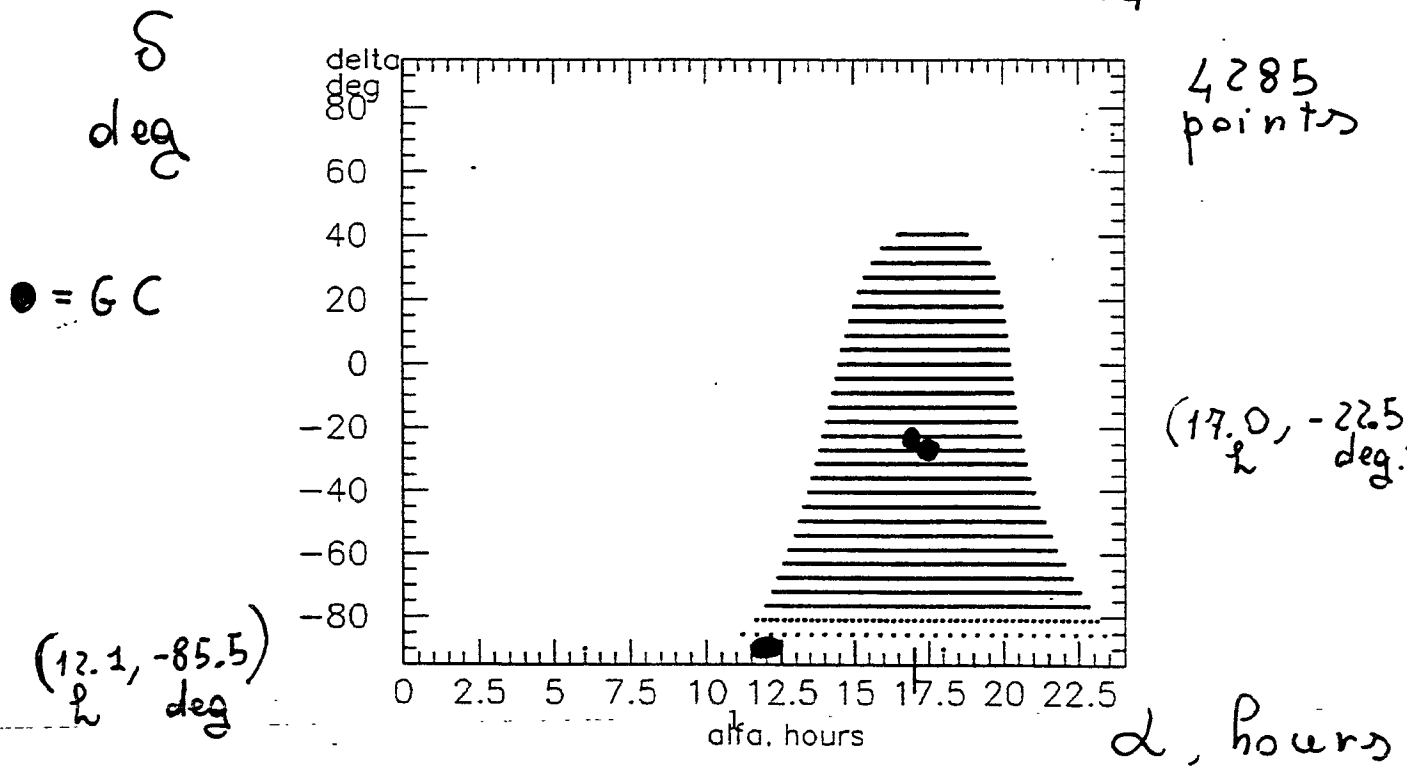

Figure 1: Sources used to map the sky, 19636 data. The best fit for frequencies is at α=17.03 hours and δ=-22.5 deg (value=0.0018). In the second figure there are shown all the points with a result better or equal to the value=0.00518, that is the value obtained for the direction of the best energy fit (4285 points).

Spectral line at 916.3 from the Explorer 1991 data base

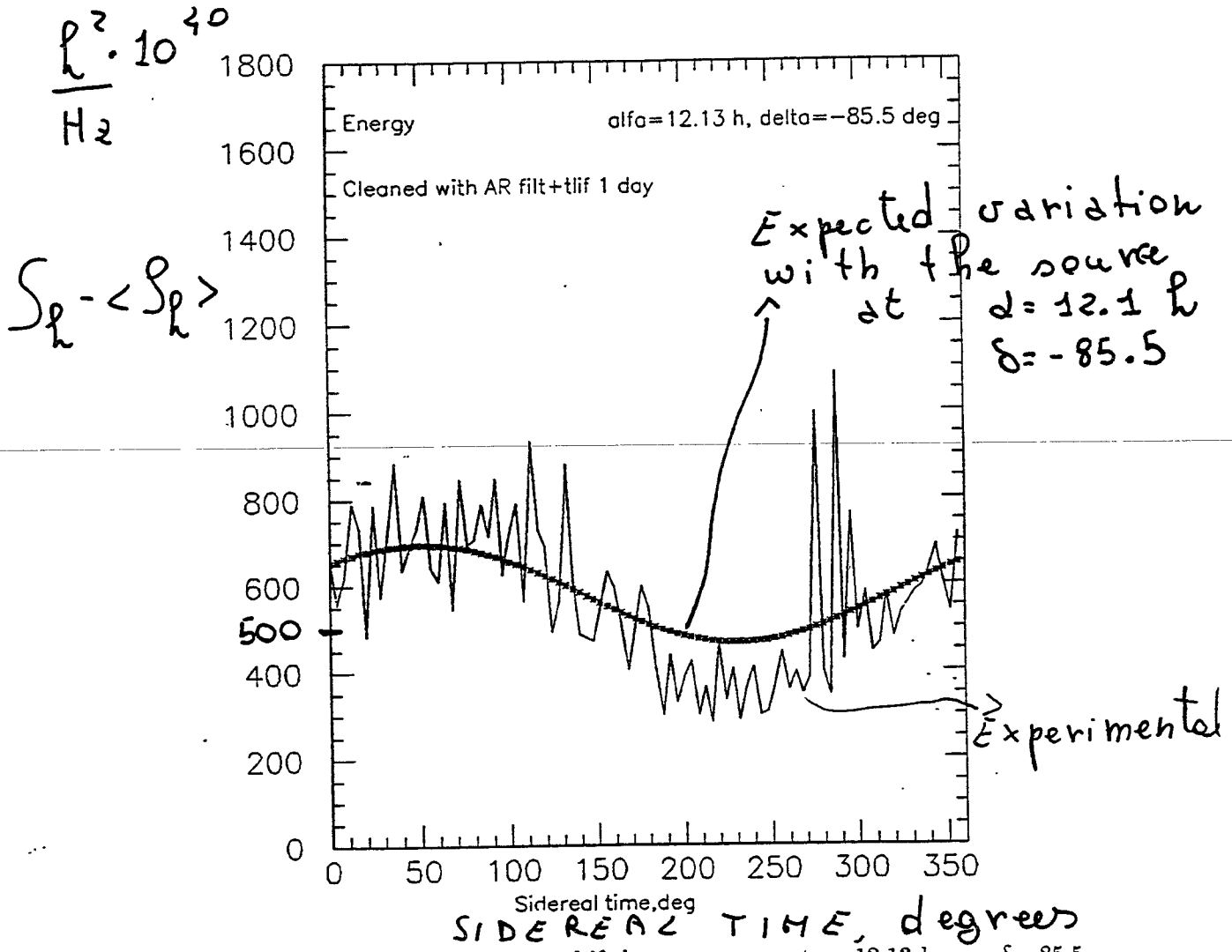

Figure 7: Experimental and expected if the source were at α=12.13 hours, δ=-85.5 degrees, that is the best fit for the energy.

8495 spectra

$$h_0 \sim \left(500 \times 10^{-40} \times 0.4 \times 10^{-3}\right)^{1/2} \sim 5 \times 10^{-21}$$

noise experim. $\sim 3 \times 10^{-22} (8495)^{-1/4} \sim 3 \times 10^{-23}$

between the resonances

$$SNR = \frac{(5 \times 10^{-21})^2}{(3 \times 10^{-23})^2} \sim 3 \cdot 10^4$$

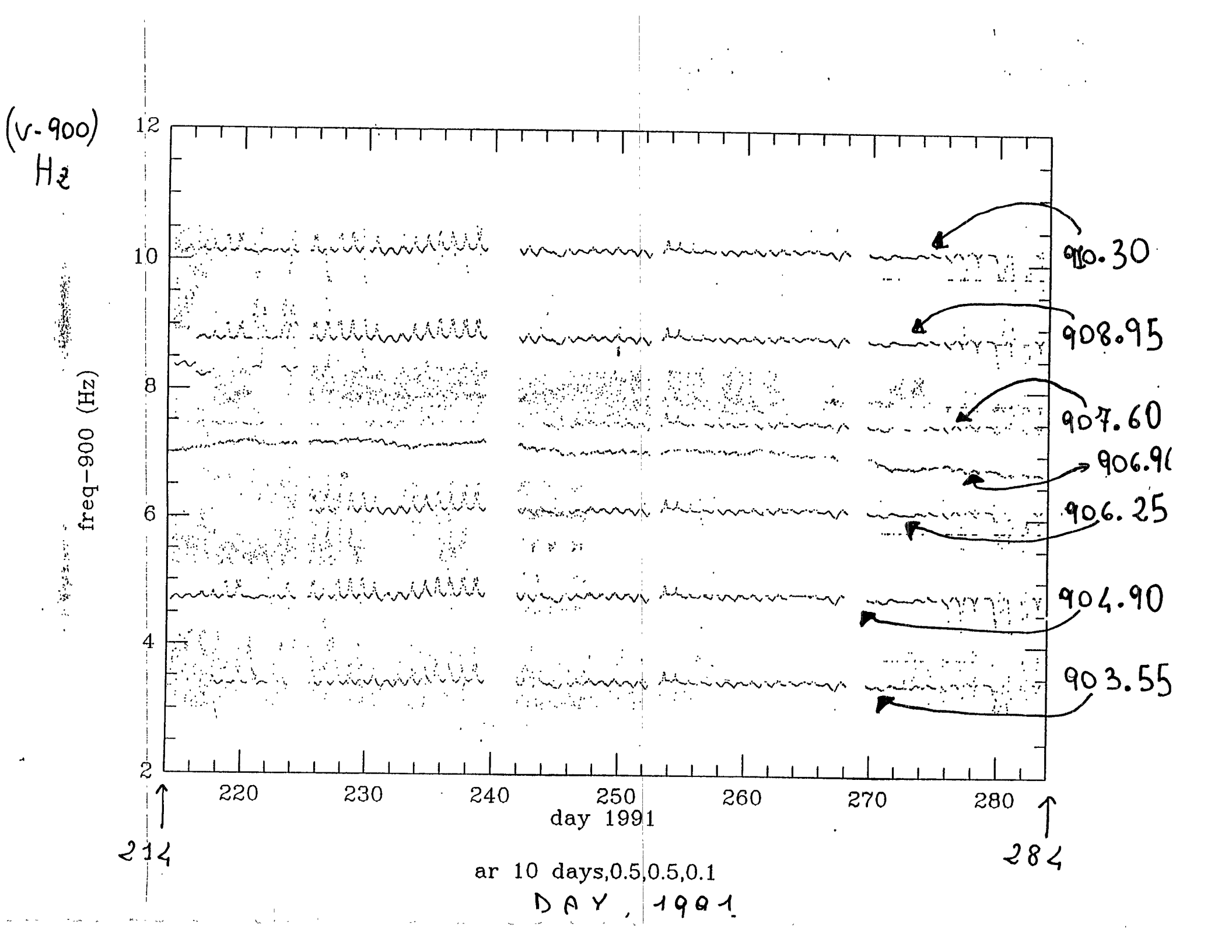
(ν-900)
Hz
freq−900 (Hz)
12
10
8
6
4
2
220
230
240
250
260
270
280
day 1991
214
284
910.30
908.95
907.60
906.91
906.25
904.90
903.55
ar 10 days,0.5,0.5,0.1
DAY, 1991

→ single, (roughly) fixed frequency

The CW Problem

for Interferometric Detectors

The CW Problem <u>is</u> a Computational Problem.

That is, looking for grav. waves from known fast pulsars (like the Crab) clearly should/will be done – but that's not a problem! However, looking for GW pulsars of unknown frequency and location <u>is</u> a well-known problem.

The "fixed frequency" source is not really at fixed frequency, since the signal is Doppler shifted by rotation of Earth & orbit round Sun, and also because pulsar will be spinning down.

So you need to search not just over frequencies f, but also over $(\theta, \phi, \dot{f}, \ddot{f}, \ldots)$, and that's a BIG computational problem.

News: Having thought about this problem some more, it looks even worse than it used to.

Point of View

Known millisecond pulsars are old, recycled pulsars with very small $\dot{P}$, and they're very stable. So recycled pulsars may not be the best candidate gravity wave sources.

The other fast pulsars are the young ones, like Crab & Vela, and they tend to have a lot of seismic activity – timing noise & glitches.

Moreover the SN rate in our galaxy is $\sim \frac{1}{40\ \text{yrs}}$ so there should ~25 NS's in our galaxy which are younger – and hopefully faster & rattier- than the Crab.

Cherchez une jeune Crab!

Some sort of hierarchical search will certainly be necessary.

E.g. consider a source which in one-year integration would have $S/N \approx 16$.

Then in a search of $\frac{365}{16} \approx 3$ weeks, $S/N \approx 4$.

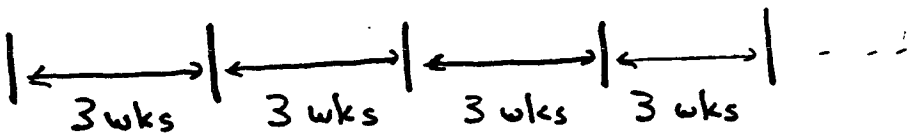

So break the year up into 3-wk segments, search thru those, and "follow up" only the "events" w/ $S/N \gtrsim 4$.

Counting up the # of required templates

$$h(t) = A \cos \Phi(t)$$

$$\Phi(t) = \Phi_0 + 2\pi\left(f_0 t + \tfrac{1}{2}\dot{f}_0 t^2 + \tfrac{1}{6}\ddot{f}_0 t^3 + \cdots\right)$$

+ Doppler corrections (θ, ϕ)

Parameters: $\underbrace{\Phi_0, f_0}_{\text{easy to search thru}}$; $\underbrace{\theta, \phi, \dot{f}_0, \ddot{f}_0, \ldots}_{\text{hard to search thru}}$

$$h(t) = \mathrm{Re}\left\{ e^{i(\Phi_0 + 2\pi f_0 t)}\, e^{iM(t)} \right\}$$

where $M(t) \equiv M(t;\ \theta, \phi, f_0, \ddot{f}_0, \ldots)$

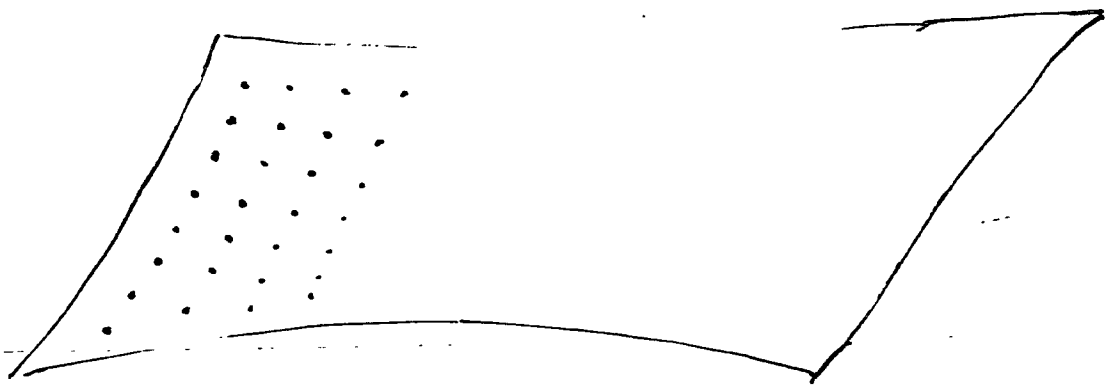

Space of $M(t, \theta, \phi, f_0, \ddot{f}_0, \ldots)$'s

Let $\mathcal{N} \equiv$ # of discrete M templates necess.

(Owen, Sathyrapakash & Dhurandhar)

$$\mathcal{N} \propto \int \sqrt{\tilde{g}}\, \underbrace{dV}_{d\theta\, d\phi\, d f_0\, d \dot{f}_0 \ldots}$$

where $\tilde{g}_{ab}$ is appropriate metric on space of $M(t)$'s.

$$\tilde{g}_{ab} = \underbrace{P_a{}^c P_b{}^d}_{\substack{\text{projects } \perp \\ \text{to space of} \\ \Phi_0, f_0}} \underbrace{g_{cd}}_{\propto \int \partial_c M(t)\, \partial_d M(t)\, dt}$$

Basically, an error in θ, ϕ, f_0, etc. can be partially compensated by an error in Φ_0, f_0, so $M(t)$ templates can be spaced a little farther apart than you might think at first.

$$\sqrt{g} \approx \text{const} \cdot \cos\theta$$

$$\Rightarrow \int \sqrt{g}\, dV \approx 2\pi \times \text{const} \times \dot{f}_{0,\max} \times \ddot{f}_{0,\max} \times \ldots$$

$\Rightarrow$ See talk by Brady & Creighton for the disappointing results

Bottom line :

Unless someone comes up w/ a fast way of doing the filtering, one will be limited – by computing power – to pulsars w/ S/N above some very high threshhold (like S/N ≈ 30 or 40) ⇒ so high that they show up w/ S/N ≈ 3 or 4 in just a few days.

Equivalently, given a source w/ S/N ≈ 10 in one year, you have to improve the detector sensitivity by a factor of 3-4 to see it.

ALL SKY SEARCH FOR CONTINUOUS WAVES

SIGNAL-NOISE INCREASE WITH TIME

- $\propto \sqrt{T}$ OBSERVATION

SIGNAL-NOISE DECREASE WITH TIME

- DOPPLER MODULATION
- AMPLITUDE MODULATION
- NEUTRON STAR / PULSAR SPIN DOWN

- PROPER MOTION
- BINARY ORBITS
- GLITCHES / TIMEING NOISE

- NON GAUSSIAN NOISE / WINDOW FUNCTION / SPECTRAL LINES

TARGET SEARCH

G.S. JONES
JONES@aei-potsdam.mpg.de
~~GREGOR~~ G.JONES@astro.cf.ac.uk

SIGNAL-NOISE

SINGLE FT $S/N \propto \frac{A_0}{6}\sqrt{T}$

MONOCHROMATIC SIGNAL
AMP = A_0
VARIANCE TIMESERIES = 6^2
OBSERVATION TIME = T

HIERARCHICAL SEARCH $\frac{S}{N} \propto \frac{A_0}{6} M^{1/4}\sqrt{T'}$

SLICE TIME = T'
SLICES AVERAGED = M

DOPPLER MODULATION

$$N_{PATCH} \propto T^4$$

STEPPING KERNEL

$$\hat{S}(\theta,\phi,f) = \int_{-\infty}^{\infty} q(\theta,\phi,f;\theta',\phi',f')\,\hat{S}(\theta',\phi',f')\,df'$$

$$q_{ER} = A \sum_{k=-\infty}^{\infty} J_k(B)\, e^{ikX}\, \frac{\mathrm{Sin}(T_{obs}\,\gamma(f-f'))}{(\gamma(f-f'))}$$

$$q_{ALL} = A_1 \sum_{K_1=-\infty}^{\infty} J_{k_1}(B_1)\, e^{iK_1X_1} \sum_{K_2=-\infty}^{\infty} J_{K_2}(B_2)\, e^{iK_2X_2} \cdots$$

$$\cdots \sum_{K_8=-\infty}^{\infty} J_{K_8}(B_8)\, e^{iK_8X_8}$$

$$\times \frac{\mathrm{Sin}(T_{obs}\,\gamma(K_1,K_2,\ldots,K_8)(f-f'))}{\gamma(K_1,K_2,\ldots K_8)(f-f')}$$

- PATCH SIZE >> ANGULAR RESOLUTION (IF ACCEPT A DROP IN S/N)
- HIERARCHICAL → T IS SMALLER ∴ NO. PATCHES SMALLER.

BINARY ORBITS

- NEXT TO IMPOSSIBLE FOR UNKOWN, BEFORE HAND, SOURCES
- TARGETED

PROPER MOTION

- SMALL POPULATION OF FAST MOVING PULSARS
- ONLY PROBLEM $T \gtrsim$ MONTHS

GLITCHES etc

- CANNOT CORRECT FOR.

DETECTOR RESPONSE

- WILL CAUSE PROBLEMS FOR STATISTICAL ANALYSIS
  - PREVIOUS ANALYSIS
    1989 100Hr GLASGOW
    1996 1.5Hr GLASGOW

DATA COMPRESSION

- SMALLER FREQUENCY RANGE IS DESIRED ABOUT $\frac{1}{10}$

- HETERODYNE / FILTER / RESAMPLE
- 'FOURIER DOMAIN SAMPLING'

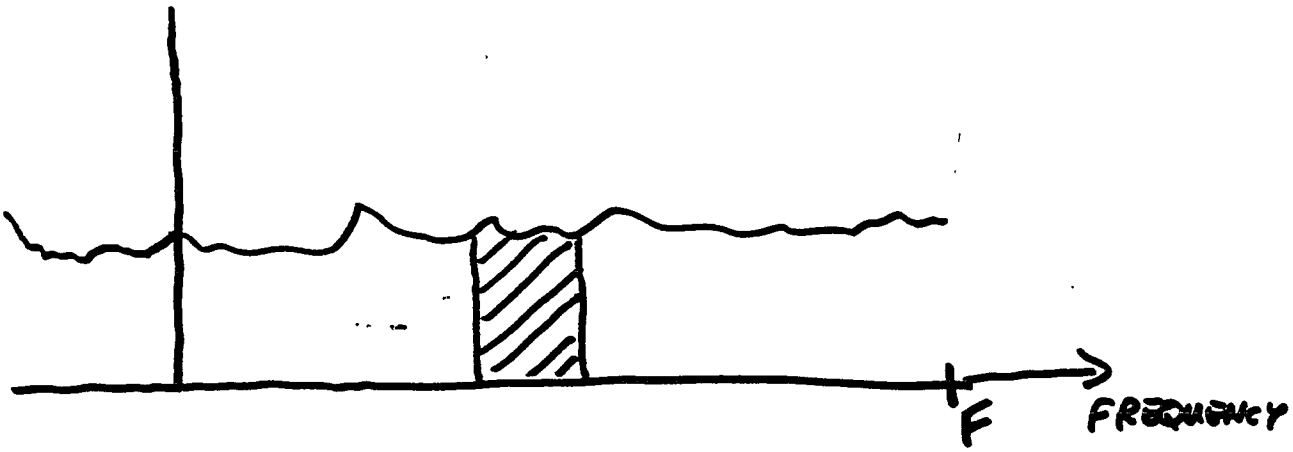

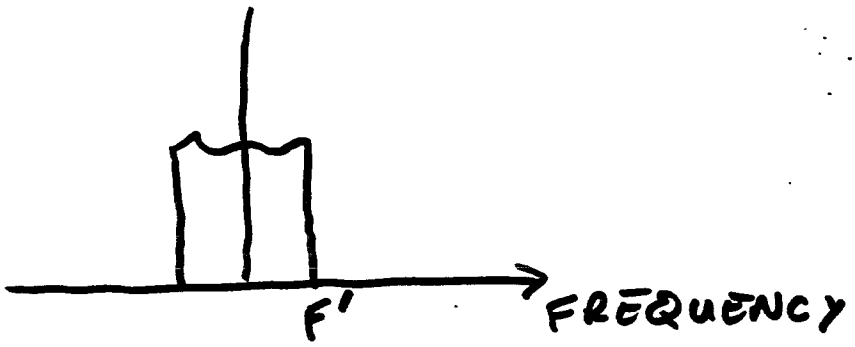

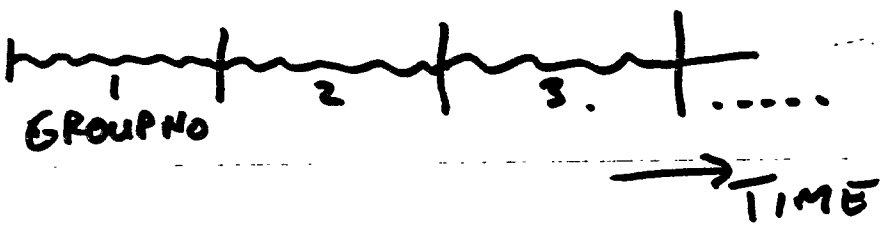

OPEN QUESTIONS AND CONCLUSIONS

- SHOULD ACCEPT CAN'T DO ALL SKY SEARCH.
- DECIDE WHAT OVERALL REGIONS TO SEARCH OVER
- LIMIT FREQUENCY RANGE?
- IN COMBINATION WITH TARGET SEARCHES.

B. Mours
L.A.P.P. ANNECY
GW Data Analysis Workshop
December 6-8, 1996

CW searches in VIRGO

- *The Simulation*
- *Single direction search*
- *All sky search*

Simulation

The Key Tool for Data Analysis

Algorithm results are easy to predict when:
- simple algorithm
- stationnary noise

This is not our case!

We need a detailled Simulation program to exercice, qualify and measure the performances of sofisticate algorithms

The VIRGO Tool: SIESTA

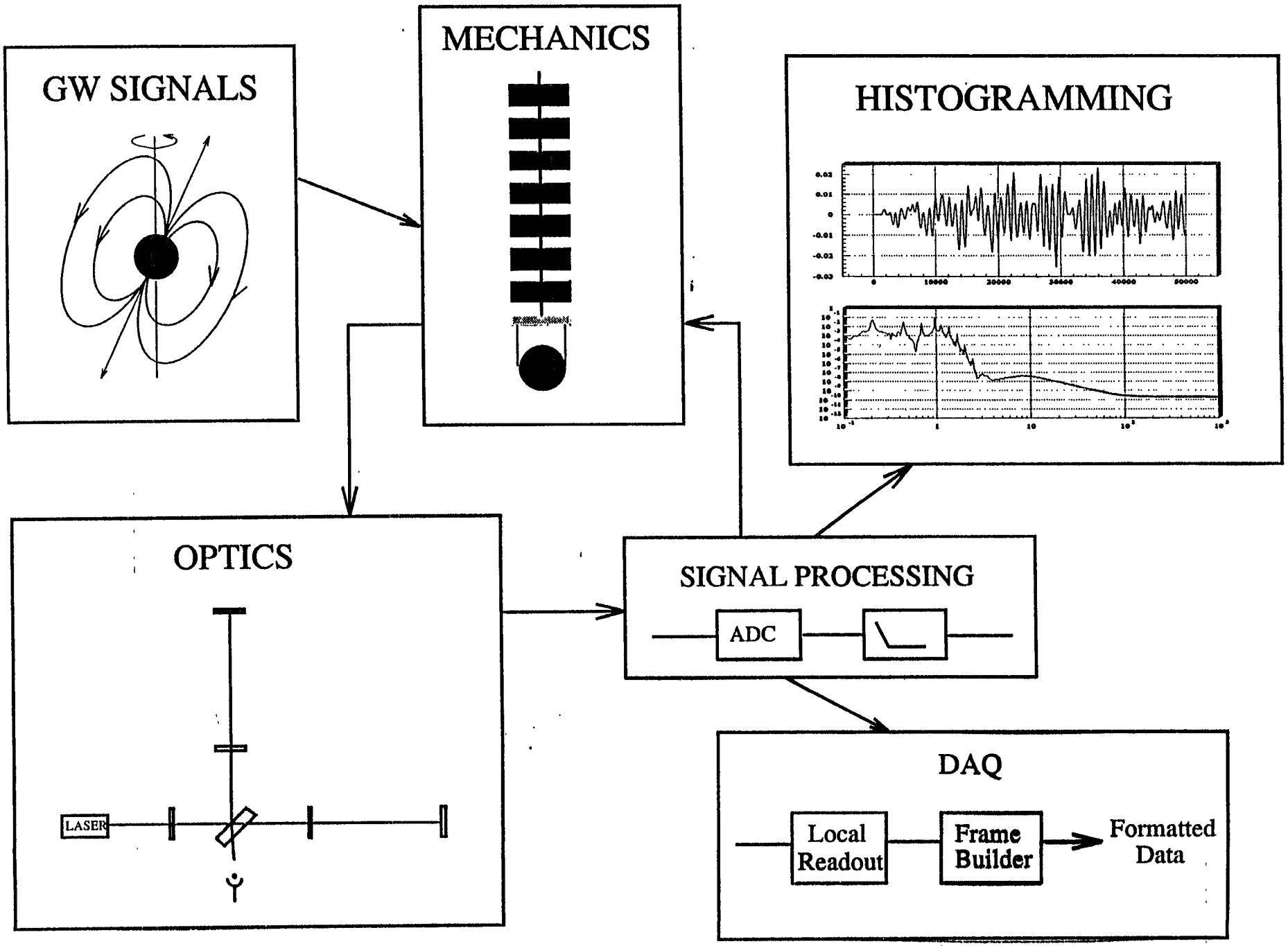
GW SIGNALS
MECHANICS
HISTOGRAMMING
OPTICS
LASER
SIGNAL PROCESSING
ADC
DAQ
Local Readout
Frame Builder
Formatted Data

Simulation of Suspended Mirrors

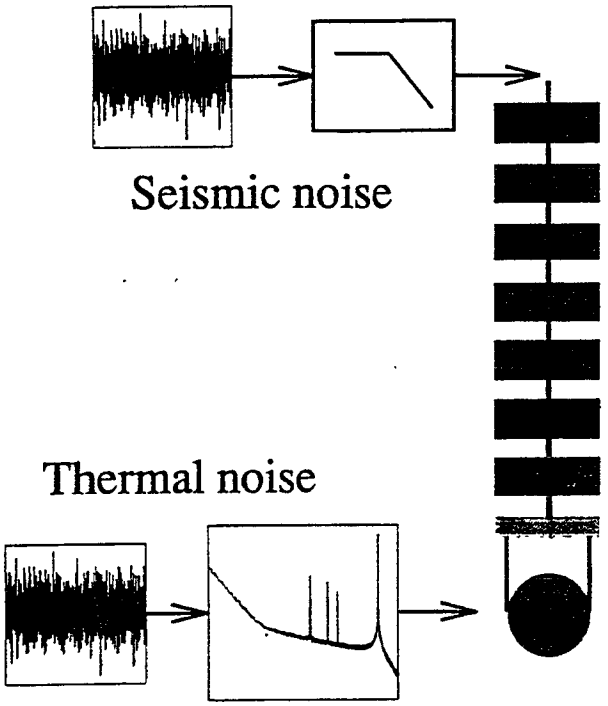

Seismic noise

Thermal noise

Numerical resolution of 1D motion equation of chain of pendula

Feedback forces

on marionette

from reference mass

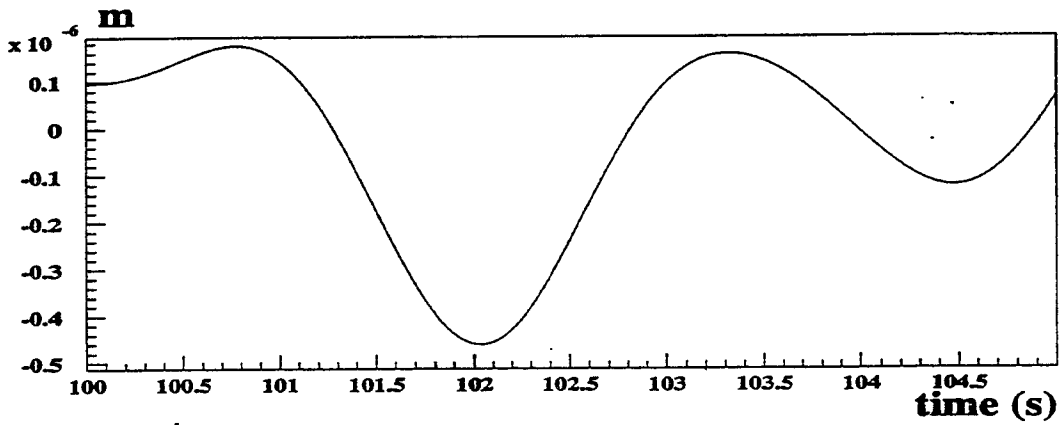

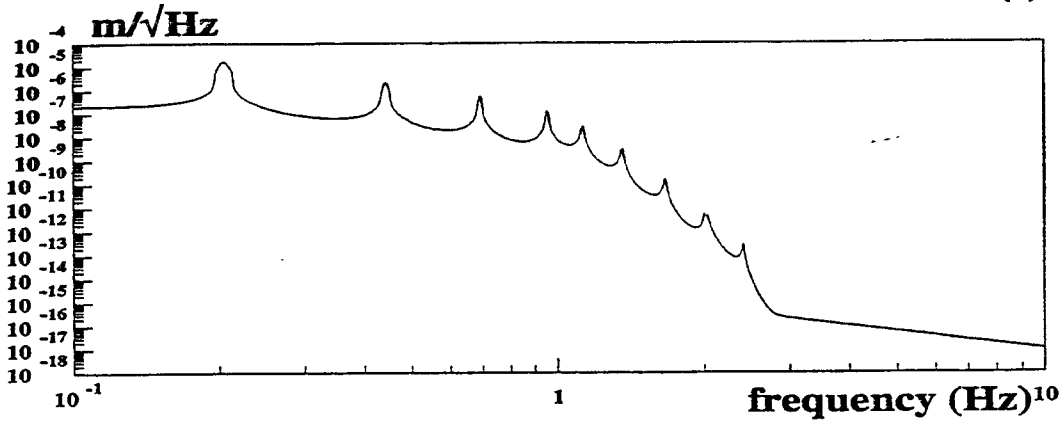

Optics Simulation Toolkit

* fast quasistatic simulations
* dynamic simulations in the linear domain

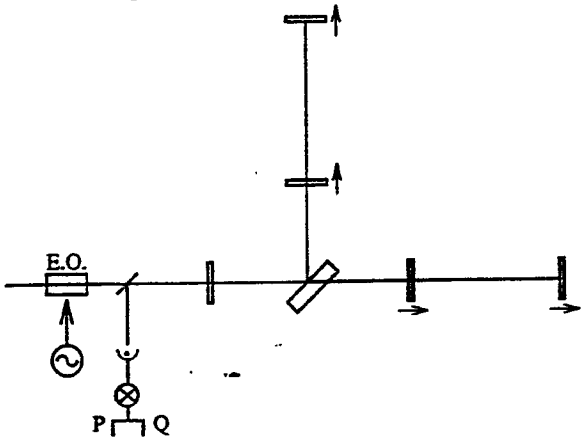

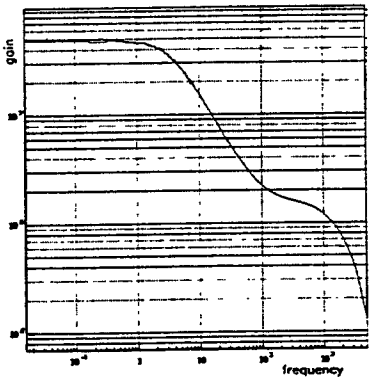

* dynamic simulations in the non-linear domain

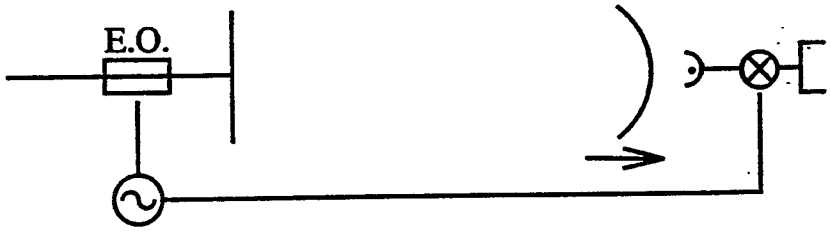

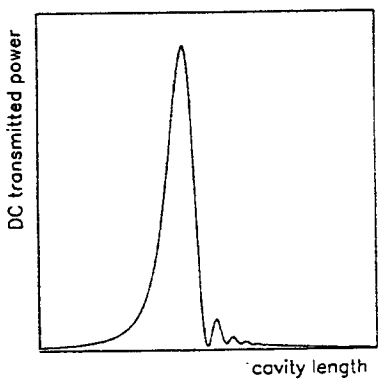

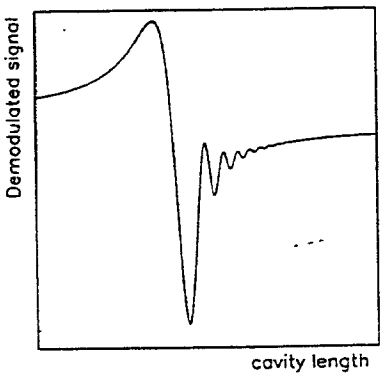

VICERE & II à Pise.

Full interferometer simulation

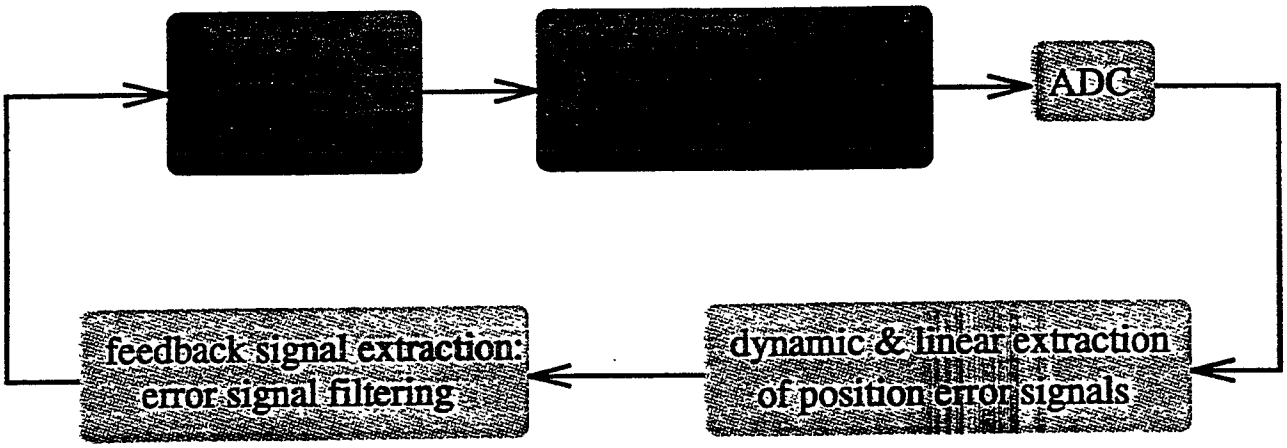

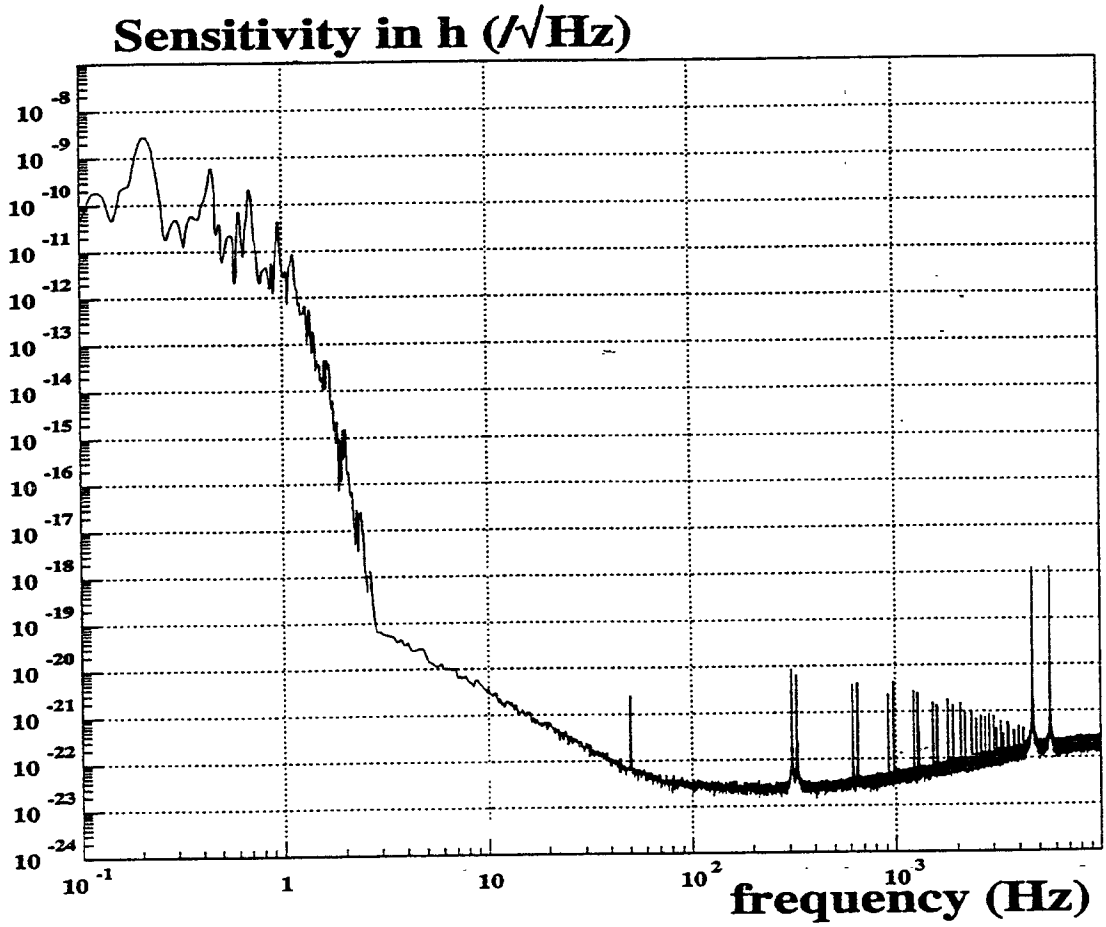

FFT of data in the time domain

Gravitational Wave event generator

- binary coalescences: up to first post-Newtonian term

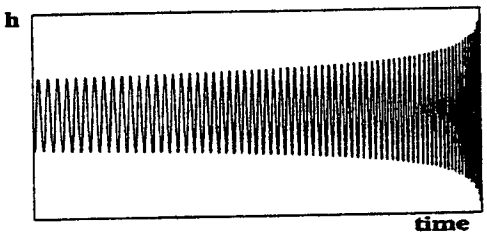

- pulsars: doppler effect simulation
  use routine from Paris "Bureau des Longitudes" to know Earth position within $\pm$ 2 km

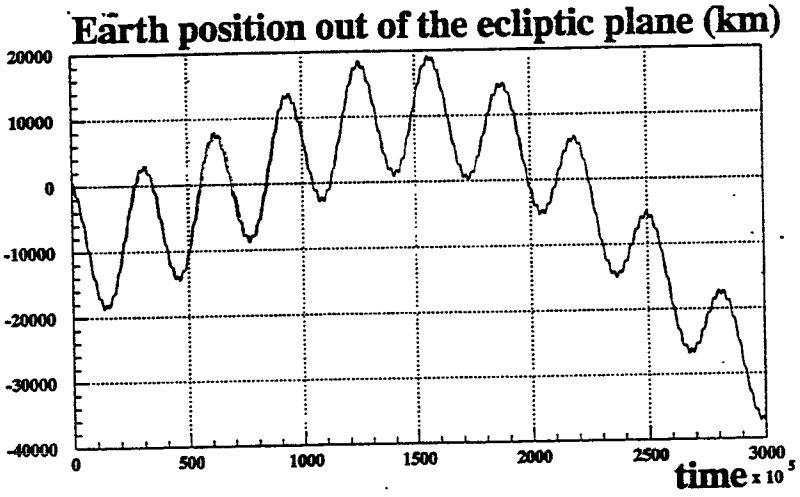

- include amplitude and phase modulation due to Earth rotation

- typical application: produce long duration formatted data with pulsar signal and typical VIRGO noise to develop blind pulsar search algorithms

Amplitude modulation

Due to the earth rotation $h(t)$ can be written as :

$$h(t) = A_1(t)\cos(\Omega t - \phi_1(t)) + A_2(t)\cos(2\Omega t - \phi_2(t))$$

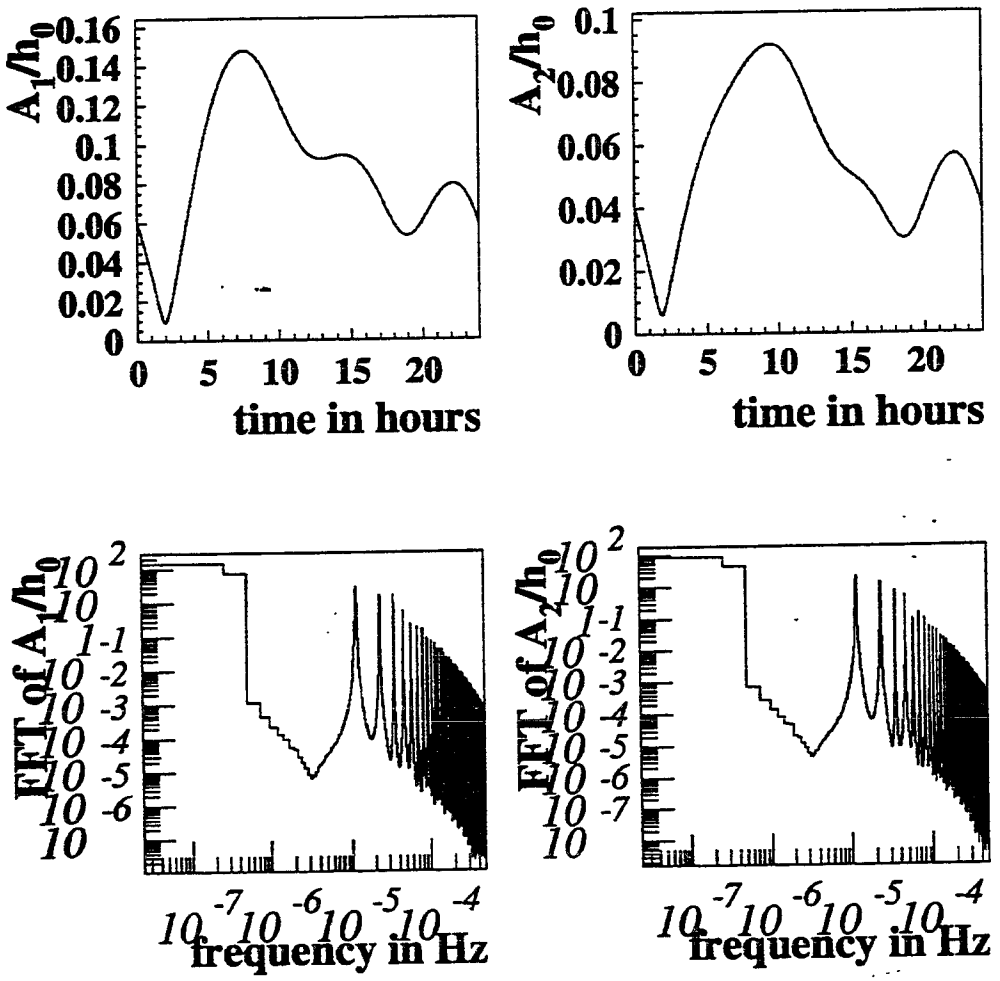

Coefficients of the amplitude modulation and their FFT for the Crab pulsar (c. f. Eric Gourgoulhon [astro-ph/9602107])

Phase modulation

Due to the earth rotation $h(t)$ can be written as :

$$h(t) = A_1(t)\cos(\Omega t - \phi_1(t)) + A_2(t)\cos(2\Omega t - \phi_2(t))$$

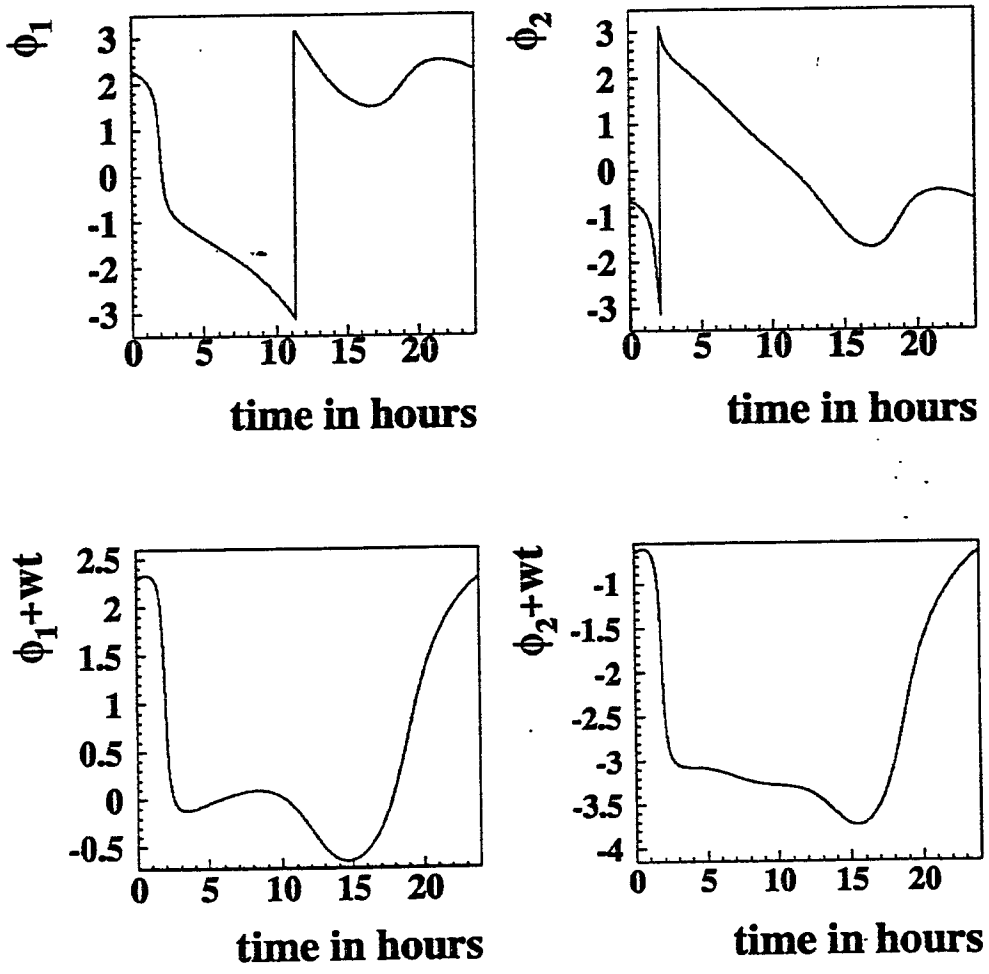

Phase coefficients for the Crab pulsar

Single search algorithm

Procedure :

- Read data @ 20kHz
- Frequency shift and mean Doppler correction
- low pass filter
- Sample data at low frequency ($\sim 1Hz$)

Advantages :

- Can perform long FFT (few months to one year) since small frequency band

Numerical check

Data Simulation with SIESTA

- Pulsar's frequency : 30.01 Hz
- Initial sampling rate : 64 Hz
- Integration time : 12 days
- $h_0 = 0.25$
- Doppler effect
- No amplitude modulation

Search at various locations (bad direction => frequency shift)

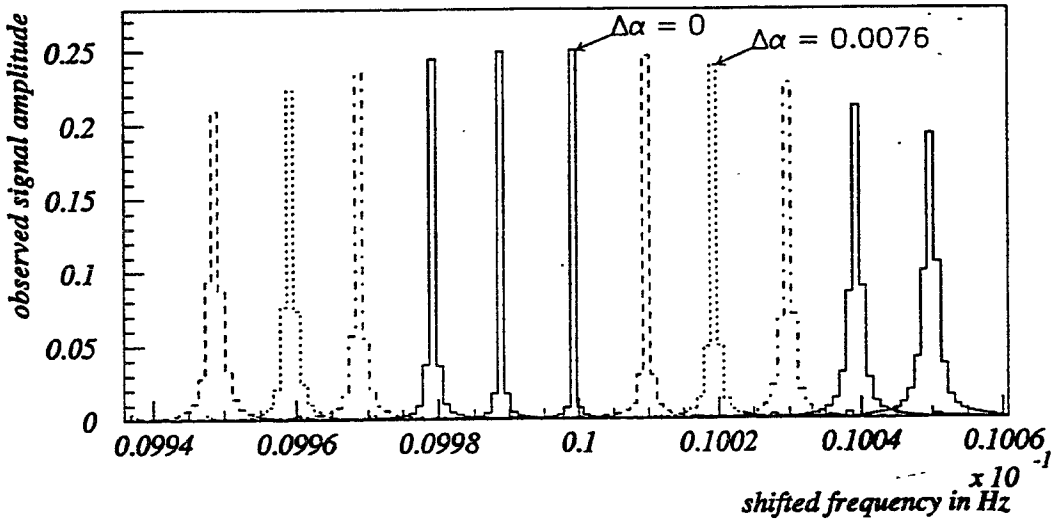

Check of losses level

Analytic curve ⇓ (NTS 95-40) ⇓ SIESTA Simulation

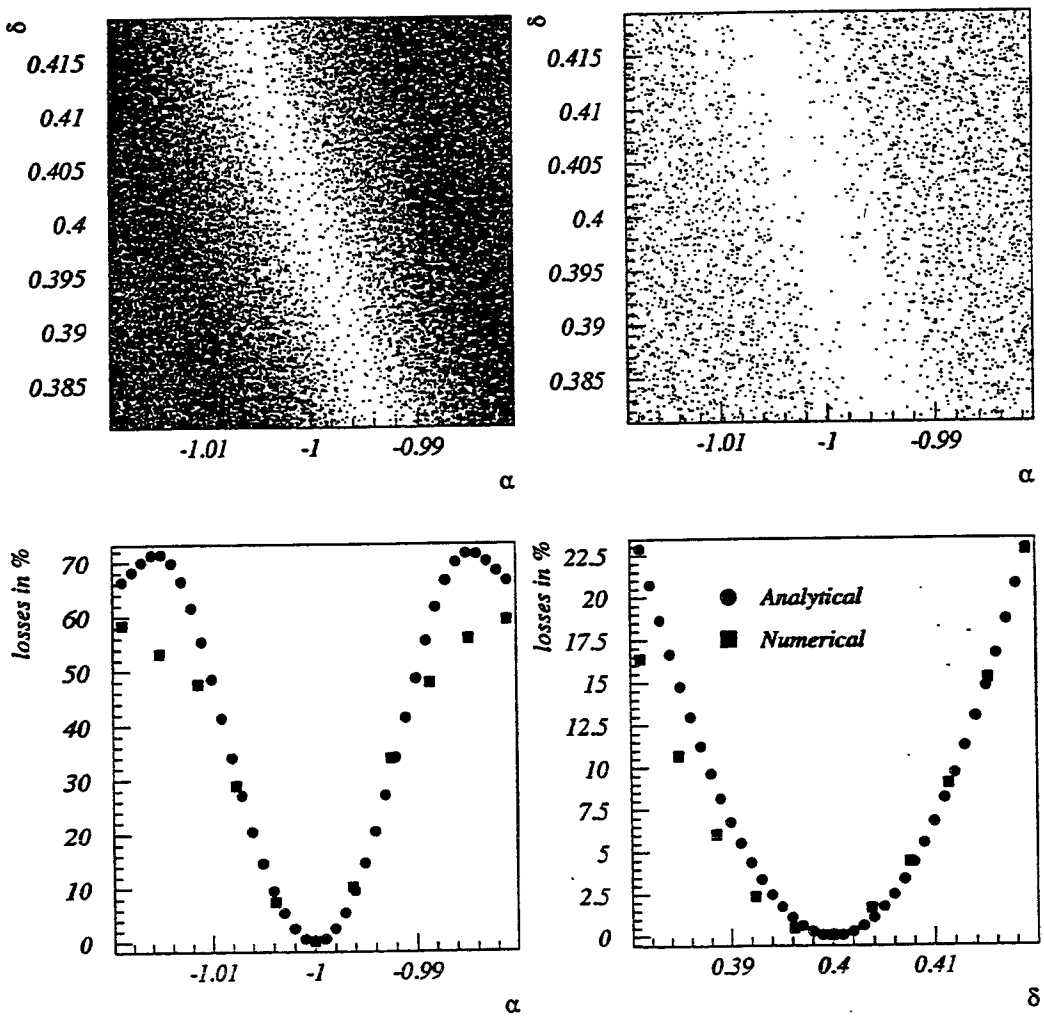

Figure 0.1: Analytical computation : NTS 95-40

Good agreement between analytical and numerical results

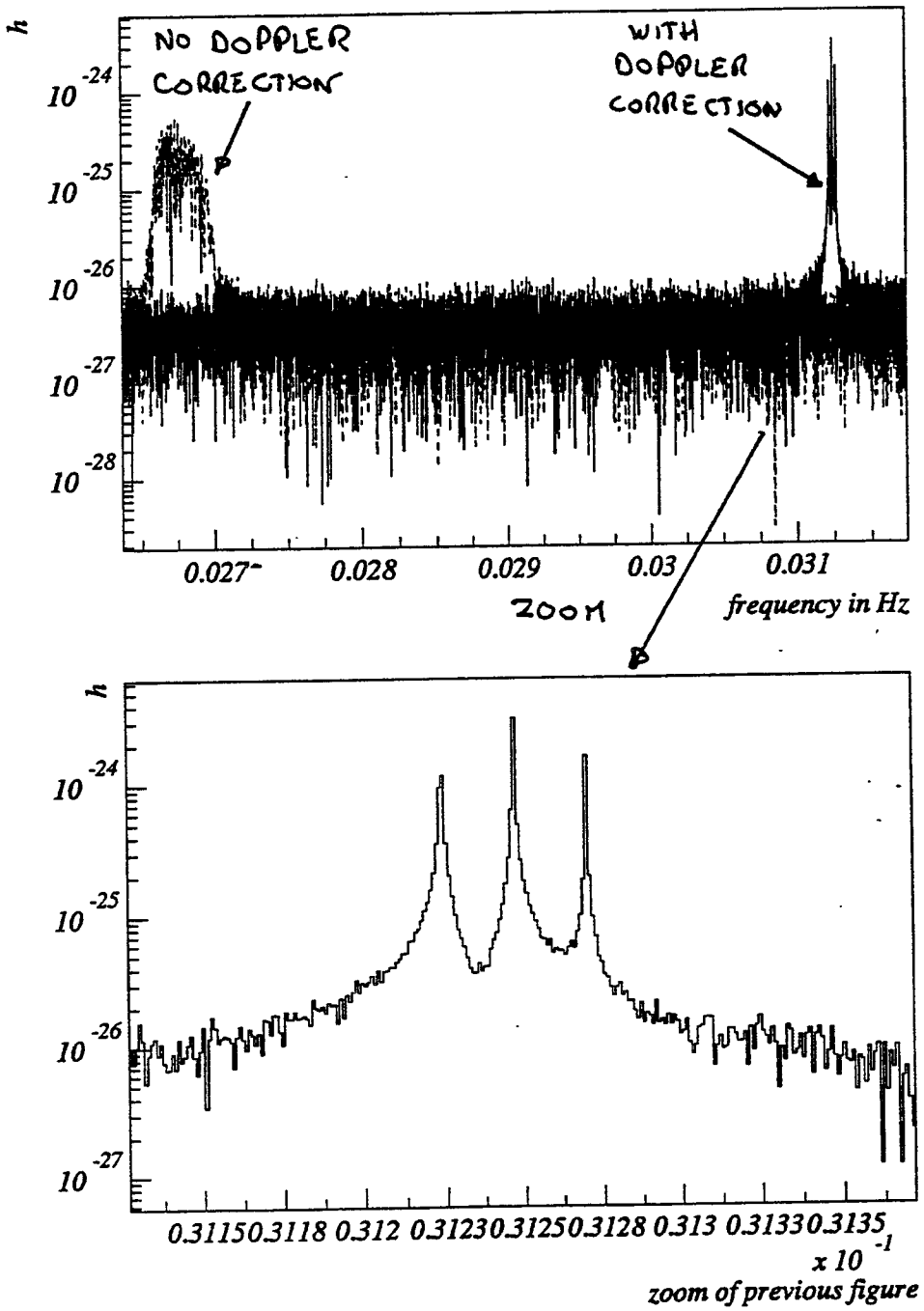

zoom of previous figure

All Sky Search

Investigations:

- Search density
- Number of search directions Vs time
- Hierarchical searches

Future:

$\Rightarrow$ Quantitative study with Monte Carlo Data

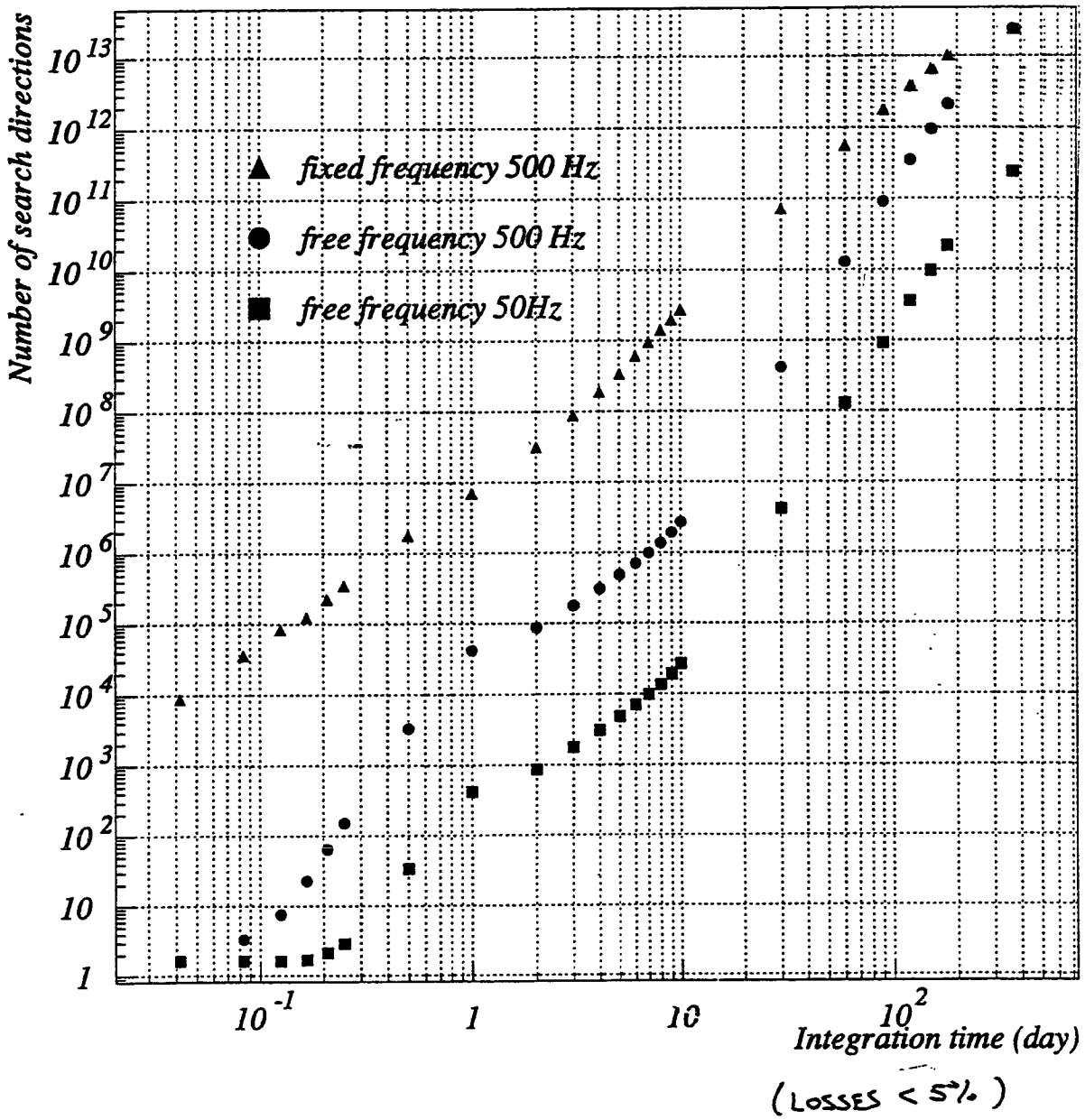
Number of search directions
10^{13}
10^{12}
10^{11}
10^{10}
10^{9}
10^{8}
10^{7}
10^{6}
10^{5}
10^{4}
10^{3}
10^{2}
10
1
fixed frequency 500 Hz
free frequency 500 Hz
free frequency 50Hz
10^{-1}
1
10
10^{2}
Integration time (day)

(LOSSES < 5%)

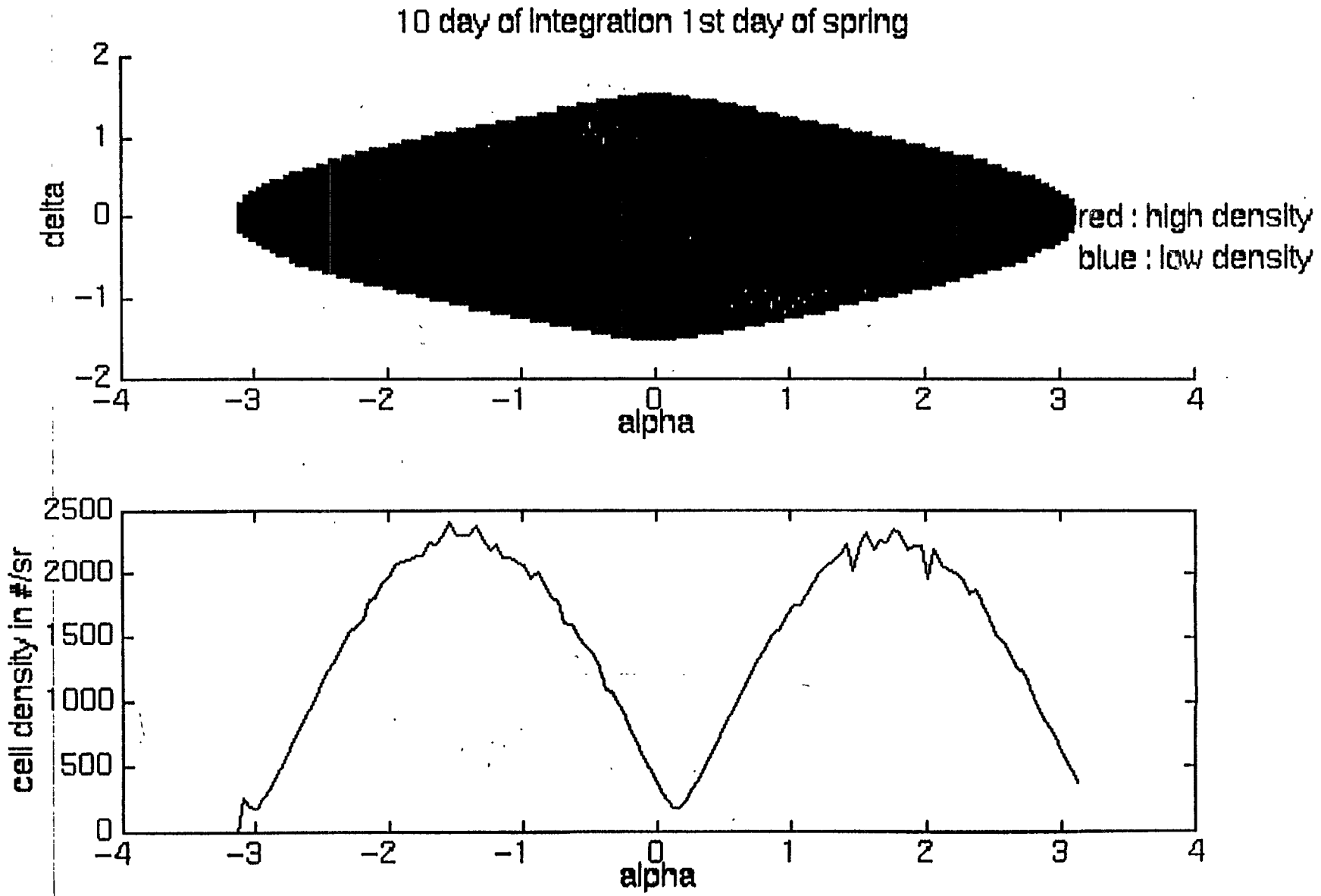
10 day of integration 1st day of spring
delta
alpha
red : high density
blue : low density
cell density in #/sr
alpha

Stochastic Background Searches: computational cost

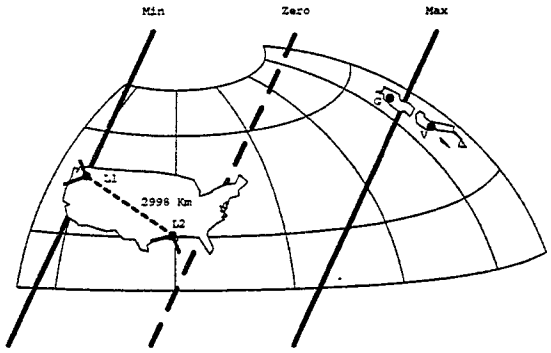

$$S = \int\int dt dt' \; h_1(t) h_2(t') Q(t-t') = 2 \int_0^\infty df \; \tilde{h}_1(f) \tilde{h}_2^*(f) \tilde{Q}(f)$$

Optimal filter: $\tilde{Q}(f) = \dfrac{\gamma(f)\Omega_{\rm gw}(f)}{f^3 P_1(f) P_2(f)}$:

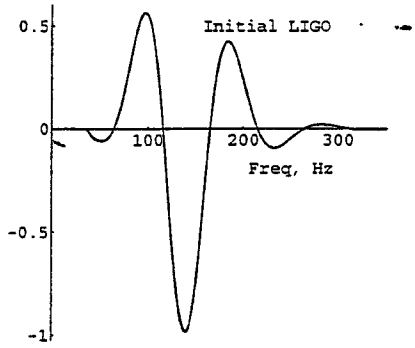

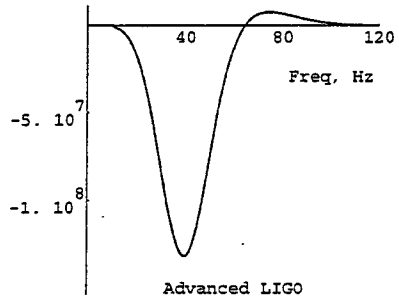

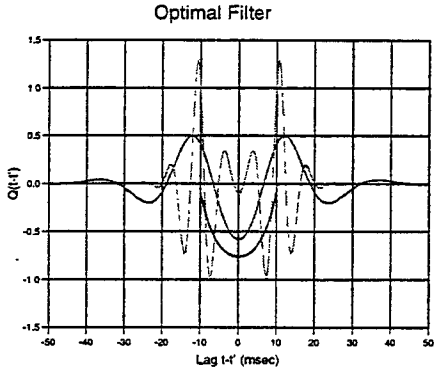

The effective bandwidth is < 300 Hz.

Strategy 1: Sample data at 16,384 samples/sec $\times$ 8 sec = 131,072 points. FFT & correlate ($\times 2$ windowing $\times 2$ detectors): one workstation, easily, in real time.

Strategy 2: Decimate data to 1024 samples/sec $\times$ 8 sec = 8192 points. FFT & correlate ($\times 2$ windowing $\times 2$ detectors): one PC, easily, in real time.

Elimination of Correlated Noise

$$\langle \tilde{n}_i^*(f)\tilde{n}_j(f')\rangle = \frac{1}{2}\Big[\delta_{ij}P_i(|f|) + \Delta_{ij}C_i(|f|)\Big]\delta(f-f')$$

$$\text{with } \delta_{ij} = \begin{pmatrix} 1 & 0 \\ 0 & 1 \end{pmatrix} \text{ and } \Delta_{ij} = \begin{pmatrix} 0 & 1 \\ 1 & 0 \end{pmatrix}.$$

If $C(f) = 0$ (no correlated noise) then for initial LIGO:

$$\Omega_{\rm gw}^{90\%} = 1.65\left[\frac{9H_0^4}{50\pi^4}T\int_0^\infty df\ \frac{\gamma^2(f)}{f^6P_1(f)P_2(f)}\right]^{-\frac{1}{2}} = 2.8\times 10^{-6}\ h_{100}^{-2}$$

This applies for $C(f) \neq 0$ iff

$$\int_0^\infty df\ C(f)\tilde{Q}(f) \ll \frac{3H_0^2}{10\pi^2}\int_0^\infty df\ \gamma(f)f^{-3}\Omega_{\rm gw}(f)\tilde{Q}(f).$$

In bandpass determined by $\tilde{Q}$ this means that

$$C(f) << \frac{3H_0^2}{10\pi^2}f^{-3}\Omega_{\rm gw} = 3\times 10^{-37}h_{100}^2\Omega_{\rm gw}f^{-3}{\rm Hz}^2$$

Initial LIGO $\Rightarrow \sqrt{C(f)} < 3\times 10^{-25}$ strain/$\sqrt{\rm Hz}$ at $f = 150$ Hz, or about 1% of total motion. Christensen has estimated the contributions of different effects:

1. Seismic noise: small at these frequencies, with planned isolation.
2. Gas bursts: also small.
3. Magnetic field fluctuations: could be dominant correlated noise source $\Rightarrow$ need to correlate magnetometers with output of detectors & veto or subtract.

Detection of Anisotropies in the Gravitational-Wave Stochastic Background

Bruce Allen
Department of Physics
University of Wisconsin - Milwaukee
PO Box 413
Milwaukee, WI 53211, USA
email: ballen@dirac.phys.uwm.edu

Adrian C. Ottewill
Department of Mathematical Physics, University College Dublin,
Belfield, Dublin 4, Ireland
email: ottewill@relativity.ucd.ie
(December 6, 1996)

By correlating the signals from a pair of gravitational-wave detectors, one can undertake sensitive searches for a stochastic background of gravitational radiation. If the stochastic background is anisotropic, then this correlated signal varies harmonically with the earth's rotation. We calculate how the harmonics of this varying signal are related to the multipole moments which characterize the anisotropy, and give a formula for the signal-to-noise ratio of a given harmonic. The specific case of the two LIGO (Laser Interferometric Gravitational Observatory) detectors, which will begin operation around the year 2000, is analyzed in detail. We consider two possible examples of anisotropy. If the gravitational-wave stochastic background contains a dipole intensity anisotropy whose origin (like that of the Cosmic Background Radiation) is motion of our local system, then that anisotropy will be observable by the advanced LIGO detector (with 90% confidence in one year of observation) if $\Omega_{\rm gw} > 5.3 \times 10^{-8} h_{100}^{-2}$. We also study the signal produced by stochastic sources distributed in the same way as the luminous matter in the galactic disk, and in the same way as the galactic halo.

I. INTRODUCTION

The design and construction of a number of new and more sensitive detectors of gravitational radiation is currently underway. These include the LIGO detector being built in the United States by a joint Caltech/MIT collaboration [1], the VIRGO detector being built near Pisa by an Italian/French collaboration [2], the GEO-600 detector being built in Hannover by an Anglo/German collaboration [3], and the TAMA-300 detector being built near Tokyo [4]. There are also several resonant bar detectors currently in operation, and several more refined bar and interferometric detectors presently in the planning and proposal stages.

When two or more of these detectors are operating, it will become possible to correlate their signals, and in this way, to search for a stochastic background of gravitational radiation. The technique for such a search was originally described in work by Michelson [5], Cristensen [6] and Flanagan [7]. A review of these techniques may be found in [8]. Such radiation might be the result of processes that took place during the very early universe. It might also result from the incoherent superposition of many faint unresolvable present-day sources such as coalescing binary systems.

The stochastic gravitational-wave background might be isotropic on the sky, or it might be anisotropic. For example, if the background results from early-universe processes, then it might be isotropic to about the same degree as the 2.7° K electromagnetic background radiation. On the other hand, if the background is due to white-dwarf binaries in our own galaxy, then they might be distributed in a pancake or bar which mimics the shape of the observed luminous matter in our galaxy. In this paper, we show how the correlated signal from a pair of gravitational wave detectors is related to multipole moments which characterize the anisotropy. This should permit a signal to be analyzed to search for (or place upper limits on) the multipole moments which characterize the anisotropy. In this paper, we will assume that the reader is already familiar with the work previously cited (references [5–8]) on stochastic background detection.

These paper is organized as follows. In Section II we show how a background of stochastic gravitational radiation may be decomposed in a plane-wave expansion, with the coefficients of the expansion treated as stochastic random variables. In Section III the properties of these random variables are related to the (frequency) spectrum and spatial distribution of the radiation, and a set of multipole moments are introduced which characterize the anisotropies of

the stochastic background. These anisotropies may be searched for by studying the variations of the detector outputs as the earth rotates relative to the fixed cosmic frame. In Section IV we show how the correlation between a pair of detectors fixed on the earth varies with time as the earth rotates, and detail how that correlation is related to the anisotropies of the stochastic gravitational background. The variation of the correlation with the earth's rotation may be decomposed into harmonics of the earth's period. In section Section V we introduce a set of functions $\gamma_{\ell m}(f)$ which are generalizations of the well-known overlap reduction function $\gamma(f)$ of references [5–8]. These functions characterize the effect of the ℓ, m anisotropy multipole on the m'th harmonic of the detector correlation. The principal result of this paper is to compute these functions for the LIGO pair of detectors. This is done by introducing two special frames of reference, fixed with respect to the earth, in Section VI, and then performing a set of integrations in Section VII. The final integrations are performed and explicit formula for the $\gamma_{\ell m}(f)$ are obtained in Section VIII. In Section IX we analyze the signal-to-noise ratios associated with the m'th harmonic, and give a formula which may be used to determine if a given anisotropy is detectable or not. Following this, we consider two specific examples of anisotropy. In Section X we consider a dipole anisotropy in the stochastic background resulting from our local proper motion. In order to predict the harmonics which result, it is necessary to adopt conventions for the normalization of the optimal filters; these choices are detailed in Section XI. In Section XII we then consider the anisotropies in the stochastic gravitational wave background that would arise from sources distributed in the same way as our galaxy, and it's halo. This is followed by a short conclusion.

Throughout this paper, c denotes the speed of light and G denotes Newton's gravitational constant.

II. THE STOCHASTIC BACKGROUND

The gravitational wave background may be described in terms of a perturbation to the Minkowski metric of space-time:

$$ds^2 = -c^2 dt^2 + d\vec{x}^2 + h_{ab}(t,\vec{x}) dx^a dx^b. \tag{2.1}$$

In transverse traceless gauge, this can be written in the form of a plane wave expansion as

$$h_{ab}(t,\vec{x}) = \sum_A \int_{-\infty}^{\infty} df \int_{S^2} d\hat{\Omega}\, h_A(f,\hat{\Omega}) e^{2\pi i f(t-\hat{\Omega}\cdot\vec{x}/c)} e^A_{ab}(\hat{\Omega}). \tag{2.2}$$

Here $h_A(f,\hat{\Omega})$ is an arbitrary complex function satisfying the relation $h_A(-f,\hat{\Omega}) = h^*_A(f,\hat{\Omega})$. The polarization states are labeled by $A = +, \times$ and $\hat{\Omega}$ is a unit vector on the two-sphere. The wave-vector of the corresponding component of the perturbation is $\vec{k} = 2\pi f\hat{\Omega}/c$. The polarization tensors e^A_{ab} appearing in these relations may be given explicitly. In standard angular coordinates (θ,ϕ) on the two-sphere one may write

$$\hat{\Omega} = \cos\phi\sin\theta\hat{x} + \sin\phi\sin\theta\hat{y} + \cos\theta\hat{z} \tag{2.3}$$
$$\hat{m} = \sin\phi\hat{x} - \cos\phi\hat{y} \tag{2.4}$$
$$\hat{n} = \cos\phi\cos\theta\hat{x} + \sin\phi\cos\theta\hat{y} - \sin\theta\hat{z} \tag{2.5}$$

and then choose

$$e^+_{ab}(\hat{\Omega}) = m_a m_b - n_a n_b \tag{2.6}$$
$$e^\times_{ab}(\hat{\Omega}) = m_a n_b + n_a m_b \tag{2.7}$$

To simplify matters later (but without any loss of generality) we assume that the $\hat{z}$ vector points along the direction of the earth's rotation axis. One can verify by inspection that $\hat{m}$ and $\hat{n}$ are a pair of orthogonal unit-length vectors in the plane perpendicular to $\hat{\Omega}$. It is simple to show that any rotation of the vectors $\hat{m}$ and $\hat{n}$ within the plane that they define simply corresponds to a trivial re-definition of the complex wave amplitudes h_+ and $h_\times$.

To describe a stochastic source, we treat the complex amplitude $h_A(f,\hat{\Omega})$ as a random variable with zero mean value. In this paper, we consider stochastic sources which are *not isotropic*. In principle, such a source has spectral properties which depends upon amplitude and frequency in an arbitrary way. For simplicity, in this paper *we consider only stochastic sources whose directional dependence is frequency-independent.* The dependence of the stochastic background on frequency and direction may be stated in terms of the expectation value of the product of two random variables $h_A(f,\hat{\Omega})$:

$$\langle h^*_A(f,\hat{\Omega}) h_{A'}(f',\hat{\Omega}')\rangle = \delta_{AA'}\delta(f-f')\delta^2(\hat{\Omega},\hat{\Omega}')H(f)P(\hat{\Omega}). \tag{2.8}$$

Here $\delta^2(\hat{\Omega},\hat{\Omega}')$ is a covariant two-dimensional delta-function on the unit two-sphere. For a general stochastic source, the quantity $H(f)P(\hat{\Omega})$ which appears on the right hand side would be an arbitrary function of frequency and direction. However our assumption that the directional dependence is frequency-independent implies that the r.h.s. factors as shown. (Note that the expressions which we later derive for Signal-to-Noise ratios and expected signal strengths may be trivially extended to include the most general case.)

III. SPECTRUM OF THE STOCHASTIC BACKGROUND

The function $H(f)$ determines the spectrum of the gravitational radiation. The energy density in gravitational waves is given by

$$\rho_{\rm gw} = \frac{c^2}{32\pi G}\langle \dot{h}_{ab}\dot{h}^{ab}\rangle, \tag{3.1}$$

where the overdot denotes a time derivative, and both tensors are evaluated at the same space-time point $(t,\vec{x})$. Substituting the plane wave expansion (2.2) into this formula and using (2.8) yields

$$\langle \dot{h}_{ab}(t,\vec{x})\dot{h}^{ab}(t,\vec{x})\rangle = \sum_A \int_{-\infty}^{\infty} df \int_{S^2} d\hat{\Omega}\, 4\pi^2 f^2 H(f) P(\hat{\Omega}) e^A_{ab}(\hat{\Omega}) e^{ab}_A(\hat{\Omega}). \tag{3.2}$$

Since $\sum_A e^A_{ab}e^{ab}_A = 4$ one has

$$\langle \dot{h}_{ab}\dot{h}^{ab}\rangle = 16\pi^2 \int d\hat{\Omega} P(\hat{\Omega}) \int_{-\infty}^{\infty} df\, f^2 H(f) = 32\pi^2 \int d\hat{\Omega} P(\hat{\Omega}) \int_0^{\infty} df\, f^2 H(f). \tag{3.3}$$

In describing gravitational wave stochastic backgrounds, it is conventional to compare the energy density to the critical energy density $\rho_{\rm critical}$ required (today) to close the universe. This critical energy density is determined by the rate at which the universe is expanding today. Let us denote the Hubble expansion rate today by

$$H_0 = 100\, h_{100}\, \frac{\rm km\,sec^{-1}}{\rm Mpc} = 3.2\times 10^{-18} h_{100}\,{\rm sec}^{-1} = 1.1\times 10^{-28} c\, h_{100}\,{\rm cm}^{-1}. \tag{3.4}$$

The value of H_0 is determined by the dimensionless factor of h_{100} which probably lies within the range $1/2 < h_{100} < 1$. The critical energy-density required to just close the universe is

$$\rho_{\rm critical} = \frac{3c^2H_0^2}{8\pi G} \approx 1.6\times 10^{-8} h_{100}^2\,{\rm ergs/cm}^3. \tag{3.5}$$

The spectrum of an *isotropic* stochastic gravitational wave background is defined by a dimensionless function of frequency f

$$\Omega_{\rm gw}(f) \equiv \frac{1}{\rho_{\rm critical}}\frac{d\rho_{\rm gw}}{d\ln f}. \tag{3.6}$$

Here $d\rho_{\rm gw}$ is the energy-density in gravitational waves contained within the frequency interval $(f, f+df)$. Using the definition $\Omega_{\rm gw}$ one obtains the relationship between the spectrum $\Omega_{\rm gw}$ and $H(f)$. For $f \geq 0$ one has

$$\Omega_{\rm gw}(f) = \frac{f}{\rho_{\rm critical}}\frac{d\rho_{\rm gw}}{df} = f\frac{8\pi G}{3c^2H_0^2}\frac{c^2}{32\pi G} 32\pi^2 f^2 H(f) \int d\hat{\Omega} P(\hat{\Omega}) = \frac{8\pi^2}{3H_0^2} f^3 H(f) \int d\hat{\Omega} P(\hat{\Omega}). \tag{3.7}$$

This formula shows the precise interpretation of $P(\hat{\Omega})$. The stochastic background energy density is made of contributions arriving from all directions $\hat{\Omega}$ on the sky. The actual value of $\Omega_{\rm gw}(f)$ is determined by the average value of $P(\hat{\Omega})$; the direction dependence of this function is the same as the direction dependence of the arriving radiation intensity.

For this reason, we *define the multipole moments* $p_{\ell m}$ of the stochastic background radiation by the expansion of $P(\hat{\Omega})$ in terms of spherical harmonic functions:

$$P(\hat{\Omega}) \equiv \sum_{\ell m} p_{\ell m} Y_{\ell m}(\hat{\Omega}) \tag{3.8}$$

where the sum is defined by

$$\sum_{\ell m} \equiv \sum_{\ell=0}^{\infty} \sum_{m=-\ell}^{\ell} = \sum_{m=-\infty}^{\infty} \sum_{\ell=|m|}^{\infty}. \tag{3.9}$$

In addition, without loss of generality we adopt the convention that the monopole moment is normalized by the condition

$$p_{00} \equiv \sqrt{4\pi} \Rightarrow \int d\hat{\Omega} P(\hat{\Omega}) \equiv 4\pi, \tag{3.10}$$

where we assume that the spherical harmonic functions are normalized in the conventional way, so that the integrals of their squares over the unit sphere gives unity. Hence the spectrum of radiation is determined entirely by $H(f)$ since for $f \geq 0$ one has

$$\Omega_{gw}(f) = \frac{32\pi^3}{3H_0^2} f^3 H(f). \tag{3.11}$$

The directionality of the arriving radiation is determined entirely by the function $P(\hat{\Omega})$. Our fundamental assumption here is that the pattern of the intensity of the stochastic background is *fixed in a frame of reference at rest with respect to the cosmological fluid.* In other words, formula (3.8) for $P(\hat{\Omega})$ is expressed in a set of coordinates $x.y,z$ which are fixed with respect to the distant stars. In those coordinates, the multipole moments $p_{\ell m}$ are constants, independent of time. The problem we address in this paper is this: how do we determine, from the data stream of a pair of interferometric detectors which are rotating with the earth, the values of (or bounds on) the multipole moments $p_{\ell m}$?

IV. DETECTION STRATEGY

To determine the multipole moments $p_{\ell m}$ the basic idea is to correlate the outputs of two gravitational wave detectors, and to look for variations of this correlated signal that are harmonics of the earth's rotational frequency. For this purpose, we need to consider the relationship between two different time (or frequency) scales that occur.

The first time scale is that defined by the light travel time ΔT between the two sites. For the remainder of this section, we will assume that the two sites are the Hanford and Livingston LIGO detectors, so that $\Delta T = 10.00$ msec. The second time scale is the period of the earth's rotation about its axis relative to the cosmic frame, $T_e = 8.6 \times 10^4$ sec $= 1$ sidereal day. Because of the enormous disparity between these two time scales, we can define a third time scale, which we will refer to as the averaging time scale, τ. We choose τ in the range

$$\Delta T << \tau << T_e, \tag{4.1}$$

for example $\tau = 30$ sec. It is then possible to examine correlations between the two detectors as a function of time, averaged over periods of length τ. Because τ is much shorter than T_e, the correlation between the two detectors will vary as the earth rotates relative to the fixed cosmological frame, because of the anisotropy in $P(\hat{\Omega})$. On the other hand, because τ is much longer than the light travel time between the two detectors, and because the detectors are sensitive to frequencies $f \approx 1/\Delta T$, there is a significant correlated signal on time scales shorter than τ.

Denote the output of the first detector by

$$s_1(t) = h_1(t) + n_1(t), \tag{4.2}$$

where h_1 is the strain due to the stochastic background and n_1 is the intrinsic noise of the first detector. In similar fashion, the output of the second detector is

$$s_2(t) = h_2(t) + n_2(t). \tag{4.3}$$

Let us use the subscript $i = 1, 2$ to label the detectors, so for example $i = 1$ denotes the Hanford, WA LIGO detector and $i = 2$ denotes the Livingston, LA LIGO detector. The response h_i of detector i to the gravitational radiation is given by

$$h_i(t) = d_i^{ab}(t) h_{ab}(t, \vec{x}_i(t)), \tag{4.4}$$

where the position of detector i's corner station is denoted by $\vec{x}_i(t)$. In this expression, the symmetric traceless tensors $d_i^{ab}(t)$ are given by

$$d_i^{ab}(t) = \frac{1}{2}\left(\hat{X}_i^a(t)\hat{X}_i^b(t) - \hat{Y}_i^a(t)\hat{Y}_i^b(t)\right) \tag{4.5}$$

where the directions of detector i's arms are defined by the unit spatial vectors $\hat{X}_i^a(t)$ and $\hat{Y}_i^a(t)$. Note that *both $d_i^{ab}(t)$ and $\vec{x}_i(t)$ are functions of time, because the earth rotates with respect to the cosmological rest frame.*

Define quantities which are the Fourier transforms of the signals, evaluated over an interval of one averaging time τ centered at time t:

$$\tilde{s}_i(f,t) = \int_{t-\tau/2}^{t+\tau/2} dt'\, e^{-2\pi i f t'} s_i(t') \text{ for } i = 1,2. \tag{4.6}$$

These Fourier transforms are easily evaluated. Substituting the plane wave expansion (2.2) into the formula for the strain (4.4) and taking the Fourier transform (4.6) we obtain

$$\tilde{s}_i(f,t) = \sum_A \int d\hat{\Omega} \int_{-\infty}^{\infty} df' e^{2\pi i(f'-f)t} \delta_\tau(f-f') h_A(f',\hat{\Omega}) d_i^{ab}(t) e_{ab}^A(\hat{\Omega}) e^{-2\pi i f' \hat{\Omega}\cdot\vec{x}_i(t)/c} + \text{noise term.} \tag{4.7}$$

In this expression, we have made use of the fact that the averaging time τ is much less than the rotation period of the earth ΔT_e, so that the vectors $X_i^a(t)$, $Y_i^a(t)$, and $\vec{x}_i(t)$ may be treated as constants and taken outside of the time integration in the Fourier transform (4.6). We have also defined the "finite time" approximation to the Dirac delta function

$$\delta_\tau(f) \equiv \int_{-\tau/2}^{\tau/2} dt'\, e^{-2\pi i f t'} = \frac{\sin(\pi f \tau)}{\pi f}, \tag{4.8}$$

which reduces to the Dirac delta function $\delta(f)$ in the limit $\tau \to \infty$, but has the property that $\delta_\tau(0) = \tau$. The final term on the right hand side of (4.7) is linearly proportional to the noise in detector i.

We now define the "signal"

$$S(t) = \int_{-\infty}^{\infty} df\, \tilde{s}_1^*(f,t)\tilde{s}_2(f,t)\tilde{Q}(f) \tag{4.9}$$

where $\tilde{Q}(f)$ is an optimal filter function, to be determined. Let us now determine the expectation value of $S(t)$ and show how it incorporates information about the multipole moments of the stochastic background. To find the expected value $S(t)$ we begin by assuming that the noise in each detector has zero mean value, and is uncorrelated with noise and gravitational strain in the other detector. Under these assumptions, we find

$$\begin{aligned}\langle S(t)\rangle = \int_{-\infty}^{\infty} df \tilde{Q}(f) \sum_A \sum_{A'} \int_{-\infty}^{\infty} df' \int_{-\infty}^{\infty} df'' \int d\hat{\Omega} \int d\hat{\Omega}' e^{-2\pi i(f'-f)t} e^{2\pi i(f''-f)t} \times \\ \delta_\tau(f-f')\delta_\tau(f-f'') d_1^{ab}(t) d_2^{cd}(t) e_{ab}^A(\hat{\Omega}) e_{cd}^{A'}(\hat{\Omega}') e^{2\pi i(f'\hat{\Omega}\cdot\vec{x}_1(t) - f''\hat{\Omega}'\cdot\vec{x}_2(t))/c} \times \\ \langle h_A^*(f',\hat{\Omega}) h_{A'}(f'',\hat{\Omega}')\rangle.\end{aligned}$$

We now substitute in the expectation value for the product of the amplitudes (2.8). The integration over f'' is now trivial. In the resulting expression, because $1/\tau$ is much smaller than the "bandwidth" $1/\Delta T$ of the signals, one of the finite-width delta functions δ_τ may be replaced by a Dirac delta function. The integration over f' is then trivial. The other finite-width delta function is then evaluated at zero argument, giving rise to a factor of τ. One thus obtains

$$\langle S(t)\rangle = \tau d_1^{ab}(t) d_2^{cd}(t) \int_{-\infty}^{\infty} df \tilde{Q}(f) H(f) \int d\hat{\Omega} P(\hat{\Omega}) e^{2\pi i f \hat{\Omega}\cdot\Delta\vec{x}(t)/c} \sum_A e_{ab}^A(\hat{\Omega}) e_{cd}^A(\hat{\Omega}) \tag{4.10}$$

where $\Delta\vec{x}(t) = \vec{x}_1(t) - \vec{x}_2(t)$ is the time-dependent separation vector between the two interferometer sites.

Not surprisingly, this previous expression can be easily simplified for the isotropic case $P(\hat{\Omega}) = 1$. In this instance, the sum over polarizations and integral over directions can be performed explicitly, yielding ($8\pi/5$ times) a time-independent function of frequency known as the overlap reduction function $\gamma(f)$. This overlap reduction function is given by

$$\gamma(f) \equiv \frac{5}{8\pi}\, d_1^{ab} d_2^{cd} \int_{S^2} d\hat{\Omega}\, e^{2\pi i f \hat{\Omega}\cdot\Delta\vec{x}/c} \left(e_{ab}^{+}(\hat{\Omega}) e_{cd}^{+}(\hat{\Omega}) + e_{ab}^{\times}(\hat{\Omega}) e_{cd}^{\times}(\hat{\Omega}) \right). \tag{4.11}$$

Notice that in (4.11) the dependence of the positions and orientations of the detectors upon time t is *not* shown; this is because $\gamma(f)$ depends only upon the *relative* positions and orientations, which is time (or earth-position) independent. Thus, in the case of an isotropic stochastic background, one finds

$$P(\hat{\Omega}) = 1 \Rightarrow \langle S(t) \rangle = \frac{8\pi}{5} \tau \int_{-\infty}^{\infty} df \tilde{Q}(f) H(f) \gamma(f). \tag{4.12}$$

This is equation (30) of reference [8]. In the present paper, we are most interested in the anisotropic case where $P(\hat{\Omega})$ varies with direction. In this case, the time variation of the tensors $d_i^{ab}(t)$ and $\Delta\vec{x}(t)$ will provide a time-dependent variation of the signal $S(t)$.

V. ROTATION HARMONICS

Because the rotation of the earth is periodic with period T_e and angular frequency $\omega_e = 2\pi/T_e$ the expected signal (4.10) varies with the same period. It can therefore be represented by the Fourier series

$$\langle S(t) \rangle = \sum_{m=-\infty}^{\infty} \langle S_m \rangle e^{im\omega_e t}. \tag{5.1}$$

Because the signal is real, the amplitudes of the different harmonics satisfy $S_m = S_{-m}^*$. The amplitudes are quantities which would be determined by Fourier transforming the actual data:

$$S_m = \frac{1}{T} \int_0^T dt\, e^{-im\omega_e t} S(t). \tag{5.2}$$

Here T represents the total observation time, which later enters into (9.4) and which is assumed to be is a multiple of the earth's rotation period T_e. The harmonic amplitudes S_m are the (at least in principle) observable quantities on which any data analysis must be based; it is their expected values $\langle S_m \rangle$ which arise in the formula for the expected signal. Note that in an actual observation or measurement, instrumental noise in the gravitational-wave detectors would prevent S_m from taking on its *expected* value. In Section IX we analyze the typical deviations of S_m from $\langle S_m \rangle$ and in this way determine how accurately S_m may in fact be measured.

Because we have assumed that the z-axis of our (cosmic) coordinate system points along the direction of the earth's axis, the m'th rotation harmonic can only result from anisotropies whose phase varies with angle ϕ as $\exp(im\phi)$. These are the anisotropies associated with the $Y_{\ell m}$. Hence

$$\langle S_m \rangle = \frac{8\pi}{5} \tau \int_{-\infty}^{\infty} df \tilde{Q}(f) H(f) \sum_{\ell=|m|}^{\infty} p_{\ell m} \gamma_{\ell m}(f) \tag{5.3}$$

The functions $\gamma_{\ell m}(f)$ are generalizations of the overlap reduction function $\gamma(f)$, which express the (frequency-dependent) contribution of the ℓ'th multipole moment to the m'th harmonic of the signal, with respect to the Earth's rotation. These are given by

$$\gamma_{\ell m}(f) = \frac{5}{8\pi} \frac{1}{2\pi} \int_0^{2\pi} d\alpha\, e^{-im\alpha} d_1^{ab}(\alpha) d_2^{cd}(\alpha) \int d\hat{\Omega}\, Y_{\ell m}(\hat{\Omega}) e^{2\pi i f \hat{\Omega}\cdot\Delta\vec{x}(\alpha)/c} \sum_A e_{ab}^A(\hat{\Omega}) e_{cd}^A(\hat{\Omega}). \tag{5.4}$$

In this expression, the angle of rotation of the earth about its axis (measured from some arbitrary fiducial point) is denoted by $\alpha \in [0, 2\pi)$ so $\alpha = \omega_e t + \text{constant} \pmod{2\pi}$. The "time-dependent" quantities d_i^{ab} and $\Delta\vec{x}$ may equivalently be expressed as functions of α.

The problem at hand is now a mathematical one – to calculate the functions $\gamma_{\ell m}(f)$ which are generalizations of the overlap reduction function $\gamma(f)$. For the monopole moment ($\ell = m = 0$) it is easy to see that the integrand above is independent of earth-position α because the overlap reduction function (4.11) only depends upon the relative orientations of the detectors, which is α-independent, giving

$$\gamma_{00}(f) = (4\pi)^{-1/2} \gamma(f). \tag{5.5}$$

In the next parts of this paper, we will show how to evaluate the other $\gamma_{\ell m}$.

Our first task is to evaluate the integrals that appear in (5.4). The product $d_1^{ab}(\alpha)d_2^{cd}(\alpha)$ is a quartic polynomial in $\sin\alpha$ and $\cos\alpha$. One approach would be to attempt to perform the integral over $\hat{\Omega}$, to obtain the resulting function of α, and then to evaluate the integral over α. However this approach is rather cumbersome.

A more promising method is to consider the projector onto the plane perpendicular to $\hat{\Omega}$, which may be calculated in terms of the vectors defined by (2.4) and (2.5):

$$Q_{ab} = \delta_{ab} - \hat{\Omega}_a\hat{\Omega}_b = \hat{m}_a\hat{m}_b + \hat{n}_a\hat{n}_b. \tag{5.6}$$

A couple minutes of algebra starting with (2.6) and (2.7) quickly establishes the identity

$$\sum_A e^A_{ab}(\hat{\Omega})e^A_{cd}(\hat{\Omega}) = Q_{ac}Q_{bd} + Q_{ad}Q_{bc} - Q_{ab}Q_{cd}. \tag{5.7}$$

We then define the set of integrals

$$C_{abcd}(\alpha) = \int d\hat{\Omega}\, Y_{\ell m}(\hat{\Omega})\mathrm{e}^{2\pi i f\hat{\Omega}\cdot\Delta\vec{x}(\alpha)/c}\hat{\Omega}_a\hat{\Omega}_b\hat{\Omega}_c\hat{\Omega}_d. \tag{5.8}$$

The desired integrals can then be expressed in terms of this quantity. For convenience, we introduce a symbol to handle the contractions that occur. This is a constant tensor defined by

$$\Theta^{pqrs}_{abcd} = 2\delta_{ac}\delta_{bd}\delta^{pq}\delta^{rs} - 4\delta_{ac}\delta^{pq}\delta_b{}^r\delta_d{}^s + \delta_a{}^p\delta_b{}^q\delta_c{}^r\delta_d{}^s. \tag{5.9}$$

Making use of the fact that each of the d_i^{ab} is symmetric in its tensor indices, and traceless, we may then write

$$\gamma_{\ell m}(f) = \frac{5}{8\pi}\frac{1}{2\pi}\int_0^{2\pi} d\alpha\, \mathrm{e}^{-im\alpha}d_1^{ab}(\alpha)d_2^{cd}(\alpha)\Theta^{pqrs}_{abcd}C_{pqrs}(\alpha). \tag{5.10}$$

From this definition it is easy to show that $\gamma_{\ell,-m} = (-1)^{\ell+m}\gamma^*_{\ell,m}$. This follows from the parity tranformation property of the spherical harmonics $Y_{\ell m}(-\hat{\Omega}) = (-1)^\ell Y_{\ell m}(\hat{\Omega})$. In order to now evaluate C_{abcd} it is convenient to introduce some additional coordinate systems.

VI. COORDINATE FRAMES

The vectors being used in this calculation are three-dimensional spatial vectors in flat Cartesian R^3. Up to this point, we have been using a coordinate system which is fixed with respect to the cosmological fluid, and in which the spatial pattern of the perturbations of the stochastic background is assumed to be time-independent. This frame of reference is the "unprimed" frame; vectors expressed with respect to these cosmic coordinates have unprimed indices. We have also assumed (without any loss of generality) that the z-axis of this cosmic frame points along the direction of the earth's rotation axis.

At this point, for calculational purposes, it is convenient to consider two additional coordinate systems. Thus, a given vector V may be expressed in terms of its components in three different frames:

$$\begin{aligned} \text{Cosmic Frame}: &\quad V^a \\ \text{Earth Frame}: &\quad V^{\bar{a}} \\ \text{Computational Frame}: &\quad V^{a'} \end{aligned}$$

The "earth frame" is a coordinate system fixed to the earth, in which the third (z-coordinate) points along the axis of the earth's rotation, in the direction of the North pole. Components of vectors in this frame are denoted with "barred" indices. The second of these new coordinate systems will be referred to as the "calculational" coordinate system. In this frame, the components of vectors are "primed". This frame is fixed with respect to the earth, and has its third (z-coordinate) pointing along the line between the two gravitational-wave detectors.

The relationship between components of vectors in these three coordinate frames may be written as matrix equations. Each of the matrices which appears is a special case of a rotation matrix which may be parametrized by Euler angles. Throughout this paper, we use the Euler angle conventions given by equations (4.83-6) of Afkin [9] which are also the conventions used in equations (4.5) and (4.43) of Rose [10]. It is convenient to define a pair of rotations about the z and y axes respectively, by

$$\mathbf{R}_z(\alpha) \equiv \begin{pmatrix} \cos\alpha & \sin\alpha & 0 \\ -\sin\alpha & \cos\alpha & 0 \\ 0 & 0 & 1 \end{pmatrix} \qquad \mathbf{R}_y(\beta) \equiv \begin{pmatrix} \cos\beta & 0 & -\sin\beta \\ 0 & 1 & 0 \\ \sin\beta & 0 & \cos\beta \end{pmatrix} \tag{6.1}$$

The most general possible rotation may be parametrized by Euler angles and is defined by the matrix $\mathbf{R}(\alpha,\beta,\gamma) = \mathbf{R}_z(\gamma)\mathbf{R}_y(\beta)\mathbf{R}_z(\alpha)$. Note that the boldface symbols here denote 3×3 square matrices.

The matrix which relates components of vectors in the cosmic and earth frames is simply rotation through angle α about the z-axis:

$$X^{\bar{a}} = R^{\bar{a}}{}_a X^a \qquad R^{\bar{a}}{}_a = \mathbf{R}(\alpha,0,0) = \mathbf{R}_z(\alpha) \tag{6.2}$$

where the first index on R labels rows and the second index labels columns, so that the operation appearing in the previous equation is ordinary multiplication of a column vector on the right by a square matrix on the left. Note that the angle $\alpha = \omega_e t$ varies with time.

Without loss of generality, assume that the freedom to choose the $\bar{x}$- and $\bar{y}$-axis in the Earth frame has been used to ensure that in this frame the separation vector $\Delta x^{\bar{a}}$ between the two detector sites has no $\bar{y}$-component. Using the two LIGO sites as an example, the Earth-frame $\bar{x}$-axis would point out from the center of the earth at an angle 38.6881° East of the 0° line of longitude (Greenwich, England). In this frame, the coordinates of the two detector sites and the detector arms directions are

$$\text{Hanford, Washington}: x_1^{\bar{a}} = \begin{pmatrix} 707.41 \\ -4329.11 \\ 4614.74 \end{pmatrix}^{\bar{a}} \text{km}, \quad \hat{X}_1^{\bar{a}} = \begin{pmatrix} -0.684779 \\ 0.476172 \\ 0.55167 \end{pmatrix}^{\bar{a}}, \quad \hat{Y}_1^{\bar{a}} = \begin{pmatrix} -0.720231 \\ -0.557622 \\ -0.412703 \end{pmatrix}^{\bar{a}}$$

$$\text{Livingston, Louisiana}: x_2^{\bar{a}} = \begin{pmatrix} 3371.80 \\ -4329.11 \\ 3240.36 \end{pmatrix}^{\bar{a}} \text{km}, \quad \hat{X}_2^{\bar{a}} = \begin{pmatrix} -0.65377 \\ -0.708366 \\ -0.266085 \end{pmatrix}^{\bar{a}}, \quad \hat{Y}_2^{\bar{a}} = \begin{pmatrix} 0.540953 \\ -0.191642 \\ -0.81893 \end{pmatrix}^{\bar{a}}.$$

It is obvious that, as claimed, the separation vector between the two sites $x_1^{\bar{a}} - x_2^{\bar{a}}$ has vanishing $\bar{y}$-component. The matrix which relates the components of the vectors in the computational and earth frames is a rotation about the $\bar{y}$ axis:

$$X^{\bar{a}} = R^{\bar{a}}{}_{a'} X^{a'} \qquad R^{\bar{a}}{}_{a'} = \mathbf{R}(0,-\beta,0) = \mathbf{R}_y(-\beta) \tag{6.3}$$

where β is a time-independent (or α-independent) angle, determined by the relative orientation of the line between the two detector sites and the earth's axis. For the two LIGO detectors, the angle relating the Earth frame and the computational frame is

$$\beta = -62.71383°. \tag{6.4}$$

Within the computational frame, the separation vector between the two sites is

$$x_1^{a'} - x_2^{a'} = 2997.98\,\text{km} \begin{pmatrix} 0 \\ 0 \\ 1 \end{pmatrix} \tag{6.5}$$

and the unit-length vectors defining the arm directions are

$$\hat{X}_1^{a'} = \begin{pmatrix} 0.176358 \\ 0.476171 \\ 0.861486 \end{pmatrix}^{a'} \qquad \hat{Y}_1^{a'} = \begin{pmatrix} -0.69696 \\ -0.557623 \\ 0.450893 \end{pmatrix}^{a'} \qquad \hat{X}_2^{a'} = \begin{pmatrix} -0.536188 \\ -0.708366 \\ 0.459042 \end{pmatrix}^{a'} \qquad \hat{Y}_2^{a'} = \begin{pmatrix} -0.479814 \\ -0.191642 \\ -0.856185 \end{pmatrix}^{a'} \tag{6.6}$$

These quantities will become useful later.

VII. COMPUTATION OF C

Our goal now is to calculate C_{abcd} as defined in (5.8). To do this, we will express the spherical harmonic functions $Y_{\ell m}(\Omega) = Y_{\ell m}(\theta,\phi)$ in terms of the "primed" coordinates in the computational frame. Combining the transformations (6.2) and (6.3) we obtain the relationship between vectors in the cosmic and computational frames:

$$V^{a'} = \mathbf{R}_y(\beta)\mathbf{R}_z(\alpha)V^a = \mathbf{R}(\alpha,\beta,0)V^a. \tag{7.1}$$

This transformation through Euler angles $\alpha, \beta, 0$ induces a simple change in the spherical harmonics. For a given value of ℓ the spherical harmonic functions in one frame are simply a sum of all the spherical harmonics with the same value of ℓ in the other frame. The relation between these two sets of functions is given by the rotation matrices D^{ℓ}_{mn}, which are closely related to Clebsch-Gordon coefficients:

$$Y_{\ell m}(\theta', \phi') = \sum_{k=-\ell}^{\ell} D^{\ell}_{km}(\alpha, \beta, 0) Y_{\ell k}(\theta, \phi). \tag{7.2}$$

(See equation (4.260) of Arfkin [9].) The inverse transformation is obtained by reversing the lower two indices on the rotation matrix and complex-conjugating:

$$Y_{\ell m}(\theta, \phi) = \sum_{k=-\ell}^{\ell} \left(D^{\ell}_{mk}(\alpha, \beta, 0)\right)^* Y_{\ell k}(\theta', \phi'). \tag{7.3}$$

The rotation matrices are conveniently expressed by equation (4.12) of Rose [10]:

$$D^{\ell}_{mk}(\alpha, \beta, \gamma) = \mathrm{e}^{-im\alpha} d^{\ell}_{mk}(\beta) \mathrm{e}^{-ik\gamma}. \tag{7.4}$$

Explicit formulae for the d^{ℓ}_{mk} may be given either in the form of a sum, or in "summed" form. The latter expression, given by equation (4.14) of Rose [10] is the most useful one for us. For $m \geq k$

$$d^{\ell}_{mk} = \left[\frac{(\ell-k)!(\ell+m)!}{(\ell+k)!(\ell-m)!}\right]^{1/2} \frac{\left(\cos\frac{\beta}{2}\right)^{2\ell+k-m} \left(-\sin\frac{\beta}{2}\right)^{m-k}}{(m-k)!} {}_2F_1(m-\ell, -k-\ell; m-k+1; -\tan^2\frac{\beta}{2}). \tag{7.5}$$

Notice that because the $m \leq \ell$ the first argument of the Gauss hypergeometric function ${}_2F_1$ is a non-positive integer the hypergeometric series ${}_2F_1$ terminates after a finite number of terms. In fact it is possible to rewrite equation Eq. (7.5) in terms of Jacobi polynomials $P_n^{(\alpha,beta)}$, for $m \geq k$

$$d^{\ell}_{mk} = (-1)^{l-m} \left[\frac{(\ell-m)!(\ell+m)!}{(\ell-k)!(\ell+k)!}\right]^{1/2} \left(\cos\frac{\beta}{2}\right)^{m+k} \left(-\sin\frac{\beta}{2}\right)^{m-k} P_{\ell-m}^{(m+k,m-k)}(-\cos\beta). \tag{7.6}$$

In the event that $m < k$ the d^{ℓ}_{mk} may be obtained from the unitarity property, equation (4.15) of Rose [10]

$$d^{\ell}_{mk}(\beta) = d^{\ell}_{km}(-\beta) = (-1)^{m-k} d^{\ell}_{km}(\beta). \tag{7.7}$$

Note also that the d^{ℓ}_{mk} are real, so that we can drop the complex conjugation that would otherwise have appeared.

The integral over the two-sphere which appears in (5.8) can also be expressed as an integral over all directions in the computational (primed) frame. In other words, $\int d\hat{\Omega} = \int d\hat{\Omega}'$. So our integral may be expressed as

$$C_{abcd}(\alpha) = \sum_{k=-\ell}^{\ell} d^{\ell}_{mk}(\beta) \mathrm{e}^{im\alpha} N^k_{\ell} \int_0^{\pi} \sin\theta' d\theta' \mathrm{e}^{2\pi i f \Delta T \cos\theta'} \mathrm{P}^k_{\ell}(\cos\theta') \int_0^{2\pi} d\phi' \mathrm{e}^{ik\phi'} \hat{\Omega}_a \hat{\Omega}_b \hat{\Omega}_c \hat{\Omega}_d, \tag{7.8}$$

where we have expressed the spherical harmonic functions in terms of associated Legendre functions P^k_{ℓ}, and $\Delta T = |x_1 - x_2|/c$ denotes the light travel time between the two detector sites (10.00 msec for the two LIGO detectors). The normalization constants N^k_{ℓ} which relate the spherical harmonics and the Legendre polynomials are

$$N^k_{\ell} = \sqrt{\frac{2l+1}{4\pi} \frac{(l-k)!}{(l+k)!}}. \tag{7.9}$$

We will eventually be contracting the four indices of C with each other and with the indices of other tensors. Of course such contractions yield the same result in any coordinate frame, and it is easier to calculate C in the calculational (primed) frame. Hence we may write $C_{abcd}(\alpha) = R_a{}^{a'} R_b{}^{b'} R_c{}^{c'} R_d{}^{d'} C_{a'b'c'd'}$ where $R_a{}^{a'} = \mathbf{R}_z(-\alpha)\mathbf{R}_y(-\beta)$, and

$$C_{a'b'c'd'} = \mathrm{e}^{im\alpha} \sum_{k=-\ell}^{\ell} d^{\ell}_{mk}(\beta) N^k_{\ell} \int_0^{\pi} \sin\theta' d\theta' \mathrm{e}^{2\pi i f \Delta T \cos\theta'} \mathrm{P}^k_{\ell}(\cos\theta') \int_0^{2\pi} d\phi' \mathrm{e}^{ik\phi'} \hat{\Omega}_{a'} \hat{\Omega}_{b'} \hat{\Omega}_{c'} \hat{\Omega}_{d'}. \tag{7.10}$$

The vector $\hat{\Omega}^{a'}$ is

$$\hat{\Omega}^{a'} = \begin{pmatrix} \cos\phi' \sin\theta' \\ \sin\phi' \sin\theta' \\ \cos\theta' \end{pmatrix}^{a'} . \tag{7.11}$$

It is clear that the integral over ϕ' in (7.10) vanishes unless $k = -4, -3, \cdots, 3, 4$. Thus even for large ℓ the range of summation over k only includes these values. There is a sense in which this reflects the fact that our signal is a product of the outputs of a pair of detectors, each of which has a quadrupole antenna pattern. It is also noteworthy that the remaining integral, over the variable θ', can also be done explicitly for any distinct values of ℓ and k.

VIII. THE REMAINING INTEGRATIONS

We are now in a position to evaluate the remaining integrals. We begin with the integral over α. We can re-write $\gamma_{\ell m}$ from (5.10) as

$$\gamma_{\ell m}(f) = \frac{5}{8\pi}\frac{1}{2\pi}\int_0^{2\pi} d\alpha\, \mathrm{e}^{-im\alpha}\mathrm{e}^{im\alpha} d_1^{a'b'}(\beta) d_2^{c'd'}(\beta) \times$$
$$\Theta^{p'q'r's'}_{a'b'c'd'} \sum_{k=-\ell}^{\ell} d^{\ell}_{mk}(\beta) N^k_\ell \int_0^{\pi} \sin\theta' d\theta'\, \mathrm{e}^{2\pi i f \Delta T \cos\theta'} \mathrm{P}^k_\ell(\cos\theta') \int_0^{2\pi} d\phi' \mathrm{e}^{ik\phi'} \hat{\Omega}_{p'}\hat{\Omega}_{q'}\hat{\Omega}_{r'}\hat{\Omega}_{s'}.$$

In this integral, we have explicitly indicated all of the dependence on α. Notice that while d_i^{ab} is a function of α, in computational coordinates $d_i^{a'b'}(\beta)$ is independent of α and depends only upon β. Likewise, the tensor $\Theta^{p'q'r's'}_{a'b'c'd'}$ defined by (5.9) has constant components in the computational frame. Hence the integral over α give a factor 2π:

$$\gamma_{\ell m}(f) = \frac{5}{8\pi} d_1^{a'b'}(\beta) d_2^{c'd'}(\beta) \times$$
$$\Theta^{p'q'r's'}_{a'b'c'd'} \sum_{k=-\ell}^{\ell} d^{\ell}_{mk}(\beta) N^k_\ell \int_0^{\pi} \sin\theta' d\theta'\, \mathrm{e}^{2\pi i f \Delta T \cos\theta'} \mathrm{P}^k_\ell(\cos\theta') \int_0^{2\pi} d\phi' \mathrm{e}^{ik\phi'} \hat{\Omega}_{p'}\hat{\Omega}_{q'}\hat{\Omega}_{r'}\hat{\Omega}_{s'}. \tag{8.1}$$

The form of this integral is interesting. The integral over ϕ' will vanish unless $k = -4, \cdots, 4$, in which case it yields a product of at most four factors of $\sin\theta'$ and $\cos\theta'$. Introducing a new variable $u = \cos\theta'$ the two integrals appearing in (8.1) may be expressed as linear combinations of the integrals

$$\int_{-1}^{1} du\, \mathrm{e}^{2\pi i f \Delta T u} \mathrm{P}^k_\ell(u) u^N (1-u^2)^{|k|/2} \tag{8.2}$$

where N is a non-negative integer bounded by $N + |k| \leq 4$. Such integrals can be expressed in closed-form as we show in the Appendix.

From this point on, we consider only the case of the two LIGO detectors. In this case the simplest way to proceed is to compute

$$s_k(\theta') = d_1^{a'b'}(\beta) d_2^{c'd'}(\beta) \Theta^{p'q'r's'}_{a'b'c'd'} \int_0^{2\pi} d\phi' \mathrm{e}^{ik\phi'} \hat{\Omega}_{p'}\hat{\Omega}_{q'}\hat{\Omega}_{r'}\hat{\Omega}_{s'}. \tag{8.3}$$

To evaluate this, we use definition (4.5) of the d_i^{ab}, the contraction operator (5.9) and the arm directions (6.6). Substituting in the vector $\hat{\Omega}^{a'}$ given by (7.11) gives elementary integrals over ϕ'. The results are easily written in terms of the variable $u = \cos\theta'$:

$$\begin{aligned}
s_0(u) &= -3.01308 + 1.75421\, u^2 + 0.945109\, u^4 \\
s_1(u) &= \left(0.5451 + 0.543353\, i - (1.6954 + 1.73284\, i)\, u^2\right) u\, (1-u^2)^{1/2} \\
s_2(u) &= \left(-0.0428705 + 1.41125\, i + (0.0119604 - 0.670812\, i)\, u^2\right) (1-u^2) \\
s_3(u) &= (-0.245744 + 0.227815 i)\, u\, (1-u^2)^{3/2} \\
s_4(u) &= (0.0492709 + 0.00345516 i)\, (1-u^2)^2 \\
s_{-k}(u) &= s_k^*(u)
\end{aligned}$$

$$s_k(u) = 0 \quad \text{for } |k| > 4$$

We then have

$$\gamma_{\ell m}(f) = \frac{5}{8\pi} \sum_{k=-\ell}^{\ell} d^{\ell}_{mk}(\beta) N^k_\ell \int_{-1}^{1} du\, e^{2\pi i f \Delta T u} P^k_\ell(u) s_k(u). \tag{8.4}$$

We now evaluate these functions for the first few multipoles. For this purpose we introduce a dimensionless frequency variable $x = 2\pi f \Delta T$. Because $\gamma_{\ell m} = (-1)^{\ell+m}\gamma^*_{\ell,-m}$ we give these functions only for $m = 0, \cdots, \ell$. They may be conveniently written in terms of spherical Bessel functions j_n. For $\ell = 0$ one has

$$\gamma_{0,0}(x) = -0.0352174 j_0(x) - 0.818115\frac{j_1(x)}{x} + 0.848647\frac{j_2(x)}{x^2}.$$

A graph of this function is shown in Figure 1.

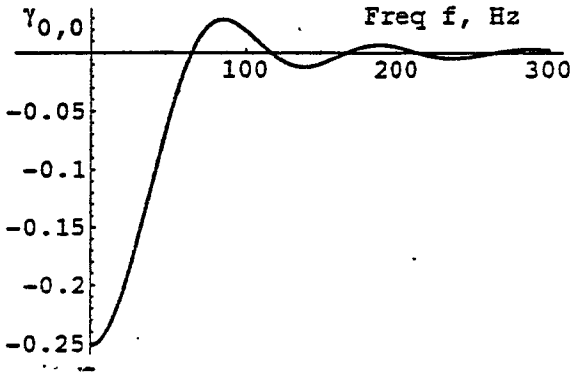

FIG. 1. The (real) function $\gamma_{0,0}(f)$ is shown for the LIGO pair of detectors.

For $\ell = 1$ one has

$$\gamma_{1,0}(x) = -0.0279637 i j_1(x) - 0.252119 i\frac{j_2(x)}{x} - 1.66955 i\frac{j_3(x)}{x^2}$$
$$\gamma_{1,1}(x) = 0.0383329 i j_1(x) - (0.327033 - 1.03547i)\frac{j_2(x)}{x} + (1.90568 - 1.77847i)\frac{j_3(x)}{x^2}.$$

A graph of these functions is shown in Figure 2.

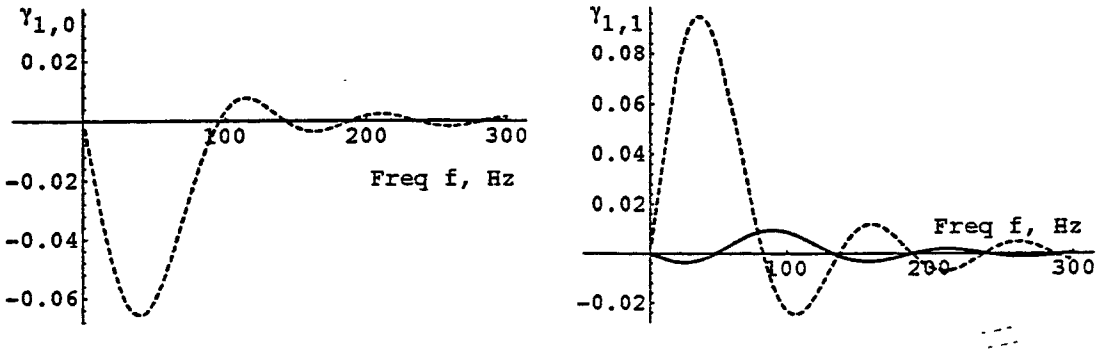

FIG. 2. The functions $\gamma_{1,m}(f)$ are shown for the LIGO pair of detectors. The real parts are shown as the solid curves, and the imaginary parts as the dotted curves.

For $\ell = 2$ one has

$$\gamma_{2,0}(x) = 0.0145494 j_0(x) + 1.00009\frac{j_1(x)}{x} - 9.39901\frac{j_2(x)}{x^2} + 28.0344\frac{j_3(x)}{x^3}$$

$$\gamma_{2,1}(x) = 0.0392947 j_0(x) + (0.385015 + 0.335238i)\frac{j_1(x)}{x} - (2.38288 + 2.48534i)\frac{j_2(x)}{x^2}$$
$$-(6.01443 - 16.1191i)\frac{j_3(x)}{x^3}$$

$$\gamma_{2,2}(x) = -0.0380887 j_0(x) - (1.05867 + 0.649899i)\frac{j_1(x)}{x} + (9.05483 + 6.80403i)\frac{j_2(x)}{x^2}$$
$$-(18.5056 + 20.4538i)\frac{j_3(x)}{x^3}.$$

A graph of these functions is shown in Figure 3.

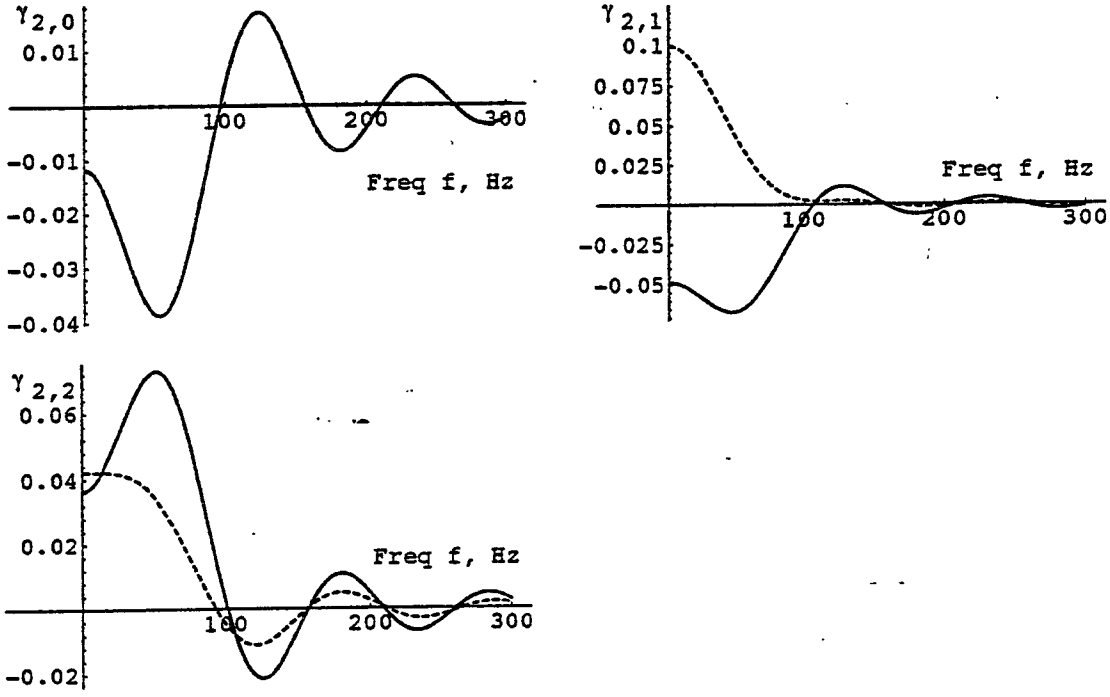

FIG. 3. The functions $\gamma_{2,m}(f)$ are shown for the LIGO pair of detectors. The real parts are shown as the solid curves, and the imaginary parts as the dotted curves.

For $\ell = 3$ one has

$$\gamma_{3,0}(x) = 0.0416301 i j_1(x) + 0.805209 i\frac{j_2(x)}{x} - 11.2779 i\frac{j_3(x)}{x^2} + 18.399 i\frac{j_4(x)}{x^3}$$

$$\gamma_{3,1}(x) = 0.00182185 i j_1(x) - (0.0155429 + 1.03107i)\frac{j_2(x)}{x} - (1.38339 - 11.1549i)\frac{j_3(x)}{x^2}$$
$$-(7.72558 + 45.6531i)\frac{j_4(x)}{x^3}$$

$$\gamma_{3,2}(x) = -0.0461979 i j_1(x) + (0.788263 - 0.534988i)\frac{j_2(x)}{x} - (7.13839 - 8.50643i)\frac{j_3(x)}{x^2}$$
$$+(42.9458 - 1.80521i)\frac{j_4(x)}{x^3}$$

$$\gamma_{3,3}(x) = 0.0365627 i j_1(x) - (0.935792 - 1.08142i)\frac{j_2(x)}{x} + (11.3339 - 13.8287i)\frac{j_3(x)}{x^2}$$
$$-(33.6244 - 32.4339i)\frac{j_4(x)}{x^3}.$$

A graph of these functions is shown in Figure 4.

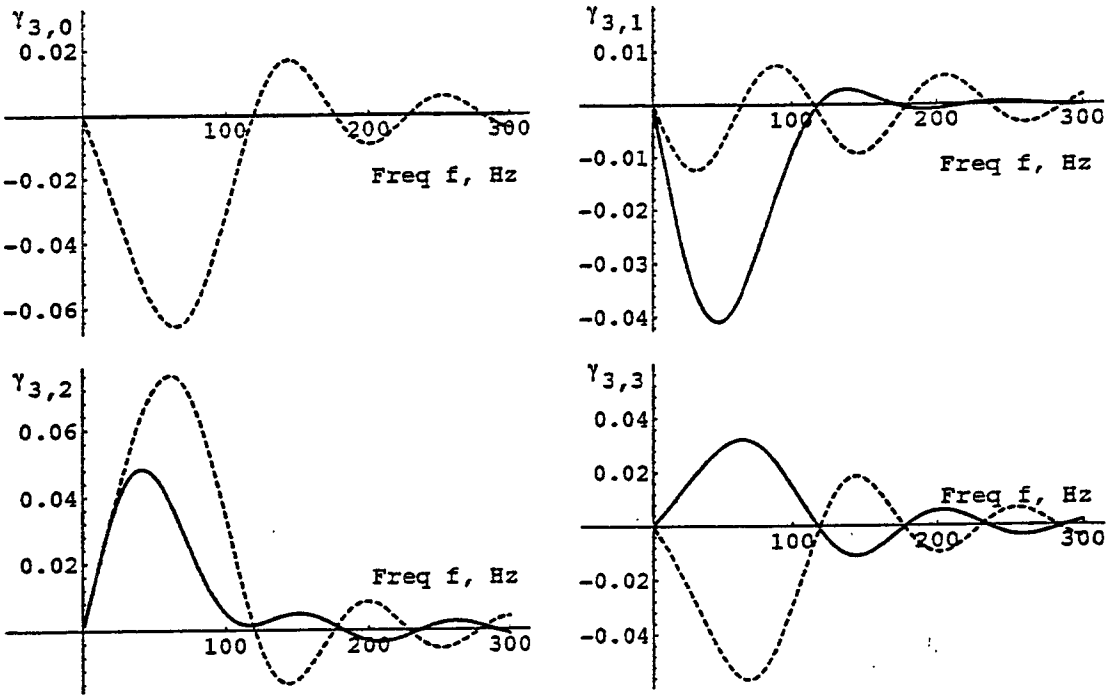

FIG. 4. The functions $\gamma_{3,m}(f)$ are shown for the LIGO pair of detectors. The real parts are shown as the solid curves, and the imaginary parts as the dotted curves.

For $\ell = 4$ one has

$$\gamma_{4,0}(x) = 0.0232299 j_0(x) - 0.899008\frac{j_1(x)}{x} + 9.78424\frac{j_2(x)}{x^2} - 88.696\frac{j_3(x)}{x^3} + 438.555\frac{j_4(x)}{x^4}$$

$$\gamma_{4,1}(x) = -0.0367891 j_0(x) - (1.10932 + 0.313862i)\frac{j_1(x)}{x} + (27.3542 + 5.98172i)\frac{j_2(x)}{x^2}$$
$$-(204.205 + 48.3679i)\frac{j_3(x)}{x^3} + (496.286 + 149.558i)\frac{j_4(x)}{x^4}$$

$$\gamma_{4,2}(x) = -0.0155407 j_0(x) + (1.05639 - 0.265167i)\frac{j_1(x)}{x} - (14.276 - 0.635514i)\frac{j_2(x)}{x^2}$$
$$+(127.588 - 28.9739i)\frac{j_3(x)}{x^3} - (551.647 - 310.656i)\frac{j_4(x)}{x^4}$$

$$\gamma_{4,3}(x) = 0.0502848 j_0(x) + (0.521081 + 1.287i)\frac{j_1(x)}{x} - (20.3464 + 20.2033i)\frac{j_2(x)}{x^2}$$
$$+(135.553 + 177.464i)\frac{j_3(x)}{x^3} - (156.429 + 719.091i)\frac{j_4(x)}{x^4}$$

$$\gamma_{4,4}(x) = -0.0344655 j_0(x) - (0.977416 + 1.17615i)\frac{j_1(x)}{x} + (24.322 + 22.0573i)\frac{j_2(x)}{x^2}$$
$$-(183.738 + 163.238i)\frac{j_3(x)}{x^3} + (458.028 + 438.49i)\frac{j_4(x)}{x^4}$$

Note that the $\gamma_{\ell m}$ with ℓ odd vanish as $f \to 0$, in contrast with the functions with ℓ even, which approach constant values at zero frequency.

IX. OBSERVABILITY AND SIGNAL-TO-NOISE RATIOS

Up to this point, we have shown how anisotropies in the gravitational-wave stochastic background give rise to periodic variations in the "signal" obtained by correlating a pair of detectors. These periodic variations are described by the Fourier series (5.1), with coefficients S_m. In this section, we address the question: how precisely can the values of these coefficients be determined, in the presence of noise in the two detectors? We answer this question by

calculating the signal-to-noise (S/N) ratios that would arise in measurements of the S_m, which also permits us to determine the best choice of the optimal filter functions $\tilde{Q}(f)$.

In carrying out this analysis, we follow the technique used in Section 3.2 of reference [8]. The following presentation will be somewhat crypic as we will assume that the reader is familiar with that material.

The noise in the detectors is characterized by a cross-correlation function

$$\langle \tilde{n}_i^*(f)\tilde{n}_j(f')\rangle = \frac{1}{2}\delta_{ij}\delta(f-f')P_i(|f|). \tag{9.1}$$

Here $i = 1, 2$ labels the two detector sites and $P_i(f)$ is the (one-sided, real) noise power spectrum of the i'th detector. For the initial and advanced LIGO detectors, these power spectra are shown in Fig. 5. For our calculations of S/N we will need to know the noise properties of the detectors averaged over our "windowing time" τ. To obtain these, we first characterize the detector noise in the time domain, by Fourier transforming (9.1). This gives

$$\begin{aligned}\langle n_i(t)n_j(t')\rangle &= \int_{-\infty}^{\infty} df\, e^{-2\pi i f t}\int_{-\infty}^{\infty} df'\, e^{2\pi i f' t'}\langle \tilde{n}_i^*(f)\tilde{n}_j(f')\rangle \\ &= \frac{1}{2}\delta_{ij}\int_{-\infty}^{\infty} df\, e^{-2\pi i f(t-t')}P_i(|f|).\end{aligned} \tag{9.2}$$

In words, this says that the Fourier transform of the noise auto-correlation function is the noise power spectrum.

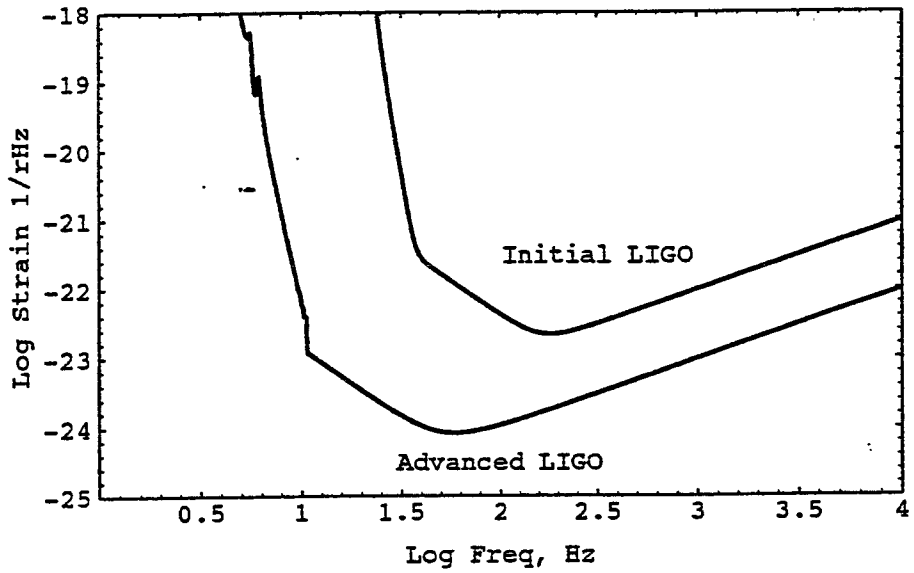

FIG. 5. The predicted noise power spectra of the initial and advanced LIGO detectors. The horizontal axis is $\log_{10}$ of frequency f, in Hz. The vertical axis shows $\log_{10}(\mathrm{P(f)/sec})^{1/2}$, or strain per root Hz. These noise power spectra are the published design goals. The bumps appearing in the low-frequency part of the advanced LIGO noise curve are obtained by folding measured seismic noise data with the predicted transfer function of the seismic isolation (stack) system.

We can now find the "windowed" version of these formulae, using the definition (4.6) of the windowed transform. Taking the windowed transforms of (9.2) yields

$$\begin{aligned}\langle \tilde{n}_i^*(f,t)\tilde{n}_j(f',t')\rangle &= \int_{t-\tau/2}^{t+\tau/2} dt''\, e^{2\pi i f t''}\int_{t'-\tau/2}^{t'+\tau/2} dt'''\, e^{-2\pi i f' t'''}\langle n_i(t'')n_j(t''')\rangle \\ &= \frac{1}{2}\delta_{ij}e^{2\pi i(ft-f't')}\int_{-\infty}^{\infty} dp\, e^{-2\pi i p(t-t')}\delta_\tau(f-p)\delta_\tau(f'-p)P_i(|p|).\end{aligned} \tag{9.3}$$

Note that in the long averaging time limit $\tau \to \infty$ this reproduces equation (9.1).

In virtually any realistic scenario, the intrinsic instrumental detector noise is expected to be much larger than the strain arising from the stochastic background of gravity waves. For this reason, if we define the "noise" in a given

measurement of S_m by $N_m \equiv S_m - \langle S_m \rangle$ then to good approximation a formula for N_m may be obtained by replacing the total detector output $s_i(t)$ which appears in (4.2) by $n_i(t)$. Using the definition of the "signal" (4.9) and the definition of the m'th harmonic (5.2) one obtains

$$N_m = \frac{1}{T}\int_0^T dt\, e^{-im\omega_e t}\int_{-\infty}^{\infty} df \tilde{n}_1^*(f,t)\tilde{n}_2(f,t)\tilde{Q}(f). \tag{9.4}$$

(Note that in this formula, we assume that the total observation time T is large compared with the earth's rotation time T_e and that during the observation time the earth has made an integral number of rotations, so that T/T_e is a large integer. We will typically take T to be 1 sidereal year.) The approximation that we make here is obviously consistent with $\langle N_m \rangle = 0$ since the noise in the two detectors is assumed to be uncorrelated, so that $\langle \tilde{n}_1^*(f,t)\tilde{n}_2(f',t')\rangle = 0$.

The "noise" arising in the measurement of S_m may be characterized by $\langle |N_m|^2\rangle = \langle |S_m|^2\rangle - |\langle S_m\rangle|^2$. We now calculate $\langle N_m^* N_{m'}\rangle$. Substituting equation (9.3) into equation (9.4) and "squaring" yields

$$\begin{aligned}\langle N_m^* N_{m'}\rangle &= \frac{1}{T^2}\int_0^T dt \int_0^T dt'\, e^{i\omega_e(mt-m't')}\int_{-\infty}^{\infty} df\, \tilde{Q}^*(f)\int_{-\infty}^{\infty} df'\, \tilde{Q}(f')\langle \tilde{n}_1^*(f,t)\tilde{n}_1(f',t')\rangle\langle \tilde{n}_2^*(f,t)\tilde{n}_2(f',t')\rangle \\ &= \frac{1}{4T^2}\int_0^T dt\int_0^T dt'\int_{-\infty}^{\infty} df\int_{-\infty}^{\infty} df'\int_{-\infty}^{\infty} dp\int_{-\infty}^{\infty} dp'\, \tilde{Q}^*(f)\tilde{Q}(f')e^{i\omega_e(mt-m't')+2\pi i(p-p')(t-t')} \\ &\quad \times \delta_\tau(f-p)\delta_\tau(f'-p)\delta_\tau(f-p')\delta_\tau(f'-p')P_1(|p|)P_2(|p'|).\end{aligned} \tag{9.5}$$

We can simplify this expression to the point where it is useful, however this is somewhat tricky – there is only one order in which the integrals above can be simply evaluated to yield useful approximations. We first do the integrals with respect to t and t' exactly. This gives

$$\begin{aligned}\langle N_m^* N_{m'}\rangle &= \frac{1}{4T^2}\int_{-\infty}^{\infty} df\int_{-\infty}^{\infty} df'\int_{-\infty}^{\infty} dp\int_{-\infty}^{\infty} dp'\, \tilde{Q}^*(f)\tilde{Q}(f')P_1(|p|)P_2(|p'|)e^{-i\omega_e T(m-m')/2} \\ &\quad \times \delta_T(p-p'+m\omega_e/2\pi)\delta_T(p-p'+m'\omega_e/2\pi)\delta_\tau(f-p)\delta_\tau(f'-p)\delta_\tau(f-p')\delta_\tau(f'-p').\end{aligned} \tag{9.6}$$

Now we note that the effective support of $\delta_T(f)$ extends over a very narrow range of frequencies (typically, $|f| < 10^{-7}$ Hz) compared with the effective support of $\delta_\tau(f)$ (whose support is typically $|f| < 10^{-2}$ Hz). In addition, none of the remaining integrand varies over such a narrow frequency range. So we are justified in replacing $\delta_T(p-p'+m\omega_e/2\pi)$ by the ordinary Dirac delta function $\delta(p-p'+m\omega_e/2\pi)$. This gives

$$\begin{aligned}\langle N_m^* N_{m'}\rangle &= \frac{1}{4T^2}\int_{-\infty}^{\infty} df\int_{-\infty}^{\infty} df'\, \tilde{Q}^*(f)\tilde{Q}(f')\int_{-\infty}^{\infty} dp'\, \delta_\tau(f-p')\delta_\tau(f'-p')e^{-i\omega_e T(m-m')/2} \\ &\quad \times \delta_T\left(\frac{\omega_e(m-m')}{2\pi}\right)\delta_\tau\left(f-p'+\frac{m\omega_e}{2\pi}\right)\delta_\tau\left(f'-p'+\frac{m\omega_e}{2\pi}\right)P_1\left(\left|p'-\frac{m\omega_e}{2\pi}\right|\right)P_2(|p'|).\end{aligned} \tag{9.7}$$

If we now additionally assume that the observation time T is much greater than the period of a single rotation $T_e = \frac{2\pi}{\omega_e}$ then to good approximation $\delta_T\left(\frac{\omega_e(m-m')}{2\pi}\right) \approx T\delta_{mm'}$. Thus

$$\begin{aligned}\langle N_m^* N_{m'}\rangle &= \frac{1}{4T}\delta_{mm'}\int_{-\infty}^{\infty} df\int_{-\infty}^{\infty} df'\, \tilde{Q}^*(f)\tilde{Q}(f')\int_{-\infty}^{\infty} dp\, \delta_\tau(f-p)\delta_\tau(f'-p) \\ &\quad \times \delta_\tau\left(f-p+\frac{m\omega_e}{2\pi}\right)\delta_\tau\left(f'-p+\frac{m\omega_e}{2\pi}\right)P_1\left(\left|p-\frac{m\omega_e}{2\pi}\right|\right)P_2(|p|).\end{aligned} \tag{9.8}$$

Next we note that the width of the $\delta_\tau(f)$ in frequency space is quite large compared to $m\omega_e$ provided that we restrict m to be fairly small: $|m| < T_e/\tau$. We also assume that the noise power spectrum $P_1(f)$ does not vary significantly over frequency scales of $\omega_e \approx 10^{-5}$ Hz. In this case we can neglect the shifting of the arguments by $m\omega_e$ above, obtaining

$$\begin{aligned}\langle N_m^* N_{m'}\rangle &= \frac{1}{4}\frac{\tau}{T}\delta_{mm'}\int_{-\infty}^{\infty} df\int_{-\infty}^{\infty} df'\, \tilde{Q}^*(f)\tilde{Q}(f')\delta_\tau^2(f-f')P_1(|f|)P_2(f|) \\ &= \delta_{mm'}\frac{\tau^2}{4T}\int_{-\infty}^{\infty} df\, |\tilde{Q}(f)|^2 P_1(|f|)P_2(|f|).\end{aligned} \tag{9.9}$$

Setting $m = m'$ we finally obtain an expression for the expected "squared noise" in a measurement of S_m:

$$\langle |N_m|^2 \rangle = \frac{\tau^2}{4T} \int_{-\infty}^{\infty} df\, |\tilde{Q}(f)|^2 P_1(|f|) P_2(|f|). \tag{9.10}$$

We can make use of this expression to find the optimal filter $\tilde{Q}(f)$.

The (squared) Signal-to-Noise ratio S/N for the m'th harmonic is now defined via the ratio of expected signal (magnitude squared) divided by expected (squared) noise. Making use of (5.3) for the former quantity, and (9.10) for the latter yields

$$\left(\frac{S}{N}\right)_m^2 \equiv \frac{|\langle S_m \rangle|^2}{\langle |N_m|^2 \rangle} = \frac{4T\left(\frac{8\pi}{5}\right)^2 \left| \tau \int_{-\infty}^{\infty} df \tilde{Q}(f) H(f) \sum_{\ell=|m|}^{\infty} p_{\ell m} \gamma_{\ell m}(f) \right|^2}{\tau^2 \int_{-\infty}^{\infty} df\, |\tilde{Q}(f)|^2 P_1(|f|) P_2(|f|)}. \tag{9.11}$$

Notice that the averaging time τ (which was earlier chosen in a rather arbitrary manner) drops out of this expression. Provided that the assumptions about τ (4.1) used in deriving this equation are satisfied, the actual value is irrelevant.

In order to find the optimal filter function, it is useful to introduce an inner product. For any complex functions of frequency $A(f)$ and $B(f)$, this defines a complex number which is denoted by (A, B). The definition is

$$(A, B) \equiv \int_{-\infty}^{\infty} df\, A^*(f) B(f) P_1(|f|) P_2(|f|). \tag{9.12}$$

This inner product is positive definite because (A, A) is real and non-negative, vanishing only if A is zero. In terms of this inner product, the Signal-to-Noise ratio may be written as

$$\left(\frac{S}{N}\right)_m^2 = 4T \left(\frac{8\pi}{5}\right)^2 \frac{\left| \left(\tilde{Q}, \frac{H(f)}{P_1(|f|) P_2(|f|)} \sum_{\ell=|m|}^{\infty} p^*_{\ell m} \gamma^*_{\ell m}(f) \right) \right|^2}{(\tilde{Q}, \tilde{Q})}. \tag{9.13}$$

The optimal choice of filter function $Q(f)$ for determining the m'th harmonic is the one which maximizes this ratio. The largest value is obtained by choosing

$$\tilde{Q}_m(f) = \frac{H(f)}{P_1(|f|) P_2(|f|)} \sum_{\ell=|m|}^{\infty} p^*_{\ell m} \gamma^*_{\ell m}(f). \tag{9.14}$$

Using the definition (3.11) of $H(f)$ in terms of the spectral function $\Omega_{\rm gw}(f)$, and substituting the optimal filter $\tilde{Q}_m$ into the expression for S/N yields

$$\left(\frac{S}{N}\right)_m^2 = \frac{9H_0^4}{50\pi^4} T \int_0^{\infty} df\, \frac{\Omega_{\rm gw}^2(f)}{f^6 P_1(f) P_2(f)} \left| \sum_{\ell=|m|}^{\infty} p_{\ell m} \gamma_{\ell m}(f) \right|^2. \tag{9.15}$$

For any given source of stochastic gravitational waves, one can use this formula for $(S/N)_m$ to determine the observation time T required to observe the m'th harmonic of the signal as the earth rotates relative to the cosmological frame.

In precise analogy with the analysis given in [8], the m'th harmonic is observable with 90% confidence if $(S/N)_m$ exceeds 1.65.

X. EXAMPLE: DIPOLE INDUCED BY PROPER MOTION

It is well known that the electromagnetic background radiation, generally referred to as the Cosmic Microwave Background Radiation (CMBR), is highly isotropic. The largest deviation from isotropy results from the motion of our local system (the solar system barycenter) with respect to the cosmological rest frame. Analysis of data from the Cosmic Background Explorer (COBE) satellite shows that our local system is moving with a velocity $\beta_{\rm proper} \equiv v/c = 0.001236$ in the direction $(l = 264°, b = 48°)$ in galactic coordinates, or equivalently $(\alpha = 168°, \delta = -7°)$ in celestial

coordinates. To lowest order in our proper velocity, this gives rise to an anisotropy in the CMBR described by the temperature distribution

$$T(\gamma) = T_0(1 + \beta_{\rm proper}\cos\gamma), \tag{10.1}$$

where γ is the angle between a point on the sky and the velocity vector of our local system, and $T_0 = 2.73$K is the mean temperature of the CMBR.

In this section, we address the question: "Would a corresponding dipole moment in the stochastic gravity wave background, arising from the proper motion of the solar system barycenter, be observable with either the initial or advanced LIGO detectors?" In the previous section, we calculated the Signal-to-Noise ratio for observations of the m'th harmonic S_m (with respect to the earth's rotation) of the signal (obtained by correlating two gravitational-wave detectors). This is determined entirely by the quantities

$$\begin{aligned} H_0 &= \text{Hubble expansion rate, sec}^{-1}. \\ T &= \text{Total observation time, sec.} \\ \gamma_{\ell m}(f) &= \text{Overlap reduction functions, dimensionless.} \\ \Omega_{\rm gw} &= \text{Fractional energy density in gravitational waves, dimensionless.} \\ p_{\ell m} &= \text{Normalized multipoles of gw stochastic background, dimensionless.} \\ P_i &= \text{Noise power spectral density of detector } i\text{, sec.} \end{aligned}$$

As an example, we use this formula to answer the question posed above.

Let us make the following reasonable assumptions:
(1) $\Omega_{\rm gw}(f)$ is constant in the LIGO band, and
(2) the stochastic gravitational-wave background is isotropic in the same rest frame as the CMBR.
The anisotropies in the stochastic background resulting from our proper motion are then described by

$$\sum_{\ell m} p_{\ell m} Y_{\ell m}(\bar\theta, \bar\phi) = 1 + \beta_{\rm proper}(\cos\bar\theta\cos 97^\circ + \sin\bar\theta\sin 97^\circ\cos\bar\phi) \tag{10.2}$$

where the angles above are standard spherical coordinates in the (barred) earth frame. One thus obtains the following multipole moments

$$\begin{aligned} p_{00} &= \sqrt{4\pi} \\ p_{1,-1} &= \beta_{\rm proper}\sqrt{\frac{2\pi}{3}}\sin 97^\circ \\ p_{1,0} &= \beta_{\rm proper}\sqrt{\frac{4\pi}{3}}\cos 97^\circ \\ p_{1,1} &= -\beta_{\rm proper}\sqrt{\frac{2\pi}{3}}\sin 97^\circ \\ p_{\ell m} &= 0 \quad \text{for } \ell > 1. \end{aligned} \tag{10.3}$$

To detect this signal, the optimal filter functions are

$$Q_m(f) = C_m \frac{1}{f^3 P_1(|f|) P_2(|f|)} \sum_{\ell=|m|}^{\infty} p^*_{\ell m}\gamma^*_{\ell m}, \tag{10.4}$$

where C_m is an (irrelevant) normalization constant. Making use of the optimal filter functions Q_0 and Q_1 for the monopole and dipole terms, we can make predictions about how large $\Omega_{\rm gw}$ needs to be in order that S_0 and S_1 are observable with a given level of confidence in a given observation time.

We can express the sensitivity of a search for the m'th harmonic in terms of the minimum value of $\Omega_{\rm gw}$ necessary to observe it with 90% confidence. For 90% confidence we need a Signal-to-Noise of 1.65. The minimum value of $\Omega_{\rm gw}$ is then given for the m'th harmonic by

$$\Omega^{(m)}_{90\%} = (1.65)\sqrt{\frac{9}{50}}\frac{H_0^2}{\pi^2}T\left[\int_0^\infty \frac{df}{f^6 P_1(f)P_2(f)}\left|\sum_{\ell=|m|}^{\infty} p_{\ell m}\gamma_{\ell m}(f)\right|^2\right]^{-\frac{1}{2}}. \tag{10.5}$$

These values are shown in Table I for the initial and advanced LIGO detectors. We note that there are potential sources of sufficient intensity that a dipole might be observable with the advanced LIGO detector. These include stochastic backgrounds due to cosmic strings or to a population of unresolved cosmological-distance supernovae.

TABLE I. Sensitivity of Initial and Advanced LIGO detectors to a dipole term in the gravitational stochastic background, arising from motion of our local system. This table shows the intensity of stochastic background required to detect either the monopole (S_0) or dipole (S_1) term in the signal, with 90% confidence, in one year of observation.

	Initial LIGO	Advanced LIGO
Monopole (m=0)	$\Omega_{90\%} = 1.6 \times 10^{-6} h_{100}^{-2}$	$\Omega_{90\%} = 1.6 \times 10^{-11} h_{100}^{-2}$
Dipole (m=1)	$\Omega_{90\%} = 2.5 \times 10^{-3} h_{100}^{-2}$	$\Omega_{90\%} = 5.3 \times 10^{-8} h_{100}^{-2}$

XI. FILTER NORMALIZATIONS AND SIGNAL STRENGTHS

Specific models for an anisotropic background predict signal harmonics S_m of definite amplitudes and phases. The phase of a given S_m depends upon the chosen origin of time; shifting the origin of time changes the phase of S_m but not its amplitude. In order to falsify or confirm a particular anisotropic model, one needs to predict the set of complex numbers S_m. However these numbers depend upon the normalization C_m of the optimal filter function $Q_m(f)$ so in order to make predictions, we need to adopt a convention for these.

We have already chosen optimal filters for which the expected value of S_m is real. At least upon first inspection, there do not appear to be any very convenient choices for the overall scale of normalization. Here, for illustrative purposes we adopt (what appears to us as) the least disagreeable of these. *We choose the normalization C_m so that the expected amplitude of the noise² is unity:* $\langle |N_m|^2 \rangle = 1$. We also assume that C_m is positive and real. Note that with this choice, the "signal" is dimensionless. From equation (9.10) this gives

$$C_m = \frac{2\sqrt{T}}{\tau} \left[\int_{-\infty}^{\infty} \frac{df}{P_1(|f|)P_2(|f|)} \left| \sum_{\ell=|m|}^{\infty} p_{\ell m} \gamma_{\ell m}(f) \right|^2 \right]^{-\frac{1}{2}} . \tag{11.1}$$

Having chosen a normalization, we can list the expected signals for a given detector. If the actual signal value exceeds 1.65 then it has been detected with 90% confidence. For example, in the case of the dipole source just discussed, the expected signals are given by (5.3) as

$$\langle S_m \rangle = \frac{3H_0^2}{10\pi^2} \sqrt{T} \Omega_{\rm gw} \left[\int_{-\infty}^{\infty} \frac{df}{P_1(|f|)P_2(|f|)} \left| \sum_{\ell=|m|}^{\infty} p_{\ell m} \gamma_{\ell m}(f) \right|^2 \right]^{\frac{1}{2}} . \tag{11.2}$$

Evaluating this for our previous example gives:

$$\langle S_0 \rangle = \begin{cases} 1.65 \sqrt{\dfrac{T}{1\ \text{year}}} \dfrac{\Omega_{\rm gw} h_{100}^2}{1.6 \times 10^{-6}} & \text{for initial LIGO} \\ 1.65 \sqrt{\dfrac{T}{1\ \text{year}}} \dfrac{\Omega_{\rm gw} h_{100}^2}{1.6 \times 10^{-11}} & \text{for advanced LIGO} \end{cases}$$

$$\langle S_1 \rangle = \begin{cases} 1.65 \sqrt{\dfrac{T}{1\ \text{year}}} \dfrac{\Omega_{\rm gw} h_{100}^2}{2.5 \times 10^{-3}} & \text{for initial LIGO} \\ 1.65 \sqrt{\dfrac{T}{1\ \text{year}}} \dfrac{\Omega_{\rm gw} h_{100}^2}{5.3 \times 10^{-8}} & \text{for advanced LIGO} \end{cases}$$

$$\langle S_m \rangle = 0 \text{ for } m \geq 2 \tag{11.3}$$

XII. GALACTIC SOURCES

In this section we consider the possibility of detecting anisotropies in the stochastic gravitational wave background assuming that this background either originates in, or is scattered in the same way as, the luminous matter in our galaxy, and for sources distributed in the same way as the galactic halo. It appears very unlikely that in the LIGO/VIRGO/GEO frequency band there are any sources of a stochastic gravitational-wave background distributed in this way. However the absence of such harmonics would be one way to demonstrate that a stochastic background had extra-galactic origin.

For the distribution of luminous matter in the galaxy we consider a set of three models constructed by Kent, Dame and Fazio [13] to model 2·4 μm data from the Infrared Telescope taken as part of the *Spacelab 2* mission. These models all assume cylindrical symmetry and take the total luminosity to consist of two components, one, $\nu_D(r,z)$, modeling the disk and the other, $\nu_B(r,z)$, modeling the central bulge, where r and z denote cylindrical polar coordinates based at the center of the Galaxy.

The first model, which we refer to as KDF1, takes

$$\nu_D(r,z) = \mu_D e^{-r/h_r} \frac{\operatorname{sech}^2\left(z/(2h_z)\right)}{4h_z} \tag{12.1}$$

$$\nu_B(r,z) = \mu_B \frac{K_0\left(\left[r^4 + \left(z/(1-\epsilon_B)\right)^4\right]^{1/4}/h_B\right)}{\pi h_B} \tag{12.2}$$

where $\mu_D = 1072\, L_\odot \mathrm{pc}^{-2}$, $h_r = 2775\,\mathrm{pc}$, $h_z = 121\,\mathrm{pc}$, $\mu_B = 6208\, L_\odot \mathrm{pc}^{-2}$, $h_B = 634\,\mathrm{pc}$ and $\epsilon_B = 0.26\,\mathrm{pc}$.

The second model (KDF2) takes

$$\nu_D(r,z) = \mu_D e^{-r/h_r} \frac{\exp\left(-\left|z/(2h_z)\right|\right)}{2h_z} \tag{12.3}$$

$$\nu_B(r,z) = \mu_B \frac{K_0\left(\left[r^4 + \left(z/(1-\epsilon_B)\right)^4\right]^{1/4}/h_B\right)}{\pi h_B} \tag{12.4}$$

where $\mu_D = 1208\, L_\odot \mathrm{pc}^{-2}$, $h_r = 2694\,\mathrm{pc}$, $h_z = 204\,\mathrm{pc}$, $\mu_B = 7710\, L_\odot \mathrm{pc}^{-2}$, $h_B = 500\,\mathrm{pc}$ and $\epsilon_B = 0.19\,\mathrm{pc}$.

The third model (KDF3) takes

$$\nu_D(r,z) = \mu_D e^{-r/h_r} \frac{\exp\left(-\left|z/(2h_z(r))\right|\right)}{2h_z(r)} \tag{12.5}$$

$$\nu_B(r,z) = \mu_B \frac{K_0\left(\left[r^4 + \left(z/(1-\epsilon_B)\right)^4\right]^{1/4}/h_B\right)}{\pi h_B} \tag{12.6}$$

where $\mu_D = 978\, L_\odot \mathrm{pc}^{-2}$, $h_r = 3001\,\mathrm{pc}$, $\mu_B = 7395\, L_\odot \mathrm{pc}^{-2}$, $h_B = 667\,\mathrm{pc}$, $\epsilon_B = 0.39\,\mathrm{pc}$ and $h_z(r)$ is now a function given by

$$h_z(r) = \begin{cases} h_{\min} & r < r_{\min} \\ h_{\min} + (h_\odot - h_{\min})\dfrac{(r - r_{\min})}{(r_\odot - r_{\min})} & r \geq r_{\min} \end{cases} \tag{12.7}$$

with $h_{\min} = 165\,\mathrm{pc}$, $r_{\min} = 5300\,\mathrm{pc}$, $h_\odot = 247\,\mathrm{pc}$ and $r_\odot = 8000\,\mathrm{pc}$, the last two quantities being the height of the galactic disk at the position of the Sun and the distance of the Sun from the Galactic center, respectively.

Finally, as a model for the galactic halo we take the model of Young [15]

$$\nu_{\mathrm{halo}} = \mu_{\mathrm{halo}} \frac{\exp\left[-7.669(R/R_e)^{1/4}\right]}{(R/R_e)^{7/8}} \qquad R > 0.2R_e \tag{12.8}$$

where R denotes the distance from the Galactic center and $R_e = 2700\,\mathrm{pc}$.

The final piece of information we need before we can calculate the multipole moments $p_{\ell m}$ for such a distribution is the direction to the Galactic center and the orientation of the Galaxy. It is standard to express this in terms of the equatorial coordinate system [14] in which the z-axis is taken along the Celestial North pole, the x-axis is taken in the direction of the (1950) vernal equinox. $90° - \delta$ and α are taken as the spherical polar coordinates corresponding to these axes. In terms of these, the direction to the Galactic center is given by

$$\alpha = 265.6° \qquad \delta = -28.9°, \tag{12.9}$$

and the direction of the Galactic North pole by

$$\alpha = 192.25° \qquad \delta = 27.4°. \tag{12.10}$$

We take the equatorial coordinate system to define our Cosmic frame. We now determine $P(\hat{\Omega})$ by choosing a direction $\hat{\Omega}$ and integrating the intensity along that direction. In this way we arrive at $p_{\ell m}$ for each model and hence by Eq. (10.5) the minimum value of Ω_{gw} necessary for detection of each multipole. To ensure convergence of the sum in this case it was necessary to include contributions to the sum for ℓ up to of order 100 (dependent on m). Tables II and III shows the intensity of the stochastic background distributed in this way required to detect multipole moments from $m = 0$ to $m = 24$ for the four models with 90% confidence in one year of observation for Inianital and Advanced LIGO respectively.

TABLE II. Sensitivity of the Initial LIGO detector to the first 25 multipoles in the gravitational stochastic background, assumed to follow the luminosity of the Galaxy or Galactic halo. This table shows the intensity of stochastic background required to detect the multipole S_m with 90% confidence in one year of observation.

m	$\Omega_{90\%}$ KDF1	$\Omega_{90\%}$ KDF2	$\Omega_{90\%}$ KDF3	$\Omega_{90\%}$ Halo
0	$1.4 \times 10^{-5} h_{100}^{-2}$	$1.4 \times 10^{-5} h_{100}^{-2}$	$1.4 \times 10^{-5} h_{100}^{-2}$	$3.9 \times 10^{-3} h_{100}^{-2}$
1	$1.4 \times 10^{-5} h_{100}^{-2}$	$1.3 \times 10^{-5} h_{100}^{-2}$	$1.3 \times 10^{-5} h_{100}^{-2}$	$3.4 \times 10^{-3} h_{100}^{-2}$
2	$1.9 \times 10^{-5} h_{100}^{-2}$	$1.9 \times 10^{-5} h_{100}^{-2}$	$1.8 \times 10^{-5} h_{100}^{-2}$	$3.6 \times 10^{-3} h_{100}^{-2}$
3	$3.0 \times 10^{-5} h_{100}^{-2}$	$2.9 \times 10^{-5} h_{100}^{-2}$	$2.9 \times 10^{-5} h_{100}^{-2}$	$4.2 \times 10^{-3} h_{100}^{-2}$
4	$4.6 \times 10^{-5} h_{100}^{-2}$	$4.4 \times 10^{-5} h_{100}^{-2}$	$4.6 \times 10^{-5} h_{100}^{-2}$	$5.0 \times 10^{-3} h_{100}^{-2}$
5	$7.3 \times 10^{-5} h_{100}^{-2}$	$6.9 \times 10^{-5} h_{100}^{-2}$	$7.1 \times 10^{-5} h_{100}^{-2}$	$6.1 \times 10^{-3} h_{100}^{-2}$
6	$7.8 \times 10^{-5} h_{100}^{-2}$	$7.4 \times 10^{-5} h_{100}^{-2}$	$7.5 \times 10^{-5} h_{100}^{-2}$	$8.1 \times 10^{-3} h_{100}^{-2}$
7	$8.6 \times 10^{-5} h_{100}^{-2}$	$8.0 \times 10^{-5} h_{100}^{-2}$	$8.3 \times 10^{-5} h_{100}^{-2}$	$1.2 \times 10^{-2} h_{100}^{-2}$
8	$1.2 \times 10^{-4} h_{100}^{-2}$	$1.1 \times 10^{-4} h_{100}^{-2}$	$1.1 \times 10^{-4} h_{100}^{-2}$	$1.7 \times 10^{-2} h_{100}^{-2}$
9	$2.0 \times 10^{-4} h_{100}^{-2}$	$2.0 \times 10^{-4} h_{100}^{-2}$	$1.9 \times 10^{-4} h_{100}^{-2}$	$2.7 \times 10^{-2} h_{100}^{-2}$
10	$3.6 \times 10^{-4} h_{100}^{-2}$	$4.0 \times 10^{-4} h_{100}^{-2}$	$3.5 \times 10^{-4} h_{100}^{-2}$	$4.3 \times 10^{-2} h_{100}^{-2}$
11	$5.0 \times 10^{-4} h_{100}^{-2}$	$5.2 \times 10^{-4} h_{100}^{-2}$	$4.9 \times 10^{-4} h_{100}^{-2}$	$7.0 \times 10^{-2} h_{100}^{-2}$
12	$6.3 \times 10^{-4} h_{100}^{-2}$	$6.2 \times 10^{-4} h_{100}^{-2}$	$6.2 \times 10^{-4} h_{100}^{-2}$	$1.2 \times 10^{-1} h_{100}^{-2}$
13	$9.2 \times 10^{-4} h_{100}^{-2}$	$8.9 \times 10^{-4} h_{100}^{-2}$	$9.0 \times 10^{-4} h_{100}^{-2}$	$2.0 \times 10^{-1} h_{100}^{-2}$
14	$1.5 \times 10^{-3} h_{100}^{-2}$	$1.5 \times 10^{-3} h_{100}^{-2}$	$1.5 \times 10^{-3} h_{100}^{-2}$	$3.1 \times 10^{-1} h_{100}^{-2}$
15	$2.4 \times 10^{-3} h_{100}^{-2}$	$2.5 \times 10^{-3} h_{100}^{-2}$	$2.4 \times 10^{-3} h_{100}^{-2}$	$5.0 \times 10^{-1} h_{100}^{-2}$
16	$3.6 \times 10^{-3} h_{100}^{-2}$	$3.7 \times 10^{-3} h_{100}^{-2}$	$3.6 \times 10^{-3} h_{100}^{-2}$	$7.8 \times 10^{-1} h_{100}^{-2}$
17	$5.1 \times 10^{-3} h_{100}^{-2}$	$5.2 \times 10^{-3} h_{100}^{-2}$	$5.1 \times 10^{-3} h_{100}^{-2}$	$1.2 \times 10^{0} h_{100}^{-2}$
18	$7.3 \times 10^{-3} h_{100}^{-2}$	$7.2 \times 10^{-3} h_{100}^{-2}$	$7.1 \times 10^{-3} h_{100}^{-2}$	$1.7 \times 10^{0} h_{100}^{-2}$
19	$1.0 \times 10^{-2} h_{100}^{-2}$	$1.0 \times 10^{-2} h_{100}^{-2}$	$1.0 \times 10^{-2} h_{100}^{-2}$	$2.4 \times 10^{0} h_{100}^{-2}$
20	$1.4 \times 10^{-2} h_{100}^{-2}$	$1.4 \times 10^{-2} h_{100}^{-2}$	$1.4 \times 10^{-2} h_{100}^{-2}$	$3.6 \times 10^{0} h_{100}^{-2}$
21	$2.1 \times 10^{-2} h_{100}^{-2}$	$2.1 \times 10^{-2} h_{100}^{-2}$	$2.0 \times 10^{-2} h_{100}^{-2}$	$5.0 \times 10^{0} h_{100}^{-2}$
22	$2.9 \times 10^{-2} h_{100}^{-2}$	$2.9 \times 10^{-2} h_{100}^{-2}$	$2.8 \times 10^{-2} h_{100}^{-2}$	$6.5 \times 10^{0} h_{100}^{-2}$
23	$4.0 \times 10^{-2} h_{100}^{-2}$	$3.9 \times 10^{-2} h_{100}^{-2}$	$3.8 \times 10^{-2} h_{100}^{-2}$	$8.9 \times 10^{0} h_{100}^{-2}$
24	$5.1 \times 10^{-2} h_{100}^{-2}$	$5.0 \times 10^{-2} h_{100}^{-2}$	$4.9 \times 10^{-2} h_{100}^{-2}$	$1.2 \times 10^{1} h_{100}^{-2}$

TABLE III. Sensitivity of the Advanced LIGO detector to the first 25 multipoles in the gravitational stochastic background, assumed to follow the luminosity of the Galaxy or Galactic halo. This table shows the intensity of stochastic background required to detect the multipole S_m with 90% confidence in one year of observation.

m	$\Omega_{90\%}$ KDF1	$\Omega_{90\%}$ KDF2	$\Omega_{90\%}$ KDF3	$\Omega_{90\%}$ Halo
0	$1.8 \times 10^{-10} h_{100}^{-2}$	$1.7 \times 10^{-10} h_{100}^{-2}$	$1.7 \times 10^{-10} h_{100}^{-2}$	$6.7 \times 10^{-8} h_{100}^{-2}$
1	$4.8 \times 10^{-10} h_{100}^{-2}$	$4.7 \times 10^{-10} h_{100}^{-2}$	$4.7 \times 10^{-10} h_{100}^{-2}$	$7.8 \times 10^{-8} h_{100}^{-2}$
2	$1.1 \times 10^{-9} h_{100}^{-2}$	$1.0 \times 10^{-9} h_{100}^{-2}$	$1.0 \times 10^{-9} h_{100}^{-2}$	$1.1 \times 10^{-7} h_{100}^{-2}$
3	$5.3 \times 10^{-9} h_{100}^{-2}$	$5.0 \times 10^{-9} h_{100}^{-2}$	$5.4 \times 10^{-9} h_{100}^{-2}$	$2.6 \times 10^{-7} h_{100}^{-2}$
4	$6.4 \times 10^{-9} h_{100}^{-2}$	$6.0 \times 10^{-9} h_{100}^{-2}$	$6.3 \times 10^{-9} h_{100}^{-2}$	$6.4 \times 10^{-7} h_{100}^{-2}$
5	$1.1 \times 10^{-8} h_{100}^{-2}$	$1.0 \times 10^{-8} h_{100}^{-2}$	$1.0 \times 10^{-8} h_{100}^{-2}$	$1.6 \times 10^{-6} h_{100}^{-2}$
6	$3.1 \times 10^{-8} h_{100}^{-2}$	$3.0 \times 10^{-8} h_{100}^{-2}$	$3.0 \times 10^{-8} h_{100}^{-2}$	$4.4 \times 10^{-6} h_{100}^{-2}$
7	$1.2 \times 10^{-7} h_{100}^{-2}$	$1.3 \times 10^{-7} h_{100}^{-2}$	$1.2 \times 10^{-7} h_{100}^{-2}$	$1.3 \times 10^{-5} h_{100}^{-2}$
8	$2.4 \times 10^{-7} h_{100}^{-2}$	$2.4 \times 10^{-7} h_{100}^{-2}$	$2.4 \times 10^{-7} h_{100}^{-2}$	$2.7 \times 10^{-5} h_{100}^{-2}$
9	$4.5 \times 10^{-7} h_{100}^{-2}$	$4.2 \times 10^{-7} h_{100}^{-2}$	$4.5 \times 10^{-7} h_{100}^{-2}$	$6.3 \times 10^{-5} h_{100}^{-2}$
10	$1.1 \times 10^{-6} h_{100}^{-2}$	$1.0 \times 10^{-6} h_{100}^{-2}$	$1.1 \times 10^{-6} h_{100}^{-2}$	$1.3 \times 10^{-4} h_{100}^{-2}$
11	$3.0 \times 10^{-6} h_{100}^{-2}$	$3.3 \times 10^{-6} h_{100}^{-2}$	$3.1 \times 10^{-6} h_{100}^{-2}$	$2.6 \times 10^{-4} h_{100}^{-2}$
12	$5.5 \times 10^{-6} h_{100}^{-2}$	$5.5 \times 10^{-6} h_{100}^{-2}$	$5.7 \times 10^{-6} h_{100}^{-2}$	$4.5 \times 10^{-4} h_{100}^{-2}$
13	$8.3 \times 10^{-6} h_{100}^{-2}$	$7.7 \times 10^{-6} h_{100}^{-2}$	$8.7 \times 10^{-6} h_{100}^{-2}$	$7.7 \times 10^{-4} h_{100}^{-2}$
14	$1.5 \times 10^{-5} h_{100}^{-2}$	$1.5 \times 10^{-5} h_{100}^{-2}$	$1.6 \times 10^{-5} h_{100}^{-2}$	$1.3 \times 10^{-3} h_{100}^{-2}$
15	$3.0 \times 10^{-5} h_{100}^{-2}$	$3.2 \times 10^{-5} h_{100}^{-2}$	$3.1 \times 10^{-5} h_{100}^{-2}$	$2.0 \times 10^{-3} h_{100}^{-2}$
16	$4.4 \times 10^{-5} h_{100}^{-2}$	$4.4 \times 10^{-5} h_{100}^{-2}$	$4.7 \times 10^{-5} h_{100}^{-2}$	$3.0 \times 10^{-3} h_{100}^{-2}$
17	$6.0 \times 10^{-5} h_{100}^{-2}$	$5.6 \times 10^{-5} h_{100}^{-2}$	$6.4 \times 10^{-5} h_{100}^{-2}$	$4.4 \times 10^{-3} h_{100}^{-2}$
18	$9.4 \times 10^{-5} h_{100}^{-2}$	$9.0 \times 10^{-5} h_{100}^{-2}$	$1.0 \times 10^{-4} h_{100}^{-2}$	$6.4 \times 10^{-3} h_{100}^{-2}$
19	$1.6 \times 10^{-4} h_{100}^{-2}$	$1.6 \times 10^{-4} h_{100}^{-2}$	$1.7 \times 10^{-4} h_{100}^{-2}$	$9.0 \times 10^{-3} h_{100}^{-2}$
20	$2.1 \times 10^{-4} h_{100}^{-2}$	$2.1 \times 10^{-4} h_{100}^{-2}$	$2.3 \times 10^{-4} h_{100}^{-2}$	$1.2 \times 10^{-2} h_{100}^{-2}$
21	$2.7 \times 10^{-4} h_{100}^{-2}$	$2.5 \times 10^{-4} h_{100}^{-2}$	$3.0 \times 10^{-4} h_{100}^{-2}$	$1.7 \times 10^{-2} h_{100}^{-2}$
22	$3.9 \times 10^{-4} h_{100}^{-2}$	$3.7 \times 10^{-4} h_{100}^{-2}$	$4.2 \times 10^{-4} h_{100}^{-2}$	$2.3 \times 10^{-2} h_{100}^{-2}$
23	$5.9 \times 10^{-4} h_{100}^{-2}$	$5.8 \times 10^{-4} h_{100}^{-2}$	$6.4 \times 10^{-4} h_{100}^{-2}$	$3.0 \times 10^{-2} h_{100}^{-2}$
24	$7.8 \times 10^{-4} h_{100}^{-2}$	$7.5 \times 10^{-4} h_{100}^{-2}$	$8.4 \times 10^{-4} h_{100}^{-2}$	$3.9 \times 10^{-2} h_{100}^{-2}$

XIII. CONCLUSION

In this paper, we have shown how the signals from a pair of gravitational wave detectors may be analyzed to search for anisotropies in the stochastic gravitational wave background. We have shown how the correlation between two detectors may be determined with an averaging time short compared to a day but long compared to the light travel time between the detectors, and how this correlation may be decomposed into harmonics of the Earth's rotation. We have calculated the signal-to-noise ratios associated with such measurements, and shown that certain types of anisotropy might reasonably be detected with instruments that will be available in the not-too-distant future.

At this point, it is difficult to proceed further without a more detailed knowledge of the instrumental data that will be forthcoming. The results given in this paper make it straightforward to predict the expected harmonic amplitudes S_m of the detector correlation for a given anisotropic distribution $p_{\ell m}$ of gravitational wave background. It is more difficult to go the other way. This would involve using a given set of observed harmonic amplitudes S_m to obtain the values of (or constraints on) the $p_{\ell m}$. There are a variety of fitting techniques that could be used – making the appropriate choice will probably require real data.

ACKNOWLEDGMENTS

This work has been partially supported by the National Science Foundation grant PHY95-07740, by the Forbairt grant SC/96/712, and by the LIGO visitors program PHY92-10038.

APPENDIX: ANALYTIC EVALUATION OF INTEGRALS

In this appendix we derive a closed form expression for the integral

$$\mathcal{I}_{\ell k}(x) = \int_{-1}^{1} du\, \mathrm{e}^{iux} \mathrm{P}_\ell^k(u) u^N (1-u^2)^{|k|/2} \tag{A1}$$

where N is a non-negative integer.

First we note that

$$\mathrm{P}_\ell^{-k}(u) = (-1)^k \frac{(l-k)!}{(l+k)!} \mathrm{P}_\ell^k(u) \tag{A2}$$

so that it is only necessary to deal with the case $k \geq 0$. For $k \geq 0$ we have

$$\mathrm{P}_\ell^k(u) = (-1)^k (1-u^2)^{k/2} \frac{d^k}{du^k} P_\ell(u) \tag{A3}$$

giving

$$\mathcal{I}_{\ell k}(x) = (-1)^k \int_{-1}^{1} du\, \mathrm{e}^{iux} u^N (1-u^2)^k \frac{d^k}{du^k} P_\ell(u). \tag{A4}$$

The presence of the factor $(1-u^2)^k$ now ensures that when we integrate by parts k times no boundary terms appear so that

$$\mathcal{I}_{\ell k}(x) = \int_{-1}^{1} du\, P_\ell(u) \frac{d^k}{du^k} \left[\mathrm{e}^{iux} u^N (1-u^2)^k\right]. \tag{A5}$$

The derivative can be expanded by the Liebniz rule to give

$$\sum_{r=0}^{k} (ix)^r p_{N+k-r}(u) \mathrm{e}^{iux} \tag{A6}$$

where $p_{N+k-r}(u)$ is a polynomial of degree $N+k-r$. Our problem is thus reduced to that of finding

$$\mathcal{J}_{\ell M}(x) = \int_{-1}^{1} du\, \mathrm{e}^{iux} u^M P_\ell(u). \tag{A7}$$

For $M = 0$ this is an elementary integral given by

$$\mathcal{J}_{\ell 0}(x) = 2 i^\ell j_\ell(x) \tag{A8}$$

where $j_\ell(x)$ denotes the spherical Bessel function of order ℓ [16]. Higher M values may then be obtained by differentiation

$$\mathcal{J}_{\ell M}(x) = (-i)^M \frac{d^M}{dx^M} \mathcal{J}_{\ell 0}(x). \tag{A9}$$

These derivatives may in turn be expressed back in terms of (undifferentiated) spherical Bessel functions using the relations [16]

$$\frac{d}{dx} j_\ell(x) = \frac{1}{2\ell+1} \left[\ell j_{\ell-1}(x) - (\ell+1) j_{\ell+1}(x)\right] \tag{A10}$$

$$= \frac{\ell}{x} j_\ell(x) - j_{\ell+1}(x). \tag{A11}$$

[1] A. Abramovici, et. al., Science, **256**, 325 (1992).
[2] B. Caron, et. al., in *Gravitational Wave Experiments, proceedings of the Edoardo Amaldi Conference*, 86 (World Scientific, Singapore, 1995).
[3] K. Danzmann, et. al, in *Gravitational Wave Experiments, proceedings of the Edoardo Amaldi Conference*, 100 (World Scientific, Singapore, 1995).
[4] K. Tsubono, et. al, in *Gravitational Wave Experiments, proceedings of the Edoardo Amaldi Conference*, 112 (World Scientific, Singapore, 1995).
[5] Michelson, Mon. Not. Roy. Astron. Soc., **227**, 933 (1987).
[6] N. Christensen, Phys. Rev. D **46**, 5250 (1992).
[7] E. Flanagan, Phys. Rev. D **48**, 2389 (1993). Note that the second term on the right hand side of equation (b6) should read $-10j_1(\alpha)$ rather than $-2j_1(\alpha)$, and that the sliding delay function shown in Figure 2 on page 2394 is incorrect.
[8] B. Allen, *The stochastic gravity-wave background: sources and detection*, in Proceedings of the Les Houches School on Astrophysical Sources of Gravitational Radiation, eds. J.A. Marck and J.P. Lasota, (Cambridge University Press, Cambridge, England,to be published)
[9] G. Arfken, *Mathematical methods for physicists*, third edition, (Academic Press, Orlando, 1985). Note that this reference uses different convensions for the normalization of Associated Legendre functions P_ℓ^m than the other references here, however the spherical harmonic functions $Y_{\ell m}$ are identical to the other references.
[10] M. E. Rose, *Elementary theory of angular momentum*, (John Wiley, New York, 1957).
[11] I. S. Gradshteyn and I.M. Ryzhik, *Table of integrals, series and products*, fourth edition, (Academic Press, San Diego, 1980).
[12] G.F. Smoot and D. Scott, Phys. Rev. D **54**, 118 (1996).
[13] S.M. Kent, T.M. Dame and G. Fazio, Ap.J., **378**, 131 (1991).
[14] D. Mihalas and J. Binney, *Galactic Astronomy*, second edition, (W.H. Freeman, San Francisco, 1981)
[15] P.J. Young, Astron.J., **81**, 807 (1976).
[16] J.D. Jackson, *Classical Electrodynamics*, second edition, (John Wiley, New York, 1975).

Time Frequency Search of GW Chirps

M. Feo, V. Pierro, I.M. Pinto, M. Ricciardi

a) A Rigorous Framework (1994-1996)

- graceful time-shifting and windowing properties of WVT -> time series splitting and splicing;
- uniform asymptotic expansion of WVT in $cT_o/\pi r_g$; proof that IFL = support of principal part of WVT irrespective of PN-order;
- study of statistical properties of WVT of noise;
- ML extraction of IFL (outperforms barycentric algo);
- 2D Kolmogorov-Smirnov data-sieving;

... chirp-model *independent; plus:*

- Generalized Hough algorithm for parameter estimation;
- Implementation of matched filter as line integral in t-f plane along estimated IFL.

a) A FORTRAN package:

- Modular
- Well documented
- Flexible

(Submitted to Phys. Rev. D, 1996)

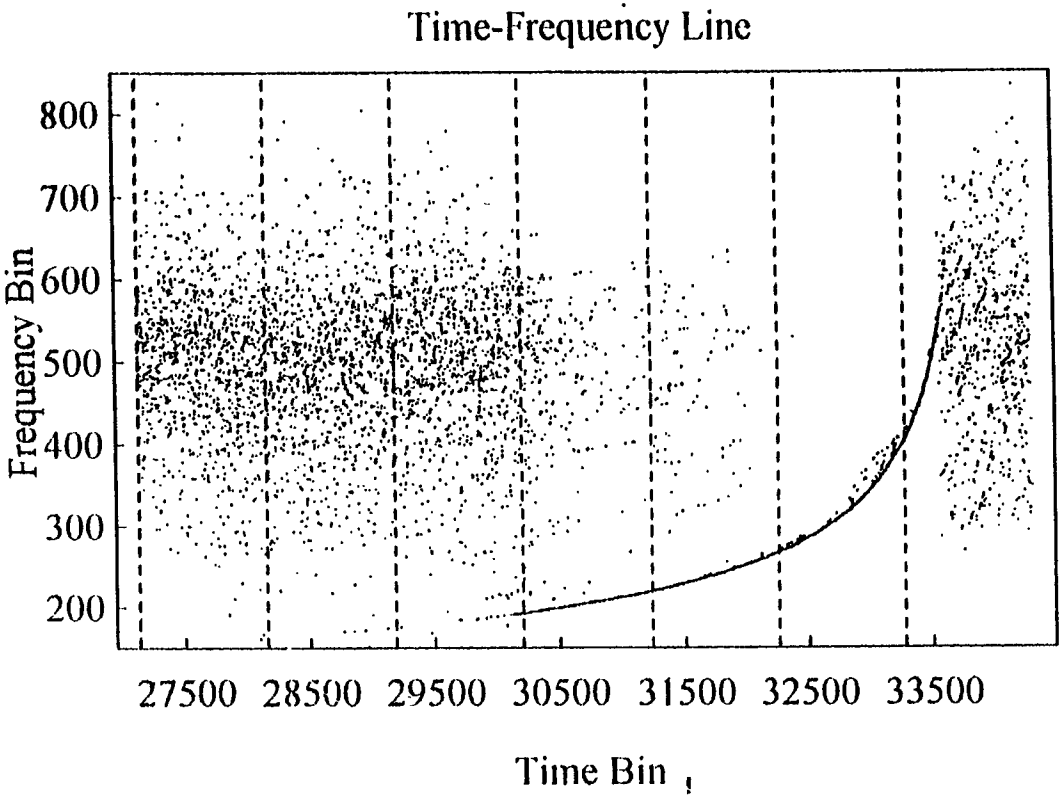
Time-Frequency Line
800
700
600
500
400
300
200
Frequency Bin
27500
28500
29500
30500
31500
32500
33500
Time Bin

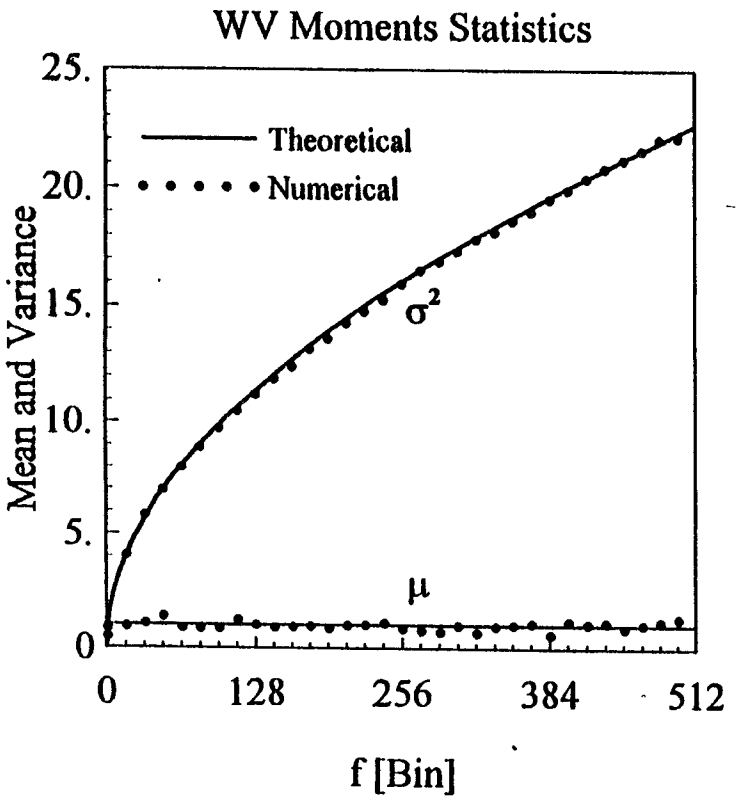
WV Moments Statistics
25.
20.
15.
10.
5.
0
Mean and Variance
Theoretical
Numerical
σ²
μ
0
128
256
384
512
f [Bin]

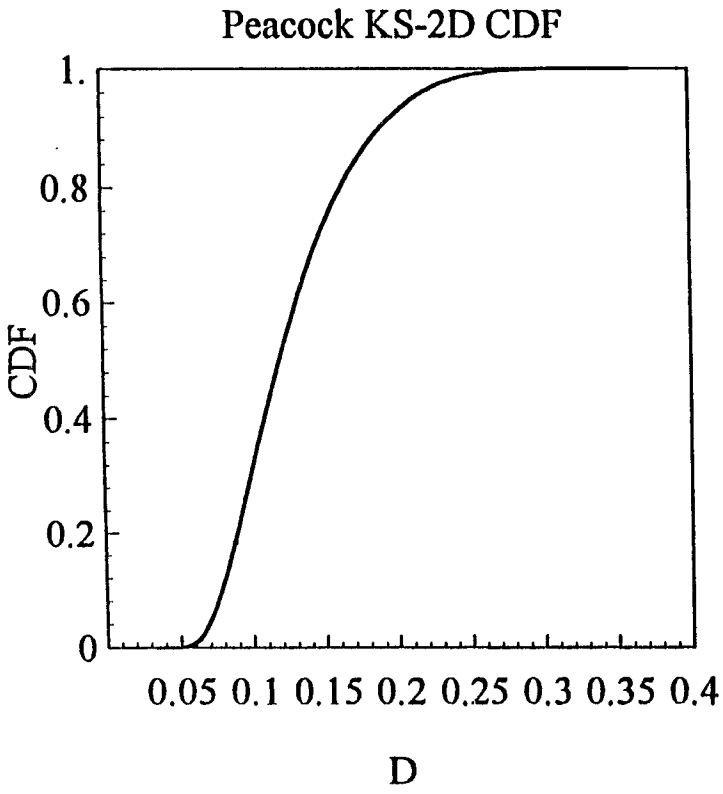
Peacock KS-2D CDF
1.
0.8
0.6
0.4
0.2
0
CDF
0.05 0.1 0.15 0.2 0.25 0.3 0.35 0.4
D

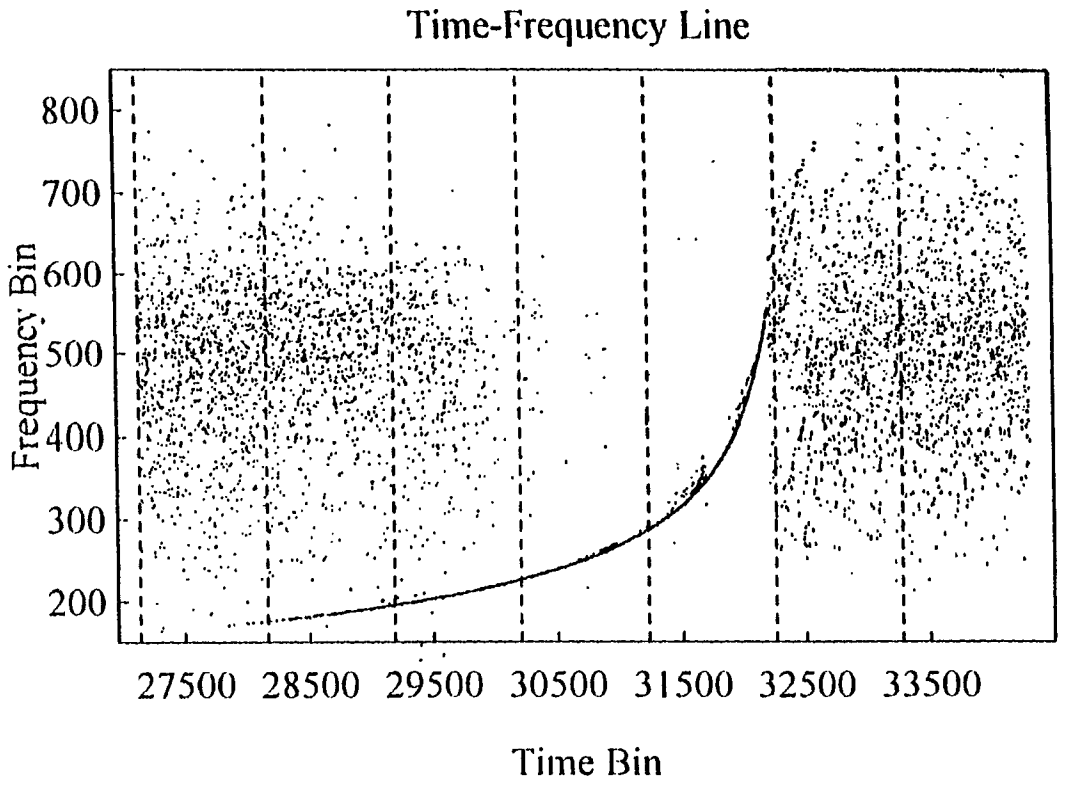
Time-Frequency Line
800
700
600
500
400
300
200
Frequency Bin
27500
28500
29500
30500
31500
32500
33500
Time Bin

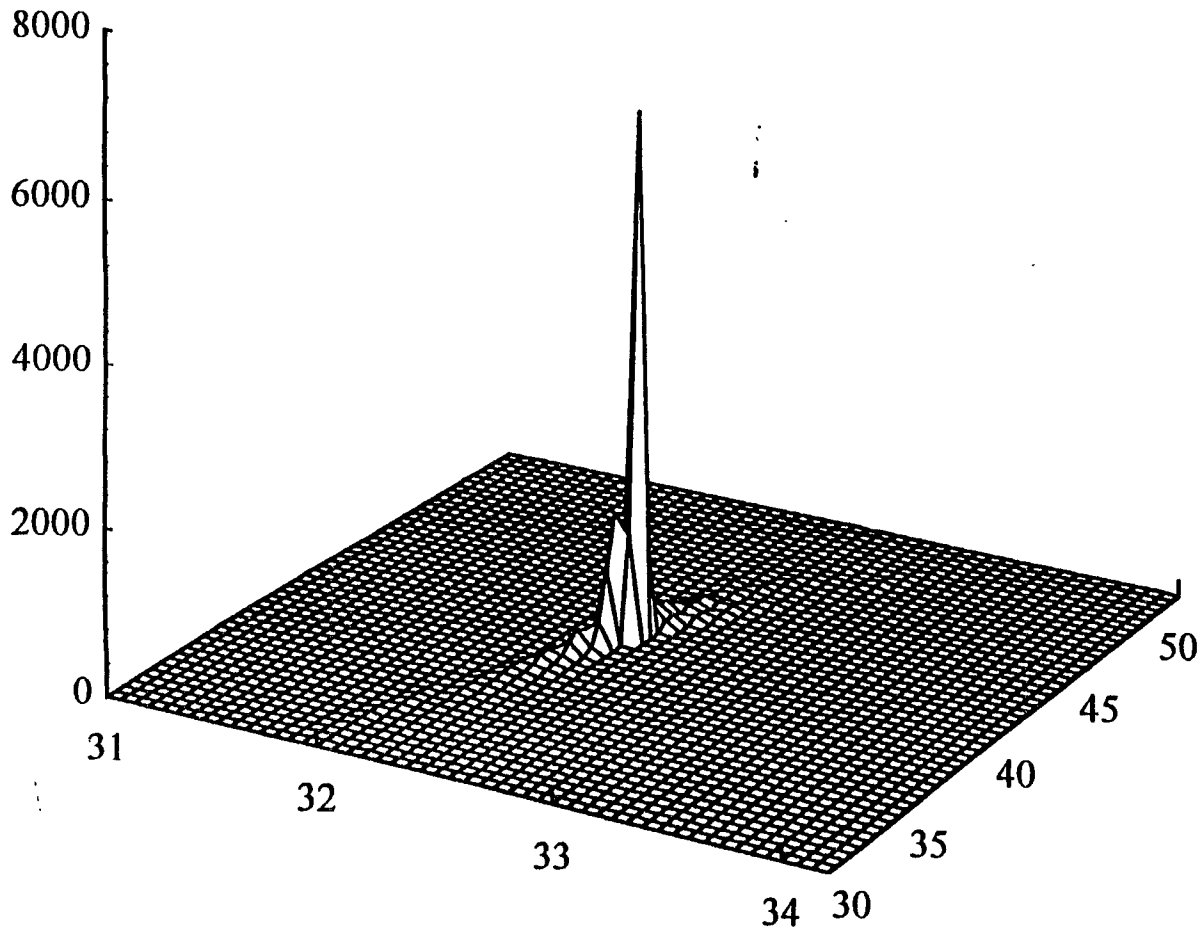
8000
6000
4000
2000
0
31
32
33
34
30
35
40
45
50

Evaluation of a Stochastic Resonance Based Detectors

V. Galdi, V. Pierro, I.M. Pinto

Comprehensive analysis of (1st order) bistable system driven by harmonic + gaussian input; special emphasis on:

- detection characteristics (ROC)
- comparison with MF in terms of ROC & comput. burden
- design optimization criteria

Main results:

- strobed strategies;
- choice of output observables ->
  - non parametric (sign counting)
  - parametric (1st moment);
- limits of adiabatic approximation;
- existence of Benzi's SR;
- comparison with MF ->
  - performance generally worse
  - computational burden might be less;
- sensitivity to Doppler modulation.

(Submitted to Phys. Rev. E, 1996)

Evaluation of a Stochastic Resonance Based Detector of Weak Harmonic Signals in Additive White Gaussian Noise

V. Galdi, V. Pierro, I. M. Pinto

D.I^3.E., University of Salerno
via Ponte Don Melillo, I-84084 Fisciano (SA), Italy
E-mail: vingal, piervin, pinto@salerno.infn.unisa.it

Keywords: Stochastic Resonance, Nonlinear Filtering, Signal Detection.

December 6, 1996

Abstract

An engineering approach to Stochastic Resonance in a framework of Signal Detection is presented. Evaluation of detection performance and comparison with usual techniques (matched filter) are developed by means of extensive Monte Carlo simulations.

1 - Introduction.

Stochastic Resonance (henceforth SR) was introduced in the early '80s by Benzi [1]. Since then, it has attracted considerable attention with reference to a variety of fields including: Signal Processing and Analysis [2],[3],[4],[5], Neuroscience [6], Electronic Devices [7], Optical and Magnetic Bistability [8],[9]. In this paper we explore the possibility of using SR for detecting weak harmonic signals in white gaussian noise. Our aim is twofold: to formulate an engineering approach providing an hopefully clear and complete view of the SR as a Signal Detection tool. In this connection we pinpoint a number of yet unclarified issues:

- Sound statistical-detection analysis;
- (Dis)assessment of resonant features;
- Convenient model parametrization in view of performance optimization.

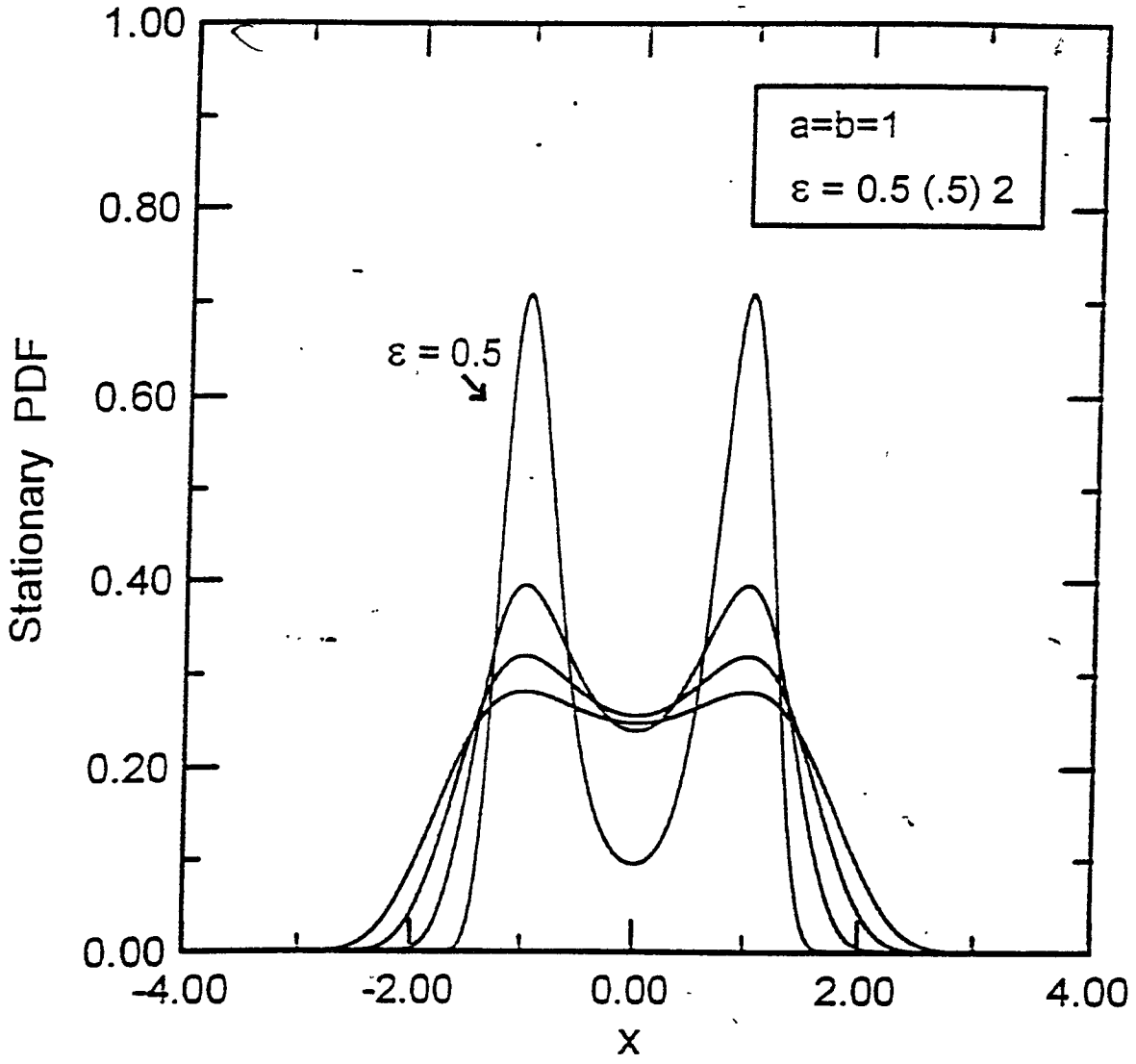

Fig. 1 - Stationary (steady state) PDF in the absence of signal.

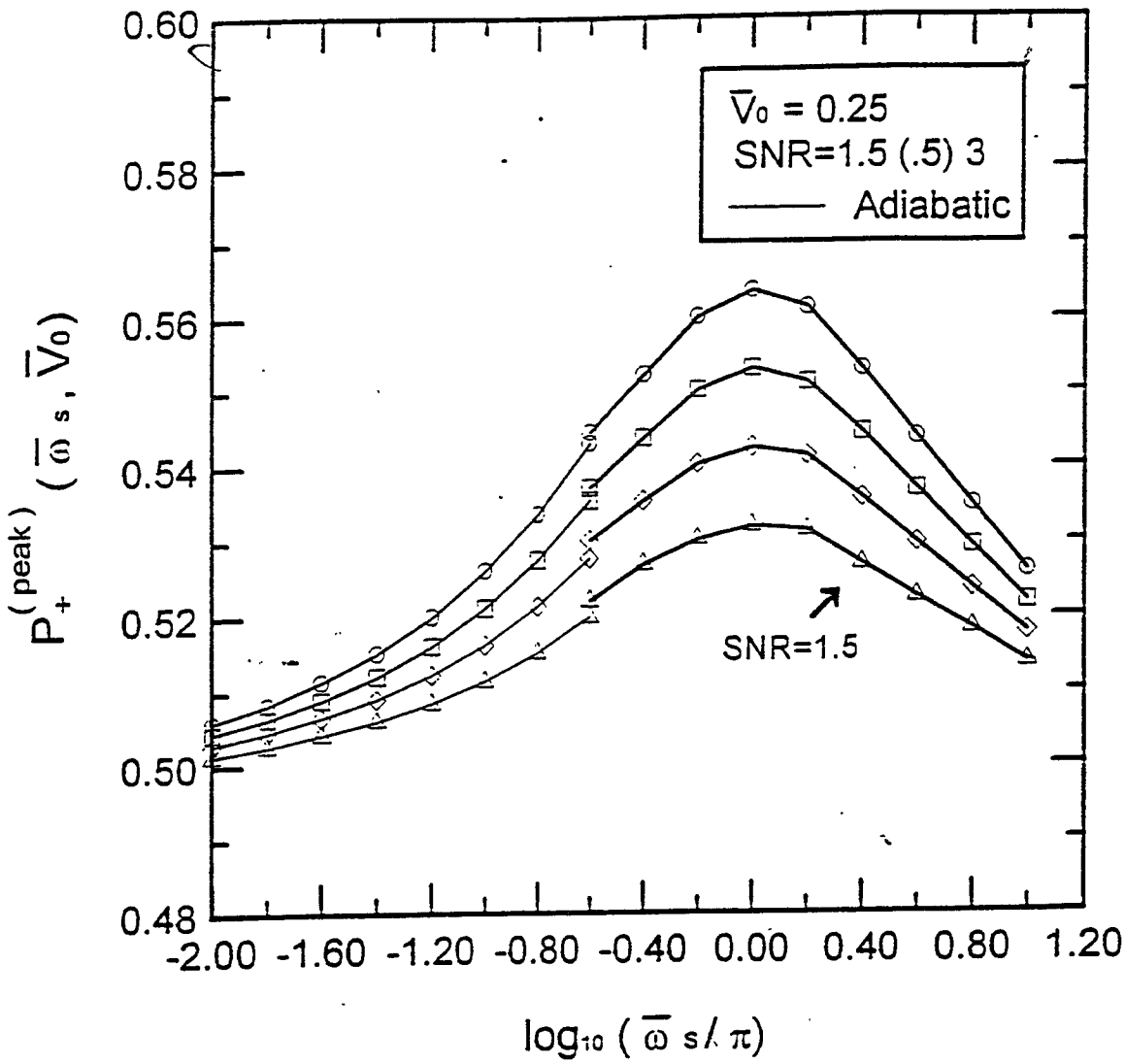

Fig. 4 - P_+ amplitude frequency response of the SR filter, for various values of SNR. Dashed curves refer to the adiabatic approximation.

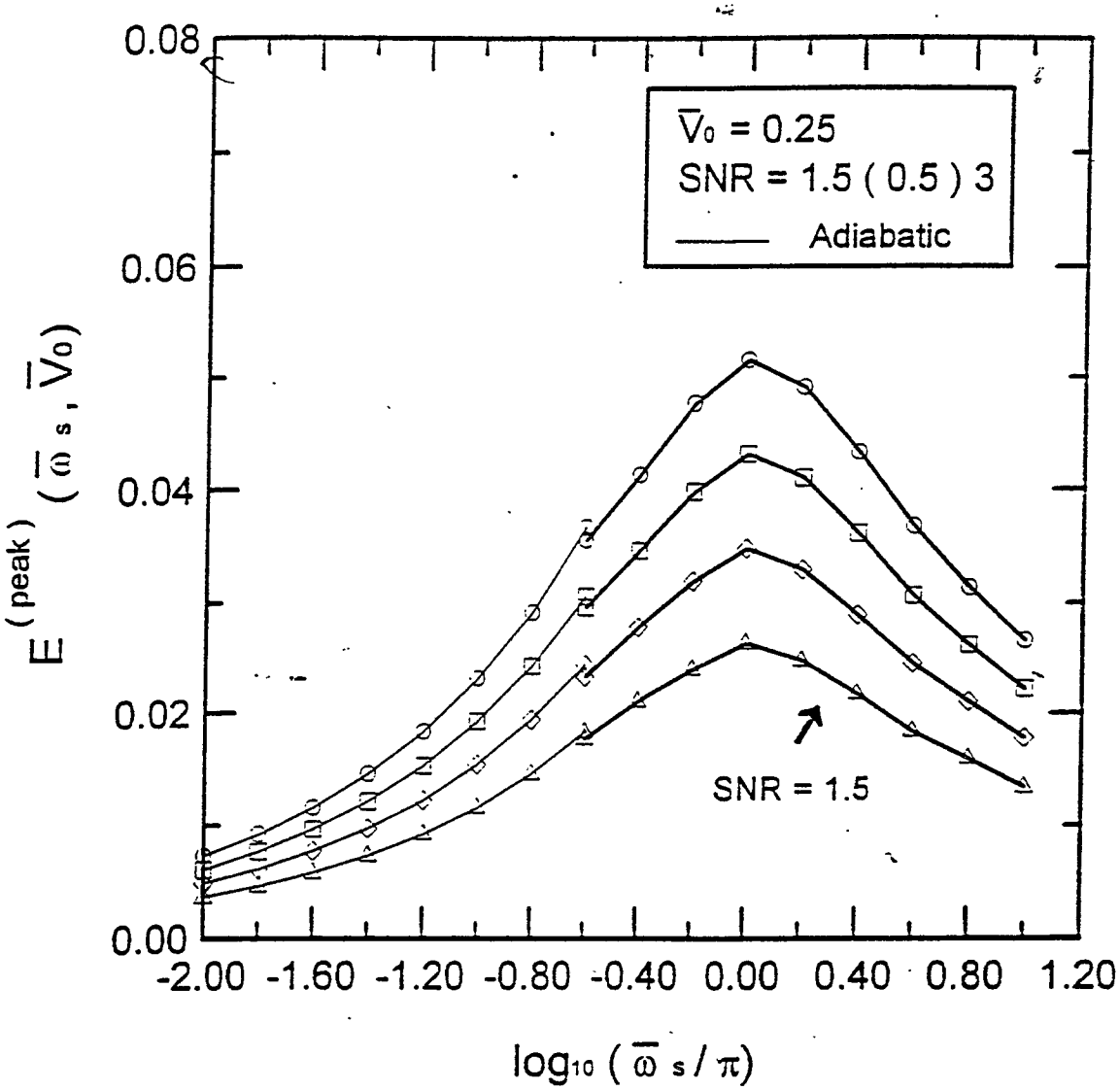

Fig. 5 - E amplitude frequency response of the SR filter, for various values of SNR. Dashed curves refer to the adiabatic approximation.

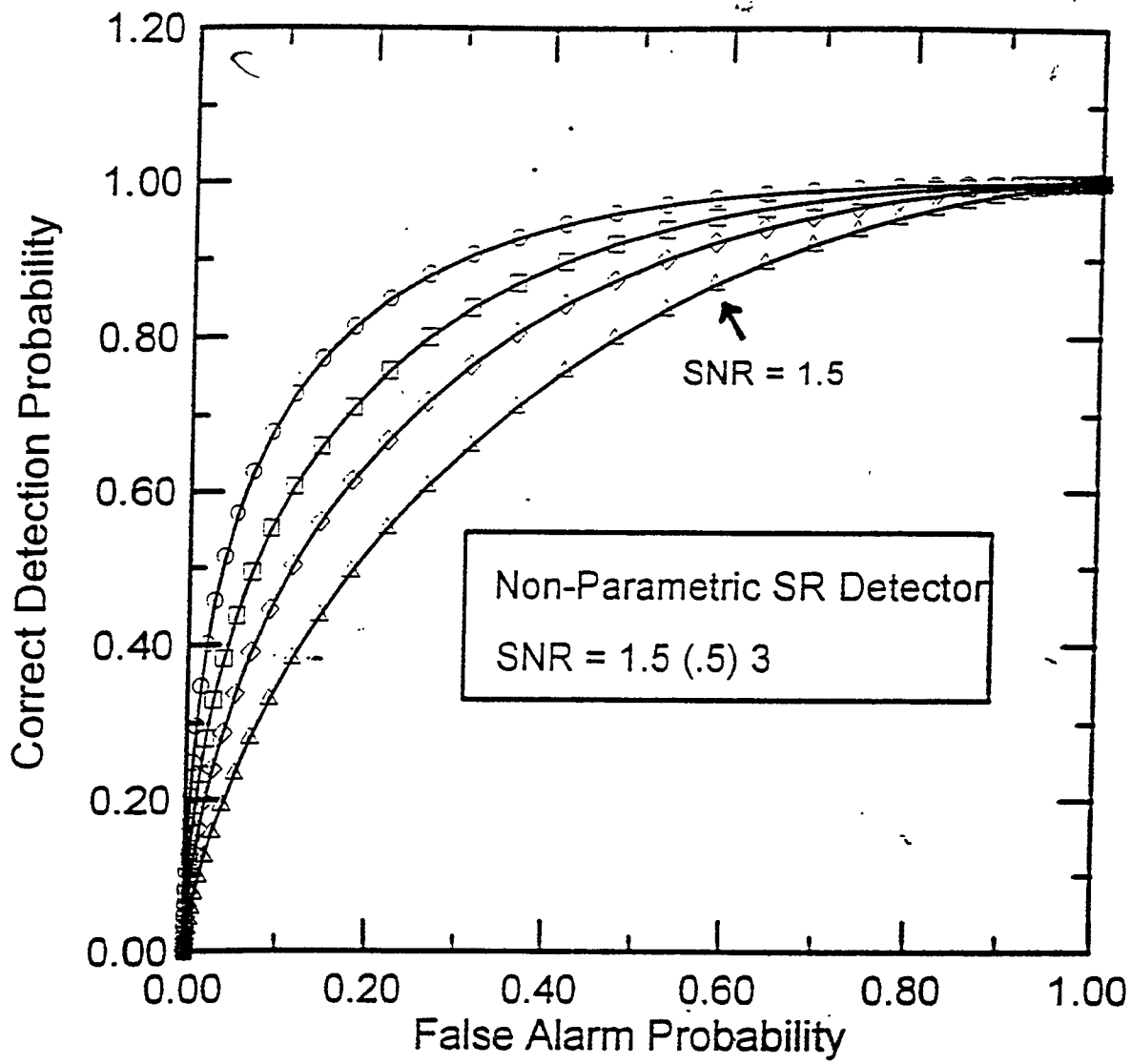

Fig. 9 - Receiver operating characteristics of a non-parametric SR detector.

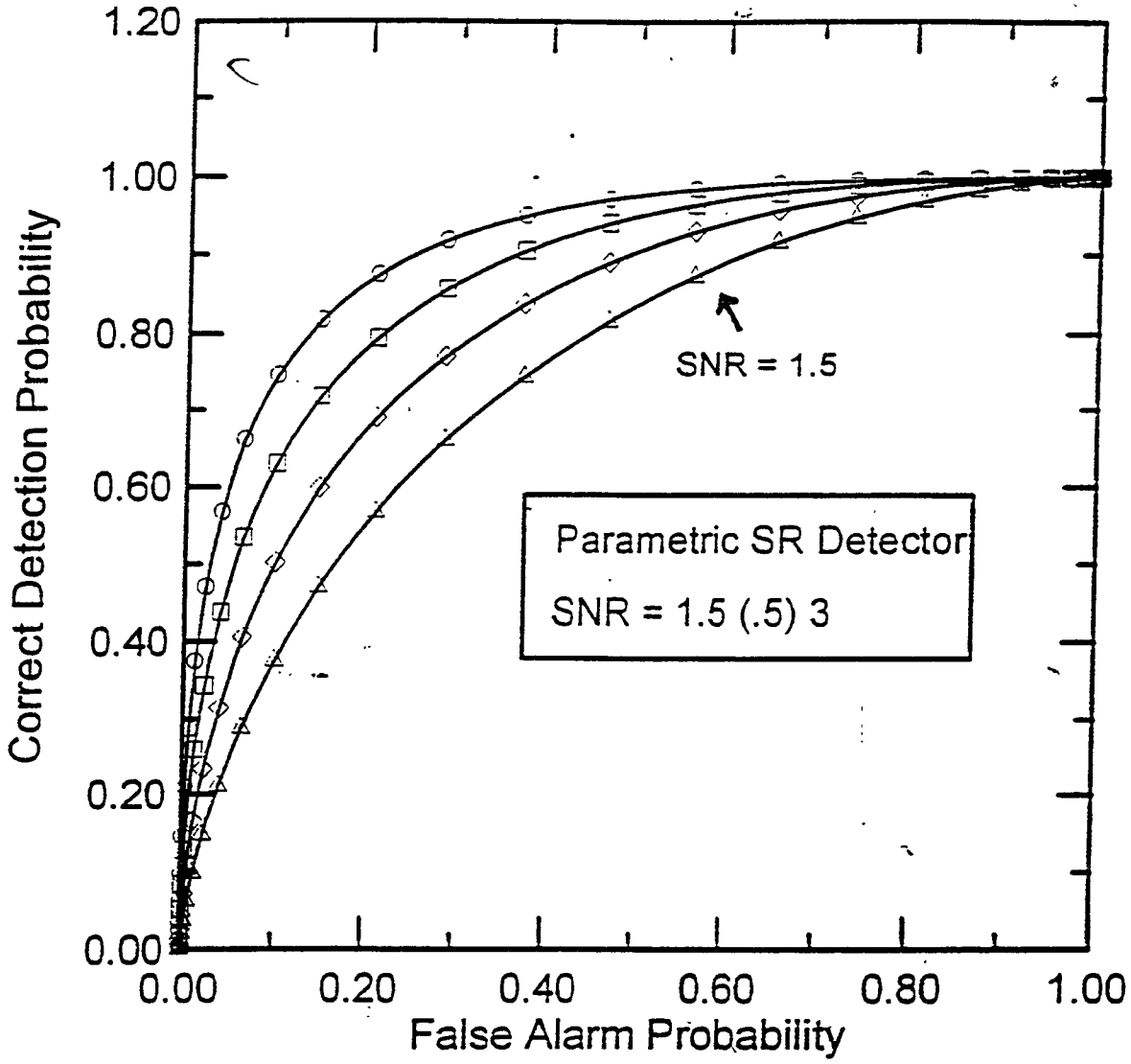

Fig. 11 - Receiver operating characteristics of a parametric SR detector.

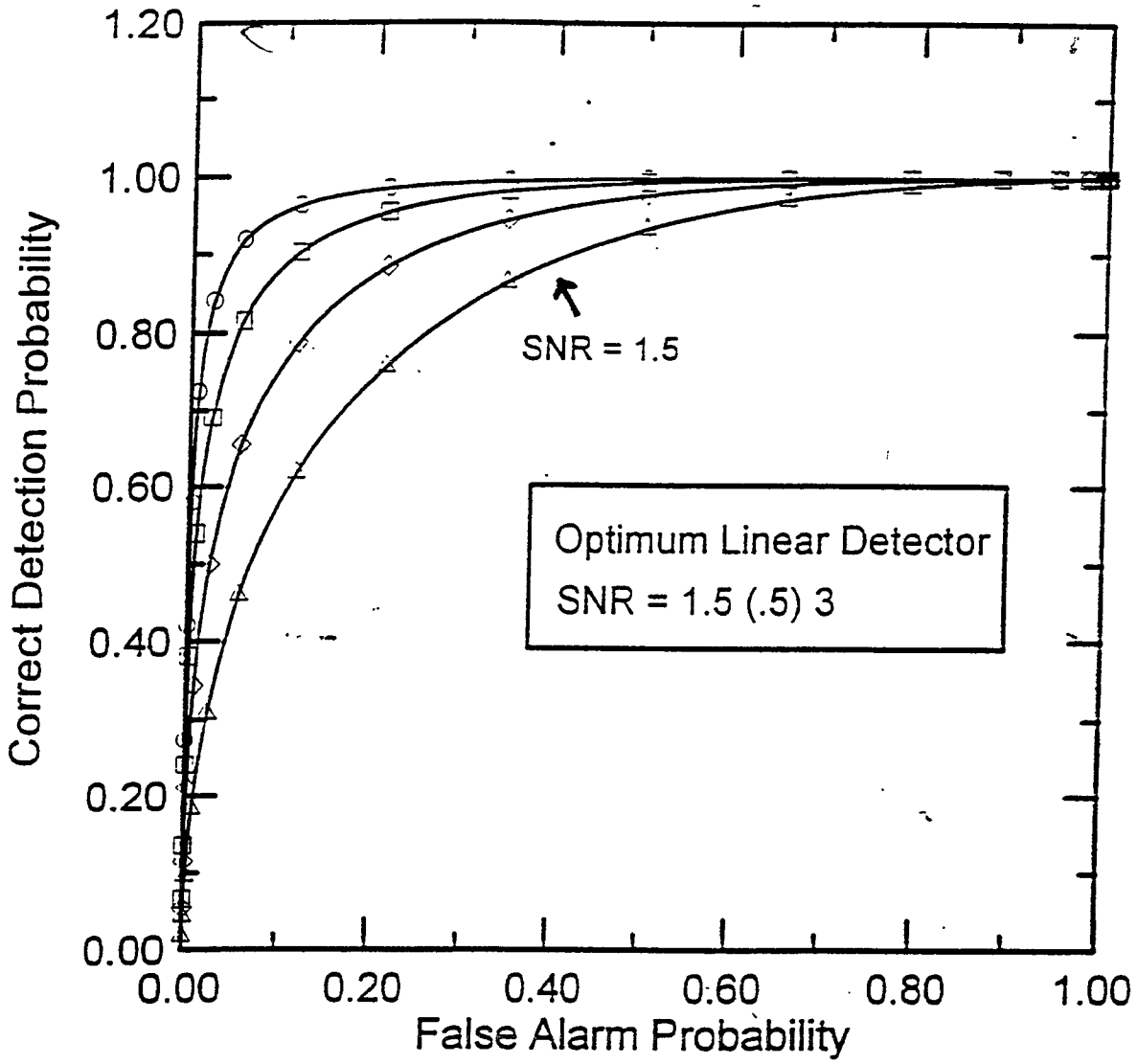

Fig. 10 - Receiver operating characteristics of an optimum linear detector.

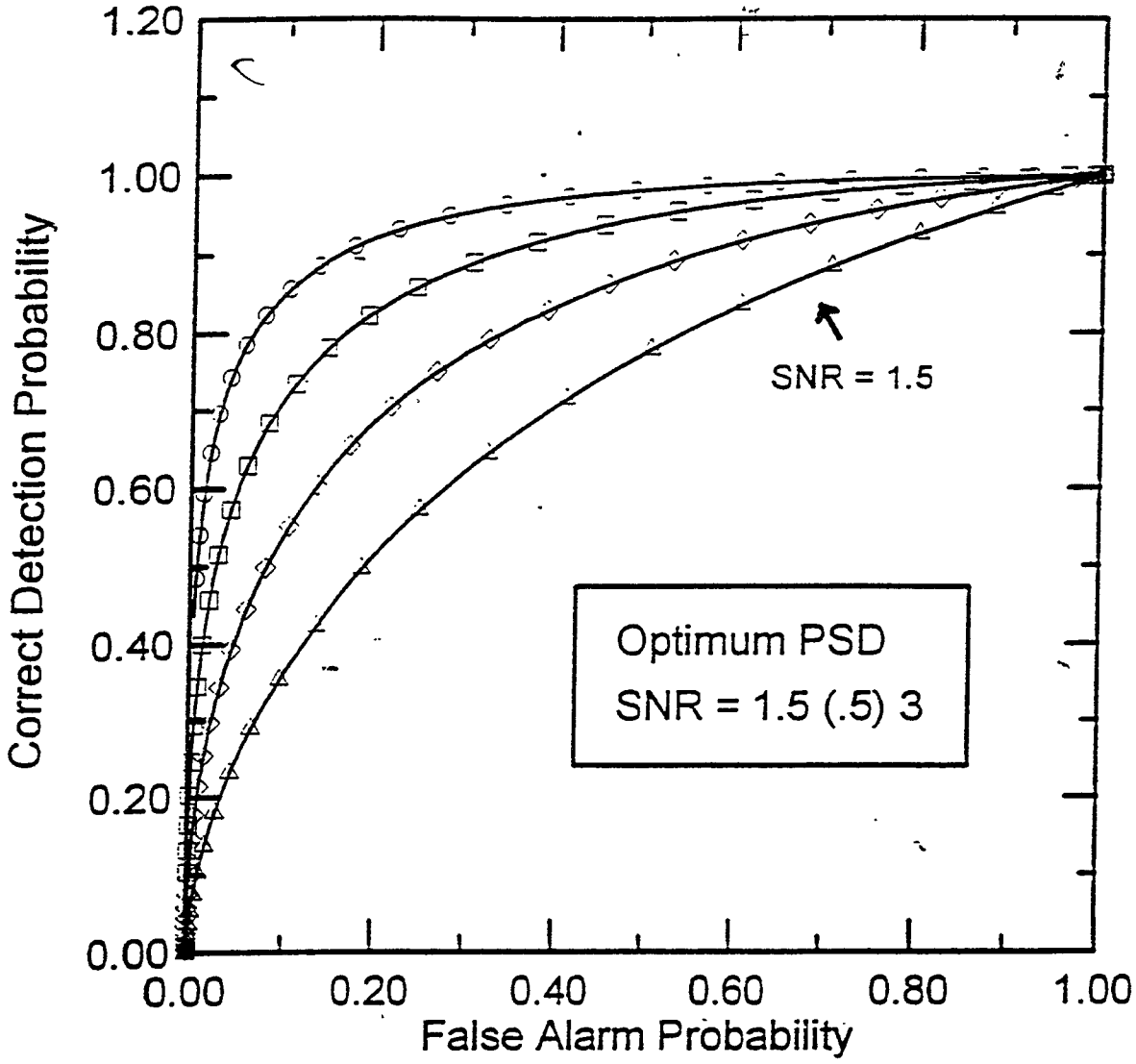

Fig. 12 - Receiver operating characteristics of an optimum phase sensitive detector.

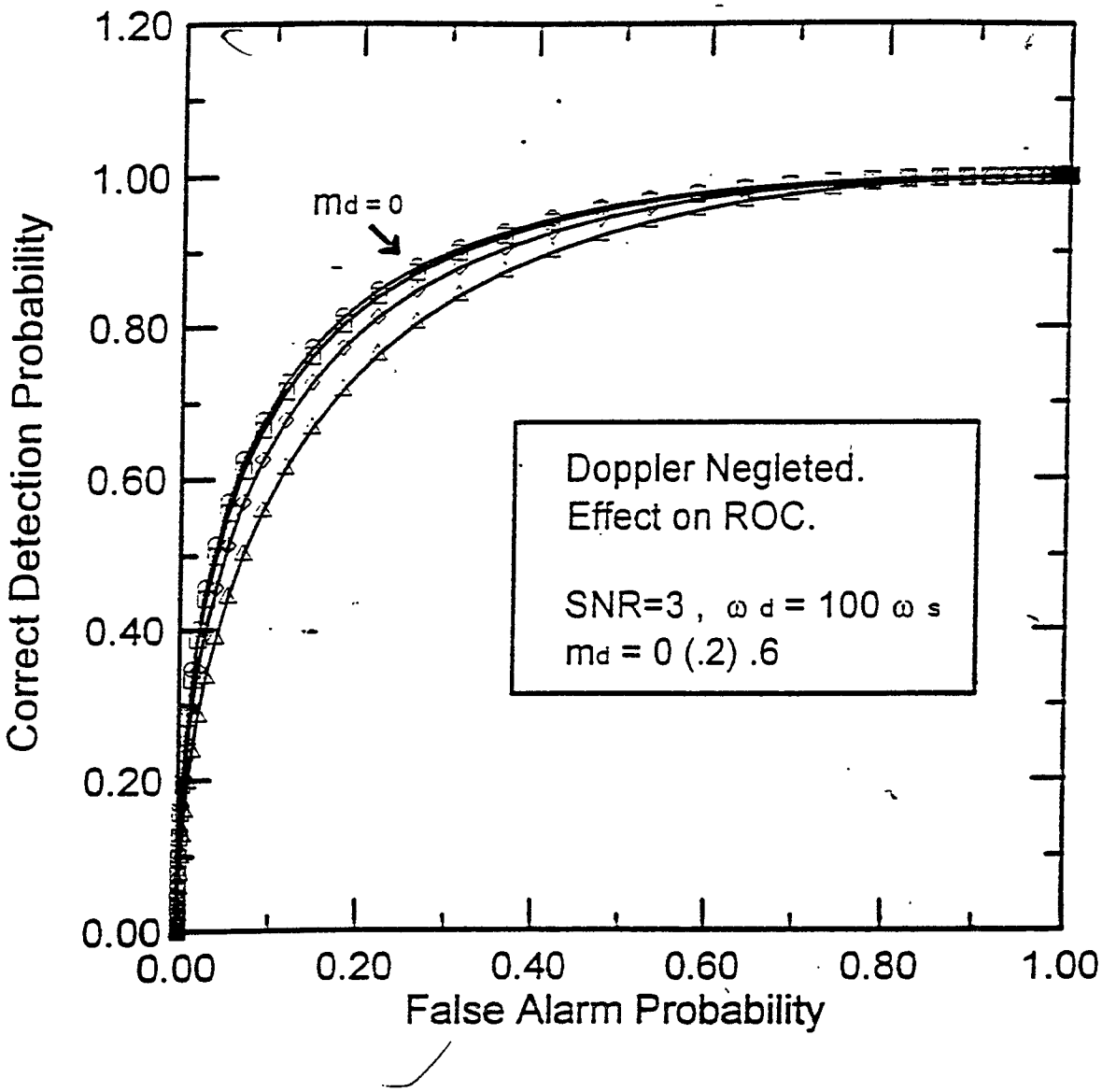

Fig. 14 - Effect on ROC of negleting Doppler modulation.
Non-parametric SR detector.

LOCALLY OPTIMUM DETECTION OF PERIODIC GRAVITATIONAL WAVES

Filomena Flagiello, Stefano Marano
email: flag@nadis.dis unina.it
DIE, Universitá di Napoli Federico II,
Via Claudio 21, I-80025, Napoli, Italia
Maurizio Longo
email: longo@cesare.diiie.unisa.it
DIIIE, Università degli Studi di Salerno
Via Melillo 1, I-84084, Fisciano (SA), Italia

LOD test Given the AM/FM model of the signal expected from periodic gravitational sources at the output of the laser interferometric antennas, we develop a locally optimum detection test for the signal.
In the signal model there are several parameters dependent upon the orientation of the antenna, the frequency and the direction of arrival of the wave. Moreover the received AM/FM signal has a narrow relative bandwidth, over which the noise has an almost flat spectrum, so it can be taken as white.
In the present analysis we assume that the observation time T is small, i.e. $T \ll 1$ month, so the FM term cointains only the contribute of the rotation of the Earth around its axis with frequency $f_1 \simeq 10^{-5}$ Hz. For a fixed frequency f_0 of the wave from the source, we suppose that the signal is known except for three parameters: α_0, the nominal strenght of the wave, θ_0, its initial phase, and ϕ, the phase in the FM term which represents the azimuth of the source in a suitable Cartesian frame. We assume θ_0 and ϕ as independent random variables uniformly distributed in $(0, 2\pi)$ while α_0 is modeled as a deterministic but unknown parameter. The AM term is not very significant so we ignore it. The locally optimum detector (LOD), i.e. asimptotically optimum for vanishing signals, is based on the statistic:

$$\Gamma \triangleq \sum_{n=-(\beta+2)}^{\beta+2} J_n^2(\beta) \left| \int_0^T r(t) e^{-i2\pi(f_0+nf_1)t} dt \right|^2$$

where $J_n(\cdot)$ is the n-th order Bessel function of first kind and β is (largest integer next to) the modulation index.

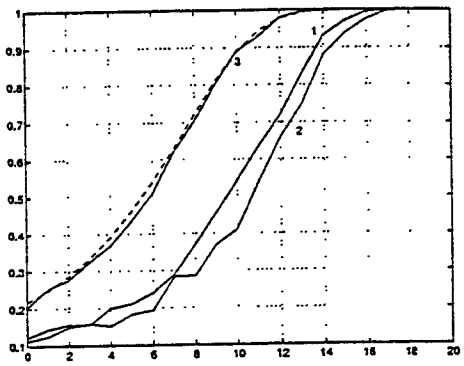

Figure 1: P_d vs SNR in dB for $\psi = \frac{\pi}{4}$, $f_0 = 100\ Hz$, $P_{fa} = 10^{-1}$, $T = 10$ days and 1) $\theta = \frac{\pi}{4}$; 2) $\theta = \frac{\pi}{2}$, 3) $\theta = 0$. The dashed line reports the performances of the noncoherent correlator.

In Fig.1 we give the performances of the LOD in term of the plot of P_d versus the Signal-to-Noise ratio.
Numerical implementation In order to construct the test we need the samples of the DFT on $N = 2BT$ points (B is the single-side band of the signal) with step M, which is the integer number of observation days. To this aim, we can perform M DFTS on $N_1 = N/M$ points and sum up. Because of the dependence of M on the observation time T, the number of additions increases linearly with T.
Also we propose the implementation of the receiver when the frequency f_0 is unknown and range over the band (f_{0min}, f_{0max}). As decision statistic we adopt the maximum of $\Gamma(f_{0i})$ where f_{0i} is taken with a given step in (f_{0min}, f_{0max}). Using an operational ambiguity function for the statistic. we deduce a step for the frequencies of $\frac{1}{T}$ and we show that in order to construct the several $\Gamma(f_{0i})$ we need the samples of a DFT over a very large number of points($\simeq 10^{10}$). The length of the DFT depends upon the receiver bandwidth we want to explore and the observation time long enough if we want a reasonable Signal-to-Noise ratio.
We are currently interested in methods for an optimum realization of the DFT dependent upon our application.

Distributed Detection of Chirp Gravitational Waves

S. Marano, University of Naples, VIRGO group
M. Medugno, CPS-CNR, Naples
M. Longo University of Salerno, VIRGO group

We deal with the simplest form of the chirp signal (i.e. Newtonian). This signal is basically characterized by two parameters: **arrival time**, t_a, and **sweep time** τ (i.e. the signal duration).

We consider the classical detection theory yielding a **bank–of–filter** detector where each filter is matched to a specific value of τ.

In our setup the lower cutoff of the antenna and the sampling frequency are respectively

$$f_0 = 10 \text{ Hz} \qquad f_c = 1 \text{ KHz}$$

As the range of **mass parameters** is $\mathcal{M} \in (0.25M_\odot, 30M_\odot)$, the range of values of sweep time is approximately

$$\tau \in (5 \text{ seconds}, 4 \text{ hours})$$

The spacing between adjacent filters in the bank can be chosen approximately constant: in the **white noise case** $\Delta\tau = 240$ ms. This is the value of $\Delta\tau$ in which the **ambiguity function** is just one half. As a conseguence of this setup we require a number of filters in the order of 60000. First investigations for the colored (VIRGO like) noise indicates that such number decreases approximately by an order of magnitude.

We investigate the computational requirements of the detector. The overall memory requirement is approximately 10^{13} bytes, while the floating point operations per second results in the order of several GFLOPS.

We investigate **distributed network computing** in order to implement such detector by **heterogeneous high performance workstations** interconnected via an Ethernet network. Our final goal is to design a distributed on-line detector running on a number of available workstations; the computation is decomposed across the workstations in such a way to minimize communications and to match the reception rate.

We derive a theoretical value of $G(w)$ (Grain): **the number of filters in the neighbour of $w = f_c\tau$ that a single "tipical" workstation is able to process in real time.** (We define "tipical" a workstation with certain well known and constant performance.) Then we define a **non–ideality factor** $\mathcal{L}$, namely a corrective factor taking into account a number of effects that previous theoretical analysis cannot include (e.g. use of "non-tipical" workstation, memory chaching management, memory paging, compiler optimization features, efficiency of fft algorithm, and so on). The value of $\mathcal{L}$ is estimated in a experimental way over three high performance workstations under Unix operating system: a Sun (Machine A) a Dec (B) and an IBM (C).

The **value of Grain to be used in a practical design** will result in $G_{act} = G/\mathcal{L}$. Sperimen-

Related Work:

Exact solution of PM equations for any orbital Eccentricity
(Nuovo Cimento B, may 1996)

Steady State Population Statistics of Compact Binaries
(Astrophysical Journal, september 20th 1996)

Effect of Residual Orbital Eccentricity on Chirp Phase Error
(Nuovo Cimento, 1996, december 1996)

Time Frequency Analysis of GW Chirps
(VIRGO Conference, 1996)

Exact Solution of Schafer-Rieth Equations
(LISA Meeting, 1996)

Fast and Accurate Waveform Templates for GW from Binary Stars with any Eccentricity (MNRAS, paper MW835)

tations are in progress to confirm this statment.

For the largest values of τ (and hence of w) our complexity analysis may be questionable, in which very long FIR filters should require a suitable segmentation to take place in the RAM memory of workstations. This is a topic of current work.

Finally, we stress that the complexity of the structure does not change very much when the unknowledge of some noise characteristics is included at design stage. In other words a **CFAR (Constant False Alarm Rate)** approach or some other kind of **spectral noise estimation** can be pursued with basically the some network of workstations.

In the next three tables the main characteristic of the machines named A, B, C, are summarized.

Machine	A
Model	SPARCstation 10
Cpu/Arch.	SPARC/sun4
Clock (Mhz)	100
Main Mem (MBy)	32
O.S. version	SunOs 4.1.3
Manifacturer	Sun
Cache (ist./d)	64K

Machine	B
Model	DEC 3000-600
Cpu/Arch.	DEC 21064/AXP
Clock (Mhz)	175
Main Mem (MBy)	64
O.S. version	DEC OSF/1 3.2
Manifacturer	Digital
Cache (ist./d)	2M

Machine	C
Model	RS/6000-3AT
Cpu/Arch.	Power2
Clock (Mhz)	59
Main Mem (MBy)	32
O.S. version	AIX 3.2.5
Manifacturer	IBM
Cache (ist./d)	32k, 64k

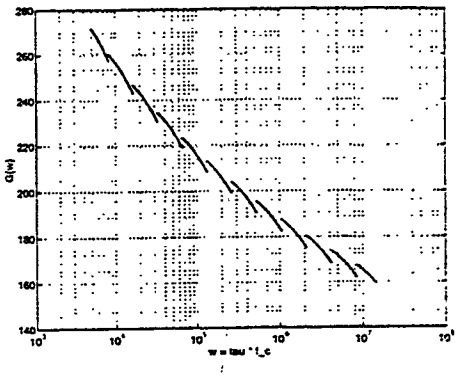

Figure 1: Theoretical value of Grain versus $w = \tau f_c$

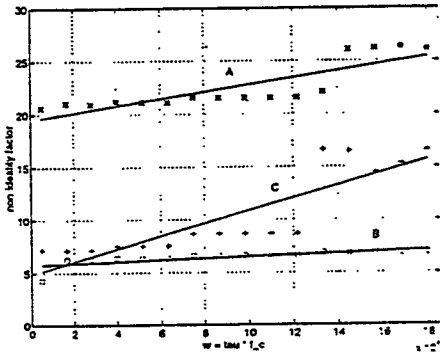

Figure 2: Experimental values of the parameter $\mathcal{L}$ versus $w = \tau f_c$ for several machines

Evaluation of a Stochastic Resonance Based Detector of Weak Harmonic Signals in Additive White Gaussian Noise

V. Galdi, V. Pierro, I. M. Pinto

D.I^3*.E., University of Salerno*
via Ponte Don Melillo, I-84084 Fisciano (SA), Italy
E-mail: vingal, piervin, pinto@salerno.infn.unisa.it

Keywords: Stochastic Resonance, Nonlinear Filtering, Signal Detection.

December 6, 1996

Abstract

An engineering approach to Stochastic Resonance in a framework of Signal Detection is presented. Evaluation of detection performance and comparison with usual techniques (matched filter) are developed by means of extensive Monte Carlo simulations.

1 - Introduction.

Stochastic Resonance (henceforth SR) was introduced in the early '80s by Benzi [1]. Since then, it has attracted considerable attention with reference to a variety of fields including: Signal Processing and Analysis [2],[3],[4],[5], Neuroscience [6], Electronic Devices [7], Optical and Magnetic Bistability [8],[9]. In this paper we explore the possibility of using SR for detecting weak harmonic signals in white gaussian noise. Our aim is twofold: to formulate an engineering approach providing an hopefully clear and complete view of the SR as a Signal Detection tool. In this connection we pinpoint a number of yet unclarified issues:

- Sound statistical-detection analysis;
- (Dis)assessment of resonant features;
- Convenient model parametrization in view of performance optimization.

The paper is organized as follows. In *Section 2* we heuristically review the SR concept and introduce the mathematical model. In *Section 3* we discuss the possible applications of SR in Signal Detection and in *Section 4* we rephrase the starting model in terms of convenient dimensionless parameters. We present the results of exaustive Monte Carlo simulations which allow a complete characterization of the SR system (like a band-pass filter) and to address the optimum detector synthesis problem. In *Section 5* we discuss some simple and efficient detection algorithms, based on the analysis of the statistical properties of the system response. We outline a comparison with traditional techniques based on (optimum) linear filtering in terms of Receiver Operating Characteristics (henceforth ROCs). Conclusions follow in *Section 6*. A number of formal developments are collected in the Appendixes.

2 - Stochastic Resonance: Heuristics.

We consider a one-dimensional nonlinear dynamical system, described by the following first order stochastic Langevin equation (henceforth SLE):

$$\begin{cases} \dot{x} = -\dfrac{d}{dx}V(x) + A\sin(\omega_s t + \phi) + \epsilon\, n(t), \\ x(0) = x_0, \end{cases} \tag{1}$$

where $n(t)$ is a stationary zero-mean white gaussian noise

$$E[n(t)n(t+\tau)] = \delta(\tau), \tag{2}$$

and $V(x)$ represents a (bistable) quartic potential :

$$V(x) = -a\frac{x^2}{2} + b\frac{x^4}{4}, \quad a, b > 0\ , \tag{3}$$

with stable stationary points at $x_m^{\pm} = \pm\sqrt{a/b}$, an unstable stationary point at $x = 0$, and a potential barrier height:

$$V_0 = \frac{a^2}{4b}. \tag{4}$$

The stochastic process $x(t)$ solution of (1), can be conveniently characterized in terms of its probability density function (henceforth PDF) $p(x,t)$, ruled by the associated Fokker-Planck Equation (henceforth FPE) [10],[11]:

$$\begin{cases} \dfrac{\partial p(x,t)}{\partial t} = \dfrac{\partial}{\partial x}\left\{\left[\dfrac{dV(x)}{dx} - A\sin(\omega_s t + \phi)\right] p(x,t)\right\} + \dfrac{\epsilon^2}{2}\dfrac{\partial^2}{\partial x^2}p(x,t), \\ p(x,0) = \delta(x - x_0). \end{cases} \tag{5}$$

Unfortunately this equation cannot be solved in closed form. Only approximate solutions, valid under special assumptions are available. In an attempt to qualitatively understand the SR mechanism, the following considerations can be useful. In the absence of noise ($\epsilon = 0$) and with a *weak* harmonic bias (*subthreshold* signal, $A < V_0$) the (deterministic) process $x(t)$ oscillates indefinitely in a neighbourhood of a stable stationary point: no transition between the two stable states is allowed. In the presence of noise only ($A = 0$) the system response $x(t)$ jumps at random times between *noisy neighbourhoods* of the stable states $x_m^{\pm}$. The first-passage time from one well of the bistable potential to reach the unstable point is itself a random variable, whose mean (Kramers time) can be expressed exactly as a double integral [10]:

$$T_k = T(x_m^{\pm} \; to \; 0) = \frac{2}{\epsilon^2} \int_0^{x_m^{\pm}} dy \;\; \exp[2V(y)/\epsilon^2] \int_{-\infty}^{y} \exp[-2V(z)/\epsilon^2] \; dz. \qquad (6)$$

Various approximations can be applied to this integral to obtain analytical estimates [12],[13]. In the following we shall refer to the estimate:

$$T_k = \frac{\sqrt{2\pi}}{a} \exp\left[\frac{2V_0}{\epsilon^2}\right], \qquad (7)$$

which provides a good approximation in the parameters range of interest [1].

As an effect of noise, switching between the stable fixed points becomes possible even for a subthreshold input signal. It can be heuristically grasped that, in particular conditions, there might be a possibility that the switching be driven by the harmonic forcing term; so that, the state of the system locks to the input signal. It can be shown that the correlation degree between the system response and the sinusoidal signal depends on the noise intensity and takes a maximum for a critical value of this latter. It was initially suggested [1] that such a behaviour results from the matching of the forcing period $T_s = 2\pi/\omega_s$ with twice the Kramers time:

$$T_s \sim 2T_k. \qquad (8)$$

This SR definition, which resembles a *classical* resonance has suffered several criticisms [14], and even denied. Some Authors introduced *alternative* definitions, more directely interpretable as a *bona fide* resonance [15].

In the following we shall try to characterize the SR with special reference to Signal Detection. A typical resonant behaviour (in the detection performance) will be indeed pointed out.

[1]Note that T_k estimate (7) is exactly twice that introduced by Benzi [1]. This latter, however, provides a good approximation only in the *high-barrier* asymptotic limit $\epsilon \to 0$. For finite ϵ the first correction is available [13]. It can be verified that (7) provides a good trade-off between ease and accuracy in the (finite) potential barrier height range of interest.

3 - SR and Signal Detection.

The possibility of using SR for detecting *weak* harmonic signals in white gaussian noise has been suggested by several Authors [2],[3],[4]. To easily understand *why* and *how* this can be achieved, we focus on SLE (1) and FPE (5).

In the absence of the harmonic signal ($A = 0$) the steady state PDF of $x(t)$ is readily obtained:

$$p_s(x) = C \exp\left[\frac{\frac{ax^2}{2} - \frac{bx^4}{4}}{\epsilon^2/2}\right], \tag{9}$$

where C is a normalization constant. *Fig. 1* shows the typical behaviour of $p_s(x)$: it is evenly distributed around the origin and clusters within two peaks centered at $x_m^{\pm}$ having (equal) widths increasing with the noise intensity, ϵ. The presence of the sinusoidal forcing term produces a *modulated*-in-time symmetry breaking in the PDF. This effect can be easily described in the *adiabatic* regime ($T_s >> T_k$), by solving perturbatively the FPE as follows [10],[14]:

$$p(x,t) = C(t) \exp\left[\frac{\frac{ax^2}{2} - \frac{bx^4}{4} + Ax\sin(\omega_s t)}{\epsilon^2/2}\right], \tag{10}$$

$C(t)$ being a normalization factor. We note a periodic simmetry breaking induced by the harmonic signal presence. This effect appears indeed in *all* regimes [2](not only in the adiabatic one!) and can be used to detect the signal presence. The detection algorithms presented in this paper are thus based on the analysis of the simplest conceivable *(a)symmetry indicators*, viz.:

$$P_+(t) = Prob\{x(t) > 0\} = \int_0^{\infty} p(x,t)dx, \tag{11}$$

$$E(t) = E[x(t)] = \int_{-\infty}^{\infty} xp(x,t)dx. \tag{12}$$

In the absence of a signal one obiouvsly has $P_+ = 0.5, E = 0$. *Fig.s 2,3* show the time evolution of P_+ and E, obtained from numerical simulations (see *Appendix C*), in the presence of signal, in the non-adiabatic regime. As one can see, after a short transient they *lock* to the signal, indipendently of the initial conditions. However, as seen from *Fig.s 2,3*, unlike the adiabatic regime (10), *phase-locking* is not achieved. and a (constant) phase lag shows up.

[2]It can be explained applying Floquét theory, [7],[16].

4 - SR characterization with reference to Signal Detection.

In the previous Section we have qualitatively analized the possibility of using SR in Signal Detection. Before proceeding to a quantitative analysis it can be convenient to define more rigorously the detection problem. For the time being we shall assume that the angular frequency ω_s as well as the initial phase ϕ (taken zero here, for simplicity) of the signal are known (coherent detection), and that we are faced with a strict detection issue, namely to decide whether the signal is present ($A \neq 0$) upon watching at the response $x(t)$ across a finite time interval, $[0, NT_s]$. To this end we capitalize on the breaking-symmetry effect induced in the PDF of $x(t)$ by the signal presence, witnessed by the time behaviour of $P_+(t), E(t)$.

We introduce some dimensionless parameters:

$$\bar{\omega}_s = \omega_s T_k \quad , \quad \textit{normalized angular frequency}, \tag{13}$$

$$\bar{V}_0 = \frac{V_0}{\epsilon^2} \quad , \quad \textit{normalized potential barrier height}, \tag{14}$$

$$SNR = \sqrt{\frac{E_s}{\epsilon^2}} = \sqrt{\frac{NT_s A^2}{2\epsilon^2}} \quad , \quad \textit{signal} - \textit{to} - \textit{noise ratio}, \tag{15}$$

where E_s represents the signal energy. Equation (1) can be rephrased in terms of the above parameters as follows:

$$\begin{cases} \dot{\bar{x}} = \bar{a}\bar{x} - \dfrac{\bar{a}^2}{4\bar{V}_0}\bar{x}^3 + SNR\sqrt{\dfrac{\bar{\omega}_s}{N\pi}}\sin(\bar{\omega}_s \bar{t}) + n(\bar{t}), \\ \bar{x}(0) = \bar{x}_0, \end{cases} \tag{16}$$

where:

$$\bar{x} = \frac{x}{\epsilon\sqrt{T_k}} \quad , \quad \bar{t} = \frac{t}{T_k}, \quad \bar{a} = a\,T_k = \sqrt{2}\pi \exp(2\bar{V}_0).$$

Now we can analyze the system response (in terms of detection performances) by varying the three fundamental parameters $\bar{\omega}_s$, $\bar{V}_0$, SNR. In *Fig.s 4,5* we report, respectively, the peak ($\max_t$) amplitude of $P_+(t)$ and $E(t)$, versus the normalized angular frequency (obtained via Monte Carlo Method, see *Appendix C*), for some typical values of SNR, at a fixed value of $\bar{V}_0$. As one can easily see, the qualitative behaviour is the same: the amplitude frequency responses show a typical resonant behaviour, reaching a maximum at:

$$\bar{\omega}_s \sim \pi \quad , \quad viz., \quad T_s \sim 2T_k, \tag{17}$$

which is exactly the Benzi condition (8) for SR. Note that our numerical results merge smoothing into the adiabatic (analytic) ones as $\bar{\omega}_s$ is decreased. In *Fig. 6* we report the corresponding phase lag with respect to the input harmonic signal, which turns

out to be the same for both P_+ and E, and almost independent of the SNR (at least in the limit of statistical error, see *Appendix C*). It is interesting to note that similar phase displacements (typical of several physical systems which exhibit SR, [7],[17],[18]) are observed in deterministic (linear) resonators. Varying $\bar{V}_0$ one obtains several families of curves like those described above (not reported for brevity) and one can readily verify that the position of the maxima (resonance condition) are always consistent with (17), and the phase displacement keeps the same qualitative behaviour, independently of $\bar{V}_0$. However, the resonance peak level depends (weakly) on $\bar{V}_0$, as shown in *Fig.s 7,8* for P_+ and E, respectively.

Optimum SR Detector Synthesis.

The above analysis shows that the peak resonance level of the (a)simmetry indicators is maximum in a relatively narrow band of frequencies, for a quite wide class of potential barrier heigths. Although we haven't yet clearly defined the detection strategy, it is not difficult to understand that the P_+ (E) resonance peak level maximization corresponds to detector performance optimization. In fact this leads to the maximization of the asymmetry effect (in the output PDF) induced by the signal presence.

Now we have all the tools to address the optimum SR detector synthesis problem. Having fixed the signal angular frequency ω_s and the noise power spectral density ϵ^2, we first have to put ourselves in the resonance condition (17) (by varying T_k). Then we can use the last degree of freedom available to maximize the resonance peak level (by varying $\bar{V}_0$). Using eq.s (4),(7) we can determine the potential parameters a, b of the SR filter.

5 - Detection Algorithms and Performance Evaluation.

In this Section we shall develop a quantitative analysis of the SR detector performance, with reference to several detection strategies. We shall assume that the SR detector has been designed according to the optimum rules defined in the previous Section. In *Appendix A* we show that there is no gain in adopting a continuous-time likelihood ratio test on the output process, since this is equivalent applying matched filtering on the input process directly. On the other hand, in *Appendix B* we show that in the adiabatic assumption, the *strobed* average strategy is equivalent to the (optimum) Neumann-Pearson ratio test [19] on the output process. This hears some heuristic hints to use the same strategy also in the optimum (non-adiabatic) operating conditions. Moreover, we will show that the strobed sign-counting strategy, which looks less computationally expensive, performs only *slightly* worse. For these reasons, we shall focus on strobed sign-counting and barycenter analysis, for the coherent and incoherent cases.

Non-Parametric Algorithms: Sign Counting.

We start examining the coherent detection. The first proposed algorithm is non-parametric [19]. The SR filter output $x(t)$, observed on a finite time interval $[0, NT_s]$, is sampled at times:

$$t_k = \frac{\frac{(2k+1)\pi}{2} - \psi}{\omega_s} \quad , \quad k = 0, 1, 2, ..., 2N-1, \tag{18}$$

when the asymmetry effect induced by the signal presence is maximum; ψ denotes the (known) phase lag introduced by the SR filter. We obtain the following time series [3]:

$$x_k = (-1)^k x(t_k) \quad , \quad k = 0, 1, 2, ..., 2N-1. \tag{19}$$

Then the signal presence can be checked adopting the following decision rule [19]. One counts the number N_+ of positive samples:

$$N_+ = \sum_{k=0}^{2N-1} U(x_k), \tag{20}$$

where $U(\cdot)$ is Heaviside's step function, and adopts the decision γ_1 (unsymmetrical distribution, signal present) iff :

$$N_+ > \Gamma, \tag{21}$$

and the decision γ_0 (symmetrical distribution, no signal present) iff:

$$N_+ \leq \Gamma, \tag{22}$$

where the threshold Γ is an integer larger than zero (unilateral symmetry- hypothesis [19]). The detector's performance is described by the following *false-alarm* and *missed-detection* probabilities, α and β:

$$\alpha = Prob\{N_+ > \Gamma \mid no\ signal\} \quad , \quad \beta = Prob\{N_+ \leq \Gamma \mid signal\}. \tag{23}$$

The stochastic variables x_k are statistically independent and identically distributed, thus [19]:

$$\alpha = I_{1/2}(\Gamma + 1, 2N - \Gamma) \quad , \quad \beta = 1 - I_{P_+}(\Gamma + 1, 2N - \Gamma), \tag{24}$$

where $P_+ = Prob\{x_k > 0\}$ and $I_p(x, y)$ is the incomplete Beta function [20].

In *Fig. 9* we report the Receiver Operating Characteristics (ROC) of the above described SR detector. By comparing *Fig. 9* with the corresponding ROC for the *optimum* linear detector [19], reported in *Fig. 10*, one finds a systematic loss of about $-4\ dB$.

[3] We rectify the negative half-wave.

How does dipend on N?
... saturation

Parametric Algorithms: Barycenter Analysis.

The second proposed algorithm is of parametric type [19] and is based on the same sampling technique introduced previously (18),(19). The decision rule is based on a test of the first moment (barycenter) of the samples distribution:

$$\mu = \frac{1}{2N} \sum_{k=0}^{2N-1} x_k. \tag{25}$$

One adopts the decision γ_1 (unsymmetrical distribution, signal present) iff:

$$\mu > \Gamma, \tag{26}$$

and the decision γ_0 (symmetrical distribution, no signal present) iff:

$$\mu \leq \Gamma, \tag{27}$$

Γ being the threshold ($\Gamma > 0$). One has [19]:

$$\alpha = 1 - F\left(\frac{\Gamma}{\sqrt{2N}\sigma_0}\right) \quad , \quad \beta = F\left(\frac{\Gamma - 2NE_1}{\sqrt{2N}\sigma_1}\right), \tag{28}$$

where:

$$E_1 = E[x_k \mid signal] \ , \ {\sigma_1}^2 = Var[x_k \mid signal], \ {\sigma_0}^2 = Var[x_k \mid no\ signal],$$

$$F(x) = \frac{1}{\sqrt{2\pi}} \int_{-\infty}^{t} \exp\left(-\frac{t^2}{2}\right) dt. \tag{29}$$

The corresponding ROC is shown in *Fig. 11.* We note a slight improvement with respect to the non-parametric strategy.

Non-Coherent detection.

In the previous Sections we have assumed the signal as perfectly known. In this connection the Optimum Linear Detector (henceforth OLD) admits an *(active)* implementation (*product-correlator*, [19], [21]) which ultimately requires an integrator and a threshold-decision unit. Thus its complexity seems comparable with the SR detector but, as shown in the previous subsections, its performance is better (by about 4 dB, by comparing *Fig.10* with *Fig.s 9,11*)

If the initial phase of the signal is unknown (non-coherent detection) an active implementation of the Optimum Phase Sensitive Detector (henceforth PSD) [19], [21] involves a loss of about -3 dB with respect to the coherent ROC, as shown in *Fig. 11.*

In *Fig. 13* we report the block-diagram of a non-coherent SR detector with non parametric strategy [4]. Using a single SR filter and a multiply displaced sampling,

[4] For the parametric strategies the basic idea is identical.

taking N_s samples in an half-period, one can obtain, at the end of the observing time interval, the most advantageous decision variable. It's not difficult to understand that this algorithm is *asymptotically efficient*; in that its ROC approach the corresponding coherent ones (*Fig. 9*), provided the observing time interval is sufficiently large ($N \sim 10^4$) and the sampling sufficiently dense (the tolerable uncertainty in the peak position is $\sim \pi/N_s$). Thus, for non-coherent detection, the SR detector performance is *asymptotically comparable* with the (active) Optimum PSD one, with almost the *same complexity*.

In principle one could apply a similar sampling technique to the OLD and thus (asymptotically) recover 3 dB, but this idea involves a considerable complexity growth. An active implementation, in fact, would require a *bank of correlators*, and so a number $2N_s$ of integrators, while SR detector requires only a *single* integrator. On the other hand, a passive implementation would require a *matched-filter* [21] and so a non-trivial frequency response shaping (frequency-domain analysis) or computationally intensive convolution operations (time-domain analysis).

Doppler Effect.

In the previous analysis we have modeled the signal to detect as a perfect sinusoidal signal. In some typical problems (e.g radar detection, gravitational waves detection) this assumption might become inaccurate due to the presence of *Doppler effect* [21]. In this subsection we face the problem of evaluating the ROC degradation of a SR based detector induced by negleting the Doppler effect. We consider the non-parametric SR coherent detector [5]. In *Section 4* we have analized the $P_+(t)$ response of an SR filter for an input sinusoidal signal $s(t) = A\sin(\omega_s t)$ (see *Fig. 2*). The steady-state behaviour can be approximatively modeled (negleting higher order harmonics) as:

$$P_+(t) \approx \frac{1}{2} + \left[P_+^{(max)} - \frac{1}{2}\right] \sin(\omega_s t + \psi), \tag{30}$$

where $P_+^{(max)}$, ψ are computed numerically (see *Appendix C*). Now we introduce the Doppler Effect in the input signal as a *slow* and *weak* angular modulation, viz.:

$$s_d(t) = A\sin\left[\omega_s t + m_d \sin(\omega_d t)\right], \quad \omega_d \ll \omega_s \quad , \quad m_d \ll 1. \tag{31}$$

We assume the ratio ω_s/ω_d to be a rational number, so that the input signal has period $T_d = 2\pi/\omega_d$. In view of the *adiabatic* assumption ($\omega_d \ll \omega_s$) we can determine the corresponding $P_+(t)$ solution by *perturbing* eq.(30):

$$P_+(t) \approx \frac{1}{2} + \left[P_+^{(max)} - \frac{1}{2}\right] \sin\left[\omega_s t + \psi + m_d \sin(\omega_d t)\right]. \tag{32}$$

[5] The analysis of the parametric detector is straightforward. For non-coherent detection we have to consider also the time-quantization error.

Adopting the sampling scheme introduced in *Section 5* with reference to coherent detection:

$$t_k = \frac{\frac{(2k+1)\pi}{2} - \psi}{\omega_s} \quad , \quad x_k = (-1)^k x(t_k) \quad , \quad k = 0, 1, 2, ..., 2N-1, \tag{33}$$

and so negleting the Doppler Effect, one has a performance degradation. One can easily estimate this degradation in the *worst case* by computing:

$$P_+^{(worst)} := \min_{k=0,1,...,2\lfloor \frac{T_d}{T_s} \rfloor - 1} \left\{ P_+^{(k)} \right\}, \tag{34}$$

where

$$P_+^{(k)} = \frac{1}{2} + \left[P_+^{(max)} - \frac{1}{2} \right] |\sin \left[\frac{(2k+1)\pi}{2} + m_d \sin \left[\frac{\omega_d}{\omega_s} \left(\frac{(2k+1)\pi}{2} - \psi \right) \right] \right]|. \tag{35}$$

One finally finds:

$$\alpha = I_{1/2}(\Gamma + 1, 2N - \Gamma) \quad , \quad \beta^{(worst)} = 1 - I_{P_+^{(worst)}}(\Gamma + 1, 2N - \Gamma). \tag{36}$$

Fig. 14 shows the ROC degradation as a function of the modulation strenght m_d.

6 - Conclusions and Recommendations.

We have characterized the SR mechanism with reference to Signal Detection. The results of extensive numerical simulations show a distinct resonant behaviour (in terms of performance) in substantial agreement with Benzi's SR condition [1]. Evaluation of the detection performance (ROC) has been accomplished with reference to statistically well-based detection strategies, using Monte Carlo Methods. Detection performance seems not much worse (in some case comparable) to the OLD ones, at the same level of complexity. As hints for future research we can cite:

- Analysis of the possible *enhancement* features of a SR device incorporated in a Signal Processing system.
- Analysis of SR in extended systems (globally coupled devices) and its application to Signal Processing. As stated in *Section 5*, a single-device SR detector seems to be in principle worse as compared to the optimum linear filter. Currently, there is a great interest in the Scientists for the use of arrays of coupled SR devices, due to the possibility of enhancing the processing performance (*Array-Enhanced SR*, [4],[5]).
- Study of SR for coloured, non-gaussian noise.

Appendix A - Continuous Strategies.

In this Appendix we show that OLD is optimum also by comparison with the *nonlinear* SR strategy. More precisely we address the general problem of finding the optimum (coherent) performance for a continuous detection strategy related to an *Itô Filter*, viz.:

$$\begin{cases} \dot{x} = a(x) + s(t) + \epsilon\, n(t), \\ x(0) = x_0, \end{cases} \qquad t \in [0,T]\,, \tag{A1}$$

$s(t)$ and $n(t)$ being, respectively, the (known) signal to detect and a stationary (zero mean) white gaussian noise, $E[n(t)n(t+\tau)] = \delta(\tau)$. Introducing a Δ-step time discretization one has :

$$\begin{array}{l} x_{k+1} - x_k = \Delta[a(x_k) + s_k + \epsilon\, n_k], \quad k = 0,1,..,N-1, \quad N = \lfloor T/\Delta \rfloor, \\ x_k = x(k\Delta), \quad s_k = s(k\Delta), \quad n_k = n(k\Delta). \end{array} \tag{A2}$$

The optimum strategy, according to Neumann-Pearson [19], is based on a test of the *maximum likelihood ratio*:

$$\begin{cases} l(x_0,...,x_N) \geq c \quad \Rightarrow \quad \textit{signal present}, \\ l(x_0,...,x_N) < c \quad \Rightarrow \quad \textit{no signal present}, \end{cases} \tag{A3}$$

$$l(x_0,...,x_N) = \frac{p(x_0,...,x_N \mid \textit{signal})}{p(x_0,...,x_N \mid \textit{no signal})}, \tag{A4}$$

$p(\cdot)$ being the joined PDF and c being a suitable threshold. Using the *short-time Euler approximation* ($\Delta \to 0$, [11],[22]) for the involved PDFs one has:

$$p(x_0,...,x_N \mid \textit{no signal}) = (2\pi\Delta\epsilon^2)^{-\frac{N}{2}} \prod_{k=0}^{N-1} \exp\left\{-\frac{[x_{k+1} - x_k - a(x_k)\Delta]^2}{2\Delta\epsilon^2}\right\}, \tag{A5}$$

$$p(x_0,...,x_N \mid \textit{signal}) = (2\pi\Delta\epsilon^2)^{-\frac{N}{2}} \prod_{k=0}^{N-1} \exp\left\{-\frac{[x_{k+1} - x_k - a(x_k)\Delta - s_k\Delta]^2}{2\Delta\epsilon^2}\right\}. \tag{A6}$$

Thus:

$$\log[l(x_0,...,x_N)] = \frac{1}{\epsilon^2} \sum_{k=0}^{N-1} \left\{ s_k\,[x_{k+1} - x_k - a(x_k)\Delta] - \frac{1}{2} s_k^2 \Delta \right\}. \tag{A7}$$

Taking $(A2)$ into account and letting $\Delta \to 0$ (*continuos strategy*), the Neumann-Pearson test $(A3)$ can be rephrased as follows:

$$\begin{cases} \dfrac{1}{\epsilon^2}\displaystyle\int_0^T s(t)z(t)\,dt \geq \log c + \frac{1}{2}\frac{E_s}{\epsilon^2} & \Rightarrow \quad \textit{signal present}, \\ \dfrac{1}{\epsilon^2}\displaystyle\int_0^T s(t)z(t)\,dt < \log c + \frac{1}{2}\frac{E_s}{\epsilon^2} & \Rightarrow \quad \textit{no signal present}, \end{cases} \tag{A8}$$

where:

$$z(t) = s(t) + \epsilon\, n(t), \qquad E_s = \int_0^T s^2(t)\,dt. \tag{A9}$$

It can be readily verify that the above decision rule is identical to that obtained applying the OLD to the *input* signal+noise mixture $z(t)$ (see [19],[21]). Thus, the optimum continuous strategy applied at the output of an Itô Filter involves *i)* the recostruction of the input signal+noise (cancelling the filter effects!) and *ii)* the application of OLD. As a conclusion, one can state that the OLD performance represents an upper-bound for *any* continuous strategy linear or nonlinear. The *strobed* strategies discussed in *Section 5* yield a good tradeoff between performance and budget (storage and computational).

Appendix B - Optimum Detection Strategy in Adiabatic Regime.

In this appendix we show that the optimum strategy in adiabatic regime is equivalent to the barycenter analyis introduced in Section 5:

$$\begin{cases} \mu \geq \Gamma & \Rightarrow \quad \textit{signal present}, \\ \mu < \Gamma & \Rightarrow \quad \textit{no signal present}, \end{cases} \tag{B1}$$

where Γ a suitable threshold,

$$\mu = \frac{1}{2N}\sum_{k=0}^{2N-1} x_k, \tag{B2}$$

and x_k is a time series defined by:

$$x_k = (-1)^k x(t_k), \qquad k = 0, 1, ..., 2N-1. \tag{B3}$$

The sampling times are defined as follows[6]:

$$t_k = \frac{(2k+1)\pi}{2\omega_s}. \tag{B4}$$

It is well known that the optimum strategy, according to Neumann-Pearson [19], is based on *maximum likelihood ratio* test:

[6]Note that the phase lag introduced by the SR filter is negligible in the adiabatic regime.

$$\begin{cases} l[x(t_0),...,x(t_{2N-1})] \geq c \quad \Rightarrow \quad signal\ present, \\ l[x_0,...,x(t_{2N-1})] < c \quad \Rightarrow \quad no\ signal\ present, \end{cases} \tag{B5}$$

$$l[x(t_0),...,x(t_{2N-1})] = \frac{p(x(t_0),...,x(t_{2N-1}) \mid signal)}{p(x(t_0),...,x(t_{2N-1}) \mid no\ signal)}, \tag{B6}$$

$p(\cdot)$ being the joined PDF and c being a suitable threshold. In the adiabatic regime ($T_s \gg T_k$) the random variables $x(t_k)$ are independent and identically distributed (*Section*3, eq. (10)), thus we can factorize the joined PDFs, obtaining the following (approximate) expressions:

$$p(x(t_0),...,x(t_{2N-1}) \mid signal) = (C_1)^{2N} \prod_{k=0}^{2N-1} \exp\left[\frac{\frac{ax(t_k)^2}{2} - \frac{bx(t_k)^4}{4} + Ax(t_k)\sin(\omega_s t_k)}{\epsilon^2/2}\right], \tag{B7}$$

$$p(x(t_0),...,x(t_{2N-1}) \mid no\ signal) = (C_0)^{2N} \prod_{k=0}^{2N-1} \exp\left[\frac{\frac{ax(t_k)^2}{2} - \frac{bx(t_k)^4}{4}}{\epsilon^2/2}\right]. \tag{B8}$$

Thus:

$$\log\{l[x(t_0),...,x(t_{2N-1})]\} \propto \sum_{k=0}^{2N-1} x(t_k)\sin(\omega_s t_k) = \sum_{k=0}^{2N-1} (-1)^k x(t_k) \propto \mu. \tag{B9}$$

The above equation immediately show the perfect equivalence between optimum (Neumann-Pearson) strategy and barycenter analysis.

Appendix C - Numerical Solution of Stochastic Differential Equations.

We consider a standard monodimensional Itô Stochastic Differential Equation (henceforth SDE) [22]:

$$\begin{cases} \dot{x} = a[x(t),t] + b[x(t),t]\ n(t), \\ x(0) = x_0, \end{cases} \tag{C1}$$

$n(t)$ being a stationary zero mean white gaussian noise

$$E[n(t)n(t+\tau)] = \delta(\tau). \tag{C2}$$

The most efficient and widely applicable numerical approach to solve seems to be the simulation of sample paths, having introduced a suitable time discretization, e.g.:

$$0 = t_0 < t_1 < ... < t_N = t, \quad t_k - t_{k-1} = \Delta = t/N. \tag{C3}$$

In many pratical situations, as in *Section 3-4*, one may only be interested in the expectation $E[g(x(t))]$ for some function g. The type of approximation required is called *weak*, because it is not necessary to have a close pathwise approximation to the Itô process. In our simulation, presented in *Section 3-4*, we have used a *weak predictor-corrector method* of order 2.0 [22] because of its numerical stability. This method uses a corrector:

$$x_{n+1} = x_n + 0.5[a(\bar{x}_{n+1} + a(x_n))]\Delta + \phi_n, \tag{C4}$$

where:

$$\phi_n = 0.25[b(\bar{x}^+) + b(\bar{x}^-) + 2b(x_n)]\Delta W + \\ +0.25[b(\bar{x}^+) - b(\bar{x}^-)][(\Delta W)^2 - \Delta]\Delta^{-1/2}, \tag{C5}$$

with supporting values:

$$\bar{x}^{\pm} = x_n + a(x_n)\Delta \pm b(x_n)\sqrt{\Delta}, \tag{C6}$$

and predictor

$$\bar{x}_{n+1} = x_n + 0.5[a(\bar{x}) + a(x_n)]\Delta + \phi_n, \tag{C7}$$

with the supporting value

$$\bar{x} = x_n + a(x_n)\Delta + b(x_n)\Delta W, \tag{C8}$$

where ΔW are independent $N(0;\Delta)$ Gaussian random variables and the time dependence is dropped for simplicity. Following the classical Monte Carlo scheme [22] we evaluate the moment $E[g(x(t))]$ using the estimator

$$\mu_M = M^{-1}\sum_{h=1}^{M} g[x_N^h], \tag{C9}$$

which represents th arithmetic mean of M independent simulations of the random variable $g(x_N)$. Obviously the result will be affected by *i)* a systematic error (effect of discretization, $\epsilon_{sys} \sim \mathcal{O}(\Delta^2)$) and *ii)* a statistical error, which in view of Central Limit Theorem is asymptotically gaussian distributed with zero average and r.m.s. deviation: $\epsilon_{stat} \sim \{M^{-1}Var[g(x_N)]\}^{-1/2}$. It is readily seen that the confidence intervals width decreases with order $M^{-1/2}$ as $M \to \infty$.

References

[1] R. Benzi et al., J. Phys. A, **14**, L453, 1981.

[2] L. Gammaitoni et al. , Phys. Lett. A, **142**, 59, 1989.

[3] V. Pierro et al. , Proc. EU.SI.P.CO. 92, Brussells, 1992

[4] M. E. Inchiosa , A. R. Bulsara, Phys. Rev. E, **53**, 53, 1996.

[5] A. R. Bulsara, L. Gammaitoni, Phys. Today, 39, March 1996.

[6] J. Collins, C. Chow , T. Imhoff, Phys. Rev. E, **52**, 315, 1995.

[7] P. Jung, P. Hanggi, Phys. Rev. A, **44**, 8032, 1991.

[8] M. Dykman et al., Phys. Lett. A, **180**, 332, 1993.

[9] B. Jost , B. Saleh , Opt. Lett. , **21**, 287, 1996.

[10] C. W. Gardiner, *Handbook of Stochastic Methods for Physics , Chemistry and Natural Sciences*, Springer-Verlag, Berlin , 1983.

[11] H. Risken, *The Fokker-Planck Equation*, Springer-Verlag, Berlin, 1984

[12] L. Ramirez-Piscina et al. , Phys. Rev. A, **40**, 2120, 1989.

[13] R.S. Larson , M.D. Kostin , J. Chem. Phys., **69**, 4821, 1978.

[14] B. McNamara, K. Wiesenfeld , Phys. Rev. A, **39**, 4854, 1989.

[15] L. Gammaitoni et al. , Phys. Rev. Lett., **74**, 1052, 1995.

[16] G. Hu et al. , Phys. Rev. A, **42**, 2030, 1990.

[17] L. Gammaitoni et al. , Phys. Lett. A, **158**, 449, 1991.

[18] N.G. Stocks et al. , J. Phys. A, **26**, L385, 1993.

[19] B. Levine, *Fondements Théouriques de la Radiotechnique Statistique*, MIR , Moskow, 1976.

[20] S. Gradshteyin, M. Ryzhik, *Table of Integrals Series and Products*, Academic Press, New York, 1976.

[21] J.V. Di Franco, W.L. Rubin, *Radar Detection*, Artech House, Dedham, 1980.

[22] P.E. Kloeden, E. Platen, *Numerical Solution of Stochastic Differential Equations*, Springer, NY, 1991.

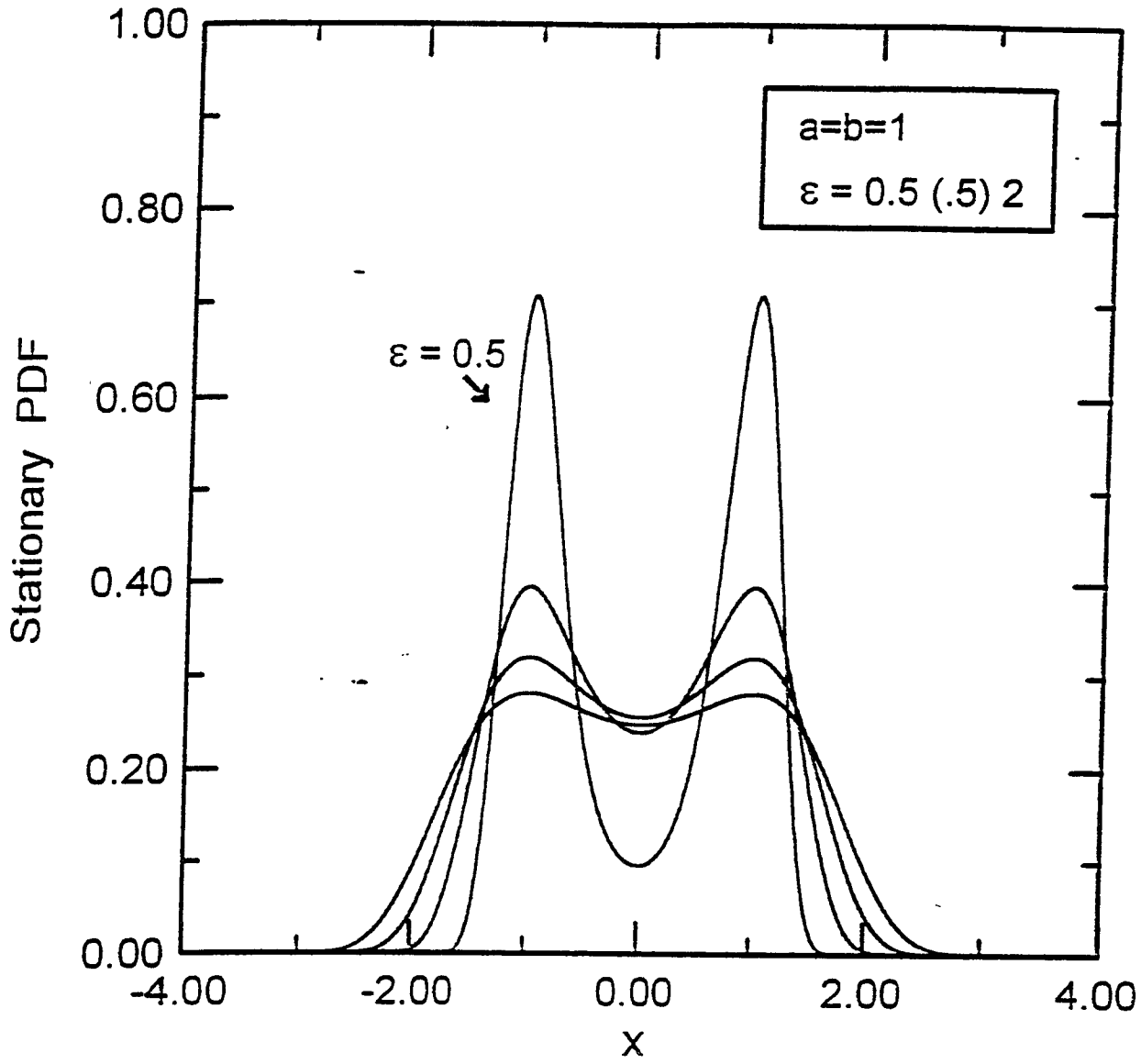

Fig. 1 - Stationary (steady state) PDF in the absence of signal.

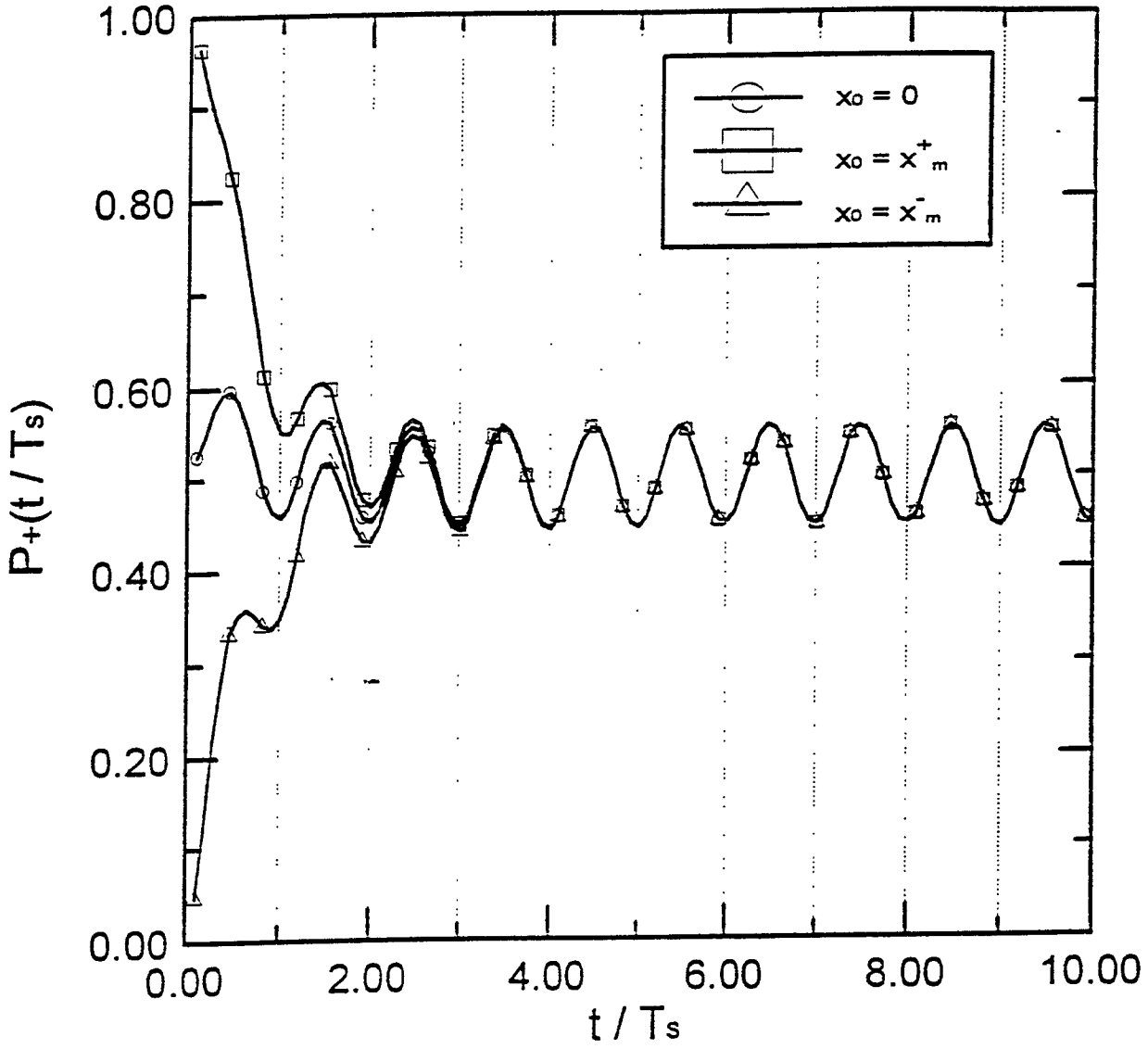

Fig. 2 - Time behaviour of the (a)symmetry indicator P_+, in the presence of an input harmonic signal, for three different initial conditions. The vertical dotted lines corresond to the zeros of the input signal.

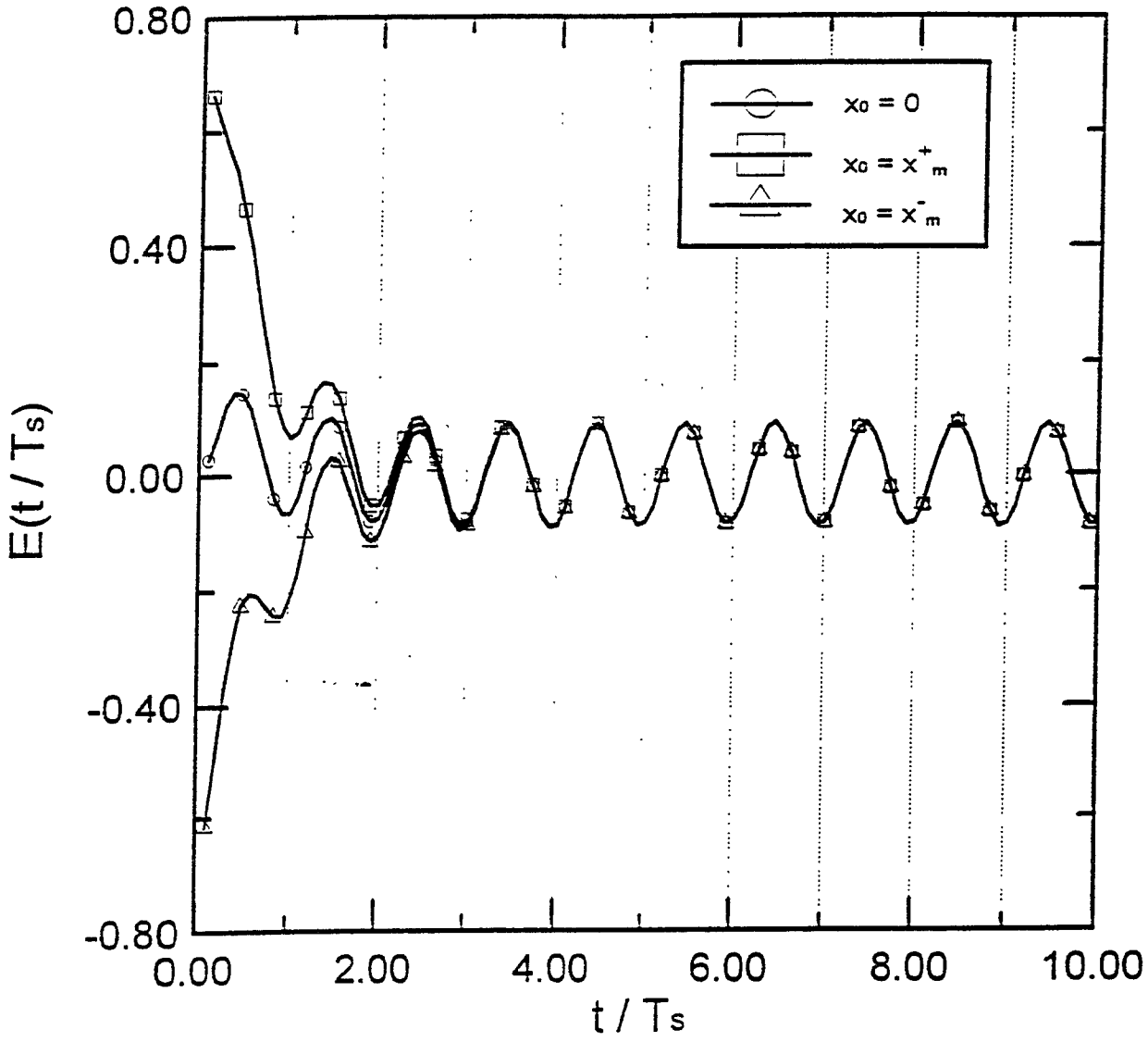

Fig. 3 - Time behaviour of the (a)symmetry indicator E, in the presence of an input harmonic signal. for three different initial conditions. The vertical dotted lines corresond to the zeros of the input signal.

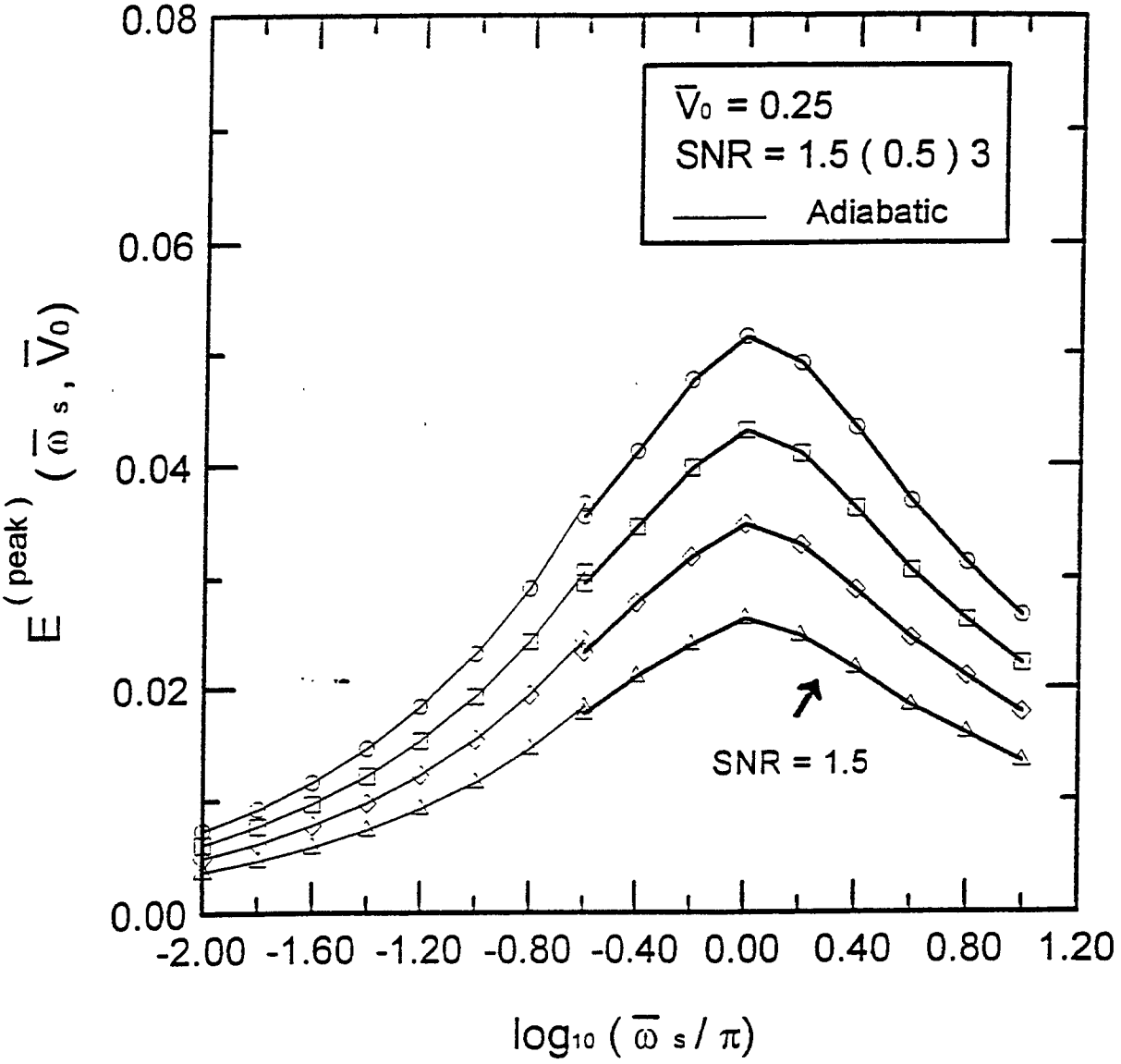

Fig. 5 - E amplitude frequency response of the SR filter, for various values of SNR. Dashed curves refer to the adiabatic approximation.

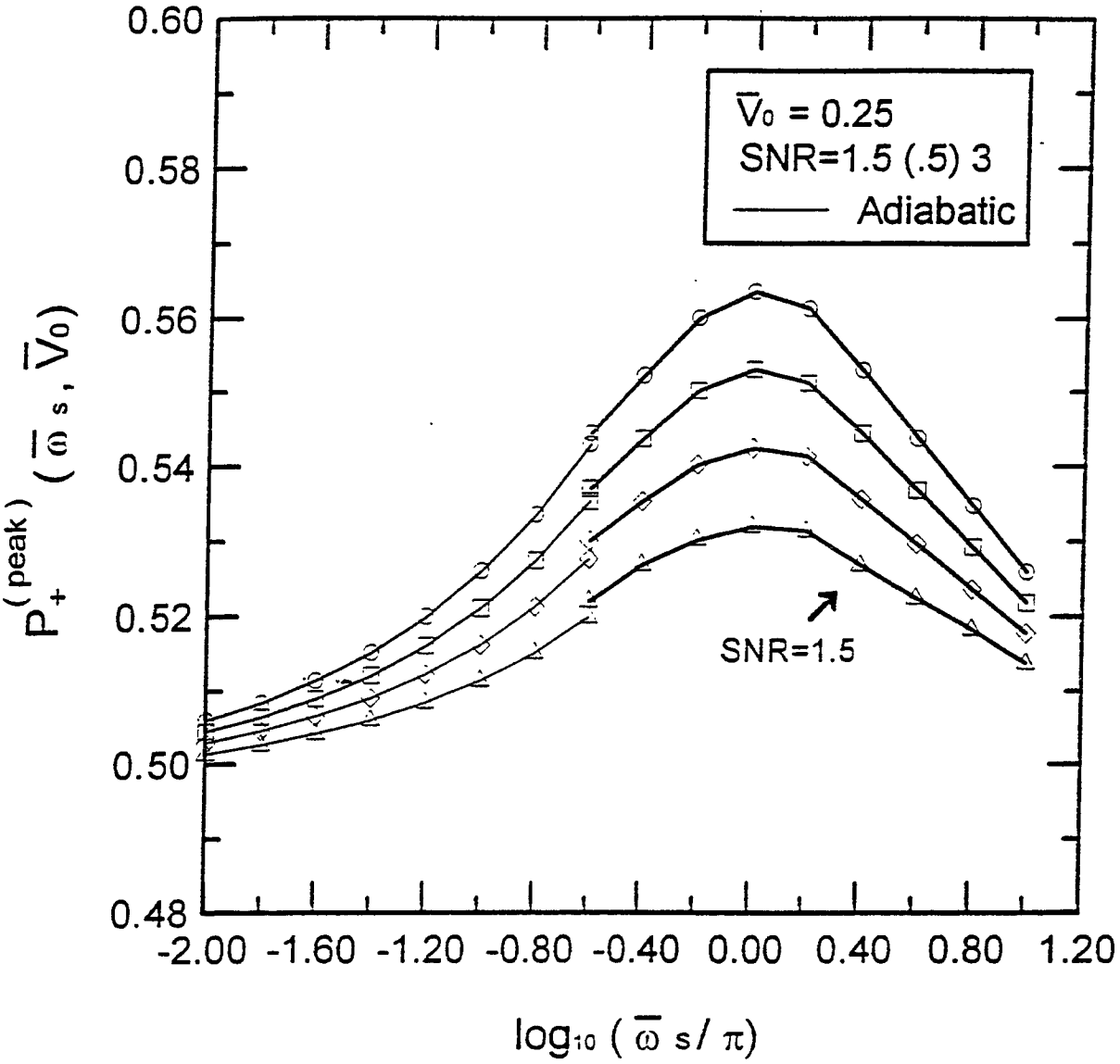

Fig. 4 - P_+ amplitude frequency response of the SR filter, for various values of SNR. Dashed curves refer to the adiabatic approximation.

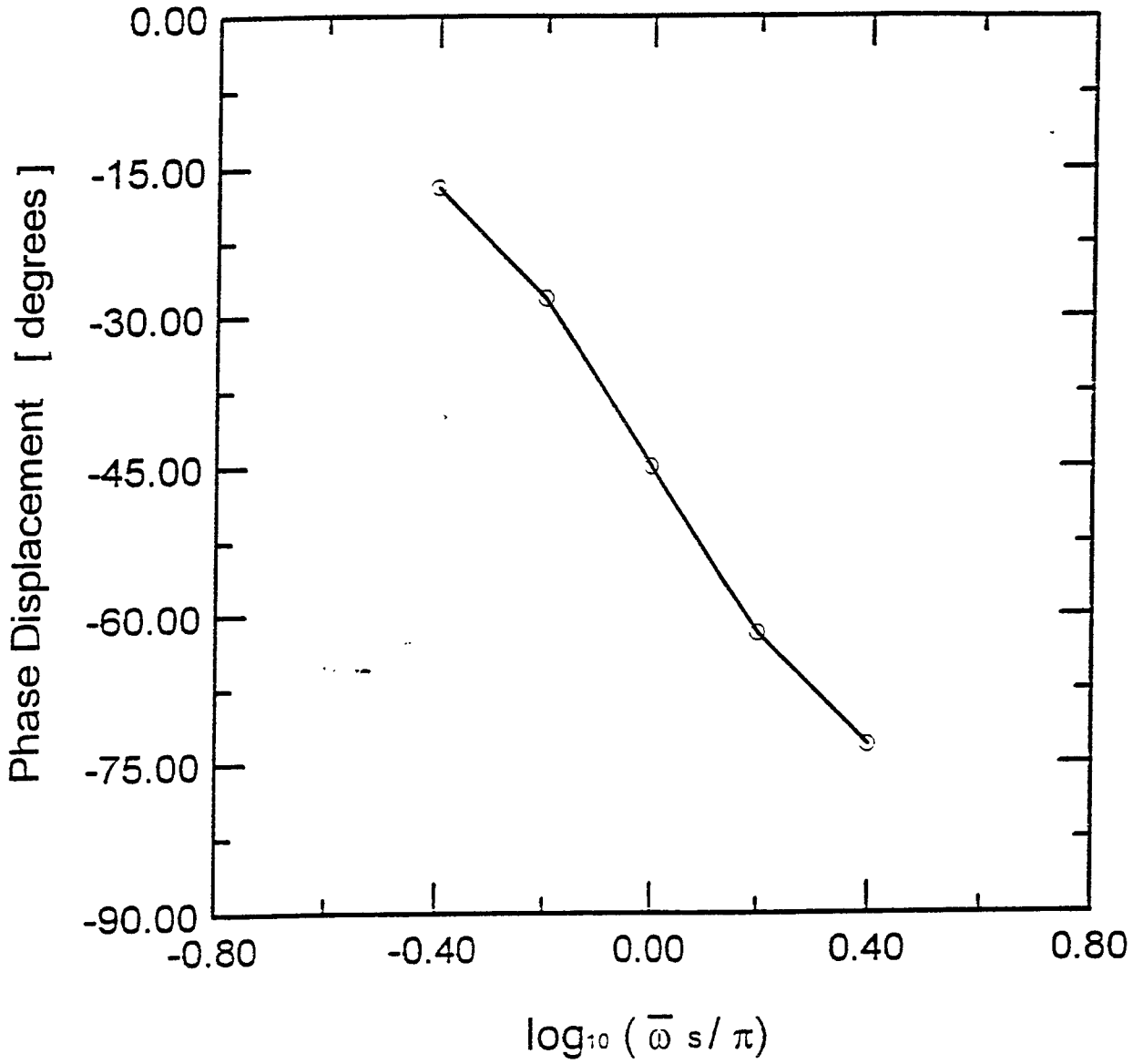

Fig. 6 - $P_+(E)$ phase frequency response.

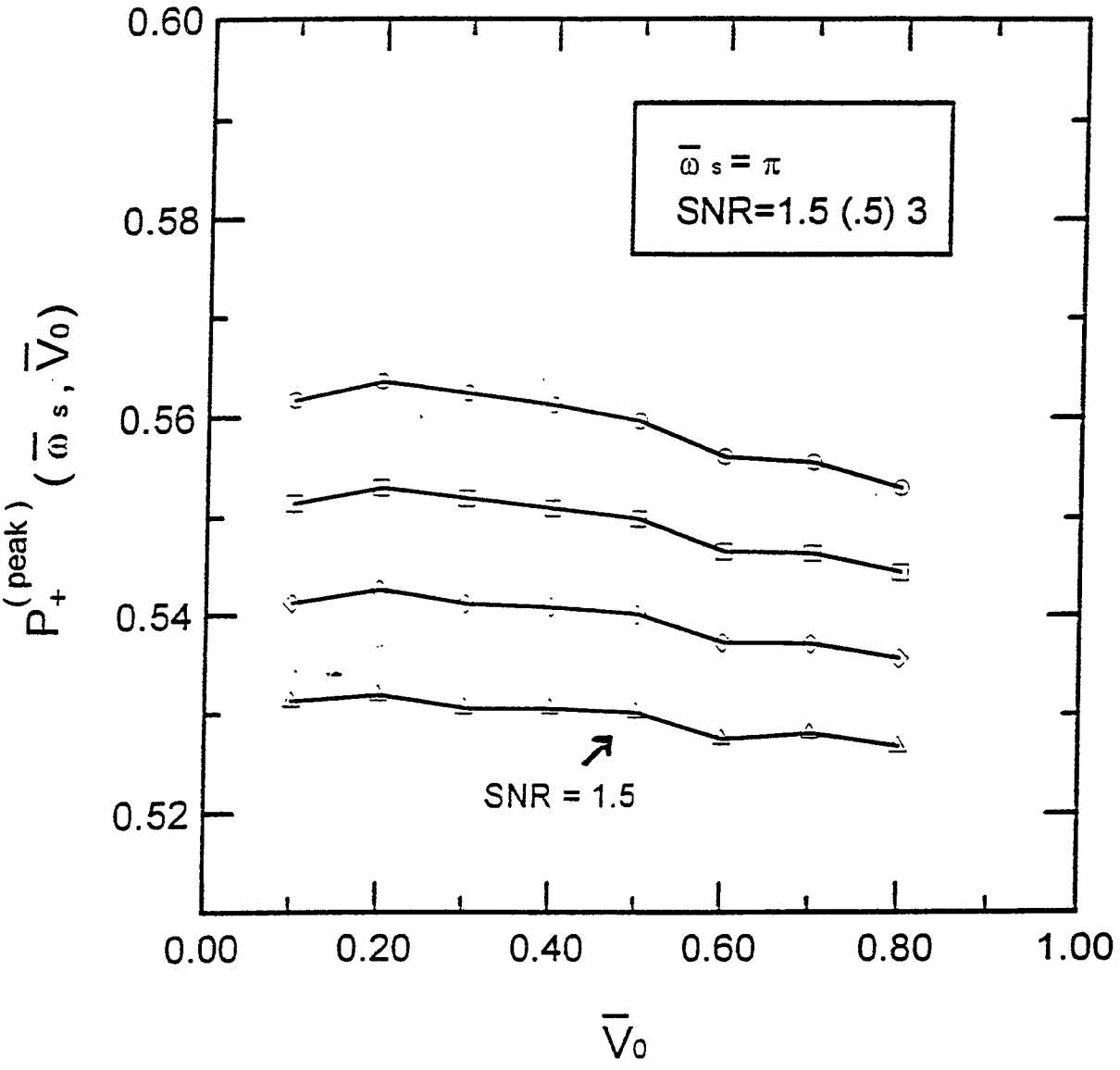

Fig. 7 - P_+ resonance peak level ($\bar{\omega}_s = \pi$) versus normalized potential barrier height.

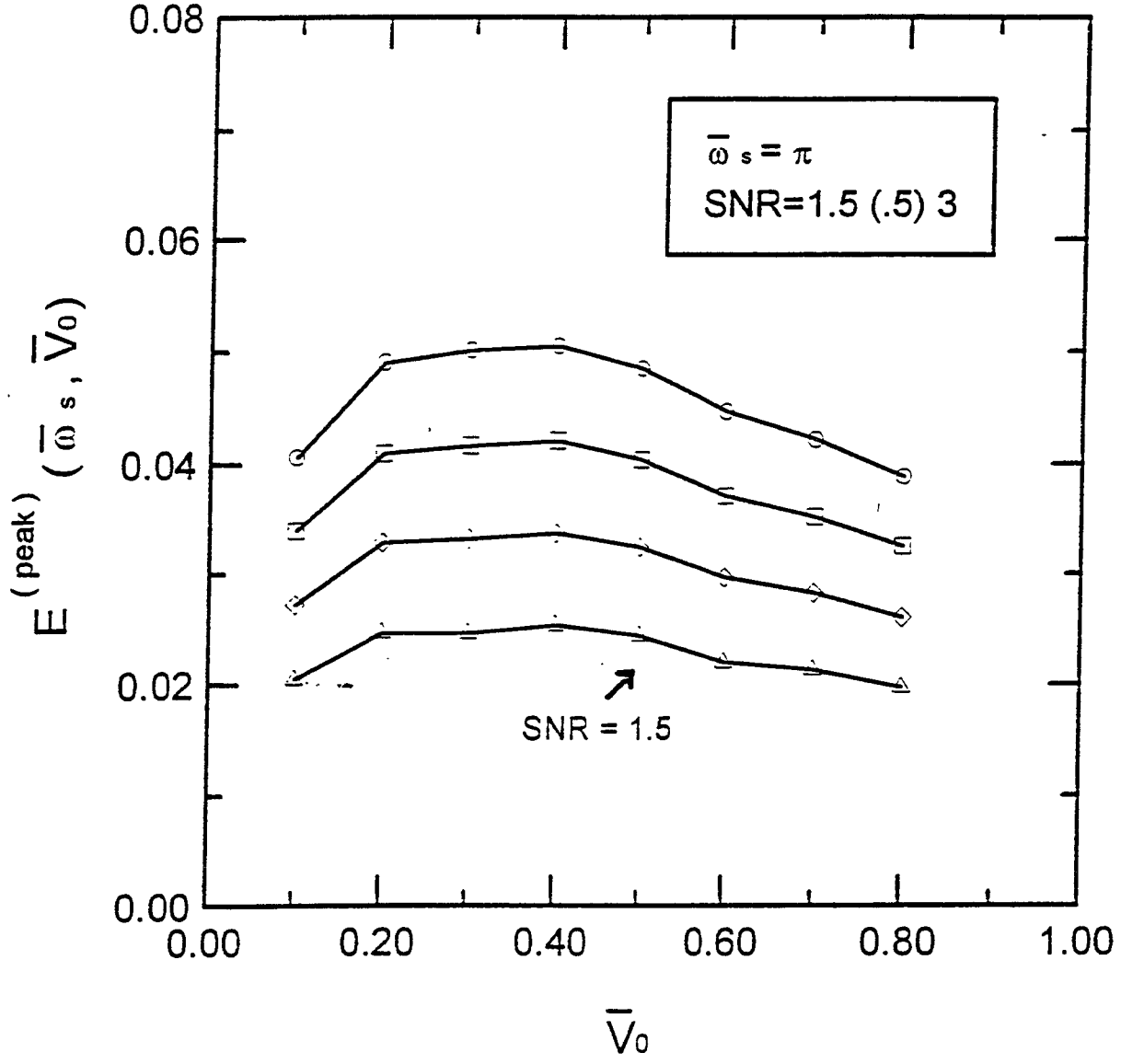

Fig. 8 - E resonance peak level ($\bar{\omega}_s = \pi$) versus normalized potential barrier height.

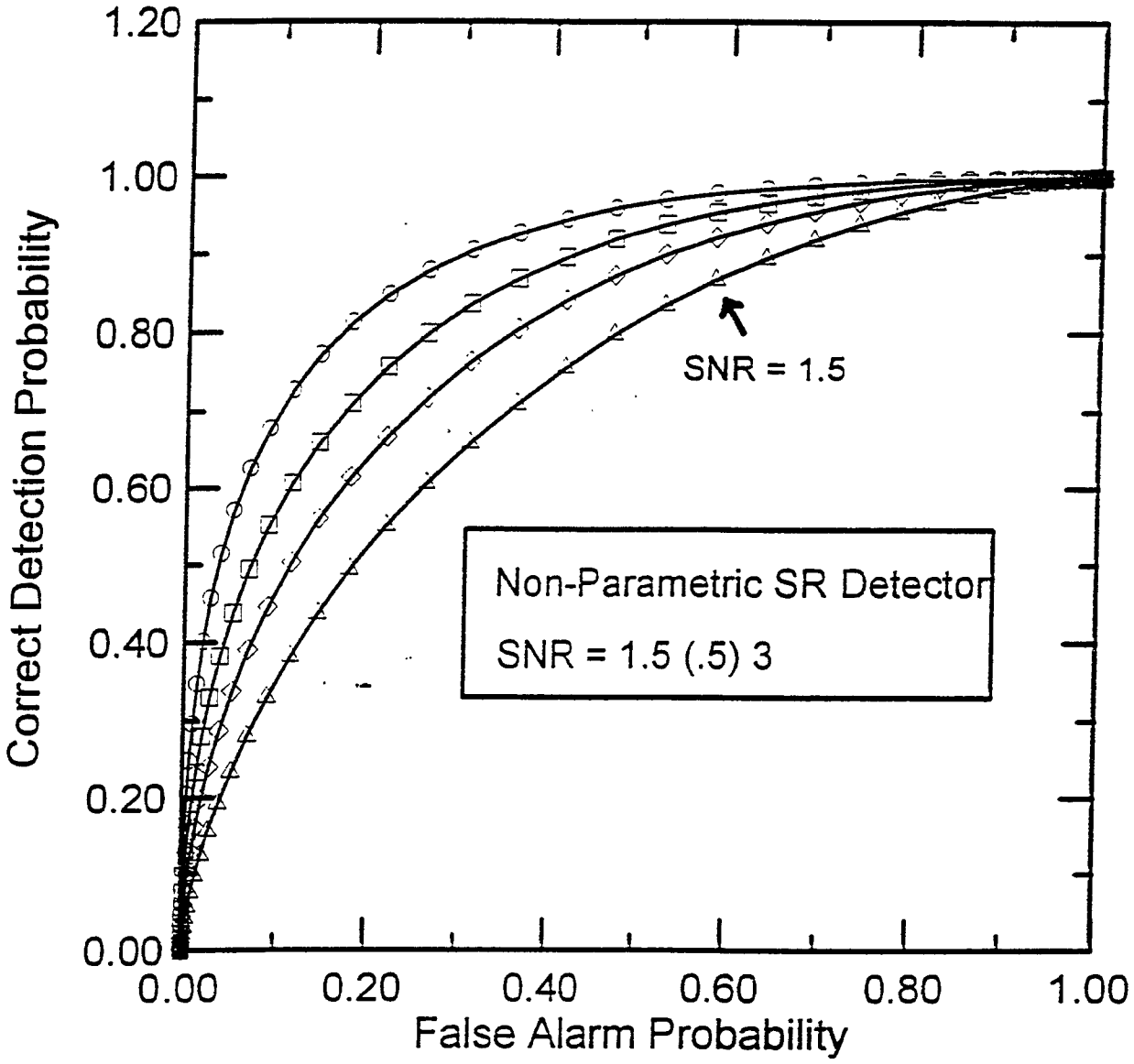

Fig. 9 - Receiver operating characteristics of a non-parametric SR detector.

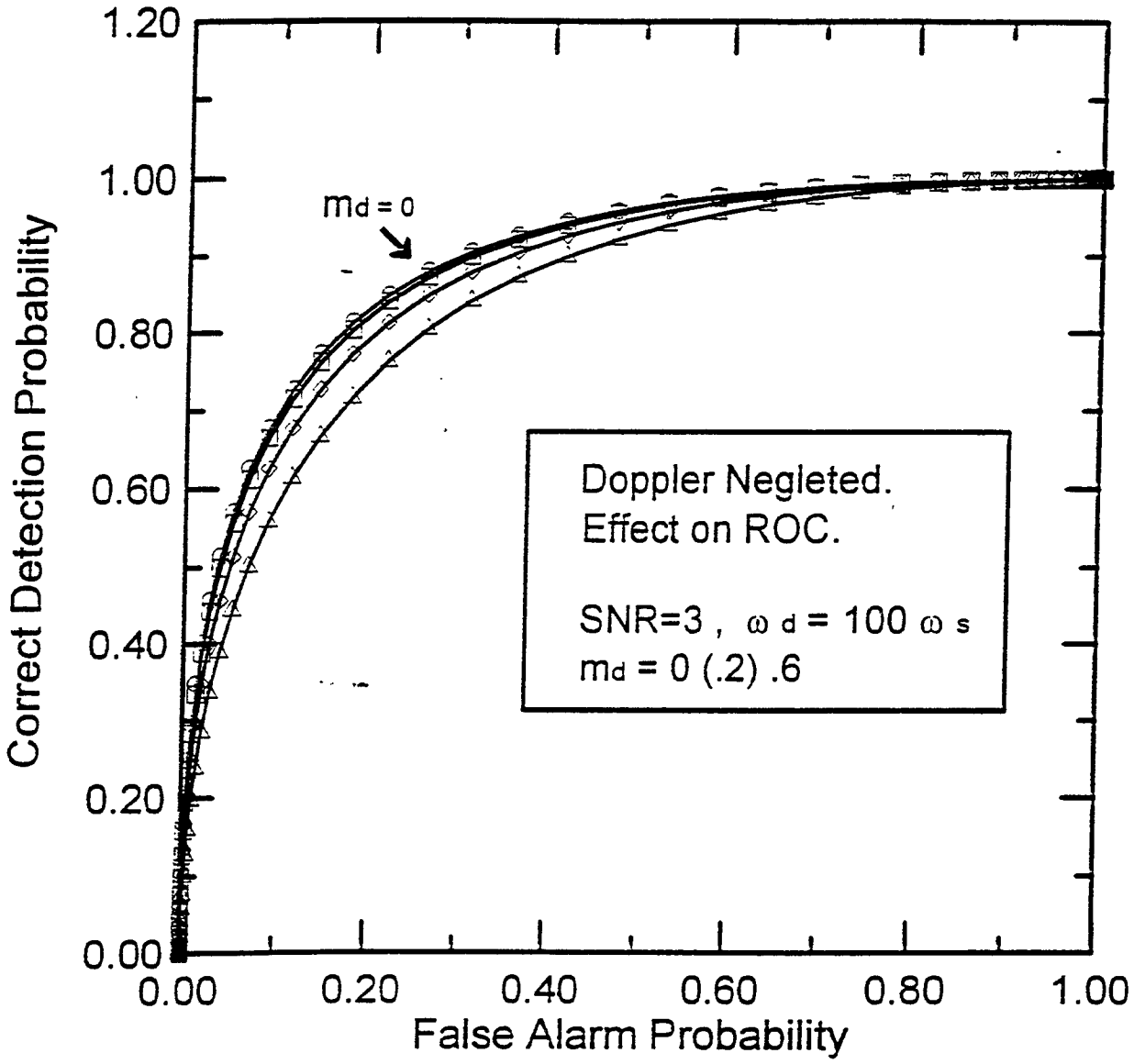

Fig. 14 - Effect on ROC of negleting Doppler modulation.
Non-parametric SR detector.

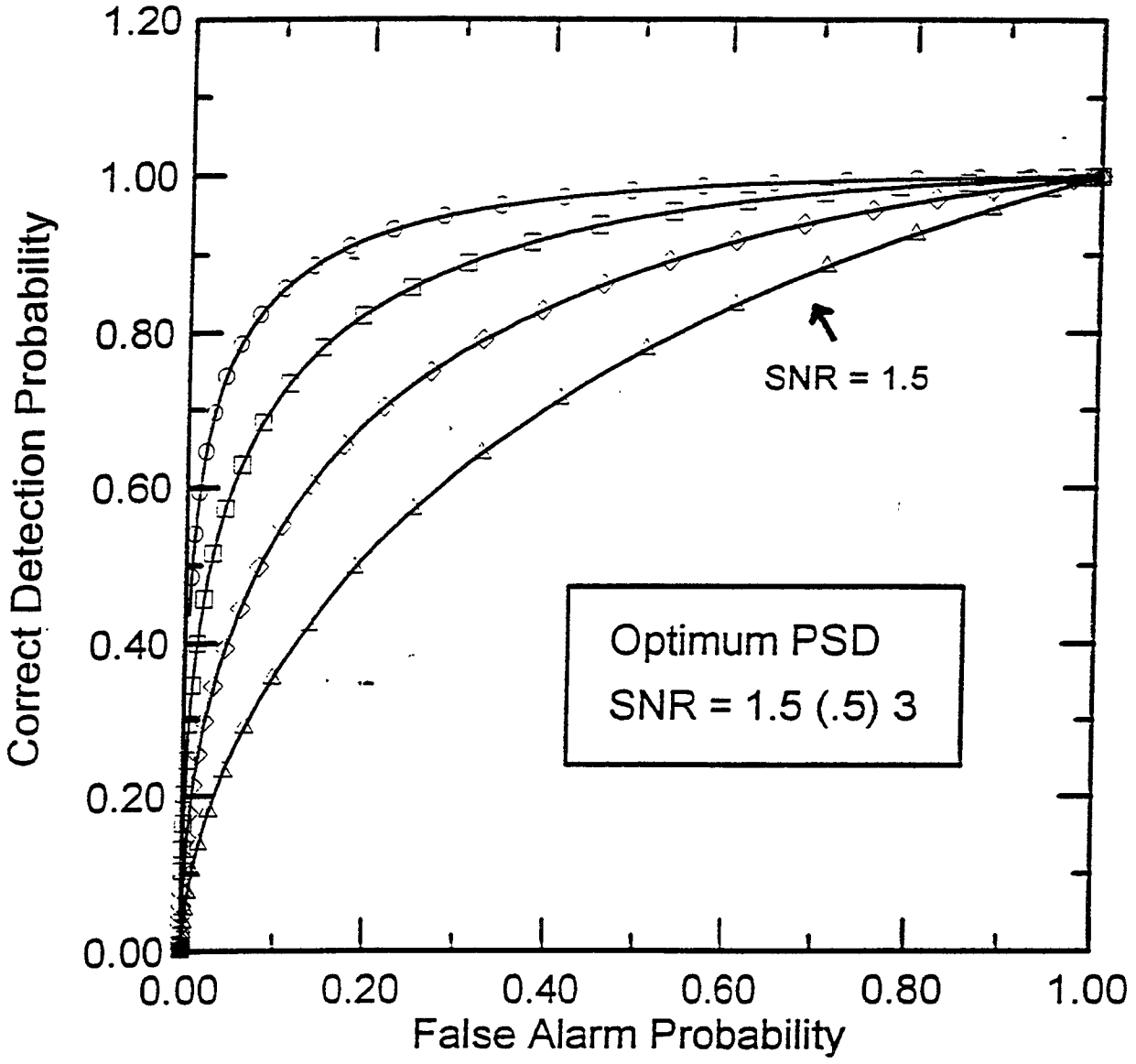

Fig. 12 - Receiver operating characteristics of an optimum phase sensitive detector.

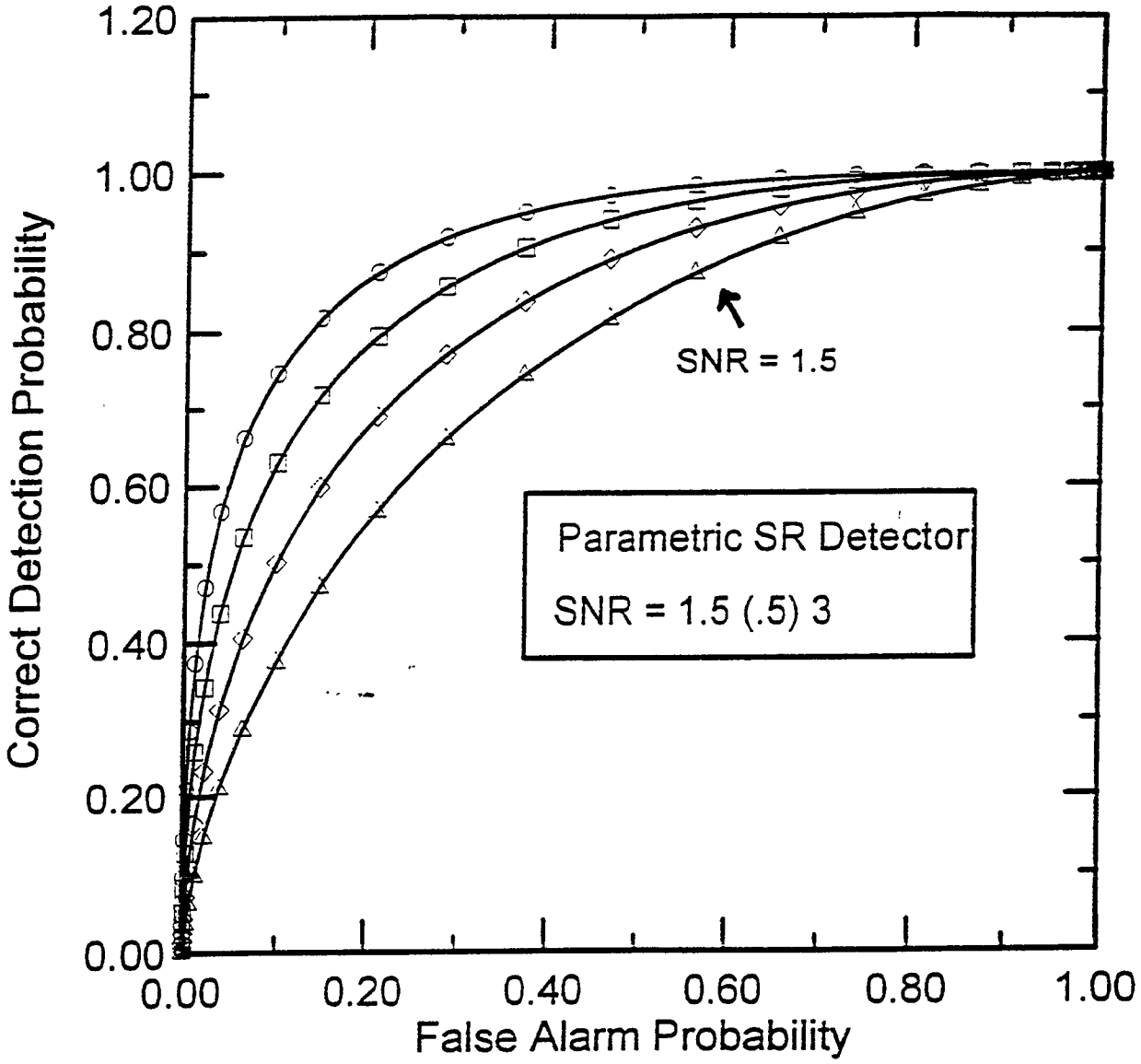

Fig. 11 - Receiver operating characteristics of a parametric SR detector.

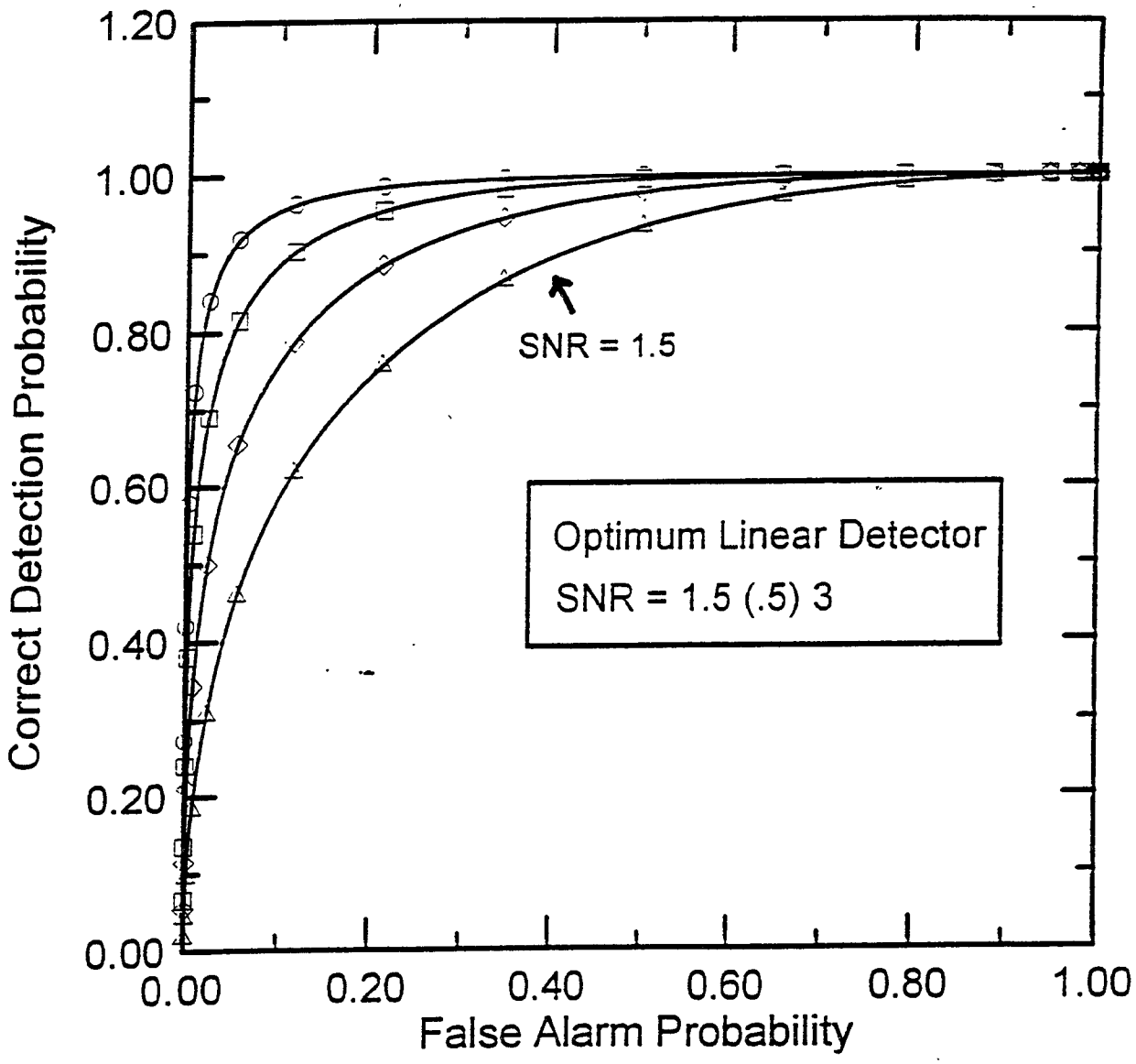

Fig. 10 - Receiver operating characteristics of an optimum linear detector.

Computational Costs

(neglecting spin effects)

	LIGO-I	GEO600
(depth at S/N = 10)	30 Mpc	7 Mpc
$m_{min} = 1\ M_\odot$ (astronomy) Longest template is 45s / 3kcycles / 1 Mbyte		
Number of templates	2×10^3	4×10^3
Total storage	2 Gbytes	4 Gbytes
CPU power	180 Mflops	470 Mflops
$m_{min} = 0.2\ M_\odot$ (nuclear physics) Longest template is 650s / 41 kcycles / 8 Mbytes		
Number of templates	1.5×10^5	3.2×10^5
Total storage	2 Tbytes	6 Tbytes $\sim m_{min}^{-13/3}$
CPU power	16 Gflops	40 Gflops $\sim m_{min}^{-8/3}$

(10% false dismissal rate)

Unresolved Issues

Broad issues:

- Hierarchical searches [Dhurandhar & Mohanty, Owen & Thorne]
- Searches for spinning, precessing binaries [Apostolatos]
- Searches for very low-mass compact objects [Thorne?]
- Multiple-interferometer searches [Finn]
- Massive systems [IBBH, Grand Challenge]

Nuts & bolts: [Lazzarini, Blackburn, Prince, Allen, Sathya...]

- Parallelizing algorithm – CPU power vs. RAM vs. disks vs. disk-memory I/O
- Windowing/gaps
- Compression?
- Nonstationary noise
- Do we need an on-line search?

Matched Filtering Binary Search

- Inspiraling binaries are the best-studied type of source.
- Research is moving from broad strategies to "nuts & bolts."

Matched filtering

- Cross-correlate template u with whitened data o/S_n:

$$\frac{S}{N} = \frac{\mathrm{Re}\int df\, \tilde{u}^*(f)\, \tilde{o}(f)/S_n(f)}{\mathrm{rms}\int df\, \tilde{u}^*(f)\, \tilde{n}(f)/S_n(f)}$$

- Template must "stay in phase" with signal over $\simeq 10^4$ cycles — form and parameters of template must be close to signal's.
- Current post-Newtonian templates are close enough.
- Potentially large parameter space:
  - Both masses are important.
  - Spins are important for some BH–NS binaries.
  - Eccentricity is negligible for almost all.
  - Angles don't matter for $T_{obs} \ll 1$ day.
- Simplest strategy: Lay out a grid in parameter space.

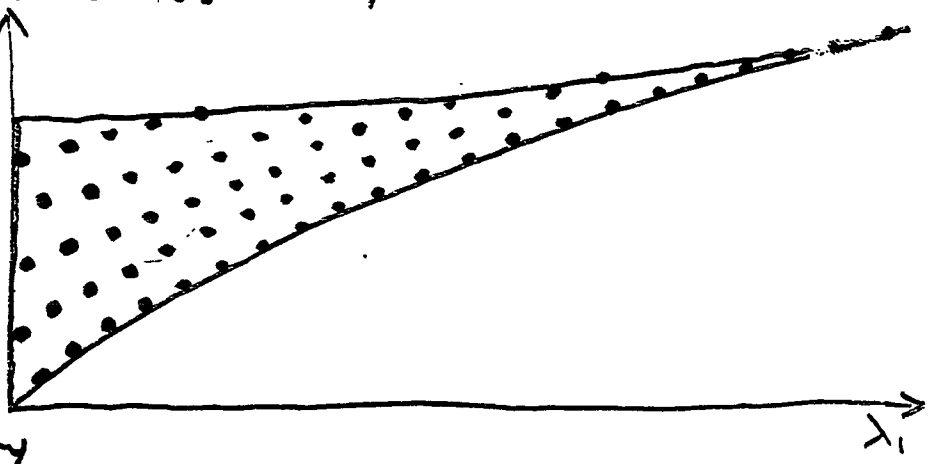

Differential geometry

- quantitatively, precisely relates $\Delta\lambda$ to S/N degradation,
- determines grid spacing and number of templates in terms of acceptable loss of S/N (event rate),
- has been applied to pulsar searches as well as inspiraling binaries,
- can be applied to other sources (e.g. black hole QNR).

All sky searches for CW sources

— computational requirements.

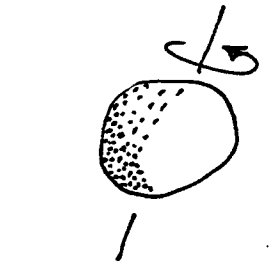

rotating neutron star

$$f(t) = f_0 \left(1 + f_1 t + f_2 t^2 + \cdots \right)$$

$\tau = \frac{1}{f_1}$: characteristic "spindown" timescale

feature of the signal @ the detector:

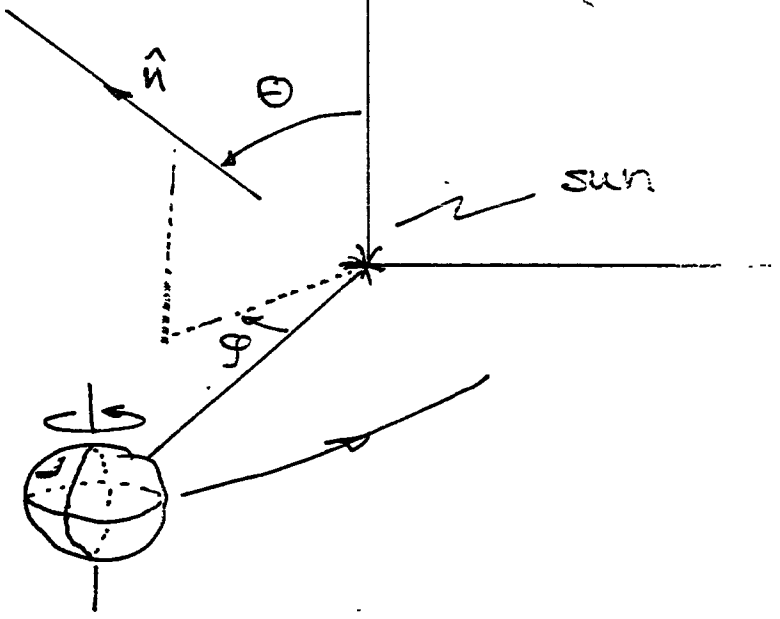

$$s_d(t) = \mathrm{Re}\left[A(t) \exp\{ i \Phi(t) \} \right]$$

$$\Phi(t) = 2\pi f_0 \int_0^t dt' \left(1 + \sum_k f_k t'^k \right)\left(1 + \frac{\vec{v}(t)}{c} \cdot \hat{n} \right)$$

$$= 2\pi f_0 t_b \left[\Theta, \varphi, f_i ; t \right]$$

Search Strategy: Brute Force

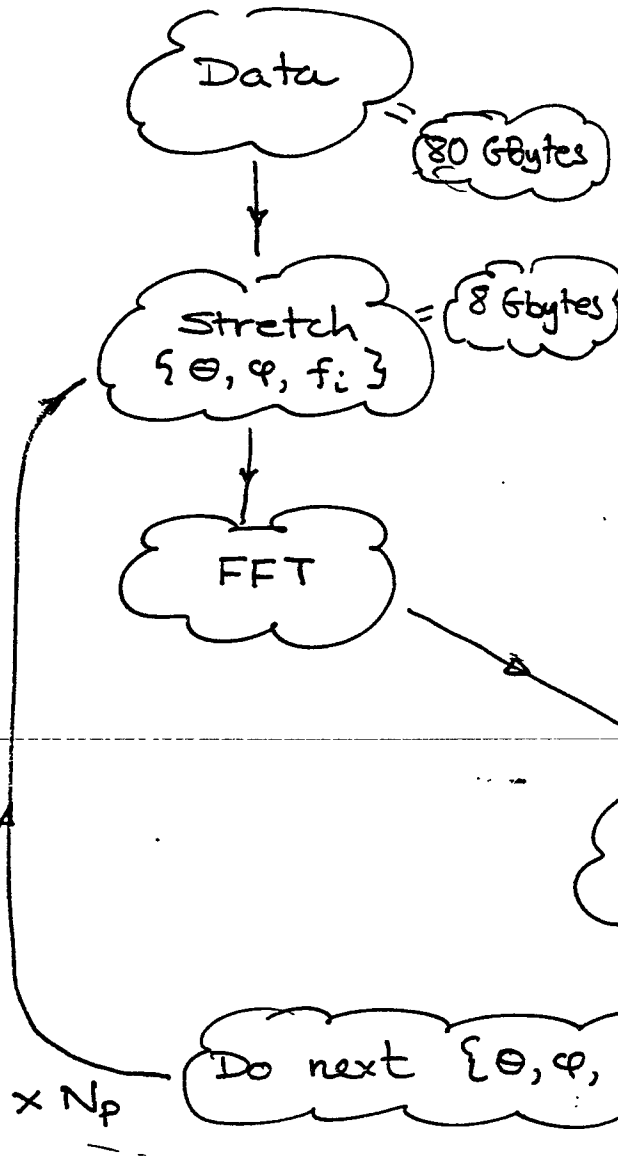

Long time series $o(t)$
$\sim 10^6 - 10^7$ secs $\Rightarrow 2\times10^9 - 2\times10^{10}$ samples
for $f_0 \leq 1$ kHz

Introduce canonical time $t_b[\theta, \varphi, f_i; t]$

$$\tilde{o}_b(f) = \int dt_b\, o(t)\, e^{2\pi i f t_b}$$

single FFT, on 100 GFlop machine of 10^6s ⟶ 1 sec.

$|\tilde{o}_b(f)|^2 \geq$ ⊕

need optimal metho to choose fewest # of points in parameter space

account for correlation between spindown + Doppler effects

+ "stepping"

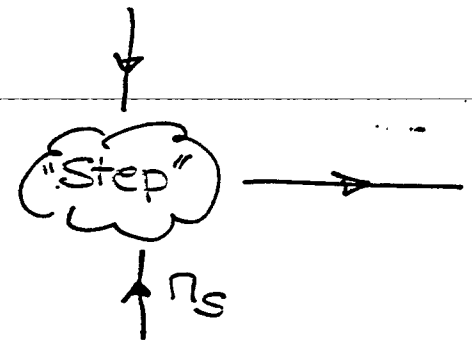

$\overline{n_s}$

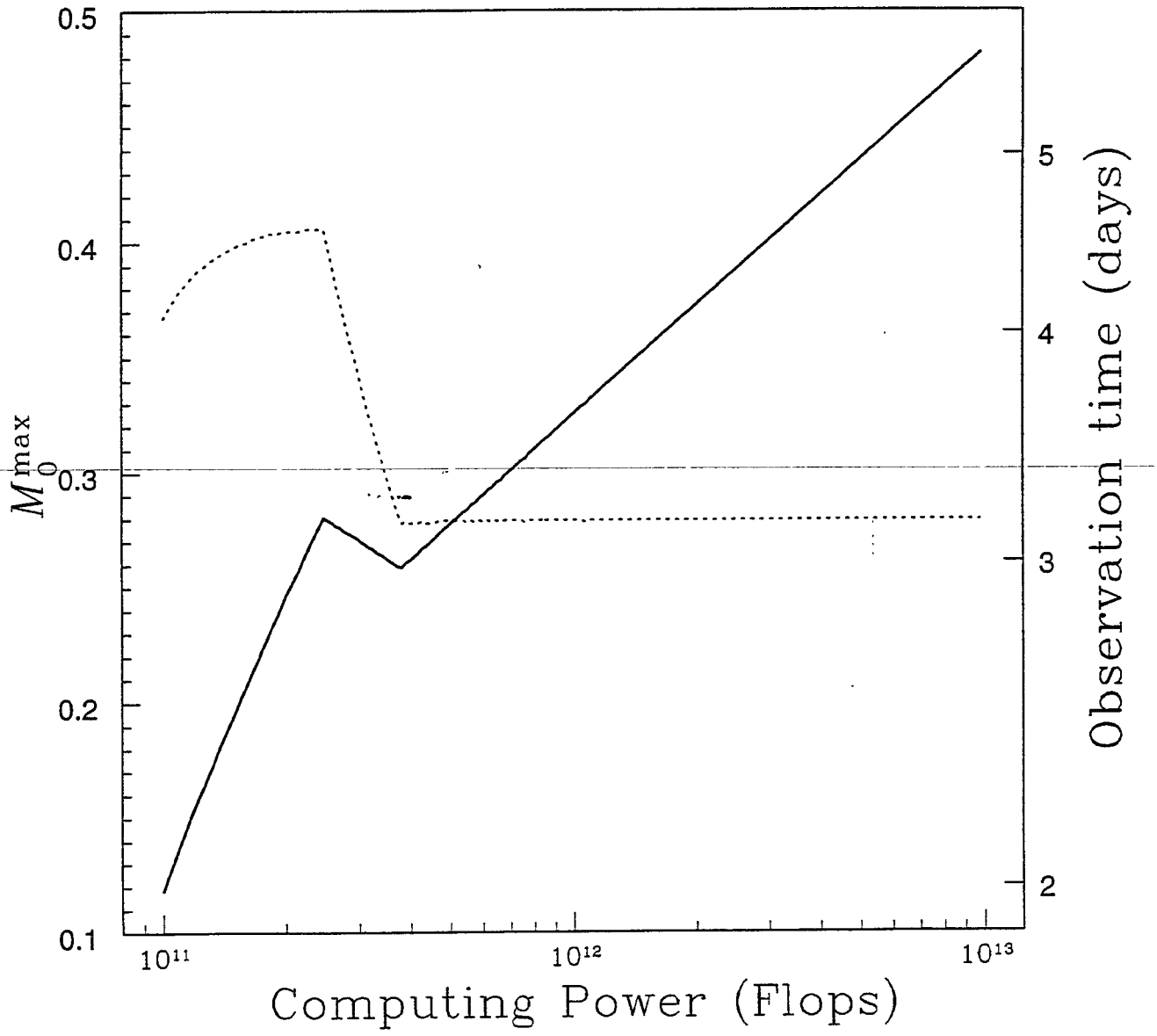
0.5
0.4
0.3
0.2
0.1
M_0^{max}
5
4
3
2
Observation time (days)
10^{11}
10^{12}
10^{13}
Computing Power (Flops)

Parameter Space: @ T. Creighton, C. Cutler, B. Schutz.

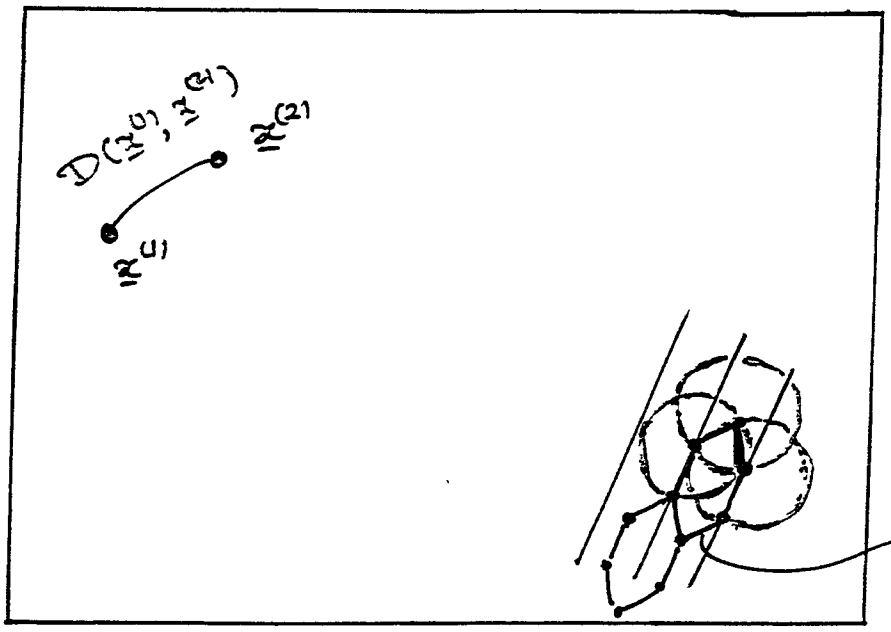

$\underline{x} = \{\theta, \varphi, f_1, f_2 \ldots\}$

$$D^2(\underline{x}^{(1)}, \underline{x}^{(2)}) = 1 - \max_f \left| \int dt_b^{(1)} \; e^{2\pi i f t_b^{(1)}} \; e^{i \underline{\Phi}(t, \underline{x}^{(2)})} \right|^2$$

Set up a lattice of points so that no $\underline{x}$ is further than M^{max} from some point on the lattice

To do so, use a "metric" defined as

$$D^2(\underline{x}^{(1)}, \underline{x}^{(2)}) \simeq \Delta \underline{x}^T \; \underline{\underline{g}} \; \Delta \underline{x}$$

$$\Delta \underline{x} = (\underline{x}^{(1)} - \underline{x}^{(2)}) \qquad \underline{\underline{g}} = \underline{\underline{g}}^T$$

Number of independent points in parameter space

$f_{max} = 200\ Hz$ $\quad \tau = 40\ Yrs$ $\quad M_{max} = 0.3$

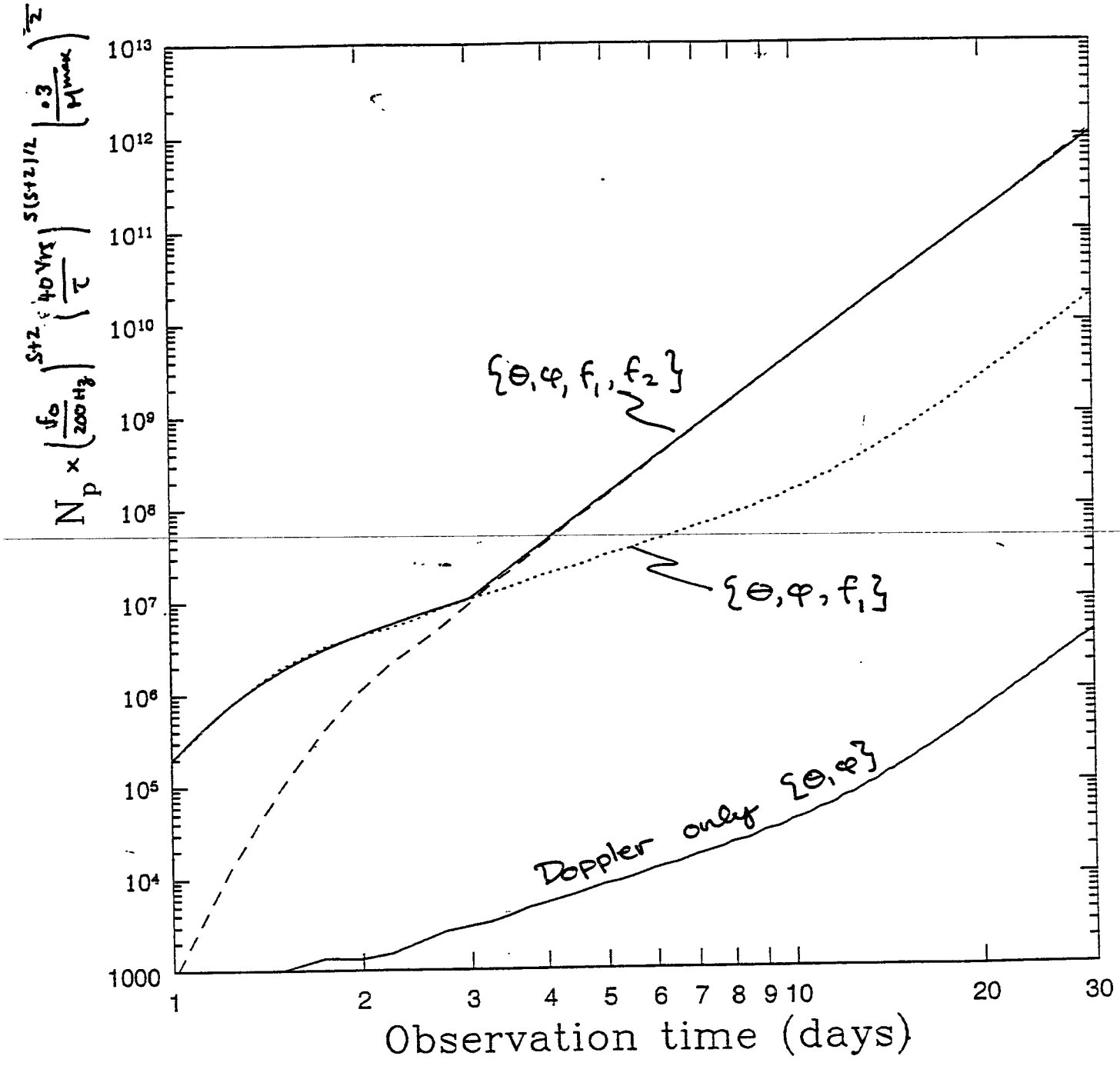

Brute force search

M^{max} + T_{obs} which maximize SNR for fixed computing power

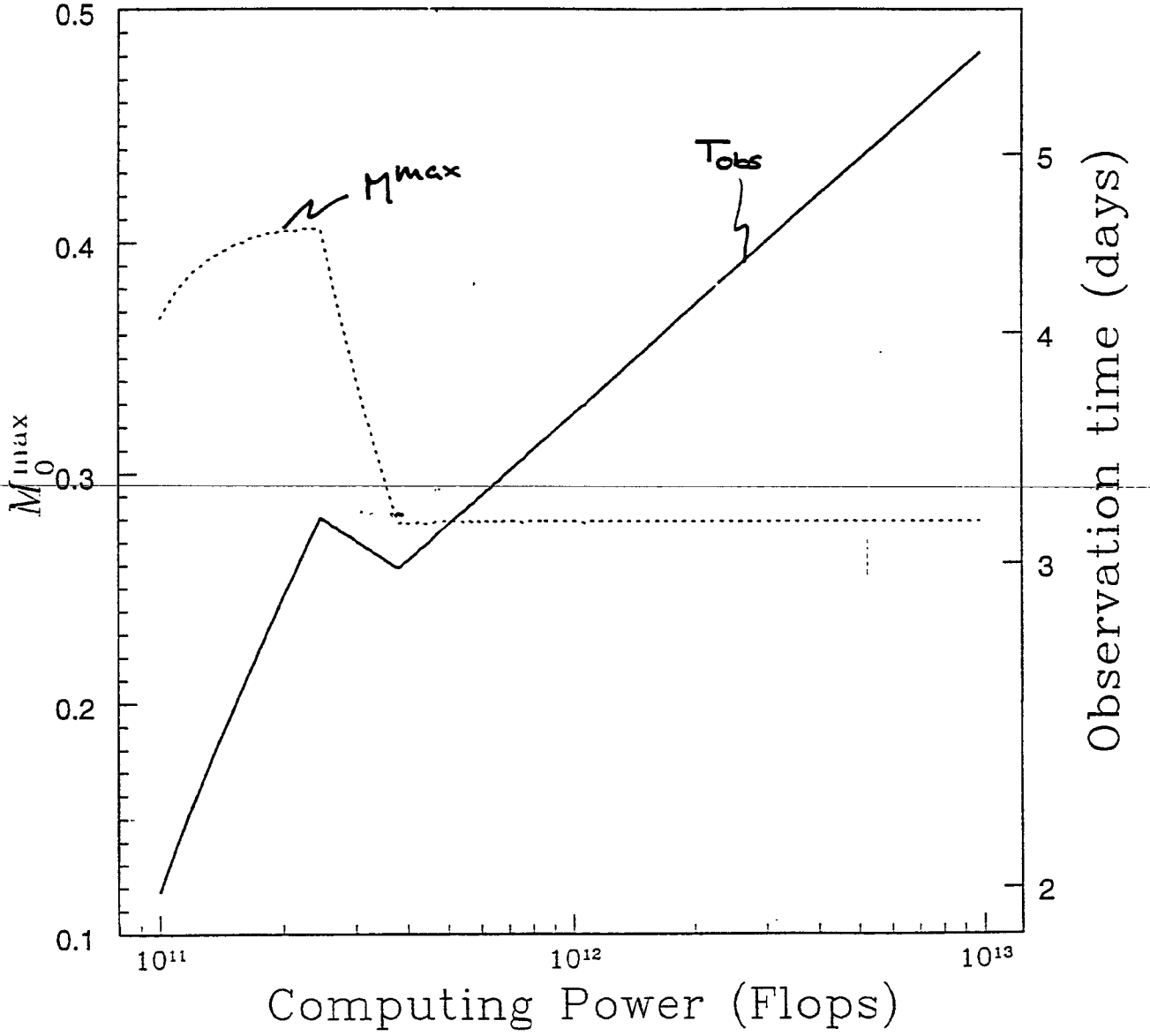

Where to ?

- promising, hierarchichal — metric formulation useful once again (Schutz + Wichden, T Creighton + PRB)
- stepping kernel + independence of position in parameter space
- Remove revolution — but not daily rotation → sidebands @ 1/day → ~~≠~~ sum. might be very useful — large correlations between revolution & spindown
- Limited searches — physical constraints
  - detector sensitivity due to amplitude modulation.
  - reduced patch number
- Simulation of all ideas in limited search
- Nightmare → I/O may impose most important constraint.

GWDAW
MIT 1996

CW Searches Hierarchically

B F Schutz
Potsdam AEI
Cardiff
schutz@aei-potsdam.mpg.de

Hierarchical search - consider angular positions only, not other parameters. (Only gets worse.)

Divide long data set into N segments. Total time T_0, split time $\tau = T/N$. Idea: Add (or combine in a filter) h successive power spectra. Lose $S/N \propto N^{1/4}$ in h (Astone). Then follow up 'accidentals' to find signal at full S/N. So one chooses $N^{1/4}$ to optimize processing speed.

Patch size on sky $\Delta\Omega = \Omega_0 \left(\frac{T}{T_0}\right)^{-4}$ $T_0 = 1\,\text{yr}$, $\Omega_0 \approx 10^{-12}$ sr

Total area of search $A \Rightarrow$ no of patches

$$n_N = \frac{A}{\Delta\Omega}\left(\frac{\tau}{T_0}\right)^{-4} = \frac{n}{N^4}, \qquad n = \frac{A}{\Delta\Omega} = \frac{4\pi}{\Omega_0}\frac{A}{4\pi}\left(\frac{T}{T_0}\right)^{-4}$$

Suppose computational cost (operations) of each patch is proportional to length of data set. Sampling rate R

Total samples $S = RT$

1-stage " $S_N = RT/N$

1-stage on data set

CW Searches Hierarchically

B F Schutz
Potsdam AEI
Cardiff
schutz@aei-potsdam.mpg.de

Hierarchical search - consider angular positions only, not other parameters. (Only gets worse.)

Divide long data set into N segments. Total time T_0, split time $\tau = T/N$. Idea: Add (or combine in a filter) successive power spectra. Lose $S/N \propto N^{1/4}$ in h (Astone). Then follow up 'accidentals' to find signal at full S/N. So one chooses $N^{1/4}$ to optimize processing speed.

Patch size on sky $\Delta\Omega = \Omega_0 \left(\frac{T}{T_0}\right)^{-4}$ $T_0 = 1\,\text{yr}$, $\Omega_0 \approx 10^{-12}$ sr

Total area of search $a \Rightarrow$ no of patches

$$n_N = \frac{a}{\Delta\Omega}\left(\frac{\tau}{T_0}\right)^{-4} = \frac{n}{N^4}, \qquad n = \frac{a}{\Delta\Omega} = \frac{4\pi}{\Omega_0}\frac{a}{4\pi}\left(\frac{T}{T_0}\right)^{-4}$$

Suppose computational cost (operations) of each patch is proportional to length of data set. Sampling rate R

Total samples $S = RT$

1-stage " $S_N = RT/N$

Cost $C = mS$ m = operations per data point

cost per stage

$$C_N = \frac{a}{\Omega_0} m \frac{RT}{N} \left(\frac{I}{\tau_0}\right)^4 \frac{1}{N^4}$$

Cost of all stages to produce summed set -

$$C_{Tot} = \frac{a}{\Omega_0} m \frac{RT}{N} \left(\frac{I}{\tau_0}\right)^4 \frac{1}{N^4} \times N$$

False alarms. After summing power spectra, there are

$$n_N \frac{RT}{N} = \frac{a}{\Omega_0} \left(\frac{I}{\tau_0}\right)^4 \frac{RT}{N^5}$$ Fourier bins. Each stage has an expected 1-σ power noise σ_p. The sum has expected noise power $\sqrt{N}\sigma_p$. A signal that has power S/N H in one stage will have S/N NH in summed power spectra. Expected number of false alarms in one bin at level NH is $\exp(-NH/\sqrt{N}\sigma_p)$

Total false alarms over all Fourier bins is

$$N_{false} = \frac{a}{\Omega_0} \left(\frac{I}{\tau_0}\right)^4 \frac{RT}{N^5} e^{-\sqrt{N} H/\sigma_p}$$

Each has to be followed up over full time-series. Each needs a search of N^4 patches and N frequency bins in each patch, so N^5 FFT's. Assume each bin can be done at a cost [redacted] m operations, so falsealarm cost is

$$C_{false} = m N^5 N_{false}$$

$$C_{\text{all stages}} = \frac{a}{f_0}\left(\frac{T}{T_0}\right)^4 m \frac{RT}{N^5}\left[N + N^5 e^{-\sqrt{N}H/\sigma_p}\right]$$

where H/σ_p is the power S/N of one stage.
Better to express this in terms of signal strength over whole observation time, $h^2 = NH/\sigma_p$ is the optimum attainable S/N,

$$C_{\text{all stages}} = \frac{a}{f_0}\left(\frac{T}{T_0}\right)^4 m RT\left[\frac{1}{N^4} + e^{-h^2/\sqrt{N}}\right]$$

↖ sensitive to non-Gaussian noise??

minimize $\frac{1}{N^4} + e^{-h^2/\sqrt{N}}$ for fixed h

h	1	5	10	15	20
N_{min}	2	7	41	124	285
$\frac{1}{N^5} + e^{-h^2/\sqrt{N}}$	0.52	3.9×10^{-1}	5.2×10^{-7}	5.9×10^{-9}	2×10^{-10}

So if one is looking for S/N = 15 in the full search, this hierarchical method saves a factor of 2×10^8 in CPU time, using 124 stages. If full-sky, 1-year search costs $\sim10^{26}$ operations ($m\sim10^9$) then with 124 stages it can be done in 10^{18} operations, ie in a few years with a 10 Gflop computer. (Uncertain scaling — no algorithms exist yet. But lesson is clear: speed improves rapidly with h.)

Experiences with the analysis of the Explorer and Nautilus datasets

Giovanni Vittorio Pallottino

ROG Collaboration (Guido Pizzella):

INFN (Istituto Nazionale di Fisica Nucleare) Rome, Frascati

University of Rome *La Sapienza*

University of Rome *Tor Vergata*

University of Aquila

CNR (Consiglio Nazionale delle Ricerche) Frascati

Activity of **Rome group** (Amaldi, Pizzella), started in the '70:

1) Experimentation on small cryogenic antennas
   which provided several important results
   and **experience**

2) Studies on g.w. detector modeling and analysis
   design criteria for large detectors
   and advanced algorithms for data analysis

3) **Construction of three cryogenic g.w. detectors**

— **ALTAIR (350 kg, 1800 Hz)** in Frascati, CNR
now used as test facility for new instrumentation

→ **EXPLORER (2300 kg, 900 Hz)** in Geneva, CERN
now operating, the first bar to operate continuously

→ **NAUTILUS (2300 kg, 900 Hz, 100 mK)** in Frascati, INF
now operating, the first ultracryogenic detector

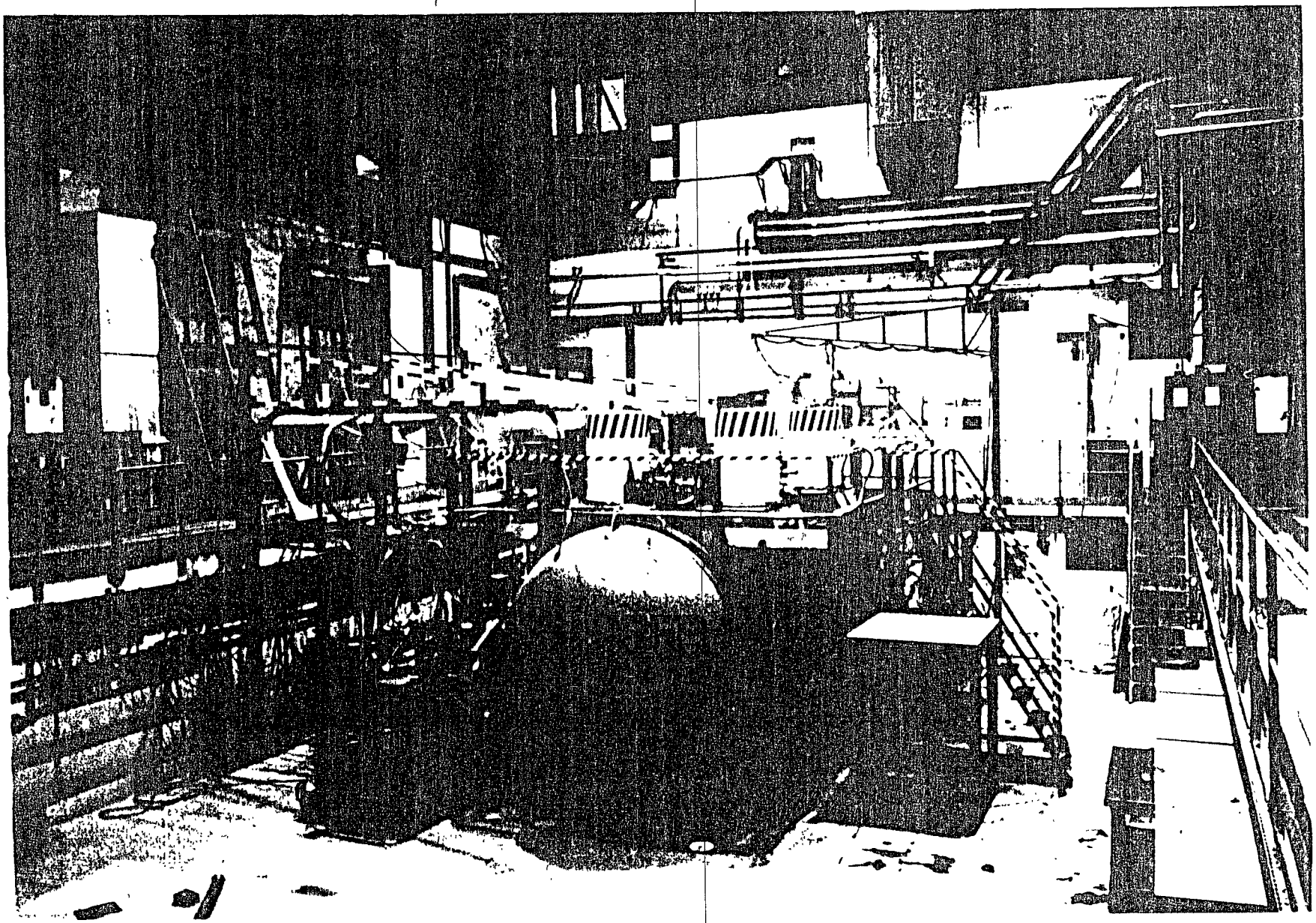

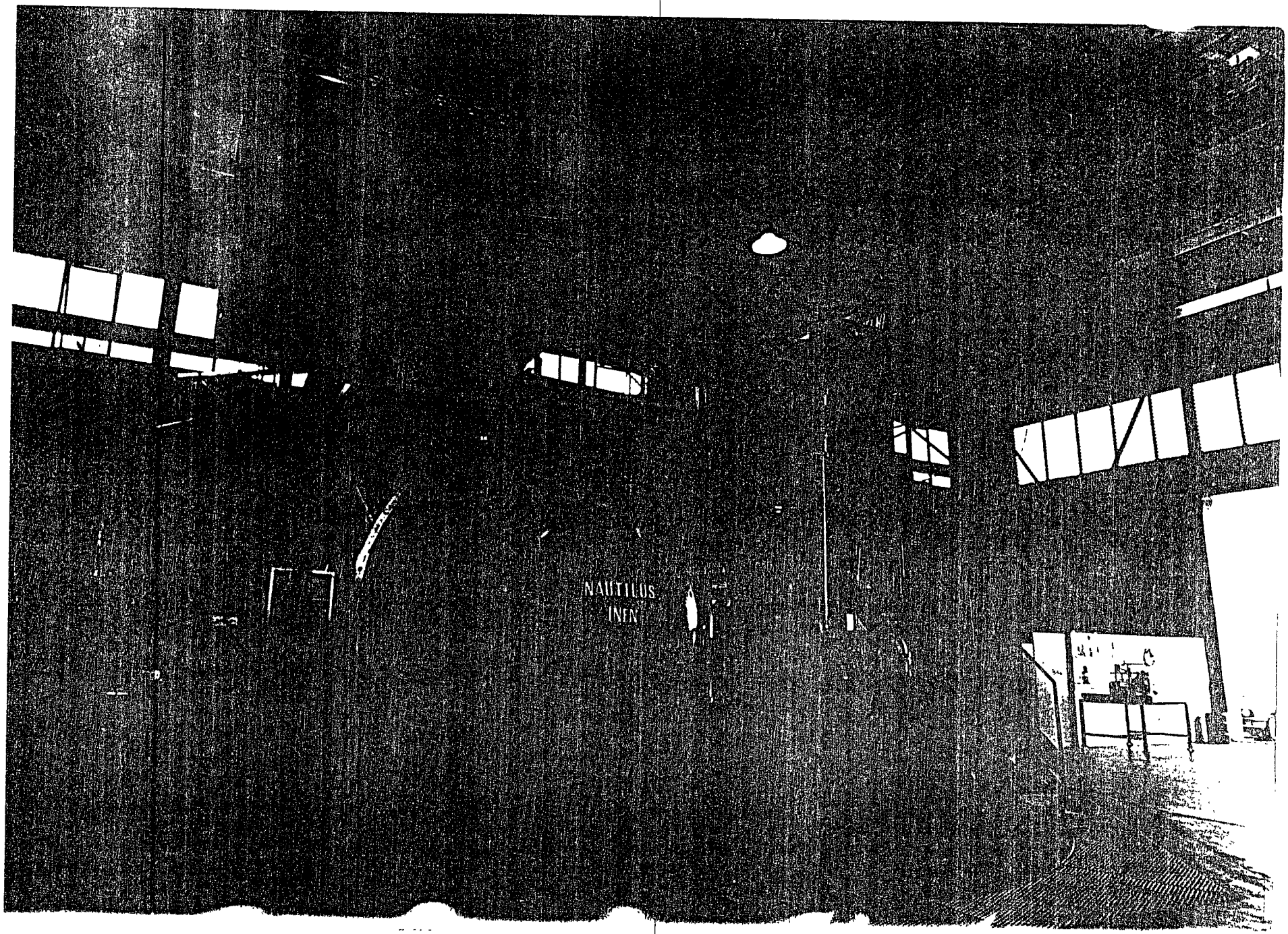
NAUTILUS
INFN

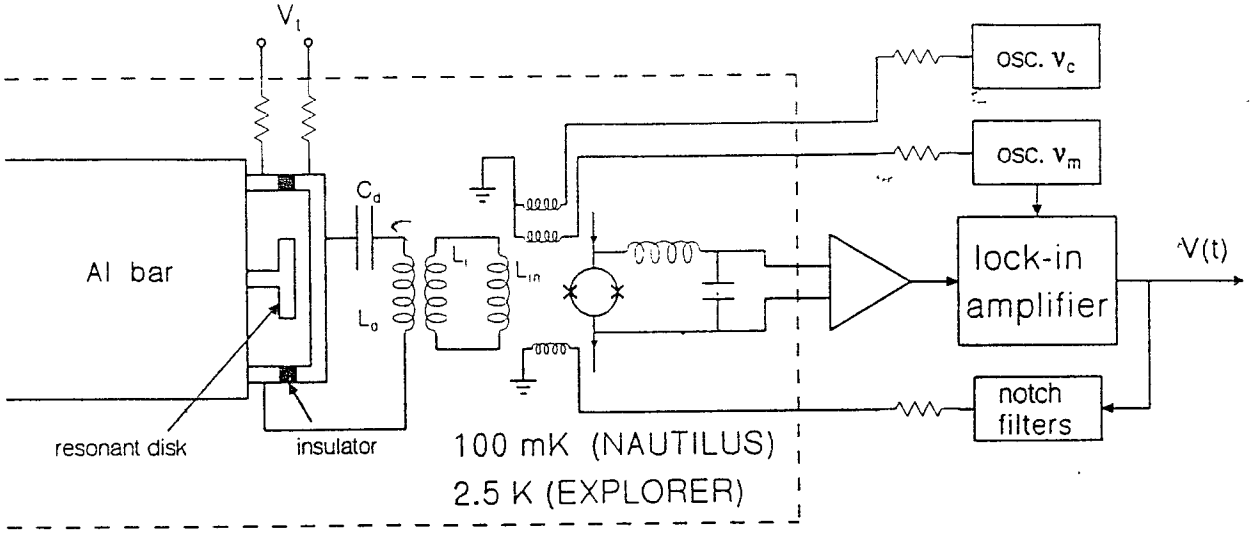
V_t
Al bar
C_d
L_o
L_i
L_{in}
resonant disk
insulator
100 mK (NAUTILUS)
2.5 K (EXPLORER)
osc. ν_c
osc. ν_m
lock-in amplifier
V(t)
notch filters

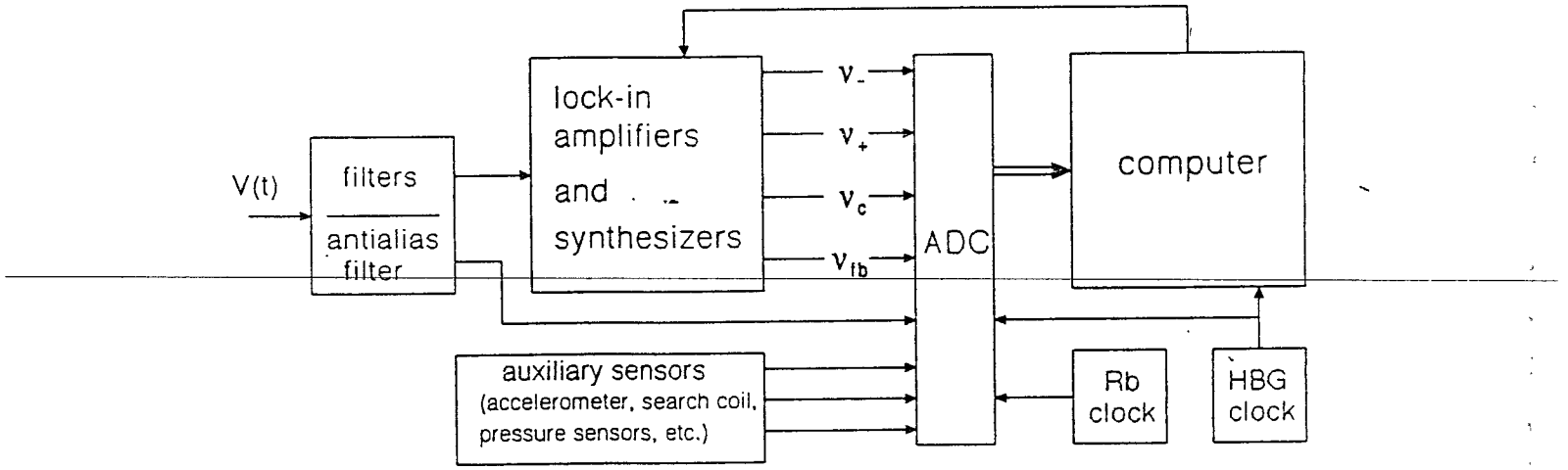
V(t)
filters
antialias filter
lock-in amplifiers and synthesizers
ν_-
ν_+
ν_c
ν_{fb}
ADC
computer
auxiliary sensors
(accelerometer, search coil, pressure sensors, etc.)
Rb clock
HBG clock

To improve the SNR we use filters based on the theo
of the optimum filter (for detecting a delta function)
We use different filters, according to

A) the sampling time of the signal to be processed
directly sampled at 220 Hz (4.5 ms) or at 5 kHz (0.2 ms)
sampled at 3.4 Hz (290 ms) after processing with lock-in

B) the parameters used for constructing the filter
fixed parameters (mathematical model of the detector)
adaptive filters, obtained from the spectrum of the data
with different adaptivity , i.e. memory, and other

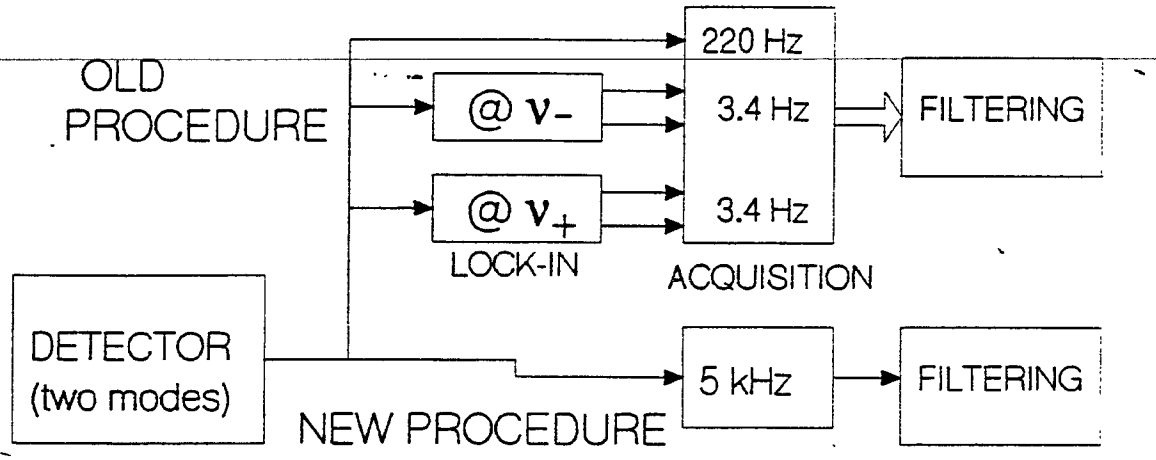

DATA ACQUISITION AND FILTERING

Procedure used until 1996

a) the signals from the lock-in's at the two modes are sampled with **$\Delta t = 290.8$ ms** and filtered with non adaptive and adaptive Wiener filters

b) the signal from the antenna (one channel) is sampled at higher rate, with **$\Delta t = 4.54$ ms** and filtered with an adaptive filter matched to a delta function

Procedure used since 1996

the signal from the antenna (one channel) is sampled with **$\Delta t = 0.2$ ms** (5 kHz) and filtered with various adaptive filters (different properties)

this procedure provides very large flexibility

What we search for?

Basically **bursts**, i.e., short events (in the ms range) with small amplitudes

to be extracted from the noise using powerful filters (exploiting the different statistical properties of the signal and of the noise)

which we model as delta functions

But we also found that our data can be used to search for:

→ periodic waves (Pia Astone reporting on that)

→ stochastic background

How do we expect the data to be?

Superposition of large well behaved noise

with Gaussian distribution

with Lorentzian spectrum at the resonant modes

and of small (as well as rare) g.w. signals

orders of magnitude below the noise

This is what we get during most of the time

(as regards, of course, the noise....)

---

while other times the matter is different

as the noise is not a stationary process

its statistics are not time-invariant

as shown by the distributions

and by the spectra

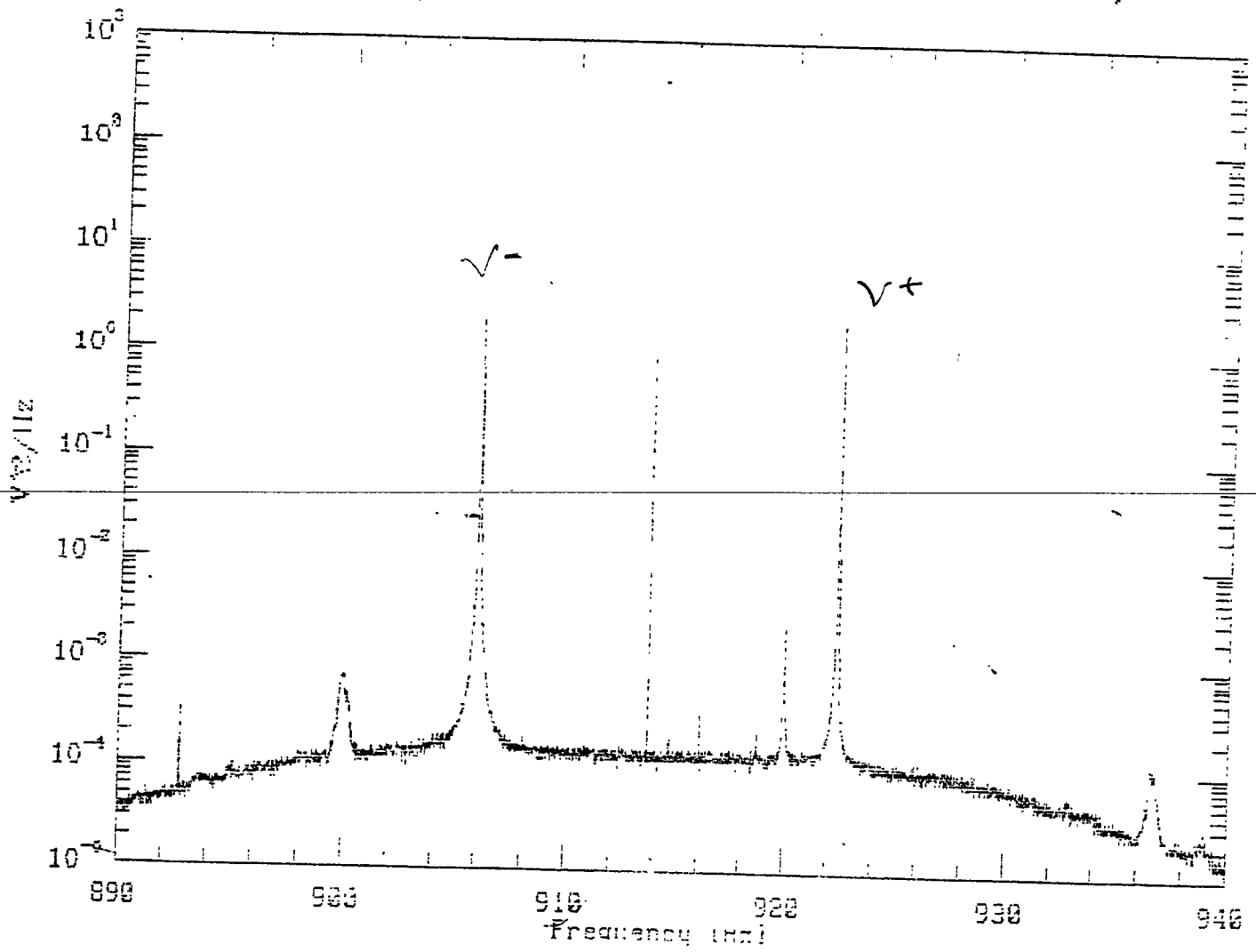
10^3
10^2
10^1
10^0
10^{-1}
10^{-2}
10^{-3}
10^{-4}
10^{-5}
$\nu-$
$\nu+$
900
908
910
920
930
940
Frequency (Hz)

Nov. 29, 1996

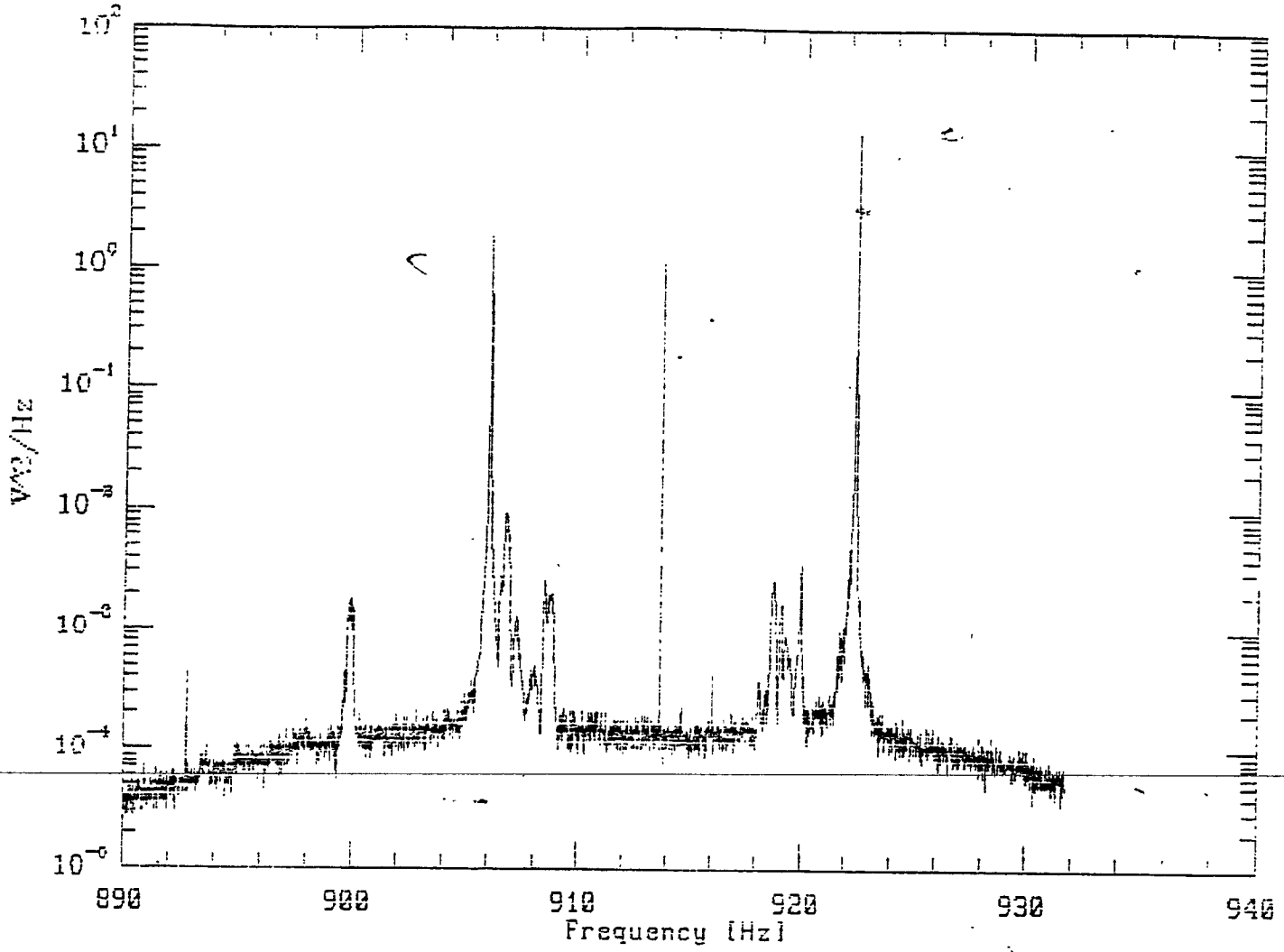
10^{2}
10^{1}
10^{0}
10^{-1}
10^{-2}
10^{-3}
10^{-4}
10^{-5}
V^2/Hz
890
900
910
920
930
940
Frequency [Hz]

Explorer Sept. 25, 1995 (7.6 hours of data)

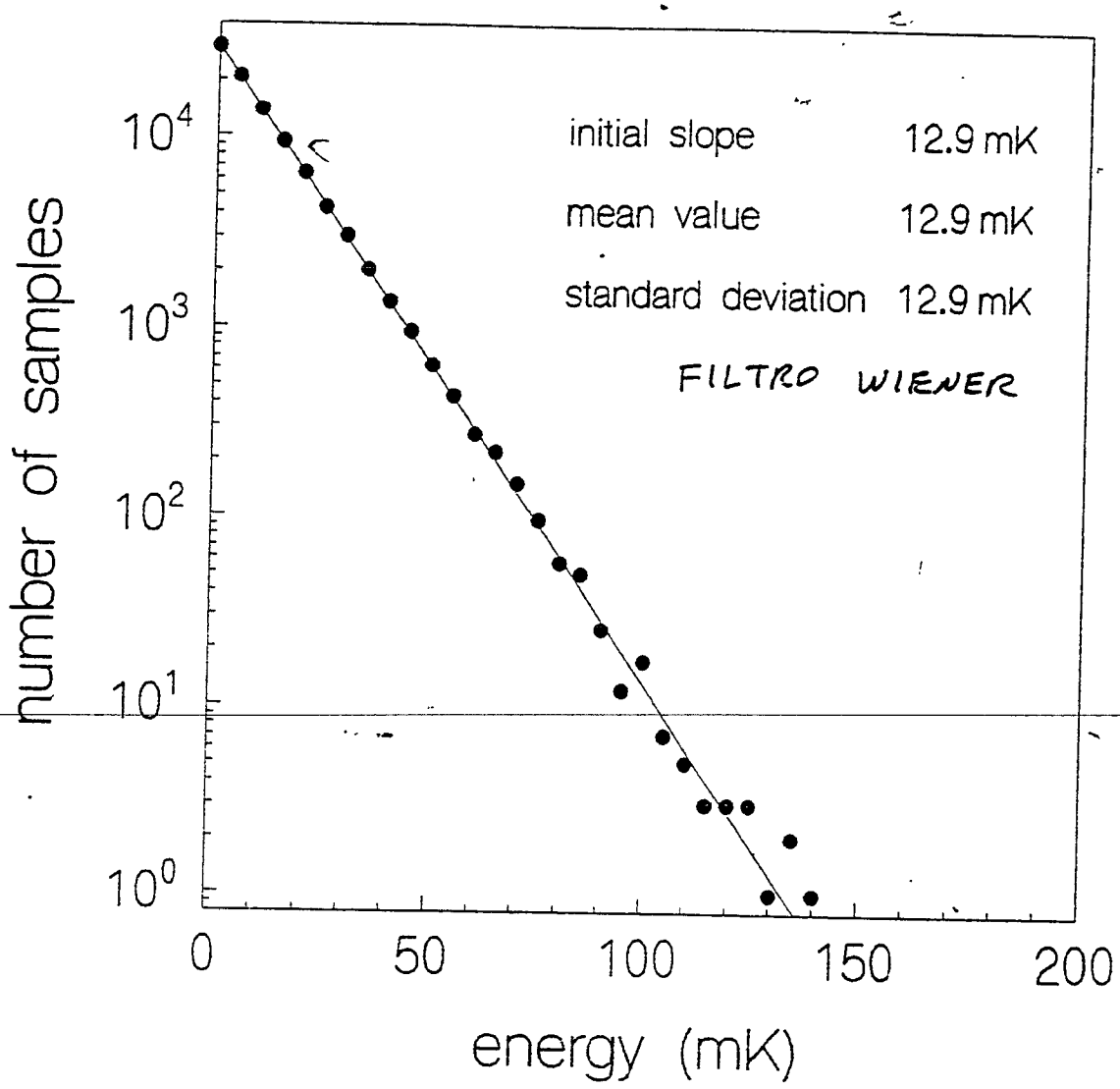

$h \simeq 8 \times 10^{-19}$

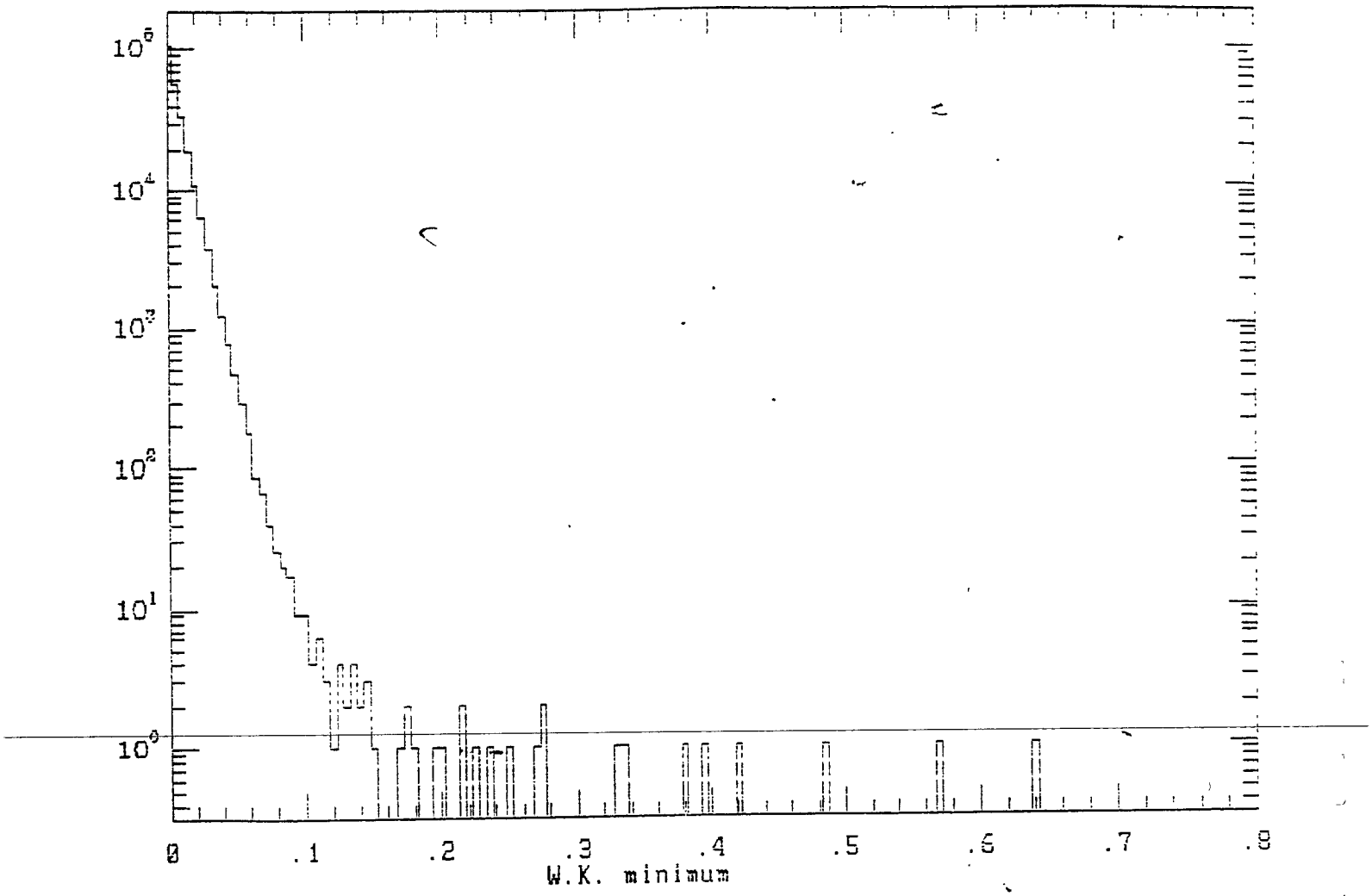

Nov 29, 1996 237'800 samples χ^2

NAUTILUS "FAST" FILTER 95

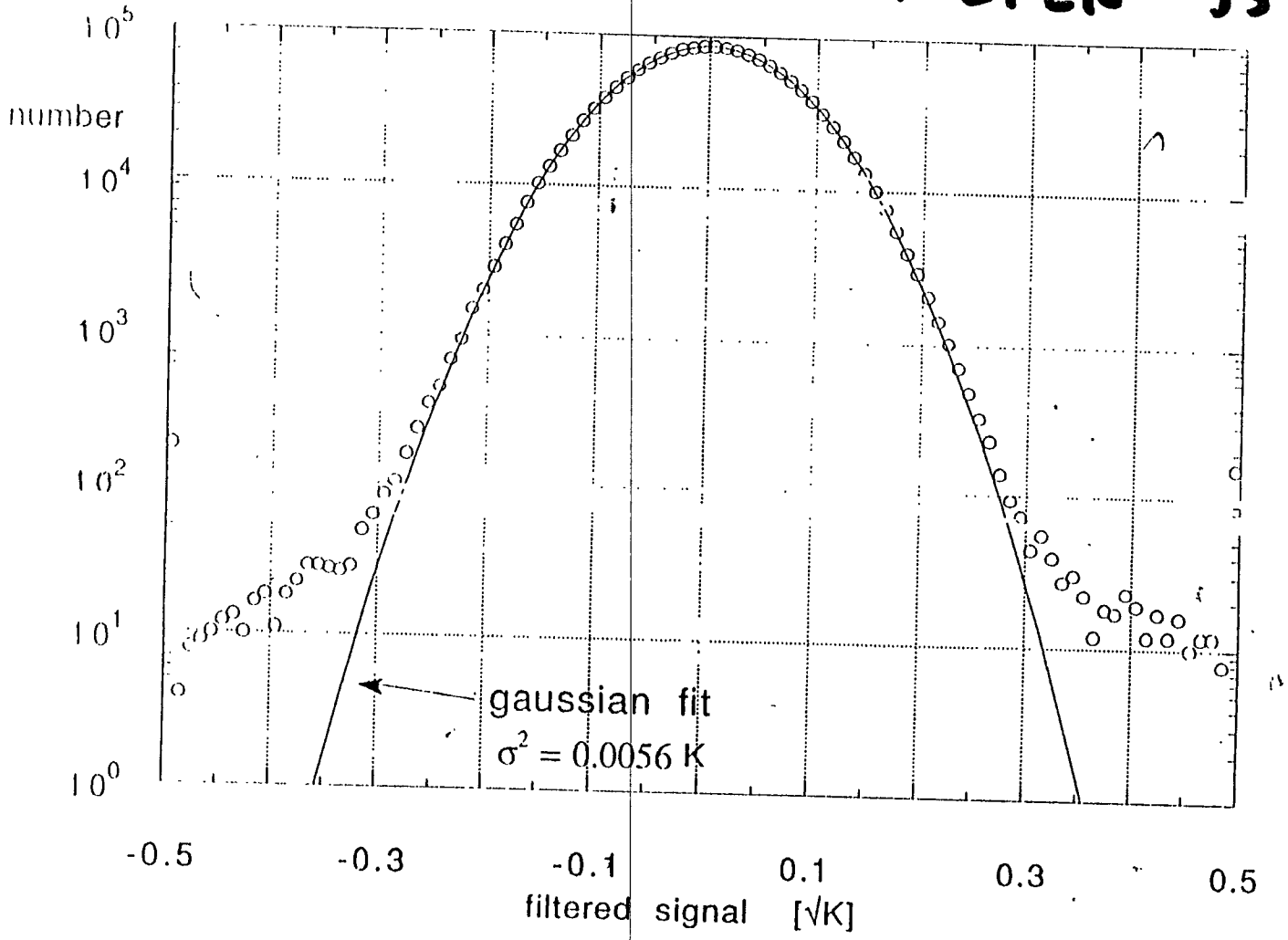

A typical distribution of the filtered data taken over days or weeks

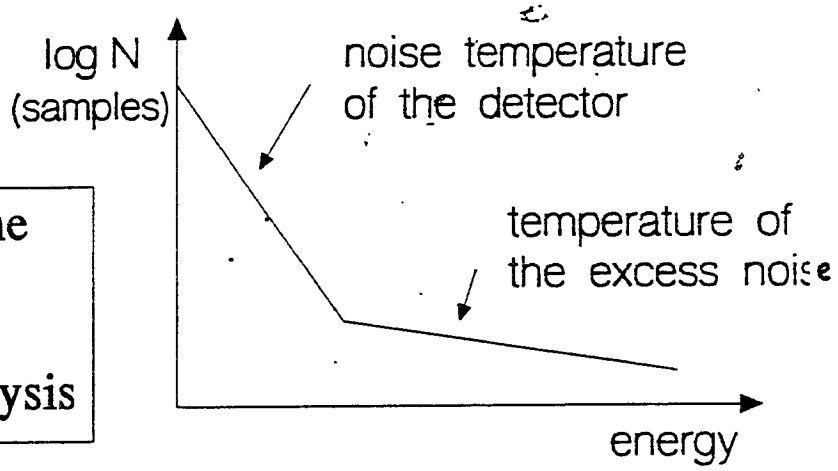

The samples of the tails are the most important for analysis

when establishing upper limits for g.w.

when selecting candidate events for coincidence analysis between two detectors

or whatever else

The rate of the excess noise is usually rather variable (sometimes the large pulses are close together)

Part of it can be eliminated if occurring when sensors of local disturbances (accelerometers, etc.) are excited

Coincidence analysis between the data of two (or more) detectors located at convenient distance

Before even daring to start this analysis one has to perform a number of tests and take various decisions

→ BE SURE OF THE TIMING OF THE DATA (know the error)

→ DECIDE WHAT TO SEARCH FOR (short bursts or what else)

→ CAREFULLY EXAMINE THE TWO STREAMS OF DATA

- the autocorrelation function, for example, provides information on the durations of the disturbances
- the distributions provide the "temperature" of the only important part of the data
- do different stretches of data have simlar properties?

→ SELECT A SUITABLE ENERGY THRESHOLD

- for a given number of events per day?
- a fixed threshold or an adaptive one (to have constant rate)?

→ DECIDE IF CONSIDER SAMPLES ABOVE THRESHOLD OR "EVENTS" (defined by max. energy, time and duration)

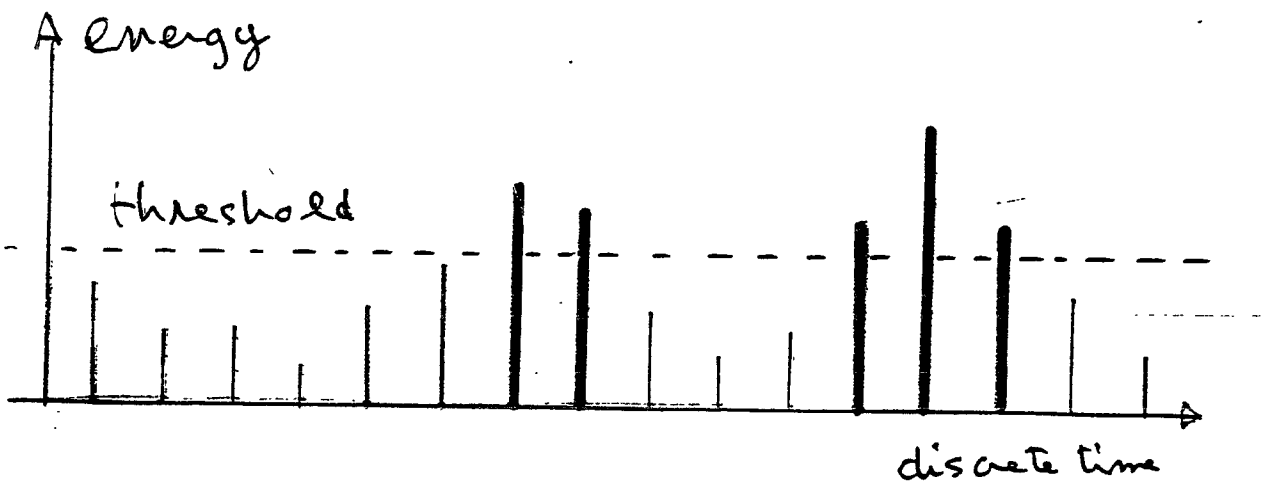

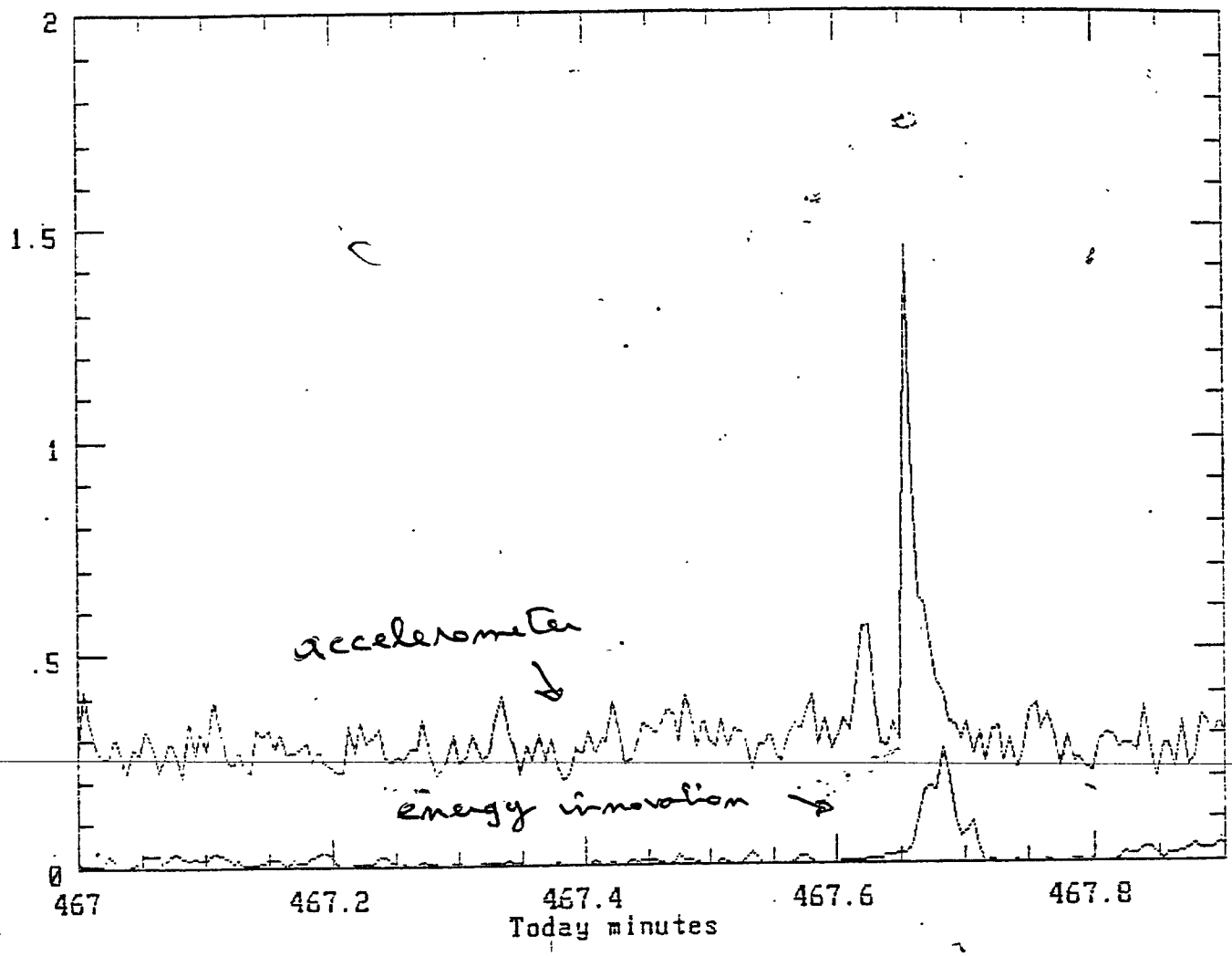

Use auxiliary channels to eliminate at least part of the disturbances

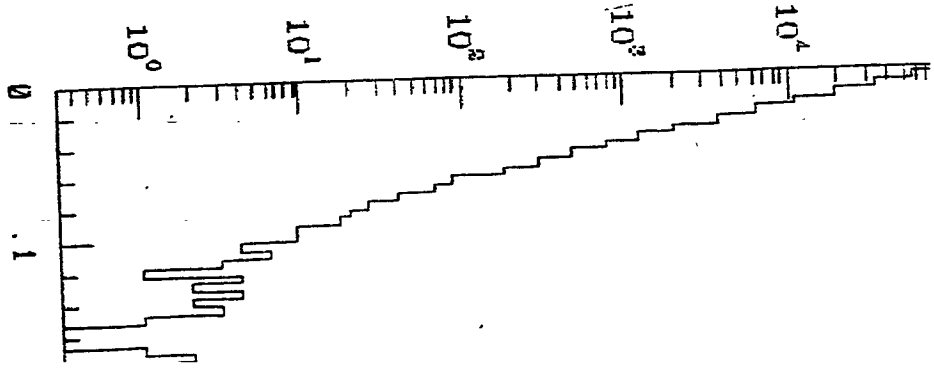

Other points:

→ Have the "events" roughly the same energy, when independently observed using the two modes of the resonant detector?

→ How long the "events" are? their duration should be related to the integration time of the filter. If much longer, they are presumably garbage

And then we have a number of choices

each at some "cost" in terms of the final probability

→ Energy threshold for defining the "events" to be analyzed or adaptivity (memory), when using a variable threshold for obtaining a given rate of "events"

→ Width of the coincidence window

A single optimum filter only exists for stationary data

which is not usually the case

Different filters may turn out to be optimum
i. e. provide maximum sensitivity (SNR improvement)
for different operating conditions of a given detector

(various filters with different adaptivity (memory)
have been discussed by Maria Alessandra Papa)

But when filtering the same data with different filters
we found very different and (disturbing) results
as regards the sets of "events" obtained with them:

the overlap between those sets of "events"
is very small, say about 5 - 10%

Some reasons why the sets of events are different

1) Most of the "events" are not *canonical*

i.e. they are not the response to a delta function excitation

but rather disturbances or tails of the thermal noise

2) Even those *canonical* contain some amount of noise

which is differently reshuffled by different filters

thus changing the observed energy of the "events"

3) Different filters may have different sensitivity

and those operating on data with longer sampling times consider

as "short" events considered "long" by other filters

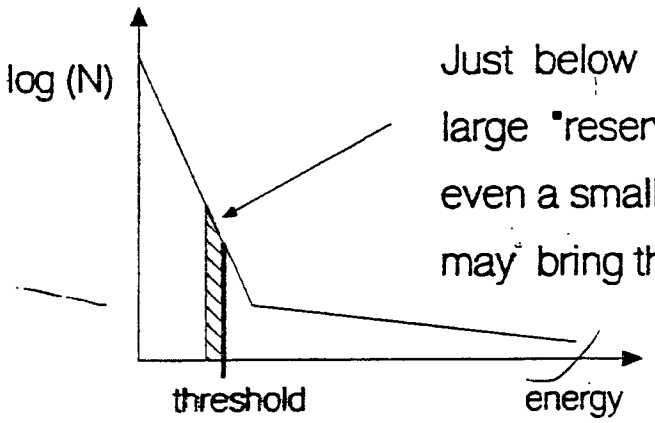

Just below the threshold there is a very large "reservoir" of (filtered) data samples even a small change of the noise may bring them above the threshold